The Equatorial Strip Sample
– A blind HI survey for gas-rich galaxies –

Diego A. Garcia-Appadoo

A thesis submitted to
Cardiff University
for the degree of

Doctor of Philosophy

September 2005

DECLARATION

This work has not previously been accepted in substance for any degree and is not being concurrently submitted in candidature for any degree.

Signed ______________________________ (candidate)

Date ____________________

STATEMENT 1

This thesis is the result of my own investigations, except where otherwise stated. The SDSS optical counterpart data for the Equatorial Strip sample was produced, as described in Chapter 3, by Andrew A. West at the University of Washington.

Other sources are acknowledged giving explicit references. A bibliography is appended.

Signed ______________________________ (candidate)

Date ____________________

STATEMENT 2

I hereby give consent for my thesis, if accepted, to be available for photocopying and for inter-library loan, and for the title and summary to be made available to outside organisations.

Signed ______________________________ (candidate)

Date ____________________

Summary

The Equatorial Strip sample comprises 1077 galaxies selected purely by their HI signature. This is a unique sample which covers a large area of sky, is free from optical selection effects and which has complete, very high quality, optical data (SDSS) for a subsample of 201 galaxies. The combination of the HI data with optical data allows us to make a comprehensive analysis and study of the properties of HI selected extragalactic sources and investigate vital global correlations which will help us to improve our understanding of gas-rich and Low Surface Brightness galaxies. The Equatorial Strip runs along the celestial equator from $-6° < \delta < +10°$ and through all R.A.s. The Equatorial Strip sample represents $\sim$ 14% of the whole sky, covering an area of 5738 deg^2 and a total volume of $\sim 2.76 \times 10^6$ Mpc^{-3}.

LSB galaxies make up 12% of the sample, however, no high luminosity or high HI mass LSB galaxies have been found. Consequently, LSB galaxies make up no more than 6% of the high luminosity, gas-rich population, and massive LSB galaxies contribute no more than 13% of the population, at the 95% confidence level.

The Bivariate Brightness Distribution and the Luminosity Function for the sample have been calculated and relationships found between surface brightness and optical luminosity, HI, baryonic and dynamical mass. From these results I find that LSB galaxies contribute 35^{+29}_{-20}% to the number density of gas-rich galaxies in the Universe but only 7^{+3}_{-2}% to the luminosity density. They also contribute 21^{+7}_{-6}% and 12 ± 3% respectively to the neutral hydrogen (HI) and baryon density of gas-rich galaxies in the Universe.

The Equatorial Strip sample has unveiled many objects not found in optical surveys, ranging from very low surface brightness, very blue galaxies to extremely gas-rich galaxies.

Preface

The data used in this thesis was the product of the HIPASS and SDSS collaborations. As a result, there are many contributors to the data collection and reduction. As part of the HIPASS collaboration, I contributed to the project as a whole by doing $\sim$ 1000 hours observing at the Parkes Telescope both as part of the main survey and the Narrow Band follow-ups, 1 week at the Australian Telescope Compact Array (ATCA) and 9 days at the 2.2 metre and NTT ESO telescopes at La Silla. I have been heavily involved in the data reduction, parameterisation of the survey and analysis of the results, both in the region of sky used for this thesis and the HIPASS survey. As a whole, all the radio data used in this thesis has been reduced and parameterised by me during a 3 month visit to Melbourne University.

As part of the HIJASS collaboration I have contributed $\sim$ 4 months observing time at the Lovell Telescope at Jodrell Bank and 10 days optical observing at the JKT telescope in La Palma.

As part of the SDSS collaboration I have contributed 9 days observing at the 1000 foot Arecibo telescope in Puerto Rico, observing gas poor galaxies in the local universe. I have also spent 3 weeks at the University of Washington in Seattle working with Julianne Dalcanton and Andrew West (SDSS collaborators) learning the intricacies of the techniques used for the reduction of SDSS optical data for nearby (extended) galaxies used in this thesis.

I have also carried out 3 weeks observing at the 100 metre Green Bank Telescope in West Virginia, for a project lead by Steve Eales (Cardiff University) aimed at detecting CO in high redshift radio galaxies.

Contents

List of Figures

List of Tables

Chapter 1

Introduction

I don't pretend to understand the Universe - it's a great deal bigger than I am.

– Thomas Carlyle (1795-1881) –

Our knowledge of the amount and distribution of matter in the universe is incomplete. The study of the structure of the universe has largely been based on optical surveys of galaxies. Through the study and cataloguing of galaxies we can learn about their properties and how these vary for different Hubble types along the Hubble sequence.

Optical surveys of galaxies primarily trace the emission from stars. However, there is strong evidence that optical light only accounts for a small fraction of the total mass of the universe (e.g. Trimble 1987). It has become apparent over the last 30 years that we may be missing a significant number of galaxies from our catalogues which could contain a significant amount of the matter in the universe (e.g. Disney 1976; Disney & Phillipps 1983; Bothun, Impey & McGaugh 1997). Optical observations are biased towards high surface brightness objects, and a substantial proportion of the optical population may be missed in typical optical surveys (Disney 1976) as any galaxies with low surface brightness will not be detected. Low Surface Brightness (LSB) galaxies are effectively hidden beneath the brightness of the night sky, leaving us to see only the highest surface brightness galaxies.

The Cosmological Principle assumes that the universe will appear homogeneous and isotropic to a typical observer. Observational cosmology is usually probed via catalogues of galaxies. Although much of the universe is dark, galaxies are the prime repositories of shining baryonic matter and their properties are used to measure the size and shape of the universe. If galaxies are to be used as effective cosmological probes, then our catalogues must be complete and homogeneous. Yet the detectability of galaxies depends very much on the cosmic environment. For example, an observer whose star was in a giant molecular cloud or near the centre of an elliptical galaxy would have difficulty discovering external galaxies and so would perceive the universe quite differently from us.

It is important to know the baryon fraction of the universe if we want to know its true nature (e.g. Fukugita, Hogan & Peebles 1998). A significant proportion of baryons could, however, be contained within LSB galaxies (e.g. Impey & Bothun 1997) and thus missing from our census, which is limited to those galaxies found in optical surveys. Put simply, we only catalogue the galaxies we can see.

Rather than tracing the stellar emission from galaxies, we can use the most abundant element in the universe, hydrogen, to trace the dynamics and distribution of matter. Neutral hydrogen (HI) emission was first detected by Ewen and Purcell (1951), who found HI in our own galaxy, the Milky Way. Kerr and Hindman (1953) were the first to detect extragalactic HI, in the Magellanic Clouds, using a 36-foot antenna in Australia. Hydrogen, in its neutral atomic state (HI), emits a photon with a wavelength of 21cm.

The 21cm line arises from a hyperfine transition in the lowest state of neutral hydrogen (cold ground state). The misaligned spins between the proton and the electron are less energetic than aligned spins but this transition is forbidden, i.e. it does not conserve spin. This means the excited state has a lifetime of 10^7 years. The probability of the transition is low ($\sim 2.868 \times 10^{-15} s^{-1}$), the spin temperature of the gas is governed by atomic collision, and the absorption and emission of photons from either an existing 21cm radiation field or indirectly from Lyman α transitions (Verschur and Kellerman 1988). This means that a bright external radiation field is not required for HI emission, and that the emission can be independent of the stellar light. In dense hydrogen gas (as in galaxies or HI clouds) de-excitation is much more likely due to collision with other atoms and this is the reason why the emission from galaxies can be detected.

This Thesis presents the results of the Equatorial Strip (ES) project, a subsample of the Parkes All Sky Survey (HIPASS) blind survey for extragalactic neutral hydrogen (HI). The HIPASS is the largest HI survey to date and the first blind HI survey to cover the whole of the southern sky and a northern extension ($+2° < \delta < +25°$). The survey, which started in 1997 and finished in 2002, was conducted with the 13-beam Multibeam receiver at the 64-m Parkes Radio Telescope in Australia.

The ES sample comprises 1077 galaxies selected solely by their HI signature. This is a unique sample which covers a large area of sky, is free from optical selection effects and which has complete, very high quality, optical data for a subsample of 201 galaxies. Up until now all previous HI surveys have relied on literature measurements of optical parameters – with the exception of HIDEEP (Minchin *et al.* 2001) which covered a far smaller area of sky (36 deg^2) - which are at best less than ideal. This sample should allow us to investigate vital global correlations which will help us to understand the role and contribution of gas rich and LSB galaxies to the Universe. This Thesis aims to improve our understanding of gas-rich and Low Surface Brightness galaxies and their contribution to the local Universe through the analysis of an HI selected sample of galaxies.

1.1 Optical Surveys and Selection Effects

It was suggested by Freeman in 1970 that all disc galaxies appear to have the same surface brightness. Freeman analysed the surface-photometry of a non-statistical sample of 36 disc galaxies finding that the B-band central surface brightness (corrected for inclination) is nearly constant at $B(0)_c = 21.65 \pm 0.30(\sigma)$ mag per square arc second (see Figure 1.1) along the entire Hubble sequence from S0 to Im. This surface brightness distribution (SBD), $\mu_B = 21.65 \pm 0.3$, from Freeman (1970) came to be known as 'Freeman's Law', even though Freeman never claimed it as a 'law'. Spiral galaxies have exponential radial profiles. We make the simplifying assumption that LSB galaxies are suitably described by exponential radial profiles but this is only valid for disc-dominated systems. It has been shown that LSB galaxies are well fit by exponential profiles (e.g. Bingelli *et al.* 1984, Caldwell & Bothun 1987, Impey *et al.* 1988, Davies *et al.* 1990).

Disney (1976) tried to find an explanation for Freeman's distribution by arguing that it is due to observational selection effects. Disney proposed that the isophotal diameter of a galaxy was the main parameter in which catalogues were based – hence LSB galaxies are discriminated against as only a small portion of the disc falls above the limiting isophote, while High Surface Brightness (HSB) galaxies would be discriminated against due to their intrinsically compact nature.

The idea that there might be selection effects due to surface brightness was not new. It was noticed by Zwicky (1957), Arp (1965) and de Vaucouleurs (1974) but Disney (1976) was the first to try to explain the observed surface brightness distribution (SBD) and the selection effects in a quantitative manner. In addition to Freeman's result (1970), which explicitly found a constant central surface brightness for spiral galaxies, Disney analysed the results of Fish (1964) for elliptical galaxies. Fish had found that the binding energy of elliptical galaxies varied as their mass to the power 3/2: $\Omega \propto M^{\frac{3}{2}}$. Disney showed that the actual measurements made were of the luminosity (L) and the scale length (α), and

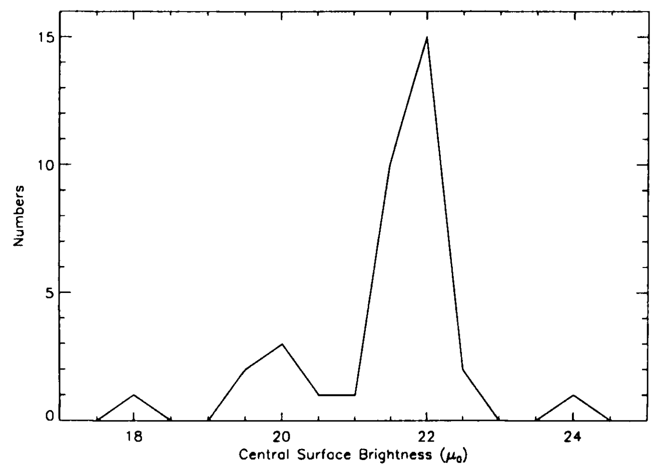

Figure 1.1: Central Surface Brightness distribution from Freeman (1970). It can be seen that the distribution is highly peaked at the 'Freeman's Law' value of $\mu_B = 21.65 \pm 0.3$.

that 'Fish's Law' therefore implied L_T/α^2 = constant. However, $L_T/\alpha^2 \propto \sigma(0)$, which is the central surface brightness, hence Fish's result implied a constant central surface brightness for ellipticals. Further analysis showed that the implied peak in the surface brightness distribution was at 14.8 $\pm$ 0.9 B mags arcsec^2, in agreement with Disney's calculation of the surface brightness which yields the maximum isophotal radius.

Kormendy (1977) offered an alternative explanation for 'Freeman's Law'; that it was an artefact of the fitting process used to determine the central surface-brightness of the exponential disc. Kormendy modelled disc and spheroidal contributions for a variety of true central disc surface-brightnesses and found that, except for particular high surface-brightness discs, the spheroid dominated down to the isophotal limit and forced the fitted central surface-brightness to be close to Freeman's value.

Disney's conclusion that selection effects were responsible for the sharp peak observed in the SBD, and that there were probably numerous LSB galaxies remaining undiscovered in the local universe, was opposed by Shostak (1977) who found no unambiguously extragalactic new sources in a neutral hydrogen survey (see Section 1.4.2).

Phillipps & Disney (1983) re-visited the work of Kormendy (1977) and showed that for galaxies with significant spheroidal components, fitting would give a central surface-brightness close to the Freeman value as the slope of the surface-brightness profile near $\mu = 25$ B_μ is the same for a spheroidal component as for a disc with $\mu_0 = 21.65$, as found by Kormendy (1977). Phillipps & Disney also showed that the hardest discs to 'hide' beneath a spheroidal component were those with $\mu_{lim} - \mu_0$ in the range 2 – 3, e.g. those near the Freeman value, as these have the largest apparent size – discs with either lower or higher surface-brightnesses than these appear smaller and are thus more easily dominated by spheroid. Domination by the spheroid, which is linked to the visibility of the disc, can therefore explain both the lack of LSB and HSB discs in Freeman's sample.

Disney & Phillipps (1983) revised the visibility function to include selection based on magnitude as well as diameter, and showed that the isophotal magnitude was considerably lower than the total magnitude for low surface-brightness galaxies. This would lead to these galaxies being excluded from catalogues as they appeared less luminous than they truly were. They also showed that, for high surface-brightness galaxies, saturation of the photographic plates meant that the measured magnitudes were considerably less than the true total magnitudes. Most catalogues will have both magnitude and diameter limits, in this case the two limits are applied simultaneously and the detection limit is the lower of the two limits at any given surface-brightness.

Figure 1.2 shows the visibility function for the selection parameters used in Disney & Phillipps (1983). The volume covered is that of an all-sky survey of both hemispheres and galaxies with $M_B = -21$, but the shape of the function is not affected by either the area or the magnitude chosen. It can be seen that it is strongly peaked in a similar manner to the surface brightness distribution of Freeman (1970), with the peak occurring where the limits due to luminosity and diameter intersect. These galaxies can be seen over a larger

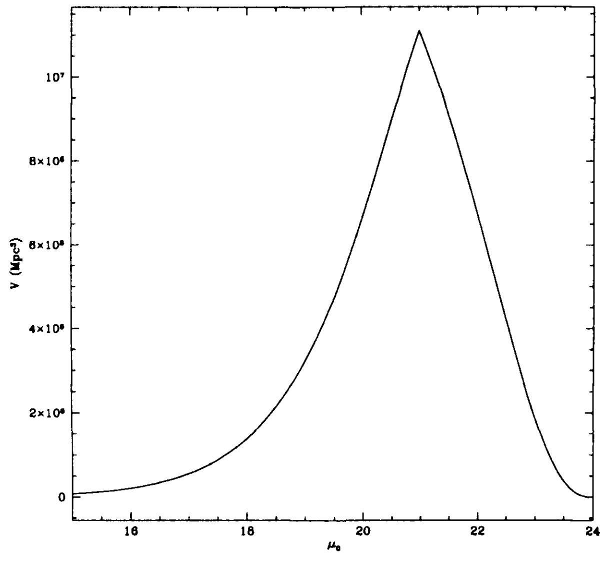

Figure 1.2: Visibility function from Disney & Phillipps (1983) for $\mu_{lim} = 24$ B$_\mu$, $m_l = 15$ B mag and $\theta_l = 20''$.

volume and hence are expected to dominate numerically.

In 1987, Bothun *et al.* reported the discovery of the first giant LSB galaxy, Malin 1. This galaxy would not have been found it were not for its bright central bulge region, which was mistaken for a dwarf in the Virgo cluster. The stacking of three deep Schmidt plates revealed a LSB disc around this central bulge which, if in Virgo, would have a diameter of $\sim$ 10 kpc. Using the 200-inch Palomar telescope to obtain optical spectroscopy showed that this central bulge had an emission-line redshift of $\sim$ 25000 km s^{-1}; indicating that either this was a background emission-line galaxy which appeared to be the core of a foreground LSB spiral due to a coincidental alignment, or the emission lines were truly those from the bulge of a giant LSB spiral.

In order to confirm which one of these hypotheses was correct, Bothun *et al.* carried out HI observations using the 1000-ft Arecibo telescope. Searches at the redshifts of Virgo

(500–3000 km s^{-1}) and Coma (5000–8000 km s^{-1}) revealed nothing, but when the telescope was tuned to the redshift of the optical emission lines (25000 km s^{-1}) HI emission from the disc was detected, revealing Malin 1 as a giant background galaxy.

Malin 1 has a central surface brightness of 26.5 B_μ and an HI content of a few times 10^{10} $M_\odot$. This remains the only known example of a giant low surface-brightness galaxy, the 'Crouching Giants' predicted by Disney (1976) but with such low central surface-brightness for the disc that it would escape detection from almost all optical surveys, were it not for the central bulge region.

1.1.1 Optical Surveys for Low Surface Brightness Galaxies

The number of galaxies for which we have photometry has greatly increased over the last 20 years. A number of surveys have been carried out to find galaxies which do not fit the 'Freeman Law' distribution. The distribution in surface brightness is continuous, but following the standard practice, we define galaxies with $\mu_0 \geq 23$ mag arcsec^{-2} and/or $\mu_{eff} \geq 24$ mag arcsec^{-2} as being low surface brightness, where μ_{eff} is the effective surface brightness, i.e. the surface brightness at the effective radius (50% of the light) and μ_0 is the central surface brightness. In terms of the narrow distribution of surface brightness distribution of Freeman (1970), a disc galaxy this diffuse should be extremely rare. In practice, LSB galaxies include objects as diverse as giant gas rich discs and dwarf spheroidals.

Most of these surveys aimed at finding LSB galaxies have shown that the number density of galaxies per magnitude of surface-brightness remains fairly constant in the field to at least $\mu_B = 23$, and deep CCD surveys have failed to find a cut-off down to $\mu_B = 25$ (see Figure 1.3, from O'Neil & Bothun 2000).

The first LSB galaxies to be discovered were dwarf spheroidals in 1938. The first to speculate on the existence of large number of LSB galaxies was Zwicky in 1957. The earliest surveys to turn up a number of LSB galaxies were the David Dunlap Observatory

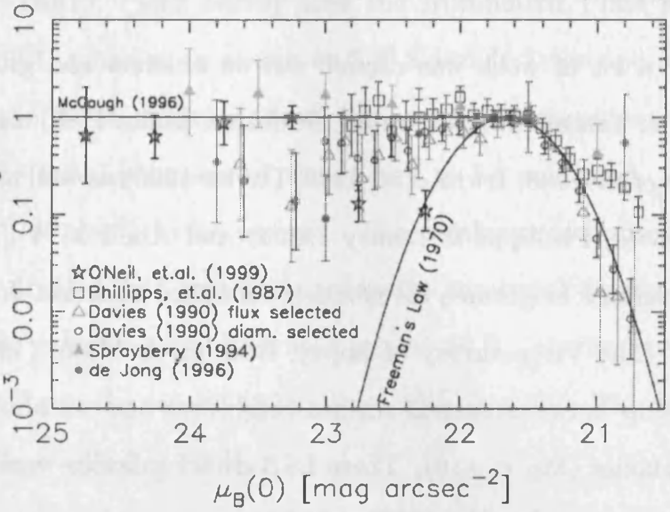

Figure 1.3: Surface Brightness distribution, from O'Neil & Bothun 2000. This SBD looks very similar to that found by McGaugh (1996), with the number per magnitude bin remaining flat down to at least $25B_{\mu}$, where statistics for galaxies run out, and turning down at the high surface-brightness end

catalogue (DDO; van den Bergh 1959) and the Uppsala General Catalogue of Galaxies (UGC; Nilson 1973). The DDO survey was aimed at finding dwarf galaxies and so most of its objects are low-mass local galaxies rather than large LSB galaxies. The UGC survey was not aimed specifically at finding LSB galaxies, but it used a large angular-size cut-off and therefore contained significantly more LSB galaxies than magnitude-limited catalogues such as that of Fisher & Tully (1981).

The first attempt to search specifically for LSB galaxies was made by Longmore *et al.* (1982). This survey attempted to find galaxies with diameters greater than 2 arcminutes on the UKST plates as the sky survey was carried out. HI follow-up observations on these objects were carried out at the Parkes Observatory. The survey concluded that LSB galaxies were systematically of lower indicative mass than 'normal' (Freeman's law) galaxies of the same type, although they have similar HI masses and physical dimensions.

As a result, LSB galaxies have a higher fractional HI mass than 'normal' galaxies.

In the 1980s, a lot of work was carried out on clusters and groups such as Virgo (Bingelli, Sandage & Tammann 1985; Impey, Bothun & Malin 1988) and Fornax (Phillipps *et al.* 1987; Davies *et al.* 1988; Irwin *et al.* 1990; Davies 1990) as well as important surveys of Abell 1367 (Davies, Phillipps & Disney 1989a) and Abell 3574 (Turner *et al.* 1993) showing that the surface brightness distribution remained constant down to the limits of survey sensitivity. The Virgo survey of Impey, Bothun, & Malin (1988) found that the observed relationship between central surface brightness and absolute magnitude broke down for dwarf galaxies ($M_B < -16$). These LSB dwarf galaxies were generally gas poor dwarf elliptical galaxies, rather than LSB spirals.

Davies *et al.* **(1994)** searched through deep CCD data using an algorithm optimised to find large low surface-brightness galaxies. This algorithm preferentially selects galaxies with scale-sizes of around 50 kpc and central surface-brightnesses about 4 magnitudes below the sky (around 25.7 $V\mu$). The survey found 19 extended LSB objects, and the authors conclude that LSB galaxies in the range $-22 < M_v < -19$ are at least an order of magnitude less common than their 'normal' surface brightness counterparts.

de Jong & van der Kruit (1994), de Jong (1996a,b,c) surveyed a statistically complete sample selected from the UGC and followed-up in B, V, R, I, H & K bands. The 86 galaxies selected have a minimum diameter of $2'$ and an axis ratio of $b/a > 0.625$. A two-dimensional decomposition technique was used to separate the components of the galaxy into a bulge, disc, and (where necessary) a bar. De Jong found that the SBD fell away slowly towards surface-brightnesses lower than the Freeman-law value, and that there was a cut-off at the high surface brightness end. This is similar to the result found by Davies (1990) for the Fornax cluster. He also found a correlation between surface brightness and Hubble type, with later types being of lower surface brightness.

Low Surface Brightness Galaxies in the Local Universe (Impey *et al.* **1996,**

Sprayberry *et al.* 1997). This survey uses the Automated Plate Measuring (APM; Kibblewhite *et al.* 1984) machine to search on UK Schmidt Telescope (UKST) B_J survey plates. The use of the APM machine allows the selection parameters to be well defined and therefore for the incompleteness of the survey to be measured, and it also allows a wide area of sky (786 deg^2) to be covered. The catalogue is limited to galaxies with $\mu_0 \gtrsim 22$ B_μ and is divided into two parts using the isophotal diameter at the limiting isophote to which the galaxies could be traced (about 26 B_μ, the first part containing 513 galaxies with $D \gtrsim 30''$ and the second 180 galaxies with $D \lesssim 30''$. The detection threshold is set at the 2σ level, $\mu = 24.5 \pm 0.5$ B_μ.

Wide Field CCD Survey for Low Surface Brightness Galaxies (O'Neil, Bothun & Cornell 1997; O'Neil *et al.* 1997). These papers present a multi-colour (U,B,V,R,I) CCD survey down to a limiting detection isophote of 26 B_μ aimed towards the Cancer and Pegasus clusters and towards known galaxies outside of clusters. The survey covers 27 square degrees, half of which is in the two clusters.

The survey was further analysed by O'Neil, Bothun & Schombert (2000) who used the refurbished Arecibo telescope to make HI observations of 43 of the LSB galaxies found, and by O'Neil & Bothun (2000) who re-examined the SBD of the galaxies. O'Neil, Bothun & Schombert find that there appears to be a lack of large, luminous, low surface brightness galaxies (e.g. Malin-1 type galaxies) in the sample. This could be an environmental effect, as the survey did not probe very low-density environments, or it could indicate that the space-density of such objects is low. They also find that their sample does *not* fit well to the Tully-Fisher (TF) relationship.

1.2 The Tully-Fisher relationship

Tully & Fisher (1977) found a relationship between the HI profile width (which is distance independent) and absolute magnitude – thus giving a velocity-independent measure of distance. Zwaan *et al.* (1995) investigated this relationship for LSB galaxies from the UGC (Nilson 1973) and from the catalogue of Schombert *et al.* (1992), and found that these LSB galaxies also fell on the Tully-Fisher (TF) relationship. However, other surveys have seen deviations from this relationship – Matthews, van Driel & Gallagher (1998) found that most of their sample of extreme late-type spiral galaxies fall below the normal TF relation and that the deviation increases with decreasing luminosity and size, implying that these lowest luminosity spirals may be a distinct class of objects that follows a different relationship from 'ordinary' spirals. These deviations from the TF relationship could not be resolved by adding in the HI content of the galaxies, implying that they are not due simply to the galaxies having evolved more slowly and preserved a larger reservoir of neutral gas than 'ordinary' spirals. The TF relation is a key relationship for studies of galaxy formation and evolutionary processes but its physical basis, however, is ill understood. The TF relation relates the luminous mass and rotational velocity of galaxies, in combination with a 'well-behaved' relation between luminous and dark matter. This implies that the TF relation is a combination of two independent relations: (i) a relation between luminosity and (luminous) mass, based mainly on the star formation history of galaxies, and (ii) a relation between mass and rotation velocity, which is the outcome of the process of galaxy formation. In Section 4.4 we use the ES sample results to study the different TF relationships for an HI selected sample.

1.3 The Bivariate Brightness Distribution (BBD)

The luminosity function (LF), usually parameterised as a Schechter function (Schechter, 1976), is often used to describe a population of galaxies. As surface brightness selection effects are not taken into account by this description, there is an implicit assumption that these can be ignored (McGaugh, 1994; Ferguson & McGaugh, 1995). However, optically selected samples are known to suffer from serious selection effects that act against low surface brightness objects, as was highlighted in the previous section. This means that luminosity functions derived from these optical samples really only describe the way the Universe is populated by relatively high surface brightness galaxies (HSBG's) which are near the peak of the 'visibility function' (Disney & Phillipps, 1983; McGaugh, Bothun & Schombert, 1995). These galaxies can be seen to much further distances than LSBG's and are therefore preferentially selected in optical surveys.

The Bivariate Brightness Distribution (BBD) determines the luminosity function as a function of surface brightness (Boyce *et al.* 1995). It describes the population of galaxies more fully than using the luminosity function alone and determines if there is a correlation between luminosity and surface brightness. If such a correlation does exist then the number of Schechter (1976) L^* galaxies has probably been determined quite accurately, as the numbers of giant low surface brightness galaxies (LSBG's) will be insignificant. However this would also suggest that a significant number of dwarf galaxies will have been missed due to SB selection effects, thus adding even greater uncertainty to the poorly determined faint end of the luminosity function. If the correlation is weak or non-existent, then the population of giant LSBG's will be significant and SB selection effects must be taken into account across the whole range of the luminosity function to make an accurate determination. In this Thesis we find the BBD for an HI selected sample (ES).

1.4 HI as a tracer of local galaxy population

The HI line is used as a kinematic tracer of the galactic potential of spiral galaxies. The 21cm line has been used to map the HI distribution and velocity field of many galaxies, leading to the recognition of dark matter and measurements of its distribution (Bosma 1978, van Albada 1985). Besides showing that galaxies have dark matter, the 21cm line can be used as a useful tracer of the local galaxy population and to determine the completeness of optically selected galaxy catalogues. Optical selection effects introduce biases in these catalogues as discussed in previous sections.

The distribution of neutral hydrogen is a key ingredient in theories of galaxy formation and evolution. Galaxies are formed when clouds of hydrogen collapse under gravity. Galaxies that contain large reservoirs of hydrogen are likely to continue star formation, while those with little hydrogen will have an ageing star population.

The cosmological neutral gas density of the universe is one of the fundamental observational parameters that must affect the formation and evolution of stars in galaxies and maps the processes that convert gas into stars. To interpret these effects it is crucial to obtain a reliable value for the present epoch. The space density of HI at the present epoch ($z = 0$) can be measured using pointed or blind HI surveys. However, HI surveys based on optical catalogues risk being biased towards galaxies with high optical brightnesses, unless the HI mass distribution follows the optical brightness distribution. Optical surveys also preclude the possibility of detecting galaxies with little or no stellar emission. The complete census of HI and its distribution among and within galaxies at present defines the relation between star formation and the raw material from which stars are made and is the logical indicator for the cosmological mass density of HI. The difficulty of blind surveys for HI is obtaining good optical data for the counterpart HI detections. In this Thesis we try to overcome this problem by obtaining high quality optical data from the Sloan Digital Sky Survey.

1.4.1 The HI mass function (HIMF)

The HI mass function (HIMF) describes the number density of neutral hydrogen clouds as a function of HI mass at the present epoch and is the HI equivalent of the optical luminosity function.

The HIMF can be constructed from a sample of sources derived from a blind HI survey. A reliable measurement of the HIMF yields a wealth of information:

- The HIMF gives an alternative view of the local galaxy population based on gas-richness rather than optical brightness.
- Integration of the HIMF yields a measurement of the mass density of neutral hydrogen, Ω_{HI}.
- The HIMF indicates which types of galaxies currently form the main reservoirs of fuel for star formation.

A fair calculation of the HIMF for HI selected galaxies requires a blind HI survey of the field, with no preference to known over or underdensities, hence the larger the area covered by the survey the better.

The faint tail of the HIMF is determined by the shape of the distribution function and its value can contribute to explaining which galaxy formation model is more likely to be correct. The hierarchical clustering scenario is presently the most widely accepted model for galaxy formation (e.g. Kaufmann 1996). In this Thesis we find the HIMF for an blind HI selected sample of over 1000 galaxies.

1.5 Extragalactic HI Surveys and Selection Effects

There have been a number of blind HI surveys since the 1970s. The first was Mathewson, Cleary, & Murray (1974), who used the Parkes 18-m dish to survey an area around the Magellanic Clouds and discovered the gas bridge of the Magellanic Stream which links the clouds to our galaxy. The first attempt to use HI to find LSBG's was carried out by Shostak (1977), who looked originally in the off-beams of pointed observations of known galaxies and followed this with two blind drift-scan surveys and a pointed absorption survey toward bright quasars.

However, one shortcoming of many HI surveys is their inability to detect low column-

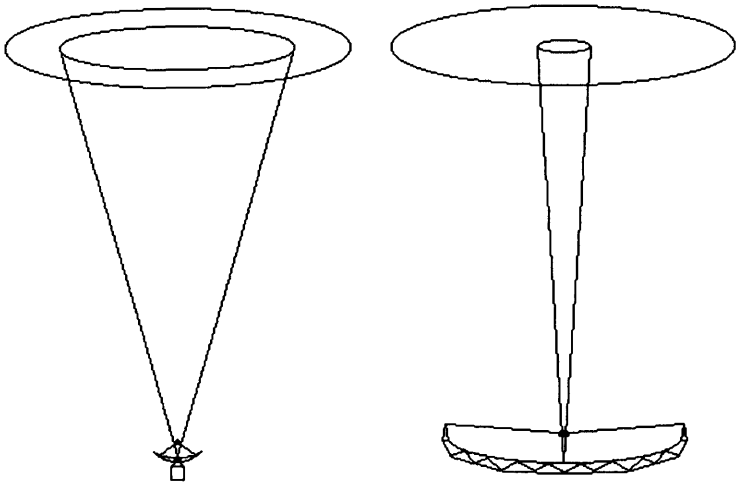

Figure 1.4: A smaller telescope (left) is less sensitive by a factor of D^2, however it has a wider beam so, in the column-density limited regime, picks up D^2 more HI than a large telescope (right).

density objects. All surveys have a column-density limit: they can only detect galaxies which have more than a certain number of atoms per square centimetre along a column through a source of a given velocity width. Below this limit, the mass in the beam falls below the detection limit, even if the total mass of the object is greater. Disney & Banks (1997) showed that the column density limit was dependent only on the integration time of the survey, the system temperature of the detector, and the velocity width of the source such that:

$$N_{\mathrm{HI}}\ (\mathrm{atoms\,cm^{-2}}) = 10^{18}\ T_s \sqrt{\frac{\Delta V(\mathrm{km\ s^{-1}})}{t_{int}(\mathrm{s})}} \tag{1.1}$$

The reason for the lack of correlation between the telescope size and the column density limit is that larger telescopes have proportionally tighter beams, so the area of the beam is proportional to D^2. This then cancels out the increase in sensitivity, which is proportional to the size of the collecting area and therefore also proportional to D^2 (see Figure 1.4).

Low Surface Brightness (LSB) galaxies are here defined as having a central surface brightness fainter than 23 B mag arcsec^{-2} (Impey & Bothun 1997) and/or $\mu_{eff} \geq 24$ mag arcsec^{-2}. They display the same range in size as seen for high surface brightness galaxies (McGaugh 1994; de Blok *et al.* 1995). LSB galaxies cover the same range of HI masses as 'normal' galaxies (Schombert *et al.* 1992) so we would naively expect them to be detected equally in an HI survey. However, LSB galaxies appear to have lower column densities than normal galaxies (de Blok, McGaugh & van der Hulst 1996) hence they are more likely to fall beneath the limiting column-density.

In 1997 Disney & Banks derived a simple scaling relationship between the average surface-brightness and the average column density over the HI disc. For any given region the HI surface density and the optical surface brightness are related by:

$$\Sigma_{\rm HI}\ (M_\odot\ pc^{-2}) = \left(\frac{M_{\rm HI}}{L_B}\right) \times \Sigma_{\rm B}\ (L_\odot\ pc^{-2}) \tag{1.2}$$

where $\Sigma_{\rm HI}$ is the HI surface density and $\Sigma_{\rm B}$ is the B-band optical surface brightness, averaged over the region and $M_{\rm HI}$ and L_B are the HI mass and the B-band luminosity within the same region. As 1 $M_\odot\ pc^{-2}$ is approximately equal to an HI column density of $10^{20.1}$ atoms pc^{-2} and 1 $L_\odot\ pc^{-2}$ is approximately equal to a surface-brightness of 27.05 B mags arcsec^{-2}, this gives the scaling relationship found by Disney & Banks (1997):

$$N_{\rm HI} \simeq 10^{20.1}\ atoms\ cm^{-2} \left(\frac{M_{\rm HI}}{L_B}\right) 10^{(0.4(27-\mu_{mean}))} \tag{1.3}$$

which is known as the Disney-Banks scaling. $N_{\rm HI}$ is the HI column density in units of atoms cm^{-2} and μ_{mean} is the average optical surface brightness in units of mags arcsec^{-2} taken over the same area as the $N_{\rm HI}$. This can be re-written as:

$$\mu_{mean} \simeq 2.5\left(30.9 + log\left(\frac{M_{\rm HI}}{L_B}\right) - log(N_{\rm HI})\right) \tag{1.4}$$

In addition to a column density limit, there is another effect that could affect the detectability of LSB galaxies compared to their 'normal' counterparts. De Blok, McGaugh & van der Hulst (1996) found that LSB galaxies have slowly rising rotation curves, as opposed to the flat rotation curves observed in 'normal' galaxies. This means that visual inspection of HI data cubes may miss LSB galaxies near the limit of detection while including HSB galaxies of the same HI flux. This should be seen in the results as a trend towards higher surface-brightness at lower integrated fluxes and at the lower ratios of peak flux to integrated flux. However, the use of an automated finder (see Chapter 2), which selects sources by integrated-flux rather than by peak-flux, lessens this effect without detracting from the advantages of visual inspection.

Another HI selection effect is that wider velocity width (ΔV) galaxies have a lower signal to noise ratio than narrower galaxies for a given HI mass. However, it is known that LSB galaxies appear to fall on the same Tully-Fisher relation as HSB galaxies (Zwaan *et al.* 1995), so the proportionality of L to ΔV would not depend on surface brightness. The implication of this is that discrimination against higher line-width galaxies will be independent of surface brightness and hence it should not affect the Surface Brightness Distribution of galaxies found in HI surveys.

1.5.1 Ionisation effects

Of course, for a galaxy to be detected by their HI content, it must contain neutral hydrogen. However, it has been proposed (Corbelli & Salpeter 1993) following very deep observations of a cut-off at $\sim 2 \times 10^{19}$ atoms cm^{-2} in the outskirts of Messier 33 and NGC 3198 (Corbelli, Schneider, & Salpeter, 1989; Maloney 1993) that neutral hydrogen will be ionised below a critical column density, very close to the Kennicutt (1989) critical density for star-formation.

However, clumping of HI may well mean that galaxies with an average surface-density below the threshold will still contain neutral hydrogen, and the small number of very deep observations means that the ionisation limit cannot yet be well determined. The closeness of the ionisation limit to the Kennicutt critical density implies that all galaxies detected in HI will contain stars and, with the exception of gas clouds associated with galaxies, a single relatively nearby, object from HIPASS (Kilborn *et al.* 2001), and the recent discovery of potentially the first 'dark galaxy' in Virgo by Minchin *et al.* (2005), this appears to be the case.

LSB galaxies obviously contain stars and are believed to have ongoing star formation, albeit at a lower rate than in 'normal' galaxies (van Zee 1995). This implies that LSB galaxies do contain neutral hydrogen, but as LSB galaxies are generally more spatially extended than 'normal' galaxies this HI is spread over a larger area, and the *average* column density seen within the beam of a single-dish telescope may therefore be well below the ionisation limit. It is also quite possible that the ionisation limit will not be the same for all galaxies, as the intergalactic UV field may well vary; for example, surveys of HVCs show that they have a cut off at $\sim 5 \times 10^{18}$ atoms cm^{-2} (Colgan, Salpeter & Terzian 1990).

1.5.2 Previous HI Surveys

In this section I will give a summary of the HI surveys leading up to HIPASS. It includes and concentrates on those which are important in the search for LSB galaxies.

Shostak (1977) uses data from 4 surveys – two drift scans (Shostak 1973, unpublished, and Shostak & Davies 1974, unpublished), a survey of the off-beams of pointed observations of known galaxies (Shostak & Roberts 1973–1974, unpublished), and an absorption survey pointed at 50 strong QSOs (Shostak & Condon 1974, unpublished).

Shostak (1977) calculates that in these surveys the average detected flux of a galaxy will be 42% of the total flux of that galaxy, the noise figures for the drift scans have been adjusted accordingly. The deeper of the two drift-scans reaches an equivalent central surface-brightness of $\mu_B = 22.7$ Bμ and is band-pass limited for $M^{\star}_{\rm HI}$ ($M^{\star}_{\rm HI}$ is the characteristic HI mass) galaxies at $14h^{-1}$ Mpc. The shallower drift-scan reaches an equivalent central surface-brightness of $\mu_B = 22.3$ Bμ over a much larger volume of detection for $M^{\star}_{\rm HI}$ galaxies.

One previously uncatalogued source was detected in these surveys, with a velocity of -353 km s^{-1} . This cannot be unambiguously defined as extra-galactic. The source is less than 5° from the galactic plane and is at a galactic velocity of -163 km s^{-1} and so may well be a high velocity cloud. The column-density limit of the drift-scans is too high to expect LSB galaxies to be found, while the pointed observations do not cover sufficient volume to unearth a hidden population – for a galaxy density for $M^{\star}_{\rm HI}$ of 1.4 ± 0.5 $100h^{-3}$ Mpc^{-3}, as found by Zwaan *et al.* (1997), the volume would have to be over 8 times larger before even a single galaxy detection was expected.

AHISS (Sorar 1994; Zwaan *et al.* 1997; Zwaan 2000) was the deepest survey prior to the multibeam surveys. It made use of the wide side-lobes of the Arecibo telescope, giving a strip 15 arcminutes wide, covering a total area of 65 deg^2, but with a variation of a factor of ten in sensitivity from the beam centre to the edges of the side-lobes. In this region (which crosses the Zone of Avoidance (ZOA) twice) 66 galaxies were found, of which 36 were previously uncatalogued. Zwaan *et al.* (1997) give the distance from the centre of the beam for each source in their Table 1 (from VLA follow-up), and this can be used to determine which galaxies fall within the FWHM of the main beam (radius 100″). Inside the FWHM there are 29 detections, of which 23 were previously uncatalogued. Excluding those galaxies identified by Zwaan *et al.* as being within the ZOA, this leaves 26 detections, of which 20 are uncatalogued, within the FWHM area.

In the AHISS sample, 5 of the 33 previously uncatalogued galaxies have no optical counterpart on the photographic sky-survey plates. However, all of the galaxies can be seen on CCD images made at the 2.5-m Isaac Newton Telescope on La Palma, and none of the galaxies has a central surface-brightness fainter than 24 B_μ – the limit predicted by the Disney–Banks scaling. Zwaan *et al.* also found that there were no galaxies in the AHISS sample with $N_{\rm HI} < 10^{19.7}$ cm^{-2}. This column-density limit is important as it is close to both the limit for star-formation found by Kennicutt (1989) and the limit for ionisation by the inter-galactic UV field found by Maloney (1993) and Corbelli & Salpeter (1993).

The **Arecibo Slice** survey (Schneider, Spitzak & Rosenberg 1998; Spitzak & Schneider 1998) is sensitive to low-mass objects over a wider area than AHISS. Despite this, the survey is not particularly sensitive to low column-density objects due to the small size of the Arecibo beam. The survey covers approximately 55 square degrees. Out of the 75 detections, 35 are in 'major' magnitude-limited catalogues. The major result from the Arecibo Slice is the HIMF, which indicates a turn-up in the lowest mass bin due to two galaxies found in that bin. This up-turn could indicate that there is a large population of gas-rich LSB galaxies which are missed by optical surveys.

The **Henning (1995) survey** (also Henning 1992, Henning & Kerr 1989, and Kerr & Henning 1987) is sensitive to $M^\star_{\rm HI}$ galaxies over a larger volume than the other surveys. However, 60% of this volume is within the ZOA and the region outside the ZOA was observed mainly during the daytime and so is of lower sensitivity than the other observations. The sensitivity also varies with declination, as points were observed for 4 minutes sec δ – the longest possible observation for something moving through the 1° east-west across the sky that was accessible to the NRAO 300 ft.

The HIMF from Henning (1995) rules out the existence of a large population of low-mass, LSB dwarf galaxies, but is inconsistent with the results of HIMFs from optically-selected samples (e.g. Briggs & Rao 1993; Solanes, Giovanelli, & Haynes 1996) which do detect low HI mass objects. This indicates that these objects should be found in a blind HI survey, as indeed they are in the Arecibo Slice and the AHISS. Banks (1998) suggests that this inconsistency could be due to the survey sensitivity being poorly understood and that the true detection limit was too high for the low-mass dwarfs to be detected.

The **ADBS (Rosenberg & Schneider 2000)** covers a large area compared to previous blind surveys; this, combined with the sensitivity of the Arecibo Telescope makes it very useful for discovering low-mass objects – 7 galaxies are found with $M_{\rm HI} < 10^8 M_\odot$. Of the 81 previously uncatalogued sources 11 are heavily obscured by the Galaxy ($A_v > 2$ mags). There remain 11 objects without obvious counterparts on the plates (generally POSS-II, although a few are POSS-I), although the authors identify 3 of these as being in regions of high stellar density and a further 3 as being near bright stars (2 of these with possible nebulosity behind the star). Of the remaining 5 sources, 1 is possibly associated with a nearby bright galaxy and the other 4 have multiple faint sources.

1.5.3 Multibeam HI surveys

The development of multibeam technology in the mid 1990s has been a big advance over single beam HI astronomy as multibeam surveys allow much larger areas to be covered much more quickly than was previously possible in single beam (on-off) observations and so can cover large areas of sky to a low limit. Table 1.1 gives the parameters for a long integration-time survey carried out at Parkes (HIDEEP, Minchin 2001), and the northern sky survey at Jodrell Bank Observatory (HIJASS, Lang 2003).

The sensitivity of these surveys to low-mass objects at a given distance might not be as good as some of the deeper surveys that have been carried out previously, but the much greater volume they cover compensates for this in terms of number of galaxies found.

The **HIDEEP Survey (Minchin *et al.* 2003)**. The HIDEEP survey covers 32 square

Table 1.1: Previous blind HI surveys

	Shostak (1977)	Henning (1995)	AHISS	Arecibo Slice	ADBS	HIJASS	HIDEEP
Telescope	Green Bank	Green Bank	Arecibo	Arecibo	Arecibo	Jodrell Bank	Parkes
	91m	91m	305m	305m	305m	76m	64-m
δv (km s^{-1})	11	22	16	16	34	18	18
Velocity (km s^{-1})	-800 to 2835	-400 to 7500	<7400	100 to 8340	<7980	-3500 to 10000	-1000 to 12700
Rms (mJy beam^{-1})	32	-	0.75	1.7	3.5	16	4
Area (deg^2)	85	7204 (pointings)	65	55	430	1115	32
Beam size (arcmin)	10.8	10.8	3.3	3.3	3.3	12	15.5
N_{HI} limit (cm^{-2})	1.6×10^{19}	-	4.3×10^{18}	9.6×10^{18}	2.8×10^{19}	7.3×10^{18}	2.2×10^{18}
Sources	1	37	66	75	265	222	173

degrees in a $4^\circ \times 8^\circ$ region centred on ($13^h40^m00^s$, -30°00′00″), near M83 in the Centaurus A group. It is much smaller survey than HIPASS and is of much longer integration time which enables it to detect low column densities and surface brightness of around 26.5 B_μ. The HIDEEP survey has an integration time 12.5 times that of HIPASS, allowing it to reach the equivalent of almost 1.4 optical magnitudes fainter and thus explore the regime between 10^{18} and 10^{19} HI atoms cm^{-2}.

The **HIPASS** survey reaches a lower column density than any previous survey (with the exception of HIDEEP); it is only marginally deeper than previous surveys but it covers the whole southern sky. The HIPASS survey is analysed in depth in the next chapter.

HIJASS - a blind HI survey of the northern sky. The HI Jodrell All-Sky Survey (HIJASS) (Lang *et al.* 2003) is the northern hemisphere analogue of HIPASS. When completed, it will provide a 21cm map of the sky at a declination $\delta > 22^\circ$. This survey is being carried out with the Lovell Telescope at the Jodrell Bank Observatory. The Lovell telescope has a multibeam receiver with 4 elements (compared to the 13 at the Parkes telescope or the 7 at Arecibo).

The technical characteristics of both surveys are very similar: a 64-MHz bandpass with 1024 channels is used to achieve a velocity resolution of 18 km s^{-1} and a spatial positional accuracy of $\sim 2.5'$. Local interference corrupts the range of useful frequencies to investigate hence restricting the velocity range to -1000 km s^{-1} to 4500 km s^{-1} and 7500 km s^{-1} to 10000 km s^{-1}.

The survey has so far covered $\sim$ 2000 deg^2, of which 1115 deg^2, including the whole strip with $70^\circ < \delta < 78^\circ$ and part of another strip at $62^\circ < \delta < 70^\circ$, has been published (Lang *et al.* 2003). Among the 222 published detections, 170 correspond to previously catalogued galaxies, 23 are associated with an optical counterpart for which we have no redshift information available, and 29 objects were previously uncatalogued.

1.6 Map of the Thesis

Chapter 2 discusses the Equatorial Strip (ES) HI sample selection and the HI properties of the galaxies found in the sample. It describes the observation techniques used and how the HI data was reduced and parameterised. Using the ES sample I produce the HI Mass function, the HI Tully-Fisher relation, and calculate the HI content of the local Universe.

Chapter 3 presents and discusses the optical properties of the ES HI sample and how the optical data for the ES sample was obtained from the Sloan Digital Sky Survey (SDSS). It describes how a control sample of optically selected galaxies chosen from the ESO-LV catalogue was compiled to be used as a comparison sample to the whole ES HI sample. I present and analyse the most interesting correlations in the optical data and I discuss the properties of the LSB galaxies in the ES sample.

Chapter 4 presents the analysis and discussion of the ES sample results. I present the HI mass to light ratio correlations, the Luminosity Function, the Bivariate Brightness Distribution and discuss the implications of these results. I present the optical and baryonic-mass Tully-Fisher relationships and I investigate the cosmological importance of gas-rich LSB galaxies.

Chapter 5 I present the main conclusions and results of this Thesis and discuss future avenues for this work.

Chapter 2

The HI Data

2.1 Overview

The Equatorial Strip (hereafter ES) sample comprises 1077 galaxies selected purely by their HI signature. This is a unique sample which covers a large area of sky, is free from optical selection effects and which has complete, very high quality, optical data (SDSS) for a subsample of 201 galaxies. The combination of the HI data with the optical data allows us to make a comprehensive analysis and study of the properties of HI selected extragalactic sources and investigate vital global correlations which will help to improve our understanding of gas-rich galaxies. The ES sample is a subset sample of galaxies selected from the HIPASS survey of the southern sky and its northern extension ($+2° < \delta < +25°$). This ES strip runs along the celestial equator from $-6° < \delta < +10°$ and through the full range of R.A.s from 0 to 24 hours. The ES sample represents $\sim$ 14% of the whole sky. The solid angle covered by this region is 1.747 steradians (5738 deg^2), and the total volume covered over the full velocity range is $\sim 2.76 \times 10^6$ Mpc^{-3}.

There are a number of important reasons for choosing this specific region of sky for our analysis. This strip is perpendicular to the plane of the Milky Way, hence largely avoiding it and minimising the areas of sky with high optical extinction. Furthermore, it is accessible from both hemispheres, allowing follow-up observations to be conducted from most of the major observatories in the world, and in particular the Sloan Digital Sky Survey (SDSS), which overlaps $\sim$ 50% in area with the ES sample, from which we obtain our optical data (see Chapter 3).

The candidate galaxy list was generated using the techniques described in Section 2.4 and by extensively searching the data cubes visually 'by eye'. Each of the galaxy candidates was then checked against the NASA/IPAC Extragalactic Database[1] (NED) for optical counterparts and the Sloan Digital Sky Survey[2] (SDSS) Data Release 2 (hereafter DR2) from which we obtained the optical data. The process and difficulties of compiling the optical sample are explored in Chapter 3.

This Chapter presents the radio HI data for the ES sample. The observations and data reduction processes are described in Section 2.2 as well as an overview of the HIPASS survey. Section 2.3 describes how the ES sample was selected and how the list was generated and parameterised. In Section 2.4 I explain what corrections are needed and what assumptions are made in order to derive the parameters obtained. Section 2.5 presents the main characteristics of the ES sample together with the catalogue itself. In Section 2.6 I present the selection limits and the completeness of the ES sample. Section 2.7 presents the HI Tully-Fisher relationship. In Section 2.8 I construct an HIMF for the ES sample and discuss its implications. Section 2.9 explores the HI content of the local universe.

[1] This research has made use of the NASA/IPAC Extragalactic Database (NED) which is operated by the Jet Propulsion Laboratory, California Institute of Technology, under contract with the National Aeronautics and Space Administration.

[2] Funding for the creation and distribution of the SDSS Archive has been provided by the Alfred P. Sloan Foundation, the Participating Institutions, the National Aeronautics and Space Administration, the National Science Foundation, the U.S. Department of Energy, the Japanese Monbukagakusho, and the Max Planck Society. The SDSS Web site is http://www.sdss.org/.

2.2 The HIPASS Survey: HI Observations and Reduction

The HI Parkes All Sky Survey (HIPASS) is the largest HI survey to date and the first blind HI survey to cover the whole of the southern sky. The survey, which started in 1997 and finished in 2002, was conducted with the 13-beam Multibeam receiver at the 64-m Parkes Radio Telescope in Australia.

2.2.1 The Multibeam System

The Parkes HI Multibeam system (Staveley-Smith *et al.* 1996) is a 13-beam system arranged to give a uniform coverage of the sky when it is scanned at an angle of 15° (see Figure 2.1 from Banks 1998). Multiple scans are carried out with slight offsets between them in order to ensure uniform sensitivity. There are two polarisations per beam, requiring 26 receivers and resulting in a total of 26 input channels.

The standard observing technique is to actively scan the sky in 8° strips at a rate of 1° min^{-1}, with scans separated by 7 arcmin in R.A., and the effective integration time at each point on the sky is 450 seconds.

To obtain spectra the multibeam correlator uses a bandpass 64-MHz wide and 1024 channels, giving a velocity range of -1280 to 12700 km s^{-1} and a channel separation of 13.2 km s^{-1}. A summary of the parameters for the survey is given in Table 2.1.

2.2.2 Data Reduction

In this section I present a brief summary of how I reduced the HI data, an in-depth description can be found in Barnes *et al.* 2001

I reduced the data using the standard multibeam reduction techniques (Barnes *et al.* 2001). The initial processing of HIPASS data was conducted 'real time' at the Parkes

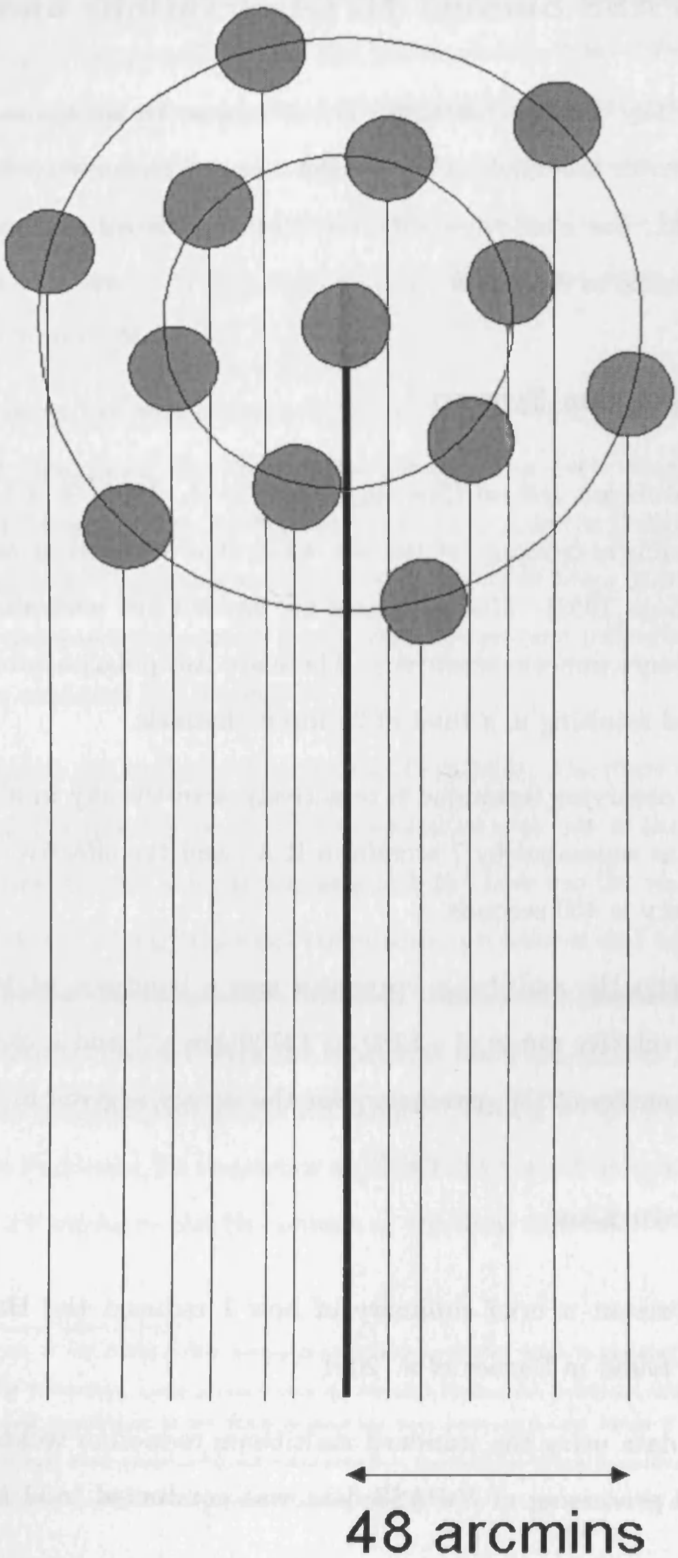

Figure 2.1: Beam scan pattern used in HIPASS .

Parameter	HIPASS value
Sky Coverage	$\delta < +25°$
Integration time per beam	450 s
Average FWHM	14.3 arcmin
Gridded FWHM	15.5 arcmin
Pixel size	4 arcmin
Velocity range	-1280 to 12700 km s^{-1}
Channel Separation	13.2 km s^{-1}
Rms noise	13 mJy beam^{-1}
3σ HI Mass Limit[a]	$10^6 D^2_{Mpc}\ M_\odot$
N_{HI} limit	7.8×10^{18} cm^{-2}

[a] For $\Delta V = 100$ km s^{-1}

Table 2.1: Main HIPASS parameters

Telescope. To correct the spectra of the standard bandpass effects they were reduced using the package LIVEDATA. This package was also used to perform the conversion to heliocentric rest-frame velocities.

The bandpass correction was performed by dividing the signal target spectrum by a reference off-source spectrum. This reference off-source spectrum represents the underlying spectral shape caused by signal filtering, as well as the temperature of the receivers, ground and sky. A reference spectrum is taken for each receiver by taking signals immediately before and after every integration as the telescope scans across the sky.

The median value for each reference channel in the reference spectrum is used to provide a robust measure of the bandpass. This can, however, create an artifact in bright HI sources by generating negative side lobes north and south of the source, as actual HI emission is included in the bandpass determination. Finally, the spectra are smoothed with a Tukey filter to suppress Gibbs ringing, resulting in a velocity resolution of 18 km s^{-1}.

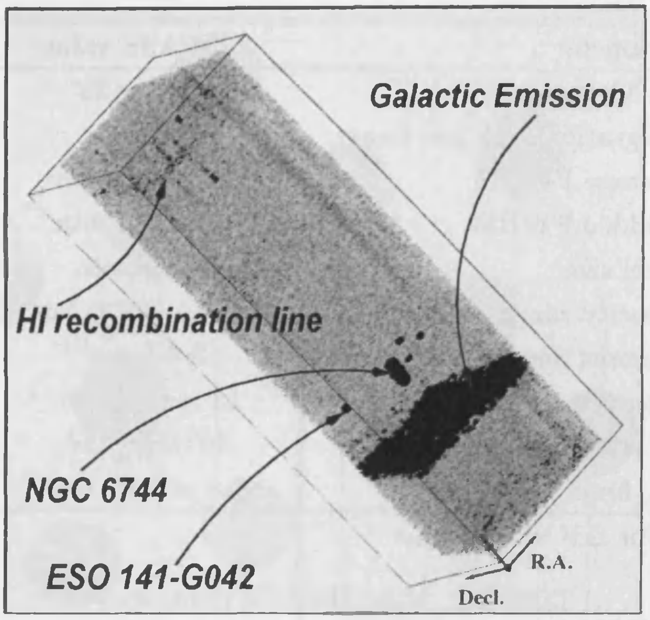

Figure 2.2: Example HIPASS cube (H041). The velocity range shown is from −1200-5000 km s^{-1}. The HI emission from our own galaxy can be seen, together with extragalactic objects and recombination lines.

The data is then processed onto three-dimensional position-position-velocity cubes (see Figure 2.2) that form the main data product of HIPASS. The bandpass-corrected spectra are gridded together using the package GRIDZILLA. The spectrum at each R.A.–Dec. pixel is taken as the median of all data within 6 arcmin of the pixel centre, multiplied by 1.28 to correctly scale point-sources flux densities. For extended sources this procedure corrupts the data, with peak flux densities for such sources being overestimated (by 1.28 for an infinitely extended source), but extended sources account for less than 2% of the overall sources and the corresponding corrections are small.

The resulting cubes from the gridding process are 8°× 8° with 4 × 4 arcmin^2 pixels in the on-sky direction and extend over the full HIPASS velocity range in the third axis (see Figure 2.2). The overlap between cubes vary, but in general is ~ 1° in R.A. and Dec. There are a total of 388 cubes that cover the southern sky plus a further 150 cubes which cover the Northern Extension ($+2° < \delta < +25°$). Apart from the declination coverage, the main difference between the two surveys is the higher level noise in northern extension, due to the northern sky being low in the horizon as seen from the Parkes telescope.

After the data has been gridded, it is further processed to remove ripple due to on-beam continuum sources. These sources set up a characteristic ripple with a frequency of 5.7 MHz ($\sim$ 1200 km s^{-1}) on the spectra due to standing waves with a wavelength of 52m set up between the prime-focus cabin and the dish surface and also give a rise in flux towards the low-frequency end of these spectra. The amplitude of the ripples and of the rise is proportional to the strength of the sources, and the phase of the ripple is constant for on-beam sources, it is therefore possible to remove these ripples using a scaled-template. An algorithm to do this, LUTHER, has been developed at the Parkes Observatory by Ian Stewart and Alan Wright and is described in Barnes *et al.* 2001.

2.3 The Equatorial Strip Sample

2.3.1 Defining the Sample and Galaxy Selection Criteria

The ES HI sample was selected from 102 data cubes (H338-H440) using a combination of automatic and interactive processes, with candidate detections first generated through an automated finder script and then manually verified. The data cubes were also searched 'by eye' using the visualisation program KVIEW (Gooch, 1995) to display a cube in two dimensions and allowing you to step through the third dimension.

To generate a consistent list of HI detections, it was necessary to impose selection criteria when cataloguing the galaxies. The selection criteria for the visually searched sample were:

- The detection must be at least 3σ above the noise in peak flux ($\sim$ 40 mJy).

- The detection must have a spatial extent either equal or greater to the beam size in order to exclude interference.
- The detection must be present in at least in two velocity planes.

Negative velocity regions were searched although they yielded no detections; however, the Galactic region from -300 km s^{-1} $< V <$ 300 km s^{-1} was not searched for galaxies to minimise confusion with Galactic sources. High Velocity Clouds (HVCs) which can be easily detected in that velocity region have been catalogued separately by Putmam *et al.* (2002).

2.3.2 Candidate generation

The ES sample was generated using an updated version of the TOPHAT finder algorithm (see Meyer *et al.* 2004 for details of the original TOPHAT) together with the visual search. The TOPHAT works by searching each spectrum in the cubes for emission on a variety of velocity width scales between 1 and 40 channels. An initial list of detections is created as follows. First, solar and continuum ripple in the spectral baselines is reduced by using a moving median filter with a width dependent on the current search scale. Spectra are then cross-correlated with a top hat filter of the appropriate size, with the convolution weighted by the noise in each velocity plane. A feature is detected in a convolved spectrum if it rises above a threshold proportional to the interquartile range values in that spectrum.

In the second stage of candidate identification, detections from all scales are 'island grouped', i.e. listing together all detections that are either adjacent or overlapping (the majority of features will be detected on multiple scales). The bounding box of these groups is then found, and the original data refitted to create the entry in the final detection list for each group.

The TOPHAT finder is very effective at filtering false detections with narrow velocity

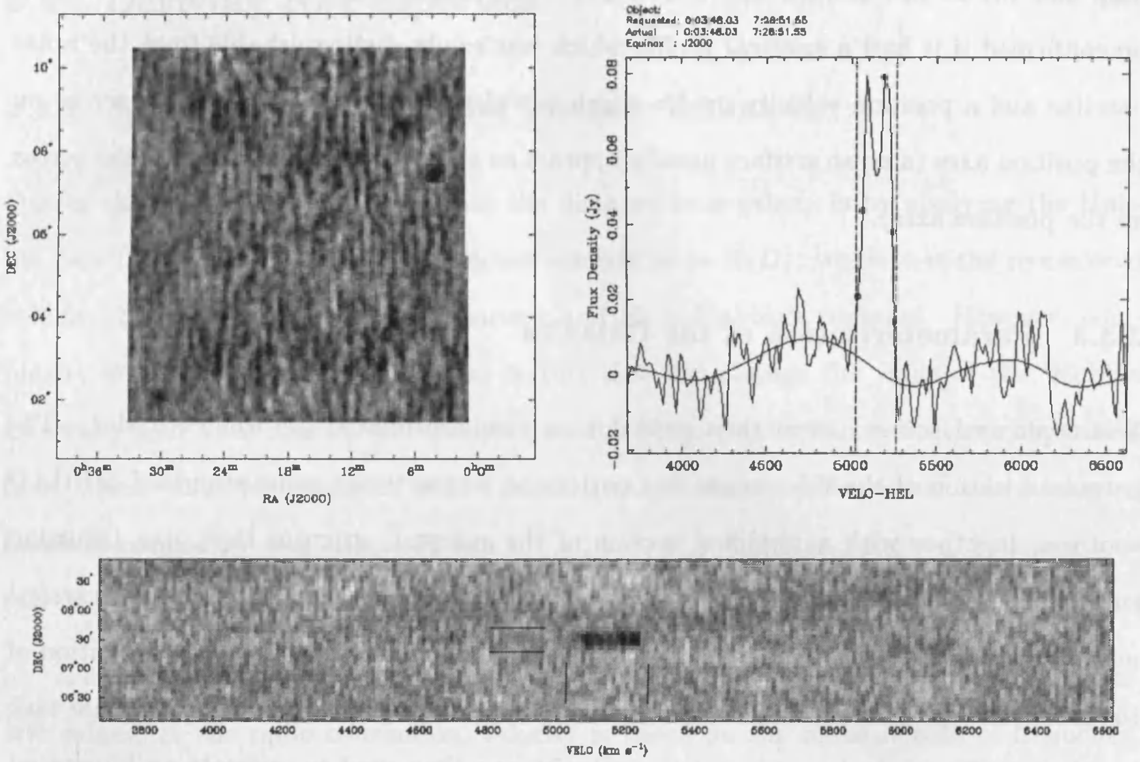

Figure 2.3: Example plots examined during the final checking and parameterisation processes: (upper left) R.A.–Dec. moment map showing the data box used for position fitting; (upper right) Spectrum within the data box – vertical lines show manually specified velocity limits within the which profile parameters are measured and the R.A.–Dec. moment map generated; (lower) Dec–Velocity moment map showing the box and profile velocity limits.

widths, as well as being quite robust against the increased level of noise and baseline ripple in the northern extension cubes. Narrow velocity width detections are usually associated with hydrogen recombination frequencies and known interference.

The results from both the TOPHAT finder and the visual search were then merged into a single list. Each candidate source was then checked manually by simultaneously displaying the source in three ways: i) as a spectrum, ii) as a zeroth (0^{th}) order moment map and iii) in the declination-velocity plane (see Figure 2.3). A source was said to be confirmed if it had a spectral profile which was easily distinguishable from the noisy baseline and a position-velocity profile which is wider than 1 or 2 pixels width across on the position axes (a noise artifact usually appears as a distinct signal 2 pixel-widths across on the position axes).

2.3.3 Parameterisation of the Galaxies

The confirmed sources were then passed to a semi-automated parameter finder. The parameterisation of the ES sources was performed interactively using standard MIRIAD routines, together with a modified version of the *mbspect* program that uses Gaussian smoothing for baseline fitting. The first stage was to fit a Gaussian to velocity integrated map (0^{th} order moment map) of each detection to determine both the central position of the galaxy as well as the spatial extent of the HI. This fitting was done using the *imfit* task in *mbspect*. The central position of the galaxies was then used to generate an integrated spectrum of the detection, using the box size based on the extent of the HI. A Gaussian is used to provide the smoothest estimate of the spectral baseline. It is important that the Gaussian is wide enough not to artificially reduce the noise of the observed spectrum, and at the same time narrow enough to fit the baseline without missing the peaks and troughs of the spectrum. Provided fitting is successful, the coordinates of the detection are taken as those of the ellipse and the moment map regenerated.

The spectra were Hanning smoothed for parameter measurement to improve signal-to-noise, giving a final velocity resolution of 26.4 km s^{-1}. This was an iterative and interactive process and when a satisfactory fit was achieved the measurement of the peak (S_{peak}) and integrated flux (S_{int}), as well as the 50% velocity width (ΔV) and heliocentric velocity ($V_{\odot}$) were recorded. The heliocentric velocity was measured as the central velocity at the 50% velocity width.

2.4 Deriving HI Properties

2.4.1 Velocity Corrections and Distance Estimates

One of the simplest ways to calculate the distance to a galaxy is by applying the Hubble Law (Hubble 1929) to the recessional velocity ($v = H_0D$), where v is the recessional velocity, D is the distance in Megaparsecs and H_0 is Hubble's constant. However, complexity arises from both cosmological factors that can change the value of the 'Hubble Constant' and local mass structures such as the Virgo cluster can distort the expansion flow. These must be corrected before an accurate distance can be estimated. I adopt a Lambda cosmology with $H_0 = 75$ km s^{-1} Mpc^{-1}, $\Omega_M = 0.3$ and $\Omega_\Lambda = 0.7$ throughout this thesis (Lahav *et al.* 2002).

The recessional velocity determined for galaxies from the HIPASS data are heliocentric values. In the radio convention, velocity is based on the measurement of frequency, giving

$$v_{radio} = c\frac{\Delta\nu}{\nu_0} \tag{2.1}$$

where ν_0 is the rest frequency of the line and $\Delta\nu$ is the shift in frequency. However, velocities are generally measured in the optical convention defined by

$$v_{optical} = c\frac{\Delta\lambda}{\lambda_0} \tag{2.2}$$

The ES sample covers a velocity range of 300 – 12 700 km s^{-1} , reaching a redshift of $z \simeq 0.04$. At these redshifts the (1 + z) effects are non-negligible in the radio frame and it is therefore necessary to convert velocities and velocity widths to the cz frame before they are used for analysis. The total effect of the (1 + z) terms, after conversion of the radial velocity to the cz frame, is substantially smaller than the measurement error on the mass and so can be neglected. Cosmological effects (1 + z) will therefore be neglected from the HI analysis.

The recessional velocities presented have been corrected for the motion of the Sun around the Galaxy (galactocentric), and also the motion of the Galaxy in the Local Group. The galactocentric correction used (de Vaucouleurs *et al.* 1991) is,

$$V_{GSR} = V_{optical} + \ 232 \text{ km s}^{-1} \ [sin(b)sin(1.7°) + cos(b)cos(1.7°)cos(l - 87.8°)] \quad (2.3)$$

The Heliocentric to Local Group correction (Karachentsev *et al.* 1996) is,

$$V_{LG} = V_{optical} + \ 316 \text{ km s}^{-1} \ [sin(b)sin(-4°) + cos(b)cos(-4°)cos(l - 93°)] \quad (2.4)$$

The Heliocentric to the CMB 3K Background (Fixsen *et al.* 1996) is,

$$V_{CMB} = V_{optical} + 371 \text{ km s}^{-1} \ [sin(b)sin(48.26°) + cos(b)cos(48.26°)cos(l - 264.14°)] \quad (2.5)$$

where $V_{optical}$ is the heliocentric velocity in the optical convention, and l and b are the Galactic Longitude and Latitude.

2.4.2 HI Mass Calculation

One of the advantages of measuring the HI content of a galaxy is that we can calculate the HI mass by applying the Rayleigh-Jeans approximation to the Plank Law:

$$T_B = \frac{c^2 I_\nu}{\nu^2 k} \quad (2.6)$$

where T_B is the brightness temperature, c is the speed of light, I_ν is the measured intensity, k is the Boltzman constant and ν is the observed frequency. This can be done because the radio emission falls on the Rayleigh-Jeans tail. In the absence of a strong background source, T_B can be expressed in relation to the kinetic temperature and the optical depth of the source by the equation:

$$T_B = (1 - e^{-\tau})\ T_{kin} \tag{2.7}$$

where τ is the optical depth and T_{kin} is the kinetic temperature of the source. For large values of τ: $T_B = T_{kin}$, and for small values of τ: $T_B = \tau\ T_{kin}$. The optical depth for HI is determined by the absorption cross section of the HI atoms at an observed frequency ν and is given by:

$$\tau = \frac{n}{1.823 \times 10^{18}\ T_{kin}} \tag{2.8}$$

where n is the column density of HI atoms in cm^{-2}. In the optically thin case ($\tau \ll 1$), the column density can be written as:

$$n = 1.823 \times 10^{18} \int T_B d\nu \tag{2.9}$$

which only depends on the integrated flux in the beam. The integral is required because most radio receivers separate the flux over multiple channels within some bandwidth. In the case of the Multibeam receiver at the Parkes telescope, the channel separation is 0.06 MHz and the bandwidth is 64 MHz.

From the column density inside the beam, the mass in HI is given by:

$$M_{\text{HI}}\,(\odot) = 2.356 \times 10^5 D^2 \int S\ dv \tag{2.10}$$

where D is the distance in Mpc and the $\int S\,dv$ is the integrated flux in Jy km s^{-1}. The distance is calculated by applying Hubble's Law and using the recessional velocity corrected with respect to the CMB background as explained in the previous section (Section 2.4.1).

This expression for the HI mass is only valid in the optically thin limit but in reality optically thick regions of HI seem to be common (Braun 1997). Although these optically thick regions may not act to saturate the entire column of HI, their contribution to the total HI mass will be underestimated. Therefore, the HI mass derived in Equation 2.10, and in this thesis is derived based on the optically thin assumption and hence should be considered a lower limit.

2.5 Characteristics of the ES Sample

In this section I will present the HI data for the 1077 sources that comprise the ES sample. Table 2.2 presents the parameters derived from the HI data; a sample page is shown, and the full catalogue can be found in Appendix A. Where appropriate I divide the sample into two sets of data: i) the 876 sources for which I do not have optical data and ii) the 201 sources for which I have SDSS optical data and which will be the basis of the analysis in Chapters 3 and 4. There are no differences in the way these samples have been selected and ii) can be thought of as a subsample with optical data of HI selected galaxies (see Chapter 3).

The HI properties found in the ES sample are given in Table 2.2. Column 1 gives the ES identification name (the prefix HIPEQ stands for HI Parkes Equatorial); Columns 2 and 3 give the right ascension and declination (J2000) in decimal degrees of the HI source from fitting the zeroth order moment map. Column 4 gives the barycentric velocity, $V_{\odot}$, measured in the radio frame and converted to the optical convention and the cz frame. Columns 5-7 give the velocity width at 50% of the peak flux (Δ_{50}), the peak flux (S_{peak})

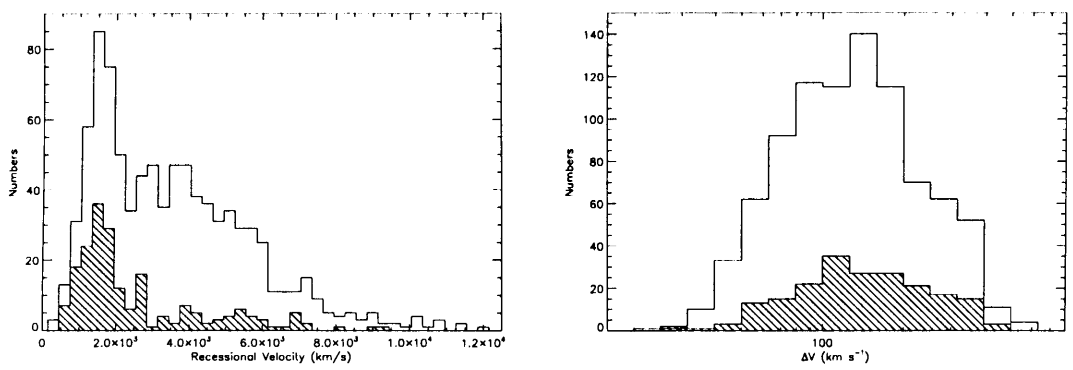

(a) (b)

Figure 2.4: Panel (a) shows the Recessional Velocity distribution of the ES sample. Panel (b) shows the distribution of the 50% velocity widths (Δ_{50}) for the ES sample in bins of 25 km s^{-1}. The unfilled histogram indicates those HI sources without optical data and the line-filled histogram the sources with optical SDSS data.

and the integrated flux (S_{int}). Column 8 gives the distance in Mpc calculated from the CMB rest-frame velocity of the sources with the conversion from the barycentric to the CMB carried out as explained in Section 2.4.1. Column 9 gives the log of the HI mass calculated using the flux from Column 7 and using Equation 2.10 derived in Section 2.4.2. The full list for the 1077 galaxies can be found in Appendix A.

The distribution of recessional velocities is shown in Figure 2.4(a) for the galaxies in the ES sample. The mean velocity is 2566 km s^{-1} and the median velocity is 1813 km s^{-1}. Figure 2.4(b) shows the distribution of the velocity widths at 50% (ΔV_{50}) for the ES sample. The largest velocity width is ΔV_{50} = 630 km s^{-1}and the smallest velocity width in the sample is ΔV_{50} = 30 km s^{-1}, which is just twice the velocity resolution of the survey. The mean velocity width is 163 km s^{-1} and the median is 136 km s^{-1}.

Figure 2.5 shows the distribution of HI masses for the ES sample. The distribution peaks at $10^{9.5} < M_{HI} < 10^{9.75}$, in agreement with the value found by other authors (e.g.

Table 2.2: HI properties of the ES sample (example Table*)

(1) Name	(2) RA (°)	(3) Dec (°)	(4) Vel (km s^{-1})	(5) W_{50} (km s^{-1})	(6) S_{peak} (Jy)	(7) S_{int} (Jy km s^{-1})	(8) Dist. (Mpc)	(9) HI mass log $M_{\odot}$
HIPEQ0001-03	0.44	-3.26	5876	128	0.075	9.60	75.3	10.11
HIPEQ0002-03	0.50	-3.28	6096	126	0.055	6.80	78.4	9.99
HIPEQ0003+07	0.95	7.48	5152	175	0.080	12.75	65.4	10.11
HIPEQ0004+07	1.07	7.37	6069	192	0.035	5.26	78.2	9.88
HIPEQ0004+05	1.15	5.84	3075	218	0.065	10.88	37.1	9.55
HIPEQ0004-01	1.19	-1.60	7386	221	0.046	9.40	96.7	10.32
HIPEQ0006+08	1.70	8.62	5172	201	0.040	7.60	66.2	9.89
HIPEQ0007+08	1.75	8.65	5137	292	0.046	10.86	65.8	10.04
HIPEQ0008-02	2.21	-2.40	3851	141	0.089	14.20	48.6	9.90
HIPEQ0011+06	2.78	6.35	6040	178	0.045	7.93	79.2	10.07
HIPEQ0012+00	3.17	0.00	11925	79	0.044	3.40	163.1	10.33
HIPEQ0014-00	3.65	0.74	3914	290	0.075	17.18	50.9	10.02
HIPEQ0014+07	3.67	7.51	3475	105	0.052	6.18	44.9	9.47
HIPEQ0017+06	4.27	6.79	5560	181	0.044	5.65	74.3	9.87
HIPEQ0019-03	4.77	-3.51	5919	177	0.050	7.90	80.0	10.08
HIPEQ0019+04	4.87	4.08	2984	532	0.077	33.49	39.7	10.09
HIPEQ0020+08	5.03	8.49	5500	65	0.037	2.15	74.4	9.45
HIPEQ0020+08	5.20	8.60	691	39	0.044	1.77	9.1	7.54
HIPEQ0022-01	5.60	-1.32	5002	85	0.109	10.20	68.3	10.05
HIPEQ0024-03	6.11	-3.86	4320	97	0.045	4.36	59.6	9.56
HIPEQ0025-02	6.44	-2.25	5592	65	0.050	9.20	77.6	10.12
HIPEQ0027-01a	6.95	-1.16	3848	223	0.039	6.60	54.2	9.66
HIPEQ0027-01	6.95	-1.80	4229	170	0.076	13.00	59.4	10.03
HIPEQ0028+02	7.03	2.60	4294	130	0.069	9.88	60.3	9.93
HIPEQ0028+03	7.06	3.36	4004	159	0.059	6.80	56.4	9.71
HIPEQ0028+05	7.13	5.00	1329	85	0.092	8.59	20.1	8.91
HIPEQ0029+01	7.44	1.75	10810	319	0.036	7.85	152.2	10.63
HIPEQ0029-05	7.45	-5.10	4072	193	0.046	7.30	57.8	9.76
HIPEQ0029+03	7.49	3.54	1339	21	0.116	4.06	20.7	8.61
HIPEQ0030+02	7.50	2.09	5269	348	0.060	12.61	74.3	10.21
HIPEQ0030+01	7.50	1.85	3396	62	0.042	2.60	48.6	9.16
HIPEQ0030+02	7.50	2.10	5268	351	0.059	12.99	74.3	10.23
HIPEQ0031+09	7.89	9.18	2135	101	0.075	6.90	31.7	9.21
HIPEQ0031+08	7.91	8.44	4272	222	0.078	16.02	60.9	10.15
HIPEQ0031-05	7.93	-5.17	4240	85	0.139	13.30	60.6	10.06
HIPEQ0031-02	7.94	-2.54	6388	252	0.046	9.30	90.3	10.25
HIPEQ0033-01	8.34	-1.12	1972	146	0.131	17.24	30.1	9.57
HIPEQ0033+02	8.43	2.68	4339	219	0.070	9.51	62.3	9.94
HIPEQ0034-02	8.54	-2.18	5296	73	0.060	4.38	75.7	9.77
HIPEQ0034+00	8.60	0.27	1510	68	0.074	5.03	24.0	8.84
HIPEQ0036+01	9.03	1.71	5525	101	0.065	6.10	79.2	9.95
HIPEQ0037+01	9.27	1.97	4577	102	0.097	20.70	66.2	10.33

* The full list can be found in Appendix A

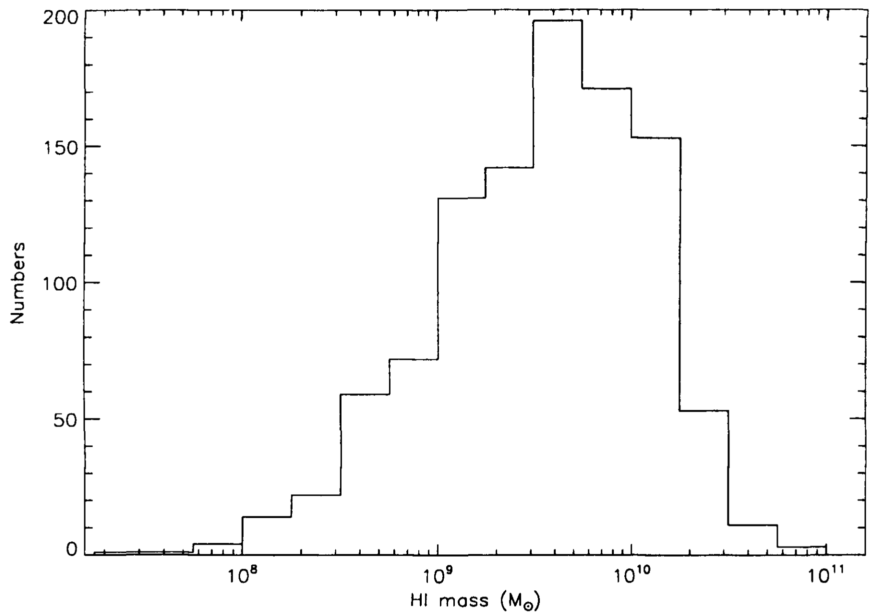

Figure 2.5: Distribution of HI masses from the ES sample for 1077 galaxies.

Zwaan *et al.* 1997, Minchin 2001, Zwaan *et al.* 2005) for $M^{\star}_{\rm HI}$ of $10^{9.75}$ $M_{\odot}$. Lower mass galaxies than this are too faint to be seen over large volumes and therefore there are fewer of these in the sample, while higher mass galaxies are too rare to be seen in large numbers.

Figures 2.6 (a) and (b) show the peak and integrated flux distributions respectively. As expected the distribution of peak fluxes peaks at the peak flux limit of $\sim$ 40 mJy. In Figure 2.6(b) we can see the distribution of integrated fluxes which peaks at around 8 Janskys. The distribution for both the ES sample with and without optical data are very similar. This is important because it indicates that the optical subsample of HI selected galaxies is representative of the sample as a whole and hence can be used to characterise the properties of HI selected galaxies. I will return to this subject in Chapter 3.

Figure 2.7 shows the spatial distribution of the ES sources. Figure 2.7(a) shows the distribution of the sources with respect to right Ascension, the Equatorial Strips covers

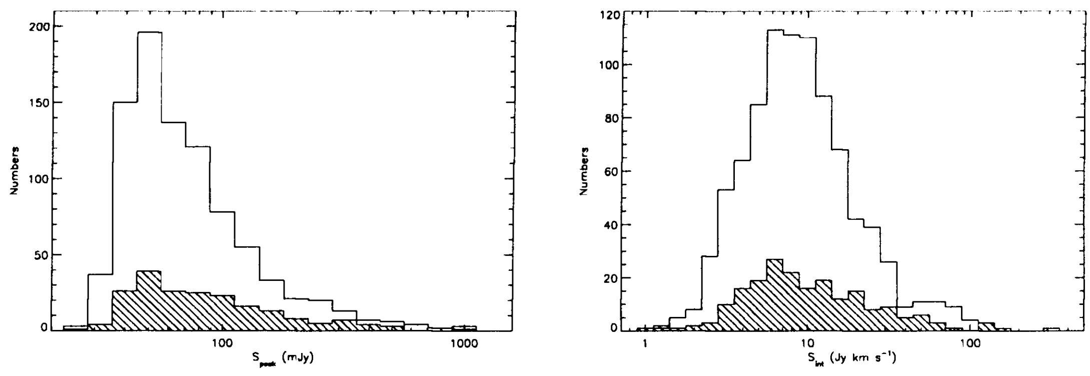

(a) (b)

Figure 2.6: (a) shows the distribution of Peak fluxes (S_{peak}). (b) shows the distribution of integrated fluxes (S_{int}) for the ES sample. The unfilled histogram indicates those HI sources without optical data and the line-filled histogram the sources with optical SDSS data.

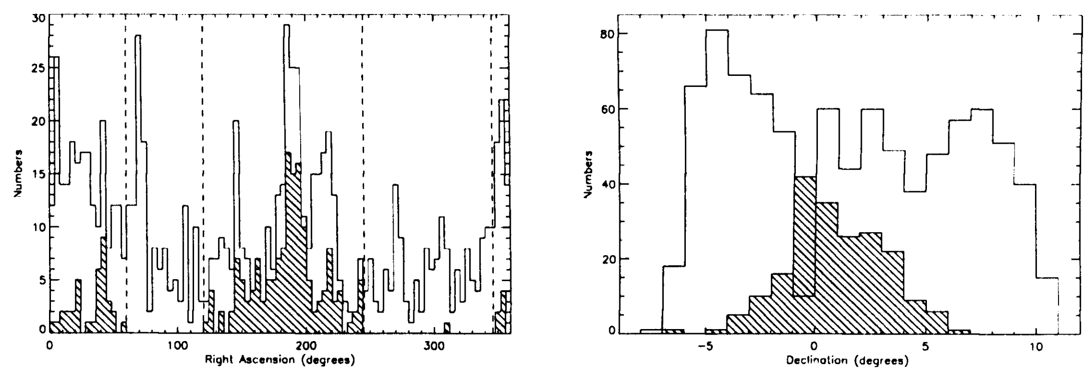

(a) (b)

Figure 2.7: Spatial distribution of the ES sample. (a) shows the distribution with respect to right Ascension. (b) shows the distribution of Declinations. The unfilled histogram indicates those HI sources without optical data and the line-filled histogram the sources with optical SDSS data.

the full range of R.A.s. The dashed vertical lines in this plot represent the R.A. limits of the SDSS survey hence explaining the lack of optical data for those regions ($60° < \delta < 120°$ and $245° < \delta < 345°$) which roughly coincide with the galactic plane. The peak seen at $\sim$ 190 degrees (12 hours) is caused by the southern extension of the Virgo cluster of galaxies. The inclusion of a significant number of cluster galaxies in the sample might affect the results of the HI analysis such as the HIMF discussed in Section 2.8. The ES sample is complete to a S_{peak} of $\sim$ 45 mJy and to an S_{int} of $\sim$ 7 Jy km s^{-1} as I will describe in the next section. Figure 2.8 shows the different bivariate distributions for the ES sample.

2.6 Completeness and Selection Limits for the ES sample

One of the main objectives of this ES sample is to extract a sample of HI-selected extragalactic objects which can be employed to study the properties of galaxies free from optical selection effects. In order to make optimal use of the sample it is essential that the completeness and reliability are well understood and quantified. Only after an accurate assessment of the completeness and reliability is it possible to extract from the sample the intrinsic properties of the local galaxy population.

Figure 2.9 shows the selection limits for the HI mass with respect to their distance. The sample is complete to an integrated flux of $\sim$ 7 Jy km s^{-1} but we have detected galaxies down to a limit of 1 Jy km s^{-1} which is similar to that of the HIDEEP survey by Minchin (2003). We have detected galaxies down to that limit thanks to the inclusion of 'by eye' detections which have been confirmed as real by Narrow Band, longer integration, follow ups.

I have analysed the form of the selections present in the ES sample by plotting the integrated flux of the galaxies against their velocity width (Figure 2.10). For a survey solely limited by the total flux (S_{int}), the selection limit would be a horizontal line. However,

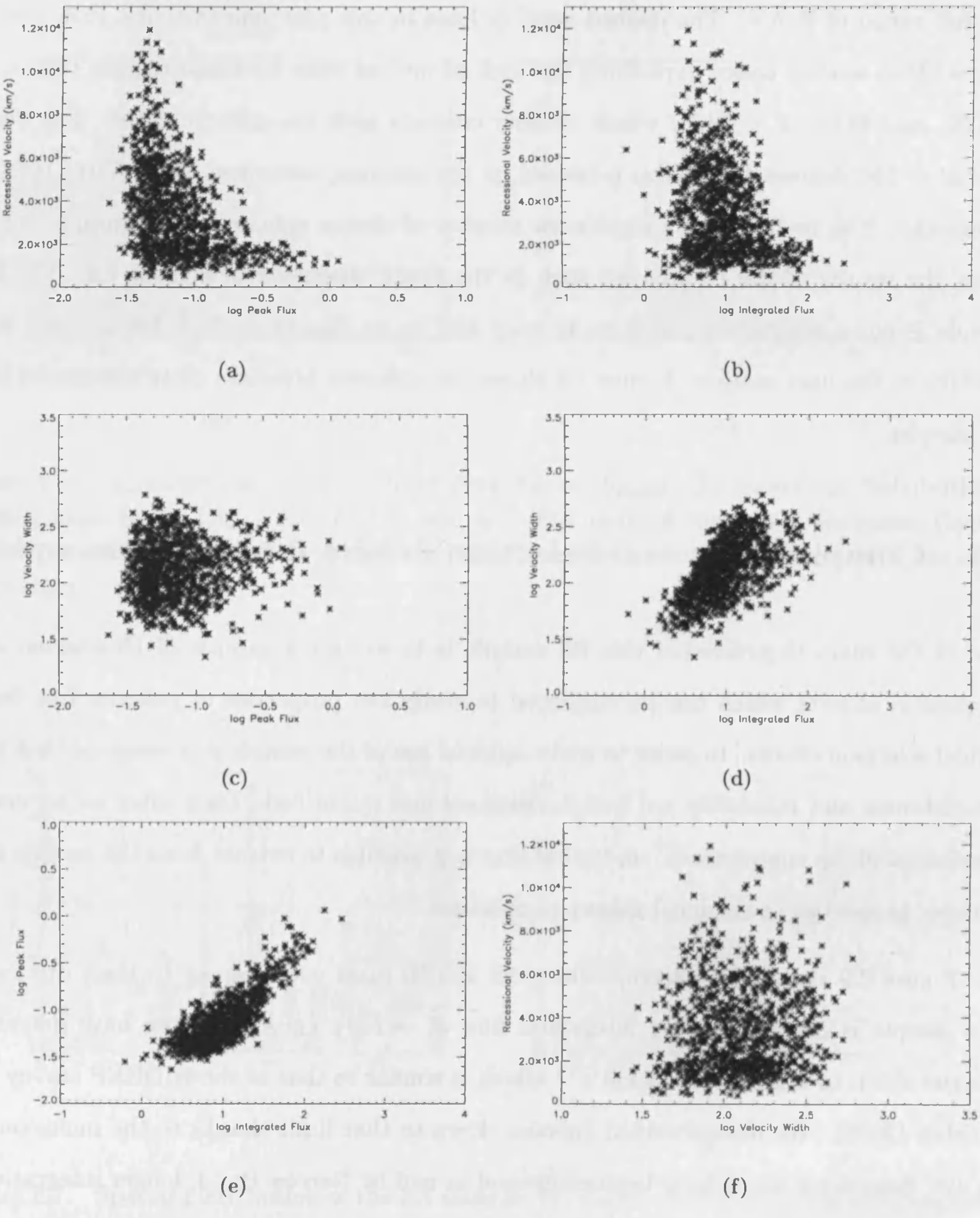

Figure 2.8: Bivariate Distributions of the ES sample. Panels (a) and (b) show respectively the distribution of peak and integrated fluxes with respect to the heliocentric recessional velocity. Panels (c) and (d) show the distribution of uncorrected velocity widths (ΔV_{50}) with respect to the peak and integrated fluxes. Panel (e) shows the relationship between the peak flux and integrated flux. Panel (f) shows the distribution of velocity widths with respect to heliocentric recessional velocities.

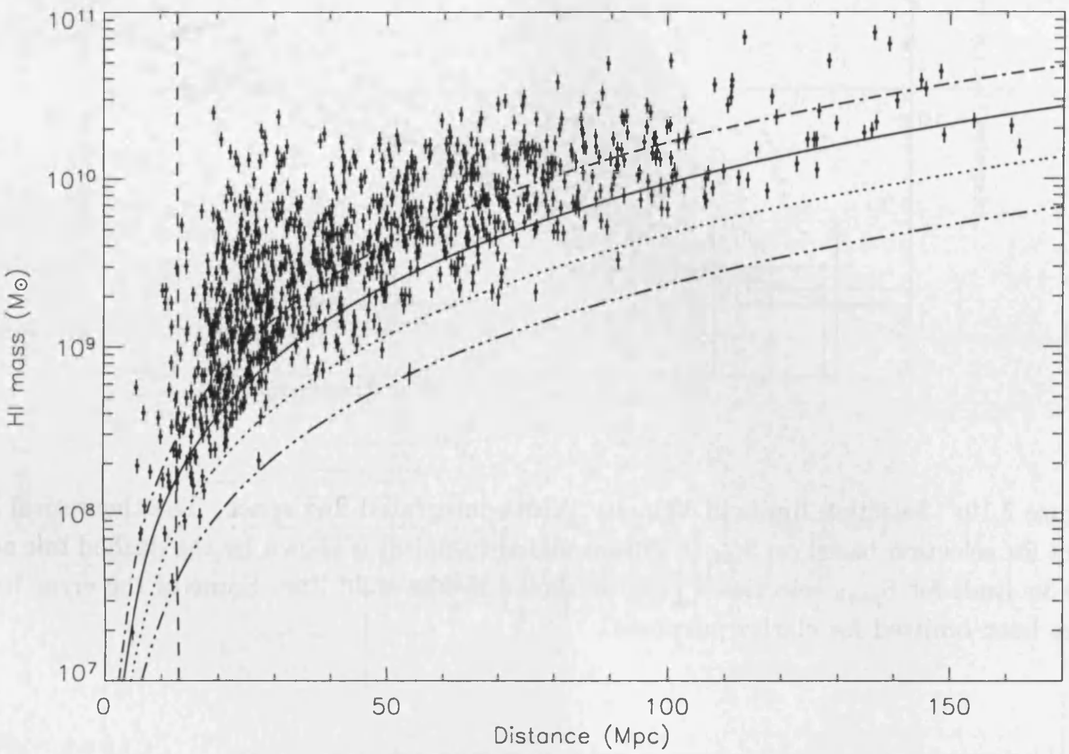

Figure 2.9: Selection limit for the Equatorial Strip sources and distribution of sources by mass and distance. The different curves show the detection limits for a limiting flux of 1, 2, 4 & 7 Jy km s^{-1} respectively; for a velocity width of 200 km s^{-1}, and a noise of 13 mJy. This is a fairly good approximation as in reality the noise varies across the data cubes and the velocity width is related to the mass of the galaxy. The sample is complete to a limiting flux of 7 Jy km s^{-1} (see section 2.6) but we can detect galaxies down to a flux of 1 Jy km s^{-1}. The dashed vertical line shows a distance of 13 Mpc or $\sim$ 1000 km s^{-1} in recessional velocity.

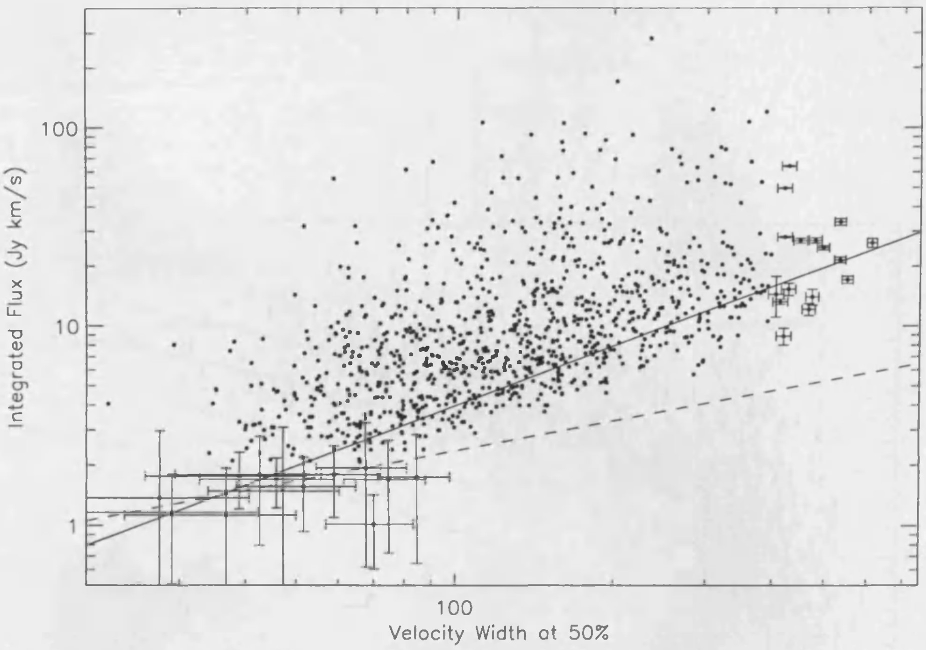

Figure 2.10: Selection limits in Velocity Width-integrated flux space. The theoretical 3σ limit for selection based on S_{int} (constant signal-to-noise) is shown by the dashed line and the 3σ limit for S_{peak} selection ($\frac{S_{int}}{\Delta V_{50}}$) is shown by the solid line. Some of the error bars have been omitted for clarity purposes.

this is clearly not the case; if the best possible selection was made, i.e. selection purely by signal-to-noise (S/N) ratio, then the selection limit would be a line with slope of 1/2 on a log-log plot (assuming $S/N \propto 1/\sqrt{\Delta V}$); this is indicated as a dashed line. The solid line in Figure 2.10 shows a selection limit based on peak flux ($S_{int} \propto \Delta V_{50}$).

It can be seen that many sources fall below the peak flux limit and for velocity widths up to $\sim$ 90 km s^{-1} the sources are being detected down to the integrated flux limit, at higher velocity widths it starts deviating from the integrated flux limit towards the peak flux limit but a substantial number of sources still are detected below that limit.

This indicates that the sample is a mixture of peak and integrated flux selected, this

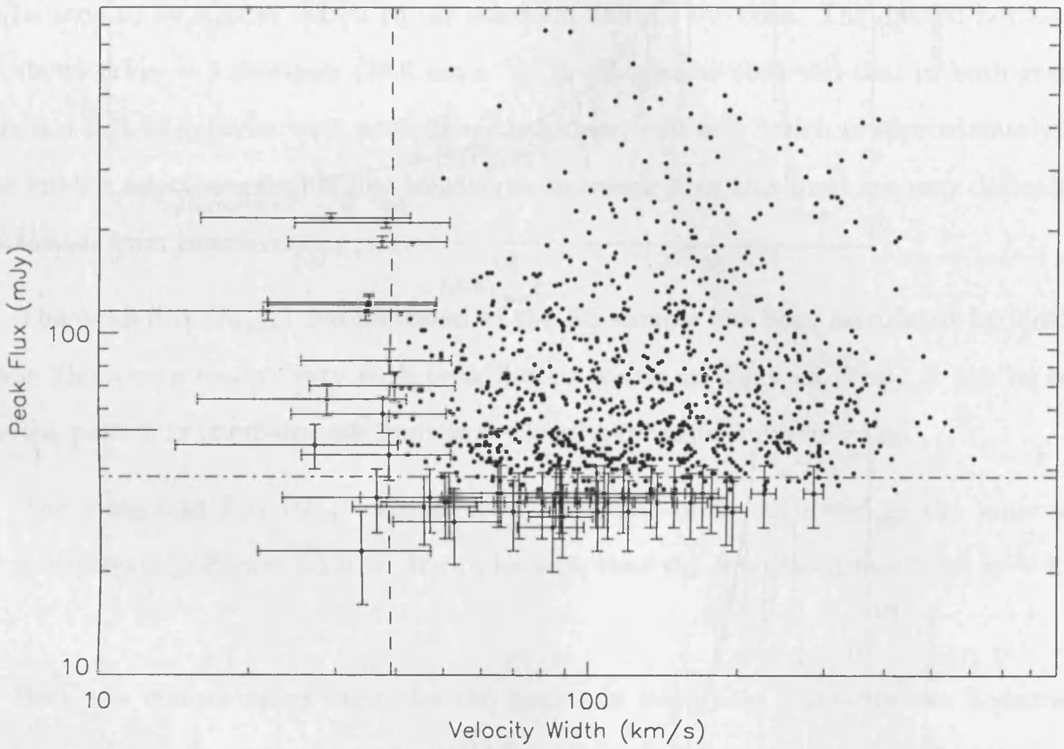

Figure 2.11: Selection limits in velocity width-peak flux space. The 3σ (39 mJy) shown here (dot-dashed line) can be seen to be a good match to the selection limit of the data. The dashed vertical line shows $\Delta V_{50} = 3$ channels (39.6 km s^{-1}). Some of the error bars have been omitted for clarity purposes.

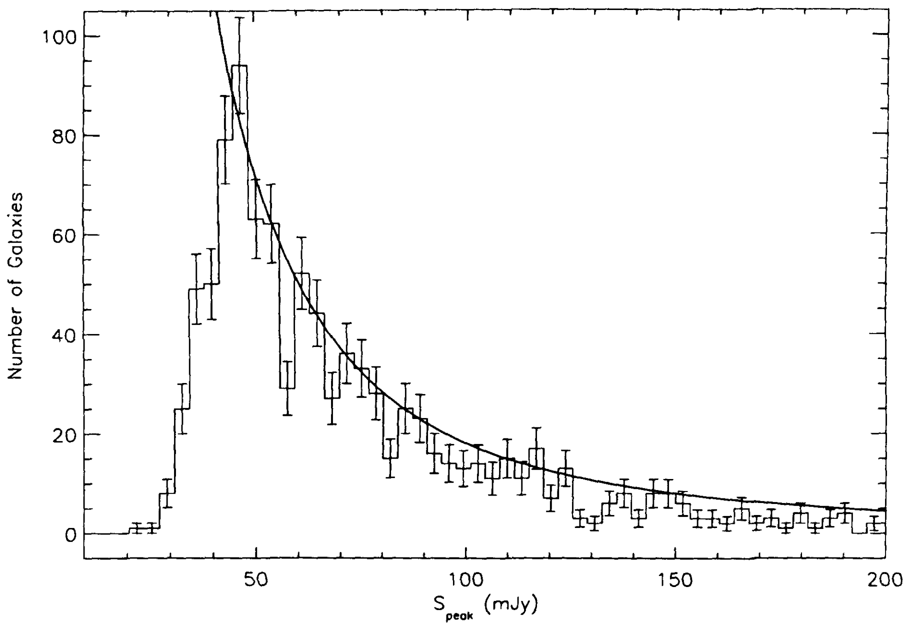

(a)

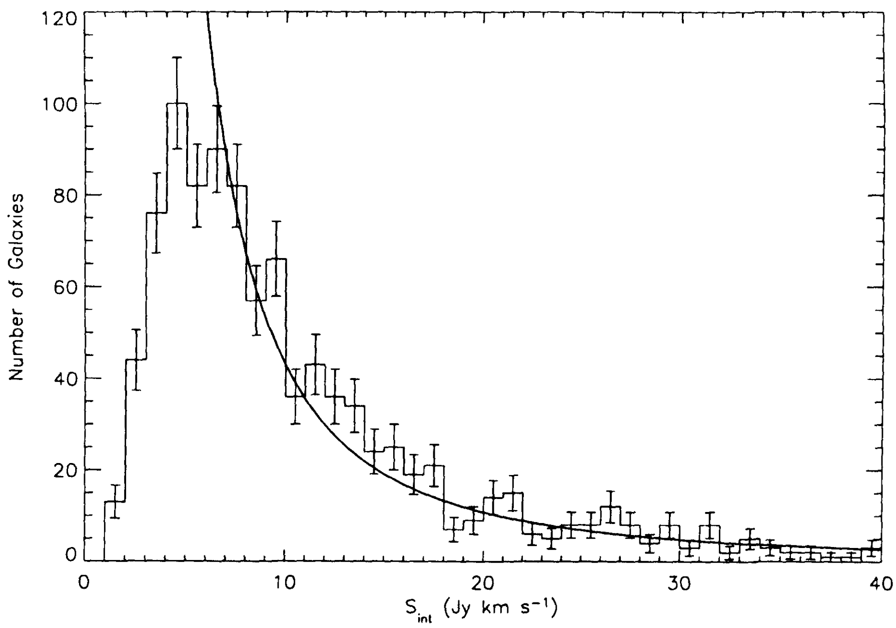

(b)

Figure 2.12: Panel (a) shows the completeness of the ES sample in peak Flux. Source count against peak flux (S_{peak}). The histogram shows the numbers found in each bin of peak flux, the curve shows represents $N(S) \sim S^{-5/2}$ as expected for a flux-limited survey. Panel (b) shows the completeness of the ES sample in integrated Flux. The histogram shows the numbers found in each bin of peak flux, the curve shows represents $N(S) \sim S^{-5/2}$ as expected for a flux-limited survey.

might be due to the inclusion of sources that were selected 'by eye' which are closer to the noise and hence more difficult to detect by the automated finders but easily detected by the brain-eye mechanism.

The peak flux selection limit is shown in Figure 2.11, it can be seen that this explains well the selection limits of the sample. The 3σ (39 mJy) used in this plot (dot-dashed line) can be seen to be a good match to the selection limit of the data. The dashed horizontal line shows ΔV_{50} = 3 channels (39.6 km s^{-1}). It can also be observed that in both graphs there is a lack of galaxies with peak fluxes less than $\sim$ 40 mJy which is approximately 3σ. This further selection effect is due to galaxies narrower than this limit are very difficult to distinguish from interference.

The peak flux (S_{peak}) completeness of the ES sample has been calculated by looking at how the source counts vary with peak flux as shown in Figure 2.12(a). It can be seen that the peak flux completeness limit is $\sim$ 45 mJy, or around 3.5 σ.

The integrated flux (S_{int}) completeness limit has been calculated in the same way and it is shown in Figure 2.12(b). It can be seen that the integrated flux limit is $\sim$ 7 Jy km s^{-1}.

Both the completeness limits for the peak and integrated fluxes for the Equatorial Sample are lower than those for the HICAT catalogue (Zwaan *et al.* 2005) which includes 4315 galaxies from the HIPASS survey. The completeness limits for HICAT are $\sim$ 64 mJy for the peak Flux and 9.2 Jy km s^{-1} for the integrated Flux. It would be expected to obtain similar completeness limits for both samples as the same rms, data and automated selection criteria has been used for both samples. However, the reason for the improvement of $\sim$ 30% and $\sim$ 25% in peak and integrated fluxes limits respectively might be due to the inclusion of sources close to the detection limits but which have been found to be real by Narrow Band radio follow-ups. The majority of sources found to be close to the detection limit were detected by the visual search whereas HICAT only included automated finder

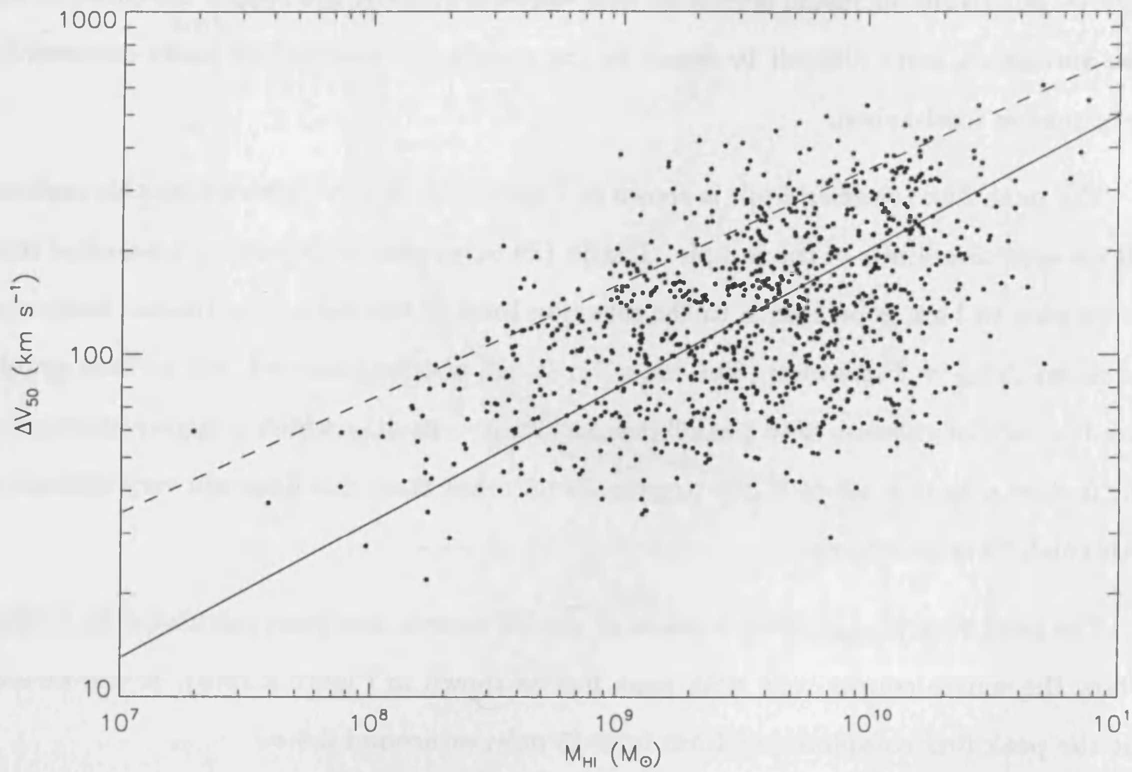

Figure 2.13: Velocity Width versus HI mass. This relationship is the HI equivalent of the Tully-Fisher relation. The best fit for the ES data is shown by the solid line. The dashed line shows the fit from Briggs & Rao's (1993) for an optically selected sample. Error bars have been omitted for clarity purposes.

detections hence having more conservative limits.

2.7 The HI Tully-Fisher relation

A correlation between the HI mass and the velocity width of the form $\Delta V \propto M_{\rm HI}^{\beta}$ is expected in the ES sample as it has been seen in optically-selected samples such as that of Briggs & Rao in 1993 who found a relation between the HI mass and the velocity width for an optically selected sample that was not corrected for inclination. This relation between the HI mass and the velocity width is the HI equivalent of the Tully-Fisher relationship (Tully *et al.* 1977) and provides a useful tool for analysing the selection effects in HI surveys where the velocity width plays an important role.

For the ES sample this relationship can be seen in Figure 2.13 where the solid line shows the best-fitting linear relation for the ES sample of $\Delta V_{50} = 0.022\ M_{\rm HI}^{0.39}$ for the ES sample while the dashed line shows the relationship found by Briggs & Rao (1993) such that $\Delta V = 0.16\ M_{\rm HI}^{0.33}$. The ES sample best-fitting slope is fairly similar to that seen in optically selected samples, suggesting that galaxies detected in HI or optical surveys seem to follow the same relationship.

2.8 The HI Mass Function of Galaxies (HIMF)

The HI mass function (HIMF), $\phi(M_{HI})$ describes the number density of neutral hydrogen as a function of HI mass at the present epoch. The concept of the HIMF was introduced by Briggs (1990) as a diagnostic tool for assessing the completeness of optical galaxy catalogues against 21-cm HI surveys. In that paper the then available luminosity functions and an adopted relation between gas richness ($M_{\rm HI}\,/L$) and luminosity were used to make the first attempts at HIMF calculations. The HIMF is determined from a flux-limited sample such that:

$$dN(M_{\rm HI}) = \phi(M_{\rm HI})V(M_{\rm HI})dM_{\rm HI} \tag{2.11}$$

where $dN(M_{\rm HI})$ is the observed number of galaxies within the mass range $(M_{\rm HI}-dM_{\rm HI}/2, M_{\rm HI}+dM_{\rm HI}/2)$, and $V(M_{\rm HI})$ is the volume in which galaxies of mass $M_{\rm HI}$ are observable to a limiting mass of $M_{{\rm HI},lim}$.

The HIMF is the HI analogue of the optical Luminosity Function (LF). This function can be represented parameterically by an analytic function such as the Schechter (Schechter 1976) function such that

$$\Phi(M_{\rm HI})d(M_{\rm HI}) = \theta^{\star}(\frac{M_{\rm HI}}{M^{\star}_{\rm HI}})^{\alpha}\ exp - (\frac{M_{\rm HI}}{M^{\star}_{\rm HI}})d(\frac{M_{\rm HI}}{M^{\star}_{\rm HI}}) \quad (2.12)$$

where α is the faint-end slope, $M^{\star}_{\rm HI}$ is the characteristic HI mass and $\theta^{\star}$ is the normalisation factor.

The HIMF is a crude but useful tool to determine quantities such as the total mass density of neutral hydrogen atoms in the local Universe, $\Omega_{\rm HI}$ ($z = 0$). It is an important factor in models of cosmology and galaxy evolution. For a good understanding of the evolution of the HI content of the Universe the measurement of a local benchmark is obviously very important.

2.8.1 The $\sum 1/V_{max}$ Method

The HIMF for the ES sample has been determined using the $\sum 1/V_{max}$ method (Schmidt 1968). The effect of galaxy clustering may influence the HIMF calculated from a flux limited sample of limited breadth and depth. The $\sum 1/V_{max}$ method assumes that the space density of galaxies is uniform (Binggeli *et al.* 1988). Zwaan *et al.* (2005) finds tentative evidence for a steepening of the low-mass end of the HIMF as a function of local galaxy density.

The main problem when applying the $\sum 1/V_{max}$ method is qunatifying the detection limits for the survey so that the maximum observable volume for each galaxy can be calculated. The The HIMF requires a flux limited sample, such as the ES sample, from which the volume within each detection would just be detectable, to the limit of the survey is calculated.

(a)

(b)

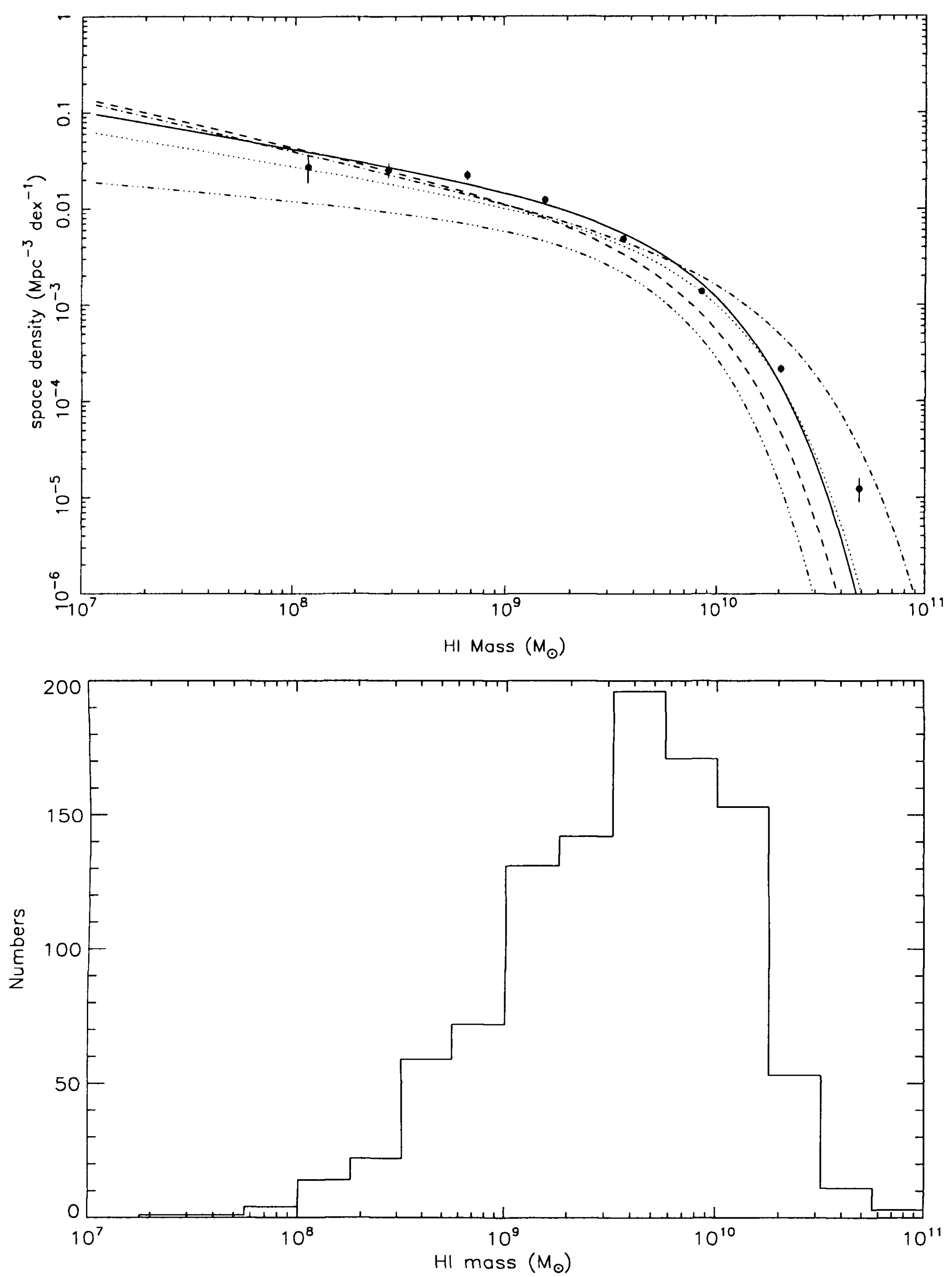

Figure 2.14: HI Mass Function for the Equatorial Strip sample (a) and HI mass distribution (b). The best fitting Schechter relation for the ES sample is shown by the solid line with a slope of $\alpha = -1.38$. The dashed line shows Henning's (2000) slope of $\alpha = -1.51$. The dot-dash line shows Kilborn's (SCC sample) slope of $\alpha = -1.52$. The dotted line shows HIPASS (HICAT) slope of $\alpha = -1.37$. The dot-dot-dash line shows Zwaan's (1997) slope of $\alpha = -1.20$.

The two main observable parameters of galaxies in the ES sample are peak flux and velocity width. If the detectability of a galaxy depends only on the peak flux density of that galaxy, then the maximum detectable distance can be calculated by simply using the inverse square law,

$$D_{max} = D\sqrt{\frac{S_p}{S_{lim}}} \tag{2.13}$$

where S_p is th epeak flux density of an individual galaxy, S_{lim} is the limiting peak flux density for the galaxy, and D is the distance. If the detectability of a galaxy depends on its total flux and velocity width, then we use the HI mass of the galaxy:

$$M_{\text{HI}} = 2.356 \times 10^5\, D^2 \int S dv\, M_\odot \tag{2.14}$$

where D is the distance to a galaxy in Mpc, and S is the spatially integrated flux density in Jy, and dv is the velocity extent of the galaxy in km s^{-1}.

From Equation 2.11 it follows that to construct an HIMF using this method:

$$\phi(M_{\text{HI}})\, dM_{\text{HI}} = \sum_{M-dM/2}^{M+dM/2} \frac{1}{V_{max,i}} \tag{2.15}$$

where dM_{HI} is a discrete mass interval, and $V_{max,i}$ is the maximum volume in which each galaxy, i, of mass M_{HI} could just be detected. Once the $1/V_{max}$ in each mass is determined it is plotted as a density histogram and a Schechter function (Schechter 1976) fitted to the data to provide an analytic form for the HIMF. The error in each point is governed by the number statistics of the sample, and can be determined by using:

$$\sigma = \left(\sum \frac{1}{V_{max}^2}\right)^{\frac{1}{2}} \tag{2.16}$$

Thus each galaxy is weighted by its contribution to the sum (Marshall 1985). At low HI masses, the effective volume surveyed is much smaller than for galaxies of higher HI mass. This means that the error at the low and high mass ends can be substantial due to poor number statistics.

A potential problem when applying the $1/V_{max}$ method to any sample (including this one) is quantifying the detection limits for the survey so that the maximum observable volume for each galaxy can be calculated accurately.

The maximum distance, D_{max}, out to which a particular galaxy of mass $M_{\rm HI}$ could be detected depends on the detectability function of the survey. As the ES sample is a bandwidth-limited survey, if the calculated D_{max} is greater than the bandwidth limit, D_{BW}, then $D_{max}= D_{BW}$. For the ES sample D_{BW} = 170 Mpc. Once the maximum detectable distance has been determined for each galaxy in the sample, this is converted into a maximum detectable volume, given by

$$V_{max} = \frac{1}{3} D^3_{max}\Omega \tag{2.17}$$

where V_{max} is the maximum volume a galaxy could have been detected in, and Ω is the solid angle of the survey, Ω = 1.747 steradians for the ES sample (5738 deg^2). For the ES sample an integrated flux limit of 7 Jy km s^{-1} has been used as this sample is complete to that limit (see Section 2.6).

The filled points in Figure 2.14 (a) show the HIMF determined by the $\sum(1/V_{max})$ method. The solid line shows the best-fitting Schechter function (see Eq 2.12) for which the Schechter parameters are $\alpha = -1.38$, $\theta^\star = 0.009$ Mpc^{-3} and $M^\star_{\rm HI} = 5.7 \times 10^9$ M$_\odot$. For comparison, also shown are the Schechter function parameters found by several other authors in previous blind HI surveys. The results from Henning (2000), Kilborn (1999), HIPASS (2004) and Zwaan (1997) are shown as dashed, dot-dash, dotted and double dot-dash lines respectively. The ES results agree very well with Zwaan's results for the whole of the HIPASS survey, they are both the largest surveys to date and the difference in the characteristic mass and normalisation factor is due to the inclusion of the Virgo cluster galaxies which affect the results by steeping the faint end slope with the inclusion of cluster members.

The $\sum(1/V_{max})$ method recovers the shape and amplitude of the HIMF simultaneously without using a Schechter function (or any other parameterisation) as an 'a priori' assumption about the intrinsic shape of the HIMF. The Schechter function is only used to enable comparison with other HI survey results based on the optically selected galaxy population, see Table 2.3 for previous calculations of these parameters. This result is consistent with the previous calculations of the HIMF and is the second to date with such large number of galaxies. Banks *et al.* (1997) found a value of $\alpha = -1.16$ and $M^{\star}_{\mathrm{HI}} = 1 \times 10^{9}$ M$_{\odot}$ for the Centaurus A group, this survey has better statistics in the faint end slope but it is in a cluster and hence might not be necessary representative of the universe as a whole.

The inclusion of a considerable number of galaxies from the southern extension of the Virgo cluster might affect the shape of the HIMF. Zwaan *et al.* 2005 finds tentative evidence for a steepening of the low-mass end of the HIMF as a function of local galaxy density. This effect becomes stronger if local densities are measured over larger scales, which indicates that environmental effects on the HI properties of galaxies are not restricted to short distance effects such as galaxy interactions.

2.9 The HI content of the local Universe

Once the HIMF has been determined, the total HI mass density (Ω_{HI}) of the local universe can be obtained by integrating under the best fit Schechter function. The integral under the Schechter function from Figure 2.14(a) is given by $\rho_{\mathrm{HI}} = \Gamma(2+\alpha)\theta^{\star}M^{\star}_{\mathrm{HI}} = 7.4 \times 10^{7}$ $h_{75}M_{\odot}$ Mpc^{-3}, where Γ is the Euler gamma function. The HI mass density from adding the data points in the HI density histogram gives the observed total HI mass density, $\sum \frac{M_{\mathrm{HI}}}{V_{max}}$.

This is slightly higher value for the total HI mass density of $\rho_{\rm HI} = 7.9 \times 10^7\ h_{75} M_\odot$ Mpc^{-3} as the Schechter fit is not a perfect fit. The HI mass density derived from the ES sample is slightly higher than previous calculations, including that of HICAT (Zwaan *et al.* 2005), and Kilborn (2001). Table 2.3 shows a comparison of the values derived from the ES sample and from previous surveys. Rao and Briggs (1993) determined $\rho_{\rm HI} = 3.6 \times 10^7$ $h_{75} M_\odot$ Mpc^{-3}, from HI observations based on optical catalogues. This is about half the HI mass density derived from the ES sample but that sample is limited by HI column density ($N_{\rm HI}$) and hence there could be more HI present therefore it can be taken as a lower limit.

The critical density of the Universe is the density at which the expansion of a Universe would eventually be halted. It is defined as (e.g. Padmanabhan, 1999):

$$\rho_c = \frac{3H_0^2}{8\pi G} \cong 1.57 \times 10^{-29}\ h_{75}^2\ g\ cm^{-3} \tag{2.18}$$

The cosmological HI mass density, $\Omega_{\rm HI}$ is defined as $\rho_{\rm HI}/\rho_c$. For the ES sample, $\Omega_{\rm HI} = 3.2 \pm 0.4 \times 10^{-4} h_{75}^{-1}$. Assuming that the percentage of He is 25% of the total gas density, $\Omega_{gas} = 4.1 \pm 0.4 \times 10^{-4} h_{75}^{-1}$.

Figure 2.15 shows the HI mass density of galaxies of different masses. The contribution of galaxies with less than 10^8 M$_\odot$ of HI to the overall HI mass density is very low. Most of the HI mass is contained in galaxies with $\sim 10^9$ - 10^{10} M$_\odot$.

The HIMF derived from the ES sample is similar to previous results, especially to the results of the HICAT catalogue. The faint-end slope of the HIMF does not seem to indicate the presence of a large, previously missed population, of gas-rich dwarf galaxies. However, the HIMF for the ES sample only covers 3 orders of magnitude in mass and therefore it does not probe directly the low mass ($M_{\rm HI} < 10^8$ M$_\odot$) regime but we do not expect galaxies with $< 10^8$ M$_\odot$ to contribute significant amounts if the extrapolation for the faint end slope of the HIMF is correct. The ALFA surveys to be carried out at the

Table 2.3: Comparison of HI parameters with previous blind HI surveys

	α	$M^{\star}_{\rm HI}$ ($M_{\odot}$)	$\theta^{\star}$	$\rho_{{\rm HI},tot}$ ($h_{75} M_{\odot}$ Mpc^{-3})	$\rho_{{\rm HI},obs}$ ($h_{75} M_{\odot}$ Mpc^{-3})	$\Omega_{\rm HI}$ (h_{75}^{-1})	Ω_{gas} (h_{75}^{-1})
This work	-1.38	5.7×10^{9}	9×10^{-3}	7.9×10^{7}	7.4×10^{7}	$3.2 \pm 0.4 \times 10^{-4}$	$4.0 \pm 0.4 \times 10^{-4}$
Zwaan *et al.* (2005)	-1.37	6.3×10^{9}	6×10^{-3}	5.4×10^{7}	...	3.5×10^{-4}	...
Kilborn (2001)	-1.52	1.1×10^{10}	3×10^{-3}	6.7×10^{7}	6.0×10^{7}	2.7×10^{-4}	3.4×10^{-4}
Henning *et al.* (2000)	-1.51	5.0×10^{9}	6×10^{-3}	5.4×10^{7}	...	2.2×10^{-4}	2.7×10^{-4}
Zwaan *et al.* (1997)	-1.2	6.3×10^{9}	6×10^{-3}	4.4×10^{7}	4.0×10^{7}	2.5×10^{-4}	3.1×10^{-4}

Arecibo telescope with its 7 beam system will help to anchor down the true value of the faint end slope of the HIMF as it will detect objects to much lower HI mass limits.

2.10 Summary of Chapter 2

In this chapter I have discussed the how the HI sample was observed, how the data was reduced and how the final catalogue was selected, generated and parameterised. I have presented the main HI characteristics of the ES sample and shown what its selection limits

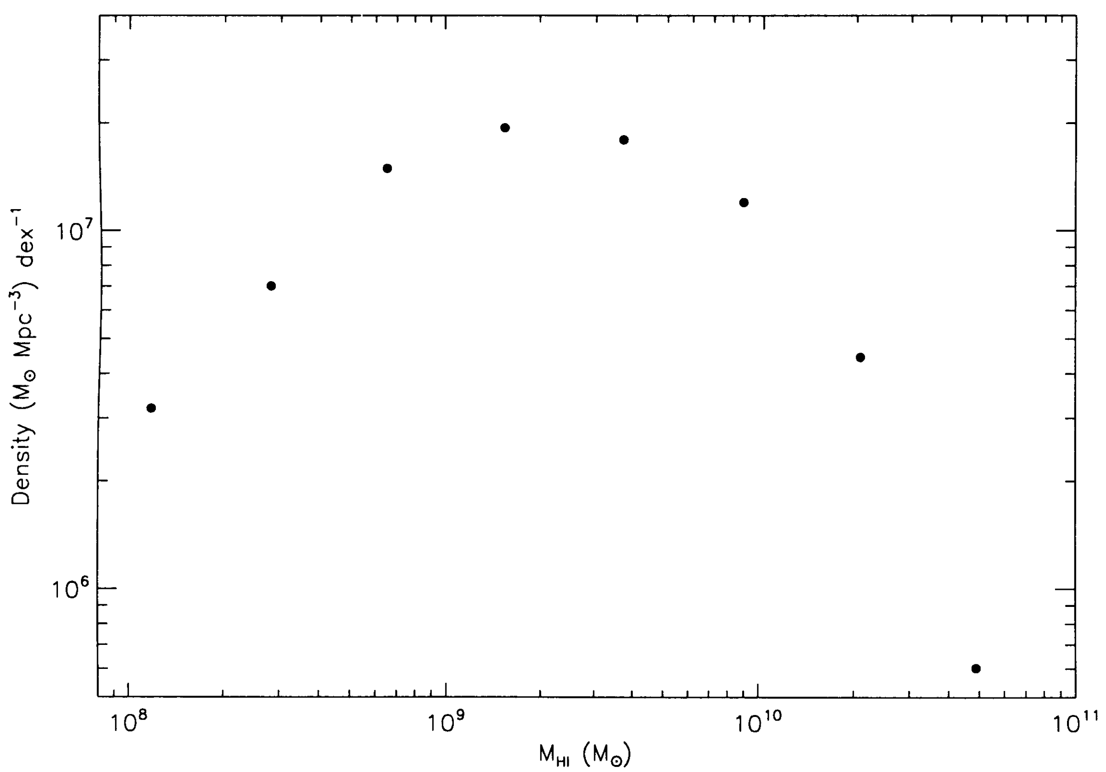

Figure 2.15: HI density of galaxies. Most of the HI mass is contained in galaxies with $10^{8.8}$ $M_\odot$ < M_{HI} < 10^{10} $M_\odot$. The contribution of galaxies with less than 10^8 $M_\odot$ of HI to the overall HI mass density is believed to be low.

and completeness are. I have presented the full catalogue with the HI parameters for the 1077 galaxies, which can be found in full in Appendix A.

I have used the HI parameters derived to determine the HI Tully-Fisher relationship for the ES sample and determined that is fairly similar to that of optically selected samples, suggesting that HI and optically selected galaxies seem to follow the same relationship.

With the HI masses derived for the ES sample I have constructed an HI Mass Function using the $1/V_{max}$ method and used it to calculate the total HI mass density of the local universe and the cosmological HI mass density. The faint-end slope of the HIMF does not seem to indicate the presence of a large, previously missed population, of gas-rich dwarf galaxies.

Chapter 3

The Optical Data

3.1 Introduction

The combination of optical and HI information for an HI selected sample is a powerful tool for analysing the properties of gas-rich galaxies. In this Chapter optical data is presented for 201 sources out of the 1077 HI sources from the ES sample presented in Chapter 2. As I will show, this subsample of 201 objects is representative of the whole HI sample and can therefore be used to characterise the whole HI sample. The optical data was obtained from the Sloan Digital Sky Survey (SDSS) which is discussed in Section 3.2. Section 3.3 explains how the process of matching HI sources with optical counterparts was carried out. For every HI detection that fell in the SDSS Data Release 2 (DR2) area we found an optical counterpart. Thus in Section 3.4 I present the optical catalogue for the ES subsample of 201 objects in Table 3.2. In order to compare our HI selected results to those of a comparable optically selected sample, in Section 3.5 I present such an optically selected sample obtained from the ESO-LV catalogue. Section 3.6 presents the correlations in the optical data both for the ES and OC samples. Finally, in Section 3.7 I present a qualitative discussion of the properties of the LSB galaxies in the ES sample.

3.2 Acquisition of optical data for the ES sample

3.2.1 The Sloan Digital Sky Survey (SDSS)

The optical data for this study comes from the Sloan Digital Sky Survey (SDSS; York *et al.* 2000; Gunn *et al.* 1998; Fukugita *et al.* 1996; Hogg *et al.* 2001; Smith *et al.* 2002; Pier *et al.* 2003) Data Release 2 (DR2; Abazajian *et al.* 2004) sky area. The DR2 area covers 3324 deg^2, about half of which overlaps with the searched HIPASS region discussed in Chapter 2 (see Figure 3.1).

The SDSS data is taken in five photometric bands (ugriz) and has point source magnitude limits of 22.0, 22.2, 22.2, 21.3 & 20.5 respectively at the 95% completeness level. The pixel scale of SDSS is 0.396″per pixel and the average seeing is 1.4″. The time delay and integrate (TDI) method for SDSS observations allows for extremely accurate flatfielding, and photometric calibration at the 2–3% level. Automatic pipelines reduce the raw data and store the derived quantities in catalogue tables.

The SDSS provides high quality photometry and spectroscopy for millions of astronomical objects. However, the publicly available photometric pipelines for galaxies with large angular extent are unreliable. The photometric software developed for SDSS was optimised for studying large scale structure traced by marginally resolved galaxies and there are several problems that occur when examining more extended nearby galaxies. At present, astronomers either incorrectly include this problematic data in their analysis of nearby galaxies or completely ignore objects closer than $z < 0.02$ to minimise their impact (Blanton *et al.* 2004). However, due to the extremely high quality of the SDSS data new tools and techniques can be developed to properly analyse nearby galaxies. Therefore, aside from the initial catalogue-matching described below, no SDSS catalogue data

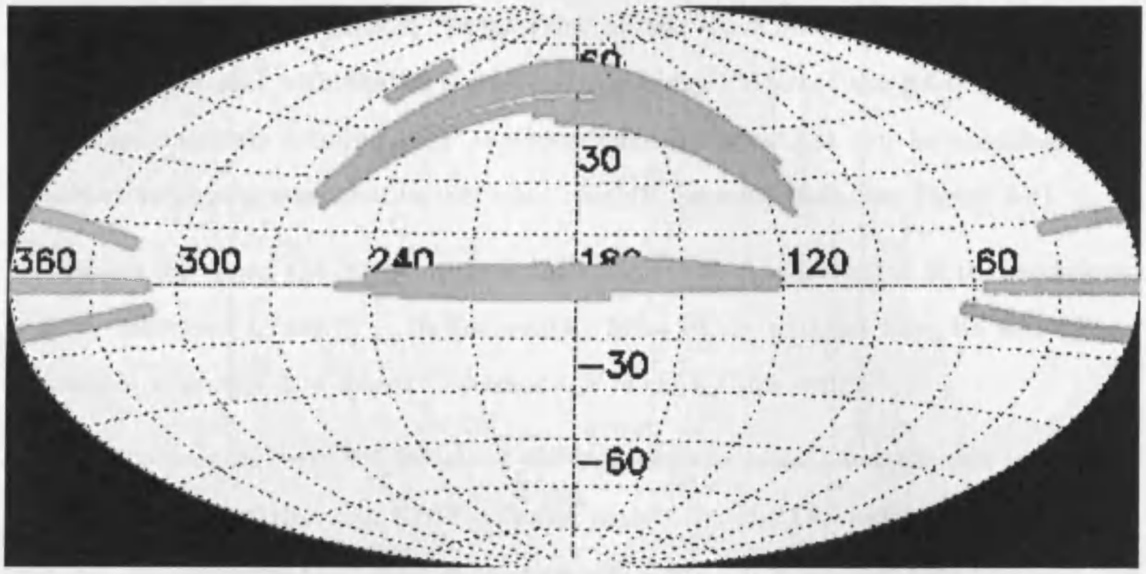

Figure 3.1: Area covered by the SDSS Data Release 2 (DR2).

was used for this study. All photometric quantities were obtained from the SDSS data using a new set of techniques optimised for reducing large galaxy photometry developed by Andrew West at the University of Washington who is my US counterpart in the ES project.

3.2.2 Matching and Confirmation of optical counterparts

Matching an HI sample with a beam size of $\sim$ 14 arcmin with an optical sample with arcsecond positional accuracy is not a trivial task. First the DR2 files for all SDSS sources within 10′ of the ES source positions. Over 1.16 million SDSS objects were found inside the HIPASS source beam areas. At every ES source position, the candidate SDSS objects were visually inspected and potential counterpart galaxies were identified. In order to be included in the final sample used in this thesis each candidate galaxy had to meet 4 selection criteria:

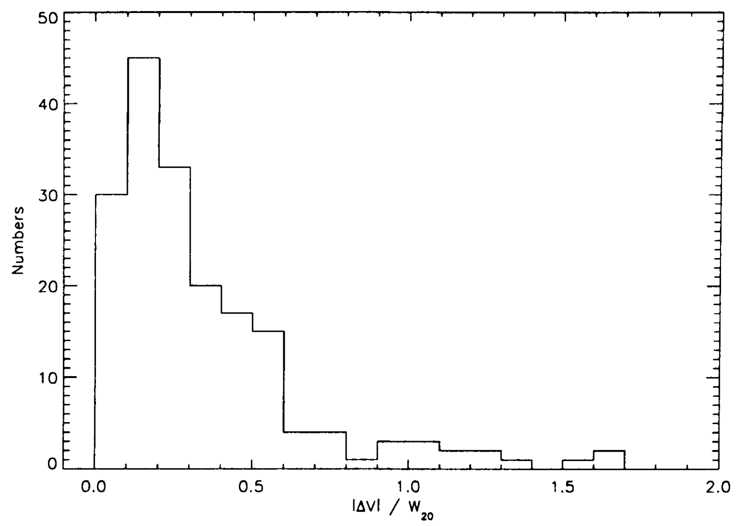

Figure 3.2: Distribution of the ratio of the absolute value of the recessional velocity difference to W_{50} HI line width for the ES galaxies that had SDSS spectra. Most of the galaxies have HI and optical velocities that match within half of the HI line width

1. The ES recessional velocity must agree to within twice the HI velocity width at 50% (W_{50}) value of the optically derived redshift (see Figure 3.2).

2. There must be no more than 1 detectable galaxy within the HIPASS beam at the same redshift.

3. The candidate galaxy must not extend across two or more SDSS fields.

4. All galaxies must be at least $1'$ away from any saturated foreground stars.

To test the first criterion, we obtained an optical redshift for each candidate galaxy. SDSS spectra were available for $\sim$ 80% of the candidate galaxies and redshifts were easily calculated from them. For the remaining candidates, we searched the NED database and acquired redshifts for all but $\sim$ 20 galaxies. The remaining sources were spectroscopically observed using the Apache Point Observatory's (APO) ARC 3.5m telescope. All of the sources were observed with long integrations on the Dual Imaging Spectrograph (DIS) with a 1.5″ slit and with the high resolution gratings. Most of the galaxies in the ES sample are currently forming stars and have emission lines that can be unambiguously identified and easily measured for accurate redshift determination (see Figure 3.4).

Figure 3.2 shows the distribution of the ratio of the absolute value of the recessional velocity difference to the W_{50} HI line width. Most of the galaxies have HI and optical recessional velocities that match to within half of the HI line width.

After obtaining redshifts for all of the candidate sources, we were able to identify 310 HIPEQ sources that had SDSS galaxies within the HIPASS beam and at the same redshift. It is important to note that *every* ES source in the SDSS area available was found to have an optical counterpart though it does not follow, because of clustering, that every optical counterpart is necessarily the 'true' match. Some could be invisible dark clouds or galaxies.

Of these 310 sources, 87 did not meet the second criterion, i.e. they had multiple SDSS galaxies within a single HIPASS beam. Some of these sources had as many as 5 galaxies at the same redshift. This criterion was applied because of the importance in knowing accurately the quantity of HI in each individual galaxy. With multiple galaxies in the HIPASS beam, only the total HI of the group is measured and not that of the individual galaxies. To avoid this spatial confusion, interferometrical HI observations would be needed to achieve much higher spatial resolution.

Twenty of the galaxies were positioned in such a way and/or had angular extents so large that they fell over multiple SDSS fields (criterion 3). At the time of sample selection, no techniques were available to accurately obtain the photometry for galaxies with flux spread over multiple fields.

Three additional galaxies were removed because of their close proximity to saturated foreground stars (criterion 4). The stars were close enough to the galaxies that scattered light would greatly affect galaxy photometry.

The ES subsample with optical counterparts therefore consists of the remaining 201 galaxies that passed all four selection criteria. Throughout the rest of this thesis, unless otherwise stated, any reference to the 'ES sample' will refer to this subsample with optical data. In the future this sample will be much larger as work on obtaining further SDSS counterparts is ongoing, with the aim ultimately obtaining optical counterparts for all the 1077 galaxies in the HI full ES sample. Their survey names, central SDSS positions, other catalogue names, and morphological types from NED can be found in Appendix C. The position centres are those used for photometry. Optical images and the HI spectrum for each source can be found in Appendix D.

Figure 3.3 shows the distribution of the position differences between the HI and optical. Most of the SDSS sources fall within $2'$ of the HIPASS position. This is consistent with the positional uncertainty in the HI of $1.3'$ found by both Meyer *et al.* (2003) and Zwaan *et al.* (2004). Figure 3.3 demonstrates the challenge of matching two surveys with drastically different angular resolutions. The observation of significant offsets in the central positions of some sources may suggest that the peak HI and peak optical positions differ by as much as a few arcminutes. HI synthesis data are required to further investigate this.

159 of the 201 galaxies have SDSS fibre spectra. The spectra were identified by visually inspecting each galaxy. Because of the deblending problems some of the galaxies have multiple spectra (as many as 5). Although these spectra are useful for obtaining redshifts, and isolated metallicity information, their small apertures ($3''$) and irregular placement make them highly susceptible to aperture effects. Because the spectral targeting engine places the fibres on both central bulges and HII regions, the spectra do not provide a uniform method of examining the global spectroscopic properties of these galaxies. We will therefore not include any analysis of the spectral data in this thesis but they will be

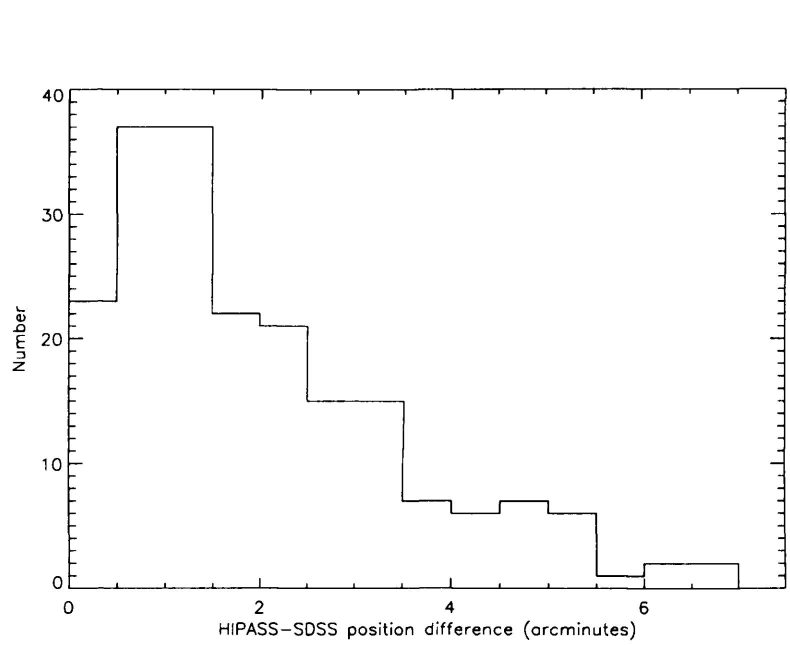

Figure 3.3: Distribution of the ES central position differences. Most of the sources fall within 2′ of the HIPEQ position. This is consistent with the positional uncertainty of 1.3′ found for HIPASS sources (Meyer *et al.* 2003, Zwaan *et al.* 2004).

used in further future analysis of the sample. A typical optical fibre spectrum is shown in Figure 3.4.

3.2.3 Photometric corrections

The photometry used in this thesis uses a modified Petrosian system (Petrosian 1976), see Lupton *et al.* (2001) for more details. This photometry method recovers most of the galaxy flux for a variety of morphological types and is robust against most changes in the surface-brightness profile. This method has fewer biases than measuring total galaxy flux with apertures based on isophotes or fractions of the central surface brightness. Elliptical apertures are used for those galaxies with high quality fits, otherwise circular apertures are utilised for the photometric pipeline.

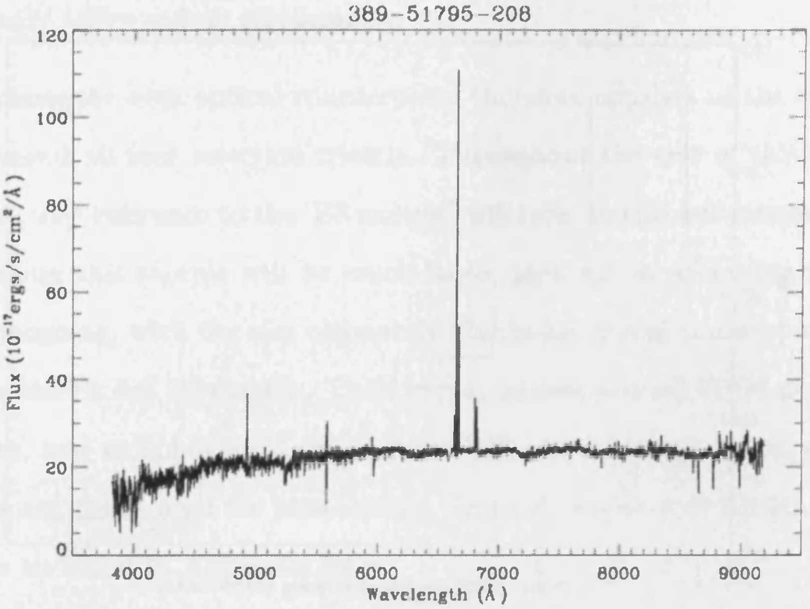

Figure 3.4: Optical Spectrum for galaxy HIPEQ0014-00.

Extinction corrections

The photometric magnitudes have been corrected for both extinction from the Milky Way as well as the internal extinction from the extragalactic object itself. The amount of Galactic extinction is determined using the Milky Way dust maps of Schlegel & Davis (1998). For the internal extinction we use the method of Tully *et al.* (1998) and calculate the internal extinction of a face-on galaxy in the I-band (γ_I), using the equation:

$$\gamma_I = 0.92 + 1.63(log(2V_{rot}) - 2.5) \tag{3.1}$$

where V_{rot} is the inclination corrected velocity width at 50% (W_{50}) derived in Chapter 2. Several galaxies have large uncertainties in the axis ratios and therefore do not have well measured inclinations which adds to the uncertainty of V_{rot}. We have then assumed an inclination of 60 degrees (the average inclination of a randomly aligned sample) for all the

Band	conversion
B =	*g + 0.39 (g - r) + 0.21*
V =	*r - 0.58 (g - r) - 0.01*
R =	*r - 0.15 (g - r) - 0.14*

Table 3.1: SDSS-Johnson filter conversion from Cross *et al.* 2004

galaxies in the sample. The value γ_I is corrected for inclination using:

$$A_I = \gamma_I \; log\left(\frac{1}{b/a}\right) \tag{3.2}$$

where b/a is the axis ratio of the galaxy. We then convert the I extinction to the SDSS bands from the relation in Schlegel *et al.* (1998). The extinction avlues values relative to I-band for u, g, r, i and z are: 2.66, 1.95, 1.42, 1.07 and 0.763 respectively. The inclination for the galaxies have been obtained using $sin(i) = 1 - cos(i)$ where

$$cos(i) = \frac{(1 - ecc^2) - 0.16^2}{1 - 0.16^2} \tag{3.3}$$

and ecc is the eccentricity found for each galaxy.

Other corrections

Out of the 201 galaxies, 34 were close to the edge of an SDSS field but were included in the sample because the majority of their light falls within one SDSS field. The optimal way to correct for this would be to mosaic the adjacent fields and re-do the photometry on the mosaicked images. The SDSS team is currently working on this process and it will be implemented at a later date. However, we are confident that the parameters currently available for those 34 galaxies are more than adequate for the purpose of this study.

Although the ES sample is nearby (< 12700 km s^{-1}), k-corrections become important for precise photometry of the more distant galaxies in the sample. We use the Blanton *et al.* (2003) convention to k-correct all of the galaxies in the sample to z = 0.

3.2.4 Conversion to the standard colour convention

Although we obtain 5 colours from the SDSS photometry (ugriz), for this study we have decided to convert those colours into the standard B,V,R Johnson filter convention to facilitate comparison with previous survey results. We use the conversions from Cross *et al.* (2004) which yields very accurate results which were derived from high-precision photometry comparison between different surveys, see Table 3.1.

3.3 The ES sample Optical Data

As discussed in the previous section, out of 1077 sources we obtained optical data for 201 sources which fulfilled our selection criteria. The optical properties of these ES sample galaxies are given in Table 3.2.

Column 1 of this table gives the ES sample ID as given in Table 2.2. Columns 2–4 give the R.A. optical position of the galaxies. Columns 5–7 give the Declination optical position of the galaxies. Column 8 gives the apparent magnitude (m_B) in the B band, converted from the Sloan colour convention using the conversion described in Table 3.1. Columns 9 and 10 give the effective radius (r_{eff}), enclosing half the light of the galaxy in arcseconds , and the effective surface brightness (μ_{eff} – i.e the surface-brightness at this radius). The effective surface brightness is the measured surface brightness within R50 which is the radii at 50% of the Petrosian flux. It is defined by taking half of the Petrosian flux and divinding by the elliptical aperture area with a semi-major axis equal to the elliptical R50. Column 11 gives the central surface-brightness (μ_0) which is defined as the surface brightness within a 3″ circular radius that is placed at the centre of each galaxy.

The positions for the centre are determined by the Sersic fit for each galaxy. No corrections for correction were made and simply measured the flux inside the fiber and divide by the circular fiber area. Column 12 gives the galaxy inclination in degrees. Columns 13 and 14 give the B−R and B−V colours respectively. The absolute magnitude (M_B) in the B band is given in Column 15. Column 16 gives the physical effective radius (R_{eff}) in kpc, calculated from the distance and r_{eff} using the distances given in Table 2.2 and Appendix B. Column 17 gives the HI Mass to B-band Luminosity ratio in solar units.

The HI properties for this subsample of 201 galaxies with optical data can be found in Appendix B. The SDSS and other catalogue names (e.g. UGC, NGC) for the 201 optical counterparts, along with Hubble types (taken from NED and the Lyon-Meudon Extragalactic Database (LEDA)) are given in Appendix C.

Table 3.2: Optical Properties of ES sources (See bottom of the Table for key)

ID Name	α_{J2000} h m s			δ_{J2000} ° ′ ″			m_B	r_{eff}	μ_{eff}	μ_0	Inc °	B-R	B-V	M_B	R_{eff} kpc	M_{HI}/L_B
1	2	3	4	5	6	7	8	9	10	11	12	13	14	15	16	17
HIPEQ0014-00	00	14	36	-00	44	42	14.11	27.0	22.40	20.81	54.7	0.93	0.59	-19.30	6.3	1.12
HIPEQ0027-01a	00	27	47	-01	09	39	15.02	22.6	22.75	21.38	60.5	0.95	0.60	-18.35	5.2	1.00
HIPEQ0033-01	00	33	22	-01	07	01	15.40	23.6	24.14	22.43	40.8	0.85	0.53	-16.30	2.5	3.70
HIPEQ0043-00	00	43	31	-00	06	49	13.72	15.6	21.25	19.74	33.8	1.15	0.73	-19.83	3.9	0.63
HIPEQ0051-00	00	51	57	-00	28	25	15.31	5.3	20.20	19.36	48.6	1.04	0.66	-15.87	0.4	2.94
HIPEQ0058+00	00	58	50	00	37	46	14.33	11.3	21.55	20.03	3.0	1.08	0.68	-19.83	3.7	0.40
HIPEQ0107+01	01	07	45	01	03	56	15.28	9.7	22.18	21.19	9.1	0.77	0.49	-12.76	0.2	0.73
HIPEQ0119+00	01	19	56	00	44	07	17.39	8.3	23.89	23.10	37.3	0.83	0.52	-16.27	2.2	1.37
HIPEQ0120-00	01	20	14	-00	11	35	15.56	17.7	22.65	22.22	64.0	0.95	0.60	-15.81	1.6	0.97
HIPEQ0122+00	01	22	09	00	56	27	13.03	57.9	22.27	21.43	75.8	0.91	0.58	-19.13	7.6	0.81
HIPEQ0123-00	01	23	07	-00	23	54	14.51	14.8	22.28	20.19	7.1	0.99	0.62	-20.39	6.8	0.28
HIPEQ0126+00a	01	26	33	00	32	58	17.19	10.3	24.11	23.21	25.0	0.88	0.56	-16.99	3.4	2.16
HIPEQ0126-00b	01	26	53	-00	39	37	16.01	3.9	20.91	20.13	33.2	0.64	0.40	-15.64	0.4	1.24
HIPEQ0154-00	01	54	55	-00	05	36	14.58	8.9	21.15	19.02	16.0	1.56	0.98	-19.74	3.2	0.38
HIPEQ0222-00	02	22	42	-00	38	31	15.42	33.1	22.92	22.37	90.0	0.99	0.62	-15.77	2.8	1.58
HIPEQ0228-01	02	28	18	-01	09	19	13.02	27.5	22.20	20.15	3.2	0.94	0.59	-18.29	2.4	0.38
HIPEQ0230+00	02	30	19	00	56	07	16.13	18.8	24.32	24.17	37.7	1.44	0.91	-15.05	1.6	0.58
HIPEQ0230-01	02	30	37	-01	05	52	12.95	16.6	20.08	18.15	58.2	1.53	0.96	-18.20	1.4	0.18
HIPEQ0231+00	02	31	42	00	53	23	15.57	15.7	22.96	21.78	40.9	0.90	0.57	-18.97	6.1	1.06
HIPEQ0236+00	02	36	18	00	45	44	15.41	16.8	22.22	21.53	68.8	1.31	0.82	-19.35	7.3	1.52
HIPEQ0238+00	02	38	45	00	31	28	16.75	14.6	24.35	23.22	43.6	0.60	0.38	-14.33	1.2	5.06
HIPEQ0240+01	02	40	18	01	14	37	16.40	20.7	24.61	23.87	31.6	0.52	0.33	-14.12	1.3	3.11
HIPEQ0241+00	02	41	44	00	26	56	11.52	108.6	22.51	20.59	65.3	1.55	0.98	-18.54	5.4	0.72
HIPEQ0244+00	02	44	10	00	43	30	15.54	21.7	23.01	22.39	65.3	0.96	0.61	-17.14	3.6	0.73
HIPEQ0246-00a	02	46	30	-00	14	09	12.67	45.8	22.23	20.02	49.8	1.23	0.77	-19.99	7.5	0.48
HIPEQ0246-00b	02	46	25	-00	30	46	11.50	40.1	21.34	19.10	15.2	1.00	0.63	-19.70	3.4	0.19
HIPEQ0249-00	02	49	33	-00	37	04	14.90	13.5	22.27	19.56	22.6	1.14	0.72	-19.77	5.6	0.36
HIPEQ0249-00a	02	49	15	-00	23	42	16.19	20.0	23.87	22.90	48.5	0.62	0.39	-16.39	3.2	1.09
HIPEQ0249-00b	02	49	48	-00	53	03	13.92	15.6	21.52	19.00	29.3	1.23	0.77	-20.90	6.9	0.43
HIPEQ0251-01	02	51	53	-01	10	02	14.67	44.2	23.68	23.04	63.8	0.79	0.50	-16.52	3.7	3.06

Table 3.2: Optical Properties of ES sources (continued)

ID Name	α_{J2000} h m s			δ_{J2000} ° ′ ″			m_B	r_{eff}	μ_{eff}	μ_0	Inc °	B-R	B-V	M_B	R_{eff} kpc	$M_{\rm HI}/L_B$
1	2	3	4	5	6	7	8	9	10	11	12	13	14	15	16	17
HIPEQ0300+00	03	00	27	00	00	15	15.51	20.3	22.73	22.04	69.1	0.88	0.55	-17.23	3.5	2.36
HIPEQ0301-00	03	01	03	-00	44	58	15.11	18.2	22.75	21.50	44.9	0.66	0.41	-17.46	2.9	1.07
HIPEQ0306-00	03	06	53	-00	47	53	13.22	11.7	20.37	18.32	16.1	1.47	0.93	-19.81	2.3	0.38
HIPEQ0316-00	03	16	44	-00	28	05	14.91	20.8	22.24	20.89	67.6	1.29	0.81	-19.88	9.1	0.23
HIPEQ0320-06	03	20	04	-06	12	30	13.45	14.9	20.57	19.31	49.1	1.06	0.67	-18.86	2.1	0.66
HIPEQ0351-00	03	51	23	-00	28	57	15.20	6.0	20.57	19.22	37.7	1.12	0.71	-20.24	3.6	0.67
HIPEQ0809+00	08	09	27	00	34	20	14.20	20.0	22.16	20.62	40.1	0.90	0.57	-18.00	2.7	0.38
HIPEQ0821+03b	08	21	44	03	21	54	14.28	13.1	21.41	19.59	34.1	1.24	0.78	-19.55	3.7	0.52
HIPEQ0821-00	08	21	40	-00	26	05	15.53	9.8	22.46	20.85	52.0	0.57	0.36	-16.69	1.3	3.31
HIPEQ0822-00	08	22	21	-01	02	11	14.53	19.8	22.17	20.29	53.0	1.01	0.64	-19.51	6.1	0.56
HIPEQ0825-00	08	25	00	-00	35	50	13.86	24.0	21.76	19.91	59.4	1.53	0.96	-20.37	8.2	0.63
HIPEQ0855+02	08	55	52	02	30	37	14.87	35.9	23.87	21.83	47.3	0.85	0.54	-18.83	9.6	0.74
HIPEQ0856+00	08	56	30	00	22	03	14.23	21.4	22.67	21.01	17.5	0.78	0.49	-18.65	3.9	0.67
HIPEQ0923-00	09	23	23	-00	43	47	14.69	20.0	22.02	20.93	64.8	0.82	0.51	-18.86	4.9	1.05
HIPEQ0930+04	09	30	21	04	09	21	14.36	26.0	22.58	20.72	54.0	1.12	0.71	-20.03	9.5	0.49
HIPEQ0936+01	09	36	45	01	13	29	17.09	3.6	21.84	21.42	66.4	0.63	0.40	-17.15	1.2	11.53
HIPEQ0942+00	09	42	02	00	20	33	12.01	31.3	21.34	19.33	13.6	1.08	0.68	-20.36	4.5	0.56
HIPEQ0944-00b	09	44	43	-00	40	20	16.03	12.7	22.92	21.97	43.0	0.76	0.48	-15.57	1.3	2.50
HIPEQ0945+01	09	45	55	01	40	52	13.31	35.2	21.61	20.69	71.8	1.07	0.67	-19.03	5.0	0.52
HIPEQ0946+02	09	46	11	02	57	21	15.11	35.2	23.50	22.05	68.5	0.96	0.60	-17.31	5.2	2.20
HIPEQ0947+00a	09	46	52	00	30	51	14.41	31.6	22.89	21.56	58.6	1.00	0.63	-17.85	4.3	1.66
HIPEQ0947+00b	09	47	14	00	55	43	15.38	26.0	23.61	22.19	48.5	0.78	0.49	-16.96	3.7	1.70
HIPEQ0953+01	09	53	43	01	35	13	12.46	73.5	21.37	20.57	90.0	0.99	0.62	-19.23	7.8	0.79
HIPEQ0954+02a	09	54	14	02	17	14	14.62	15.4	22.52	21.09	2.3	0.80	0.50	-20.44	7.7	0.38
HIPEQ0955+04a	09	55	22	04	15	57	12.64	29.7	21.16	18.83	53.7	1.02	0.64	-19.66	4.2	0.19
HIPEQ0958+01	09	58	33	01	41	53	17.26	13.2	24.56	24.35	47.7	0.47	0.29	-15.04	1.8	6.95
HIPEQ1000+03	10	00	46	03	20	13	14.07	23.5	21.58	20.16	70.0	1.35	0.85	-18.47	3.7	1.45
HIPEQ1010+05	10	10	25	05	08	40	15.51	6.3	21.46	20.10	36.5	1.05	0.66	-18.37	1.8	1.35
HIPEQ1014+03	10	14	12	03	28	27	11.17	65.3	21.61	18.79	45.1	1.45	0.91	-20.44	6.6	0.51
HIPEQ1015+02	10	15	51	02	42	36	15.03	40.1	23.91	22.26	61.2	0.68	0.43	-16.66	4.2	1.94

Table 3.2: Optical Properties of ES sources (continued)

ID	α_{J2000}			δ_{J2000}			m_B	r_{eff}	μ_{eff}	μ_0	Inc	B-R	B-V	M_B	R_{eff}	M_{HI}/L_B
Name	h m s			°′″							°				kpc	
1	2	3	4	5	6	7	8	9	10	11	12	13	14	15	16	17
HIPEQ1026+03	10	26	44	03	51	28	13.55	34.3	22.42	20.78	51.8	0.86	0.54	-19.08	5.6	0.87
HIPEQ1028+03	10	28	33	03	36	43	15.54	25.3	22.65	22.35	83.6	0.50	0.32	-15.98	2.5	1.10
HIPEQ1031+04	10	31	15	04	28	06	13.95	57.8	22.80	21.57	86.1	0.63	0.40	-17.60	5.7	1.87
HIPEQ1039+01	10	39	20	01	42	41	14.88	12.8	22.40	21.89	19.6	0.92	0.58	-15.90	0.9	0.54
HIPEQ1041+00	10	41	53	00	47	35	14.91	15.5	22.63	21.29	19.1	0.93	0.58	-19.61	6.0	0.63
HIPEQ1046+01	10	46	14	01	49	07	13.27	63.4	22.40	20.87	83.6	1.10	0.69	-18.01	5.5	1.41
HIPEQ1050+01	10	50	05	01	16	06	17.52	10.2	23.54	23.19	58.4	1.06	0.66	-14.57	1.3	5.97
HIPEQ1051+04a	10	51	39	04	35	27	14.43	26.7	22.62	21.54	57.2	0.94	0.59	-16.93	2.4	1.01
HIPEQ1052+00	10	52	52	00	02	48	15.60	4.7	20.32	19.83	43.1	0.80	0.50	-16.72	0.7	1.47
HIPEQ1053+02	10	53	14	02	34	14	15.78	9.0	22.53	22.04	55.7	0.60	0.38	-15.60	0.8	2.74
HIPEQ1055+02	10	55	37	02	25	26	16.22	6.3	22.17	20.85	49.2	0.57	0.36	-15.15	0.6	1.57
HIPEQ1101+03	11	01	14	03	38	08	12.12	77.7	21.94	20.61	77.3	0.96	0.61	-19.37	7.5	0.38
HIPEQ1109-00	11	09	27	-00	04	53	14.58	14.2	21.43	20.13	56.2	1.27	0.80	-19.17	3.9	2.02
HIPEQ1110+01	11	10	55	01	08	14	15.94	9.7	22.84	21.88	68.5	0.78	0.49	-15.36	0.9	1.88
HIPEQ1113+05	11	13	01	05	16	55	14.73	15.1	22.29	21.39	27.4	0.62	0.39	-18.21	2.8	0.47
HIPEQ1117+04a	11	17	25	04	35	01	12.95	12.1	20.06	17.54	24.3	1.21	0.76	-19.12	1.5	0.33
HIPEQ1119+02	11	20	12	02	32	56	13.81	31.2	23.24	22.14	36.1	0.66	0.42	-18.29	4.0	1.07
HIPEQ1124+03	11	24	28	03	18	09	13.20	32.3	22.73	21.14	67.9	0.68	0.43	-18.63	3.6	0.67
HIPEQ1127-01	11	27	05	-00	58	37	14.71	19.0	22.86	21.29	20.6	0.92	0.58	-16.54	1.6	1.02
HIPEQ1131-02	11	31	28	-02	17	40	13.43	29.0	22.68	20.35	4.3	1.03	0.65	-20.74	9.6	0.65
HIPEQ1133-03	11	33	46	-03	25	13	14.90	22.6	23.01	22.28	44.7	0.79	0.50	-17.21	2.9	2.11
HIPEQ1136+00	11	36	30	00	49	40	14.96	5.7	20.72	20.49	55.9	0.51	0.32	-16.50	0.5	0.98
HIPEQ1138+03	11	38	49	03	35	48	14.80	13.4	22.29	19.40	12.6	1.25	0.79	-19.70	5.1	0.67
HIPEQ1143-01	11	43	56	-01	15	45	17.83	9.0	24.39	24.24	30.4	0.75	0.47	-14.38	1.2	2.33
HIPEQ1145+02	11	45	03	02	10	25	17.31	16.3	24.83	24.72	40.0	0.76	0.48	-14.00	1.4	6.99
HIPEQ1148-02	11	48	48	-02	02	14	14.17	38.2	23.47	20.93	41.6	0.85	0.54	-18.07	5.2	1.96
HIPEQ1151-02	11	51	55	-02	38	23	15.41	9.5	21.55	20.81	49.4	0.97	0.61	-18.35	2.6	1.45
HIPEQ1152+01	11	52	20	01	44	49	14.48	16.3	22.11	19.79	33.4	0.88	0.56	-20.21	6.9	0.47
HIPEQ1152-02	11	52	49	-02	28	52	14.51	4.9	19.95	19.68	48.6	0.41	0.26	-16.88	0.5	0.71
HIPEQ1152-03b	11	52	33	-03	40	36	14.66	19.3	23.06	22.37	29.1	0.75	0.47	-17.48	2.5	0.64

Table 3.2: Optical Properties of ES sources (continued)

ID	α_{J2000}			δ_{J2000}			m_B	r_{eff}	μ_{eff}	μ_0	Inc	B-R	B-V	M_B	R_{eff}	M_{HI}/L_B
Name	h m s			° ′ ″							°				kpc	
1	2	3	4	5	6	7	8	9	10	11	12	13	14	15	16	17
HIPEQ1155+01	11	55	35	01	15	24	13.47	47.4	23.38	21.05	34.5	1.07	0.67	-18.92	6.9	0.51
HIPEQ1200-00	12	00	43	-00	00	16	15.40	33.3	24.31	22.17	38.6	0.95	0.60	-17.04	4.9	1.51
HIPEQ1200-01	12	00	24	-01	05	13	11.06	40.4	20.89	18.49	18.7	1.26	0.79	-20.87	4.8	0.26
HIPEQ1202+01	12	02	38	01	59	55	12.67	25.3	21.59	18.70	8.6	1.43	0.90	-19.80	3.8	0.33
HIPEQ1204-01	12	04	16	-01	32	15	15.71	23.4	24.36	23.80	19.7	0.85	0.54	-16.23	2.8	2.53
HIPEQ1204-02	12	04	47	-02	43	13	14.76	14.7	22.40	19.54	17.5	1.32	0.83	-19.88	6.0	0.39
HIPEQ1210+02	12	10	57	02	01	49	15.62	23.2	24.27	23.36	12.1	0.90	0.57	-16.15	2.5	2.82
HIPEQ1215+04a	12	15	50	04	41	27	15.06	12.8	21.68	20.91	56.4	0.77	0.48	-17.59	2.1	0.61
HIPEQ1216-03	12	15	56	-03	35	08	14.75	15.2	22.63	20.86	0.7	0.98	0.62	-19.58	5.4	0.68
HIPEQ1218+00	12	17	56	00	27	29	15.51	26.4	24.40	23.38	37.7	1.02	0.64	-15.67	2.2	5.03
HIPEQ1218-01	12	18	11	-01	04	50	14.66	13.1	21.70	20.39	39.7	1.24	0.78	-19.87	5.1	1.01
HIPEQ1219+03	12	19	00	03	58	34	14.35	11.9	21.56	19.61	14.4	0.88	0.56	-17.64	1.4	0.17
HIPEQ1220+00	12	20	19	00	20	35	15.89	19.2	22.90	22.59	71.1	0.57	0.36	-15.21	1.5	1.54
HIPEQ1220+01	12	20	29	01	27	36	15.13	30.1	22.35	21.61	90.0	0.99	0.62	-16.95	3.8	1.04
HIPEQ1221+03	12	21	01	03	44	00	14.46	29.0	22.35	20.53	72.1	1.50	0.95	-18.49	5.5	1.41
HIPEQ1223-03b	12	23	54	-03	24	47	13.19	31.5	21.18	19.88	74.1	1.44	0.91	-19.29	4.8	0.31
HIPEQ1224+00	12	23	59	00	33	06	17.45	9.4	24.17	23.70	19.3	0.87	0.55	-15.08	1.5	11.38
HIPEQ1224+03b	12	24	41	03	18	53	14.20	21.6	22.86	20.99	19.0	0.85	0.53	-16.94	1.8	0.77
HIPEQ1225+00	12	25	26	00	34	59	13.18	22.7	21.55	17.93	32.4	1.19	0.75	-19.43	3.7	0.12
HIPEQ1226+02	12	26	54	02	30	51	12.85	23.2	20.76	20.07	56.4	1.03	0.65	-19.32	3.0	0.29
HIPEQ1227+01	12	27	35	01	34	12	16.61	14.0	24.20	23.72	42.1	0.53	0.33	-15.08	1.5	21.89
HIPEQ1228+02	12	28	55	02	44	31	14.78	41.3	23.71	22.72	62.6	0.83	0.52	-17.25	5.1	1.64
HIPEQ1228+03	12	28	58	03	35	29	11.67	21.0	20.02	16.92	22.0	1.43	0.90	-19.43	1.7	0.05
HIPEQ1229+00	12	29	46	00	51	31	17.00	15.9	23.19	22.90	81.0	1.01	0.64	-15.69	2.6	4.09
HIPEQ1230+02	12	30	13	02	38	20	15.61	14.6	23.39	23.03	48.6	0.64	0.40	-16.50	1.9	0.96
HIPEQ1230+03	12	30	33	03	35	00	15.85	5.6	21.56	20.72	33.8	0.63	0.40	-18.51	2.0	1.37
HIPEQ1232+00a	12	32	31	00	24	04	13.16	61.9	23.44	22.00	45.4	0.96	0.60	-18.82	7.5	1.14
HIPEQ1232+00b	12	32	44	00	07	36	11.38	182.2	22.42	21.70	90.0	1.38	0.87	-20.09	17.4	0.63
HIPEQ1233-02	12	33	34	-02	38	05	15.17	31.6	24.42	23.84	40.4	0.96	0.61	-17.71	5.8	1.17
HIPEQ1236+03	12	36	33	03	07	11	16.11	21.1	23.36	22.78	69.4	0.80	0.50	-15.77	2.4	2.69

Table 3.2: Optical Properties of ES sources (continued)

ID Name	α_{J2000} h m s			δ_{J2000} ° ′ ″			m_B	r_{eff}	μ_{eff}	μ_0	Inc °	B-R	B-V	M_B	R_{eff} kpc	M_{HI}/L_B
1	2	3	4	5	6	7	8	9	10	11	12	13	14	15	16	17
HIPEQ1239-00	12	39	17	-00	31	24	12.32	51.9	21.56	20.65	69.7	0.87	0.55	-19.06	4.7	2.01
HIPEQ1241+01	12	41	01	01	24	25	15.01	8.2	21.03	20.30	40.3	1.04	0.65	-17.16	1.1	1.39
HIPEQ1241-02	12	41	21	-02	59	51	14.86	15.4	21.74	20.73	61.0	1.06	0.67	-17.02	1.8	0.63
HIPEQ1242+03b	12	42	36	03	58	08	13.07	26.9	21.68	19.57	39.2	1.20	0.75	-17.72	1.9	0.17
HIPEQ1242-00	12	42	21	-00	03	38	12.31	41.0	21.29	20.87	62.1	1.06	0.67	-19.88	5.4	0.49
HIPEQ1242-01a	12	42	21	-01	21	39	14.09	19.1	22.16	21.06	27.1	0.83	0.52	-17.33	1.8	1.36
HIPEQ1242-01b	12	42	59	-01	12	38	14.12	34.1	22.36	21.21	71.8	1.14	0.72	-19.25	7.8	1.54
HIPEQ1243-00	12	43	57	-00	35	35	12.83	42.1	22.60	20.55	28.2	1.00	0.63	-20.16	8.1	0.43
HIPEQ1244+00	12	44	36	00	28	10	13.73	57.5	23.63	22.04	54.4	0.74	0.46	-17.79	5.6	0.34
HIPEQ1244-02	12	44	27	-02	18	55	15.19	24.6	23.55	22.10	40.3	0.73	0.46	-16.86	3.1	1.75
HIPEQ1245-00	12	45	16	-00	27	55	11.49	58.6	21.09	19.56	67.3	1.47	0.93	-20.47	7.0	0.45
HIPEQ1249+03	12	49	08	03	23	20	12.86	19.2	20.95	19.40	26.5	0.94	0.59	-17.89	1.3	1.13
HIPEQ1249+04	12	49	15	04	35	58	15.38	21.1	23.37	22.03	42.5	0.70	0.44	-17.63	4.1	1.54
HIPEQ1250+05	12	50	00	05	19	34	12.17	33.8	21.47	19.79	28.1	0.82	0.52	-18.41	2.1	0.54
HIPEQ1253+01	12	53	28	01	15	21	12.80	47.5	21.71	20.52	73.3	1.35	0.85	-18.67	4.5	0.27
HIPEQ1253+02	12	53	36	02	11	21	12.06	35.3	21.67	18.44	12.3	1.44	0.91	-19.18	3.0	0.12
HIPEQ1253+04	12	53	11	04	28	10	13.39	9.4	19.57	18.41	46.8	0.80	0.51	-17.33	0.6	0.62
HIPEQ1255+00	12	55	08	00	09	26	12.83	44.3	22.95	20.24	9.8	1.04	0.65	-18.88	4.7	0.48
HIPEQ1255+02	12	55	17	02	52	27	13.92	12.8	20.34	19.00	63.3	1.40	0.88	-19.18	2.6	0.76
HIPEQ1255-00	12	55	40	-00	15	59	16.01	27.8	23.50	22.99	78.4	0.93	0.58	-15.42	2.6	1.30
HIPEQ1256+03	12	56	11	03	51	58	16.09	16.6	24.06	23.01	32.2	0.47	0.29	-14.50	1.1	6.13
HIPEQ1257+02	12	57	57	02	40	53	15.43	16.3	23.44	22.63	33.8	0.79	0.50	-15.69	1.3	1.07
HIPEQ1257-01	12	57	09	-01	42	02	14.12	26.2	21.67	20.83	74.9	1.12	0.70	-19.01	5.4	1.32
HIPEQ1258+02	12	58	34	02	49	25	14.48	36.8	23.37	21.23	56.2	0.85	0.54	-18.59	7.3	0.82
HIPEQ1300+02a	13	00	01	02	02	45	14.90	12.5	22.37	21.49	22.4	0.98	0.61	-16.13	1.0	0.37
HIPEQ1300+02b	13	00	39	02	30	31	11.86	37.3	21.30	18.76	32.7	0.98	0.62	-19.31	3.1	0.21
HIPEQ1303+03	13	03	09	03	59	38	14.61	24.3	23.45	21.76	4.7	0.77	0.48	-18.53	5.0	0.77
HIPEQ1304-02	13	04	30	-02	54	14	16.39	9.4	22.69	22.03	40.8	1.05	0.66	-15.25	1.0	3.35
HIPEQ1304-03	13	04	32	-03	33	58	13.06	58.8	23.56	22.84	25.9	0.72	0.45	-18.70	6.4	1.03
HIPEQ1307-00	13	07	42	-00	51	47	13.99	15.8	21.67	20.44	25.8	0.88	0.56	-20.43	5.9	0.78

Table 3.2: Optical Properties of ES sources (continued)

ID Name	α_{J2000} h m s			δ_{J2000} ° ′ ″			m_B	r_{eff}	μ_{eff}	μ_0	Inc °	B-R	B-V	M_B	R_{eff} kpc	M_{HI}/L_B
1	2	3	4	5	6	7	8	9	10	11	12	13	14	15	16	17
HIPEQ1308-02	13	08	40	-02	08	49	14.38	17.4	22.39	20.64	17.1	1.02	0.64	-20.01	6.4	0.64
HIPEQ1311+03a	13	11	28	03	25	01	15.84	11.1	21.73	21.05	69.4	0.84	0.53	-17.41	2.4	2.43
HIPEQ1312+03	13	12	06	03	08	37	15.18	8.4	21.28	19.52	37.9	1.22	0.77	-20.12	4.7	0.81
HIPEQ1312+05	13	12	06	05	30	45	16.72	12.7	24.09	23.42	49.8	0.68	0.43	-14.35	1.0	2.88
HIPEQ1313+06	13	13	12	06	04	09	14.28	15.2	22.03	19.92	13.9	1.20	0.76	-20.68	7.2	0.61
HIPEQ1317-00	13	17	32	-00	59	59	15.90	18.2	22.75	22.19	72.1	0.49	0.31	-15.67	1.8	1.68
HIPEQ1318-01	13	18	16	-01	13	19	14.22	21.8	22.66	20.55	20.7	1.14	0.72	-20.31	8.5	0.39
HIPEQ1320+05	13	20	36	05	24	51	15.25	21.6	22.69	22.08	66.7	1.03	0.65	-15.89	1.8	0.90
HIPEQ1327+02	13	26	20	02	06	42	16.58	10.5	23.62	23.09	59.7	0.62	0.39	-14.77	0.9	10.73
HIPEQ1329-00	13	29	30	-00	22	46	16.19	18.1	23.43	22.48	59.4	0.92	0.58	-17.19	4.1	3.05
HIPEQ1332+01	13	32	25	01	51	21	14.07	12.5	21.30	18.74	21.2	1.28	0.81	-19.32	2.9	0.26
HIPEQ1335+01	13	35	35	01	26	23	13.90	22.2	22.22	19.50	32.4	1.17	0.74	-20.45	7.9	0.40
HIPEQ1341+05	13	41	20	05	06	14	15.01	14.5	22.49	20.23	27.3	0.92	0.58	-19.93	6.8	1.29
HIPEQ1348+03	13	48	08	03	57	20	12.37	55.3	22.63	20.65	34.8	1.04	0.66	-19.05	5.1	0.18
HIPEQ1352+02a	13	52	52	02	46	43	13.53	34.5	22.82	19.21	32.0	1.36	0.85	-20.56	11.0	0.50
HIPEQ1352-01	13	52	54	-01	05	24	12.36	58.2	22.81	21.24	29.7	1.03	0.65	-19.38	6.3	0.39
HIPEQ1400+02	14	00	59	02	01	04	14.96	21.4	21.95	21.28	77.9	0.99	0.62	-18.61	5.4	1.11
HIPEQ1411-01	14	11	39	-01	09	19	12.97	70.7	22.35	21.37	82.6	0.85	0.53	-18.95	8.3	1.47
HIPEQ1415+04	14	15	30	04	23	55	15.35	7.5	21.63	20.44	4.8	0.86	0.54	-19.18	2.9	0.66
HIPEQ1416+03	14	16	55	03	49	15	16.41	15.4	24.18	24.26	90.0	0.92	0.58	-15.40	1.7	3.89
HIPEQ1422-00	14	22	26	-00	23	12	12.25	56.0	22.51	20.27	36.4	0.96	0.60	-19.75	6.8	0.34
HIPEQ1429-00	14	29	33	-00	00	50	14.33	23.5	22.50	21.13	46.7	0.75	0.47	-17.55	2.7	3.98
HIPEQ1432+00	14	32	29	00	16	19	14.45	23.7	21.61	20.74	79.0	1.14	0.72	-17.56	2.9	0.42
HIPEQ1433+01	14	33	40	01	30	50	17.06	17.7	24.75	23.87	64.8	0.52	0.33	-15.13	2.4	3.35
HIPEQ1433+02	14	33	13	02	55	29	14.81	13.7	21.96	20.56	38.9	0.71	0.45	-17.00	1.5	0.64
HIPEQ1437+02	14	37	42	02	18	12	12.66	51.1	21.63	20.93	75.8	1.49	0.94	-19.46	6.6	0.43
HIPEQ1437-00	14	37	50	-00	23	36	12.84	22.0	20.76	18.87	51.5	1.02	0.64	-19.41	3.0	0.12
HIPEQ1439+02	14	39	05	02	57	56	15.77	19.8	24.12	23.12	34.4	1.00	0.63	-16.13	2.3	1.84
HIPEQ1439-00	14	39	50	-00	41	19	13.30	54.6	23.00	21.12	58.4	0.95	0.60	-18.82	7.0	0.91
HIPEQ1440+02	14	40	54	02	10	55	14.27	13.7	21.50	20.63	34.7	0.77	0.48	-17.70	1.6	0.25

Table 3.2: Optical Properties of ES sources (continued)

ID Name 1	α_{J2000} h m s 2	3	4	δ_{J2000} ° ′ ″ 5	6	7	m_B 8	r_{eff} 9	μ_{eff} 10	μ_0 11	Inc ° 12	B-R 13	B-V 14	M_B 15	R_{eff} kpc 16	M_{HI}/L_B 17
HIPEQ1440-00	14	40	24	-00	17	14	12.84	37.3	21.63	18.99	61.9	1.69	1.07	-19.42	5.1	1.06
HIPEQ1444+01a	14	44	27	01	42	45	12.60	30.1	21.49	18.68	38.1	1.25	0.79	-19.29	3.5	0.58
HIPEQ1500+01	15	00	05	01	54	09	12.25	35.4	21.38	18.56	43.8	1.41	0.89	-19.32	3.5	0.16
HIPEQ1504+02	15	04	29	02	20	48	15.29	10.9	22.24	20.82	19.9	0.86	0.54	-20.28	6.9	0.99
HIPEQ1504-00	15	04	30	-00	51	01	14.98	30.7	22.92	21.97	73.7	0.95	0.60	-17.15	4.0	1.38
HIPEQ1507+01	15	07	15	01	32	01	11.87	53.7	22.47	18.51	5.0	1.35	0.85	-20.94	9.5	0.15
HIPEQ1542+00	15	41	59	00	41	45	14.04	52.5	22.68	21.72	86.1	1.20	0.76	-18.16	7.0	1.23
HIPEQ1544+02	15	44	52	02	29	47	14.98	12.3	22.24	21.03	14.8	1.13	0.71	-18.66	3.2	1.25
HIPEQ1545+00	15	45	23	00	47	42	15.30	19.4	23.54	21.80	11.4	0.98	0.62	-18.32	5.0	1.40
HIPEQ1601+01a	16	01	29	01	42	42	12.93	43.0	22.44	20.82	45.5	0.87	0.55	-19.24	5.7	0.21
HIPEQ1609-00	16	09	43	-00	05	35	15.97	16.5	23.89	22.49	48.5	0.38	0.24	-15.67	1.7	2.54
HIPEQ1613-00	16	13	31	-00	51	56	14.59	10.4	21.65	20.84	28.6	0.50	0.32	-17.73	1.5	0.77
HIPEQ1614+00	16	14	36	00	50	18	14.14	35.0	23.59	22.27	16.6	0.76	0.48	-18.07	4.7	0.55
HIPEQ1614-00	16	14	24	-00	12	41	13.84	65.5	22.68	21.40	90.0	1.43	0.90	-18.42	9.0	1.95
HIPEQ2036-04	20	36	20	-04	38	14	13.86	30.2	22.76	19.66	37.5	1.57	0.99	-20.63	11.6	0.74
HIPEQ2314+00	23	14	16	00	08	03	14.51	9.2	21.20	20.45	9.5	0.94	0.59	-19.14	2.4	0.28
HIPEQ2324-00	23	24	27	-00	05	28	14.49	20.7	23.04	21.32	61.2	0.60	0.38	-17.98	3.1	1.04
HIPEQ2335+01	23	35	26	01	11	38	16.14	20.1	24.40	23.23	32.2	1.10	0.69	-16.23	2.9	4.05
HIPEQ2336+00	23	36	43	00	19	57	12.88	24.4	21.48	18.32	28.7	1.22	0.77	-19.49	3.5	0.44
HIPEQ2337+00	23	37	22	00	23	33	14.53	34.3	24.07	23.14	31.6	0.92	0.58	-17.92	5.1	0.92
HIPEQ2340+01	23	40	15	01	13	55	15.07	13.9	21.98	20.55	51.8	1.14	0.71	-16.44	1.4	1.53

(1) Name
(2)-(4) Right Ascension
(5)-(7) Declination
(8) Apparent Magnitude (B)
(9) Effective Radius in arcseconds
(10) Effective Surface-Brightness
(11) Central Surface-Brightness
(12) Galaxy inclination °
(13) B-R colour
(14) B-V colour
(15) Absolute Magnitude
(16) Effective Radius in kpc
(17) HI mass to B band Luminosity ratio

3.4 The Optical Comparison (OC) sample

In previous sections we have presented the optical counterparts of the ES HI sample. However, it is useful to compare those results to those of an optically selected sample of similar characteristics; this allows one to highlight potential key differences. Although there have been many recent major optical catalogues (e.g. SDSS, 2dF) they tend to be of high redshift objects for large scale structure and cosmological purposes and not intended for 'local' universe studies. We have decided to compile an optical comparison sample (hereafter OC) from the ESO-LV catalogue (Lauberts & Valentijn, 1989) for the reasons described below.

The ESO-LV catalogue contains a total of 15457 galaxies published by the European Southern Observatory, in 1989. As of its publication date, the catalogue was the largest collection, by far, of magnitudes and diameters measured by machine. The reason for choosing the ESO-LV catalogue over any other catalogues is that it provides similar optical data to that obtained for the ES sample, such as B band apparent magnitude and effective surface-brightnesses. In addition we can obtain HI data from the HIPASS survey as they are both surveys of the southern sky. This allows us to make direct, like with like, comparisons between the two samples, an HI selected sample (ES) and an optically selected sample (OC).

3.4.1 Selection criteria for the OC sample

The selection criteria for the OC sample were determined by the need to make it as similar as possible to the ES sample. For that reason the sources selected had to fulfill all of the following requirements:

- The sources need to have 'no near first companion' within a 7 arcminutes radius; this is roughly half the diameter of the Parkes beam and it is the same criteria as for the ES sample. The reason for this is to select 'isolated' galaxies and not pairs or groups of galaxies so we can get accurate HI masses for each individual galaxy.

- The sources have to be bigger than 3 arcmin in r_{25} in diameter. This is to select 'local' sources and obtain a manageable sample size, comparable to the ES sample. The final OC sample contains 236 sources compared to the 201 in the ES sample.
- The sources need to have an optical redshift roughly less than 12700 km s^{-1}. This is to make sure that both samples cover the same volume of space.
- The sources need to have HI data to allow one to calculate the same parameters as in the ES sample. All the HI data for the OC sample has been obtained from the HIPASS survey. The down-side of this criterion is that these sources are necessarily gas-rich compared to a typical optically selected sample.

Figure 3.5 shows the distributions of the HI parameters for the OC sample. Table 3.3 lists the HI parameters derived for both samples. How some of the paramaters were obtained, such as the N_{HI} is discussed in Section 4.3.2.

The OC sample has a similar velocity distribution but much higher Integrated and Peak HI fluxes. This is to be expected as the sources in the OC sample are optically selected and hence they are generally bigger in size, more massive and are optically brighter.

No optical comparison sample will be ideal or free from selection effects of its own. By insisting on an optically selected sample with measured HI we have necessarily selected in favour of gas-rich galaxies. Because dwarf galaxies are rare in optically selected samples (i.e. the optical Luminosity Function) our OC sample will mostly consist of giant gas-rich galaxies, i.e. giant spirals. Size selection such as the one used for the OC sample includes more LSB galaxies than a magnitude selected sample. However, within its limitations, it still a useful exercise to compare the two samples as well as with those in the literature.

	ES sample		OC Sample	
Parameter	mean	median	mean	median
S_{peak} (Jy)	0.11	0.073	0.40	0.187
S_{int} (Jy km s^{-1})	15.94	8.64	76.92	40.00
Δ_{50} (km s^{-1})	163	136	275	260
$V_{\odot}$ (km s^{-1})	2566	1813	1758	1626
M_{HI} ($M_{\odot}$)	4.2×10^{9}	2.5×10^{9}	6.7×10^{9}	4.5×10^{9}
L_B ($L_{\odot}$)	6.5×10^{9}	3.5×10^{9}	1.5×10^{10}	9.2×10^{9}
N_{HI} (cm^{-2})	7.1×10^{20}	3.3×10^{20}	2.2×10^{21}	1.9×10^{21}
μ^B_{eff}	22.43	22.42	22.91	22.81
m_B	14.47	14.58	12.27	12.30
M_B	−18.00	−18.35	−19.28	−19.39
M_{HI} / L_B	1.51	0.95	0.72	0.54
R_{eff} (kpc)	4.03	3.56	12.27	12.30
B−R	0.97	0.95	1.20	1.20

Table 3.3: Comparison of the HI and optical parameters for the ES and OC samples.

Throughout this Thesis, where relevant and appropriate, I will show plots of the OC sample alongside those of the ES sample.

3.5 Correlations in the optical data

In this Section I present the most interesting correlations found in both the ES and OC samples. Many of the correlation plots shown in this section are looking at the same set of variables in different ways. This is a useful way of finding interesting correlations which migh not appear apparent otherwise.

The distribution of effective surface brightnesses for the ES sample and the OC sample are shown in Figures 3.6(a) and 3.6(b) respectively. It can be seen that the ES sample spans 5 magnitudes in effective surface-brightness, which is a larger range than seen for the OC sample. The ES sample distribution appears to show an intriguing 'dip' and seems

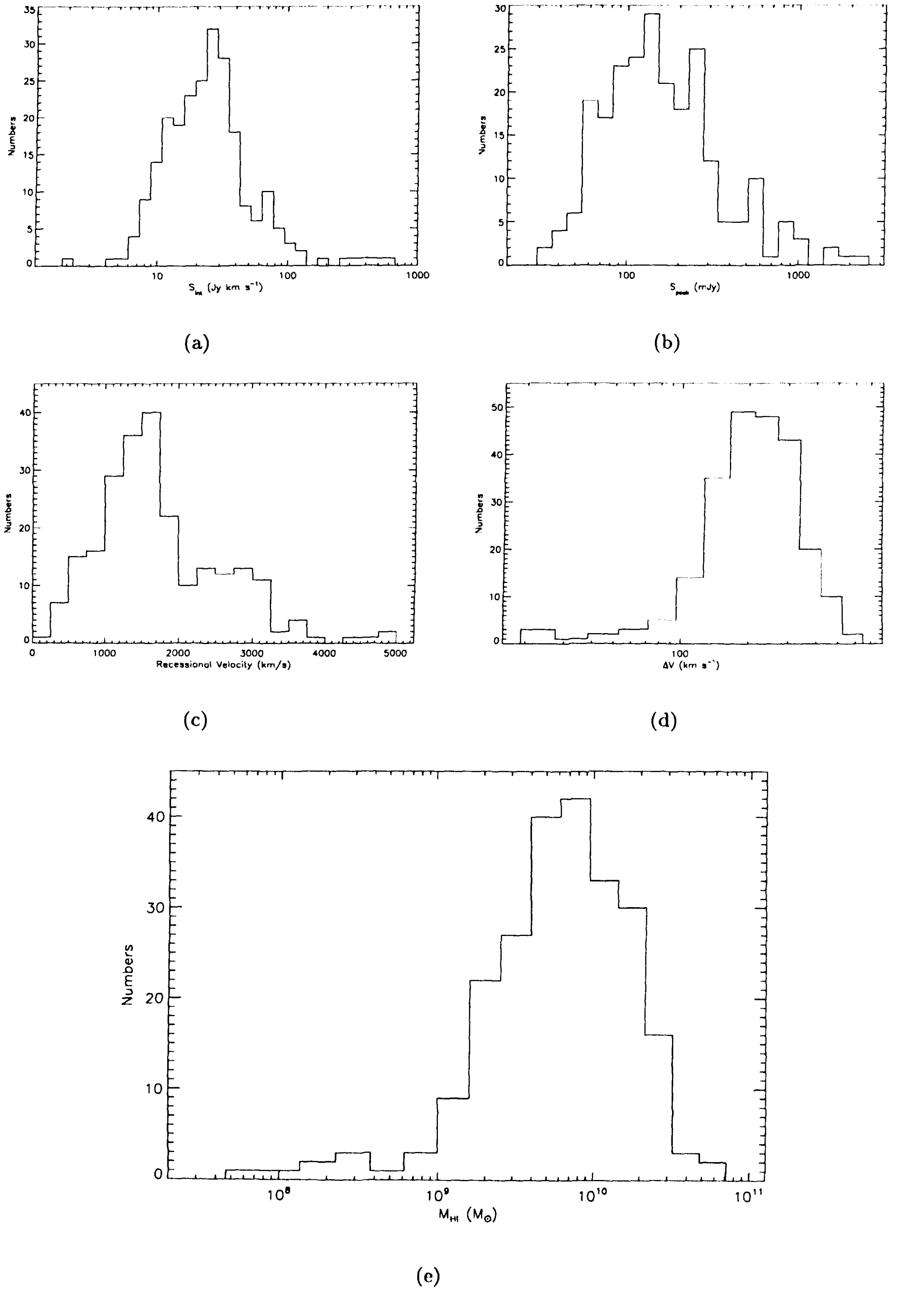

Figure 3.5: HI properties of the OC sample: Distributions of (a) integrated flux (S_{int}), (b) peak flux (S_{peak}), (c) recessional velocity ($V_{\odot}$), (d)velocity width (W_{50}) and (e) HI mass for the optical comparison sample.

to be bimodal, with one peak roughly at ($21 < \mu_{eff} < 22$) and a second higher and fainter peak at $22 < \mu_{eff} < 23$. This feature could be due to large scale structure which would then reflect into a bimodality in the surface-brightness distribution. Otherwise, the probability of finding such a small number of galaxies in the bins between $21.8 < \mu_{eff} < 22.2$ is low suggesting that the bimodality might be real. This feature cannot be seen in the OC sample, Figure 3.6(b).

As previously discussed, we have chosen to define Low Surface Brightness (LSB) galaxies as those with $\mu_0 > 23$ and/or $\mu_{eff} > 24$. Based on these criteria, there are 25 LSB galaxies in the ES sample (12%); I will investigate the properties of these LSB galaxies in Section 3.6.

The number of galaxies in each apparent magnitude bin for the ES sample and the OC sample are shown in Figures 3.7(a) and 3.7(b) respectively. The ES sample spans 7 magnitudes in apparent magnitude whereas the OC sample only spans 5. This is not surprising because the combination of surface-brightness selection effects combined with angular size selection will restrict the range in apparent magnitudes. The distribution of absolute magnitudes for the ES sample and the OC sample are shown in Figures 3.7(c) and 3.7(d) respectively. For the ES sample, the distribution in absolute magnitude is wider than that in apparent magnitude by 1 magnitude and spans 8 magnitude bins. Thus the distribution of absolute magnitudes spans more orders of magnitude than the HI mass distribution (see Chapter 2) indicating that there is a wide range of values for M_{HI}/L_B (see Chapter 4).

The distribution of galaxies in the ES sample by apparent effective radius is shown in Figure 3.8(a). Most galaxies in the ES sample appear to have optical sizes $1 < r_{eff} < 30$ arcseconds peaking at $r_{eff} \sim 15$ arcseconds with no one size dominating. Figures 3.8(b) and 3.8(c) show the distribution of absolute effective radius for the ES sample and OC sample respectively. The distribution of absolute sizes for the ES sample shows most

(a)

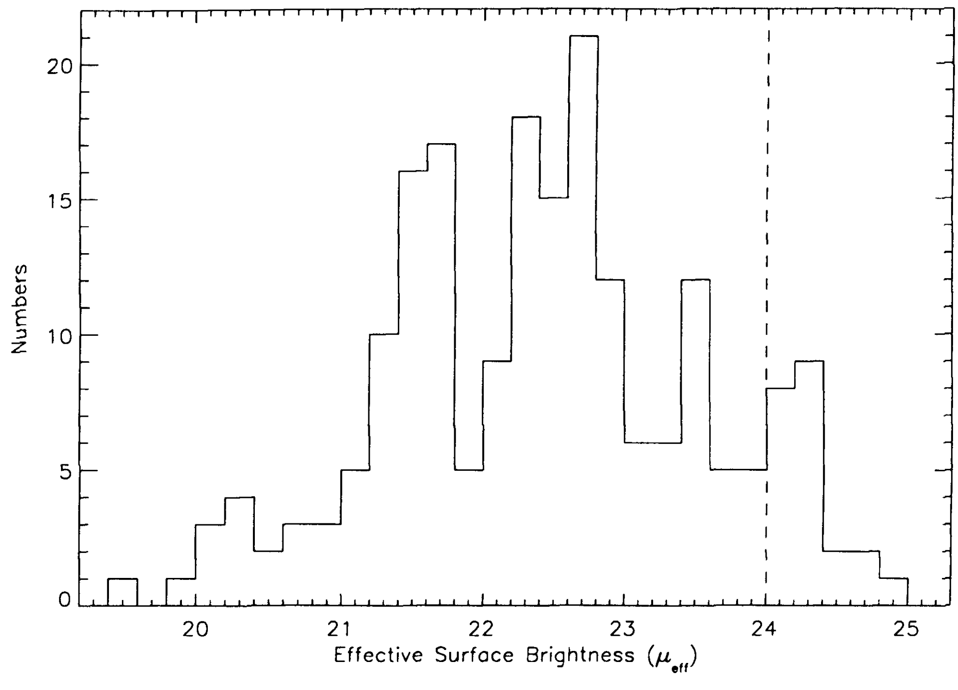

(b)

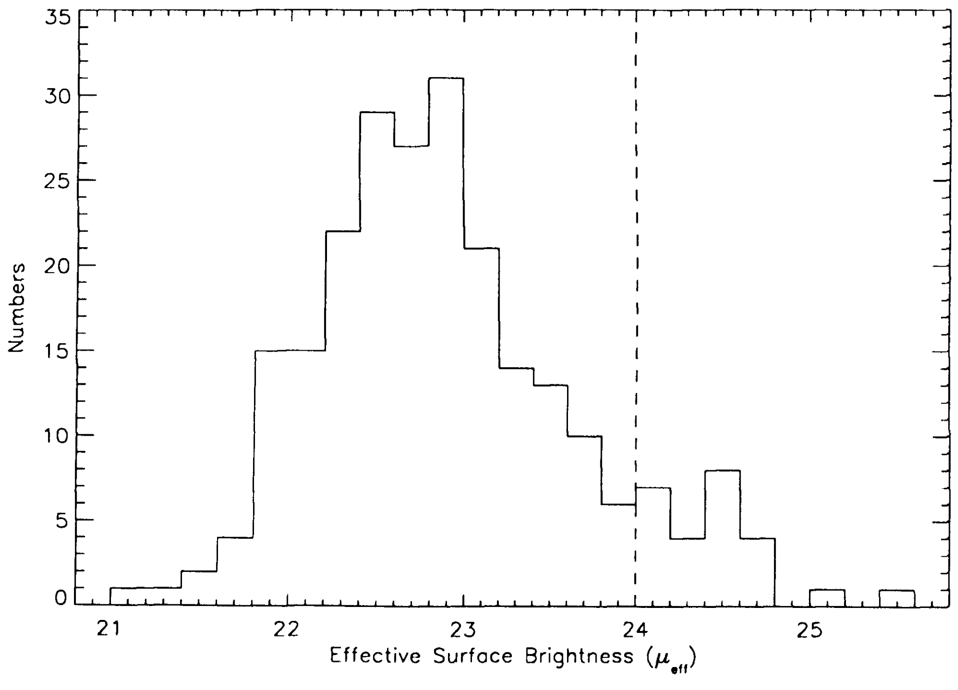

Figure 3.6: Effective Surface-Brightness distribution for the ES sample (a) and OC sample (b). The ES sample SBD appears to be bimodal with one peak roughly at $21 < \mu_{eff} < 22$ and a second peak which is higher and fainter at $22 < \mu_{eff} < 23$. Galaxies with $\mu_{eff} > 24$ are LSB galaxies, this is indicated by the vertical dashed line. The OC sample does not show the bimodality observed in the ES sample.

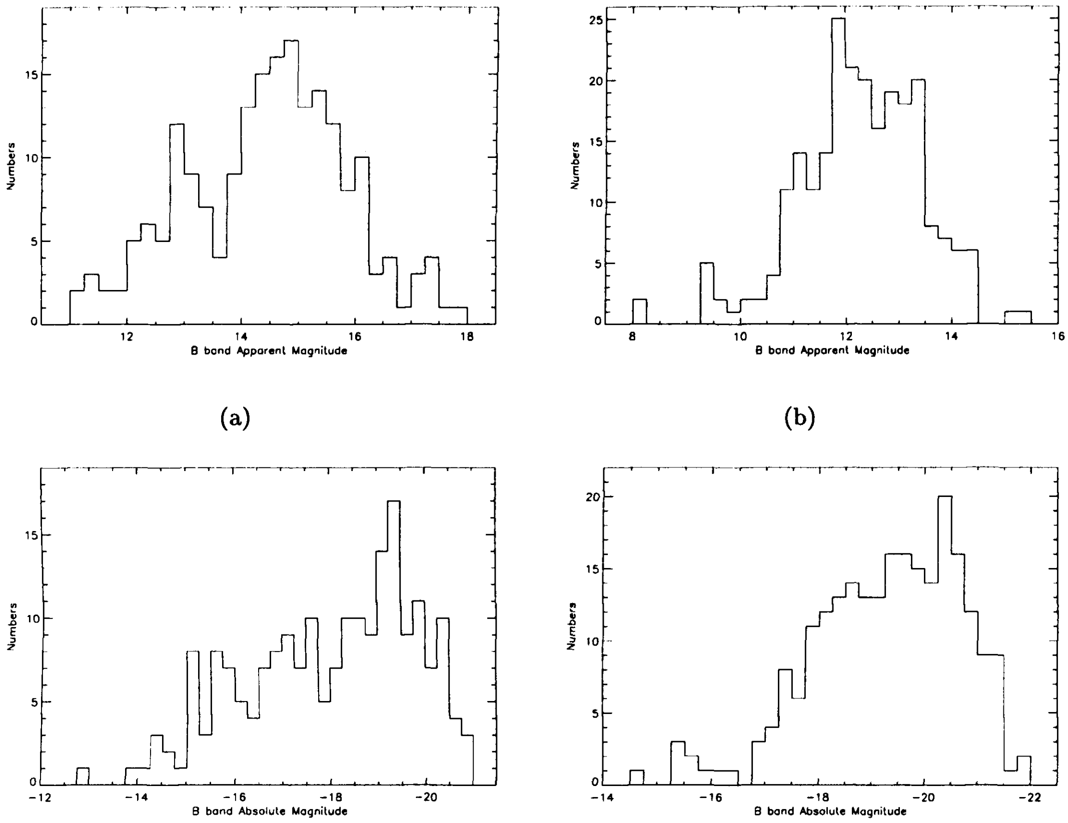

(a) (b)

(c) (d)

Figure 3.7: Panels 3.7(a) and 3.7(b) show the number of galaxies in apparent magnitude bins for the ES sample and OC sample respectively. Panels 3.7(c) and 3.7(d) show the distribution of absolute magnitudes for the ES sample and OC sample respectively. For the ES sample the apparent magnitude peaks at $14.5 < m_B < 15.5$ and at $-19 < M_B < -20$ for absolute magnitude.

galaxies having sizes between 1 and 10 kpc fairly evenly distributed.

Figure 3.9 examines the distributions of the apparent effective radius in terms of the apparent magnitude. It appears that there is a weak correlation between apparent effective radius and apparent magnitude. This might imply that it is unlikely that there is a physical link between size and luminosity hence implying that there is no bias towards detecting any particular surface-brightness.

In Figure 3.10 the relationship between effective radius and absolute magnitude is shown. Figure 3.11 shows the variation of apparent effective radius with effective surface-brightness. It can be seen that there is no correlation .

The relationship between apparent magnitude and effective surface brightness for the ES sample is shown in Figure 3.12(a). There is a strong correlation (r_s = 0.53, s = 7e-16) and the best-fitting linear relation is given by μ_{eff} = (0.63 $\pm$ 0.08) m_B + (13.3 $\pm$ 0.2), which has a scatter of $\sim$ 1.2 magnitudes. Such correlation is very surprising and was previously found by Minchin *et al.* (2003) in the HIDEEP sample. Figure 3.12(b) shows the same relation for the OC sample, in this case there is very little (r_s = 0.16, s = 0.01), if any, correlation and the best-fitting relation has a slope which is almost flat with μ_{eff} = (0.07 $\pm$ 0.04) m_B + (22.03 $\pm$ 0.52). The comparison between the two samples seems to support the explanation that the lack of correlation observed in the OC sample is a selection effect as the ES sample is free from optical selection effects.

Figure 3.13(a) shows a strong correlation (r_s = 0.52, s = 1e-15), this time between the absolute magnitude and the effective surface-brightness in the ES sample. The best fitting linear relationship has the form:

$$\mu_{eff} = (0.50 \pm 0.05)\ M_B + (31.4 \pm 0.2) \tag{3.4}$$

with a scatter of $\sim$ 1 magnitude. This scatter seems to be too narrow to be explained by

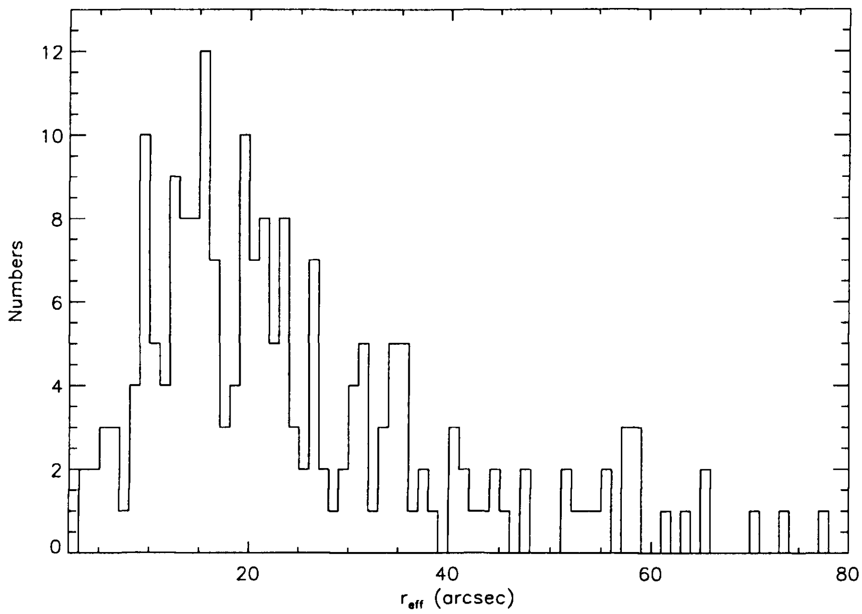

(a)

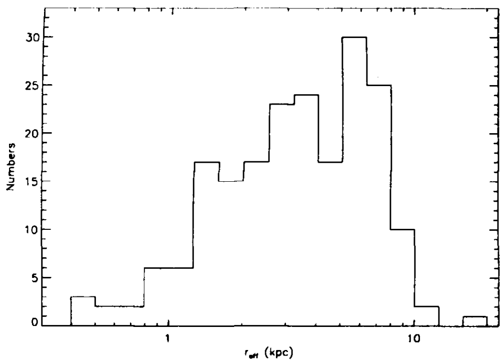

(b)

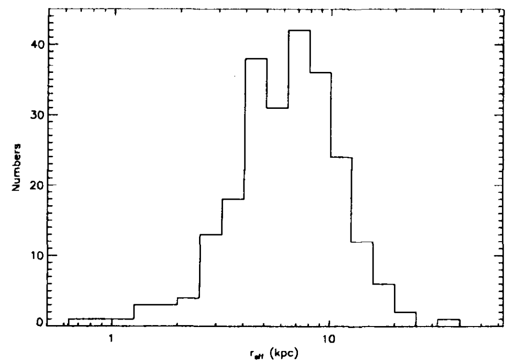

(c)

Figure 3.8: Number of galaxies per bin of apparent effective radius for the ES sample (a) and absolute effective radius for the ES sample (b) and OC sample (c). Most galaxies in the ES sample appear to have optical sizes $1'' < r_{eff} < 30''$.

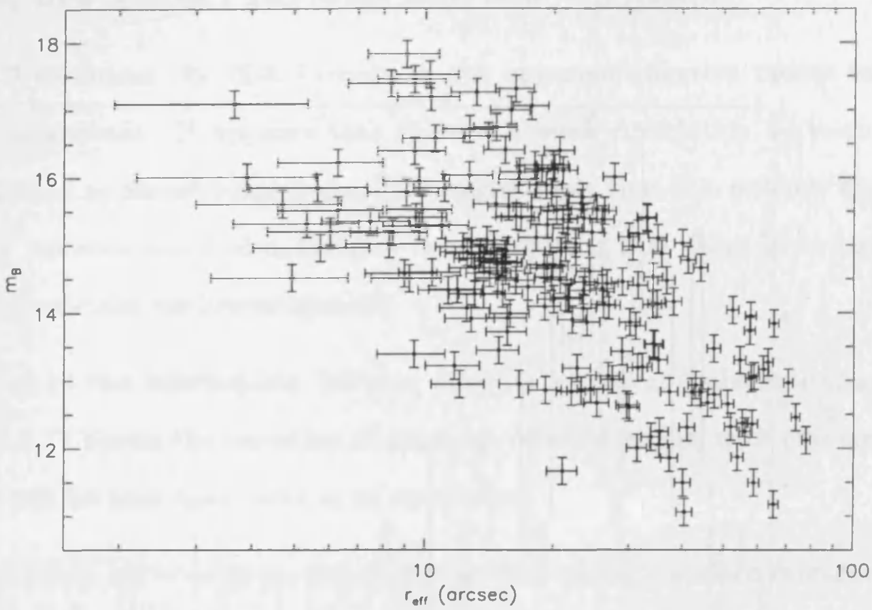

Figure 3.9: Comparison between effective radius and magnitude. There is correlation between apparent effective radius and apparent magnitude.

the relationship observed between the surface-brightness and apparent magnitude seen in Figure 3.12 and hence must have a physical explanation. There appears to be a lack of bright, low surface-brightness galaxies and a similar lack, though not as severe, of faint, high surface brightness galaxies. This is investigated further in Chapter 4 where volume corrections for the HI masses are used to construct the bivariate brightness distribution (BBD). Figure 3.13(b) shows the same relationship for the OC sample. In this case, there is very little ($r_s = 0.052$, s = 0.42), if any, correlation and the best fitting linear relationship has an almost flat slope with μ_{eff} = (0.04 ± 0.03) M_B + (23.78 ± 0.04).

A relationship between μ_{eff} and M_B was also found by Binggeli & Cameron (1991) for their study of galaxies in Virgo. However, they found a relationship such that $< \mu >_{eff} = 0.75\ B_T + 11.5$ (where B_T is the apparent B-band magnitude, at a con-

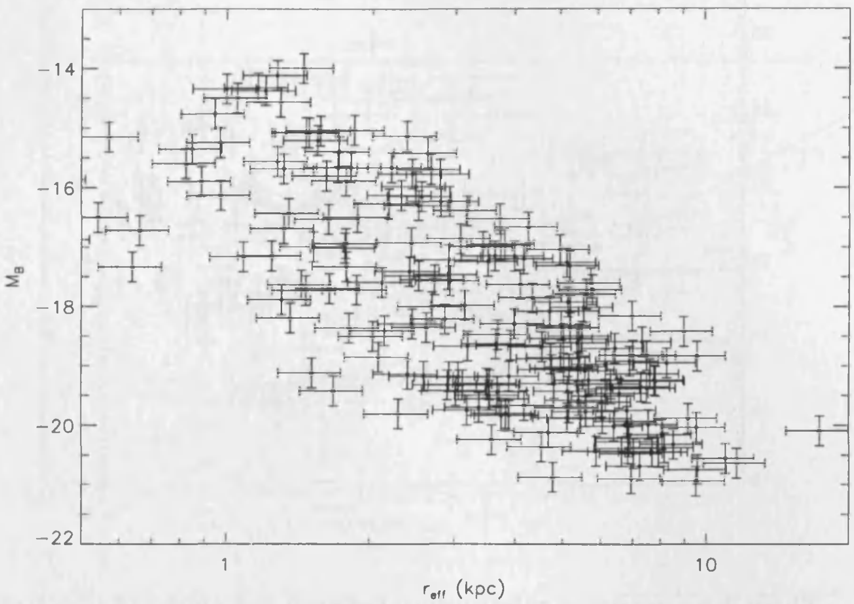

Figure 3.10: Comparison between effective radius and absolute magnitude in the ES sample.

stant distance-modulus for galaxies in Virgo, and $< \mu >_{eff}$ is the mean B-band surface-brightness within the effective radius, which is different from the definition of μ_{eff} used for the ES sample); this has a similar scatter but a steeper slope compared to the ES sample, even though in the ES sample there is a considerable number of galaxies that belong to the southern extension of the Virgo cluster – i.e. the surface-brightness falls off considerably quicker with decreasing luminosity than has been found in the ES sample. This is most likely due to differences in the morphological types studied, since the ES sample by definition consists of gas-rich galaxies which are mainly field spirals, while Binggeli & Cameron sample consists of dwarf galaxies (mainly dwarf ellipticals) within the Virgo cluster. The ES sample, unlike the sample from Binggeli & Cameron, does not suffer from optical selection effects.

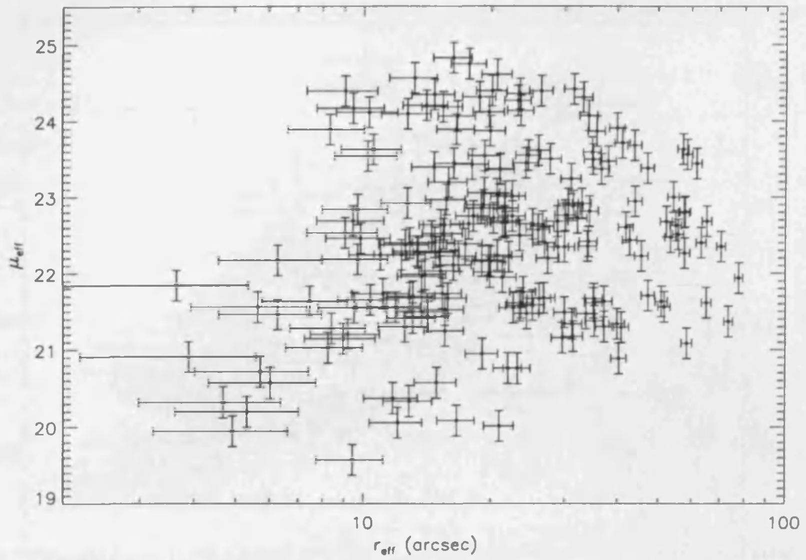

Figure 3.11: There is no apparent relationship between the apparent effective radius and the surface-brightness. For a given radius there is a wide range of values for the effective surface-brightness.

The distribution of Central Surface-Brightnesses (μ_0) for the ES sample is shown in Figure 3.14. The distribution peaks at $20.5 < \mu_0 < 21.0$ which is about 1 magnitude brighter than the Freeman value. However, there is a second peak at $\mu_0 \sim 22$ magnitudes arcsec^{-2}, which is fainter than the Freeman value, and a third peak at the Low Surface Brightness limit ($\mu_0 > 23.0$). There are 25 galaxies in the ES sample which fall in our definition of Low Surface Brightness galaxies (those to the right of the dashed line in Figure 3.14), and this is $\sim$ 12% of the total sample. This is discussed further in Section 3.6.

Figure 3.15(a) shows relationship between the Central Surface Brightnesses (μ_0) and the apparent magnitude. Again, there is a surprising correlation ($r_s = 0.53$, s = 6e-16) similar to that found in Figure 3.12 between the effective surface-brightness and the apparent magnitude. The best fitting (least squares) linear relationship is:

(a)

(b)

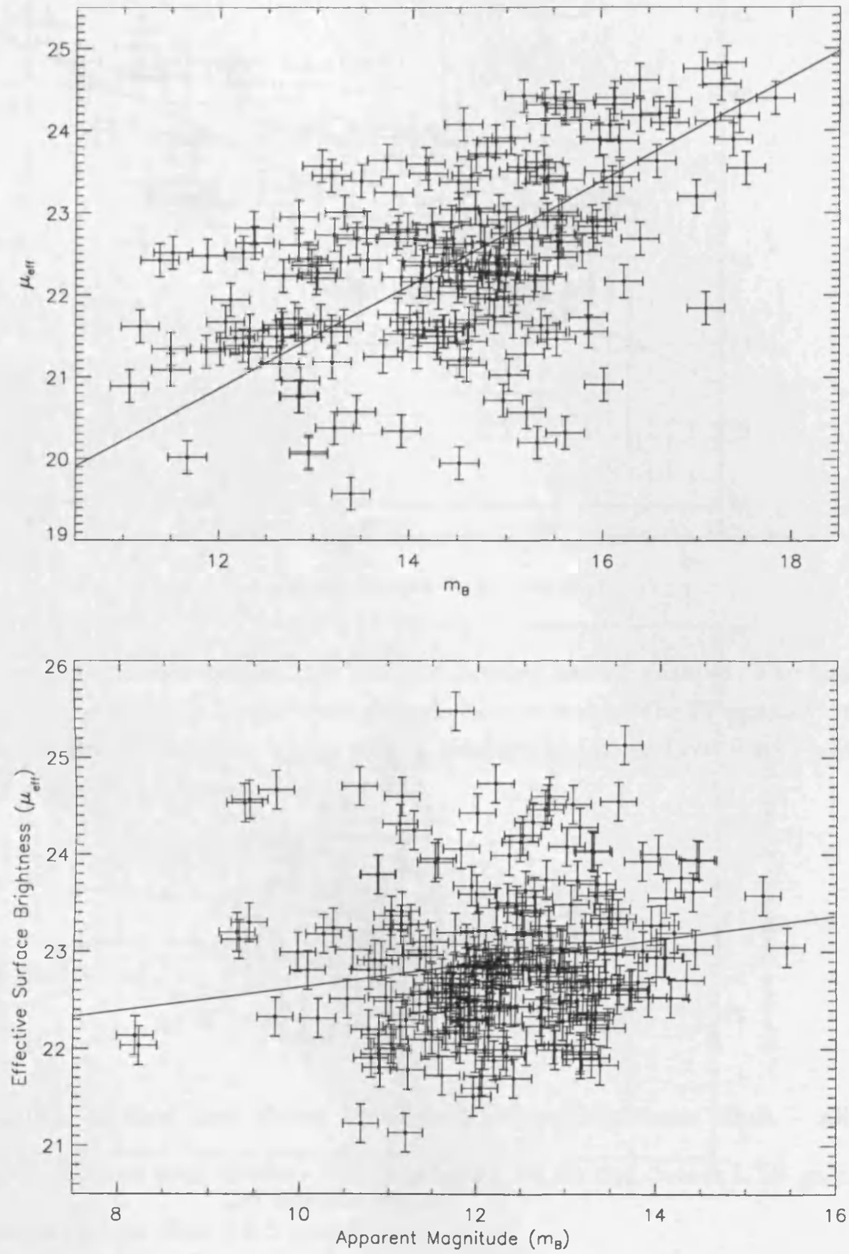

Figure 3.12: (a) The surprising correlation between the apparent magnitude and the effective surface-brightness in the ES sample. (b) The same correlation for the OC sample appears not to exist suggesting that a selection effect may be at work.

(a)

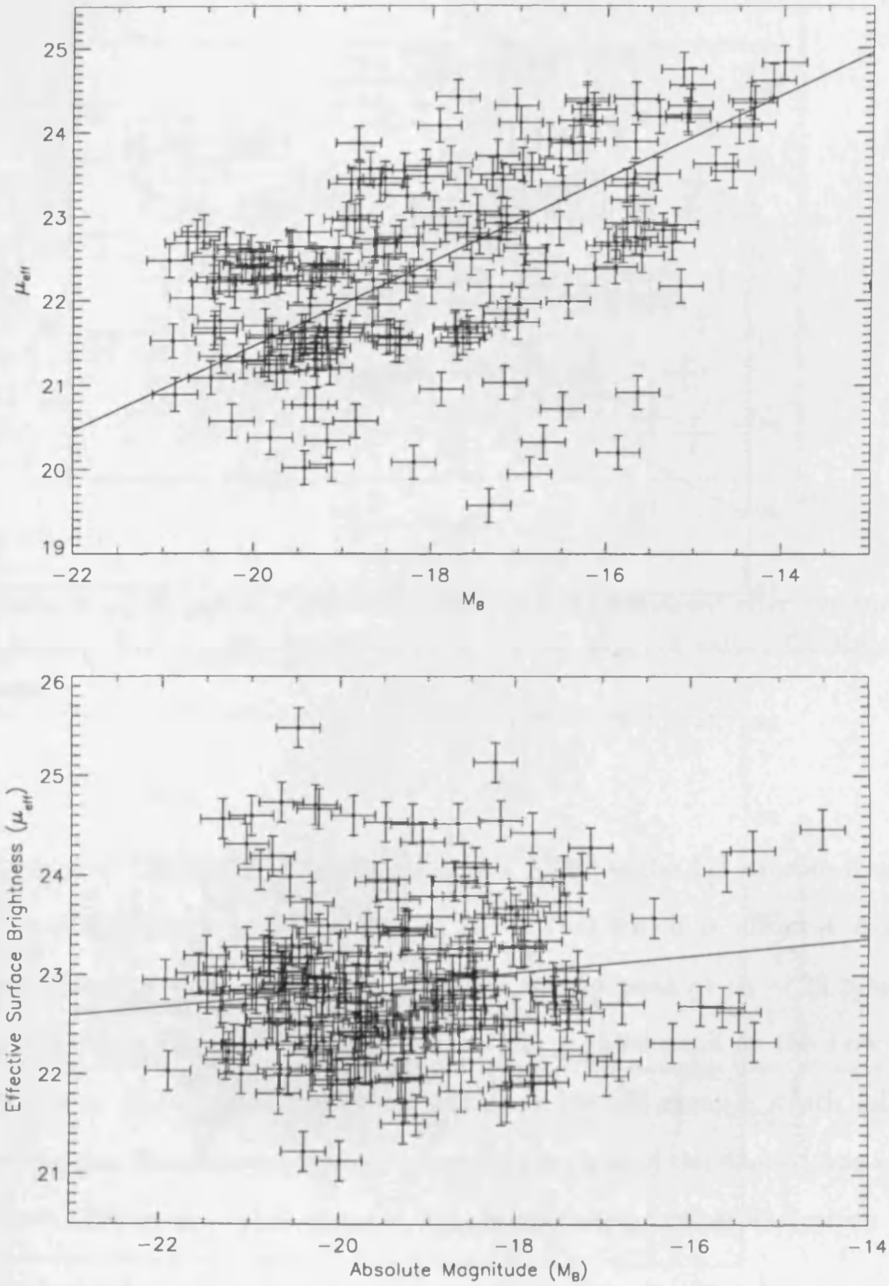

(b)

Figure 3.13: (a) the correlation between the absolute magnitude and the effective surface-brightness for the ES sample. This interesting correlation might be explained as being due to a near constant HI surface density and a near constant ratio of HI size to optical size. (b) the same correlation for the OC sample but in this case appears not to exist.

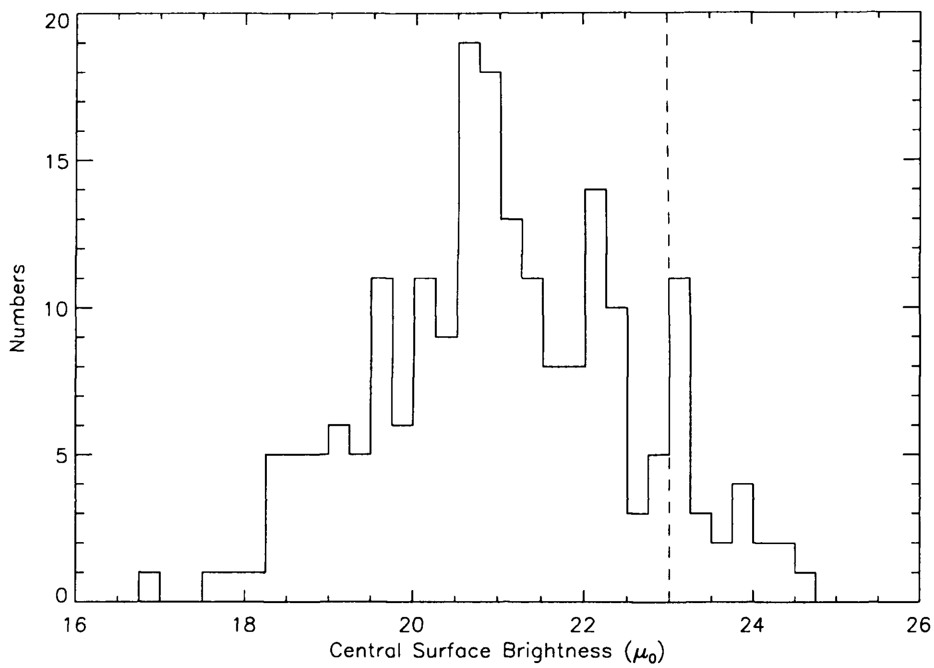

Figure 3.14: Central Surface-Brightness Distribution for the ES sample. The highest peak is at $20.5 < \mu_0 < 21.0$ which is about 1 magnitude brighter than the Freeman value. There are 25 galaxies in the ES sample which fall in our definition of Low Surface-Brightness galaxies to the right of the vertical dashed line.

$$\mu_0 = (1.08 \pm 0.01)\ m_B + (5.26 \pm 0.26) \tag{3.5}$$

The horizontal dashed line shows the Low Surface-Brightness limit – all galaxies above it are LSB. The vertical dashed line shows that we do not detect LSB galaxies with apparent magnitudes less than 14.5 magnitudes.

It is possible that this relationship could arise from a combination of observational selection and physical properties – if galaxies of a narrow range of flux are selected (as they are bound to be in a mainly flux-limited sample such as this), and the mean HI column densities of all these galaxies fall within a narrow range, then the HI sizes of these galaxies

(a)

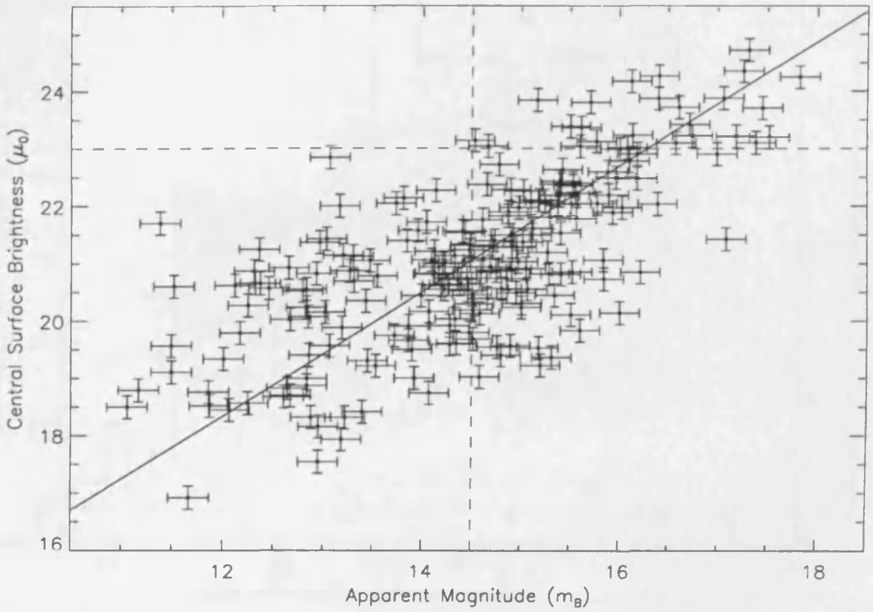

(b)

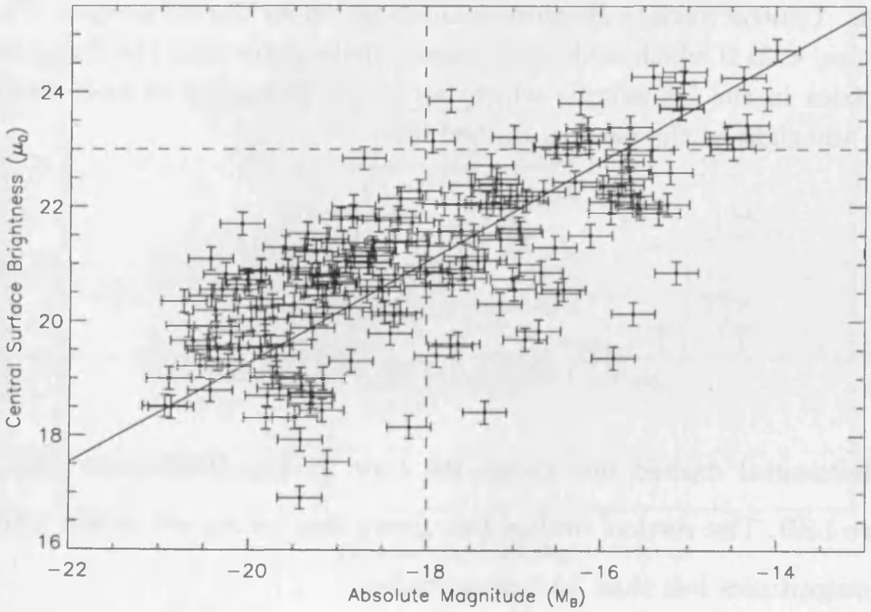

Figure 3.15: Correlation between the Central Surface-Brightness (μ_0) and the (a) apparent magnitude (m_B) and (b) absolute magnitude (M_B) for the ES sample.

would also fall in a narrow range. If HI size is linked to optical size as found by Cayette *et al.* (1994) and Salpeter & Hoffman (1996), then this will lead to all galaxies having similar optical sizes (as seen in Figure 3.8(a)). This would lead to a 1:1 relationship between apparent magnitude and effective surface-brightness, which is exactly what we observe (see Equation 3.4). This was first noticed by Minchin *et al.* (2003) in the HIDEEP sample.

Low column density galaxies would be expected to occupy the top left corner of this plot, and high column density galaxies the bottom right corner. If the hypothesis proposed to explain this relationship is indeed true, this implies that galaxies with high or low mean column densities do not exist or are not observed. For high column density galaxies this is not unexpected as the mean column density will always be lower than the peak. However, for low column densities galaxies there is no reason why they should not be detected in the ES sample if they do exist and have HI masses above the detection limit. This, therefore, implies that these galaxies either do not exist or they have been ionised by the intergalactic UV field and no longer contain significant amounts of neutral hydrogen.

Figure 3.15(b) shows the correlation between μ_0 with absolute magnitude ($r_s = 0.72$, $s = 2e\text{-}33$). The best-fitting linear relationship is $\mu_0 = (0.87 \pm 0.01)\ m_B + (36.66 \pm 0.25)$. There appears to be a lack of bright, low surface-brightness which would appear in the top right corner.

The distribution of the B−R, B−V and V−R colours for the galaxies in the ES sample are shown in Figure 3.16. The mean B−R colour is 0.97 ± 0.04, the mean B−V colour is 0.61 ± 0.04 and the mean V−R colour is 0.35 ± 0.04. This compares with B−V = 0.75 ± 0.03 and V−R = 0.53 for 'normal' galaxies (de Jong & van der Kruit 1994). Thus, the ES sample is considerably bluer. This is investigated further in the next Section.

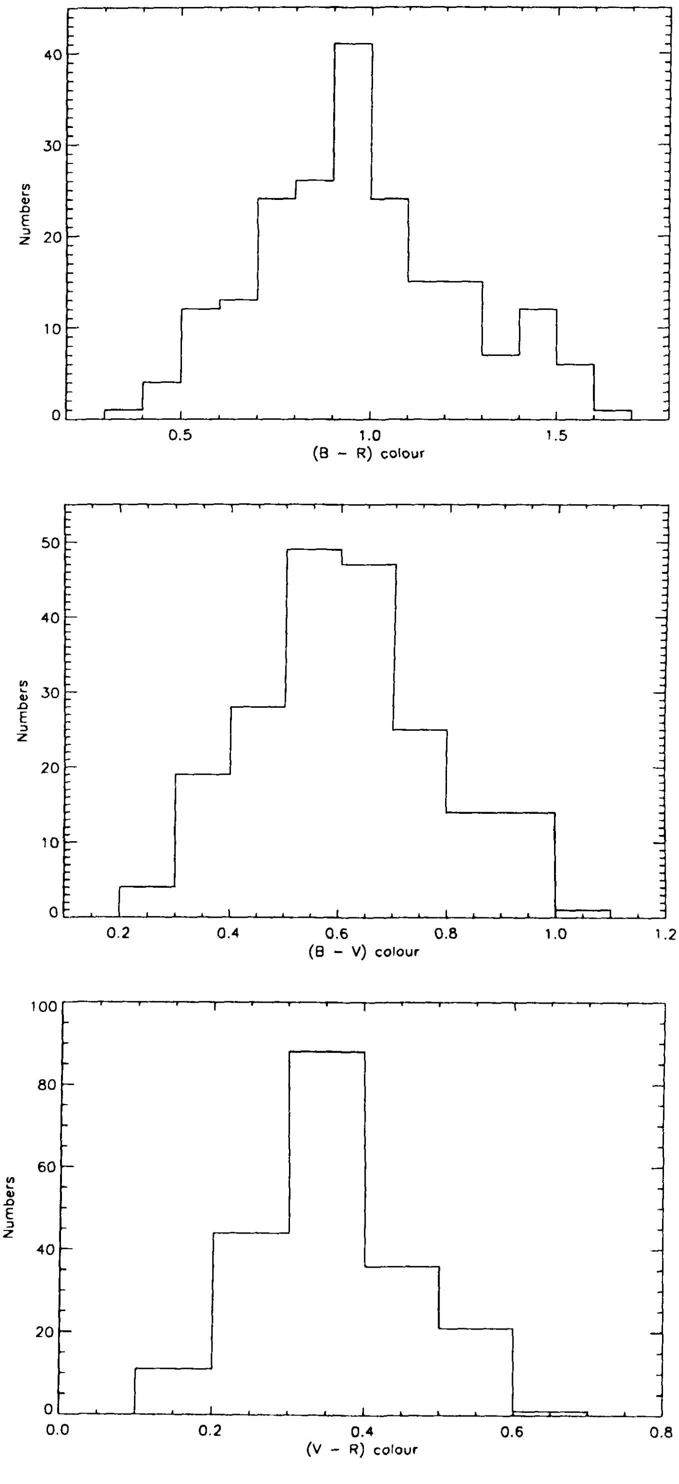

Figure 3.16: Galaxy colours for the ES sample. From upper to lower panels, B - R, B - V and V - R colours. Galaxies in the ES sample are bluer than those selected from optical samples.

3.6 LSB Galaxies in the ES sample

There are 201 galaxies in the ES sample for which we have optical data. Out of those, 25 (12% of the total sample) fulfill our definition of LSB galaxies, i.e. $\mu_0 > 23$ and/or $\mu_{eff} > 24$. The LSB galaxies under consideration here fall far from the Freeman value, with typical central surface brightnesses of $\mu_0 \approx 23.6$ B. In Chapter 1 I emphasised how the substantial optical selection effects selects against the detection of galaxies that are unevolved or diffuse. Thus it is interesting to look at objects which do not suffer from such optical selection effects.

Here I briefly summarise the characteristics of the LSB galaxies in the ES sample and show some striking and exciting examples.

	ES sample	
Parameter	mean	median
S_{peak} (Jy)	0.11	0.095
S_{int} (Jy km s^{-1})	9.02	6.70
Δ_{50} (km s^{-1})	83	83
$V_\odot$ (km s^{-1})	1810	1523
M_{HI} ($M_\odot$)	1.1×10^9	8.9×10^8
L_B ($L_\odot$)	4.4×10^8	1.8×10^8
N_{HI} (cm^{-2})	5.9×10^{20}	3.4×10^{20}
μ_{eff} (B)	24.19	24.20
μ_0 (B)	23.56	23.38
m_B	16.37	16.40
M_B	−15.52	−15.13
M_{HI} / L_B	4.7	3.1
R_{eff} (kpc)	2.18	1.83
B − R	0.80	0.82
B − V	0.50	0.52
V − R	0.29	0.30

Table 3.4: Properties of LSB galaxies in the ES sample

Table 3.4 presents the main parameters of the LSB galaxies found in the ES sample. By definition these galaxies are almost 2 magnitudes fainter in their central surface-brightness (μ_0) than the $\mu_0 \sim 21.65$ value found by Freeman (1970) and almost 2.5 magnitudes fainter than the sample as a whole.

As expected, their HI properties are broadly similar to the rest of the ES sample, as an HI sample is not affected by optical selection effects. The peak and integrated fluxes values for the LSB galaxies are similar to those of the whole ES sample but their velocity widths and effective radii are about half that of the ES sample as a whole. Their HI masses are about 4 times lower but their HI-mass to light ratio is 3 times higher, so these are gas-rich objects indeed. The mean M_{HI}/L_B value for the galaxies in the ES sample with absolute magnitudes greater than -15 or the 'dwarfs' in the sample is 5.53 and a median value of 5.85.

What makes these objects most strikingly different from the rest of the ES sample is their luminosity. They are $\sim$ 15 times fainter in their blue luminosity and contain about 4 times less HI.

Another defining characteristic in LSB disc galaxies is their blue colour. McGaugh & Bothun (1994) found $B - V = 0.49 \pm 0.04$ for their LSB sample, while for the ES sample we get $V - R = 0.29$ and $B - V = 0.50 \pm 0.03$, similar in colour to that of an actively star forming Sc galaxy. This compares with $B - V = 0.75 \pm 0.03$ and $V - R = 0.53$ for normal spirals that are on average 2 magnitudes brighter in effective surface brightness (de Jong & van der Kruit 1994). LSB galaxies in general are about 0.25 magnitudes bluer in $B - V$ than high surface-brightness galaxies.

The colour pictures for the 201 galaxies in the ES sample together with their HI spectra can be found in Appendix D and also on my website[1].

This population of galaxies is very different from 'normal' HSB field spirals and LSB

[1]http://www.astro.cf.ac.uk/pub/Diego.Garcia/galaxies/index.html

Name	μ_0	μ_{eff}
HIPEQ1416+03	24.26	24.18
HIPEQ1143-01	24.39	24.24
HIPEQ0958+01	24.56	24.35
HIPEQ1145+02	24.82	24.72

Table 3.5: Lowest LSB galaxies in the ES sample

dwarfs in clusters. Figure 3.17 shows the 4 galaxies with the lowest surface-brightnesses in the ES sample, their surface-brightness parameters are shown in Table 3.5. (It is worth comparing this figure with Figure 3.18 which shows the LSB galaxies in the OC sample, they both have the same grey-scale contrast level.) In general, LSB galaxies are late type (Sc and later) spiral and irregular galaxies and frequently irregular or amorphous appearance of the disc often result in a dwarf classification. These are extraordinarily diffuse objects, with an 'inchoate' structure and lacking any kind of central condensation or organisation. We know of no other galaxies like them. They would never have been found in optical surveys while previous blind HI surveys lacked sufficiently good optical data to identify them. Thus, they represent a new and exciting population.

They are extremely diffuse objects, have much bluer colours than 'normal' galaxies and are very gas-rich, all of which suggests that they are either: a) young objects or b) old objects with puzzlingly low star formation rates and hence large reservoirs of atomic hydrogen. However, if the latter is true, and they are not forming stars, then this does not explain why they are so blue.

HIPEQ0958+01 is a very interesting object – apart from being one of the lowest surface-brightness objects, it has the bluest colours of the whole ES sample with B − V = 0.29, B − R = 0.47 and V − R = 0.17. It appears to have a single HII region off-centre embedded in an amorphous disc.

These objects (see also McGaugh *et al.* 1995) are morphologically similar to the irregular faint blue galaxies resolved by the HST. They typically lack the old red disc conspicuous in higher surface-brightness galaxies. Together with their blue colours, this suggests that LSB galaxies are relatively young. Unlike the HST objects, however, these objects are close enough for a detailed investigation of their ages and star formation histories.

3.6.1 Are there giant LSB galaxies in the OC sample?

Once the OC sample was compiled we noticed that there were some objects which appear to fit our definition of Giant LSB galaxies, i.e. galaxies with low effective surface brightness but with high luminosity. Upon further investigation it was found that none of these objects is actually an LSB galaxy as we define them; most of them are either very nearby, extended, highly disturbed interacting systems, healthy bright spiral galaxies or ringed elliptical galaxies; the three 'lowest surface-brightness' objects in the OC sample are shown in Figure 3.18. It can be seen that these objects appear to have extended halos which could in part be responsible for their 'LSB' classification; however, they all have well defined, bright cores and hence they would not be defined as LSB under our definition of LSB galaxies. Conversely, due to our strict selection criteria (see Section 3.3), none of the objects in the ES sample are multiple or interacting systems.

For the reasons outlined above we have concluded, as shown in Figure 3.18, that there are no 'true' Giant LSB galaxies in the OC sample but since these 'apparently LSB' objects remain in the OC sample we warn the reader of their existence. These objects will create an artificial feature in the BBD which will be discussed in Section 4.2 - Figure 4.11 - as they will appear to be 'Malin 1' type 'Crouching Giants' or giant Low Surface Brightness galaxies, where in fact we believe this not to be case. This once again highlights the importance of good, homogeneous optical data for this kind of study, and thus the uniqueness and superiority of the ES sample.

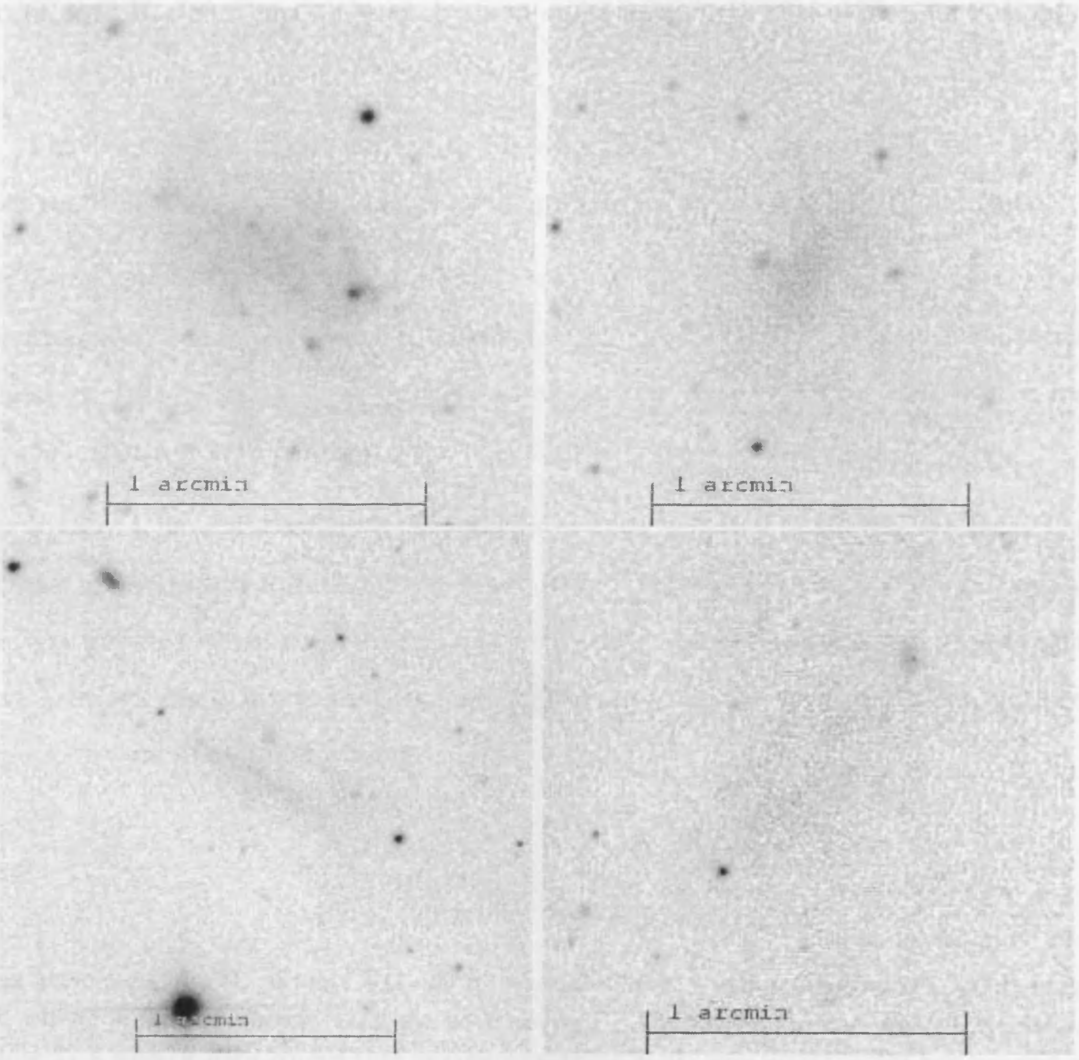

Figure 3.17: LSB galaxies in the ES sample. From top left to bottom right: HIPEQ1416+03, HIPEQ1143-01, HIPEQ0958+01 and HIPEQ1145+02. These 4 galaxies are the lowest surface-brightness objects in the ES sample (see Table 3.5).

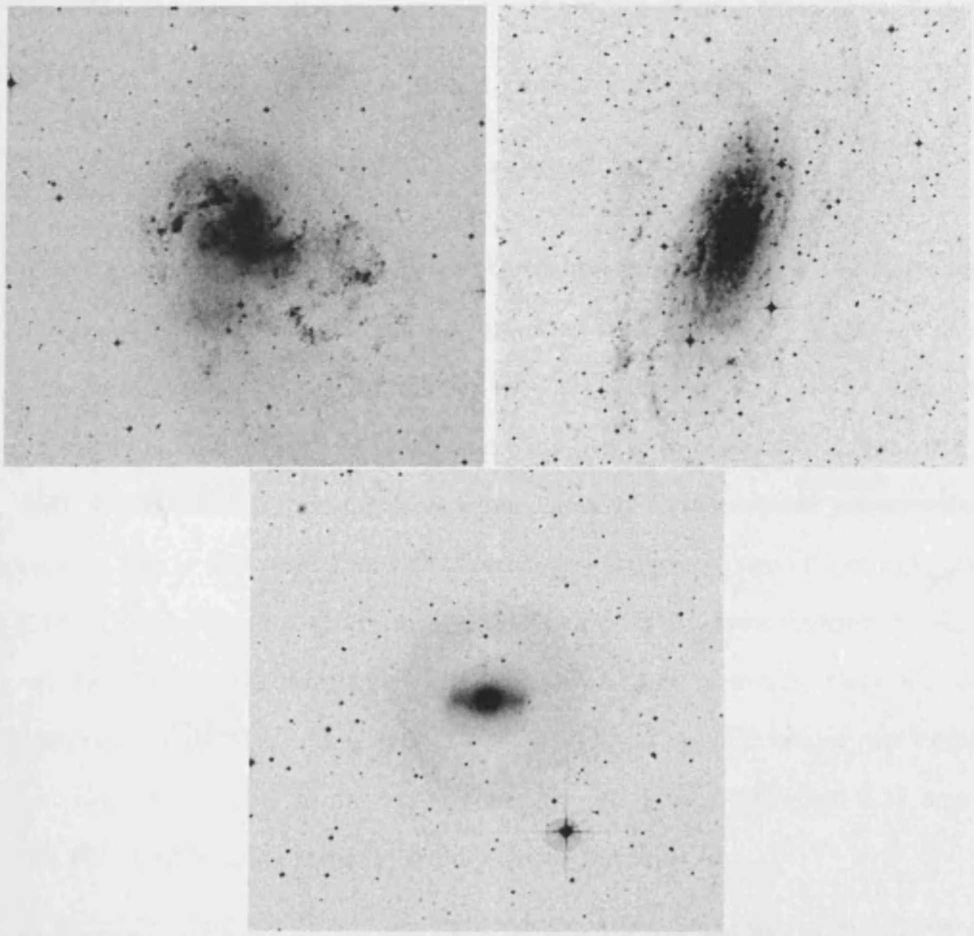

Figure 3.18: 'Low Surface-Brightness' Galaxies in the OC sample. It can be clearly seen that these objects are not actually LSB galaxies as we have chosen to define them. All the images are 15′ × 15′ in size. It is worth comparing this figure with Figure 3.17 which presents the 4 lowest surface-brightness objects in the ES sample. Both figures have the same grey-scale contrast levels.

3.7 Summary of Chapter 3

In this chapter I have discussed how the optical sample was obtained from the SDSS data. Of the 1077 HI detections we have obtained multi-wavelength optical data for 201 objects which main properties have been presented.

I have selected and presented an optically-selected comparison sample (OC) extracted from the ESO-LV sample,and compared its properties to the HI-selected ES sample.

In Section 3.6 I have presented the main correlations in the optical data. There are strong correlations between the effective surface brightness (μ_{eff}) and central surface-brightness (μ_0) of galaxies, with their apparent and absolute magnitudes where more luminous galaxies have higher surface-brightnesses.

Finally I have discussed the properties of LSB galaxies in the ES sample. These galaxies are extremely diffuse objects, have much bluer colours than 'normal' galaxies and are very gas-rich which suggests that they are either young objects or old objects which have been left undisturbed leading them to have very low star formation rates and hence large reservoirs of atomic hydrogen.

Chapter 4

Analysis and Discussion

The combination of optical and HI information for an HI selected sample is a powerful tool for analysing the properties of gas-rich galaxies. The only selection effect in the ES sample is its selection by HI mass but this can be corrected, giving an optically unbiased look at the luminosity function, the surface brightness distribution and the bivariate luminosity – surface brightness distribution. This combination of data also allows us to investigate the Tully-Fisher relationships for the ES sample, both the traditional velocity width – optical luminosity and velocity width – baryonic mass relationships are investigated. The HI radii of the galaxies can be estimated from their optical radii and hence their column densities and dynamical masses estimated.

The cosmological importance of LSB galaxies can be estimated by combining the surface brightness distribution with the relationships found between surface brightness and optical luminosity, HI mass, baryonic mass and dynamical mass. This allows for the contribution of LSB galaxies to the number density, luminosity density, HI density, baryon density of the Universe to be calculated.

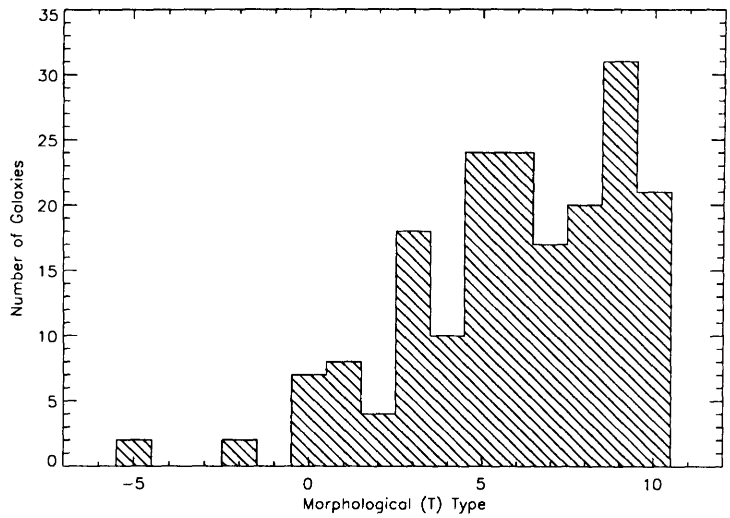

Figure 4.1: Distribution of Morphological Type in the ES sample

4.1 Correlations with HI mass to light ratio

Roberts & Haynes (1994) found that for a roughly flux limited sample of galaxies included both in the UGC and RC3 the median value of M_{HI}/L_B increased with Hubble type; these results from Roberts & Haynes are listed in Table 4.1. For galaxies in the UGC sample, this gives an average of $M_{\mathrm{HI}}/L_B = 0.31$ if E and S0 galaxies are excluded.

The distribution of galaxy types for the ES sample is shown in Figure 4.1; Hubble types for the ES sample, as described in Chapter 3, are listed in Appendix C. It can be clearly seen that this sample is dominated by late type galaxies which is expected since early type galaxies (ellipticals) have lower HI content and hence will not be preferentially selected in an HI sample.

The distribution of M_{HI}/L_B for the ES sample is shown in Figure 4.2(a). This sample has a median $M_{\mathrm{HI}}/L_B = 0.91 \pm 0.16$, which is considerably more gas rich than optically selected samples (e.g. Roberts & Haynes 1994). However, this is not surprising as gas-rich

	E, S0	S0a, Sa	Sab, Sb	Sbc, Sc	Scd, Sd	Sm, Im
$M_{\rm HI}/L_B$	0.04	0.12	0.21	0.29	0.36	0.66

Table 4.1: $M_{\rm HI}/L_B$ along the Hubble sequence from Roberts & Haynes (1994)

galaxies are much more likely to be detected in an HI survey than in optical survey. The distribution of $M_{\rm HI}/L_B$ for the optical comparison (OC) sample is shown in Figure 4.2(b). This OC sample has a median $M_{\rm HI}/L_B = 0.54 \pm 0.13$ which is relatively high for an optically selected sample, but it is not surprising as it is most probably due to a selection effect which was introduced when selecting the optical sample – the fact that we only chose galaxies with HI data. That means that these galaxies will be more gas-rich than your 'normal' optically selected galaxy but even then the ES sample still almost twice as gas-rich as the optically selected OC sample.

From Figure 4.1 it can be seen that more than two thirds of the ES sample are Sc or later type galaxies with the highest bin being that of Sm galaxies. The mean value of the $M_{\rm HI}/L_B$ is three times higher than that of the optically selected UGC sample from Roberts & Haynes (1994) of $M_{\rm HI}/L_B = 0.31$.

The ES sample can be arbitrarily divided into 4 groups based on their $M_{\rm HI}/L_B$ values:

Moderately gas poor galaxies with $\mathbf{0 < M_{HI}/L_B < 0.31}$. The $M_{\rm HI}/L_B$ of these galaxies is lower than the average sample of Roberts & Haynes. There are 28 galaxies in this group which is $\sim$ 14% of the total number in the ES sample.

Moderately gas-rich galaxies with $\mathbf{0.31 < M_{HI}/L_B < 1.0}$. These galaxies have HI mass to light ratios higher than the average of the sample of Roberts & Haynes. However, in these galaxies there is probably still more mass in their stars than in their gas. This group contains 78 galaxies and constitutes the largest fraction of the ES sample (39%).

(a)

(b)

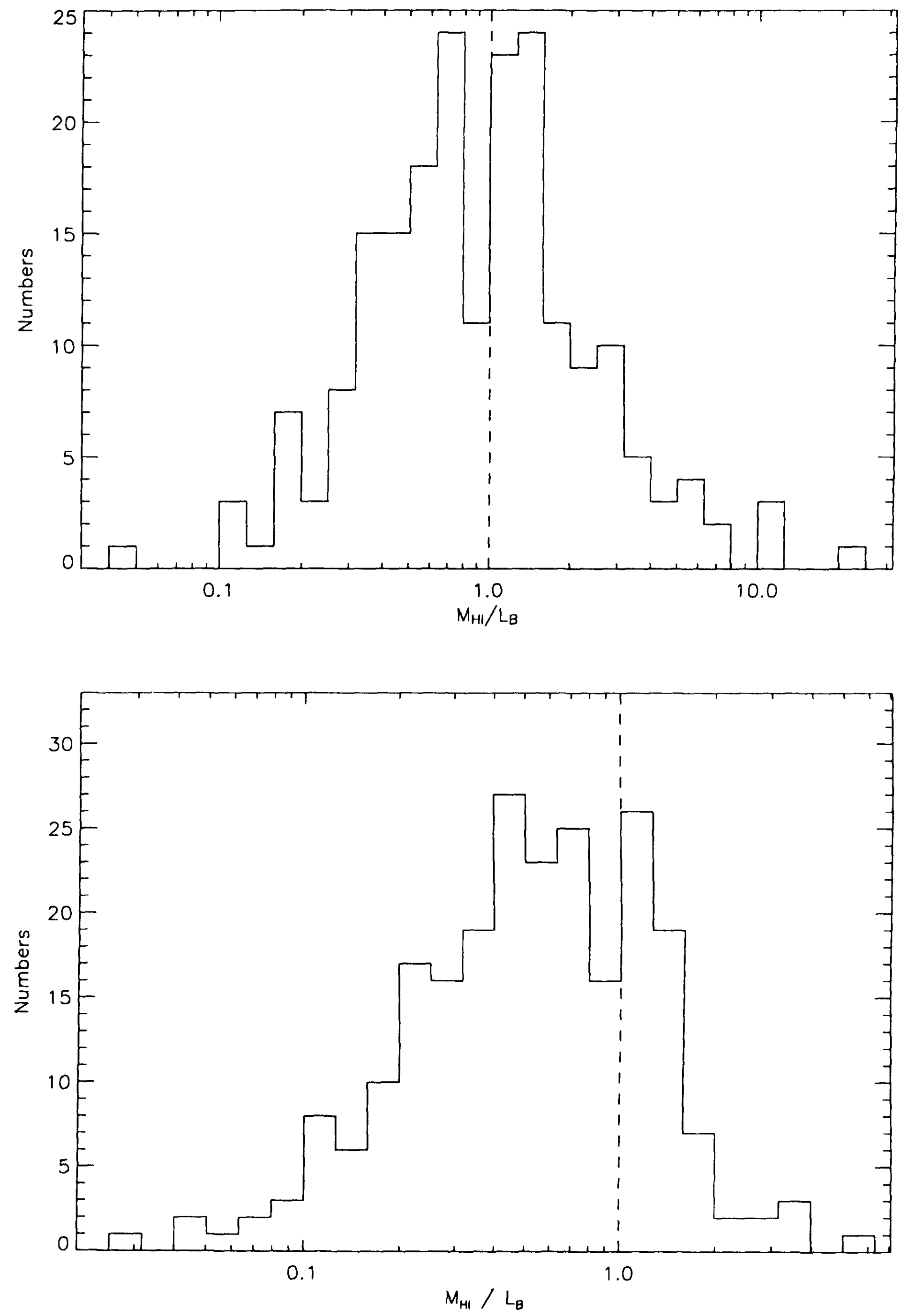

Figure 4.2: Distribution of HI mass to light ratios for the ES asmple (a) and OC sample (b). It can be seen that the ES sample is considerably more gas-rich than the OC sample, as selection by HI flux will preferentially pick out gas-rich galaxies. The ES sample has a median of $M_{\rm HI}/L_B = 0.91$, the median for the OC sample is $M_{\rm HI}/L_B = 0.54$. The vertical shows the $M_{\rm HI}/L_B = 1$ boundary and objects above it are dominated by their gas.

Gas-rich galaxies with $1.0 < \mathbf{M_{HI}/L_B} < 3.0$. These galaxies are uncommon in optically selected samples as they might contain more mass in their gas than in their stars. This is true if $M_\star/L_B = 1$ as M_{HI}/L_B is not the same as $M_{HI} > M_\star$ unless that is the case. There are almost as many objects in this group as in the previous one representing $\sim 37\%$ of the ES sample.

Extremely gas-rich galaxies with $3.0 < \mathbf{M_{HI}/L_B} < 22.0$. The baryonic mass in these galaxies is dominated by their gas, with the proportion of mass in stars and gas being reversed from the 'normal' galaxies in optically selected samples. These galaxies are very rare in optical samples and are not particularly common even in HI selected samples, implying that their rarity is not entirely an optical selection effect. There are 21 galaxies in this group (10% of the overall ES sample), with 4 galaxies having $M_{HI}/L_B > 11$ and one object (HIPEQ1227+01) with $M_{HI}/L_B \sim 22$, this is the Giovanelli & Haynes cloud (1989).

Figures 4.3(a) and 4.3(b) show how the M_{HI}/L_B varies with HI mass for the ES sample and OC sample respectively. Minchin *et al.* (2003) suggested that less massive galaxies have higher HI mass to light ratios, but for the ES sample we find a very weak correlation ($r_s = -0.15$, $s = 0.034$). We can see a slightly stronger correlation for the OC sample ($r_s = 0.21$, $s = 0.0012$) but this instead indicates a trend for M_{HI}/L_B to increase with HI mass and is probably due to selection effects. This is not the case in the ES sample, moreover, the fact that for the ES sample there is little correlation between M_{HI}/L_B and M_{HI} and that in fact the highest M_{HI}/L_B are for galaxies with $M_{HI} > 10^9$ $M_\odot$ suggests that it may not be the case that less massive galaxies have higher HI mass to light ratios.

There is a much stronger correlation ($r_s = 0.68$, $s = 3\text{e-}28$) seen between M_{HI}/L_B and absolute magnitude for the ES sample which is shown in Figure 4.4(a). Higher HI mass to light ratios are seen in fainter galaxies. The best-fitting linear relationship found has the form:

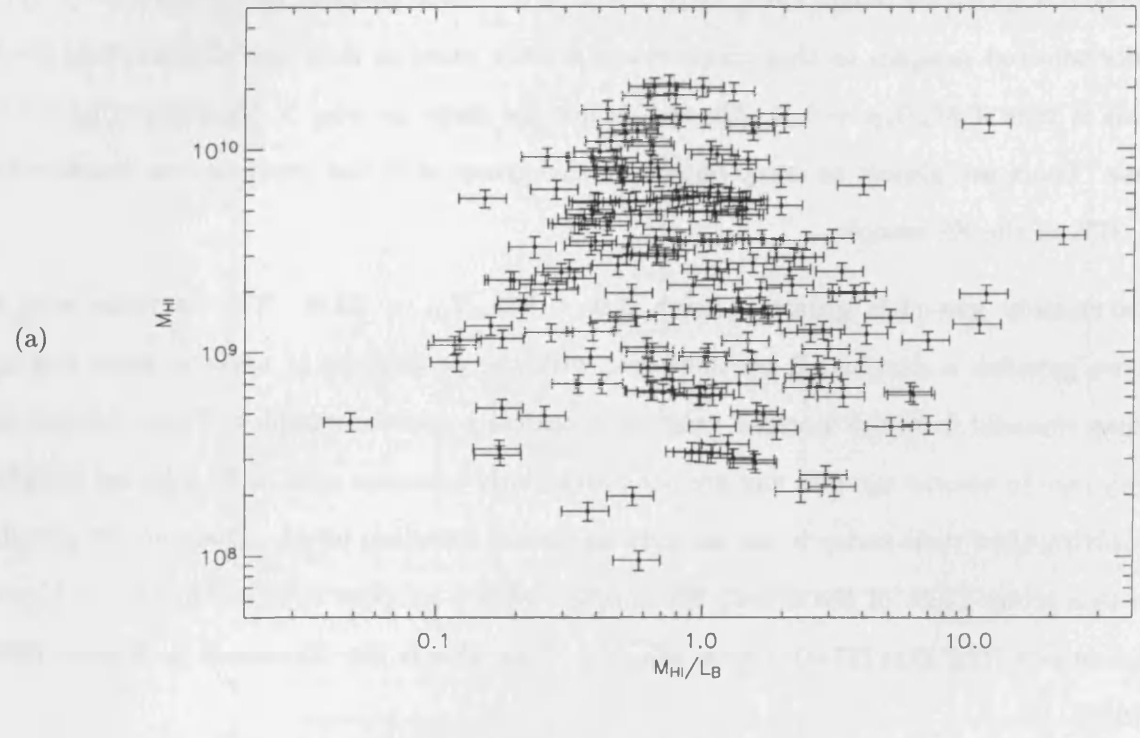

Figure 4.3: Correlation of HI mass with HI mass to light ratio for the ES sample (a) and OC sample (b). For both samples there is a lack of low mass, low $M_{\rm HI}/L_B$ galaxies, with most galaxies with $M_{\rm HI}/L_B < 1$ having $M_{\rm HI} > 10^9 M_\odot$.

(a)

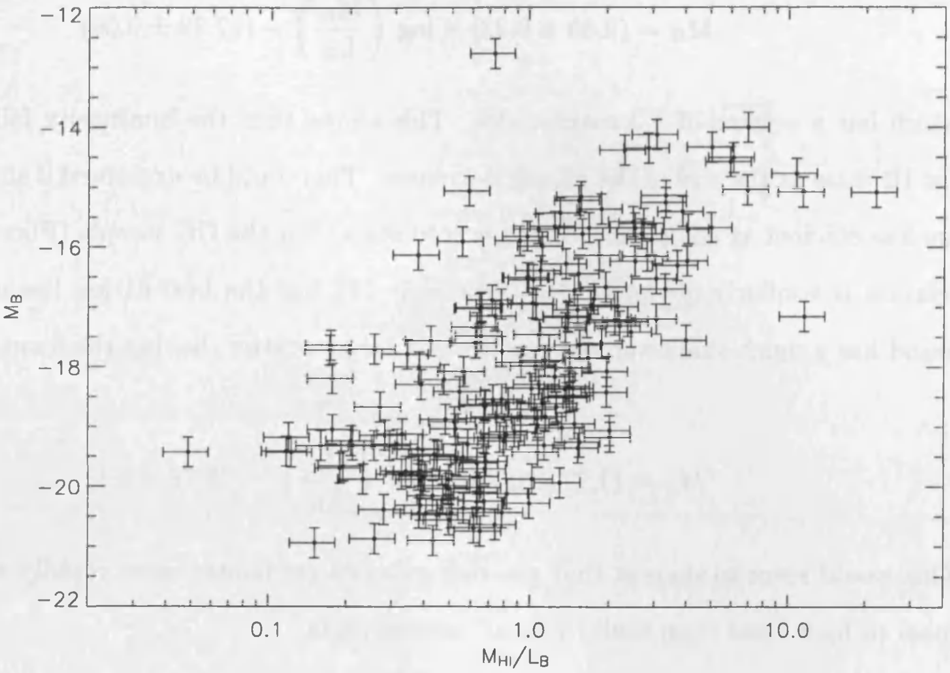

(b)

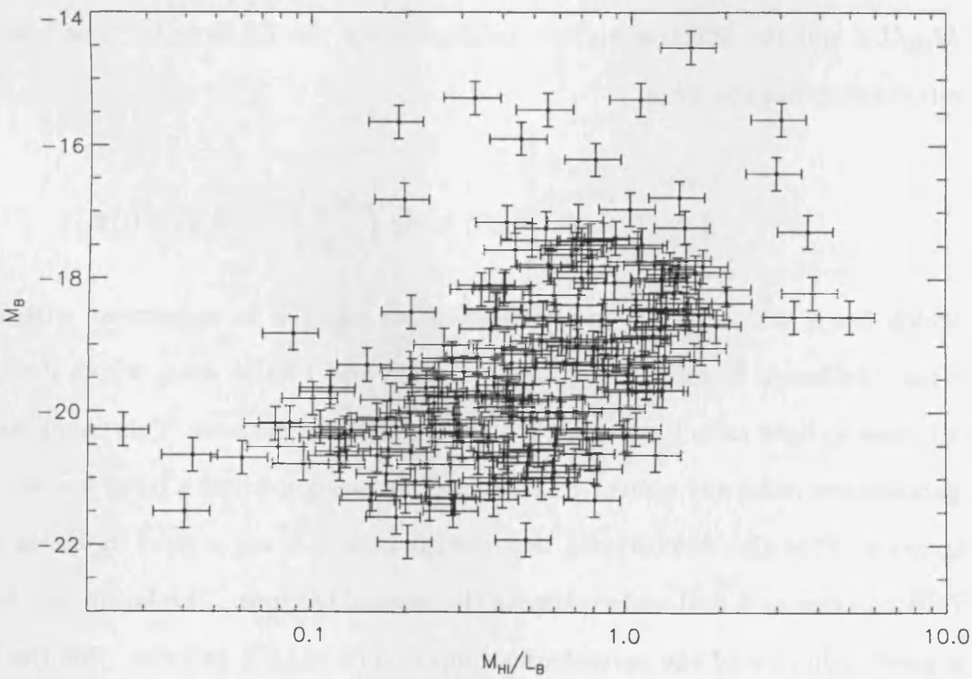

Figure 4.4: Correlation of absolute B-band magnitude with HI mass to light ratio for the ES sample (a) and OC sample (b). Higher HI mass to light ratios are seen in fainter galaxies.

$$M_B = (2.80 \pm 0.23) \times \log\left(\frac{\mathrm{M_{HI}}}{\mathrm{L_B}}\right) - (17.89 \pm 0.09) \tag{4.1}$$

which has a scatter of 1.2 magnitudes. This shows that the luminosity falls faster than the HI mass as the size of the galaxy decreases. This could be explained if smaller galaxies are less efficient at converting their gas into stars. For the OC sample (Figure 4.4(b)) the relation is similarly obvious ($r_s = 0.54$, s = 1e-19) but the best-fitting linear relationship found has a much shallower slope and has a larger scatter, having the form:

$$M_B = (1.77 \pm 0.20) \times \log\left(\frac{\mathrm{M_{HI}}}{\mathrm{L_B}}\right) - (18.76 \pm 0.1) \tag{4.2}$$

This would seem to suggest that gas-rich galaxies get fainter more rapidly with increased mass to light ratio than their 'optical' counterparts.

In Figure 4.5(a) a similar correlation ($r_s = 0.56$, s = 5e-18) can be seen between the M_{HI}/L_B and the effective surface brightness for the ES sample. The best-fitting linear relationship has the form:

$$\mu_{eff} = (1.50 \pm 0.15) \times \log\left(\frac{\mathrm{M_{HI}}}{\mathrm{L_B}}\right) + (22.50 \pm 0.06) \tag{4.3}$$

which has a scatter of 1.3 magnitudes. This result is in agreement with those from de Blok, McGaugh & van der Hulst (1996) in B and I band data, which indicated that the HI mass to light ratio increased with lower surface brightness. This could imply that these galaxies are relatively unevolved and have not yet converted a large fraction of their mass to stars. This also demostrates that the luminosity is not a good indicator of the mass of LSB galaxies as it will underestimate the mass of baryons. The luminosity is therefore not a good indicator of the cosmological importance of LSB galaxies. For the OC (optically selected) sample the correlation is weaker ($r_s = 0.37$, s = 3e-9), with a shallower slope and a larger scatter than the relationship for the ES sample, the best-fitting linear relationship

(a)

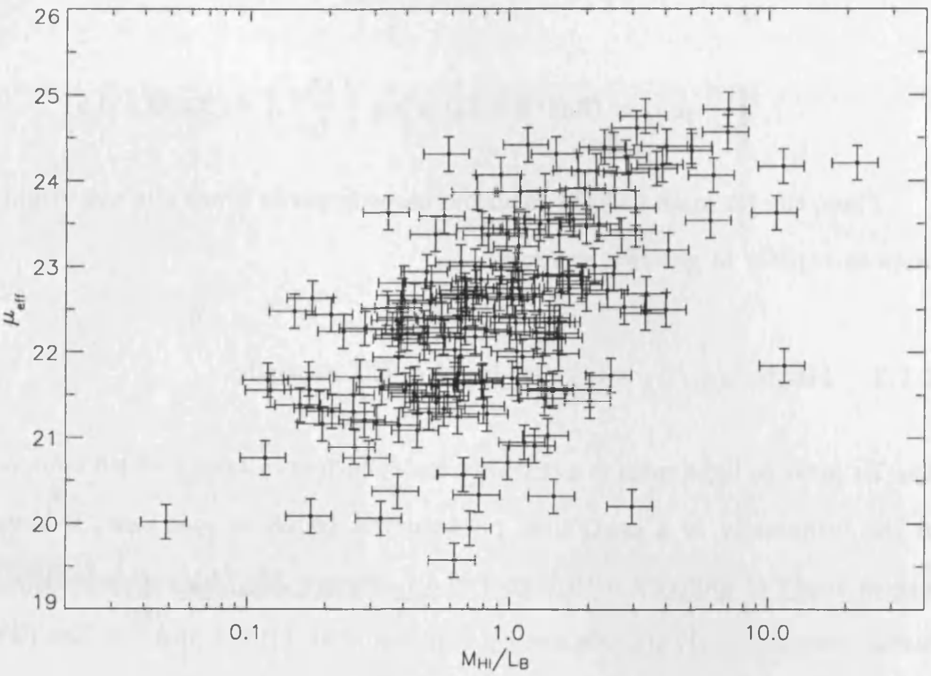

(b)

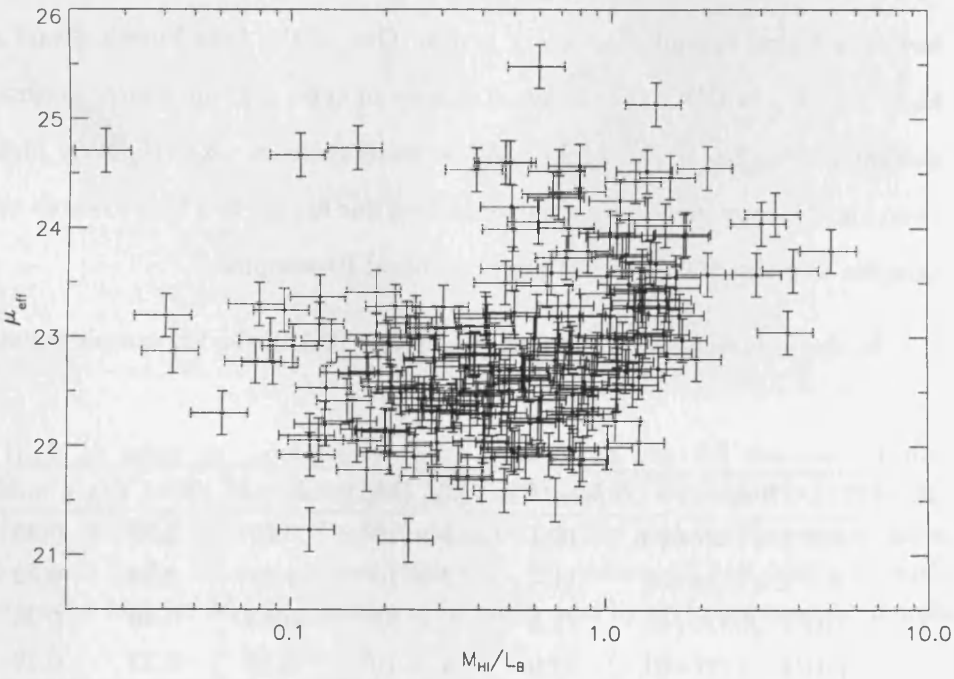

Figure 4.5: Correlation of effective surface brightness with HI mass to light ratio for the ES sample (a) and OC sample (b). The HI mass to light ratio increases towards lower surface-brightness more than twice as rapidly in gas-rich galaxies.

for the OC sample having the form:

$$\mu_{eff} = (0.60 \pm 0.12) \times \log\left(\frac{\mathrm{M_{HI}}}{\mathrm{L_B}}\right) + (23.09 \pm 0.6) \tag{4.4}$$

Thus, the HI mass to light ratio increases towards lower surface-brightness more than twice as rapidly in gas-rich galaxies.

4.1.1 High $M_{\rm HI}/L_B$ objects in the ES sample

The HI mass to light ratio is a distance independent quantity which compares the HI mass to the luminosity in a particular photometric band, in this case, B-band. To date the largest study of galaxies with higher than average $M_{\rm HI}/L_B$ ratios is that of gas-rich, low surface brightness dwarf galaxies by van Zee *et al.* (1997) and van Zee (2000, 2001).

For most galaxies $M_{\rm HI}/L_B$ is typically less than 1 $\mathrm{M_\odot/L_\odot}$, with late type galaxies having a larger spread than early types. One of the best known dwarf galaxies with a high $M_{\rm HI}/L_B$ is DDO 154, a dwarf galaxy of type Sm, for which Hoffman *et al.* (1993) measured $M_{\rm HI}/L_B = 11\ \mathrm{M_\odot/L_\odot}$. While many galaxies with relatively high $M_{\rm HI}/L_B$ have been found, many more have gone unnoticed due in part to a bias towards optically selected samples and the limitations of previous blind HI samples.

In the previous Section I have shown that 10% of the ES sample is extremely gas-rich

Name	$M_{\rm HI}/L_B$	$\mathrm{M_{HI}}$ ($\mathrm{M_\odot}$)	B − R	B − V	V − R	μ_0
HIPEQ1327+02	10.7	1×10^9	0.62	0.39	0.23	23.10
HIPEQ1224+00	11.4	2×10^9	0.87	0.54	0.32	23.70
HIPEQ0936+01	11.5	1×10^{10}	0.63	0.40	0.23	21.42
HIPEQ1227+01	21.9	4×10^9	0.52	0.33	0.19	23.72

Table 4.2: Highest HI mass to blue luminosity ratio galaxies in the ES sample

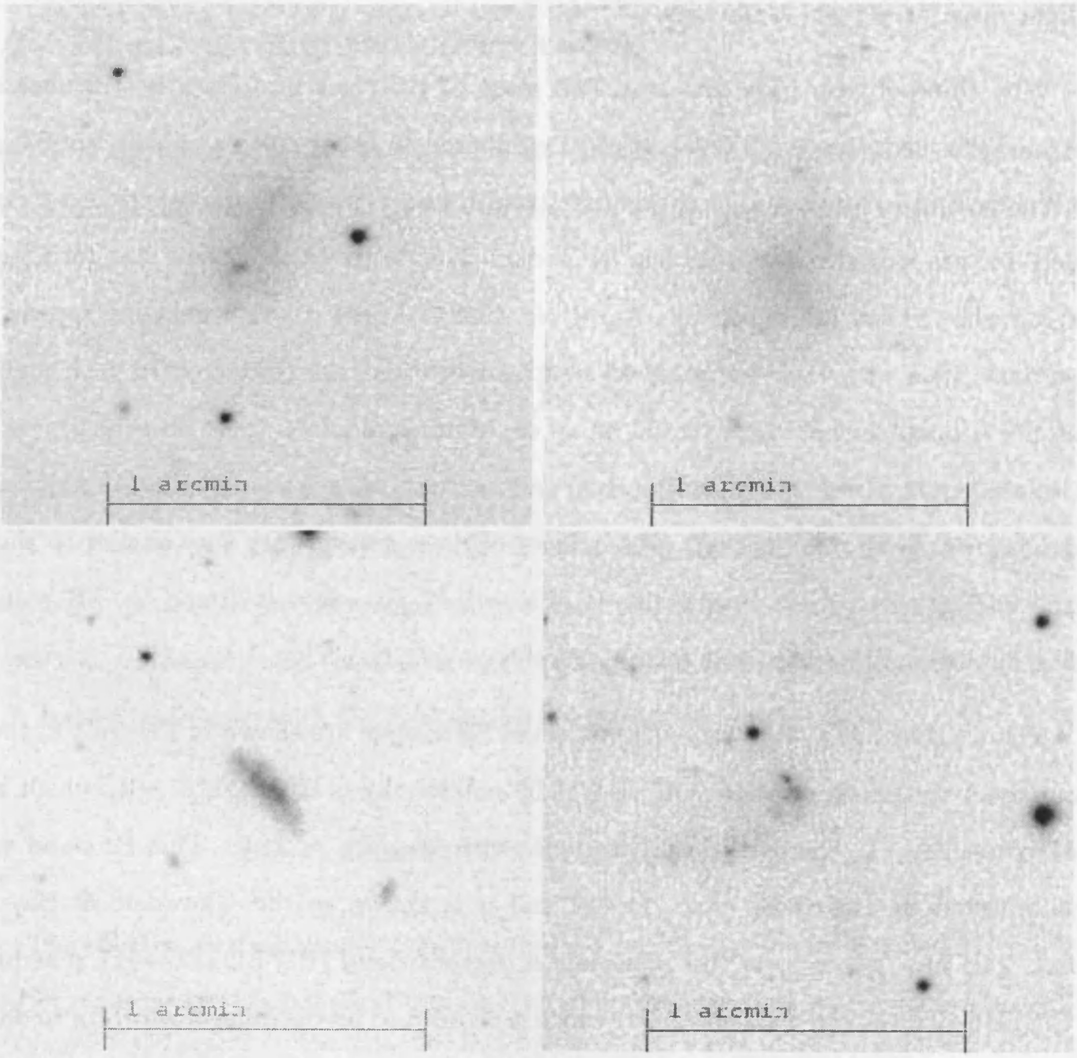

Figure 4.6: High HI mass to Luminosity ratio galaxies in the ES sample. From top left to bottom right (with increasing M_{HI}/L_B) HIPEQ1327+02, HIPEQ1224+00, HIPEQ0936+01 and HIPEQ1227+01. These 4 galaxies are the highest HI mass to blue luminosity ratio objects in the ES sample (see Table 4.2). We believe HIPEQ1227+01 with $M_{\mathrm{HI}}/L_B \sim 22$ to be the highest M_{HI}/L_B galaxy to be confirmed by accurate measurements to date.

($M_{\rm HI}/L_B > 3$) with 4 galaxies having $M_{\rm HI}/L_B > 10$ (see Figure 4.6 and Table 4.2). The lack of high $M_{\rm HI}/L_B$ bright galaxies suggests that there is a physical limit to the HI mass to light ratio for a given luminosity.

Why these objects have not converted most of their gas into stars is still unclear. These objects have 'normal' amounts of HI compared to other galaxies of the same type but they are underluminous. We have already seen (see Figure 4.4) that there is a strong 'trend' for gas-rich galaxies to be less luminous. This suggests that their star formation has, somehow, been inhibited (van Zee *et al.* 1996). These gas-rich galaxies appear to have done little with their unprocessed neutral hydrogen (HI) compared to their stellar content. A possible explanation could be an environmental effect; these objects appear to be isolated systems, which are undisturbed and hence could lack the stimulation necessary to trigger regular star formation. The colours of these galaxies are very similar to those of the LSB galaxies, if not bluer, with B − V = 0.47, B − R = 0.76 and V − R = 0.28 which implies that they are star forming at the present epoch.

The 4 highest $M_{\rm HI}/L_B$ ratio objects in the ES sample are shown in Figure 4.6, their parameters are shown in Table 4.2. Especially noteworthy is HIPEQ1227+01, which has the highest $M_{\rm HI}/L_B$ ratio in the ES sample, with $M_{\rm HI}/L_B = 21.9$. This HI cloud was first detected by Giovanelli *et al.* (1989) and it is known as the Giovanelli & Haynes cloud. The $M_{\rm HI}/L_B$ ratio of the Giovanelli & Haynes cloud (HIPEQ1227+01) is as high as ESO215-G?009 (Warren *et al.* 2004) which is claimed to be the highest $M_{\rm HI}/L_B$ to date. However, ESO215-G?009 is a nearby ($\sim$ 4.2 Mpc) dwarf galaxy with large uncertainties in its distance and lies a region with high galactic extinction and has an estimated baryonic mass of 2×10^8 $M_\odot$. HIPEQ1227+01 on the other hand is at a distance of $\sim$ 22 Mpc, is the second bluest galaxy in the ES sample after HIPEQ0958+01 (see Section 3.6) and has an estimated baryonic mass of 4×10^9 $M_\odot$ – which is 20 times higher than ESO215-G?009. We believe that HIPEQ1227+01 is the highest $M_{\rm HI}/L_B$ galaxy to be confirmed by accurate measurements to date. Most, but not all, gas-rich galaxies in the ES sample are LSB, with a mean $\mu_{eff} \approx 23.79$ and $\mu_0 \approx 23.04$.

4.2 HI mass weighted correlations

As shown in Figure 4.7(a) it can be seen that the absolute magnitude in the ES sample is very strongly correlated with the HI mass and has a best-fitting linear relationship of the form:

$$M_B = (-2.68 \pm 0.14) \times \log\,(\mathrm{M_{HI}}) + (7.09 \pm 1.29) \qquad (4.5)$$

Since there is no optical selection involved in the ES sample, this cannot be a selection effect. However, the same correlation in the OC sample could well be a selection effect since both quantities are dependant on distance to get into the sample. Figure 4.7(b) shows the relationship for the OC sample which has a similarly strong correlation but with a shallower slope, with the best-fitting linear relationship given by

$$M_B = (-2.06 \pm 0.12) \times \log\,(\mathrm{M_{HI}}) + (0.54 \pm 1.18) \qquad (4.6)$$

The effective surface brightness appears to be weakly correlated ($r_s = -0.27$, s = 7e-5) with HI mass for the ES sample (Figure 4.7(c)) and even more weakly correlated ($r_s = 0.19$, s = 2e-3) for the OC sample (Figure 4.7(d)).

The implications of these correlations are that the distributions shown in Chapter 3 for the absolute magnitude and surface brightness are not sampling the same volume in each bin, i.e. the fainter bins which correspond to the lower HI masses, cover a smaller volume. In order to correctly determine the luminosity function (LF) and the surface brightness distribution, it is necessary to correct for this selection effect.

This correction can be made using the HI Mass Function (HIMF). In Chapter 2 I

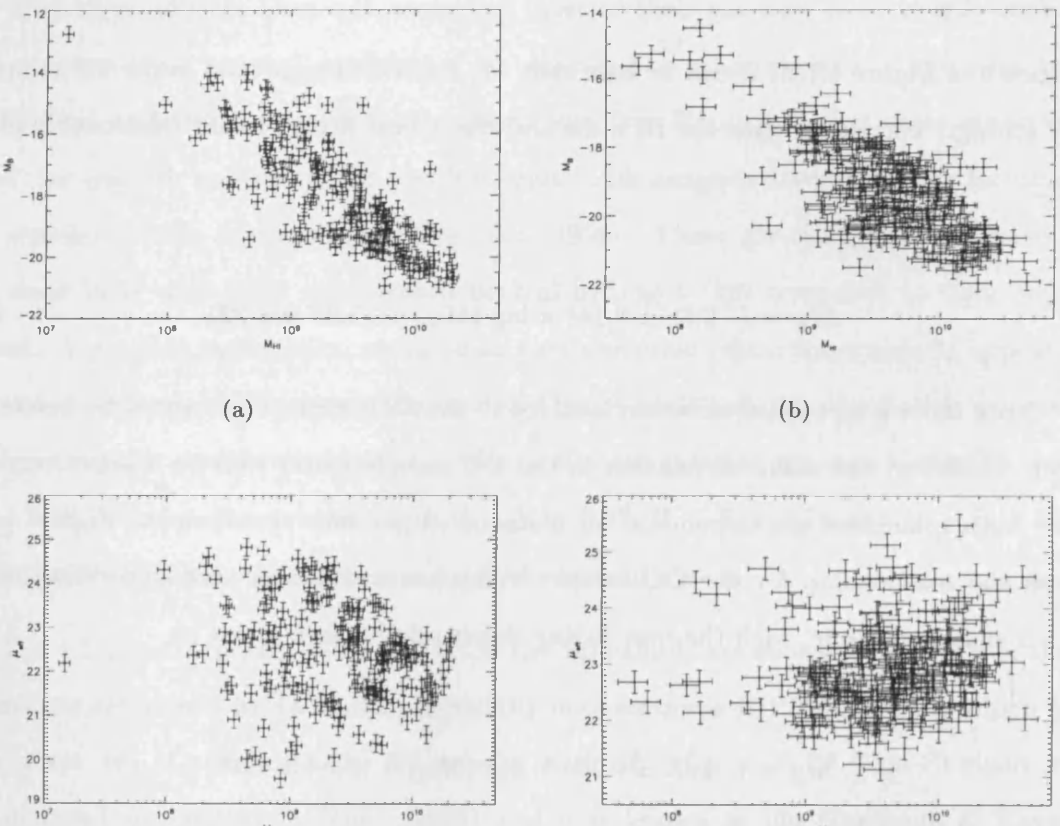

(a) (b)

(c) (d)

Figure 4.7: Upper Panel: The correlation of absolute B band magnitude with HI mass for the ES sample (a) and OC sample (b). Lower panel: The correlation of effective surface brightness with HI mass for the ES sample (c) and OC sample (d). As both these parameters are correlated with HI mass, selection by HI mass will give a biased distribution of these properties unless a correction is applied.

created the HIMF for the ES sample region and I calculated Schechter function parameters with $\alpha = -1.38$ and $M^{\star}_{\rm HI} = 10^{9.75}$ M$_{\odot}$ (see section 2.8). The HIMF shows how many galaxies would be expected in each bin if all bins sampled the same volume in the absence of large scale structure. This can then be used to correct each bin by weighting it according to the number of galaxies actually found in that bin and dividing it by the number expected from the HIMF. This gives the distributions of absolute magnitude and effective surface brightness free of HI selection effects (Minchin 1999).

4.2.1 The Bivariate Brightness Distribution (BBD)

As shown in Section 3.6 the luminosity and surface brightness appear to be correlated (see Figure 3.13(a)), so the the distributions of luminosity and surface brightness on their own do not yield that much information. However,we can instead use the bivariate brightness distribution (BBD) which is the joint distribution in the M_B, μ^B_{eff} plane.

If correctly determined, the BBD ensures that the surface brightness selection effects have not affected the determination of luminosity function, i.e. the space density of galaxies as a function of luminosity. There is normally an implicit (and incorrect) assumption that these selection effects can be ignored in constructing the LF (e.g. Ferguson & McGaugh 1995). It is virtually impossible to obtain an accurate BBD from an optically selected sample but it should be much easier from an HI selected sample (Boyce & Phillipps 1995) as you only have to correct for the HI mass selections.

The BBD gives important information on the contribution of LSB galaxies to the universe; if LSB galaxies are generally faint dwarf galaxies then their contribution to the total light and mass of the universe is not great compared to that of 'normal' surface brightness giant galaxies, but if LSB galaxies occupy the same range of luminosities as 'normal' galaxies, then they could make a significant contribution.

The unweighted BBD of galaxies from the ES sample is shown in Figure 4.8. It

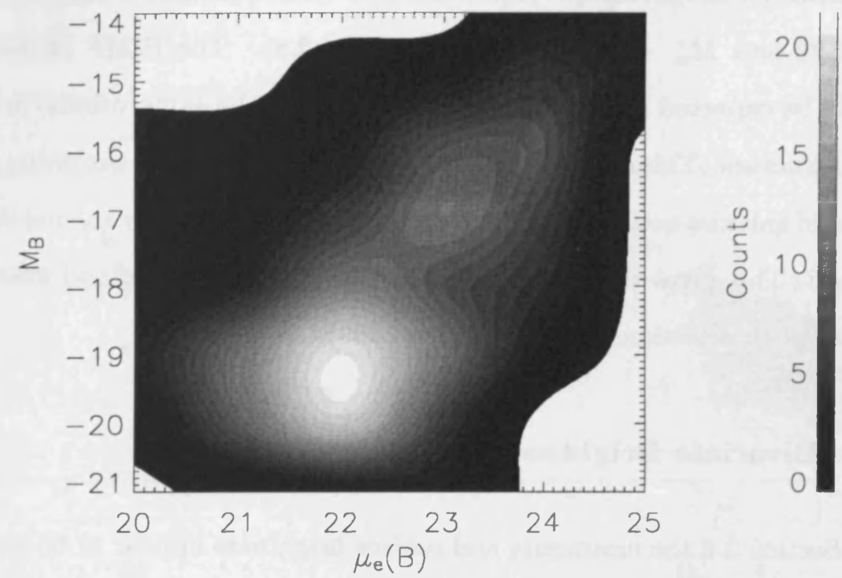

Figure 4.8: Uncorrected bivariate brightness distribution of ES galaxies. The blank areas around the image indicate where there is no data.

shows the correlation between luminosity and surface brightness and illustrates the conventional emphasis on the overwhelming importance of high surface brightness giant galaxies. However, such galaxies tend to have larger HI masses and can be seen over greater volumes.

Figure 4.9 shows the BBD of galaxies for the comparison sample, without any weighting for HI mass being applied. It shows again the correlation between luminosity and surface brightness and illustrates even more dramatically the conventional emphasis on the overwhelming importance of high surface brightness giant galaxies. However, the peak of the distribution seems to be shifted about one magnitude towards fainter effective surface brightnesses and one magnitude towards brighter absolute magnitudes.

The corrected BBD showing the true space density of galaxies is shown in Figure 4.10. After applying the HIMF weighted correction the resulting BBD can be seen that

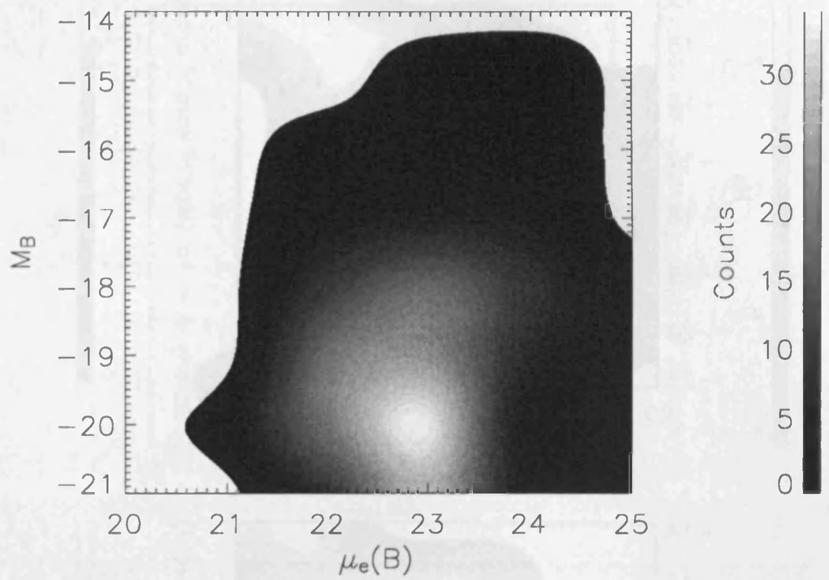

Figure 4.9: Uncorrected bivariate brightness distribution for the OC sample. The blank areas around the image indicate where there is no data.

there is much more uniform population distribution in the absolute magnitude-surface brightness plane compared to that seen in the unweighted BBD. The HIMF weighted BBD is obviously dependent on the HIMF used to construct it. However, my result for the HIMF is in excellent agreement with the best HIMF calculations to date (Zwaan *et al.* 2004).

A steeper HIMF would yield a higher density at low luminosities and low surface brightnesses; while a shallower HIMF decreases the density all around, with the density of low luminosity, low surface brightness galaxies falling slightly more than that of high luminosity, high surface brightness galaxies.

We have defined LSB galaxies to be those with central surface brightness in the B band dimmer than 23 mag arcsec^{-2} ($\mu_0^B > 23$) and/or effective surface brightnesses

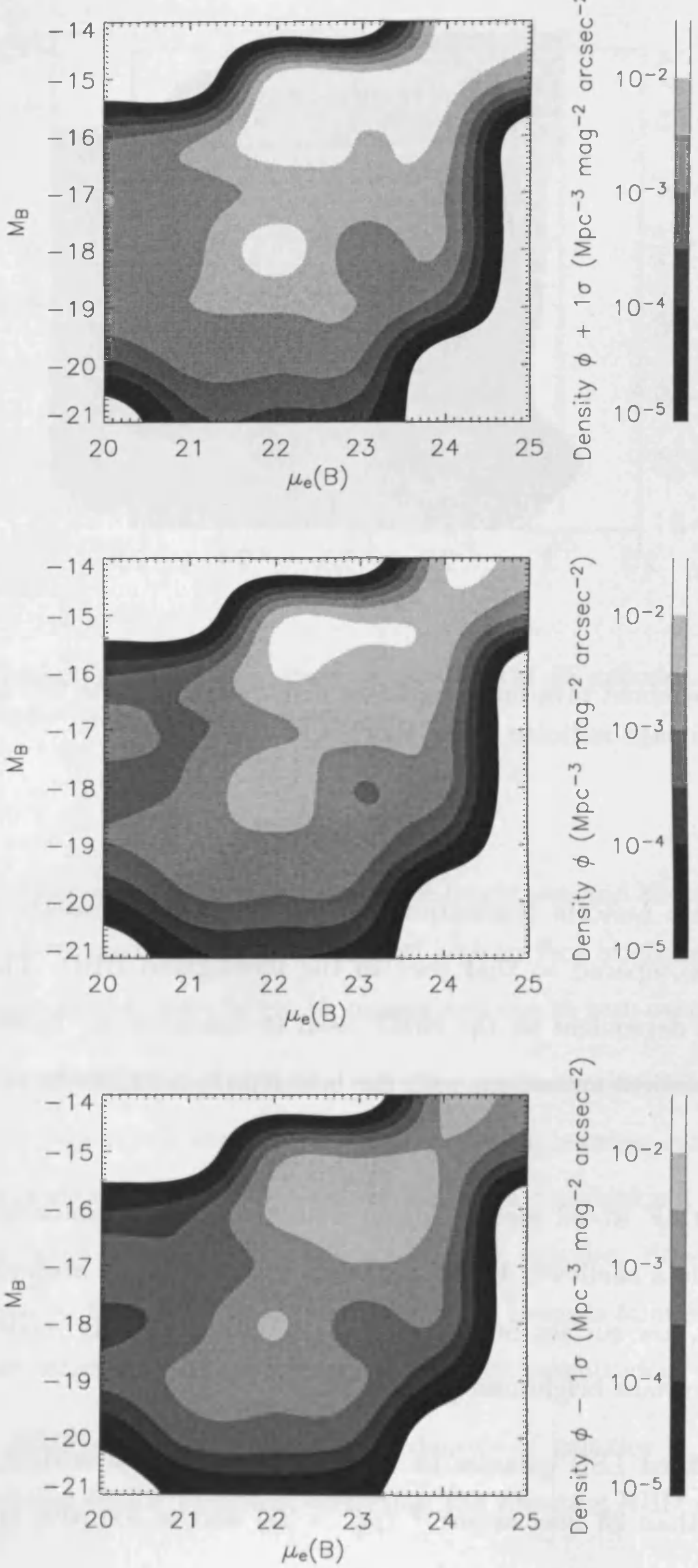

Figure 4.10: The Bivariate Brightness Distribution of HI selected galaxies. The central panel shows the best estimate of the BBD formed using HIMF weighting. The upper and lower panels show the BBD $+1\sigma$ in each bin and BBD -1σ in each bin respectively.

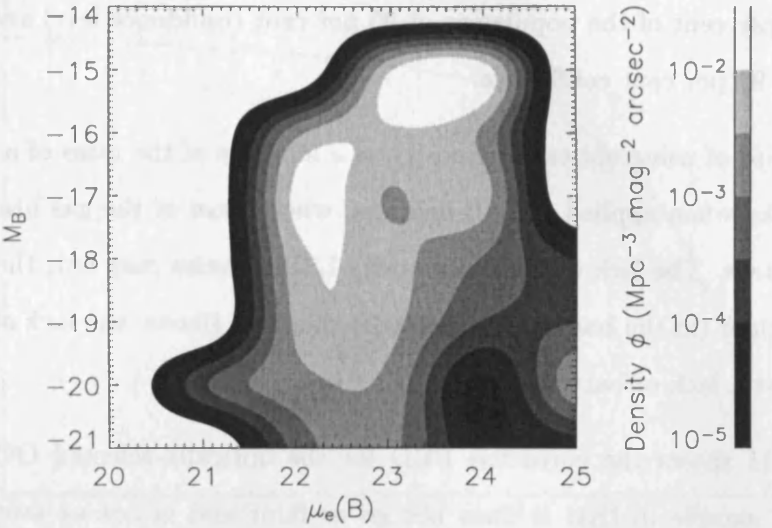

Figure 4.11: The Bivariate Brightness Distribution of the OC sample. The plot shows the best estimate of the BBD formed using the same HIMF weighting used for the ES sample.

($\mu^B_{eff} > 24$). Using this definition, we can set limits on the population of giant LSB galaxies as follows.

There is a clear deficiency of high luminosity, low surface brightness 'Crouching Giant' galaxies (LSB galaxies with $L_B > 10^{10} L_\odot$): of 44 galaxies with $L_B > 10^{10} L_\odot$, not one is an LSB galaxy. By applying the binomial theorem, we can calculate that the probability of finding *no* LSB galaxies in a sample of 44 is less than 0.05 if LSB galaxies make up more than 6 per cent of the population and 0.001 if LSB galaxies make up more than 12 per cent of the population. We can therefore rule out that LSB galaxies make up more than 6 per cent of the high luminosity, gas-rich population at 95 per cent confidence and that they make up more than 12 per cent with 99 per cent confidence.

Of the 22 HI-massive galaxies in the ES sample ($M_{HI} > 10^{10} M_\odot$) not one is an LSB galaxy. By the same method used above HI-massive LSB galaxies therefore contribute no more than 13 per cent of the population at 95 per cent confidence level and no more than 18 per cent at 99 per cent confidence.

The concept of using optical luminosity as a measure of the mass of a galaxy appears somewhat shaky when applied to LSB galaxies, where most of the gas has often not been converted to stars. The lack of high luminosity LSB galaxies may not, therefore, indicate a real lack of giant (in the baryonic sense) LSB galaxies. Hence, the lack of LSB, massive-HI does suggest a lack of baryonic giants.

Figure 4.11 shows the corrected BBD for the optically-selected OC sample. It is unlike the ES sample in that it does not go as faint and is not as evenly distributed. However, it shows a very interesting feature which, if real, would indicate the existence of abundant giant low surface brightness galaxies or 'Crouching Giants'. The overdensity in the bottom right part of the plot ($\mu_{eff}(B) \sim 25$ and $M_B \sim -20$) would indicate the existence of a population of very low surface brightness galaxies with high luminosity which could dominate the luminosity density of the universe. However, we have shown in Section 3.6.1 that the galaxies in those bins seem to have been misclassified and hence that this feature is most likely not real.

4.2.2 Luminosity Function (LF)

The Luminosity function of galaxies (LF) is fundamental for observational cosmology. Accurate knowledge of the luminosity function is required to test cosmological models and to understand galaxy evolution. The luminosity function of galaxies can be created by collapsing the BBD (Figure 4.10) along the surface brightness axis, to form the optical luminosity function. The resulting luminosity function $\phi(L_B)$ is shown in Figure 4.12 as solid points with 1σ error bars. The data is binned in 1 magnitude bins and to enable direct comparison with published luminosity functions we have chosen to use the absolute

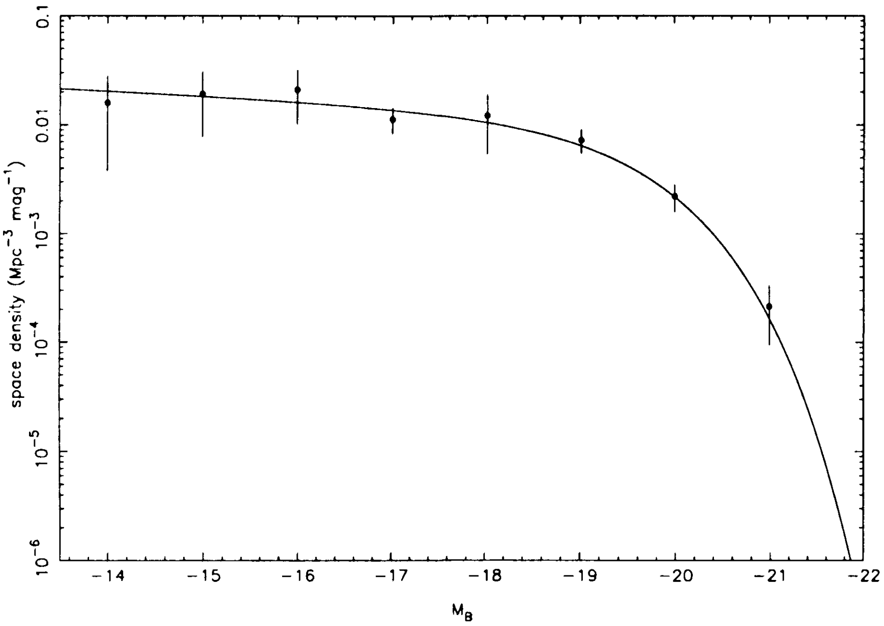

Figure 4.12: Luminosity Function of ES galaxies corrected with HIMF weighting. The best fit has a slope of $\alpha = -1.11^{+0.13}_{-0.09}$.

magnitude uncorrected for opacity effects in the galactic disc.

$$\phi(L)\, dL = \phi^\star \left(\frac{L}{L^\star}\right)^\alpha e^{-\frac{L}{L^\star}}\, d\left(\frac{L}{L^\star}\right) \tag{4.7}$$

In a similar manner to the HIMF in Section 2.8, in order to parameterise the LF, we fit a Schechter (1976) function, where α is the faint end slope, $\phi^\star$ is the normalisation factor and $L^\star$ is the characteristic absolute magnitude at the boundary between the exponential and power law part or the 'knee' of the Schechter function.

The best-fitting Schechter function, which is determined by minimising χ^2 for the expected number of galaxies per bin is shown as a solid curve in Figure 4.12. The best fitting Schechter parameters are found to be $\alpha = -1.11^{+0.13}_{-0.09}$, $L^\star_B = -19.46^{+0.55}_{-0.40}$ and $\phi^\star = (1.12 \pm 0.17) \times 10^{-2}$ Mpc^{-3}. This is a very interesting result as it would be expected to get a steeper slope due to the morphological type of the galaxies in the ES sample being dominated by late type.

It is interesting to compare the luminosity function for HI selected galaxies to the luminosity functions of optically selected galaxies found by other authors. There are a vast number of luminosity functions based on optical redshift surveys in the literature which typically contain a few thousand galaxies. The estimate of the luminosity function for the ES sample is in good agreement with optically selected, especially with that of the SDSS (Blanton *et al.* 2000) which is to date the biggest optical survey and obtained a slope of $\alpha = -1.20$. However, it is particularly striking that the value for the faint end slope ranges from -0.80 for the APM survey (Loveday 1992) to ~ -1.50 for the 2dF survey (Folkes 1999). On the other hand, the normalisation value and the characteristic luminosity or 'knee' are quite similar for all surveys. This most likely reflects the difficulty constraining the faint-end of the LF due to the relatively poor number statistics at the faint-end.

4.2.3 Luminosity density of gas-rich galaxies

A more fundamental parameter is the luminosity density – the integrated light from the whole population of galaxies. It is also a more robust way of comparing galaxy samples than by Schechter function parameters. As discussed by Lilly *et al.* (1996), this parameter is, in principle, less dependent on the details of galaxy evolution than the luminosity function. The integral luminosity density can be determined by integrating the luminosity function (LF) weighted by the luminosity, which gives $\rho_{L_B} = \phi^\star\, L_B^\star\, \Gamma(2+\alpha)$, where Γ is the Euler gamma function.

We find a value of $\rho_{L_B} = (12.3 \pm 1.3) \times 10^7\, h_{75}\, L_\odot^B\, Mpc^{-3}$ for the luminosity density of gas-rich galaxies in the ES sample. The mean value of ρ_{L_B} for the main optically selected galaxy samples is $10.1 \times 10^7\, h_{75}\, L_\odot^B\, Mpc^{-3}$. These results agree remarkably well with each other and they exceed the luminous density of late type irregular galaxies found by Markze *et al.* (1994b) and is 15–30% of the luminous density of the luminous density for all morphological types found by the optical samples.

We can then use the Lilly *et al.* (1996) conversion to get a value of $\rho_{L_B} = (4.0 \pm 0.5) \times 10^{19}\, h_{75}^{-2}\, W\, Hz^{-1}\, Mpc^{-3}$, which is approximately 50% of the integral luminosity density of the local Universe (Lilly *et al.* 1996).

4.3 Optical parameters, HI flux and column densities

4.3.1 Dependence of HI flux on optical parameters

The interesting and unexpected result, described in Chapter 3, that the surface brightness (both the effective and central) and apparent magnitude are linked suggests that there is not a straight correlation between apparent magnitude and HI flux, but rather that the HI flux may depend on other parameters, in particular the size of the galaxy. Figure 4.13(a) shows the strong relationship ($r_s = -0.64$, s = 1e-24) between integrated flux and apparent magnitude for the ES sample; which you would expect since they are equally distance dependant, however, this relationship has a large scatter. The best-fitting (least squares) linear relationship has the form:

$$\log S_{int} = (-0.19 \pm 0.01)\, m_B + (3.73 \pm 0.21) \tag{4.8}$$

As shown in Figure 4.13(b) there is similarly a strong correlation for the OC sample ($r_s = -0.56$, s = 5e-21), for which the best-fitting linear relation is given by $\log S_{int} = (-0.21 \pm 0.02)\ m_B + (4.27 \pm 0.23)$, which is in excellent agreement with that of the ES sample.

Figure 4.14(a) shows there is also a strong correlation ($r_s = 0.64$, s = 3e-25) between effective angular radius and HI flux for the ES sample. The best linear fit to the data

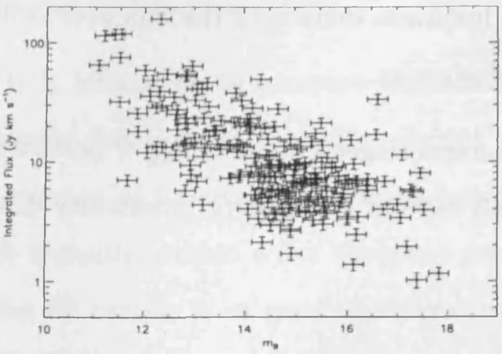

(a)

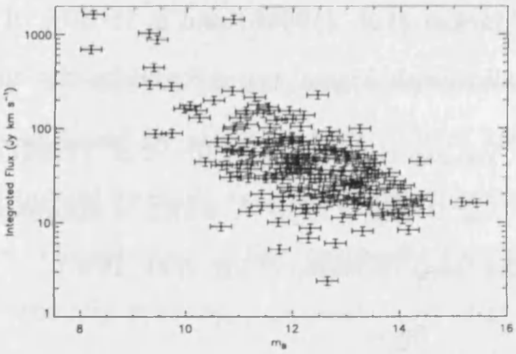

(b)

Figure 4.13: Correlation between apparent magnitude and HI flux (S_{int}) for the ES sample (a) and OC sample (b). Their slope is almost identical. Apparently brighter galaxies have higher HI fluxes

is given by $\log S_{int} = (0.91 \pm 0.07) \log r_{eff} - (0.21 \pm 0.10)$. This supports the idea that the average surface density of HI does not change much, so optically larger galaxies with correspondingly larger HI discs have higher HI fluxes. If the central surface brightnesses of galaxies and the average surface density of HI were constant, then a correspondence between optical and HI sizes would lead to a correspondence between optical luminosity and HI flux.

However, the central surface brightnesses of galaxies are not constant - although the observed central surface brightness of a sample of galaxies often is. It is possible that observed correlations between luminosity and HI flux in optically selected samples are due to surface brightness selection effects. Figure 4.14(b) shows the relationship between effective radius and HI flux for the OC sample ($r_s = 0.56$, s = 3e-21). The best-fitting linear relationship has a shallower slope than the relationship found for the ES sample, given by $\log S_{int} = (0.60 \pm 0.04) \log r_{eff} - (0.89 \pm 0.18)$.

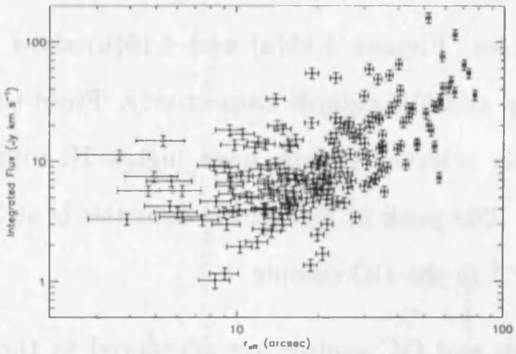

(a)

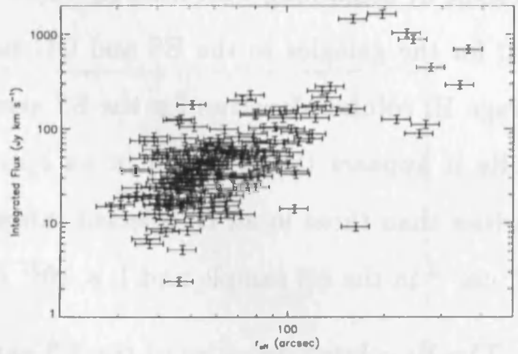

(b)

Figure 4.14: Correlation between effective radius and HI flux (S_{int}) for the ES sample (a) and OC sample (b). The slope in the ES sample is steeper than that of the optically selected OC sample.

4.3.2 Estimated HI column densities

From the optical size it is possible to estimate the size of the HI disc and hence get an estimate of the HI column density. To do this, it is necessary to rely on data from optically selected samples in order to relate the HI size of the galaxy to the effective radius. These relationships will therefore have been derived from samples with surface brightness close to the Freeman value, and they might not be applicable to LSB galaxies.

From the ESO-LV catalogue, which gives effective diameters and the diameter to the 25 B_μ isophote, it is possible to calculate that $r_{B25} \approx (2.15 \pm 0.67) \times r_{eff}$. Salpeter & Hoffman (1996) found that $r_{\rm HI} \approx (2.34 \pm 0.14) \times r_{B25}$ for an optically selected sample and we can combine these to give

$$r_{\rm HI} \approx (5.03 \pm 1.59) \times r_{eff} \tag{4.9}$$

Equation 4.9 has been used to calculate the HI radii of the galaxies in the ES sample and thus, by combining with their HI fluxes we have calculated the average column density of HI for the galaxies in the ES and OC samples. Figures 4.15(a) and 4.15(b) show the average HI column densities for the ES sample and OC sample respectively. From these results it appears that galaxies in an optically selected sample have higher HI column densities than those in an HI selected sample. The peak in HI column densities is at 3×10^{20} cm^{-2} in the ES sample and 1×10^{21} cm^{-2} in the OC sample.

The HI column densities of the ES sample and OC sample are compared to the effective surface brightnesses in Figures 4.16(a) and 4.16(b) respectively. It can be seen that no galaxies have particularly low average column densities – even if the radii of the HI discs used are too small by a factor of 2 then the lowest column densities would still be around $10^{19.6}$ cm^{-2}. There is a tendency ($r_s = -0.40$, s = 3e-9) for lower surface brightness galaxies to have lower column densities both in the ES and OC samples. There seems to be a lack of high column density, low surface brightness galaxies. The best-fitting linear relation gives $\log(N_{HI}) = -0.16 \times \mu_{eff} + 24.35$ with a large scatter of 0.3 dex. The linear relationship for the OC sample is extremely similar to that for the ES sample.

Giovanelli & Haynes (1988) give values of log $M_{\rm HI}/D^2_{Holm}$ (where D_{Holm} is the Holmberg diameter in kpc) for galaxies of different morphological types which are consistently around $\approx 8 \times 10^{20}$ cm^{-2}. This should be approximately twice the value calculated here for N_{HI}, and it does appear from the values calculated that most galaxies in the ES sample have $N_{HI} \approx 4 \times 10^{20}$ cm^{-2}. The column densities from the ES sample appear, therefore, to be consistent with those from the optically selected sample of Giovanelli & Haynes, despite having considerably higher values of $M_{\rm HI}/L_B$.

There appears to be a sharp cut-off at around 2×10^{19} cm^{-2} even though our detection sensitivity is significantly lower at $N_{HI} \sim 8 \times 10^{18}$ cm^{-2}. Minchin (2003) found the same cut off in his deep (HIDEEP) survey which went down to an even lower limit of $N_{HI} \sim 2 \times 10^{18}$ cm^{-2}, which we would imply that there is no low column density

(a)

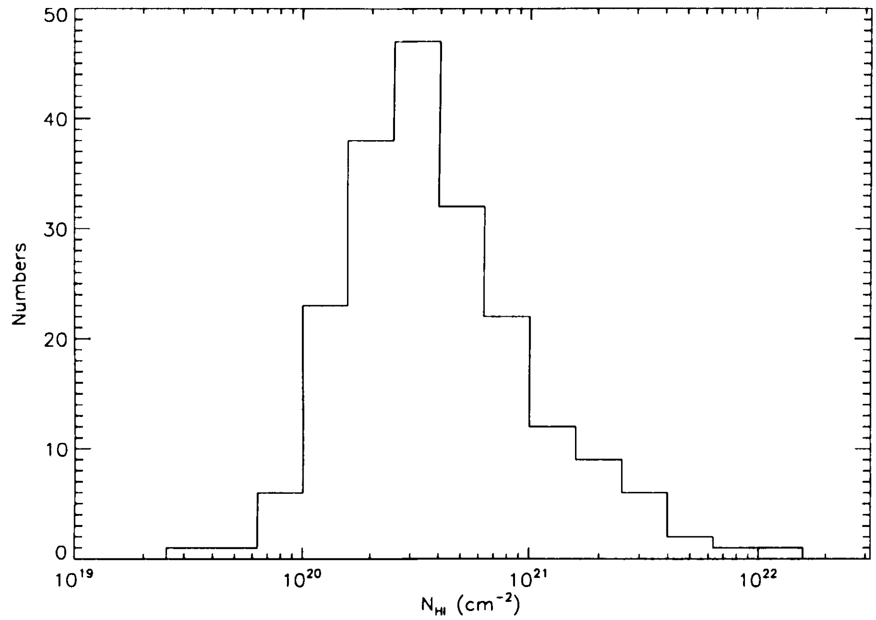

(b)

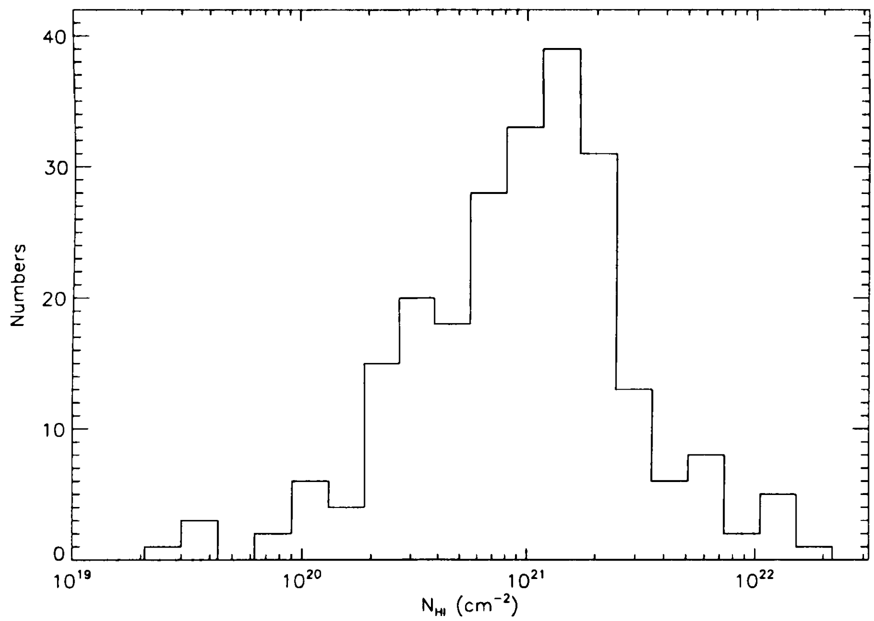

Figure 4.15: Average HI column density distribution for the ES sample (a) and OC sample (b). The peak in HI column densities is at 3 $\times$ 10^{20} cm^{-2} in the ES sample and 1 $\times$ 10^{21} cm^{-2} in the OC sample.

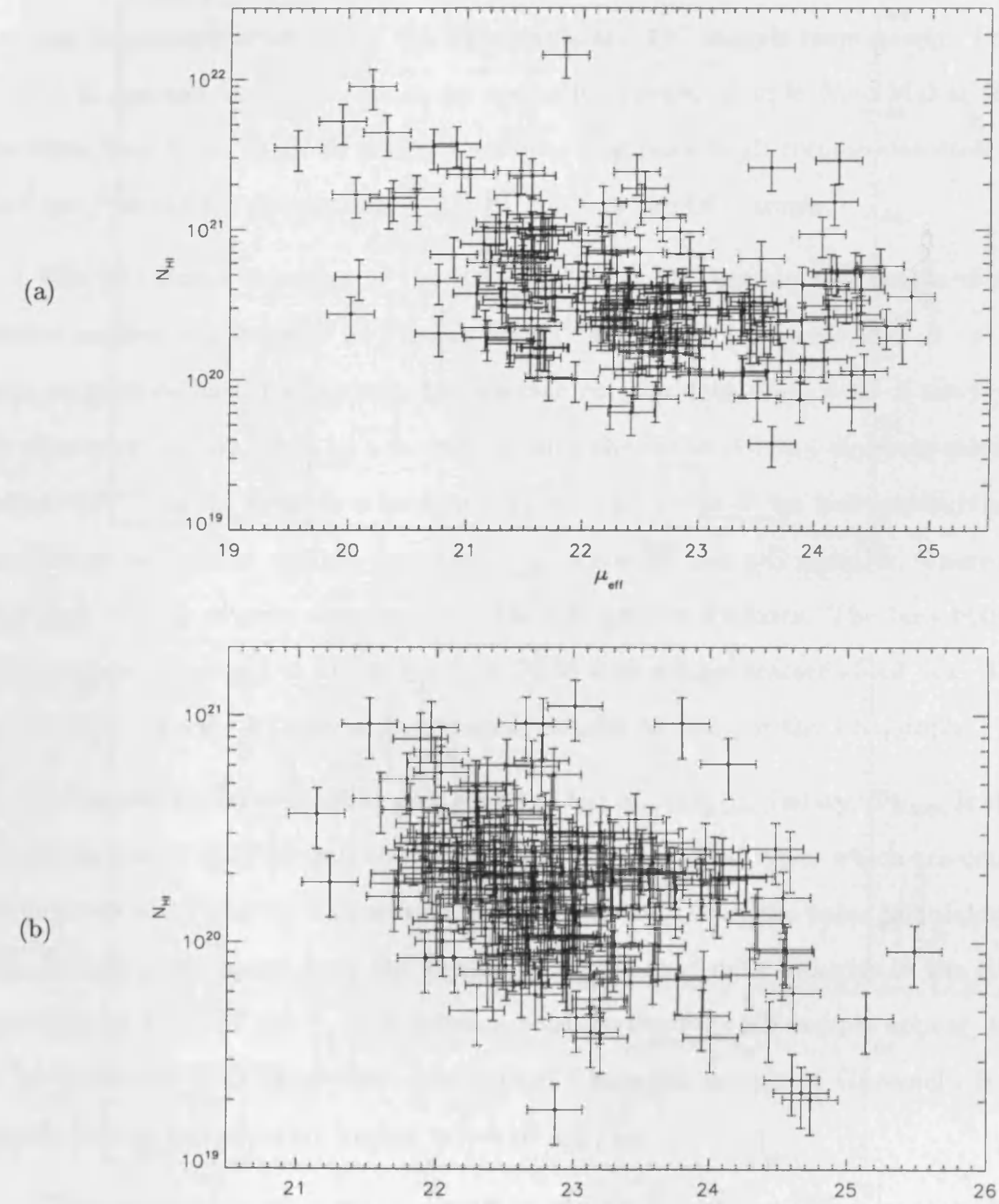

Figure 4.16: Comparison between effective surface brightness and estimated average HI column density for the ES sample (a) and OC sample (b).

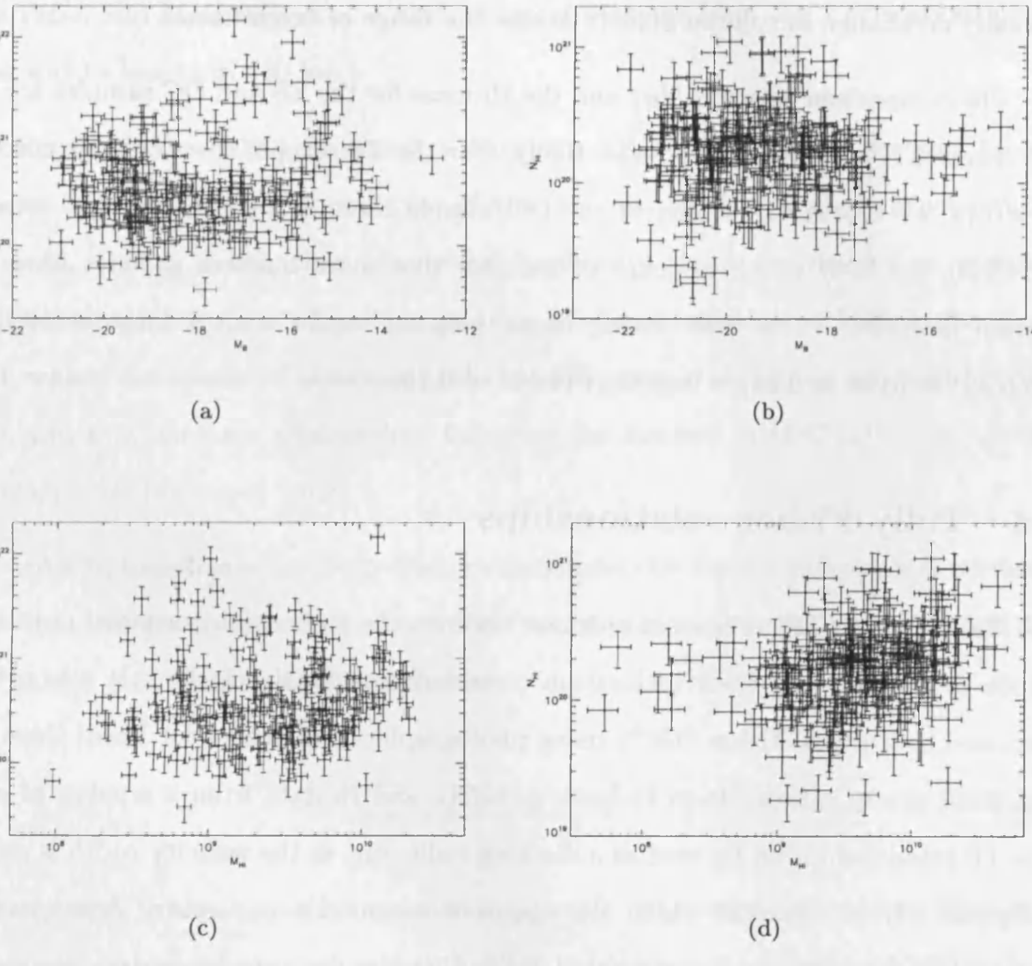

Figure 4.17: Upper panel: comparison between average HI column density and absolute magnitude for the ES sample (a) and OC sample (b). Lower panel: comparison between average HI column density and HI mass for the ES sample (c) and OC sample (d).

population of HI rich galaxies that would be missed by the ES sample.

Other comparisons with the estimated HI column density are given in Figure 4.17. The comparison between absolute magnitude and N_{HI} for the ES sample and the OC sample respectively are shown in Figures 4.17(a) and 4.17(b). It can be seen that there is virtually no change in column density across the range of brightnesses.

The comparison between N_{HI} and the HI mass for the ES and OC samples are shown in Figures 4.17(c) and 4.17(d) respectively. For the ES sample there is little correlation ($r_s = 0.14$, $s = 0.049$). However, in the OC sample there is a much stronger correlation ($r_s = 0.30$, $s = 1\text{e-}6$) which appears to indicate that more massive galaxies have higher column densities. The best fitting linear relation, again with a large scatter, gives $\log(N_{HI}) = (0.39 \pm 0.04) \times \log(M_{HI})\ (18.46 \pm 0.18)$.

4.4 Tully-Fisher relationships

The Tully-Fisher (TF) relationship is one between the inclination corrected optical magnitude of galaxies and their inclination corrected rotational velocity. It was originally discussed by Tully & Fisher (1977) using photographic magnitudes for Local Group, M81 and M101 group galaxies from Holmberg (1958), and HI data from a number of sources. The TF relationship can be used as a distance indicator, as the velocity width is measured independently of distance, whilst the apparent magnitude is distance dependent. The distance to a galaxy can be estimated by finding the distance necessary to correct the observed apparent magnitude to the absolute magnitude predicted by the velocity width.

The application of the Tully-Fisher (TF) relationship to different types of galaxies has been much discussed in recent years. Zwaan *et al.* (1995) found that LSB galaxies seemed to fall on the same TF relationship as 'normal' galaxies, however other authors have found types of galaxies that deviate from the TF relation. Matthews, van Driel & Gallagher

(1998) found that most of their sample of extremely late-type, low-luminosity spirals fell below the standard TF relationship, with the deviation increasing with decreasing size and luminosity. O'Neil, Bothun & Schombert (2000) found deviations in high velocity-width ($\Delta V > 200$km s^{-1}) galaxies, with these deviations increasing with increasing HI mass to light ratio, and McGaugh *et al.* (2000) found deviations from the TF relationship for galaxies widths less than 180 km s^{-1} .

McGaugh *et al.* (2000) proposed a baryonic TF relationship to account for the deviations they saw. They found that if the TF relationship was constructed using $M_{bary} = M_\star + M_{gas}$ rather than the optical luminosity alone, the deviations vanished. The TF relationship for the ES sample galaxies has been investigated both in the B and R-band, where the results of Courteau (1997) and Burton *et al.* (2001) are used for comparison, and as a baryonic relationship, following the method of McGaugh *et al.* (2000). These results are presented below.

In order to investigate the Tully-Fisher relationship for the ES sample, it is necessary to make an estimate of their inclination. This has been carried out using the optical axis ratio obtained (see Chapter 3) and equation:

$$\cos^2 i = \frac{(b/a)^2 - r_0^2}{1 - r_0^2} \tag{4.10}$$

(Holmberg 1958) where r_0 is the assumed axial ratio of an edge-on system. This is an unknown value which falls in the range 0.11 – 0.20. I have assumed a value of 0.16 with the errors on the inclinations modified to take the possible range of values into account – this makes very little difference except for very edge on systems. Only those systems where the implied inclination was between 40° and 80° were used for defining the Tully-Fisher relationship, as this is where the inclinations are most reliable, but inclinations have been found for all the ES sample galaxies. The distribution of inclinations is shown in Figure 4.18. The velocity widths were corrected using:

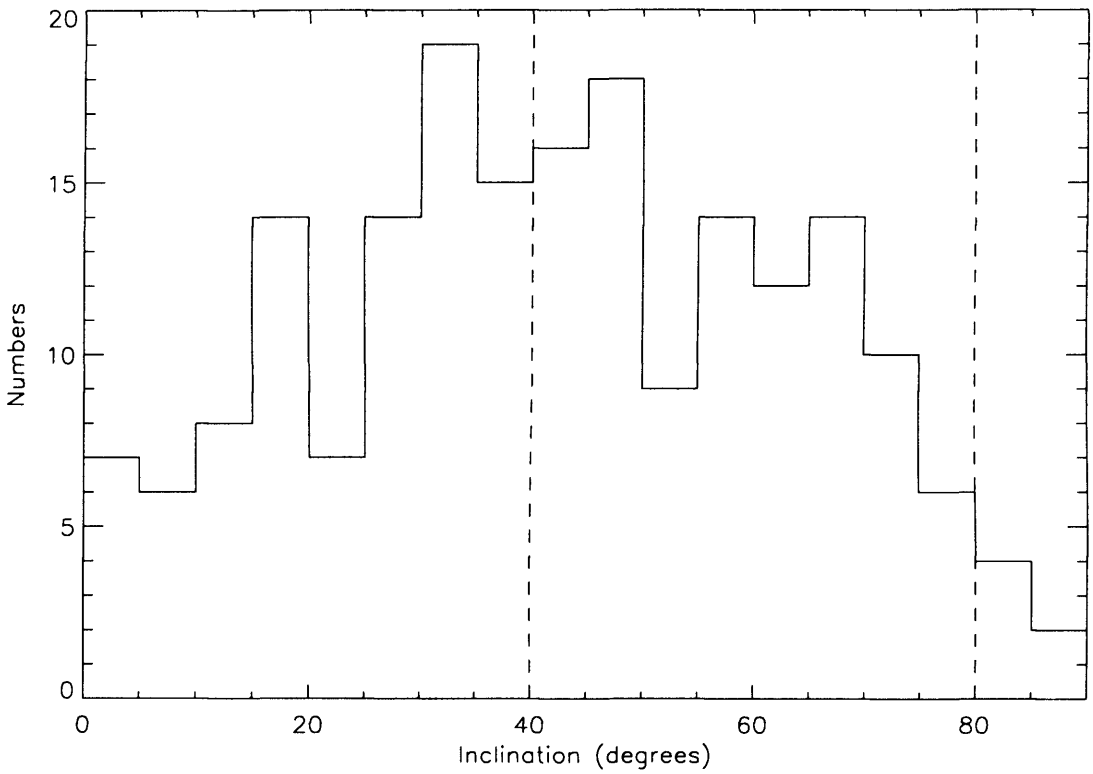

Figure 4.18: Distribution of galaxy inclinations for the ES sample. The dashed lines at 40° and 80° indicate the boundaries of the range of inclinations taken as useful for analysing Tully-Fisher relationships. There are 99 galaxies in the ES sample that fall in that category and they are the ones used to determine the B-band, R-band and baryonic TF relationships for the ES sample.

$$\Delta V(0) = \frac{\Delta V_{50}}{\sin i} \tag{4.11}$$

(Tully & Fisher 1977) where $\Delta V(0)$ is the corrected velocity width. The errors of $\Delta V(0)$ have been estimated using the error of 16 km s^{-1} on ΔV_{50} and an assumed error of 10% in b/a. I follow Burton *et al.* (2001) by using $\eta = \log \Delta V(0) - 2.5$ in defining the TF relationship as $M_B = \Delta TF + \alpha_{TF}\eta$. The absolute magnitudes of the galaxies were corrected according to the prescription of Courteau (1997), who used $M_B = M_B - A_{i,B}$ where the internal absorption, $A_{i,B}$ is given by

$$A_{i,B} = 0.95\,[\log(a/b) - 0.418] \tag{4.12}$$

This corrects all the galaxies to the magnitude they would have at an inclination of 70°. However, this makes no allowance for the surface brightness of galaxies – LSB galaxies are thought to contain less dust than 'normal' galaxies, which would lead to them having a smaller internal extinction and thus being overcorrected here and appearing brighter than they truly are. As most LSB galaxies are low-luminosity galaxies, this would have the effect of making the slope of the TF relationship shallower.

The B and R-band Tully-Fisher relationships found for the ES sample are shown in Figures 4.19(a) and 4.19(b) respectively. The best-fitting linear relationship is indicated by the solid line. The parameters of the linear relationship are given in Table 4.3. These TF relationships found for the ES sample are consistent with previous values from the literature, some of which are shown for comparison in Table 4.3.

It is possible that a 'baryonic' TF relationship for the ES sample may provide a better fit. The baryonic mass for the ES sample has been found by combining the HI mass and optical luminosity using:

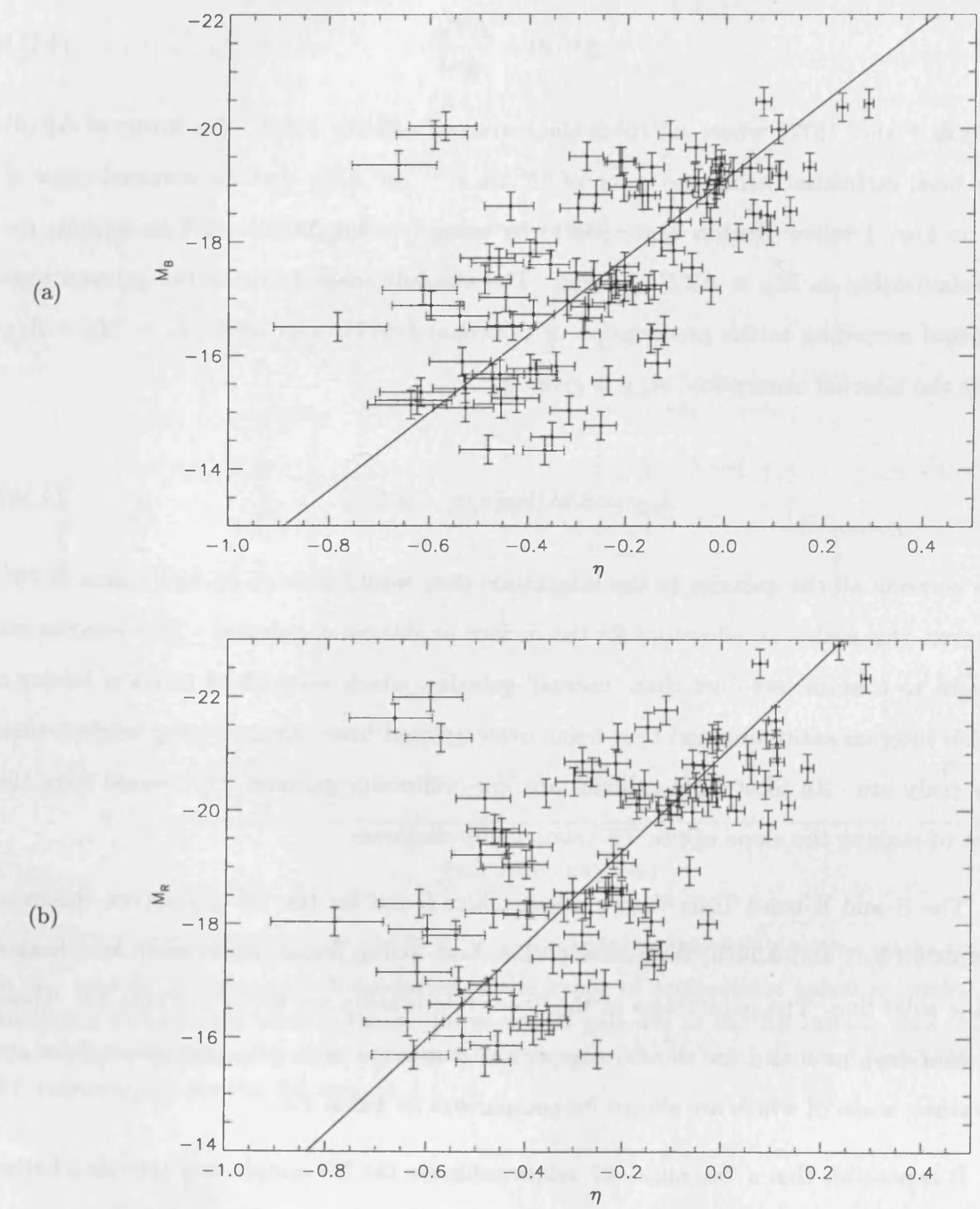

Figure 4.19: Tully-Fisher (TF) relationships for ES sample of galaxies: (a) in the B-band and (b) in the R-band.

Table 4.3: Tully-Fisher parameters

Sample	band	α_{TF}	Δ_{TF}
ES sample	**B**	-6.85 ± 0.18	-19.10 ± 0.47
Pierce & Tully (1992)	B	-7.48 ± 0.24	-19.55 ± 0.32
ES sample	**R**	-8.33 ± 0.21	-20.97 ± 0.47
Pierce & Tully (1992)	R	-8.23 ± 0.14	-20.46 ± 0.22
HIDEEP (2001)	R	-9.84 ± 1.32	-20.18 ± 0.03
Courteau (1997)	R	-7.18 ± 0.26	-20.98 ± 0.05

$$M_{baryonic} = 1.4\ M_{\rm HI}\ +\ \Upsilon_\star^B\ L_B \tag{4.13}$$

where $\Upsilon_\star^B$ is the stellar mass to B-band light. This has been estimated, as in McGaugh *et al.* (2000) using the model of de Jong (1996) for a 12 Gyr old, solar metallicity stellar population with a constant star formation rate and a Salpeter initial mass function, corrected to B-band using the average colours in that paper (also used by McGaugh *et al.* for their correction to H-band). This gives a value of $\Upsilon_\star^B \approx 1.4$, which I have used in my calculations.

Once the baryonic mass has been calculated, the baryonic TF relationship can be found. This is shown in Figure 4.20. The line indicates the best-fitting linear relation, which is given by $\log(M_{bary}) = (3.10 \pm 0.53) \times \eta + (10.34 \pm 0.19)$. Minchin (2001) found $\log(M_{bary}) = (3.20 \pm 0.42) \times \eta + (10.213 \pm 0.068)$ and McGaugh *et al.* (2000) found $\log(M_{bary}) = (3.98 \pm 0.12) \times \eta + (10.32 \pm 0.01)$). The best-fitting line is within 2σ of both the best-fits from McGaugh *et al.* (2000) and Minchin (2001).

The ES sample data is consistent with both previous optical and baryonic TF relationships. The baryonic TF found for the ES sample appears to be slightly shallower than previous determinations (e.g. Minchin 2001, McGaugh *et al.* 2000), however, this sample

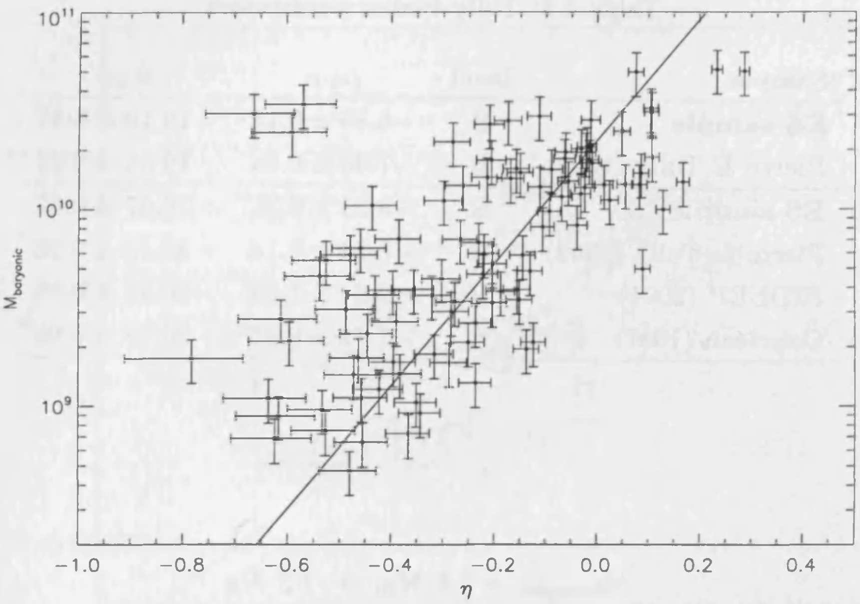

Figure 4.20: Baryonic Tully-Fisher relationship for the ES sample. The solid line shows the best-fitting linear relation to the ES data.

is more uniform than that of McGaugh *et al.* (2000) which draws its optical data from a number of different surveys.

4.5 Dynamical Masses

It is possible to make a rough estimate of the dynamical masses of the ES galaxies using the standard relation:

$$M_{dyn} = \frac{R_{\rm HI} \times (\Delta V(0))^2}{\rm G} \tag{4.14}$$

I have estimated $R_{\rm HI}$ as in Section 4.3 using $r_{\rm HI} = 5.03 \pm 1.59 \times r_{eff}$ and converted the result to kpc using the distances to the ES sample galaxies. $\Delta V(0)$ has been calculated using the same method as for the Tully-Fisher relationship in Section 4.3. The distribution of dynamical masses is shown in Figure 4.21.

The relationship between the dynamical mass of the ES sample galaxies and HI mass to light ratio of these galaxies is shown in Figure 4.22. As $M_{\rm HI}/L_B$ is distance independent, this correlation could not be directly due to distance dependence. However, that the HI mass to light ratio is larger in galaxies with smaller dynamical masses is expected, as similar relationships between the HI mass to light ratio and luminosity HI mass have already been seen.

Figure 4.23 shows how the surface brightness of galaxies varies with dynamical mass

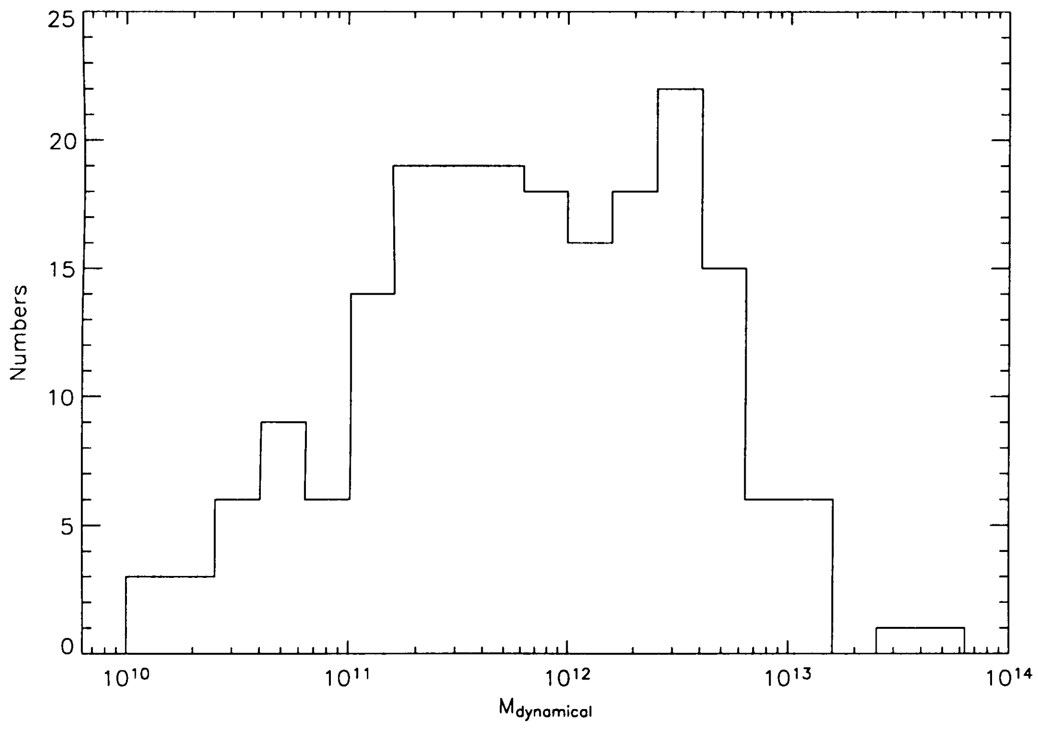

Figure 4.21: Distribution of approximate dynamical masses in units of solar mass. The distribution is similar in shape to the distributions of HI mass and of absolute magnitude and has a total width of 3.5 dex.

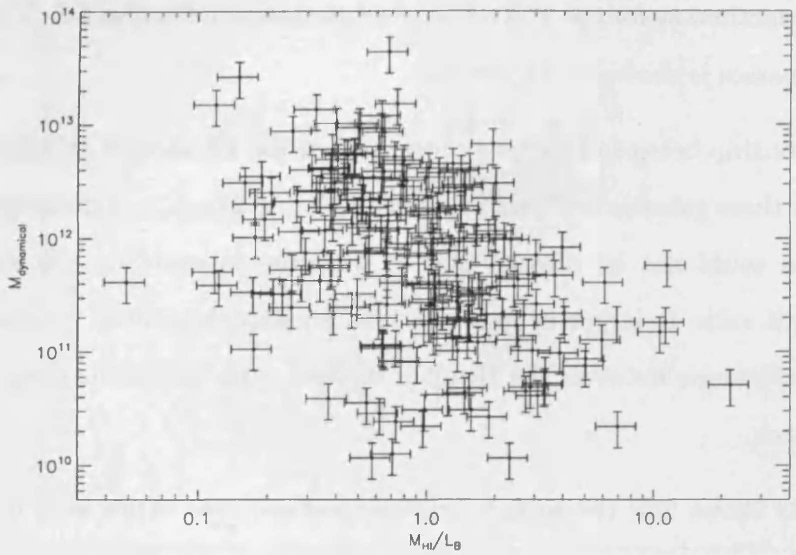

Figure 4.22: Variation of HI mass to light ratio with approximate dynamical mass. It can be seen that there is a trend for less massive galaxies to have higher HI mass to light ratios. Most low mass galaxies found in the ES sample are gas-rich.

for the ES sample. It can be seen that there is a correlation here ($r_s = -0.29$, $s = 2e\text{-}5$), with the more massive galaxies having higher surface-brightnesses. This is expected, as similar correlations have already been seen between surface brightness and HI mass and optical luminosity. However, there are some giant galaxies with low effective surface brightnesses - HIPEQ2337+00 is the largest LSB galaxy with μ_{eff} = 24.10, μ_0 = 23.14, $M_{HI} = 2 \times 10^9$ $M_{\odot}$. While this is similar to the result for M_{HI}, it is very different from the result for L_B. It appears that LSB galaxies can be 'giant' in the sense of containing a lot of mass or neutral hydrogen without meeting the standard definition of a giant galaxy - i.e. having a high luminosity.

The correlation between the dynamical mass to light ratio (M_{dyn}/L_B) and the effective surface brightness ($r_s = 0.38$, $s = 2e\text{-}8$) is shown in Figure 4.24. The best-fitting linear relationship, shown by the solid line in Figure 4.24, has a slope of 0.21 ± 0.011 which is in excellent agreement with the prediction from the $\Upsilon\Sigma$–relation (Zwaan *et al.* 1995), which had a slope of 0.2. It is also in good agreement with the result found by de Blok, McGaugh & van der Hulst (1996) using radio synthesis imaging to map the HI distribution of galaxies and thus accurately determine their dynamical masses.

The $\Upsilon\Sigma$ relation was derived by Zwaan *et al.* 1995 as a necessary consequence of their result that LSB and 'normal' galaxies sat on the same TF relationship. It is derived from

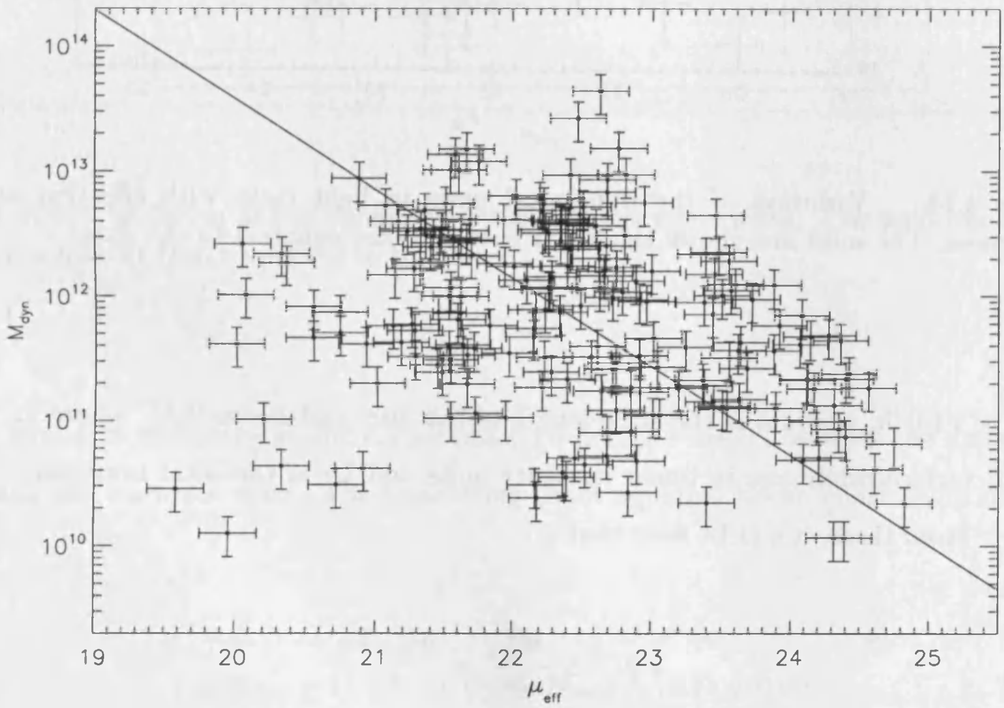

Figure 4.23: Relationship between surface-brightness and dynamical mass. There is a correlation seen here, with the more massive galaxies having higher surface-brightnesses. However, 'giant' LSB galaxies with $M_{dyn} \gtrsim 10^{12} M_\odot$ can be found. HIPEQ2337+00 with $\mu_{eff} = 24.10$, $\mu_0 = 23.14$ and $M_{HI} = 2 \times 10^9$ $M_\odot$ is the largest LSB galaxy with $M_{dyn} \approx 7 \times 10^{11}$ $M_\odot$. Large LSB galaxies are not identified as such by their optical properties, even when they contain very large amounts of neutral hydrogen or have very high dynamical masses.

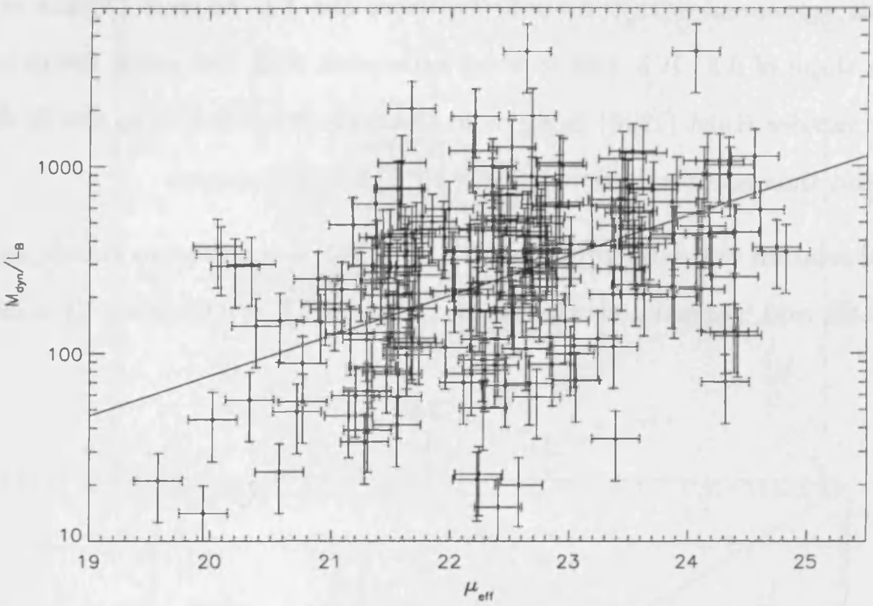

Figure 4.24: Variation of the dynamical mass to light ratio with effective surface-brightness. The solid line shows the linear best-fit (least squares) to the data.

$M_{dyn} \propto V(0)^2 h$, where h is the scale-length of the disc, and $L_T \propto \Sigma_0 h^2$, where Σ_0 is the central surface-brightness in linear intensity units and L_T is the total luminosity of the galaxy. From these, it can be seen that

$$V(0)^4 \propto \frac{M_{dyn}^2}{h^2} \propto \frac{M_{dyn}^2 \Sigma_0}{L_T} \tag{4.15}$$

(Equation 1 in Zwaan *et al.* 1995) which can be rearranged to give

$$L_T \propto \frac{V(0)^4}{\Sigma_0 (M_{dyn}/L_T)^2} \tag{4.16}$$

For the Tully-Fisher relation, $L_T \propto V(0)^4$, to hold for all galaxies as Σ_0 varies, it is therefore necessary that $\Sigma_0 (M_{dyn}/L_T)^2$ (or $\Sigma \Upsilon^2$) remains constant.

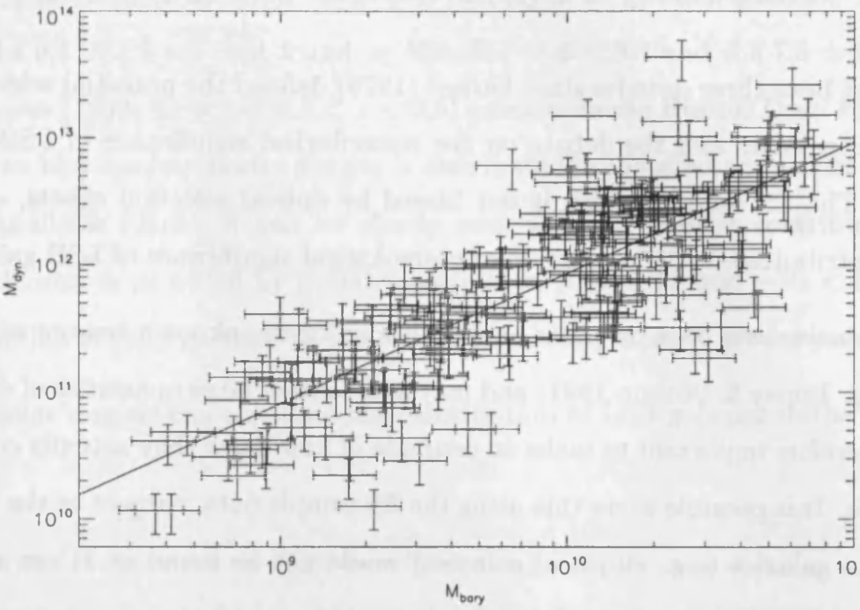

Figure 4.25: Variation of the dynamical mass with baryonic mass. The solid line shows the linear best-fit (least squares) to the data.

Figure 4.25 shows the strong correlation ($r_s = 0.81$, s = 1e-31) between the dynamical mass and the baryonic mass. The best-fitting (least squares) linear relationship has the form:

$$\log M_{dyn} = (1.03 \pm 0.05) \log M_{bary} + (1.65 \pm 0.05) \tag{4.17}$$

It can be clearly seen that there is a 1:1 correspondance between the dynamical and baryonic masses. This implies that most galaxies have about 2 orders of magnitude more mass in their dynamical mass than in their baryonic mass implying that galaxies contain ~ 100 times more dark matter than baryonic matter.

4.6 Cosmological contribution of gas-rich LSB Galaxies

It has almost been three decades since Disney (1976) defined the potential selection effects against LSB galaxies and the debate on the cosmological significance of LSB galaxies is still open. The ES sample, which is not biased by optical selection effects, can make a valuable contribution to the discussion of cosmological significance of LSB galaxies.

LSB galaxies have been proposed as repositories for an unknown amount of the missing baryons (e.g. Impey & Bothun 1997) and may also contain large quantities of dark matter, thus it is therefore important to make an estimate of how much they actually contribute to the Universe. It is possible to do this using the ES sample data, subject to the assumption that HI poor galaxies (e.g. elliptical galaxies) would not be found at 21 cm and that we do not detect sufficient numbers of dwarf galaxies ($M_{HI} < 10^8$ $M_{\odot}$) to say anything about their contribution. In this section I analyse the contribution of the LSB galaxies in the ES sample to the total contribution of HI rich galaxies using the HIMF weighting described in Section 4.2.1 to correct the numbers in each surface brightness bin.

Figure 4.26 shows the volume corrected surface brightness distribution of the ES sample. This seems to be consistent with a flat surface brightness distribution between $22 < \mu_{eff} < 24$, a downturn at the bright end and possibly at the low surface brightness end ($\mu_{eff} > 24$), though the errors in that bin are big and the flat trend between at $22 < \mu_{eff} < 24$ continuing at lower surface brightnesses cannot be discounted. The contribution of LSB galaxies to the total number density in the ES sample is 35^{+29}_{-20} per cent, which is lower (at the 95%) than the 62 ± 37 per cent calculated by Minchin *et al.* 2004 for a sample half the size.

To compare the contribution to the luminosity density made by galaxies of different surface brightnesses, we need to weight the surface brightness distribution in Figure 4.26 with the luminosities of the galaxies, and this is shown in Figure 4.27. The luminosity density is peaked at $\mu_{eff} \sim 22$. Gas-rich LSB galaxies do not appear to emit much light with only 7^{+3}_{-2} per cent of the total luminosity density of all gas-rich galaxies. This is very similar to the 6.7 ± 2.8 per cent found by Minchin *et al.* 2004 and the 7.3 ± 3.6 per cent found by Driver (1999) for local ($0.3 < z < 0.5$) galaxies in the Hubble Deep Field. Figure 4.27 (a) shows how the luminosity density is distributed in the effective surface brightness-absolute magnitude plane. It can be clearly seen that the highest contribution to the luminosity density is provided by galaxies with $21 < \mu_{eff} < 23$ and $-20 < M_B < -18$. The contribution of LSB galaxies to the overall luminosity density is very modest.

In a similar way we can calculate the contribution of LSB galaxies to the neutral gas

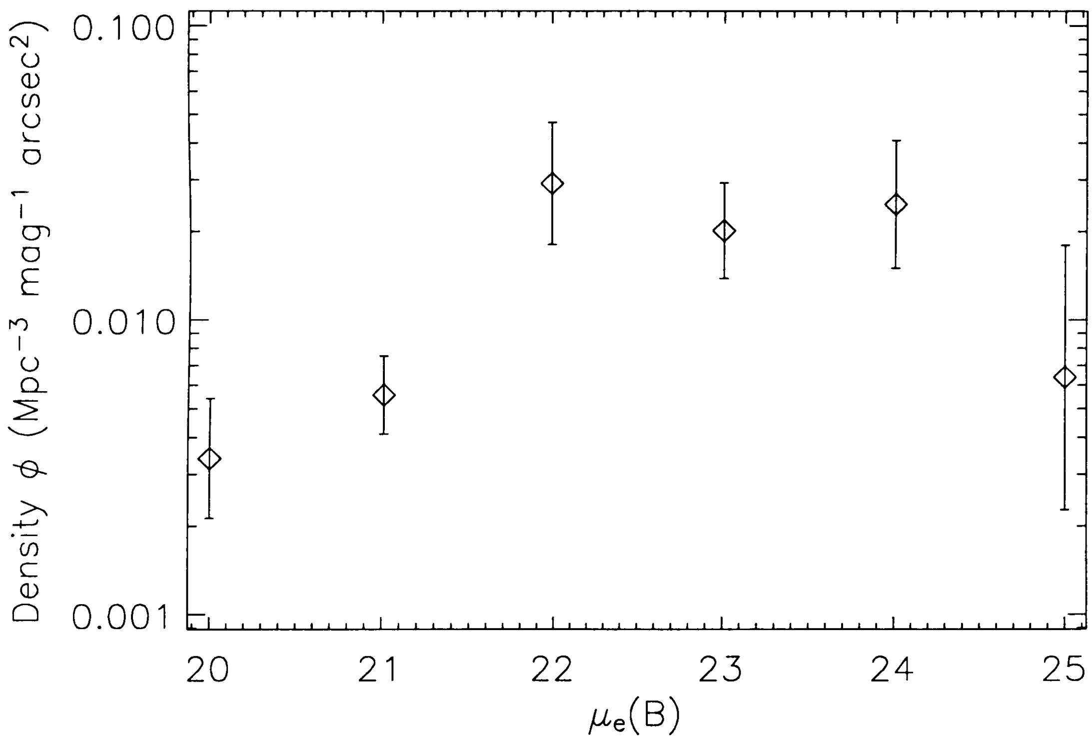

Figure 4.26: Corrected surface brightness distribution of ES galaxies. The contribution of LSB galaxies to the overall number density of the ES sample is 35^{+29}_{-20} %.

(a)

(b)

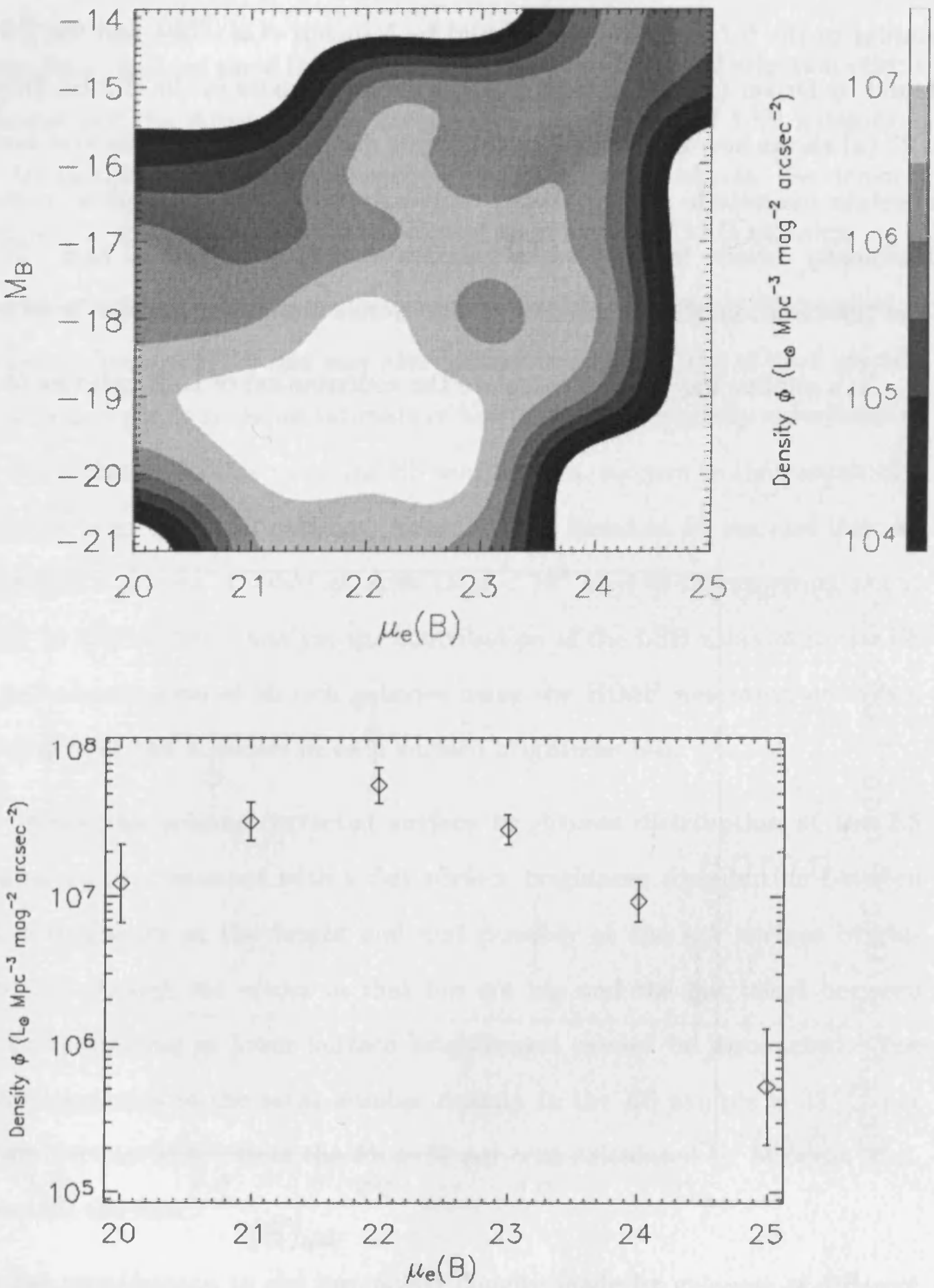

Figure 4.27: Corrected Luminosity density-surface brightness distribution of ES galaxies. Figure 4.27(a) clearly shows that the highest contribution to the luminosity density is provided by galaxies with $21 < \mu_{eff} < 23$ and $-20 < M_B < -18$. Figure 4.27(b) shows that the peak of the density occurs at $\mu_{eff} \sim 22$. The contribution of LSB galaxies to the overall luminosity density is very modest, 7^{+3}_{-2} %.

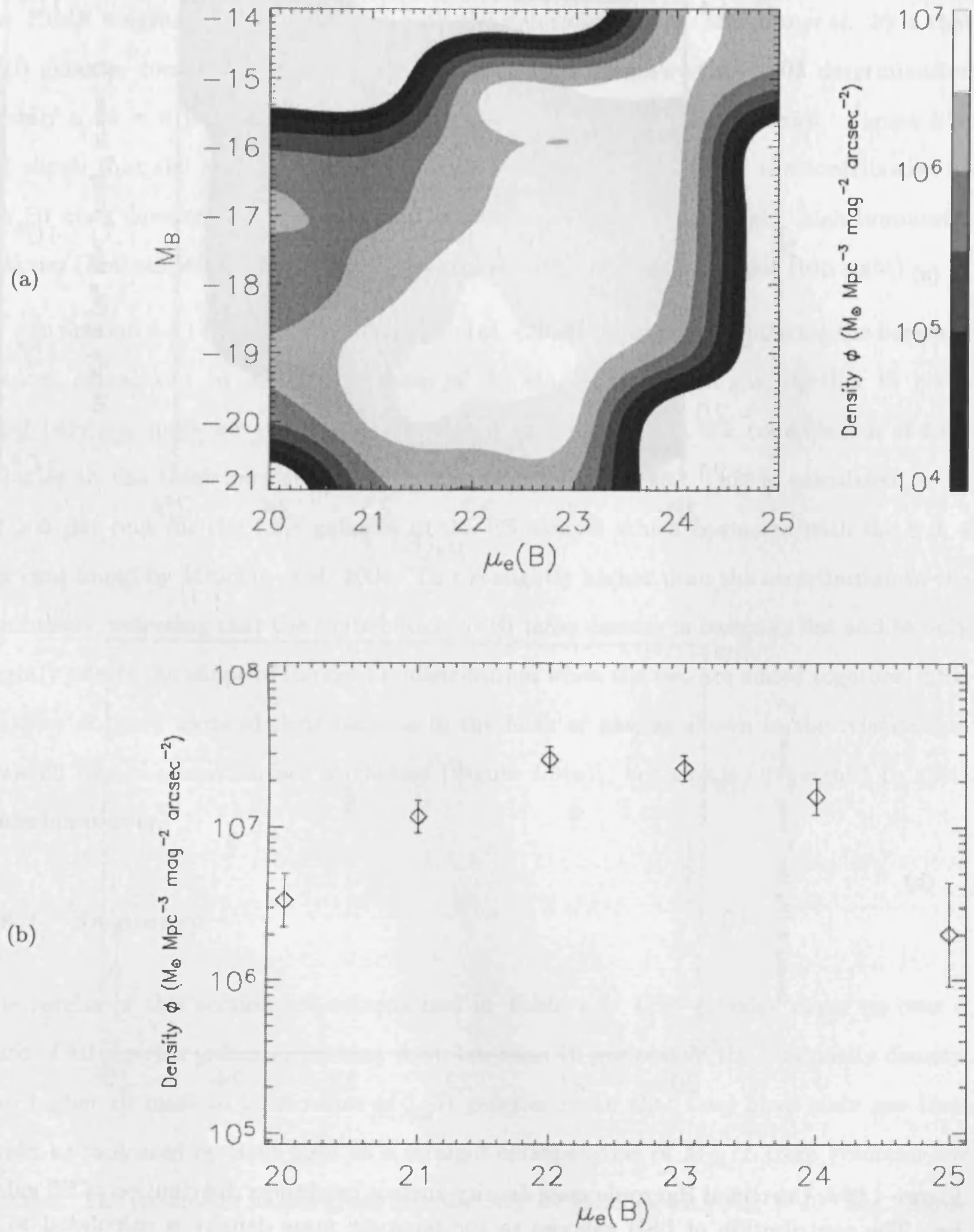

Figure 4.28: Corrected HI mass density-surface brightness distribution of ES galaxies. Panel 4.28(a) shows the contribution to the HI mass density is fairly evenly shared by a wide variety of galaxies, from bright, high luminosity galaxies (bottom left) to low surface brightness, low luminosity galaxies (top right).

(a)

(b)

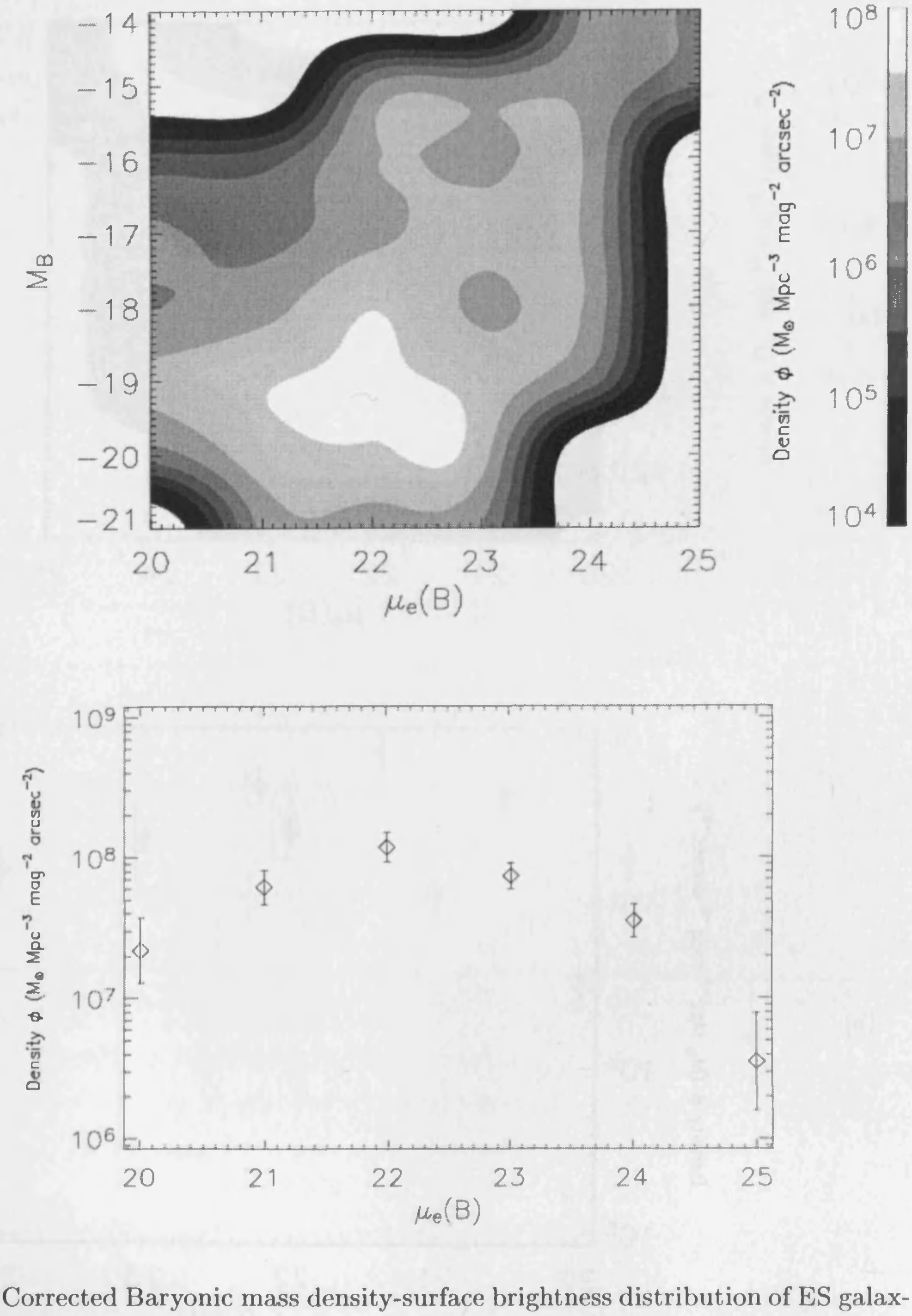

Figure 4.29: Corrected Baryonic mass density-surface brightness distribution of ES galaxies. The contribution of LSB galaxies to the baryonic mass density is calculated to be $12 \pm 3\,\%$.

(HI) density and this is shown in Figure 4.28. This amounts to 21^{+7}_{-6} per cent of all HI with the HIMF weighting. This compares with the determination by Minchin *et al.* 2004 that LSB galaxies contribute 32 ± 11 per cent and with Zwaan's *et al.* 2003 determination of only a 15 ± 6 per cent contribution to the HI density by LSB galaxies. Figure 4.28 (a) shows that the HI mass density is not peaked. This means that the contribution to the HI mass density is shared by a wide variety of galaxies, from bright, high luminosity galaxies (bottom left) to low surface brightness, low luminosity galaxies (top right).

In Section 4.4 I followed the McGaugh *et al.* (2000) method in calculating the baryonic content of galaxies by adding the mass of the stars and the HI gas together to get a total baryonic mass for the galaxy (see Equation 4.13). Thus, the contribution of LSB galaxies to the total baryon density is shown in Figure 4.29. This is calculated to be 12 ± 3 per cent for the LSB galaxies in the ES sample which compares with the 9 ± 4 per cent found by Minchin *et al.* 2004. This is slightly higher than the contribution to the luminosity, reflecting that the contribution to HI mass density is basically flat and so only slightly affects the shape of the density distribution when the two are added together. LSB galaxies do have more of their baryons in the form of gas, as shown in the relationship between $M_{\rm HI}/L_B$ and surface brightness (Figure 4.5(a)), but this is outweighed by their underluminosity.

4.6.1 Summary

The results of this section are summarised in Table 4.4. LSB galaxies make up over a third of all gas-rich galaxies, yet they have less than 10 per cent of the luminosity density. The higher HI mass to light ratios of LSB galaxies mean that they have more gas than would be indicated by their light on a straight extrapolation of $M_{\rm HI}/L$ from Freeman-law galaxies. The parameter values given here are only for galaxies with $M_{\rm HI} > 10^8$ $M_\odot$. These are almost entirely spiral galaxies. Dwarf galaxies, even gas-rich ones, tend to have lower

Quantity	Percentage LSB contribution
Number density	35^{+29}_{-20}
Luminosity density	7^{+3}_{-2}
Neutral hydrogen density	21^{+7}_{-6}
Baryon density	$12\ ^{+3}_{-3}$

Table 4.4: Cosmological contribution of gas-rich LSB galaxies

masses than this, while elliptical galaxies are too gas poor to be detected. Most dwarf galaxies have low surface brightnesses; therefore, if these were included, it is likely that the total contribution from LSB galaxies would be higher. These values should therefore be seen as lower estimates to the total contribution of LSB galaxies.

This survey does not find any giant LSB galaxies. Thus we find that LSB galaxies make up no more 13% of the population of luminous ($L_B > 10^{10} M_\odot$) galaxies (to 95% confidence limit). Once volumetric corrections are made, the number of galaxies per unit volume is fairly flat as we go to lower surface brightnesses. Furthermore, LSB galaxies contribute about 21% of the neutral hydrogen density but only 7% of the luminosity density.

Chapter 5

Conclusions

5.1 Conclusions

I have studied the Equatorial Strip (ES) region of sky covering 5738 deg^2 using the Parkes HI multibeam system. The survey revealed 1077 sources over three decades in HI mass and a volume of $\sim 2.76 \times 10^6$ Mpc^{-3}. We have obtained photometric optical data from the SDSS (DR2) for 201 sources which have been identified as the optical counterparts to the HI sources; these cover a range of 5 magnitudes in effective surface brightness (μ_{eff}), 7 magnitudes in central surface brightness (μ_0) and 8 magnitudes in absolute magnitude (M_B).

We define LSB galaxies as those with $\mu_0^B > 23$ and/or $\mu_{eff}^B > 24$. 25 galaxies fulfill this criteria in the ES sample (12%). There is a clear deficiency of high luminosity, low surface brightness 'Crouching Giant' galaxies (LSB galaxies with $L_B > 10^{10} L_\odot$). There are 44 galaxies with $L_B > 10^{10} L_\odot$ in the ES sample but not one is an LSB galaxy. Thus LSB galaxies make up no more than 6% of the high luminosity, gas-rich population at the

95% confidence level and they make up no more than 12% at 99% confidence.

Of the 22 HI-massive galaxies in the ES sample ($M_{\rm HI} > 10^{10} M_{\odot}$) not one is an LSB galaxy. By the same method used above massive LSB galaxies therefore contribute no more than 13 per cent of the population at 95 per cent confidence level and no more than 18 per cent at 99 per cent confidence.

I have found a correlation between the HI mass and the velocity width of the form $\Delta V_{50} = 0.022\ M_{\rm HI}^{0.39}$ which is fairly similar to that seen in optically selected samples, suggesting that galaxies detected in HI and optical surveys seem to follow the same relationship.

Using the HI masses derived for the ES sample I have constructed an HI Mass Function using the $1/V_{max}$ method. I have found that the HIMF is well fitted by a Schechter function with parameters $\alpha = -1.38$ and $M_{\rm HI}^{\star} = 5.7 \times 10^9$ $M_{\odot}$. I have then used these values to calculate the total HI mass density of the local universe, $\rho_{\rm HI} = 7.4 \times 10^7\ h_{75} M_{\odot}$ Mpc^{-3}, the cosmological HI mass density, $\Omega_{\rm HI} = 3.2 \pm 0.4 \times 10^{-4} h_{75}^{-1}$ and assuming that the percentage of He is 25%, the total gas density, $\Omega_{gas} = 4.1 \pm 0.4 \times 10^{-4} h_{75}^{-1}$.

A relationship has been found between M_B and μ_{eff} – more luminous galaxies have higher surface brightnesses. The best fitting slope is 0.50 ± 0.05, significantly shallower than the slope of 0.75 found by Bingelli & Cameron (1991) for dwarf galaxies in the Virgo cluster. The same relationship still holds for the central surface brightness (μ_0) but this time with a best fitting slope of 0.87 ± 0.01 (see Figure 3.15).

I have shown there is relationship between the HI mass to luminosity ratio and the effective surface brightness with a best fitting linear relationship which is given by $\mu_{eff} = (0.60 \pm 0.12) \times log\left(\frac{M_{\rm HI}}{L_B}\right) + (23.09 \pm 0.6)$. This result is in agreement with those from de Blok, McGaugh & van der Hulst (1996) in B and I band data, which indicated that the HI mass to light ratio increases with lower surface-brightness. This could imply that these galaxies are relatively unevolved and have not yet converted a large fraction of their mass to stars. This also indicates that the luminosity is not a good indicator of the mass of LSB galaxies as it will underestimate the mass of baryons. Their luminosity is therefore not a good indicator of the cosmological importance of LSB galaxies.

I have derived estimates of HI column densities for the ES sample galaxies using their measured HI masses and relationships found in the literature between optical and HI radii of optically selected samples of galaxies. This gives the result that most galaxies in the ES sample have average column densities of around 3×10^{20} atoms cm^{-2}, with the lowest being 5×10^{19} atoms cm^{-2}. This is well above the column density limit for the ES sample of $\approx 8 \times 10^{18}$ atoms cm^{-2} for a galaxy with $\Delta V = 100$ km s^{-1}. This implies that it is highly unlikely that we are missing a large population of low column density galaxies.

The same radii used to calculate the column densities, together with the optical inclinations and the HI velocity widths were used to calculate the dynamical masses, M_{dyn}, for the ES sample. Again, it was found that LSB galaxies are generally less massive than 'normal' galaxies.

I have investigated the Tully-Fisher (TF) relationship for the ES sample. It has been suggested (Matthews *et al.* 1998) that most of their sample of extremely late-type, low-luminosity spirals fell below the standard TF relationship, with the deviation increasing with decreasing size and luminosity. I investigate the TF relationship in the B and R-bands and my results are consistent with previous values from optically selected samples. I calculated the 'baryonic' Tully-Fisher relation and I find a best fitting linear relationship of $\log(M_{bary}) = (3.10 \pm 0.53) \times \eta + (10.34 \pm 0.19)$ which is slightly shallower but consistent with the values found by Minchin (2001) and McGaugh (2000) (3.20 ± 0.42 and 3.98 ± 0.12 respectively).

I have calculated the Bivariate Brightness Distribution (BBD) for the ES sample. The BBD is the bivariate distribution of galaxies as a function of luminosity and surface brightness and it describes the contribution of galaxies of different luminosities and surface brightnesses to the Universe. It is virtually impossible to obtain an accurate BBD from an optically selected sample (Boyce & Phillipps 1995) but it is in principle much easier from an HI selected sample as you only have to correct for the HI mass selections. I then apply an HIMF weighted correction and the resulting BBD shows the true space density of galaxies.

This corrected surface brightness distribution is then used to estimate the cosmological contribution of LSB galaxies. By combining the SBD with the relationships found between surface brightness and optical luminosity, HI mass, baryonic mass and dynamical mass. This allows for the contribution of LSB galaxies to the number density, luminosity density, HI density, baryon density of the Universe to be calculated. I find that LSB galaxies contribute $35^{+29}_{-20}\%$ to the number density of gas-rich galaxies in the Universe. They contribute only $7^{+3}_{-2}\%$ to the luminosity density of the Universe. They also contribute $21^{+7}_{-6}\%$ and $12 \pm 3\%$ to the neutral hydrogen (HI) and baryon density of gas-rich galaxies in the Universe.

It can be seen from my results that LSB galaxies make up over a third of all gas-rich galaxies, yet they constitute less than 10 per cent of the luminosity density in the Universe. The higher HI mass to light ratios of LSB galaxies mean that they have more gas than would be indicated by their light on a straight extrapolation of M_{HI}/L from Freeman-law galaxies.

It can also be seen that the luminosity is a poor tracer of the dynamical mass of LSB galaxies in the same way that it is a poor tracer of the baryonic mass. Zwaan *et al.* (1997) found that in order to explain their observation that LSB galaxies fall on the same Tully-Fisher (TF) relationship as 'normal' galaxies, the product $\Upsilon^2\Sigma$ must remain constant (where Υ is the mass to light ratio, and Σ is the surface-brightness in linear units of intensity). This means that as the surface brightness falls, the luminosity is an increasingly bad indicator of the true mass. That $\Upsilon^2\Sigma$ remains constant is also seen in the ES data (Section 4.5).

That the $\Upsilon^2\Sigma$ relation is seen to hold for the ES sample implies that the ES galaxies should all fall on a single TF relationship. This has been investigated in Section 4.5, where it has been found that the ES data can be fitted with a single slope. This slope is consistent with the B and R-band TF relationship of Pierce & Tully (1992) although with a much wider scatter, which may be due to the wider spread of morphological types. The data is also consistent with the baryonic TF relationship of McGaugh *et al.* (2000).

The ES sample has uncovered some extraordinary objects such as the LSB galaxies described in Chapter 3. Being free from optical selection effects, the ES sample does not discriminate against LSB galaxies. These objects deviate more than 6σ from the Freeman value in their central surface brightness (μ_0). LSB galaxies have very blue colours which are similar to those of an actively star-forming Sc galaxy which is on average 2 magnitudes brighter in its effective surface brightness (de Jong & van der Kruit 1994). LSB galaxies in general are about 0.25 magnitudes bluer in B−V than high surface brightness galaxies. This population of galaxies is very different from 'normal' HSB field spirals and LSB dwarfs in clusters. These are extraordinarily diffuse objects, with an 'inchoate' structure and with bulge components which are faint or totally undetectable in most cases.

Apart from LSB galaxies, 10% of the ES sample is made up of extremely gas-rich galaxies ($M_{\rm HI}/L_B > 3$) with 4 galaxies having $M_{\rm HI}/L_B > 10$. Why these objects have not converted most of their gas into stars still unclear. These objects have 'normal' amounts of HI compared to other galaxies of the same type but they are underluminous. These gas-rich galaxies appear to have done little with their unprocessed neutral hydrogen (HI) compared to their stellar content. The colours of these galaxies are very similar to those of the LSB galaxies, i.e. very blue.

I have calculated the Luminosity function (LF) for the ES sample corrected with HIMF weighting using the HIMF. The best fitting Schechter parameters are found to be

$\alpha = -1.11^{+0.13}_{-0.09}$, $L^{\star}_{B} = -19.46^{+0.55}_{-0.40}$ and $\phi^{\star} = (1.12 \pm 0.17) \times 10^{-2}$ Mpc^{-3}. The estimate of the luminosity function for the ES sample is in good agreement with optically selected samples. We find a value of $\rho_{L_B} = (12.3 \pm 1.3) \times 10^{7} h_{75} L^{B}_{\odot} Mpc^{-3}$ for the luminosity density of gas-rich galaxies in the ES sample which is slightly higher than the mean value for optical selected samples.

5.2 Future Work

The Equatorial Strip sample is very much an ongoing project. For this thesis we have obtained optical data for 201 galaxies but we hope to soon have data for a much larger proportion of the whole ES sample.

The greater numbers of galaxies with both HI and optical data will improve the accuracy of the SBD and of the relationships between surface brightness and luminosity, HI mass, baryonic mass and dynamical mass. This will decrease the error bars and enable tighter limits to be put on the contribution of LSB galaxies to the cosmic luminosity, neutral hydrogen, baryonic and mass densities of gas-rich galaxies.

Our analysis of the ES sample has unveiled some very intriguing and interesting objects which merit further follow up. Further follow ups are planned using radio-synthesis telescopes such as the VLA, WSRT and GMRT as we need higher resolution 21 cm maps to investigate objects such as HIPEQ1227+01 which has the highest $M_{\rm HI}/L_B$ of ~ 22 for a non-dwarf galaxy ($M_{\rm HI} \approx 4 \times 10^{9}$ M$_{\odot}$) and HIPEQ0958+01 which is the second lowest surface brightness object in the ES sample and has the bluest colours in the whole sample. HI interferometrical data will provide accurate HI column densities and rotational velocities. The information provided by the optical spectra will allows us to determine the metallicity and star formation rates for all the objects in the sample and especially for those extremely gas-rich galaxies. This will allow us to determine if these objects are 'young' or have had very low star formation rates throughout their history.

Appendix A

The ES Sample

The Equatorial Strip Sample

The following 1077 galaxies were detected in the Equatorial Strip region discussed in Chapter 2 of this thesis. This list gives the main HI parameters for all those sources. The columns in the table are as follows.

ES HI Parameters

(1) Name for the Equatorial Strip HIPASS galaxies

(2) Right Ascension in degrees

(3) Declination in degrees

(4) Heliocentric Velocity in km s^{-1}

(5) Total velocity width at 50% (uncorrected for inclination effects)

(6) Peak Flux in Janskys

(7) Integrated Flux in Janskys km s^{-1}

(8) Distance in Mega Parsecs (see section 2.4.1)

(9) log of the HI mass (see section 2.4.2)

(1) Name	(2) RA (°)	(3) Dec (°)	(4) Vel (km s^{-1})	(5) W_{50} (km s^{-1})	(6) S_{peak} (Jy)	(7) S_{int} (Jy km s^{-1})	(8) Dist. (Mpc)	(9) HI mass log $M_\odot$
HIPEQ0001-03	0.44	-3.26	5876	128	0.075	9.60	75.3	10.11
HIPEQ0002-03	0.50	-3.28	6096	126	0.055	6.80	78.4	9.99
HIPEQ0003+07	0.95	7.48	5152	175	0.080	12.75	65.4	10.11
HIPEQ0004+07	1.07	7.37	6069	192	0.035	5.26	78.2	9.88
HIPEQ0004+05	1.15	5.84	3075	218	0.065	10.88	37.1	9.55
HIPEQ0004-01	1.19	-1.60	7386	221	0.046	9.40	96.7	10.32
HIPEQ0006+08	1.70	8.62	5172	201	0.040	7.60	66.2	9.89
HIPEQ0007+08	1.75	8.65	5137	292	0.046	10.86	65.8	10.04
HIPEQ0008-02	2.21	-2.40	3851	141	0.089	14.20	48.6	9.90
HIPEQ0011+06	2.78	6.35	6040	178	0.045	7.93	79.2	10.07
HIPEQ0012+00	3.17	0.00	11925	79	0.044	3.40	163.1	10.33
HIPEQ0014-00	3.65	0.74	3914	290	0.075	17.18	50.9	10.02
HIPEQ0014+07	3.67	7.51	3475	105	0.052	6.18	44.9	9.47
HIPEQ0017+06	4.27	6.79	5560	181	0.044	5.65	74.3	9.87
HIPEQ0019-03	4.77	-3.51	5919	177	0.050	7.90	80.0	10.08
HIPEQ0019+04	4.87	4.08	2984	532	0.077	33.49	39.7	10.09
HIPEQ0020+08	5.03	8.49	5500	65	0.037	2.15	74.4	9.45
HIPEQ0020+08	5.20	8.60	691	39	0.044	1.77	9.1	7.54
HIPEQ0022-01	5.60	-1.32	5002	85	0.109	10.20	68.3	10.05
HIPEQ0024-03	6.11	-3.86	4320	97	0.045	4.36	59.6	9.56
HIPEQ0025-02	6.44	-2.25	5592	65	0.050	9.20	77.6	10.12
HIPEQ0027-01a	6.95	-1.16	3848	223	0.039	6.60	54.2	9.66
HIPEQ0027-01	6.95	-1.80	4229	170	0.076	13.00	59.4	10.03
HIPEQ0028+02	7.03	2.60	4294	130	0.069	9.88	60.3	9.93
HIPEQ0028+03	7.06	3.36	4004	159	0.059	6.80	56.4	9.71
HIPEQ0028+05	7.13	5.00	1329	85	0.092	8.59	20.1	8.91
HIPEQ0029+01	7.44	1.75	10810	319	0.036	7.85	152.2	10.63
HIPEQ0029-05	7.45	-5.10	4072	193	0.046	7.30	57.8	9.76
HIPEQ0029+03	7.49	3.54	1339	21	0.116	4.06	20.7	8.61
HIPEQ0030+02	7.50	2.09	5269	348	0.060	12.61	74.3	10.21
HIPEQ0030+01	7.50	1.85	3396	62	0.042	2.60	48.6	9.16
HIPEQ0030+02	7.50	2.10	5268	351	0.059	12.99	74.3	10.23
HIPEQ0031+09	7.89	9.18	2135	101	0.075	6.90	31.7	9.21
HIPEQ0031+08	7.91	8.44	4272	222	0.078	16.02	60.9	10.15
HIPEQ0031-05	7.93	-5.17	4240	85	0.139	13.30	60.6	10.06
HIPEQ0031-02	7.94	-2.54	6388	252	0.046	9.30	90.3	10.25
HIPEQ0033-01	8.34	-1.12	1972	146	0.131	17.24	30.1	9.57
HIPEQ0033+02	8.43	2.68	4339	219	0.070	9.51	62.3	9.94
HIPEQ0034-02	8.54	-2.18	5296	73	0.060	4.38	75.7	9.77
HIPEQ0034+00	8.60	0.27	1510	68	0.074	5.03	24.0	8.84
HIPEQ0036+01	9.03	1.71	5525	101	0.065	6.10	79.2	9.95
HIPEQ0037+01	9.27	1.97	4577	102	0.097	20.70	66.2	10.33
HIPEQ0037+08	9.48	8.63	5182	339	0.056	13.86	74.6	10.26

Continued on Next Page...

(1) Name	(2) RA (°)	(3) Dec (°)	(4) Vel (km s^{-1})	(5) W_{50} (km s^{-1})	(6) S_{peak} (Jy)	(7) S_{int} (Jy km s^{-1})	(8) Dist. (Mpc)	(9) HI mass log $M_{\odot}$
HIPEQ0039+03	9.88	3.99	5246	205	0.048	8.26	75.8	10.05
HIPEQ0041-05	10.29	-5.34	3646	124	0.047	6.50	54.0	9.65
HIPEQ0041-01	10.32	-1.69	5399	131	0.044	5.00	78.1	9.86
HIPEQ0041-01	10.43	-1.99	2033	75	0.051	3.70	32.1	8.95
HIPEQ0043-00	10.88	0.11	4124	287	0.064	13.81	60.6	10.08
HIPEQ0043-04	10.96	-4.20	7067	118	0.047	11.40	101.4	10.44
HIPEQ0043+01	10.98	1.89	4472	165	0.042	6.25	65.4	9.80
HIPEQ0046-01	11.53	-1.71	4221	145	0.043	6.60	62.0	9.78
HIPEQ0046-02	11.75	-2.71	7330	87	0.041	7.70	105.1	10.30
HIPEQ0048-02	12.01	-2.75	4331	112	0.083	19.80	63.4	10.27
HIPEQ0048+04	12.02	4.10	1961	121	0.042	4.53	31.1	9.01
HIPEQ0049-01	12.39	-1.79	3987	203	0.058	10.10	58.6	9.91
HIPEQ0050-05	12.54	-5.18	5642	240	0.050	10.90	81.3	10.23
HIPEQ0051-03	12.85	-3.14	4139	104	0.050	8.40	60.4	9.86
HIPEQ0051+03	12.93	3.15	1946	117	0.033	3.69	30.5	8.91
HIPEQ0051-00	12.99	0.47	1616	173	0.117	14.84	26.0	9.37
HIPEQ0052-03	13.07	-3.95	1528	154	0.079	11.00	24.8	9.20
HIPEQ0053+05	13.26	6.00	5116	49	0.050	2.42	73.5	9.49
HIPEQ0054-02	13.60	-2.26	5517	88	0.033	2.80	78.9	9.61
HIPEQ0058+00	14.71	0.63	5338	156	0.048	4.97	75.4	9.82
HIPEQ0059+00	14.79	0.93	5431	128	0.042	4.90	76.6	9.83
HIPEQ0101+07	15.35	7.62	2191	143	0.116	15.44	31.6	9.56
HIPEQ0102-04	15.58	-4.49	1824	47	0.086	4.20	26.5	8.84
HIPEQ0103-03	15.79	-3.60	2711	83	0.113	9.40	38.3	9.51
HIPEQ0103-04	15.88	-4.62	5905	158	0.036	5.30	82.0	9.92
HIPEQ0104-06	16.24	-6.20	1088	193	0.450	86.85	15.8	9.71
HIPEQ0105-06	16.28	-6.28	2341	163	0.062	10.11	32.7	9.41
HIPEQ0105-04	16.32	-4.37	1905	131	0.043	4.60	26.7	8.89
HIPEQ0106+03	16.51	3.40	5435	84	0.027	1.75	74.6	9.36
HIPEQ0106-02	16.61	-2.17	4035	83	0.040	5.10	55.3	9.57
HIPEQ0107+01	16.94	1.07	626	59	0.063	3.81	8.7	7.83
HIPEQ0108+01	17.14	1.64	2123	95	0.121	16.40	28.6	9.50
HIPEQ0108+01	17.20	1.38	5525	88	0.029	6.30	75.0	9.92
HIPEQ0108-05	17.25	-5.51	2364	151	0.052	7.50	31.8	9.25
HIPEQ0109-02	17.42	-2.26	1974	153	0.116	15.20	26.2	9.39
HIPEQ0109-01	17.47	-1.74	3902	34	0.023	2.30	52.4	9.17
HIPEQ0110+00	17.70	0.23	5428	158	0.036	4.90	73.1	9.79
HIPEQ0111+01	17.85	1.30	6913	132	0.070	9.10	93.5	10.27
HIPEQ0112+00	18.24	0.98	1272	160	0.537	76.90	15.7	9.65
HIPEQ0113-06	18.25	-6.14	2223	252	0.084	21.17	28.6	9.61
HIPEQ0115-00	18.88	0.85	1897	178	0.174	28.00	23.4	9.56
HIPEQ0117-01	19.48	-1.97	6039	115	0.111	11.80	79.4	10.24
HIPEQ0119-01	19.81	-1.68	4905	69	0.040	3.70	63.4	9.54

Continued on Next Page...

(1) Name	(2) RA (°)	(3) Dec (°)	(4) Vel (km s^{-1})	(5) W_{50} (km s^{-1})	(6) S_{peak} (Jy)	(7) S_{int} (Jy km s^{-1})	(8) Dist. (Mpc)	(9) HI mass log $M_\odot$
HIPEQ0119+03	19.93	3.44	2329	366	0.071	19.44	28.1	9.56
HIPEQ0119+00	19.98	0.74	4294	70	0.030	1.02	54.8	8.86
HIPEQ0120-00	20.06	0.19	1712	129	0.039	3.88	19.6	8.55
HIPEQ0120+05	20.19	5.73	2149	83	0.042	3.19	25.4	8.68
HIPEQ0121+01	20.25	1.40	4894	309	0.042	8.92	62.8	9.92
HIPEQ0121+03	20.36	3.94	5149	104	0.049	3.92	66.2	9.61
HIPEQ0121+05	20.42	5.29	2240	448	0.098	26.96	26.4	9.65
HIPEQ0122+00	20.54	0.94	2325	266	0.159	33.23	27.5	9.77
HIPEQ0123-00	20.78	0.40	7283	60	0.049	2.95	95.6	9.80
HIPEQ0123+06	20.93	6.68	2317	40	0.114	5.01	27.0	8.94
HIPEQ0124+03	21.13	3.80	2147	111	0.172	28.09	24.6	9.60
HIPEQ0124+01	21.16	1.71	5156	152	0.067	10.60	65.7	10.03
HIPEQ0125-04	21.25	-4.71	5940	117	0.041	10.70	76.6	10.17
HIPEQ0125+08	21.41	8.03	2898	59	0.115	9.19	34.6	9.41
HIPEQ0126-03	21.55	-3.96	2082	136	0.049	6.20	23.5	8.91
HIPEQ0126+06	21.55	6.28	2113	40	0.076	3.16	23.9	8.63
HIPEQ0126-06	21.56	-6.07	1940	249	0.086	16.14	21.7	9.25
HIPEQ0126+00a	21.64	0.55	5337	68	0.045	1.94	67.9	9.32
HIPEQ0126-00	21.72	0.66	1898	99	0.039	3.29	20.9	8.53
HIPEQ0129+10	22.39	10.01	9234	87	0.043	3.44	122.2	10.08
HIPEQ0132+04	23.16	4.53	1957	132	0.078	10.63	21.3	9.06
HIPEQ0134+04	23.73	4.41	1945	107	0.157	15.54	21.2	9.22
HIPEQ0135+01	23.89	2.00	2592	111	0.060	6.66	30.0	9.15
HIPEQ0138+07	24.60	7.54	4228	218	0.069	9.72	52.6	9.80
HIPEQ0140+05	25.02	5.75	3271	315	0.071	18.29	39.7	9.83
HIPEQ0140-05	25.06	-5.64	1373	59	0.047	1.80	14.1	7.93
HIPEQ0141-05	25.27	-5.54	1646	181	0.073	12.10	17.9	8.96
HIPEQ0142+02	25.62	2.93	1753	79	0.112	8.87	19.5	8.90
HIPEQ0143+08	25.80	8.93	5470	427	0.073	15.34	70.4	10.25
HIPEQ0144+04	26.16	4.89	1612	84	0.047	4.03	18.1	8.49
HIPEQ0145-00	26.25	0.27	5362	150	0.051	4.00	69.4	9.66
HIPEQ0146+04	26.57	4.25	1795	113	0.048	5.50	20.9	8.75
HIPEQ0146-03	26.58	-3.78	5500	51	0.098	5.50	71.6	9.82
HIPEQ0149+05	27.28	5.95	1489	381	0.055	16.05	17.5	9.07
HIPEQ0150+02	27.56	2.32	1685	72	0.053	3.50	20.5	8.54
HIPEQ0150+06	27.65	6.11	1560	192	0.043	6.55	18.9	8.74
HIPEQ0150-01	27.74	-1.44	5764	116	0.044	4.90	76.5	9.83
HIPEQ0151-04	27.86	-4.07	10802	161	0.041	6.90	147.8	10.55
HIPEQ0151-05	28.00	-5.50	1749	153	0.147	22.30	22.0	9.41
HIPEQ0152-03	28.19	-3.46	5346	183	0.049	8.80	71.3	10.02
HIPEQ0154-00a	28.52	0.72	4974	224	0.059	11.10	66.6	10.06
HIPEQ0154-00	28.73	0.09	5662	93	0.042	3.76	76.3	9.71
HIPEQ0155+03	28.97	3.49	4776	71	0.074	5.04	64.4	9.69

Continued on Next Page...

(1) Name	(2) RA (°)	(3) Dec (°)	(4) Vel (km s^{-1})	(5) W_{50} (km s^{-1})	(6) S_{peak} (Jy)	(7) S_{int} (Jy km s^{-1})	(8) Dist. (Mpc)	(9) HI mass log $M_\odot$
HIPEQ0156+03	29.11	3.45	4782	62	0.061	3.43	64.6	9.53
HIPEQ0156-01	29.20	-1.99	4649	52	0.047	9.40	63.0	9.94
HIPEQ0157+03	29.48	3.42	4766	258	0.064	13.94	64.9	10.14
HIPEQ0158+04	29.52	4.36	4689	302	0.055	10.62	63.9	10.01
HIPEQ0158+03	29.57	3.10	5434	170	0.041	6.45	74.2	9.92
HIPEQ0158+03	29.68	3.29	3431	178	0.039	6.15	46.8	9.50
HIPEQ0159+09	29.93	9.91	6024	111	0.040	4.47	82.8	9.86
HIPEQ0159-05	29.93	-5.96	1597	362	0.074	20.80	22.4	9.39
HIPEQ0202-04	30.60	-4.21	5116	80	0.044	3.50	71.2	9.62
HIPEQ0204-04	31.10	-4.95	3996	88	0.065	7.60	56.4	9.76
HIPEQ0204-06	31.12	-6.20	1356	164	0.163	25.40	20.6	9.40
HIPEQ0204+06	31.13	6.64	3319	253	0.048	9.87	47.0	9.71
HIPEQ0205+06	31.33	6.11	3373	102	0.082	8.14	48.0	9.65
HIPEQ0208+07	32.22	7.98	3403	342	0.071	12.55	49.3	9.86
HIPEQ0210-01	32.62	-1.45	3646	54	0.084	4.90	53.1	9.51
HIPEQ0210+06	32.68	6.77	1595	102	0.095	9.00	25.2	9.13
HIPEQ0211+03	32.78	3.84	3212	206	0.091	15.90	47.2	9.92
HIPEQ0215+06	33.85	6.00	1545	217	0.596	92.53	25.2	10.14
HIPEQ0216+01	34.02	1.80	6163	158	0.053	7.90	88.6	10.16
HIPEQ0217-05	34.32	-5.46	5483	63	0.037	5.70	79.3	9.93
HIPEQ0217+06	34.44	6.29	1552	61	0.150	9.55	25.5	9.17
HIPEQ0221-04	35.34	-4.39	2418	157	0.038	5.30	37.4	9.24
HIPEQ0221-05	35.40	-5.52	2475	116	0.246	47.30	38.2	10.21
HIPEQ0222-03	35.68	-3.97	2375	104	0.110	10.80	36.8	9.54
HIPEQ0222-00	35.68	0.64	1535	144	0.059	7.27	25.4	9.04
HIPEQ0223-04	35.97	-4.62	2358	101	0.139	13.20	36.5	9.62
HIPEQ0224-02	36.05	-2.17	1476	97	0.037	3.40	24.6	8.68
HIPEQ0227-01	36.85	-1.11	1438	69	0.036	2.40	23.7	8.50
HIPEQ0228-01a	37.07	-1.33	1846	87	0.032	2.40	29.1	8.68
HIPEQ0228-01	37.08	-1.16	1605	155	0.131	16.00	25.9	9.40
HIPEQ0230+00	37.58	0.94	1523	27	0.047	1.37	24.4	8.28
HIPEQ0230-01	37.65	-1.10	1501	331	0.042	7.84	24.1	9.03
HIPEQ0230-03	37.67	-3.80	1719	88	0.187	16.40	27.0	9.45
HIPEQ0230-02	37.67	-2.92	6113	168	0.079	25.30	87.1	10.66
HIPEQ0231+00	37.92	0.89	6167	129	0.041	4.23	87.7	9.88
HIPEQ0235+06	38.94	6.33	6164	203	0.088	14.99	86.6	10.42
HIPEQ0236+00a	39.02	0.44	2754	63	0.064	7.40	39.7	9.44
HIPEQ0236+00	39.08	0.76	6794	64	0.038	7.00	95.3	10.18
HIPEQ0236+00b	39.15	0.00	1213	85	0.049	3.70	18.8	8.49
HIPEQ0236+07	39.16	7.35	5834	79	0.044	3.81	81.7	9.78
HIPEQ0238-01	39.56	-1.30	2759	157	0.091	10.60	39.2	9.58
HIPEQ0238+00	39.69	0.52	1452	94	0.078	6.82	21.3	8.86
HIPEQ0239+03	39.85	3.41	5132	225	0.063	14.26	71.3	10.23

Continued on Next Page...

(1) Name	(2) RA (°)	(3) Dec (°)	(4) Vel (km s^{-1})	(5) W_{50} (km s^{-1})	(6) S_{peak} (Jy)	(7) S_{int} (Jy km s^{-1})	(8) Dist. (Mpc)	(9) HI mass log $M_{\odot}$
HIPEQ0240+01	40.07	1.24	1176	54	0.095	5.74	17.2	8.60
HIPEQ0240-06	40.13	-6.09	1319	87	0.118	9.67	19.1	8.92
HIPEQ0241+00	40.43	0.45	992	388	0.410	119.34	14.2	9.76
HIPEQ0242+00	40.67	0.01	1314	254	0.110	23.80	18.3	9.27
HIPEQ0243+04	40.85	4.98	4032	338	0.064	15.21	54.9	10.03
HIPEQ0243+01	40.92	1.39	1304	79	0.772	61.50	17.8	9.66
HIPEQ0244+00	41.04	0.72	2771	70	0.034	2.99	37.5	9.00
HIPEQ0244+09	41.24	9.24	3767	167	0.039	5.21	50.7	9.50
HIPEQ0246+03	41.57	3.58	6628	373	0.054	14.78	89.9	10.45
HIPEQ0246-00a	41.60	0.51	1509	217	0.165	32.09	19.7	9.47
HIPEQ0246-00b	41.62	0.24	2744	309	0.155	27.59	36.4	9.93
HIPEQ0247-00	41.85	0.33	6430	361	0.047	16.97	86.8	10.48
HIPEQ0247+03	41.98	3.89	1022	89	0.765	67.38	12.6	9.40
HIPEQ0248-02	42.13	-2.10	7261	90	0.049	4.41	98.1	10.00
HIPEQ0248+02	42.18	2.08	10929	157	0.054	8.48	150.0	10.65
HIPEQ0249+02	42.28	2.14	1101	58	0.945	55.35	13.3	9.37
HIPEQ0249-00a	42.31	0.40	2642	122	0.041	2.45	34.1	8.83
HIPEQ0249+01	42.32	1.96	3010	64	0.042	2.40	39.1	8.94
HIPEQ0249-02	42.35	-2.66	1164	88	0.143	12.60	14.2	8.77
HIPEQ0249-00b	42.39	0.62	6493	118	0.025	2.63	87.0	9.67
HIPEQ0249-00	42.45	0.88	6953	259	0.040	7.84	93.3	10.21
HIPEQ0250+02	42.56	2.05	1099	70	0.059	4.37	13.0	8.24
HIPEQ0251+03	42.77	3.36	2978	44	0.047	2.14	38.1	8.86
HIPEQ0251+04	42.79	4.46	1010	66	0.090	5.98	11.5	8.27
HIPEQ0251-01	42.97	-1.17	1498	105	0.278	27.99	17.9	9.32
HIPEQ0253+06	43.29	6.53	5326	317	0.038	8.52	69.7	9.99
HIPEQ0253+02	43.45	2.34	6585	320	0.036	8.79	87.0	10.20
HIPEQ0254+02	43.52	2.96	3004	259	0.090	16.75	37.6	9.75
HIPEQ0257+01	44.32	1.34	1748	172	0.063	10.84	19.9	9.00
HIPEQ0257-02	44.46	-2.33	1679	185	0.236	39.30	18.8	9.52
HIPEQ0258-04	44.59	-4.25	2497	98	0.041	5.70	29.8	9.08
HIPEQ0259+02	44.95	2.76	2814	239	0.088	16.32	33.8	9.64
HIPEQ0300+00	45.11	0.00	2832	212	0.052	9.89	33.9	9.43
HIPEQ0301-00	45.26	0.75	2625	111	0.073	6.50	31.0	9.17
HIPEQ0305-00	46.35	0.35	7585	126	0.040	4.70	99.0	10.04
HIPEQ0306-00	46.72	0.80	3186	197	0.080	13.10	38.1	9.65
HIPEQ0308-02	47.16	-2.98	2616	261	0.046	9.40	30.3	9.31
HIPEQ0309-04	47.36	-4.86	3325	120	0.039	7.50	40.0	9.45
HIPEQ0311-04	47.77	-4.25	2307	88	0.087	7.80	26.2	9.10
HIPEQ0312-05	48.18	-5.26	2292	93	0.046	7.00	26.1	9.05
HIPEQ0312+04	48.20	4.72	5785	244	0.093	16.80	73.9	10.33
HIPEQ0314-02	48.54	-2.82	1911	111	0.479	106.20	21.1	10.05
HIPEQ0314-04	48.67	-4.77	2371	116	0.123	14.90	27.4	9.42

Continued on Next Page...

(1) Name	(2) RA (°)	(3) Dec (°)	(4) Vel (km s^{-1})	(5) W_{50} (km s^{-1})	(6) S_{peak} (Jy)	(7) S_{int} (Jy km s^{-1})	(8) Dist. (Mpc)	(9) HI mass log $M_{\odot}$
HIPEQ0315-03	48.97	-3.65	4222	99	0.074	9.70	52.8	9.80
HIPEQ0316-00	49.18	0.47	6826	75	0.040	1.70	88.9	9.50
HIPEQ0317-00	49.45	0.13	6721	610	0.043	26.23	87.6	10.68
HIPEQ0320-06	50.02	-6.21	2314	227	0.092	18.64	27.5	9.52
HIPEQ0320+01	50.06	1.34	6906	133	0.035	4.00	90.6	9.89
HIPEQ0320-03	50.06	-3.65	6083	75	0.056	4.40	79.2	9.81
HIPEQ0320-02	50.08	-2.08	11298	80	0.050	4.00	153.0	10.34
HIPEQ0322-04	50.69	-4.19	4070	150	0.115	14.80	52.1	9.98
HIPEQ0324-04	51.21	-4.22	1866	60	0.050	3.00	22.6	8.56
HIPEQ0326+08	51.62	8.01	2489	276	0.075	17.47	31.4	9.61
HIPEQ0328-04	52.23	-4.24	8265	215	0.049	10.53	112.1	10.49
HIPEQ0335-04	53.91	-4.25	5957	74	0.039	8.50	82.0	10.13
HIPEQ0336-04	54.11	-4.70	6655	56	0.050	2.80	91.9	9.75
HIPEQ0337-05	54.26	-5.03	4307	183	0.081	14.50	59.7	10.08
HIPEQ0337-04	54.35	-4.89	5738	292	0.044	11.00	79.5	10.21
HIPEQ0338-04	54.60	-4.31	4235	60	0.043	7.10	59.1	9.77
HIPEQ0339+08	54.89	8.52	6585	107	0.034	3.12	91.8	9.79
HIPEQ0340+05	55.22	5.37	6014	61	0.048	3.64	84.2	9.78
HIPEQ0341-04	55.38	-4.25	5623	61	0.050	6.30	79.1	9.97
HIPEQ0341-01	55.44	-1.99	3512	68	0.121	7.90	50.1	9.67
HIPEQ0341-04	55.48	-4.71	4382	192	0.062	18.40	62.1	10.22
HIPEQ0343-04	55.81	-4.73	5632	231	0.050	11.55	79.7	10.24
HIPEQ0345+05	56.25	5.91	5982	335	0.047	11.05	84.8	10.27
HIPEQ0345+08	56.27	8.87	1746	39	0.070	3.03	26.8	8.71
HIPEQ0345+02	56.40	2.21	4214	146	0.050	5.14	60.6	9.65
HIPEQ0346-04	56.66	-4.44	4069	77	0.072	15.10	58.9	10.09
HIPEQ0348+01	57.25	1.18	4252	124	0.072	9.30	61.8	9.92
HIPEQ0351-00	57.85	0.48	9031	117	0.036	3.74	128.7	10.16
HIPEQ0354+06	58.68	6.62	3430	246	0.045	8.01	51.0	9.69
HIPEQ0359+01	59.78	1.36	4017	139	0.064	8.20	59.1	9.83
HIPEQ0400+00	60.03	0.75	3657	143	0.069	8.90	54.1	9.79
HIPEQ0402-01	60.72	-1.99	4822	109	0.041	4.40	69.9	9.70
HIPEQ0403-01	60.92	-1.93	1016	91	0.103	9.50	18.0	8.86
HIPEQ0404-02	61.10	-2.17	996	178	0.225	39.40	17.7	9.46
HIPEQ0409+08	62.31	8.64	3455	186	0.104	20.65	49.8	10.08
HIPEQ0411-03	62.88	-3.80	3555	61	0.070	8.80	50.8	9.73
HIPEQ0412+02	63.20	2.38	4936	391	0.067	15.90	69.3	10.26
HIPEQ0414+02	63.59	2.79	3316	265	0.053	10.97	46.7	9.75
HIPEQ0414+02	63.69	2.65	3303	252	0.037	8.22	46.4	9.62
HIPEQ0415+00	63.88	0.92	3628	102	0.041	3.70	50.6	9.35
HIPEQ0415+02	63.92	2.48	3541	137	0.063	7.85	49.4	9.65
HIPEQ0416+02	64.10	2.32	3545	154	0.038	5.40	49.2	9.49
HIPEQ0419+02	64.96	2.11	4151	180	0.051	8.34	56.4	9.80

Continued on Next Page...

(1) Name	(2) RA (°)	(3) Dec (°)	(4) Vel (km s^{-1})	(5) W_{50} (km s^{-1})	(6) S_{peak} (Jy)	(7) S_{int} (Jy km s^{-1})	(8) Dist. (Mpc)	(9) HI mass log $M_{\odot}$
HIPEQ0421+10	65.29	10.16	7503	88	0.050	4.42	102.4	10.04
HIPEQ0424-03	66.10	-3.65	4887	116	0.090	10.70	65.1	10.03
HIPEQ0426-04	66.61	-4.59	3563	90	0.049	5.70	46.4	9.46
HIPEQ0429-04	67.35	-4.74	4555	111	0.037	6.90	59.1	9.75
HIPEQ0429+03	67.45	3.69	4735	367	0.056	15.61	61.4	10.14
HIPEQ0430+06	67.50	6.99	4302	92	0.097	8.43	55.4	9.78
HIPEQ0430-00	67.69	0.34	3751	137	0.032	6.10	47.7	9.51
HIPEQ0430-01	67.73	-1.99	2630	108	0.096	11.10	32.4	9.44
HIPEQ0430-05	67.74	-5.79	4501	51	0.041	7.30	58.0	9.76
HIPEQ0431-04	67.90	-4.59	4143	92	0.079	7.10	52.9	9.67
HIPEQ0432+01	68.00	1.22	3656	66	0.104	12.60	46.1	9.80
HIPEQ0433+00	68.26	0.60	5579	134	0.040	4.90	72.3	9.78
HIPEQ0435+02	68.99	2.23	3551	113	0.061	6.50	43.8	9.47
HIPEQ0436-00	69.16	0.14	3766	77	0.103	25.50	46.6	10.12
HIPEQ0436-03	69.17	-3.18	5169	334	0.062	24.90	65.9	10.41
HIPEQ0437-04	69.42	-4.77	3952	129	0.092	11.30	49.1	9.81
HIPEQ0438+00	69.65	0.19	7961	214	0.062	13.27	104.5	10.53
HIPEQ0438+02	69.71	2.89	4548	272	0.098	22.23	57.0	10.23
HIPEQ0438+00	69.73	0.30	3352	51	0.047	2.20	40.6	8.93
HIPEQ0439-04	69.86	-4.93	4426	154	0.055	8.47	55.4	9.79
HIPEQ0440+01	70.04	1.46	10235	154	0.042	6.30	136.6	10.44
HIPEQ0440-00	70.12	0.80	2803	302	0.052	15.70	33.0	9.61
HIPEQ0440-01	70.13	-1.99	3473	72	0.064	8.20	42.2	9.54
HIPEQ0441-01	70.34	-1.83	3526	79	0.043	6.50	42.8	9.45
HIPEQ0441-02	70.36	-2.85	867	188	0.497	77.40	6.8	8.93
HIPEQ0441-01	70.40	-1.28	8734	194	0.042	7.00	115.2	10.34
HIPEQ0442+00	70.73	0.62	4748	133	0.109	13.20	59.4	10.04
HIPEQ0443+03	70.88	3.04	3474	83	0.070	5.78	41.9	9.38
HIPEQ0443-05	70.95	-5.35	5085	278	0.061	15.30	64.1	10.17
HIPEQ0444-02	71.13	-2.83	3684	67	0.053	3.60	44.9	9.23
HIPEQ0445-04	71.42	-4.88	4899	88	0.047	6.60	61.6	9.77
HIPEQ0446-02	71.54	-2.07	4575	70	0.052	8.50	57.1	9.81
HIPEQ0446+08	71.63	8.32	4575	236	0.048	7.91	57.0	9.78
HIPEQ0446-03	71.67	-3.89	3007	49	0.108	6.30	35.7	9.28
HIPEQ0447-04	71.77	-4.17	3006	158	0.057	9.30	35.7	9.45
HIPEQ0447+00	71.78	0.07	4595	103	0.034	3.30	57.4	9.41
HIPEQ0447+01	71.97	1.78	4481	192	0.049	7.35	55.8	9.73
HIPEQ0448+00	72.13	0.24	771	105	0.180	16.60	5.5	8.08
HIPEQ0448-03	72.21	-3.89	2955	54	0.047	4.80	35.1	9.14
HIPEQ0450+07	72.65	7.02	3882	328	0.078	25.32	47.8	10.14
HIPEQ0450+06	72.68	6.02	4549	290	0.062	13.73	57.0	10.02
HIPEQ0452-04	73.01	-4.95	3703	79	0.057	4.20	45.7	9.32
HIPEQ0452-05	73.22	-5.52	3183	133	0.064	8.20	38.7	9.46

Continued on Next Page...

(1) Name	(2) RA (°)	(3) Dec (°)	(4) Vel (km s^{-1})	(5) W_{50} (km s^{-1})	(6) S_{peak} (Jy)	(7) S_{int} (Jy km s^{-1})	(8) Dist. (Mpc)	(9) HI mass log $M_{\odot}$
HIPEQ0453-03	73.29	-3.04	4720	95	0.051	6.10	59.8	9.71
HIPEQ0453-04	73.38	-4.40	4005	76	0.066	7.10	50.0	9.62
HIPEQ0454-05	73.55	-5.60	4588	37	0.185	7.50	58.2	9.78
HIPEQ0456-04	74.07	-4.43	4039	113	0.071	7.70	51.1	9.67
HIPEQ0456+01	74.21	1.02	8463	83	0.051	4.80	112.6	10.16
HIPEQ0457+00	74.38	0.73	3940	63	0.053	6.50	49.9	9.58
HIPEQ0458-00	74.50	0.11	5229	90	0.041	12.20	67.8	10.12
HIPEQ0459+05	74.86	5.59	4611	252	0.045	9.84	59.6	9.92
HIPEQ0500-03	75.08	-3.32	3771	157	0.095	13.00	48.4	9.86
HIPEQ0501-04	75.42	-4.25	4197	138	0.150	20.90	54.6	10.17
HIPEQ0502+00	75.65	0.28	4980	78	0.046	7.10	65.6	9.86
HIPEQ0503+00	75.90	0.66	4370	107	0.044	9.20	57.5	9.86
HIPEQ0513-03	78.37	-3.28	4091	176	0.033	5.20	56.8	9.60
HIPEQ0519-04	79.80	-4.47	3902	53	0.055	3.10	55.8	9.36
HIPEQ0520+08	80.20	8.82	4635	195	0.136	26.36	66.1	10.43
HIPEQ0521+04	80.26	4.02	4043	342	0.102	17.78	58.1	10.15
HIPEQ0524-05	81.01	-5.34	3860	61	0.069	7.80	56.3	9.77
HIPEQ0524+07	81.08	7.41	4333	103	0.072	8.25	62.7	9.88
HIPEQ0524+04	81.25	4.52	520	165	0.239	33.26	11.2	8.99
HIPEQ0527-05	81.99	-5.27	2487	322	0.082	26.40	38.1	9.96
HIPEQ0531+08	82.78	8.34	958	89	0.062	5.48	17.6	8.60
HIPEQ0533-03	83.42	-3.47	6610	74	0.043	6.20	95.0	10.12
HIPEQ0538++00	84.52	0.40	5811	154	0.054	8.32	83.6	10.14
HIPEQ0538+02	84.71	2.47	7137	150	0.043	6.53	102.0	10.20
HIPEQ0540-01	85.15	-1.36	5404	54	0.079	4.30	77.7	9.79
HIPEQ0541+06	85.45	6.68	458	59	0.110	7.22	10.1	8.24
HIPEQ0543-01	85.94	-1.59	5536	189	0.031	5.20	78.9	9.88
HIPEQ0545+05	86.26	5.07	387	121	0.616	71.97	8.5	9.09
HIPEQ0553+09	88.38	9.60	8578	221	0.046	9.40	118.7	10.49
HIPEQ0555-02	88.86	-2.57	4358	125	0.054	6.80	59.4	9.75
HIPEQ0555+03	88.93	3.39	805	117	0.147	17.33	11.1	8.70
HIPEQ0556-05	89.25	-5.37	2393	79	0.077	5.90	32.2	9.16
HIPEQ0602-03	90.70	-3.31	2616	183	0.042	7.20	33.3	9.28
HIPEQ0603+08	90.95	8.65	5289	200	0.062	10.60	69.5	10.08
HIPEQ0604-02	91.07	-2.18	3995	105	0.044	4.10	51.7	9.41
HIPEQ0605-02	91.48	-2.40	2587	126	0.042	5.20	32.1	9.10
HIPEQ0613+04	93.37	4.38	4679	344	0.039	8.97	59.0	9.87
HIPEQ0615+00	93.78	0.21	2527	88	0.168	31.10	29.4	9.80
HIPEQ0621-05	95.28	-5.86	881	117	0.089	9.60	7.0	8.04
HIPEQ0621+00	95.45	0.37	3000	166	0.143	40.20	35.5	10.08
HIPEQ0632-01	98.05	-1.65	6829	194	0.030	5.20	89.6	9.99
HIPEQ0633+04	98.40	4.70	4469	29	0.217	8.02	57.2	9.79
HIPEQ0636+00	99.14	0.95	2842	153	0.105	15.40	35.7	9.67

Continued on Next Page...

(1) Name	(2) RA (°)	(3) Dec (°)	(4) Vel (km s^{-1})	(5) W$_{50}$ (km s^{-1})	(6) S_{peak} (Jy)	(7) S_{int} (Jy km s^{-1})	(8) Dist. (Mpc)	(9) HI mass log M$_\odot$
HIPEQ0636+04	99.20	4.03	3487	186	0.051	6.89	44.5	9.51
HIPEQ0637+03	99.41	3.41	3385	156	0.061	7.06	43.4	9.50
HIPEQ0640-01	100.23	-1.72	2707	112	0.072	6.91	35.2	9.31
HIPEQ0653-03	103.27	-3.97	2930	74	0.067	4.80	42.0	9.30
HIPEQ0653-03	103.32	-3.87	2674	160	0.051	7.20	38.6	9.40
HIPEQ0656+06	104.09	6.01	6229	136	0.074	10.13	88.1	10.27
HIPEQ0656-03	104.09	-3.72	2570	86	0.042	4.30	38.0	9.16
HIPEQ0656+06	104.12	6.24	6636	218	0.061	11.81	93.8	10.39
HIPEQ0657-05	104.33	-5.07	2771	112	0.083	17.20	40.9	9.83
HIPEQ0657-05	104.48	-5.33	2824	108	0.239	24.80	41.8	10.01
HIPEQ0659-01	104.84	-1.53	1854	171	0.145	20.10	28.9	9.60
HIPEQ0700-02	105.10	-2.39	1826	52	0.058	3.10	28.7	8.78
HIPEQ0701+01	105.27	1.92	1971	62	0.072	11.40	30.7	9.40
HIPEQ0702-03	105.64	-3.30	2599	00	0.052	4.20	39.5	9.19
HIPEQ0703+03	105.78	3.17	3504	99	0.041	3.54	51.8	9.35
HIPEQ0705+02	106.42	2.62	1734	45	0.102	4.66	28.0	8.94
HIPEQ0709-05	107.39	-5.43	1920	265	0.086	20.10	30.7	9.65
HIPEQ0710+05	107.53	5.25	3566	136	0.082	9.07	52.9	9.78
HIPEQ0722+04	110.69	4.46	1141	322	0.090	29.88	18.2	9.37
HIPEQ0730+07	112.50	7.24	3870	90	0.048	5.15	53.1	9.53
HIPEQ0731+08	112.83	8.02	1871	53	0.043	2.11	25.5	8.51
HIPEQ0731+00	112.87	0.06	1498	38	0.083	3.30	20.5	8.51
HIPEQ0734+04	113.55	4.54	1233	149	0.092	12.95	16.0	8.89
HIPEQ0736+04	114.23	4.21	2747	276	0.045	8.80	35.6	9.42
HIPEQ0737+03	114.49	3.32	1187	78	0.149	12.59	14.2	8.78
HIPEQ0738-01	114.51	-1.46	1397	45	0.068	3.10	17.1	8.33
HIPEQ0739-00	114.83	0.73	1573	141	0.056	7.40	19.0	8.80
HIPEQ0739-02	114.89	-2.62	1744	52	0.093	5.20	21.3	8.75
HIPEQ0740-01	115.11	-1.57	1573	94	0.068	9.60	18.7	8.90
HIPEQ0745+07	116.31	7.98	5025	324	0.065	12.59	64.5	10.09
HIPEQ0745+04	116.45	4.97	2743	245	0.070	12.33	33.2	9.50
HIPEQ0746-05	116.64	-5.77	1457	130	0.080	9.50	15.8	8.74
HIPEQ0800++02	120.24	2.29	4966	279	0.090	25.11	62.6	10.36
HIPEQ0803+08	120.95	8.70	4891	116	0.061	6.70	61.8	9.78
HIPEQ0806+08	121.67	8.05	4524	345	0.047	11.00	57.3	9.93
HIPEQ0809+00	122.36	0.57	1798	151	0.045	5.29	20.8	8.73
HIPEQ0818+04	124.55	4.63	4163	49	0.085	4.48	55.4	9.51
HIPEQ0820-05	125.12	-5.13	4399	126	0.063	7.94	59.5	9.82
HIPEQ0821+03	125.41	3.18	2676	282	0.049	8.90	36.2	9.44
HIPEQ0821-00	125.42	0.43	1802	72	0.156	13.74	24.4	9.29
HIPEQ0821+03b	125.43	3.37	4057	255	0.045	6.82	55.1	9.69
HIPEQ0821-00	125.42	0.43	1957	72	0.145	13.00	26.5	9.33
HIPEQ0822-01	125.59	-1.04	4460	132	0.051	5.78	60.9	9.70

Continued on Next Page...

(1) Name	(2) RA (°)	(3) Dec (°)	(4) Vel (km s^{-1})	(5) W$_{50}$ (km s^{-1})	(6) S_{peak} (Jy)	(7) S_{int} (Jy km s^{-1})	(8) Dist. (Mpc)	(9) HI mass log M$_{\odot}$
HIPEQ0823-04	125.86	-4.93	7097	293	0.077	21.40	97.8	10.68
HIPEQ0825-00	126.25	0.60	4914	467	0.055	12.12	67.9	10.12
HIPEQ0826+02	126.60	2.59	5614	87	0.043	3.22	78.0	9.66
HIPEQ0826-04	126.62	-4.06	5556	57	0.046	3.30	77.3	9.67
HIPEQ0831+07	127.87	7.02	1838	125	0.065	6.95	27.7	9.10
HIPEQ0834-05	128.70	-5.07	4901	228	0.042	8.00	70.4	9.97
HIPEQ0835-04	128.91	-4.08	4348	112	0.090	9.30	62.9	9.94
HIPEQ0836+05	129.15	5.25	1853	59	0.044	2.41	29.0	8.68
HIPEQ0838-02	129.52	-2.42	1916	56	0.076	4.50	30.2	8.98
HIPEQ0839-02	129.95	-2.53	5538	84	0.050	5.20	79.9	9.89
HIPEQ0840-04	130.15	-4.11	4436	55	0.054	5.00	64.8	9.69
HIPEQ0842+00	130.73	0.66	10494	53	0.039	3.50	149.9	10.27
HIPEQ0848-02	132.08	-2.99	4119	65	0.034	5.10	60.5	9.64
HIPEQ0851-02	132.93	-2.19	3524	252	0.115	29.20	52.0	10.27
HIPEQ0851-02	132.99	-2.40	3448	135	0.102	12.60	50.9	9.89
HIPEQ0855+02	133.97	2.51	3779	127	0.057	5.60	54.7	9.60
HIPEQ0856-03	134.02	-3.35	2263	294	0.062	19.10	34.1	9.72
HIPEQ0856+00	134.12	0.37	2493	146	0.069	9.20	37.1	9.47
HIPEQ0857+09	134.35	9.91	3712	226	0.048	9.06	53.3	9.78
HIPEQ0858-03	134.68	-3.73	2955	94	0.061	13.30	42.8	9.76
HIPEQ0858+06	134.70	6.29	3790	119	0.127	13.83	54.1	9.98
HIPEQ0858-04	134.71	-4.92	3930	62	0.100	17.60	56.1	10.12
HIPEQ0859+06	134.76	6.75	3579	41	0.069	3.18	51.1	9.29
HIPEQ0906+06	136.66	6.31	1433	147	0.109	14.20	19.8	9.12
HIPEQ0908+05	137.08	5.92	1310	67	0.057	3.44	17.6	8.40
HIPEQ0908-01	137.13	-1.75	8276	73	0.036	2.60	113.6	9.90
HIPEQ0909+05	137.26	5.20	597	36	0.033	1.13	7.8	7.21
HIPEQ0910+07	137.64	7.18	1500	99	0.083	8.64	19.5	8.89
HIPEQ0912+09	138.09	9.96	2108	222	0.088	15.05	27.1	9.42
HIPEQ0916+06	139.05	6.33	3627	157	0.061	6.10	46.6	9.49
HIPEQ0917-04	139.30	-4.75	3715	142	0.090	15.10	47.6	9.91
HIPEQ0921+03	140.47	3.06	3464	242	0.046	9.43	43.0	9.61
HIPEQ0923-00	140.85	0.73	3471	234	0.051	9.44	42.8	9.61
HIPEQ0929+07	142.31	7.77	6441	71	0.089	6.49	83.0	10.02
HIPEQ0929+07	142.45	7.75	2124	396	0.070	22.97	23.7	9.48
HIPEQ0930+04	142.59	4.16	5244	69	0.087	5.99	66.3	9.79
HIPEQ0934+00	143.65	0.13	5076	208	0.066	12.10	64.0	10.07
HIPEQ0935+05	143.77	5.16	1992	177	0.039	5.11	21.8	8.76
HIPEQ0935-05	143.95	-5.58	1583	49	0.087	4.60	16.5	8.47
HIPEQ0936+01	144.19	1.22	4875	271	0.052	11.32	61.3	10.00
HIPEQ0938+09	144.56	9.55	3312	337	0.090	23.02	40.0	9.94
HIPEQ0939+00	144.76	0.65	2129	66	0.043	3.30	24.1	8.65
HIPEQ0940-03	145.08	-3.88	1509	53	0.079	4.00	15.9	8.38

Continued on Next Page...

(1) Name	(2) RA (°)	(3) Dec (°)	(4) Vel (km s^{-1})	(5) W$_{50}$ (km s^{-1})	(6) S_{peak} (Jy)	(7) S_{int} (Jy km s^{-1})	(8) Dist. (Mpc)	(9) HI mass log M$_\odot$
HIPEQ0941-02	145.28	-2.73	1718	128	0.041	4.50	18.9	8.58
HIPEQ0942+00	145.51	0.34	1880	129	0.490	59.19	21.2	9.80
HIPEQ0942+09	145.74	9.50	3180	109	0.230	26.09	38.9	9.97
HIPEQ0943-05	145.86	-5.32	1997	143	0.122	17.20	23.1	9.34
HIPEQ0943-05	145.90	-5.92	2131	89	0.111	9.60	25.0	9.15
HIPEQ0944-00a	146.03	0.65	1639	62	0.121	11.80	18.3	8.97
HIPEQ0944-00	146.18	0.67	1220	125	0.055	6.50	12.8	8.40
HIPEQ0944+09	146.19	9.59	540	79	0.066	5.35	3.7	7.23
HIPEQ0945+06	146.34	6.39	3046	196	0.050	7.96	37.6	9.42
HIPEQ0945+01	146.48	1.68	1853	265	0.079	16.60	21.6	9.26
HIPEQ0946-03	146.52	-3.96	4982	137	0.055	10.80	64.4	10.02
HIPEQ0946+02	146.55	2.96	1927	177	0.070	13.41	22.7	9.21
HIPEQ0946+05	146.56	5.71	3048	274	0.055	11.60	37.9	9.59
HIPEQ0947+00a	146.72	0.51	1763	212	0.113	19.31	20.7	9.29
HIPEQ0947+00b	146.81	0.93	1850	113	0.077	8.05	21.9	8.96
HIPEQ0947-02	146.89	-2.03	1513	161	0.074	10.50	17.5	8.88
HIPEQ0947+02	146.97	2.65	1860	200	0.106	15.80	22.2	9.26
HIPEQ0948-03	147.10	-3.76	4046	104	0.046	6.30	52.2	9.61
HIPEQ0948+02	147.24	2.45	6006	129	0.053	5.91	79.3	9.94
HIPEQ0949+00	147.45	0.62	1993	133	0.242	31.40	24.6	9.65
HIPEQ0950+09	147.72	9.01	5126	320	0.065	14.98	67.6	10.21
HIPEQ0951+07	147.81	7.83	555	98	0.262	24.24	5.6	8.25
HIPEQ0951+01	147.95	1.42	1929	94	0.062	5.90	24.3	8.91
HIPEQ0952+05	148.08	5.79	5629	66	0.043	3.09	75.0	9.61
HIPEQ0953+07	148.43	7.79	5273	51	0.032	1.57	70.5	9.26
HIPEQ0953+01	148.43	1.59	1284	330	0.213	55.14	16.2	9.53
HIPEQ0954+02a	148.56	2.29	7192	61	0.054	3.64	97.4	9.91
HIPEQ0954+01	148.65	1.91	1922	127	0.054	6.30	25.1	8.97
HIPEQ0954+09	148.67	9.27	1479	205	0.080	11.61	19.1	9.00
HIPEQ0955+04a	148.84	4.27	1813	222	0.057	11.50	23.8	9.19
HIPEQ0958+01	149.64	1.70	1805	113	0.057	5.82	24.8	8.92
HIPEQ1000+03	150.19	3.34	2053	361	0.076	23.07	28.8	9.65
HIPEQ1002+03	150.52	3.41	5634	96	0.049	6.23	78.2	9.95
HIPEQ1002-06	150.65	-6.01	659	128	0.190	21.06	10.7	8.75
HIPEQ1004+01	151.18	1.69	1270	121	0.046	5.75	19.4	8.71
HIPEQ1007+06	151.81	6.96	9113	91	0.044	5.41	128.3	10.32
HIPEQ1007+10	151.85	10.36	540	55	0.084	4.71	10.2	8.06
HIPEQ1010+05	152.60	5.14	4067	126	0.042	5.67	58.7	9.66
HIPEQ1014+07	153.50	7.04	1211	215	0.217	37.60	20.5	9.57
HIPEQ1014+03	153.55	3.47	1217	434	0.326	115.35	20.7	10.07
HIPEQ1015+07	153.87	7.32	3716	290	0.041	6.38	54.7	9.65
HIPEQ1015+02	153.96	2.71	1273	144	0.098	12.71	21.7	9.15
HIPEQ1017-03	154.26	-3.47	1449	176	0.115	17.80	24.2	9.39

Continued on Next Page...

(1) Name	(2) RA (°)	(3) Dec (°)	(4) Vel (km s^{-1})	(5) W_{50} (km s^{-1})	(6) S_{peak} (Jy)	(7) S_{int} (Jy km s^{-1})	(8) Dist. (Mpc)	(9) HI mass log $M_\odot$
HIPEQ1017+04	154.27	4.34	1341	66	0.096	7.80	22.7	8.98
HIPEQ1018+09	154.50	9.82	2200	495	0.057	24.82	34.2	9.84
HIPEQ1018+07	154.63	7.03	3655	237	0.076	17.33	54.1	10.08
HIPEQ1019+02	154.80	2.98	4291	354	0.049	12.68	62.9	10.07
HIPEQ1026+03	156.68	3.86	2141	241	0.122	22.28	33.2	9.76
HIPEQ1028+03	157.14	3.61	1147	110	0.045	4.53	19.6	8.61
HIPEQ1029+06	157.39	6.06	3536	256	0.053	9.47	51.7	9.78
HIPEQ1030-02	157.52	-2.67	4440	85	0.034	2.80	64.1	9.43
HIPEQ1031+04	157.81	4.47	1173	180	0.204	33.01	19.4	9.47
HIPEQ1034-02	158.54	-2.35	2128	97	0.065	5.70	31.8	9.13
HIPEQ1039-00	159.80	0.39	5852	187	0.046	11.80	81.3	10.26
HIPEQ1039+01	159.83	1.71	707	48	0.072	4.10	11.2	8.08
HIPEQ1041+00	160.47	0.79	5541	104	0.046	4.56	76.2	9.79
HIPEQ1046+01	161.56	1.82	983	233	0.256	46.78	12.7	9.25
HIPEQ1050+01	162.52	1.27	1589	120	0.030	3.94	19.6	8.55
HIPEQ1050-02	162.69	-2.15	4634	136	0.049	7.00	60.9	9.79
HIPEQ1051+05	162.81	5.84	1011	157	0.261	35.14	11.5	9.04
HIPEQ1051+03	162.90	3.45	1067	67	0.165	11.35	12.1	8.60
HIPEQ1051+04a	162.91	4.59	1037	154	0.099	11.50	11.7	8.57
HIPEQ1051+10	162.95	10.14	2688	255	0.116	21.10	33.9	9.76
HIPEQ1052+03	163.07	3.74	3597	266	0.084	17.58	46.2	9.95
HIPEQ1052+00	163.22	0.05	1809	88	0.069	5.67	21.8	8.80
HIPEQ1053+07	163.25	7.63	3355	78	0.075	6.27	42.7	9.43
HIPEQ1053+02	163.31	2.57	1045	88	0.105	9.00	11.4	8.44
HIPEQ1055+02	163.90	2.42	1040	84	0.037	3.44	10.7	7.97
HIPEQ1101+03	165.31	3.64	1122	303	0.149	35.89	10.7	8.98
HIPEQ1105-00	166.45	0.03	1083	234	0.933	282.50	9.7	9.79
HIPEQ1106+07	166.71	7.21	1418	185	0.054	8.02	14.1	8.57
HIPEQ1108-05	167.11	-5.12	11351	65	0.042	2.50	152.5	10.14
HIPEQ1109-00	167.36	0.08	3810	337	0.082	19.89	46.5	10.01
HIPEQ1110+01	167.73	1.14	991	71	0.075	5.34	8.4	7.95
HIPEQ1112+10	168.17	10.25	1280	40	0.057	2.43	12.4	7.94
HIPEQ1113+05	168.25	5.28	2525	83	0.053	4.02	29.2	8.91
HIPEQ1117-05	169.35	-5.31	4085	50	0.038	4.30	51.1	9.42
HIPEQ1117+04a	169.35	4.58	1573	351	0.061	14.55	16.9	8.99
HIPEQ1118-02	169.57	-2.03	7430	79	0.035	2.90	97.6	9.81
HIPEQ1119-03	169.78	-3.04	7863	94	0.032	3.40	103.9	9.94
HIPEQ1119+03	169.79	3.60	7005	193	0.051	8.92	91.8	10.25
HIPEQ1120+02	170.05	2.55	1593	100	0.218	21.61	17.7	9.20
HIPEQ1120-03	170.18	-3.16	7725	291	0.038	9.60	102.3	10.37
HIPEQ1122-04	170.60	-4.75	1071	104	0.060	5.90	11.3	8.25
HIPEQ1124+00	171.03	0.66	7985	63	0.051	3.20	106.7	9.93
HIPEQ1124+03	171.12	3.30	1368	107	0.226	23.51	15.7	9.14

Continued on Next Page...

(1) Name	(2) RA (°)	(3) Dec (°)	(4) Vel (km s^{-1})	(5) W_{50} (km s^{-1})	(6) S_{peak} (Jy)	(7) S_{int} (Jy km s^{-1})	(8) Dist. (Mpc)	(9) HI mass log $M_\odot$
HIPEQ1126+10	171.50	10.00	1153	76	0.064	5.22	13.3	8.33
HIPEQ1127-00	171.77	0.98	962	83	0.096	8.94	11.1	8.41
HIPEQ1127-04	171.94	-4.91	1041	76	0.081	6.50	12.4	8.37
HIPEQ1128+09	172.11	9.40	1733	405	0.074	14.45	21.8	9.21
HIPEQ1128+09	172.15	9.11	6134	268	0.069	17.85	82.1	10.45
HIPEQ1130+09	172.53	9.28	1008	347	0.212	41.98	12.5	9.19
HIPEQ1131-02	172.87	-2.29	4677	107	0.153	18.47	62.9	10.24
HIPEQ1132+00	173.05	0.79	6073	71	0.041	7.50	82.4	10.08
HIPEQ1133-03	173.44	-3.42	1604	139	0.128	15.51	21.8	9.24
HIPEQ1136+00a	174.11	0.80	4302	50	0.032	3.60	59.3	9.48
HIPEQ1136+00	174.12	0.83	1099	90	0.078	6.84	15.9	8.61
HIPEQ1137-05	174.48	-5.61	2248	80	0.064	9.60	31.9	9.36
HIPEQ1138+03	174.70	3.60	5492	102	0.054	5.43	76.4	9.87
HIPEQ1143-01	175.98	-1.26	1692	29	0.064	1.16	26.0	8.27
HIPEQ1144-03	176.17	-3.80	1764	187	0.059	8.20	27.1	9.15
HIPEQ1145+09	176.25	9.17	2852	121	0.072	8.36	41.8	9.54
HIPEQ1145+02	176.26	2.17	1007	41	0.122	5.58	17.0	8.58
HIPEQ1146-03	176.70	-3.83	5440	52	0.064	8.60	77.8	10.09
HIPEQ1148-02	177.20	-2.04	1725	223	0.168	28.49	27.4	9.70
HIPEQ1149-05	177.35	-5.14	1831	67	0.076	11.10	28.9	9.34
HIPEQ1150-00	177.63	0.55	1930	57	0.047	5.80	30.4	9.10
HIPEQ1151-02	177.98	-2.64	3832	224	0.036	6.69	56.4	9.70
HIPEQ1152+01	178.08	1.75	6022	136	0.036	5.09	86.6	9.95
HIPEQ1152-03	178.11	-3.87	1729	183	0.070	11.00	27.9	9.31
HIPEQ1152-03b	178.14	-3.68	1635	61	0.091	5.93	26.7	9.00
HIPEQ1152-02	178.20	-2.48	1054	60	0.114	7.45	18.9	8.80
HIPEQ1152-04	178.23	-4.42	1622	163	0.191	29.40	26.5	9.69
HIPEQ1153-03	178.40	-3.99	1727	159	0.101	15.70	28.0	9.46
HIPEQ1155+06	178.84	6.11	5873	229	0.058	11.07	84.7	10.27
HIPEQ1155+01	178.90	1.26	1879	176	0.095	14.12	30.1	9.48
HIPEQ1155+06	178.98	6.76	2482	419	0.186	49.71	38.2	10.23
HIPEQ1158-01	179.69	-1.45	1567	72	0.048	5.20	25.9	8.91
HIPEQ1159-02	179.76	-2.59	1685	113	0.043	4.90	27.5	8.94
HIPEQ1200-01	180.10	-1.09	1459	319	0.242	65.30	24.3	9.96
HIPEQ1200-00	180.18	0.00	1928	54	0.124	7.06	30.6	9.19
HIPEQ1200-03	180.21	-3.41	1591	46	0.042	3.50	26.1	8.75
HIPEQ1202+01	180.66	2.00	1966	303	0.100	18.75	30.9	9.63
HIPEQ1204-01	181.07	-1.54	1468	96	0.103	8.83	24.0	9.08
HIPEQ1204-02	181.20	-2.72	5887	43	0.094	3.25	84.3	9.74
HIPEQ1205+08	181.39	8.94	6252	160	0.038	4.55	89.1	9.93
HIPEQ1208+02	182.00	2.82	1320	201	0.426	69.63	21.3	9.87
HIPEQ1210+02	182.74	2.03	1331	83	0.125	10.74	20.8	9.04
HIPEQ1211+02	182.75	2.03	1331	82	0.118	9.77	20.7	9.00

Continued on Next Page...

(1) Name	(2) RA (°)	(3) Dec (°)	(4) Vel (km s^{-1})	(5) W_{50} (km s^{-1})	(6) S_{peak} (Jy)	(7) S_{int} (Jy km s^{-1})	(8) Dist. (Mpc)	(9) HI mass log $M_{\odot}$
HIPEQ1211+02	182.87	2.94	1289	95	0.078	6.57	20.0	8.79
HIPEQ1213+07	183.45	7.25	2521	66	0.034	2.08	36.0	8.80
HIPEQ1213+07	183.47	7.23	2634	296	0.040	6.61	37.5	9.34
HIPEQ1214+07	183.53	7.80	1215	115	0.063	6.63	18.2	8.72
HIPEQ1214+05	183.63	5.82	2045	261	0.100	21.44	29.3	9.64
HIPEQ1214+09	183.67	9.20	1777	120	0.043	4.53	25.6	8.85
HIPEQ1215+09	183.81	9.55	597	192	0.038	6.52	9.6	8.15
HIPEQ1215+04a	183.96	4.69	2179	116	0.041	3.91	30.8	8.94
HIPEQ1215+09	183.98	9.67	2203	35	0.123	4.82	31.0	9.04
HIPEQ1215-03	183.98	-3.59	5055	127	0.047	5.74	70.1	9.82
HIPEQ1217+10	184.25	10.01	1179	62	0.114	7.99	16.9	8.73
HIPEQ1217+07	184.47	7.19	3687	324	0.082	18.20	50.6	10.04
HIPEQ1217+00	184.48	0.46	933	60	0.335	21.19	13.4	8.95
HIPEQ1218+06	184.50	6.67	734	115	0.083	7.50	10.6	8.30
HIPEQ1218-01	184.55	-1.08	5587	298	0.058	9.29	76.8	10.11
HIPEQ1218+07	184.59	7.65	3911	146	0.057	6.95	53.5	9.67
HIPEQ1218+08	184.72	8.85	2454	174	0.074	10.87	33.5	9.46
HIPEQ1219+03	184.75	3.98	1516	56	0.042	2.13	20.9	8.34
HIPEQ1219+06	184.95	6.98	7028	55	0.092	5.60	96.2	10.09
HIPEQ1219+06	184.96	6.67	480	41	0.061	2.65	6.6	7.44
HIPEQ1220+00	185.08	0.34	890	71	0.066	4.57	12.1	8.19
HIPEQ1220+01	185.12	1.46	1588	184	0.043	6.26	21.4	8.83
HIPEQ1221+03	185.25	3.73	2553	343	0.096	15.57	34.2	9.63
HIPEQ1221+04	185.47	4.49	1562	159	0.633	84.88	20.5	9.93
HIPEQ1222-04	185.61	-4.65	5118	101	0.045	11.20	68.9	10.10
HIPEQ1222+04	185.62	4.58	1264	110	0.166	13.91	16.3	8.94
HIPEQ1222+09	185.65	9.40	1240	291	0.045	10.54	15.9	8.80
HIPEQ1223+05	185.78	5.30	1649	303	0.055	9.72	21.3	9.02
HIPEQ1223-03b	185.97	-3.41	1989	372	0.051	11.12	25.7	9.24
HIPEQ1223+00	186.00	0.55	2040	84	0.096	8.00	26.4	9.12
HIPEQ1224+03	186.14	4.00	1721	157	0.043	5.89	21.8	8.82
HIPEQ1224+03b	186.17	3.31	923	51	0.197	10.73	11.1	8.49
HIPEQ1225+04	186.33	4.93	2513	333	0.062	11.04	32.3	9.43
HIPEQ1225+05	186.34	5.74	1127	139	0.047	5.83	13.6	8.40
HIPEQ1225+00	186.36	0.58	2130	99	0.044	4.40	27.1	8.88
HIPEQ1225+02	186.41	2.17	1498	65	0.105	7.07	18.5	8.76
HIPEQ1225+07	186.45	7.23	985	284	0.116	27.91	11.5	8.94
HIPEQ1226+05	186.50	5.83	1530	133	0.061	7.41	18.8	8.79
HIPEQ1226-01	186.58	-1.27	2124	99	0.068	6.50	26.8	9.04
HIPEQ1226+08	186.68	8.89	1268	87	0.296	25.70	15.1	9.14
HIPEQ1226+02	186.73	2.51	1679	187	0.087	14.27	20.6	9.15
HIPEQ1227+06	186.75	6.28	1425	114	0.043	4.03	17.1	8.44
HIPEQ1227+07	186.78	7.27	925	147	0.213	25.01	10.3	8.80

Continued on Next Page...

(1) Name	(2) RA (°)	(3) Dec (°)	(4) Vel (km s^{-1})	(5) W_{50} (km s^{-1})	(6) S_{peak} (Jy)	(7) S_{int} (Jy km s^{-1})	(8) Dist. (Mpc)	(9) HI mass log $M_{\odot}$
HIPEQ1227+05	186.78	5.90	1112	153	0.101	15.47	12.9	8.78
HIPEQ1227+09	186.85	9.36	433	62	0.066	4.78	3.7	7.18
HIPEQ1227+01	186.90	1.57	1286	63	0.493	33.32	15.1	9.25
HIPEQ1228+08	187.11	8.74	1112	171	0.070	10.20	12.5	8.57
HIPEQ1228+04	187.17	4.30	4149	379	0.054	14.70	53.6	10.00
HIPEQ1228+02	187.23	2.74	1559	168	0.087	13.52	18.4	9.03
HIPEQ1228+03	187.24	3.59	894	126	0.060	7.06	9.4	8.17
HIPEQ1229+07	187.42	7.81	2322	144	0.046	6.43	28.4	9.09
HIPEQ1229+00	187.44	0.86	2223	109	0.046	4.38	27.1	8.88
HIPEQ1230+02	187.55	2.64	1628	39	0.097	3.70	19.0	8.50
HIPEQ1230+03	187.64	3.58	5137	121	0.042	4.23	66.7	9.65
HIPEQ1230+01	187.75	1.00	6721	230	0.055	12.65	88.6	10.37
HIPEQ1231+03	187.90	3.96	1720	158	0.302	45.18	19.8	9.62
HIPEQ1232+00a	188.13	0.40	1520	157	0.302	41.47	17.0	9.45
HIPEQ1232+00b	188.18	0.13	1127	304	0.505	118.38	11.6	9.58
HIPEQ1233-00	188.30	0.51	831	43	0.047	3.00	7.5	7.60
HIPEQ1233+08	188.37	8.67	1224	182	0.329	50.71	12.7	9.29
HIPEQ1233-02	188.39	-2.63	2462	68	0.092	6.74	29.5	9.14
HIPEQ1233-04	188.41	-4.89	1392	134	0.148	16.90	15.1	8.96
HIPEQ1234+02	188.54	2.66	1731	358	0.414	107.25	19.4	9.98
HIPEQ1234+08	188.58	8.20	1946	268	0.342	65.73	22.3	9.89
HIPEQ1234+06	188.60	6.41	1995	156	0.347	56.36	22.9	9.84
HIPEQ1234+02	188.62	2.22	1790	325	0.321	77.93	20.2	9.87
HIPEQ1236+03	189.14	3.12	1432	119	0.059	6.54	14.9	8.54
HIPEQ1236+06	189.14	6.64	1069	49	0.284	14.34	10.0	8.53
HIPEQ1237+06	189.25	6.94	1626	113	0.070	7.47	17.5	8.73
HIPEQ1239-04	189.78	-4.55	2470	69	0.071	4.80	28.7	8.97
HIPEQ1239-00	189.82	0.52	1070	199	1.055	159.45	9.7	9.55
HIPEQ1239+07	189.85	7.93	2063	109	0.059	6.15	23.1	8.89
HIPEQ1239-03	189.86	-3.77	2656	132	0.097	12.20	31.2	9.45
HIPEQ1240-05	190.05	-5.79	1178	167	0.401	59.40	11.2	9.24
HIPEQ1240-05	190.16	-5.13	2787	154	0.124	33.00	32.9	9.92
HIPEQ1241+01	190.25	1.41	1695	143	0.080	9.25	18.0	8.85
HIPEQ1241-02	190.34	-3.00	1431	99	0.057	4.86	14.4	8.38
HIPEQ1241-04	190.37	-4.14	3183	69	0.043	2.70	38.2	8.97
HIPEQ1241-03	190.38	-3.03	1548	102	0.047	4.60	16.0	8.44
HIPEQ1242+03	190.50	3.32	3933	62	0.043	2.82	48.3	9.19
HIPEQ1242-00	190.59	0.06	1708	216	0.211	39.32	18.1	9.48
HIPEQ1242-01a	190.59	-1.36	1101	144	0.169	21.04	9.9	8.69
HIPEQ1242+03b	190.65	3.97	742	140	0.049	6.88	5.0	7.61
HIPEQ1242-01b	190.75	-1.21	3172	293	0.119	23.27	37.9	9.90
HIPEQ1243+07	190.80	7.63	1306	66	0.043	2.82	12.6	8.02
HIPEQ1243+00	190.90	0.69	4407	97	0.042	4.50	54.7	9.50

Continued on Next Page...

(1) Name	(2) RA (°)	(3) Dec (°)	(4) Vel (km s^{-1})	(5) W_{50} (km s^{-1})	(6) S_{peak} (Jy)	(7) S_{int} (Jy km s^{-1})	(8) Dist. (Mpc)	(9) HI mass log $M_\odot$
HIPEQ1243-00	190.99	0.59	2605	193	0.167	21.27	30.1	9.66
HIPEQ1244-05	191.02	-5.70	1551	128	0.319	34.00	16.0	9.31
HIPEQ1244+00	191.15	0.47	1167	103	0.109	7.33	10.7	8.30
HIPEQ1244-02	191.11	-2.32	1576	108	0.114	9.89	16.2	8.79
HIPEQ1245-00	191.28	0.48	1780	176	0.374	93.80	19.0	9.90
HIPEQ1245-06	191.44	-6.07	1471	218	0.125	27.25	14.9	9.15
HIPEQ1246+05	191.70	5.96	830	127	0.086	9.54	6.2	7.94
HIPEQ1247-00	191.78	0.76	4042	104	0.030	3.30	49.8	9.28
HIPEQ1247+04	191.95	4.33	982	51	0.593	31.82	8.3	8.71
HIPEQ1247-03	191.97	-3.29	1202	64	0.067	4.50	11.3	8.13
HIPEQ1248+08	192.11	8.49	1000	420	0.135	28.12	8.6	8.69
HIPEQ1248-05	192.15	-5.29	1418	42	0.069	3.80	14.3	8.26
HIPEQ1249+03	192.28	3.39	723	156	0.425	54.57	4.9	8.49
HIPEQ1249+04	192.31	4.60	2642	74	0.097	7.28	30.8	9.21
HIPEQ1249-05	192.36	-5.19	4552	140	0.074	20.60	57.0	10.20
HIPEQ1249-04	192.38	-4.02	1614	141	0.100	12.90	17.0	8.94
HIPEQ1249-04	192.43	-4.57	1533	100	0.129	13.20	16.0	8.90
HIPEQ1250+05	192.50	5.33	649	168	0.341	48.73	4.0	8.27
HIPEQ1250-05	192.66	-5.26	4921	78	0.050	11.30	62.2	10.01
HIPEQ1250-04	192.68	-4.13	1624	141	0.098	13.30	17.3	8.97
HIPEQ1251-04	192.96	-4.58	2939	90	0.047	7.10	35.2	9.32
HIPEQ1251-05	192.97	-5.21	4765	183	0.054	7.80	60.2	9.82
HIPEQ1252-05	193.17	-5.86	3938	160	0.044	5.70	49.0	9.51
HIPEQ1253+04	193.30	4.47	718	75	0.227	18.31	5.4	8.10
HIPEQ1253-04	193.36	-4.95	1468	53	0.077	4.40	15.6	8.40
HIPEQ1253+01	193.37	1.26	1138	278	0.071	13.74	11.1	8.60
HIPEQ1253+02	193.40	2.19	999	426	0.057	12.02	9.2	8.38
HIPEQ1253-06	193.45	-6.60	1550	142	0.314	44.59	16.8	9.47
HIPEQ1254+02	193.70	2.68	923	142	0.133	16.90	8.4	8.45
HIPEQ1255+00	193.78	0.16	1311	187	0.153	23.53	13.7	9.02
HIPEQ1255-03	193.81	-3.40	1548	42	0.183	8.60	17.0	8.77
HIPEQ1255+02	193.82	2.87	2759	363	0.056	13.92	33.3	9.56
HIPEQ1255+08	193.83	8.01	2774	53	0.048	3.49	33.5	8.97
HIPEQ1255-00	193.92	0.27	1115	92	0.043	3.44	11.2	8.01
HIPEQ1255+04	193.95	4.30	757	257	0.358	78.23	6.4	8.88
HIPEQ1255+10	193.97	10.20	2680	197	0.041	7.62	32.3	9.27
HIPEQ1256+03	194.05	3.87	654	189	0.112	15.19	5.1	7.97
HIPEQ1257-01	194.29	-1.70	2821	293	0.083	19.82	34.6	9.75
HIPEQ1257-04	194.31	-4.14	1624	121	0.156	17.70	18.5	9.15
HIPEQ1257-05	194.32	-5.33	1382	148	0.234	29.40	15.2	9.21
HIPEQ1257+02	194.49	2.68	923	102	0.049	4.85	9.1	7.98
HIPEQ1258+02	194.64	2.82	2731	132	0.069	8.90	33.7	9.38
HIPEQ1258-06	194.69	-6.11	1602	137	0.070	8.38	18.6	8.83

Continued on Next Page...

(1) Name	(2) RA (°)	(3) Dec (°)	(4) Vel (km s^{-1})	(5) W_{50} (km s^{-1})	(6) S_{peak} (Jy)	(7) S_{int} (Jy km s^{-1})	(8) Dist. (Mpc)	(9) HI mass log $M_\odot$
HIPEQ1258-04	194.72	-4.88	1377	46	0.091	4.70	15.5	8.43
HIPEQ1300+02a	195.00	2.05	876	51	0.056	2.73	9.0	7.72
HIPEQ1300+02b	195.16	2.51	960	99	0.196	25.63	10.3	8.81
HIPEQ1300-00	195.21	0.00	1302	188	0.078	12.80	15.0	8.83
HIPEQ1301-01	195.26	-1.96	1604	58	0.106	9.90	19.1	8.93
HIPEQ1301-05	195.28	-5.53	1157	64	0.041	2.60	13.2	8.03
HIPEQ1301-04	195.39	-4.80	3133	168	0.057	8.90	40.0	9.53
HIPEQ1303+03	195.79	3.99	2844	112	0.078	7.44	36.5	9.37
HIPEQ1303+07	195.83	7.83	2902	217	0.074	14.82	37.3	9.69
HIPEQ1304-02	196.12	-2.90	1266	78	0.078	6.24	15.6	8.55
HIPEQ1304-03	196.13	-3.57	1358	114	0.383	41.30	16.9	9.44
HIPEQ1305-06	196.27	-6.49	1167	288	0.220	63.36	14.5	9.50
HIPEQ1305-07	196.31	-7.89	1272	60	0.085	5.10	16.0	8.49
HIPEQ1307-00	196.93	0.86	5324	190	0.071	13.34	71.9	10.21
HIPEQ1308-02	197.17	-2.15	5260	175	0.050	7.64	71.4	9.96
HIPEQ1309-05	197.33	-5.32	3252	134	0.062	8.60	44.1	9.59
HIPEQ1311+03a	197.87	3.42	3008	160	0.055	7.53	41.3	9.48
HIPEQ1312+05	198.03	5.51	909	80	0.051	3.98	13.1	8.21
HIPEQ1312-06	198.01	-6.99	1485	160	0.200	32.00	21.0	9.52
HIPEQ1312+03	198.03	3.14	8069	116	0.040	4.63	111.6	10.13
HIPEQ1312-04	198.07	-4.34	3259	72	0.101	12.70	45.1	9.78
HIPEQ1312+07	198.14	7.18	901	120	0.079	7.52	13.2	8.49
HIPEQ1313+06	198.30	6.07	6906	191	0.043	7.99	95.6	10.24
HIPEQ1313+10	198.34	10.20	1153	80	0.181	15.18	16.7	9.00
HIPEQ1315+00	198.92	0.49	3142	93	0.047	4.00	44.5	9.27
HIPEQ1316+08	199.00	8.01	7025	77	0.047	3.68	98.0	9.92
HIPEQ1317-00	199.38	1.00	1223	105	0.047	4.95	19.0	8.63
HIPEQ1318-01	199.57	-1.22	5638	102	0.060	5.30	79.5	9.90
HIPEQ1318-05	199.60	-5.73	5811	62	0.047	4.20	81.9	9.82
HIPEQ1320+05	200.15	5.41	959	85	0.059	4.83	16.2	8.47
HIPEQ1320+09	200.16	9.80	1131	148	0.113	15.49	18.4	9.09
HIPEQ1326+02	201.58	2.11	1085	153	0.113	16.86	19.0	9.16
HIPEQ1327+09	201.79	9.94	1048	42	0.044	1.79	18.4	8.16
HIPEQ1328+02	202.18	2.26	1019	49	0.043	2.26	18.3	8.25
HIPEQ1328-02	202.25	-2.02	3813	132	0.054	6.60	56.3	9.69
HIPEQ1329-00	202.37	0.38	3213	160	0.048	6.88	48.1	9.57
HIPEQ1329+00	202.40	0.79	3333	46	0.031	1.70	49.7	9.00
HIPEQ1329-01	202.49	-1.71	4192	348	0.098	16.49	61.5	10.17
HIPEQ1330+07	202.67	7.92	995	104	0.049	5.22	18.0	8.60
HIPEQ1332+01	203.10	1.86	3235	107	0.048	4.05	48.5	9.35
HIPEQ1332-03	203.17	-3.07	4489	248	0.048	12.40	65.7	10.10
HIPEQ1335+01	203.90	1.44	5160	239	0.054	7.52	74.8	10.00
HIPEQ1336+03	204.02	3.65	6676	78	0.043	3.53	95.8	9.88

Continued on Next Page...

(1) Name	(2) RA (°)	(3) Dec (°)	(4) Vel (km s^{-1})	(5) W_{50} (km s^{-1})	(6) S_{peak} (Jy)	(7) S_{int} (Jy km s^{-1})	(8) Dist. (Mpc)	(9) HI mass log $M_\odot$
HIPEQ1336+08	204.02	8.86	1156	129	0.085	10.15	20.1	8.99
HIPEQ1336+07	204.13	7.37	6880	84	0.075	5.91	98.5	10.13
HIPEQ1337+07	204.37	7.65	1042	160	0.152	22.26	18.5	9.25
HIPEQ1337+08	204.39	8.89	1153	266	0.397	71.38	20.0	9.83
HIPEQ1337+05	204.44	5.22	6645	134	0.043	5.02	95.2	10.03
HIPEQ1338+08	204.67	8.44	1017	120	0.049	4.86	18.0	8.57
HIPEQ1339-02	204.75	-2.28	8877	160	0.032	4.60	126.5	10.24
HIPEQ1341-04	205.30	-4.31	6832	154	0.043	6.40	97.4	10.16
HIPEQ1341+05	205.33	5.10	6843	229	0.045	8.64	97.5	10.29
HIPEQ1341-02	205.45	-2.76	8918	93	0.037	3.00	126.7	10.05
HIPEQ1345+08	206.35	8.80	6109	91	0.051	4.28	86.4	9.88
HIPEQ1345-05	206.42	-5.97	1590	160	0.167	21.50	24.6	9.49
HIPEQ1348-05	207.02	-5.87	5019	82	0.039	4.20	70.8	9.69
HIPEQ1348+03	207.03	3.96	1157	196	0.093	13.36	18.1	9.01
HIPEQ1351-02	208.00	-2.19	4441	83	0.138	11.20	61.6	10.00
HIPEQ1352-06	208.03	-6.06	3006	209	0.173	27.81	42.0	10.06
HIPEQ1352+02a	208.22	2.78	4575	280	0.069	12.90	63.2	10.08
HIPEQ1352-01	208.23	-1.09	1388	204	0.210	29.88	19.8	9.44
HIPEQ1354-04	208.55	-4.81	4500	66	0.115	17.60	61.8	10.20
HIPEQ1354+05	208.57	5.24	1432	194	0.109	17.76	19.9	9.22
HIPEQ1355-05	208.95	-5.97	2154	171	0.084	13.80	29.3	9.45
HIPEQ1356+05	209.04	5.03	1234	275	0.287	53.31	16.7	9.54
HIPEQ1357+06	209.37	6.15	4301	284	0.034	5.72	57.9	9.65
HIPEQ1400+02	210.25	2.02	3564	240	0.044	7.73	46.7	9.60
HIPEQ1401-03	210.33	-3.90	3351	149	0.035	4.00	43.8	9.26
HIPEQ1401-05	210.37	-5.81	1652	127	0.044	4.30	20.7	8.64
HIPEQ1401-01	210.44	-1.32	7572	83	0.040	4.00	102.0	9.99
HIPEQ1403+09	210.83	9.80	7059	58	0.042	2.81	94.3	9.77
HIPEQ1403+09	210.84	9.43	4568	42	0.110	5.12	59.7	9.63
HIPEQ1403-06	210.86	-6.05	2615	324	0.242	52.80	33.2	10.14
HIPEQ1404+08	211.22	8.81	1237	168	0.075	10.59	14.0	8.69
HIPEQ1405-03	211.30	-3.36	1762	216	0.068	11.70	21.1	9.09
HIPEQ1406-05	211.63	-5.44	2997	124	0.224	29.90	37.5	10.00
HIPEQ1408-06	212.04	-6.09	2636	180	0.080	13.21	32.2	9.51
HIPEQ1408+07	212.11	7.06	5826	274	0.038	8.78	75.8	10.07
HIPEQ1410-02	212.56	-2.58	1762	192	0.153	26.30	19.9	9.39
HIPEQ1411-01	212.91	-1.16	1539	241	0.372	64.39	16.6	9.62
HIPEQ1411-05	212.93	-5.85	4854	41	0.051	3.20	61.8	9.46
HIPEQ1415-04	213.77	-4.34	2883	169	0.121	21.40	34.3	9.77
HIPEQ1415-03	213.84	-3.06	9634	63	0.042	4.50	128.2	10.24
HIPEQ1415+04	213.88	4.40	5673	60	0.053	3.24	72.4	9.60
HIPEQ1415-04	213.98	-4.07	2798	59	0.146	9.10	33.0	9.37
HIPEQ1416+03	214.23	3.82	1466	100	0.076	7.15	14.9	8.57

Continued on Next Page...

(1) Name	(2) RA (°)	(3) Dec (°)	(4) Vel (km s^{-1})	(5) W_{50} (km s^{-1})	(6) S_{peak} (Jy)	(7) S_{int} (Jy km s^{-1})	(8) Dist. (Mpc)	(9) HI mass log $M_\odot$
HIPEQ1417-01	214.34	-1.53	1609	65	0.052	3.20	16.8	8.33
HIPEQ1418+05	214.58	5.62	5189	531	0.055	21.54	65.5	10.34
HIPEQ1419-02	214.90	-2.10	1824	101	0.035	3.50	19.6	8.50
HIPEQ1419+09	214.93	9.38	1280	139	0.178	24.59	12.2	8.94
HIPEQ1420+03	215.11	3.99	1743	161	0.089	10.92	18.4	8.94
HIPEQ1421+03	215.38	3.40	1492	266	0.061	12.96	15.1	8.84
HIPEQ1421-03	215.47	-3.76	2852	70	0.049	6.30	33.5	9.22
HIPEQ1422-00	215.61	0.39	1626	196	0.165	28.63	16.9	9.29
HIPEQ1422-04	215.73	-4.71	2858	123	0.036	4.00	33.7	9.03
HIPEQ1423+01	215.85	1.72	1544	222	0.126	23.70	15.8	9.15
HIPEQ1423-05	215.95	-6.00	2692	209	0.056	9.67	31.5	9.35
HIPEQ1424+08	216.13	8.31	1256	96	0.046	4.05	12.0	8.14
HIPEQ1424-03	216.16	-3.21	2968	64	0.139	26.30	35.3	9.89
HIPEQ1426-05	216.50	-5.41	1795	96	0.050	5.00	19.5	8.65
HIPEQ1426+08	216.74	8.72	1358	138	0.083	9.94	13.6	8.64
HIPEQ1427-02	216.75	-2.22	7335	77	0.045	7.50	95.8	10.21
HIPEQ1427+00	216.82	1.00	7897	80	0.065	12.30	103.7	10.49
HIPEQ1428-03	217.07	-3.60	2915	185	0.047	7.50	35.0	9.33
HIPEQ1429-00	217.39	0.01	1532	197	0.294	49.76	16.4	9.50
HIPEQ1429+07	217.45	7.68	4225	419	0.035	8.88	53.0	9.77
HIPEQ1430+03	217.53	3.23	1839	137	0.055	7.12	20.6	8.85
HIPEQ1430+07	217.69	7.28	1348	181	0.143	19.55	14.1	8.96
HIPEQ1431+05	217.80	5.99	7318	391	0.047	10.58	96.2	10.36
HIPEQ1431+06	218.00	6.21	2344	205	0.148	26.02	27.8	9.68
HIPEQ1432+00	218.12	0.27	1655	194	0.037	4.62	18.6	8.58
HIPEQ1432+09	218.18	9.90	1371	191	0.272	41.46	14.8	9.33
HIPEQ1433+02	218.30	2.92	1483	87	0.055	5.18	16.5	8.52
HIPEQ1433+04	218.35	4.45	1573	99	0.438	42.04	17.7	9.49
HIPEQ1433+06	218.39	6.79	2121	169	0.034	5.36	25.1	8.90
HIPEQ1433+01	218.42	1.51	1816	66	0.055	3.38	21.1	8.55
HIPEQ1433+05	218.47	5.46	7323	232	0.041	6.66	96.8	10.17
HIPEQ1435-04	218.83	-4.77	7227	225	0.036	6.90	95.9	10.18
HIPEQ1435+05	218.86	5.29	1626	94	0.096	7.98	18.9	8.83
HIPEQ1437+02	219.43	2.30	1751	293	0.109	25.25	21.3	9.43
HIPEQ1437-00	219.46	0.39	1873	151	0.048	5.79	23.0	8.86
HIPEQ1439+02	219.77	2.97	1568	95	0.073	6.07	19.2	8.72
HIPEQ1439+05	219.80	5.36	1498	122	0.492	56.21	18.3	9.65
HIPEQ1439-00	219.96	0.69	1753	183	0.192	29.40	21.9	9.52
HIPEQ1440-00	220.10	0.29	1883	172	0.305	52.59	23.9	9.85
HIPEQ1440+02	220.22	2.18	1629	121	0.030	3.35	20.6	8.52
HIPEQ1441-01	220.47	-1.83	1910	80	0.064	5.10	24.7	8.87
HIPEQ1442+00	220.62	0.69	1982	172	0.049	8.40	25.9	9.12
HIPEQ1443+04	220.76	4.88	1639	301	0.094	20.66	21.4	9.35

Continued on Next Page...

(1) Name	(2) RA (°)	(3) Dec (°)	(4) Vel (km s^{-1})	(5) W_{50} (km s^{-1})	(6) S_{peak} (Jy)	(7) S_{int} (Jy km s^{-1})	(8) Dist. (Mpc)	(9) HI mass log $M_\odot$
HIPEQ1444+01a	221.11	1.71	1566	324	0.146	35.25	20.9	9.56
HIPEQ1444+01	221.23	1.99	1993	66	0.074	5.91	26.8	9.00
HIPEQ1445+07	221.32	7.87	1681	37	0.210	8.33	22.6	9.00
HIPEQ1447+10	221.93	10.32	2254	292	0.047	11.48	31.1	9.42
HIPEQ1448-03	222.18	-3.71	1043	111	0.220	24.50	15.2	9.13
HIPEQ1452-02	223.02	-2.53	2085	184	0.097	13.10	30.3	9.45
HIPEQ1452-03	223.15	-3.54	2075	160	0.191	27.90	30.3	9.78
HIPEQ1453+03	223.46	3.56	1563	138	0.486	92.34	23.6	10.08
HIPEQ1454+01	223.53	1.78	4424	48	0.051	2.50	62.7	9.36
HIPEQ1454-03	223.64	-3.60	4415	76	0.040	2.40	62.7	9.35
HIPEQ1455-01	223.95	-1.34	1949	111	0.043	4.00	29.4	8.91
HIPEQ1456+05	224.20	5.12	1171	86	0.051	4.46	19.1	8.58
HIPEQ1458-01	224.58	-1.08	2198	427	0.191	64.20	33.3	10.23
HIPEQ1458+06	224.69	6.73	1671	130	0.037	4.62	26.2	8.87
HIPEQ1500+01	225.02	1.90	1338	323	0.048	13.52	22.0	9.19
HIPEQ1503-03	225.94	-3.36	6534	196	0.061	11.90	93.7	10.39
HIPEQ1504+00	226.11	0.80	4973	80	0.032	2.40	72.1	9.47
HIPEQ1504+02	226.12	2.35	9255	171	0.039	5.08	132.0	10.32
HIPEQ1504-00	226.12	0.85	1793	197	0.054	9.47	28.8	9.27
HIPEQ1507+01	226.81	1.53	2530	205	0.104	18.12	38.9	9.81
HIPEQ1512+01	228.03	1.73	2136	158	0.087	13.00	33.5	9.54
HIPEQ1521-05	230.28	-5.66	9025	123	0.042	4.60	127.5	10.25
HIPEQ1521+05	230.48	5.08	1471	174	0.237	33.16	22.9	9.61
HIPEQ1533-01	233.29	-1.65	2935	133	0.078	11.50	39.4	9.62
HIPEQ1537+05	234.39	5.97	1445	190	0.224	34.81	17.8	9.41
HIPEQ1541+00	235.50	0.70	2064	163	0.107	19.00	24.9	9.44
HIPEQ1541+00	235.50	0.70	1910	250	0.114	20.08	22.8	9.39
HIPEQ1544+02	236.22	2.50	3824	104	0.082	8.61	48.1	9.67
HIPEQ1545+00	236.35	0.80	3784	115	0.062	7.15	47.5	9.58
HIPEQ1546+06	236.53	6.91	1408	114	0.058	6.16	15.1	8.52
HIPEQ1549+05	237.25	5.20	2152	196	0.197	32.73	24.6	9.67
HIPEQ1601+01a	240.37	1.71	1916	234	0.057	9.41	21.0	8.99
HIPEQ1605-04	241.42	-4.57	1690	90	0.084	7.20	18.6	8.77
HIPEQ1607+07	241.83	8.00	2799	278	0.039	8.27	33.8	9.35
HIPEQ1608+07	242.09	7.54	1364	212	0.097	14.83	14.6	8.87
HIPEQ1609+08	242.36	8.75	3022	75	0.149	11.05	37.3	9.56
HIPEQ1609-04	242.40	-4.62	914	71	0.096	7.20	9.0	8.14
HIPEQ1609-00	242.43	0.09	1491	98	0.075	6.98	16.7	8.66
HIPEQ1609+00	242.49	0.72	2227	166	0.114	27.70	26.7	9.67
HIPEQ1613-00	243.38	0.87	2086	151	0.055	7.56	25.7	9.07
HIPEQ1614+02	243.58	2.51	4774	76	0.040	3.14	62.6	9.46
HIPEQ1614-00	243.60	0.21	2018	362	0.172	38.19	25.1	9.75
HIPEQ1614+00	243.65	0.84	1972	114	0.080	8.25	24.5	9.07

Continued on Next Page...

(1) Name	(2) RA (°)	(3) Dec (°)	(4) Vel (km s^{-1})	(5) W_{50} (km s^{-1})	(6) S_{peak} (Jy)	(7) S_{int} (Jy km s^{-1})	(8) Dist. (Mpc)	(9) HI mass log $M_{\odot}$
HIPEQ1618+07	244.70	7.41	1434	244	0.122	24.61	18.5	9.30
HIPEQ1619+01	244.83	1.72	1636	151	0.073	9.90	21.4	9.03
HIPEQ1619+01	244.97	1.95	5104	85	0.053	4.40	68.9	9.69
HIPEQ1621-02	245.44	-2.28	1785	90	0.163	34.30	24.3	9.68
HIPEQ1638-04	249.55	-4.85	1690	169	0.073	11.20	27.2	9.29
HIPEQ1639+07	249.84	7.73	3548	377	0.085	29.33	52.4	10.28
HIPEQ1641+05	250.35	5.66	3650	385	0.045	15.03	54.0	10.01
HIPEQ1641-05	250.49	-5.02	1739	289	0.240	54.70	28.2	10.01
HIPEQ1642+02	250.66	2.44	7137	208	0.042	6.49	102.3	10.20
HIPEQ1645-03	251.30	-3.21	6170	146	0.050	6.50	88.9	10.08
HIPEQ1647-00	251.98	0.38	2450	63	0.124	9.30	37.7	9.49
HIPEQ1651-03	252.91	-3.09	7185	138	0.036	4.00	102.6	10.00
HIPEQ1656+08	254.17	8.02	1465	60	0.067	4.09	23.0	8.71
HIPEQ1709-04	257.35	-4.94	7359	92	0.047	4.30	100.4	10.01
HIPEQ1710+07	257.50	7.82	2566	109	0.051	4.33	34.0	9.07
HIPEQ1722-05	260.58	-5.73	1752	135	0.213	29.90	19.8	9.44
HIPEQ1728+07	262.04	7.41	1684	135	0.133	16.33	17.9	9.09
HIPEQ1731-04	262.93	-4.15	7129	69	0.051	3.60	92.5	9.86
HIPEQ1732+07	263.10	7.08	1644	363	0.330	67.56	17.1	9.67
HIPEQ1733+05	263.49	5.46	2824	158	0.087	9.40	33.1	9.38
HIPEQ1735+02	263.89	2.79	9970	129	0.041	4.94	132.6	10.31
HIPEQ1740+10	265.17	10.37	2408	412	0.043	13.24	28.1	9.39
HIPEQ1742+09	265.67	9.07	1515	352	0.068	17.28	16.3	9.04
HIPEQ1747+04	266.77	4.21	7943	79	0.043	3.21	105.8	9.93
HIPEQ1748-01	267.18	-1.21	4619	93	0.040	3.00	60.1	9.41
HIPEQ1754+02	268.68	2.92	1749	182	0.067	9.44	22.8	9.06
HIPEQ1755-04	268.76	-4.67	9137	100	0.052	4.70	125.1	10.24
HIPEQ1756-05	269.17	-5.21	9406	93	0.074	13.10	129.5	10.71
HIPEQ1758+09	269.56	9.68	6293	82	0.112	9.27	86.1	10.21
HIPEQ1758+00	269.69	0.66	3975	43	0.056	2.70	54.3	9.27
HIPEQ1759+07	269.80	7.15	1883	208	0.084	14.99	26.0	9.38
HIPEQ1759+06	269.83	6.31	1801	245	0.150	31.12	24.9	9.66
HIPEQ1800+07	270.01	7.19	3635	363	0.049	13.69	50.0	9.91
HIPEQ1800-03	270.11	-4.00	4434	226	0.035	6.30	61.2	9.75
HIPEQ1801+06	270.48	6.97	1949	310	0.251	56.85	27.7	10.01
HIPEQ1803-02	270.77	-2.96	3765	178	0.065	10.80	52.8	9.85
HIPEQ1805-03	271.30	-3.37	1835	44	0.068	3.10	27.2	8.73
HIPEQ1807-02	271.80	-2.82	1869	142	0.287	35.30	28.2	9.82
HIPEQ1809-05	272.44	-5.84	3115	133	0.034	6.60	45.7	9.51
HIPEQ1810+01	272.55	1.55	1922	61	0.054	7.40	29.5	9.18
HIPEQ1810-01	272.68	-1.11	2217	103	0.044	5.80	33.7	9.19
HIPEQ1814-02	273.60	-2.41	1981	80	0.066	17.30	31.1	9.60
HIPEQ1815-02	273.88	-2.89	1980	54	0.060	12.60	31.2	9.46

Continued on Next Page...

(1) Name	(2) RA (°)	(3) Dec (°)	(4) Vel (km s^{-1})	(5) W_{50} (km s^{-1})	(6) S_{peak} (Jy)	(7) S_{int} (Jy km s^{-1})	(8) Dist. (Mpc)	(9) HI mass log $M_{\odot}$
HIPEQ1817-04	274.27	-4.07	3163	106	0.044	4.30	47.4	9.36
HIPEQ1819-01	274.80	-1.15	3111	177	0.046	7.30	46.8	9.58
HIPEQ1819+01	274.88	1.19	2673	114	0.113	12.80	40.8	9.70
HIPEQ1823+00	275.88	0.29	3020	131	0.099	12.00	45.5	9.77
HIPEQ1824-01	276.25	-1.47	3087	192	0.122	30.50	46.3	10.19
HIPEQ1827+09	276.99	9.67	3780	166	0.055	7.03	55.3	9.70
HIPEQ1832+06	278.05	6.42	2797	88	0.073	6.88	41.2	9.44
HIPEQ1853+09	283.49	9.86	4657	321	0.083	20.48	60.2	10.24
HIPEQ1856-03	284.00	-3.18	1708	62	0.150	19.60	19.7	9.25
HIPEQ1858+00	284.68	0.31	6278	72	0.089	7.80	81.6	10.09
HIPEQ1901+06	285.40	6.87	2914	77	0.147	11.45	34.8	9.51
HIPEQ1901-04	285.43	-4.50	1673	145	0.168	23.10	18.1	9.25
HIPEQ1910+00	287.61	0.57	1625	70	0.103	13.90	16.9	8.97
HIPEQ1912-03	288.12	-3.95	5929	230	0.045	8.60	75.9	10.07
HIPEQ1914+10	288.74	10.29	653	81	0.270	21.75	4.2	7.95
HIPEQ1929+08	292.28	8.11	3065	220	0.080	16.31	40.0	9.79
HIPEQ1932-00	293.24	0.61	1501	78	0.090	6.80	20.2	8.81
HIPEQ1935+01	293.79	1.24	10293	324	0.048	14.10	142.9	10.83
HIPEQ1937+09	294.38	9.32	3111	79	0.048	2.94	43.3	9.11
HIPEQ1938+08	294.69	8.80	3059	296	0.036	6.73	43.0	9.47
HIPEQ1938-01	294.70	-1.40	6338	98	0.045	4.50	88.2	9.92
HIPEQ1940+00	295.11	0.67	1381	88	0.048	4.00	20.8	8.61
HIPEQ1943-01	295.83	-1.16	1431	100	0.060	6.00	22.3	8.85
HIPEQ1951+01	297.95	1.49	1346	87	0.048	3.90	22.7	8.67
HIPEQ1953+08	298.48	8.17	2128	67	0.076	5.85	33.3	9.18
HIPEQ1954+05	298.72	5.90	3280	178	0.077	12.04	49.0	9.83
HIPEQ1957+05	299.35	5.87	3216	473	0.051	14.01	48.2	9.88
HIPEQ1958+02	299.70	2.60	7393	145	0.071	7.85	105.9	10.32
HIPEQ1959+04	299.84	4.53	3373	358	0.069	21.67	50.3	10.11
HIPEQ2003-03	300.90	-3.71	2375	258	0.047	10.40	36.4	9.51
HIPEQ2004+07	301.05	7.39	5829	139	0.069	9.29	83.5	10.18
HIPEQ2009-06	302.35	-6.27	1418	96	0.375	36.00	22.4	9.63
HIPEQ2011+05	302.99	5.77	5152	154	0.133	22.40	72.5	10.44
HIPEQ2012-03	303.20	-3.93	1458	155	0.046	6.40	22.0	8.86
HIPEQ2015-03	303.96	-3.12	3644	80	0.041	2.60	50.8	9.20
HIPEQ2015-02	303.97	-2.91	5745	188	0.037	9.20	79.7	10.14
HIPEQ2017+00	304.26	0.56	3836	108	0.043	6.30	53.0	9.62
HIPEQ2018-00	304.69	0.13	5705	113	0.086	24.20	78.2	10.54
HIPEQ2020-04	305.15	-4.91	1506	118	0.117	11.50	20.3	9.05
HIPEQ2021-02	305.41	-2.58	5211	66	0.047	7.10	70.5	9.92
HIPEQ2025+05	306.32	5.27	4779	124	0.060	6.22	63.3	9.77
HIPEQ2029-02	307.45	-2.14	5825	244	0.051	11.60	76.5	10.20
HIPEQ2029+07	307.46	7.90	1640	157	0.047	5.68	19.2	8.69

Continued on Next Page...

(1) Name	(2) RA (°)	(3) Dec (°)	(4) Vel (km s^{-1})	(5) W_{50} (km s^{-1})	(6) S_{peak} (Jy)	(7) S_{int} (Jy km s^{-1})	(8) Dist. (Mpc)	(9) HI mass log $M_{\odot}$
HIPEQ2030+06	307.59	6.71	10172	549	0.052	17.10	137.5	10.88
HIPEQ2030+01	307.62	1.37	3885	201	0.082	13.50	49.6	9.89
HIPEQ2030+01	307.65	1.84	3872	192	0.038	6.90	49.3	9.60
HIPEQ2030+09	307.68	9.20	4529	74	0.122	9.31	58.3	9.87
HIPEQ2032-02	308.19	-2.07	6021	109	0.064	7.50	78.5	10.04
HIPEQ2036+03	309.01	3.48	5719	317	0.057	13.08	73.6	10.22
HIPEQ2036-04	309.08	-4.64	6097	371	0.058	14.15	78.9	10.32
HIPEQ2036+02	309.20	2.94	5650	106	0.063	5.67	72.5	9.85
HIPEQ2037+08	309.43	8.70	521	42	0.048	2.30	2.5	6.54
HIPEQ2040+02	310.06	2.67	5835	303	0.045	11.68	74.6	10.19
HIPEQ2042+04	310.75	4.93	5647	173	0.055	8.37	71.8	10.01
HIPEQ2044-01	311.19	-1.70	4278	97	0.056	9.90	53.0	9.82
HIPEQ2047+07	311.91	7.20	2397	157	0.040	5.43	27.4	8.98
HIPEQ2058+04	314.73	4.54	3942	273	0.077	20.11	50.3	10.08
HIPEQ2100-01	315.02	-1.94	5996	147	0.051	6.60	78.9	9.99
HIPEQ2104+09	316.15	9.60	4838	280	0.074	14.30	64.1	10.14
HIPEQ2109-03	317.50	-3.60	8321	83	0.051	3.90	114.5	10.08
HIPEQ2109-03	317.50	-3.64	2358	77	0.061	9.20	32.1	9.35
HIPEQ2113+08	318.27	8.83	5990	120	0.059	7.15	82.7	10.06
HIPEQ2114+01	318.59	1.95	3591	69	0.043	2.88	50.2	9.23
HIPEQ2116+05	319.12	5.84	3578	51	0.059	3.33	50.6	9.30
HIPEQ2126-01	321.61	-1.81	437	109	0.032	2.90	10.3	7.86
HIPEQ2131+02	322.88	2.49	3249	75	0.133	11.08	48.7	9.79
HIPEQ2132+07	323.22	7.97	3451	65	0.046	3.15	51.3	9.29
HIPEQ2138+08	324.55	8.98	1104	109	0.113	11.76	19.2	9.01
HIPEQ2139+06	324.94	6.31	4778	154	0.055	7.45	69.1	9.92
HIPEQ2146+01	326.54	1.09	4535	117	0.052	5.90	64.5	9.76
HIPEQ2147-04	326.97	-4.16	5257	110	0.042	7.30	74.1	9.97
HIPEQ2149+00	327.28	0.40	4834	82	0.080	7.20	67.9	9.89
HIPEQ2150+02	327.74	2.68	3944	100	0.045	4.32	55.1	9.49
HIPEQ2154+02	328.64	2.96	3934	97	0.059	6.02	53.8	9.61
HIPEQ2154+06	328.68	6.47	8128	148	0.034	3.72	112.0	10.04
HIPEQ2157-01	329.29	-1.52	3593	69	0.039	2.60	48.4	9.16
HIPEQ2157+08	329.30	8.29	3444	37	0.058	2.11	46.2	9.03
HIPEQ2158+01	329.51	1.02	3199	315	0.059	13.90	42.7	9.78
HIPEQ2208+03	332.03	3.60	3961	148	0.037	5.00	50.2	9.47
HIPEQ2208+04	332.04	4.72	4023	188	0.039	6.25	51.0	9.58
HIPEQ2209+02	332.47	2.02	3790	99	0.035	3.27	47.4	9.24
HIPEQ2217+10	334.46	10.20	3593	47	0.033	1.49	43.6	8.82
HIPEQ2224-03	336.00	-3.51	2923	87	0.107	9.70	34.6	9.44
HIPEQ2225+06	336.38	6.39	8149	65	0.045	2.75	107.0	9.87
HIPEQ2229+07	337.37	7.73	2049	190	0.058	9.91	23.3	9.10
HIPEQ2234-04	338.74	-4.68	989	92	0.107	10.60	10.3	8.43

Continued on Next Page...

(1) Name	(2) RA (°)	(3) Dec (°)	(4) Vel ($km\ s^{-1}$)	(5) W_{50} ($km\ s^{-1}$)	(6) S_{peak} (Jy)	(7) S_{int} ($Jy\ km\ s^{-1}$)	(8) Dist. (Mpc)	(9) HI mass log $M_\odot$
HIPEQ2235+06	338.90	6.28	2432	123	0.043	4.80	29.9	9.00
HIPEQ2235-02	338.92	-2.70	3083	178	0.089	13.40	38.8	9.68
HIPEQ2236-02	339.13	-2.90	1791	103	0.140	14.00	21.5	9.18
HIPEQ2239-05	339.76	-5.83	2884	233	0.071	12.10	37.1	9.59
HIPEQ2239-04	339.77	-4.76	914	57	0.142	8.50	10.5	8.34
HIPEQ2241+00	340.39	0.41	1880	161	0.121	17.40	24.2	9.38
HIPEQ2244+10	341.05	10.03	7066	227	0.044	7.56	96.2	10.22
HIPEQ2245+06	341.30	6.44	1915	224	0.165	29.53	25.8	9.66
HIPEQ2245+08	341.41	8.02	7566	68	0.061	5.72	103.7	10.16
HIPEQ2250+00	342.59	0.86	1786	53	0.028	2.80	25.7	8.64
HIPEQ2250+07	342.72	7.21	3176	105	0.087	9.18	44.6	9.63
HIPEQ2251-05	342.83	-5.56	3939	112	0.052	9.80	55.3	9.85
HIPEQ2251+07	342.88	7.27	3177	103	0.079	8.20	44.8	9.59
HIPEQ2252+06	343.21	6.12	3477	180	0.062	10.04	49.3	9.76
HIPEQ2255-05	343.90	-5.53	3102	72	0.064	10.30	45.0	9.69
HIPEQ2256+03	344.04	3.96	4746	138	0.051	5.96	67.6	9.81
HIPEQ2256+05	344.07	5.40	7146	182	0.053	9.40	100.9	10.35
HIPEQ2257-00	344.37	1.00	3297	151	0.054	12.20	48.1	9.82
HIPEQ2257-02	344.43	-2.48	3104	117	0.099	11.90	45.5	9.76
HIPEQ2258-03	344.50	-3.77	3949	92	0.228	31.40	57.1	10.38
HIPEQ2259-05	344.90	-5.01	2943	71	0.054	5.20	43.7	9.37
HIPEQ2303++01	345.85	1.90	5362	80	0.050	4.00	77.4	9.75
HIPEQ2305+00	346.31	0.83	7658	145	0.069	8.70	109.5	10.39
HIPEQ2307+09	346.77	10.00	4808	283	0.044	12.35	69.9	10.15
HIPEQ2307+02	346.82	2.19	5147	129	0.051	5.86	74.7	9.89
HIPEQ2312+03	348.10	3.65	4952	64	0.051	3.23	71.9	9.59
HIPEQ2313+06	348.28	6.30	3517	164	0.057	8.59	52.1	9.74
HIPEQ2313+06	348.32	6.44	4756	479	0.086	27.04	69.0	10.48
HIPEQ2314-02	348.56	-2.71	3761	191	0.109	20.90	55.4	10.18
HIPEQ2314+00	348.57	0.13	4333	71	0.061	2.98	63.2	9.45
HIPEQ2314+04	348.68	4.53	2654	379	0.177	53.46	40.2	10.31
HIPEQ2316+05	349.00	5.20	9567	145	0.048	6.74	136.1	10.47
HIPEQ2317+06	349.50	6.60	4868	349	0.088	20.42	69.9	10.37
HIPEQ2318+06	349.73	6.87	4126	193	0.037	5.44	59.6	9.66
HIPEQ2319+10	349.92	10.17	3511	246	0.136	30.03	50.9	10.26
HIPEQ2320+08	350.05	8.03	2789	105	0.064	7.70	41.0	9.48
HIPEQ2320+02	350.20	2.51	4043	81	0.116	9.40	58.1	9.87
HIPEQ2320-04	350.21	-4.94	5791	118	0.041	5.90	82.2	9.97
HIPEQ2321+09	350.40	9.08	2831	74	0.067	5.17	41.3	9.32
HIPEQ2321+01	350.46	1.73	3013	142	0.055	6.80	43.8	9.49
HIPEQ2322+01	350.72	1.44	8633	387	0.060	23.22	121.5	10.91
HIPEQ2324-00	351.11	0.09	2679	114	0.100	11.23	38.6	9.60
HIPEQ2324+08	351.12	8.46	3637	100	0.078	6.45	51.5	9.61

Continued on Next Page...

(1) Name	(2) RA (°)	(3) Dec (°)	(4) Vel (km s^{-1})	(5) W_{50} (km s^{-1})	(6) S_{peak} (Jy)	(7) S_{int} (Jy km s^{-1})	(8) Dist. (Mpc)	(9) HI mass log $M_{\odot}$
HIPEQ2324-02	351.19	-2.02	5206	45	0.102	4.80	73.1	9.78
HIPEQ2326-04	351.66	-4.98	5832	138	0.043	6.20	81.3	9.98
HIPEQ2328+03	352.19	3.50	5053	230	0.081	15.04	69.8	10.24
HIPEQ2330+03	352.63	3.94	5522	265	0.037	7.55	75.7	10.01
HIPEQ2330-02	352.69	-2.43	10122	132	0.035	4.40	140.4	10.31
HIPEQ2331+01	352.77	1.57	1425	206	0.039	7.00	19.6	8.80
HIPEQ2331-02	352.99	-2.17	2581	120	0.054	5.90	35.0	9.23
HIPEQ2332-05	353.08	-5.63	5273	171	0.037	4.80	71.8	9.77
HIPEQ2332+09	353.23	9.78	8479	266	0.054	13.33	116.2	10.63
HIPEQ2333+04	353.32	4.39	5705	85	0.041	3.49	77.3	9.69
HIPEQ2333-02	353.35	-2.70	2418	131	0.079	10.20	32.3	9.40
HIPEQ2333-03	353.38	-3.06	5353	99	0.044	5.50	72.5	9.83
HIPEQ2334-04	353.67	-4.51	2431	87	0.102	19.90	32.1	9.68
HIPEQ2335+01	353.86	1.19	2576	83	0.130	9.53	33.8	9.41
HIPEQ2336+02	354.05	2.16	2775	172	0.131	21.74	36.2	9.83
HIPEQ2336-04	354.09	-4.88	5945	110	0.084	8.40	79.8	10.10
HIPEQ2336+00	354.18	0.33	2574	251	0.105	21.12	33.4	9.74
HIPEQ2337-05	354.30	-5.73	2395	90	0.042	3.50	30.9	8.89
HIPEQ2337+00	354.34	0.39	2658	111	0.118	9.50	34.3	9.42
HIPEQ2338-05	354.68	-5.76	2154	99	0.091	9.30	27.1	9.21
HIPEQ2338+05	354.69	5.46	5589	141	0.056	7.55	74.0	9.99
HIPEQ2338-06	354.70	-6.52	1985	319	0.250	79.75	24.8	10.06
HIPEQ2339+07	354.88	7.81	3392	57	0.045	2.77	43.6	9.09
HIPEQ2340+01	355.06	1.23	1857	187	0.059	9.62	22.6	9.06
HIPEQ2341+03	355.37	3.72	2858	153	0.124	21.80	35.8	9.82
HIPEQ2341-03	355.48	-3.57	7006	144	0.057	7.80	92.9	10.20
HIPEQ2343-01	355.97	-1.56	6782	74	0.056	4.70	89.3	9.95
HIPEQ2344-06	356.05	-6.15	2093	152	0.111	15.01	24.9	9.34
HIPEQ2346+03	356.67	3.81	2905	221	0.094	18.83	35.2	9.74
HIPEQ2347+06	356.85	6.80	3238	85	0.044	3.80	39.6	9.15
HIPEQ2348+04	357.18	4.18	2924	155	0.106	14.97	35.1	9.64
HIPEQ2351+03	357.97	3.12	5238	240	0.047	7.11	66.4	9.87
HIPEQ2353+07	358.48	7.94	5053	155	0.038	4.68	63.7	9.65
HIPEQ2354-02	358.62	-2.51	7008	225	0.034	6.20	90.9	10.08
HIPEQ2356-00	359.06	0.94	7441	189	0.064	11.30	96.8	10.40
HIPEQ2356+06	359.12	6.42	1531	45	0.063	2.85	15.6	8.21
HIPEQ2356+01	359.21	1.38	2652	157	0.062	13.00	30.8	9.46
HIPEQ2358+04	359.57	4.80	3008	108	0.046	4.10	35.6	9.09
HIPEQ2359+02	359.82	2.70	2600	146	0.047	4.55	30.1	8.99
HIPEQ2359+04	359.87	4.78	3811	318	0.061	12.52	46.6	9.81

Appendix B

The ES Sample - Optical Subsample

The Equatorial Strip - Optical Subsample

The following 201 galaxies were detected in the Equatorial Strip region discussed in Chapter 2 of this thesis. This list gives the main HI parameters for all those sources. This sources are included in the previous list of 1077 galaxies and are shown in a separate appendix for reference purposes. The columns in the table are as follows.

ES HI Parameters

(1) Name for the Equatorial Strip HIPASS galaxies

(2) Right Ascension in degrees

(3) Declination in degrees

(4) Heliocentric Velocity in km s^{-1}

(5) Total velocity width at 50% (uncorrected for inclination effects)

(6) Peak Flux in Janskys

(7) Integrated Flux in Janskys km s^{-1}

(8) Distance in Mega Parsecs (see section 2.4.1)

(9) log of the HI mass (see section 2.4.2)

(1) Name	(2) RA (°)	(3) Dec (°)	(4) Vel (km s^{-1})	(5) W_{50} (km s^{-1})	(6) S_{peak} (Jy)	(7) S_{int} (Jy km s^{-1})	(8) Dist. (Mpc)	(9) HI mass log $M_{\odot}$
HIPEQ0014-00	3.65	0.74	3914	290	0.075	17.18	50.9	10.02
HIPEQ0027-01a	6.95	-1.16	3848	223	0.039	6.60	54.2	9.66
HIPEQ0033-01	8.34	-1.12	1972	146	0.131	17.24	30.1	9.57
HIPEQ0043-00	10.88	0.11	4124	287	0.064	13.81	60.6	10.08
HIPEQ0051-00	12.99	0.47	1616	173	0.117	14.84	26.0	9.37
HIPEQ0058+00	14.71	0.63	5338	156	0.048	4.97	75.4	9.82
HIPEQ0107+01	16.94	1.07	626	59	0.063	3.81	8.7	7.83
HIPEQ0119+00	19.98	0.74	4294	70	0.030	1.02	54.8	8.86
HIPEQ0120-00	20.06	0.19	1712	129	0.039	3.88	19.6	8.55
HIPEQ0122+00	20.54	0.94	2325	266	0.159	33.23	27.5	9.77
HIPEQ0123-00	20.78	0.40	7283	60	0.049	2.95	95.6	9.80
HIPEQ0126+00a	21.64	0.55	5337	68	0.045	1.94	67.9	9.32
HIPEQ0126-00	21.72	0.66	1898	99	0.039	3.29	20.9	8.53
HIPEQ0154-00	28.73	0.09	5662	93	0.042	3.76	76.3	9.71
HIPEQ0222-00	35.68	0.64	1535	144	0.059	7.27	25.4	9.04
HIPEQ0228-01	37.08	-1.16	1605	155	0.131	16.00	25.9	9.40
HIPEQ0230+00	37.58	0.94	1523	28	0.047	1.37	24.4	8.28
HIPEQ0230-01	37.65	-1.10	1501	331	0.042	7.84	24.1	9.03
HIPEQ0231+00	37.92	0.89	6167	129	0.041	4.23	87.7	9.88
HIPEQ0236+00	39.08	0.76	6794	64	0.038	7.00	95.3	10.18
HIPEQ0238+00	39.69	0.52	1452	94	0.078	6.82	21.3	8.86
HIPEQ0240+01	40.07	1.24	1176	54	0.095	5.74	17.2	8.60
HIPEQ0241+00	40.43	0.45	992	388	0.410	119.34	14.2	9.76
HIPEQ0244+00	41.04	0.72	2771	70	0.034	2.99	37.5	9.00
HIPEQ0246-00a	41.60	0.51	1509	217	0.165	32.09	19.7	9.47
HIPEQ0246-00b	41.62	0.24	2744	309	0.155	27.59	36.4	9.93
HIPEQ0249-00a	42.31	0.40	2642	122	0.041	2.45	34.1	8.83
HIPEQ0249-00b	42.39	0.62	6493	118	0.025	2.63	87.0	9.67
HIPEQ0249-00	42.45	0.88	6953	259	0.040	7.84	93.3	10.21
HIPEQ0251-01	42.97	-1.17	1498	105	0.278	27.99	17.9	9.32
HIPEQ0300+00	45.11	0.00	2832	212	0.052	9.89	33.9	9.43
HIPEQ0301-00	45.26	0.75	2625	111	0.073	6.50	31.0	9.17
HIPEQ0306-00	46.72	0.80	3186	197	0.080	13.10	38.1	9.65
HIPEQ0316-00	49.18	0.47	6826	75	0.040	1.70	88.9	9.50
HIPEQ0320-06	50.02	-6.21	2314	227	0.092	18.64	27.5	9.52
HIPEQ0351-00	57.85	0.48	9031	117	0.036	3.74	128.7	10.16
HIPEQ0809+00	122.36	0.57	1798	151	0.045	5.29	20.8	8.73
HIPEQ0821-00	125.42	0.43	1802	72	0.156	13.74	24.4	9.29
HIPEQ0821+03b	125.43	3.37	4057	255	0.045	6.82	55.1	9.69
HIPEQ0822-01	125.59	-1.04	4460	132	0.051	5.78	60.9	9.70
HIPEQ0825-00	126.25	0.60	4914	467	0.055	12.12	67.9	10.12
HIPEQ0855+02	133.97	2.51	3779	127	0.057	5.60	54.7	9.60
HIPEQ0856+00	134.12	0.37	2493	146	0.069	9.20	37.1	9.47

Continued on Next Page...

(1) Name	(2) RA (°)	(3) Dec (°)	(4) Vel (km s^{-1})	(5) W_{50} (km s^{-1})	(6) S_{peak} (Jy)	(7) S_{int} (Jy km s^{-1})	(8) Dist. (Mpc)	(9) HI mass log $M_\odot$
HIPEQ0923-00	140.85	0.73	3471	234	0.051	9.44	42.8	9.61
HIPEQ0930+04	142.59	4.16	5244	69	0.087	5.99	66.3	9.79
HIPEQ0936+01	144.19	1.22	4875	271	0.052	11.32	61.3	10.00
HIPEQ0942+00	145.51	0.34	1880	129	0.490	59.19	21.2	9.80
HIPEQ0944-00	146.18	0.67	1220	125	0.055	6.50	12.8	8.40
HIPEQ0945+01	146.48	1.68	1853	265	0.079	16.60	21.6	9.26
HIPEQ0946+02	146.55	2.96	1927	177	0.070	13.41	22.7	9.21
HIPEQ0947+00a	146.72	0.51	1763	212	0.113	19.31	20.7	9.29
HIPEQ0947+00b	146.81	0.93	1850	113	0.077	8.05	21.9	8.96
HIPEQ0953+01	148.43	1.59	1284	330	0.213	55.14	16.2	9.53
HIPEQ0954+02a	148.56	2.29	7192	61	0.054	3.64	97.4	9.91
HIPEQ0955+04a	148.84	4.27	1813	222	0.057	11.50	23.8	9.19
HIPEQ0958+01	149.64	1.70	1805	113	0.057	5.82	24.8	8.92
HIPEQ1000+03	150.19	3.34	2053	361	0.076	23.07	28.8	9.65
HIPEQ1010+05	152.60	5.14	4067	126	0.042	5.67	58.7	9.66
HIPEQ1014+03	153.55	3.47	1217	434	0.326	115.35	20.7	10.07
HIPEQ1015+02	153.96	2.71	1273	144	0.098	12.71	21.7	9.15
HIPEQ1026+03	156.68	3.86	2141	241	0.122	22.28	33.2	9.76
HIPEQ1028+03	157.14	3.61	1147	110	0.045	4.53	19.6	8.61
HIPEQ1031+04	157.81	4.47	1173	180	0.204	33.01	19.4	9.47
HIPEQ1039+01	159.83	1.71	707	48	0.072	4.10	11.2	8.08
HIPEQ1041+00	160.47	0.79	5541	104	0.046	4.56	76.2	9.79
HIPEQ1046+01	161.56	1.82	983	233	0.256	46.78	12.7	9.25
HIPEQ1050+01	162.52	1.27	1589	120	0.030	3.94	19.6	8.55
HIPEQ1051+04a	162.91	4.59	1037	154	0.099	11.50	11.7	8.57
HIPEQ1052+00	163.22	0.05	1809	88	0.069	5.67	21.8	8.80
HIPEQ1053+02	163.31	2.57	1045	88	0.105	9.00	11.4	8.44
HIPEQ1055+02	163.90	2.42	1040	84	0.037	3.44	10.7	7.97
HIPEQ1101+03	165.31	3.64	1122	303	0.149	35.89	10.7	8.98
HIPEQ1109-00	167.36	0.08	3810	337	0.082	19.89	46.5	10.01
HIPEQ1110+01	167.73	1.14	991	71	0.075	5.34	8.4	7.95
HIPEQ1113+05	168.25	5.28	2525	83	0.053	4.02	29.2	8.91
HIPEQ1117+04a	169.35	4.58	1573	351	0.061	14.55	16.9	8.99
HIPEQ1120+02	170.05	2.55	1593	100	0.218	21.61	17.7	9.20
HIPEQ1124+03	171.12	3.30	1368	107	0.226	23.51	15.7	9.14
HIPEQ1127-00	171.77	0.98	962	83	0.096	8.94	11.1	8.41
HIPEQ1131-02	172.87	-2.29	4677	107	0.153	18.47	62.9	10.24
HIPEQ1133-03	173.44	-3.42	1604	139	0.128	15.51	21.8	9.24
HIPEQ1136+00	174.12	0.83	1099	90	0.078	6.84	15.9	8.61
HIPEQ1138+03	174.70	3.60	5492	102	0.054	5.43	76.4	9.87
HIPEQ1143-01	175.98	-1.26	1692	29	0.064	1.16	26.0	8.27
HIPEQ1145+02	176.26	2.17	1007	41	0.122	5.58	17.0	8.58
HIPEQ1148-02	177.20	-2.04	1725	223	0.168	28.49	27.4	9.70

Continued on Next Page...

(1) Name	(2) RA (°)	(3) Dec (°)	(4) Vel (km s^{-1})	(5) W_{50} (km s^{-1})	(6) S_{peak} (Jy)	(7) S_{int} (Jy km s^{-1})	(8) Dist. (Mpc)	(9) HI mass log $M_{\odot}$
HIPEQ1151-02	177.98	-2.64	3832	224	0.036	6.69	56.4	9.70
HIPEQ1152+01	178.08	1.75	6022	136	0.036	5.09	86.6	9.95
HIPEQ1152-03b	178.14	-3.68	1635	61	0.091	5.93	26.7	9.00
HIPEQ1152-02	178.20	-2.48	1054	60	0.114	7.45	18.9	8.80
HIPEQ1155+01	178.90	1.26	1879	176	0.095	14.12	30.1	9.48
HIPEQ1200-01	180.10	-1.09	1459	319	0.242	65.30	24.3	9.96
HIPEQ1200-00	180.18	0.00	1928	54	0.124	7.06	30.6	9.19
HIPEQ1202+01	180.66	2.00	1966	303	0.100	18.75	30.9	9.63
HIPEQ1204-01	181.07	-1.54	1468	96	0.103	8.83	24.0	9.08
HIPEQ1204-02	181.20	-2.72	5887	43	0.094	3.25	84.3	9.74
HIPEQ1210+02	182.74	2.03	1331	83	0.125	10.74	20.8	9.04
HIPEQ1215+04a	183.96	4.69	2179	116	0.041	3.91	30.8	8.94
HIPEQ1215-03	183.98	-3.59	5055	127	0.047	5.74	70.1	9.82
HIPEQ1217+00	184.48	0.46	933	60	0.335	21.19	13.4	8.95
HIPEQ1218-01	184.55	-1.08	5587	298	0.058	9.29	76.8	10.11
HIPEQ1219+03	184.75	3.98	1516	56	0.042	2.13	20.9	8.34
HIPEQ1220+00	185.08	0.34	890	71	0.066	4.57	12.1	8.19
HIPEQ1220+01	185.12	1.46	1588	184	0.043	6.26	21.4	8.83
HIPEQ1221+03	185.25	3.73	2553	343	0.096	15.57	34.2	9.63
HIPEQ1223-03b	185.97	-3.41	1989	372	0.051	11.12	25.7	9.24
HIPEQ1223+00	186.00	0.55	2040	84	0.096	8.00	26.4	9.12
HIPEQ1224+03b	186.17	3.31	923	51	0.197	10.73	11.1	8.49
HIPEQ1225+00	186.36	0.58	2130	99	0.044	4.40	27.1	8.88
HIPEQ1226+02	186.73	2.51	1679	187	0.087	14.27	20.6	9.15
HIPEQ1227+01	186.90	1.57	1286	63	0.493	33.32	15.1	9.25
HIPEQ1228+02	187.23	2.74	1559	168	0.087	13.52	18.4	9.03
HIPEQ1228+03	187.24	3.59	894	126	0.060	7.06	9.4	8.17
HIPEQ1229+00	187.44	0.86	2223	109	0.046	4.38	27.1	8.88
HIPEQ1230+02	187.55	2.64	1628	39	0.097	3.70	19.0	8.50
HIPEQ1230+03	187.64	3.58	5137	121	0.042	4.23	66.7	9.65
HIPEQ1232+00a	188.13	0.40	1520	157	0.302	41.47	17.0	9.45
HIPEQ1232+00b	188.18	0.13	1127	304	0.505	118.38	11.6	9.58
HIPEQ1233-02	188.39	-2.63	2462	68	0.092	6.74	29.5	9.14
HIPEQ1236+03	189.14	3.12	1432	119	0.059	6.54	14.9	8.54
HIPEQ1239-00	189.82	0.52	1070	199	1.055	159.45	9.7	9.55
HIPEQ1241+01	190.25	1.41	1695	143	0.080	9.25	18.0	8.85
HIPEQ1241-02	190.34	-3.00	1431	99	0.057	4.86	14.4	8.38
HIPEQ1242-00	190.59	0.06	1708	216	0.211	39.32	18.1	9.48
HIPEQ1242-01a	190.59	-1.36	1101	144	0.169	21.04	9.9	8.69
HIPEQ1242+03b	190.65	3.97	742	140	0.049	6.88	5.0	7.61
HIPEQ1242-01b	190.75	-1.21	3172	293	0.119	23.27	37.9	9.90
HIPEQ1243-00	190.99	0.59	2605	193	0.167	21.27	30.1	9.66
HIPEQ1244-02	191.11	-2.32	1576	108	0.114	9.89	16.2	8.79

Continued on Next Page...

(1) Name	(2) RA (°)	(3) Dec (°)	(4) Vel (km s^{-1})	(5) W$_{50}$ (km s^{-1})	(6) S_{peak} (Jy)	(7) S_{int} (Jy km s^{-1})	(8) Dist. (Mpc)	(9) HI mass log M$_{\odot}$
HIPEQ1244+00	191.15	0.47	1167	103	0.109	7.33	10.7	8.30
HIPEQ1245-00	191.32	0.47	1510	348	0.331	75.70	15.3	9.62
HIPEQ1249+03	192.28	3.39	723	156	0.425	54.57	4.9	8.49
HIPEQ1249+04	192.31	4.60	2642	74	0.097	7.28	30.8	9.21
HIPEQ1250+05	192.50	5.33	649	168	0.341	48.73	4.0	8.27
HIPEQ1253+04	193.30	4.47	718	75	0.227	18.31	5.4	8.10
HIPEQ1253+01	193.37	1.26	1138	278	0.071	13.74	11.1	8.60
HIPEQ1253+02	193.40	2.19	999	426	0.057	12.02	9.2	8.38
HIPEQ1255+00	193.78	0.16	1311	187	0.153	23.53	13.7	9.02
HIPEQ1255+02	193.82	2.87	2759	363	0.056	13.92	33.3	9.56
HIPEQ1255-00	193.92	0.27	1115	92	0.043	3.44	11.2	8.01
HIPEQ1256+03	194.05	3.87	654	189	0.112	15.19	5.1	7.97
HIPEQ1257-01	194.29	-1.70	2821	293	0.083	19.82	34.6	9.75
HIPEQ1257+02	194.49	2.68	923	102	0.049	4.85	9.1	7.98
HIPEQ1258+02	194.64	2.82	2731	132	0.069	8.90	33.7	9.38
HIPEQ1300+02a	195.00	2.05	876	51	0.056	2.73	9.0	7.72
HIPEQ1300+02b	195.16	2.51	960	99	0.196	25.63	10.3	8.81
HIPEQ1303+03	195.79	3.99	2844	112	0.078	7.44	36.5	9.37
HIPEQ1304-02	196.12	-2.90	1266	78	0.078	6.24	15.6	8.55
HIPEQ1304-03	196.13	-3.57	1358	114	0.383	41.30	16.9	9.44
HIPEQ1307-00	196.93	0.86	5324	190	0.071	13.34	71.9	10.21
HIPEQ1308-02	197.17	-2.15	5260	175	0.050	7.64	71.4	9.96
HIPEQ1311+03a	197.87	3.42	3008	160	0.055	7.53	41.3	9.48
HIPEQ1312+03	198.03	3.14	8069	116	0.040	4.63	111.6	10.13
HIPEQ1312+05	198.03	5.51	909	80	0.051	3.98	13.1	8.21
HIPEQ1313+06	198.30	6.07	6906	191	0.043	7.99	95.6	10.24
HIPEQ1317-00	199.38	1.00	1223	105	0.047	4.95	19.0	8.63
HIPEQ1318-01	199.57	-1.22	5638	102	0.060	5.30	79.5	9.90
HIPEQ1320+05	200.15	5.41	959	85	0.059	4.83	16.2	8.47
HIPEQ1326+02	201.58	2.11	1085	153	0.113	16.86	19.0	9.16
HIPEQ1329-00	202.37	0.38	3213	160	0.048	6.88	48.1	9.57
HIPEQ1332+01	203.10	1.86	3235	107	0.048	4.05	48.5	9.35
HIPEQ1335+01	203.90	1.44	5160	239	0.054	7.52	74.8	10.00
HIPEQ1341+05	205.33	5.10	6843	229	0.045	8.64	97.5	10.29
HIPEQ1348+03	207.03	3.96	1157	196	0.093	13.36	18.1	9.01
HIPEQ1352+02a	208.22	2.78	4575	280	0.069	12.90	63.2	10.08
HIPEQ1352-01	208.23	-1.09	1388	204	0.210	29.88	19.8	9.44
HIPEQ1400+02	210.25	2.02	3564	240	0.044	7.73	46.7	9.60
HIPEQ1411-01	212.91	-1.16	1539	241	0.372	64.39	16.6	9.62
HIPEQ1415+04	213.88	4.40	5673	60	0.053	3.24	72.4	9.60
HIPEQ1416+03	214.23	3.82	1466	100	0.076	7.15	14.9	8.57
HIPEQ1422-00	215.61	0.39	1626	196	0.165	28.63	16.9	9.29
HIPEQ1429-00	217.39	0.01	1532	197	0.294	49.76	16.4	9.50

Continued on Next Page...

(1) Name	(2) RA (°)	(3) Dec (°)	(4) Vel (km s^{-1})	(5) W_{50} (km s^{-1})	(6) S_{peak} (Jy)	(7) S_{int} (Jy km s^{-1})	(8) Dist. (Mpc)	(9) HI mass log $M_{\odot}$
HIPEQ1432+00	218.12	0.27	1655	194	0.037	4.62	18.6	8.58
HIPEQ1433+02	218.30	2.92	1483	87	0.055	5.18	16.5	8.52
HIPEQ1433+01	218.42	1.51	1816	66	0.055	3.38	21.1	8.55
HIPEQ1437+02	219.43	2.30	1751	293	0.109	25.25	21.3	9.43
HIPEQ1437-00	219.46	0.39	1873	151	0.048	5.79	23.0	8.86
HIPEQ1439+02	219.77	2.97	1568	95	0.073	6.07	19.2	8.72
HIPEQ1439-00	219.96	0.69	1753	183	0.192	29.40	21.9	9.52
HIPEQ1440-00	220.10	0.29	1883	172	0.305	52.59	23.9	9.85
HIPEQ1440+02	220.22	2.18	1629	121	0.030	3.35	20.6	8.52
HIPEQ1444+01a	221.11	1.71	1566	324	0.146	35.25	20.9	9.56
HIPEQ1500+01	225.02	1.90	1338	323	0.048	13.52	22.0	9.19
HIPEQ1504+02	226.12	2.35	9255	171	0.039	5.08	132.0	10.32
HIPEQ1504-00	226.12	0.85	1793	197	0.054	9.47	28.8	9.27
HIPEQ1507+01	226.81	1.53	2530	205	0.104	18.12	38.9	9.81
HIPEQ1541+00	235.50	0.70	1910	250	0.114	20.08	22.8	9.39
HIPEQ1544+02	236.22	2.50	3824	104	0.082	8.61	48.1	9.67
HIPEQ1545+00	236.35	0.80	3784	115	0.062	7.15	47.5	9.58
HIPEQ1601+01a	240.37	1.71	1916	234	0.057	9.41	21.0	8.99
HIPEQ1609-00	242.43	0.09	1491	98	0.075	6.98	16.7	8.66
HIPEQ1613-00	243.38	0.87	2086	151	0.055	7.56	25.7	9.07
HIPEQ1614-00	243.60	0.21	2018	362	0.172	38.19	25.1	9.75
HIPEQ1614+00	243.65	0.84	1972	114	0.080	8.25	24.5	9.07
HIPEQ2036-04	309.08	-4.64	6097	371	0.058	14.15	78.9	10.32
HIPEQ2314+00	348.57	0.13	4333	71	0.061	2.98	63.2	9.45
HIPEQ2324-00	351.11	0.09	2679	114	0.100	11.23	38.6	9.60
HIPEQ2335+01	353.86	1.19	2576	83	0.130	9.53	33.8	9.41
HIPEQ2336+00	354.18	0.33	2574	251	0.105	21.12	33.4	9.74
HIPEQ2337+00	354.34	0.39	2658	111	0.118	9.50	34.3	9.42
HIPEQ2340+01	355.06	1.23	1857	187	0.059	9.62	22.6	9.06

Appendix C

The ES Sample - Optical Subsample ID's

The Equatorial Strip - Optical Subsample ID's & Morphological Type

The following 201 galaxies were detected in the Equatorial Strip region discussed in Chapter 2 and 3 of this thesis. This list gives the optical ID's for these galaxies. The columns in the table are as follows.

ES Optical Parameters

(1) SDSS ID name for the ES galaxies

(2) Right Ascension

(3) Declination

(4) Other Catalogue Names

(5) HIPEQ Name

(6) Morphological Type

(7) T type

Table C.1: Galaxy Names.

		RA			DEC				Morph.	T
SDSS Name	h	m	s	°	′	″	Other Name	HIPASS Name	Type	Type
SDSSJ001431.87-004415.0	00	14	31.87	-00	44	15.0	UGC00139	HIPEQ0014-00	SAB(s)c	5
SDSSJ002749.46-011160.0	00	27	49.46	-01	11	60.0	UGC00272	HIPEQ0027-01a	SAB(s)d	7
SDSSJ003321.96-010718.8	00	33	21.96	-01	07	18.8	UGC00328	HIPEQ0033-01	SB(rs)dm	8
SDSSJ004327.77-000730.4	00	43	27.77	-00	07	30.4	NGC0237	HIPEQ0043-00	SAB(rs)cd	6
SDSSJ005159.59-002911.8	00	51	59.59	-00	29	11.8	ARK018	HIPEQ0051-00	Sb	3
SDSSJ005848.82+003512.1	00	58	48.82	+00	35	12.1	IC1607/UGC00611	HIPEQ0058+00	Sb	3
SDSSJ010746.30+010349.0	01	07	46.30	+01	03	49.0	UGC00695	HIPEQ0107+01	Scc	5
SDSSJ011958.78+004318.5	01	19	58.78	+00	43	18.5	LSBCF827-05	HIPEQ0119+00	Sdd	7
SDSSJ012006.58-001219.1	01	20	06.58	-00	12	19.1	UGC00866	HIPEQ0120-00	Sdmm	8
SDSSJ012209.10+005644.9	01	22	09.10	+00	56	44.9	NGC0493	HIPEQ0122+00	SAB(s)ccd	6
SDSSJ012313.63-002307.4	01	23	13.63	-00	23	07.4	UGC00929	HIPEQ0123-00	Scdd	6
SDSSJ012629.18+003257.5	01	26	29.18	+00	32	57.5	UGC01018	HIPEQ0126+00a	Imm	10
SDSSJ012646.39-003845.6	01	26	46.39	-00	38	45.6	UM323	HIPEQ0126-00b	BCDD	6
SDSSJ015440.92-000837.3	01	54	40.92	-00	08	37.3	UGC01382	HIPEQ0154-00	E	-5
SDSSJ022229.88-003704.1	02	22	29.88	-00	37	04.1	UGC01839	HIPEQ0222-00	Sdm	8
SDSSJ022827.74-010908.6	02	28	27.74	-01	09	08.6	NGC0941	HIPEQ0228-01	SAB(rs)c	5
SDSSJ023017.09+005619.3	02	30	17.09	+00	56	19.3	UGC01981	HIPEQ0230+00	IB(s)m	9
SDSSJ023033.12-010632.4	02	30	33.12	-01	06	32.4	NGC0955	HIPEQ0230-01	Sab	2
SDSSJ023143.25+001738.4	02	31	43.25	+00	17	38.4	UGC01998	HIPEQ0231+00	Scd	6
SDSSJ023623.52+004229.2	02	36	23.52	+00	42	29.2	UGC02091	HIPEQ0236+00	Sc	5
SDSSJ023848.50+003114.2	02	38	48.50	+00	31	14.2	APMUKSB023614+001818	HIPEQ0238+00	LSB	
SDSSJ024022.80+011349.1	02	40	22.80	+01	13	49.1	UGC02162	HIPEQ0240+01	IB(s)m	9
SDSSJ024144.78+002642.4	02	41	44.78	+00	26	42.4	NGC1055	HIPEQ0241+00	SBb	3
SDSSJ024420.93+004034.3	02	44	20.93	+00	40	34.3	UGC02216	HIPEQ0244+00	Im	10
SDSSJ024633.55-001450.6	02	46	33.55	-00	14	50.6	NGC1090	HIPEQ0246-00a	SB(rs)bc	4
SDSSJ024625.32-002956.4	02	46	25.32	-00	29	56.4	NGC1087	HIPEQ0246-00b	SAB(rs)c	5
SDSSJ024940.92-003125.0	02	49	40.92	-00	31	25.0	CGCG389-028	HIPEQ0249-00	SB(rs)b	3
SDSSJ024852.54-002101.4	02	48	52.54	-00	21	01.4	UGCA042	HIPEQ0249-00a	dI	10
SDSSJ024927.74-005225.3	02	49	27.74	-00	52	25.3	UGC02311	HIPEQ0249-00b	SB(r)b	3

Continued on Next Page...

Table C.1: – *continued*

SDSS Name	RA h	m	s	DEC °	′	″	Other Name	HIPASS Name	Morph. Type	T Type
SDSSJ025151.62-011026.8	02	51	51.62	-01	10	26.8	UGC02345	HIPEQ0251-01	SB(rs)m	9
SDSSJ030040.08+000113.1	03	00	40.08	+00	01	13.1	UGC02479	HIPEQ0300+00	Sdm	8
SDSSJ030103.14-004435.9	03	01	03.14	-00	44	35.9	UGC02482	HIPEQ0301-00	Sdm	8
SDSSJ030652.42-004741.3	03	06	52.42	-00	47	41.3	NGC1211	HIPEQ0306-00	SB(r)0/a	0
SDSSJ031631.90-002803.7	03	16	31.90	-00	28	03.7	UGC02628	HIPEQ0316-00	SB(s)bc	4
SDSSJ032009.53-061542.5	03	20	09.53	-06	15	42.5	NGC1299	HIPEQ0320-06	SB(rs)b	3
SDSSJ035140.44-003038.2	03	51	40.44	-00	30	38.2	ARK103	HIPEQ0351-00	Spiral	
SDSSJ080924.12+003634.6	08	09	24.12	+00	36	34.6	UGC04254	HIPEQ0809+00	SB(rs)m	9
SDSSJ082210.58+031604.4	08	22	10.58	+03	16	04.4	IC0503	HIPEQ0821+03b	SBa	1
SDSSJ082126.21-002510.2	08	21	26.21	-00	25	10.2	UGC04358	HIPEQ0821-00	IrS	
SDSSJ082228.66-010244.2	08	22	28.66	-01	02	44.2	UGC04370	HIPEQ0822-00	SB(rs)d	7
SDSSJ082501.90-003530.1	08	25	01.90	-00	35	30.1	NGC2590	HIPEQ0825-00	SA(s)bc	4
SDSSJ085552.25+023125.0	08	55	52.25	+02	31	25.0	UGC04673	HIPEQ0855+02	SB(s)d	7
SDSSJ085640.66+002231.4	08	56	40.66	+00	22	31.4	UGC04684	HIPEQ0856+00	SA(rs)dm	8
SDSSJ092315.60-004341.2	09	23	15.60	-00	43	41.2	UGC04996	HIPEQ0923-00	SAB(s)bc	4
SDSSJ093015.17+040838.4	09	30	15.17	+04	08	38.4	NGC2900	HIPEQ0930+04	SBcd	6
SDSSJ093626.76+011129.8	09	36	26.76	+01	11	29.8	new	HIPEQ0936+01		
SDSSJ094203.46+002012.5	09	42	03.46	+00	20	12.5	NGC2967	HIPEQ0942+00	SA(s)c	5
SDSSJ094446.32-004118.2	09	44	46.32	-00	41	18.2	new	HIPEQ0944-00b		
SDSSJ094603.48+014004.4	09	46	03.48	+01	40	04.4	UGC05228	HIPEQ0945+01	SB(s)c	5
SDSSJ094551.91+025839.4	09	45	51.91	+02	58	39.4	UGC05224	HIPEQ0946+02		8
SDSSJ094653.81+003028.4	09	46	53.81	+00	30	28.4	UGC05238	HIPEQ0947+00a	SB(s)dm	8
SDSSJ094705.30+005752.9	09	47	05.30	+00	57	52.9	UGC05242	HIPEQ0947+00b	SB(s)m	9
SDSSJ095340.78+013443.7	09	53	40.78	+01	34	43.7	NGC3044	HIPEQ0953+01	B(s)c	5
SDSSJ095359.23+020019.8	09	53	59.23	+02	00	19.8	[ISI96]0951+0214	HIPEQ0954+01a	dI	10
SDSSJ095410.58+021714.3	09	54	10.58	+02	17	14.3	CGCG035-083	HIPEQ0954+02a	...	1
SDSSJ095517.76+041613.1	09	55	17.76	+04	16	13.1	NGC3055	HIPEQ0955+04a	SAB(s)c	5
SDSSJ095829.09+014137.3	09	58	29.09	+01	41	37.3	LSBCL1-099	HIPEQ0958+01		9
SDSSJ100026.98+032228.6	10	00	26.98	+03	22	28.6	UGC05376	HIPEQ1000+03	Sdm	8

Continued on Next Page...

Table C.1: – *continued*

SDSS Name	RA h	m	s	DEC °	′	″	Other Name	HIPASS Name	Morph. Type	T Type
SDSSJ101037.22+050900.7	10	10	37.22	+05	09	00.7	CGCG036-048	HIPEQ1010+05		
SDSSJ101414.21+032802.6	10	14	14.21	+03	28	02.6	NGC3169	HIPEQ1014+03	SA(s)a	1
SDSSJ101555.25+024112.5	10	15	55.25	+02	41	12.5	UGC05539	HIPEQ1015+02	IBm	10
SDSSJ102641.71+035141.8	10	26	41.71	+03	51	41.8	NGC3246	HIPEQ1026+03	SABdm	8
SDSSJ102837.97+033336.4	10	28	37.97	+03	33	36.4	UGC05677	HIPEQ1028+03	Sdm	8
SDSSJ103113.51+042810.9	10	31	13.51	+04	28	10.9	UGC05708	HIPEQ1031+04	SBd	7
SDSSJ103925.13+014306.6	10	39	25.13	+01	43	06.6	UGC05797	HIPEQ1039+01	dIn	10
SDSSJ104153.42+004735.5	10	41	53.42	+00	47	35.5	UGC05823	HIPEQ1041+00	Im	10
SDSSJ104612.53+014850.8	10	46	12.53	+01	48	50.8	NGC3365	HIPEQ1046+01	Scd	6
SDSSJ105008.95+011555.4	10	50	08.95	+01	15	55.4	LSBCL1-134	HIPEQ1050+01	dI	10
SDSSJ105134.94+043459.5	10	51	34.94	+04	34	59.5	UGC05974	HIPEQ1051+04a	Scd	6
SDSSJ105248.70+000202.4	10	52	48.70	+00	02	02.4	CGCG010-041	HIPEQ1052+00		
SDSSJ105318.74+023734.7	10	53	18.74	+02	37	34.7	LSBCL1-137	HIPEQ1053+02	dIn	10
SDSSJ105538.95+022340.6	10	55	38.95	+02	23	40.6	CGCG038-051	HIPEQ1055+02		
SDSSJ110116.15+033741.5	11	01	16.15	+03	37	41.5	NGC3495	HIPEQ1101+03	Sd	7
SDSSJ110925.18-000548.8	11	09	25.18	-00	05	48.8	IC0673	HIPEQ1109-00	(R)SAB(rs)c	5
SDSSJ111054.58+010532.3	11	10	54.58	+01	05	32.3	CGCG011-018	HIPEQ1110+01	dIn	10
SDSSJ111312.17+051201.4	11	13	12.17	+05	12	01.4	CGCG039-073	HIPEQ1113+05		5
SDSSJ111730.14+043318.7	11	17	30.14	+04	33	18.7	NGC3604	HIPEQ1117+04a	SA(s)a	1
SDSSJ112015.41+023138.3	11	20	15.41	+02	31	38.3	UGC06345	HIPEQ1119+02	IB(s)m	9
SDSSJ112424.70+031934.0	11	24	24.70	+03	19	34.0	NGC3664	HIPEQ1124+03	SB(s)m	9
SDSSJ112712.14-005941.3	11	27	12.14	-00	59	41.3	UGC06457	HIPEQ1127-01	dIn	10
SDSSJ113131.99-021833.1	11	31	31.99	-02	18	33.1	UGC06510	HIPEQ1131-02	SAB(rs)cd	6
SDSSJ113345.17-032616.8	11	33	45.17	-03	26	16.8	CGCG012-022	HIPEQ1133-03	SAB(s)dm	8
SDSSJ113636.62+004900.1	11	36	36.62	+00	49	00.1	UGC06578	HIPEQ1136+00		-2
SDSSJ113854.82+033449.4	11	38	54.82	+03	34	49.4	MRK1302	HIPEQ1138+03	(R)SB(r)b	3
SDSSJ114345.46-011634.3	11	43	45.46	-01	16	34.3	new	HIPEQ1143-01		
SDSSJ114454.07+020949.3	11	44	54.07	+02	09	49.3	new	HIPEQ1145+02	Im	10
SDSSJ114850.33-020155.9	11	48	50.33	-02	01	55.9	UGC06780	HIPEQ1148-02	SAB(s)d	7

Continued on Next Page...

Table C.1: – *continued*

SDSS Name	RA h	m	s	DEC °	′	″	Other Name	HIPASS Name	Morph. Type	T Type
SDSSJ115156.30-023833.0	11	51	56.30	-02	38	33.0	UGC06838	HIPEQ1151-02	SAab	2
SDSSJ115243.42+014428.0	11	52	43.42	+01	44	28.0	UGC06854	HIPEQ1152+01	SB(rs)bc	4
SDSSJ115237.22-022810.2	11	52	37.22	-02	28	10.2	UGC06850	HIPEQ1152-02	BCD	6
SDSSJ115231.30-034028.2	11	52	31.30	-03	40	28.2	UGCA249	HIPEQ1152-03b	IB(s)m	9
SDSSJ115536.94+011412.5	11	55	36.94	+01	14	12.5	UGC06903	HIPEQ1155+01	SB(s)cd	6
SDSSJ120047.64-000122.8	12	00	47.64	-00	01	22.8	NGC4030b	HIPEQ1200-00	SAB(s)m	9
SDSSJ120023.33-010559.3	12	00	23.33	-01	05	59.3	NGC4030	HIPEQ1200-01	SA(s)bc	4
SDSSJ120242.34+015837.2	12	02	42.34	+01	58	37.2	NGC4045	HIPEQ1202+01	SAB(r)a	1
SDSSJ120420.35-013149.8	12	04	20.35	-01	31	49.8	UGC07053	HIPEQ1204-01	IAB(s)m	9
SDSSJ120447.16-024314.2	12	04	47.16	-02	43	14.2	UGC07065	HIPEQ1204-02	(R)SB(r)0/a	0
SDSSJ121103.74+020022.7	12	11	03.74	+02	00	22.7	UGC07178	HIPEQ1210+02	IAB(rs)m	10
SDSSJ121600.55+043902.2	12	16	00.55	+04	39	02.2	VCC0172	HIPEQ1215+04a	IAm	10
SDSSJ121608.40-033413.1	12	16	08.40	-03	34	13.1	CGCG013-114	HIPEQ1216-03	SAB(s)cd	6
SDSSJ121756.38+002600.6	12	17	56.38	+00	26	00.6	UGC07332	HIPEQ1218+00	IB(s)m	10
SDSSJ121808.69-010352.2	12	18	08.69	-01	03	52.2	NGC4202	HIPEQ1218-01	SAB(rs)bc	4
SDSSJ121909.84+035122.7	12	19	09.84	+03	51	22.7	UGC07354	HIPEQ1219+03	E	-5
SDSSJ122021.24+002204.1	12	20	21.24	+00	22	04.1	CGCG014-010	HIPEQ1220+00	Sm?	9
SDSSJ122027.50+012811.3	12	20	27.50	+01	28	11.3	UGC07394	HIPEQ1220+01	SAd	7
SDSSJ122102.33+034317.0	12	21	02.33	+03	43	17.0	NGC4289	HIPEQ1221+03	SA(s)cd	6
SDSSJ122412.53+003358.3	12	24	12.53	+00	33	58.3	DDO121	HIPEQ1223+00	IB(s)m	9
SDSSJ122353.76-032635.2	12	23	53.76	-03	26	35.2	NGC4348	HIPEQ1223-03b	SAbc	4
SDSSJ122430.53+000418.5	12	24	30.53	+00	04	18.5	KDG118	HIPEQ1224+00	Irr	10
SDSSJ122439.91+031810.1	12	24	39.91	+03	18	10.1	VCC0739	HIPEQ1224+03b	S	7
SDSSJ122542.79+003420.3	12	25	42.79	+00	34	20.3	NGC4385	HIPEQ1225+00	SB(rs)0	0
SDSSJ122658.44+022936.6	12	26	58.44	+02	29	36.6	NGC4409	HIPEQ1226+02	SB(r)bc	4
SDSSJ122745.86+013601.8	12	27	45.86	+01	36	01.8	HI1225+01	HIPEQ1227+01	dIn	10
SDSSJ122901.87+024324.6	12	29	01.87	+02	43	24.6	UGC07612	HIPEQ1228+02	Sm	9
SDSSJ122858.90+033413.4	12	28	58.90	+03	34	13.4	NGC4457	HIPEQ1228+03	(R)SAB(s)0/a	0
SDSSJ122932.66+005021.5	12	29	32.66	+00	50	21.5	UGC07625	HIPEQ1229+00	Sm	9

Continued on Next Page...

Table C.1: – *continued*

SDSS Name	RA h	m	s	DEC °	′	″	Other Name	HIPASS Name	Morph. Type	T Type
SDSSJ123013.78+023728.6	12	30	13.78	+02	37	28.6	UGC07642	HIPEQ1230+02	Sdm	8
SDSSJ123012.00+033440.8	12	30	12.00	+03	34	40.8	VCC1262	HIPEQ1230+03	BCD	6
SDSSJ123228.08+002319.3	12	32	28.08	+00	23	19.3	NGC4517A	HIPEQ1232+00a	SB(rs)dm	8
SDSSJ123244.76+000655.1	12	32	44.76	+00	06	55.1	NGC4517	HIPEQ1232+00b	SA(s)cd	6
SDSSJ123346.42-023916.9	12	33	46.42	-02	39	16.9	UGC07710	HIPEQ1233-02	IAB(s)m	9
SDSSJ123641.74+030626.3	12	36	41.74	+03	06	26.3	UGC07780	HIPEQ1236+03	Sdm	8
SDSSJ123918.14-003153.0	12	39	18.14	-00	31	53.0	NGC4592	HIPEQ1239-00	SA(s)dm	8
SDSSJ124111.45+012435.3	12	41	11.45	+01	24	35.3	UGC07841	HIPEQ1241+01	SA(r)b	3
SDSSJ124122.80-030332.0	12	41	22.80	-03	03	32.0	CGCG014-104	HIPEQ1241-02	SA0	0
SDSSJ124231.01+035727.0	12	42	31.01	+03	57	27.0	NGC4630	HIPEQ1242+03b	IB(s)m	9
SDSSJ124231.87-000454.8	12	42	31.87	-00	04	54.8	NGC4632	HIPEQ1242-00	SAc	5
SDSSJ124232.42-012102.9	12	42	32.42	-01	21	02.9	NGC4629	HIPEQ1242-01a	SAB(s)m	9
SDSSJ124257.31-011346.9	12	42	57.31	-01	13	46.9	UGC07883	HIPEQ1242-01b	SA(s)cd	6
SDSSJ124350.98-003345.4	12	43	50.98	-00	33	45.4	NGC4653	HIPEQ1243-00	SAB(rs)cd	6
SDSSJ124428.39+002757.2	12	44	28.39	+00	27	57.2	UGC07911	HIPEQ1244+00	(R)SB(s)m	9
SDSSJ124433.29-021909.8	12	44	33.29	-02	19	09.8	UGC07913	HIPEQ1244-02	SAB(s)m	9
SDSSJ124508.16-002742.8	12	45	08.16	-00	27	42.8	NGC4666	HIPEQ1245-00	SABc	5
SDSSJ124911.52+032322.6	12	49	11.52	+03	23	22.6	NGC4701	HIPEQ1249+03	SA(s)cd	6
SDSSJ124914.88+043926.3	12	49	14.88	+04	39	26.3	UGC07976	HIPEQ1249+04	Sdm	8
SDSSJ124957.72+051840.7	12	49	57.72	+05	18	40.7	NGC4713	HIPEQ1250+05	SAB(rs)d	7
SDSSJ125321.41+011606.2	12	53	21.41	+01	16	06.2	NGC4771	HIPEQ1253+01	SAd	7
SDSSJ125329.04+021006.6	12	53	29.04	+02	10	06.6	NGC4772	HIPEQ1253+02	SA(s)a	1
SDSSJ125314.47+042749.7	12	53	14.47	+04	27	49.7	NGC4765	HIPEQ1253+04	S0/a	0
SDSSJ125512.67+000659.8	12	55	12.67	+00	06	59.8	UGC08041	HIPEQ1255+00	SB(s)d	7
SDSSJ125515.50+025347.0	12	55	15.50	+02	53	47.0	NGC4799	HIPEQ1255+02	S	6
SDSSJ125539.36-001547.9	12	55	39.36	-00	15	47.9	UGC08048	HIPEQ1255-00	Sm	9
SDSSJ125604.42+034846.4	12	56	04.42	+03	48	46.4	UGC08055	HIPEQ1256+03	ImV	8
SDSSJ125744.35+024128.3	12	57	44.35	+02	41	28.3	UGC08074	HIPEQ1257+02	Sm	9
SDSSJ125712.14-014224.5	12	57	12.14	-01	42	24.5	UGC08067	HIPEQ1257-01	Sb	3

Continued on Next Page...

Table C.1: – *continued*

SDSS Name	RA h	m	s	DEC °	′	″	Other Name	HIPASS Name	Morph. Type	T Type
SDSSJ125822.30+024733.4	12	58	22.30	+02	47	33.4	UGC08084	HIPEQ1258+02	SB(s)dm	8
SDSSJ125958.03+020259.3	12	59	58.03	+02	02	59.3	UGC08105	HIPEQ1300+02a	dIn	9
SDSSJ130036.55+023002.2	13	00	36.55	+02	30	02.2	NGC4900	HIPEQ1300+02b	SB(rs)c	5
SDSSJ130305.74+035929.0	13	03	05.74	+03	59	29.0	UGC08153	HIPEQ1303+03	Sd	7
SDSSJ130431.87-025917.5	13	04	31.87	-02	59	17.5	LCRSB130157.2-024313	HIPEQ1304-02		
SDSSJ130431.82-033425.3	13	04	31.82	-03	34	25.3	UGCA322	HIPEQ1304-03	SAB(s)dm	8
SDSSJ130738.66-005632.6	13	07	38.66	-00	56	32.6	IC0849	HIPEQ1307-00	SAB(rs)cd	6
SDSSJ130843.06-020806.0	13	08	43.06	-02	08	06.0	UGC08223	HIPEQ1308-02	SBcd	6
SDSSJ131123.21+032441.8	13	11	23.21	+03	24	41.8	UGC08263	HIPEQ1311+03a	SBc	5
SDSSJ131207.15+031156.4	13	12	07.15	+03	11	56.4	NGC5013	HIPEQ1312+03	Sb	3
SDSSJ131205.95+052836.5	13	12	05.95	+05	28	36.5	UGC08276	HIPEQ1312+05	Im	10
SDSSJ131320.83+060341.4	13	13	20.83	+06	03	41.4	NGC5027	HIPEQ1313+06	SB(r)b	3
SDSSJ131742.65-010005.4	13	17	42.65	-01	00	05.4	UM559	HIPEQ1317-00		
SDSSJ131810.03-011438.0	13	18	10.03	-01	14	38.0	UGC08360	HIPEQ1318-01	SAB(r)cd	6
SDSSJ132032.18+052422.7	13	20	32.18	+05	24	22.7	UGC08382	HIPEQ1320+05	IBm	10
SDSSJ132811.81+021643.7	13	28	11.81	+02	16	43.7	LEDA135827	HIPEQ1327+02	dIn	9
SDSSJ132925.42-002355.0	13	29	25.42	-00	23	55.0	UGC08473	HIPEQ1329-00	Im	10
SDSSJ133230.72+015051.0	13	32	30.72	+01	50	51.0	UGC08521	HIPEQ1332+01	(R)SB(r)ab	2
SDSSJ133524.50+012437.4	13	35	24.50	+01	24	37.4	NGC5227	HIPEQ1335+01	(R)SB(r)b	3
SDSSJ134105.11+050619.8	13	41	05.11	+05	06	19.8	UGC08657	HIPEQ1341+05	Sbc	4
SDSSJ134816.08+035702.5	13	48	16.08	+03	57	02.5	NGC5300	HIPEQ1348+03	SAB(r)c	5
SDSSJ135256.54+024902.3	13	52	56.54	+02	49	02.3	NGC5335	HIPEQ1352+02a	SB(r)b	3
SDSSJ135254.50-010653.3	13	52	54.50	-01	06	53.3	NGC5334	HIPEQ1352-01	SB(rs)c	5
SDSSJ140045.77+020117.0	14	00	45.77	+02	01	17.0	UGC08924	HIPEQ1400+02	Sc	5
SDSSJ141137.73-010929.9	14	11	37.73	-01	09	29.9	NGC5496	HIPEQ1411-01	SBcd	6
SDSSJ141526.33+042429.9	14	15	26.33	+04	24	29.9	NGC5521	HIPEQ1415+04	S	5
SDSSJ141657.05+035003.1	14	16	57.05	+03	50	03.1	KKR05	HIPEQ1416+03	Im	10
SDSSJ142223.59-002318.2	14	22	23.59	-00	23	18.2	NGC5584	HIPEQ1422-00	SAB(rs)cd	6
SDSSJ142934.68-000106.2	14	29	34.68	-00	01	06.2	UGC09299	HIPEQ1429-00	SAB(s)d	7

Continued on Next Page...

Table C.1: – *continued*

SDSS Name	RA h	m	s	DEC °	′	″	Other Name	HIPASS Name	Morph. Type	T Type
SDSSJ143228.32+001739.5	14	32	28.32	+00	17	39.5	UGC09348	HIPEQ1432+00	S0	-2
SDSSJ143353.30+012905.6	14	33	53.30	+01	29	05.6	[ISI96]1431+0142	HIPEQ1433+01	dI	10
SDSSJ143245.22+025452.6	14	32	45.22	+02	54	52.6	CGCG047-085	HIPEQ1433+02	SB	5
SDSSJ143741.16+021728.0	14	37	41.16	+02	17	28.0	NGC5690	HIPEQ1437+02	Sc	5
SDSSJ143753.52-002355.7	14	37	53.52	-00	23	55.7	NGC5691	HIPEQ1437-00	SAB(s)a	1
SDSSJ143904.27+025657.5	14	39	04.27	+02	56	57.5	UGC09432	HIPEQ1439+02	Im	9
SDSSJ143949.46-004309.5	14	39	49.46	-00	43	09.5	NGC5705	HIPEQ1439-00	SB(rs)d	7
SDSSJ144058.25+021112.1	14	40	58.25	+02	11	12.1	NGC5725	HIPEQ1440+02	SB(s)d	7
SDSSJ144056.14-001905.9	14	40	56.14	-00	19	05.9	NGC5719	HIPEQ1440-00	SAB(s)ab	2
SDSSJ144424.50+014048.0	14	44	24.50	+01	40	48.0	NGC5740	HIPEQ1444+01a	SAB(rs)b	3
SDSSJ150000.26+015329.0	15	00	00.26	+01	53	29.0	NGC5806	HIPEQ1500+01	SAB(s)b	3
SDSSJ150429.71+021959.5	15	04	29.71	+02	19	59.5	CGCG048-099	HIPEQ1504+02		
SDSSJ150430.10-005105.4	15	04	30.10	-00	51	05.4	UGC09682	HIPEQ1504-00	SB(s)m	9
SDSSJ150707.68+013240.2	15	07	07.68	+01	32	40.2	NGC5850	HIPEQ1507+01	SB(r)b	3
SDSSJ154159.81+004246.1	15	41	59.81	+00	42	46.1	UGC09977	HIPEQ1542+00	Sc	5
SDSSJ154500.26+022803.7	15	45	00.26	+02	28	03.7	CGCG050-091	HIPEQ1544+02		
SDSSJ154514.35+004619.6	15	45	14.35	+00	46	19.6	UGC10005	HIPEQ1545+00	SA(s)d	7
SDSSJ160134.06+014228.1	16	01	34.06	+01	42	28.1	IC1158	HIPEQ1601+01a	SAB(r)c	5
SDSSJ160943.90-000651.8	16	09	43.90	-00	06	51.8	UGC10229	HIPEQ1609-00	Im	10
SDSSJ161329.16-005301.3	16	13	29.16	-00	53	01.3	VV370	HIPEQ1613-00	Sm	9
SDSSJ161433.00+004920.3	16	14	33.00	+00	49	20.3	UGC10290	HIPEQ1614+00	SB(s)m	9
SDSSJ161424.84-001229.9	16	14	24.84	-00	12	29.9	UGC10288	HIPEQ1614-00	Sc	5
SDSSJ203623.33-043709.5	20	36	23.33	-04	37	09.5	NGC6941	HIPEQ2036-04	SAB(rs)b	3
SDSSJ231432.98+001407.4	23	14	32.98	+00	14	07.4	UGC12446	HIPEQ2314+00	Sa	1
SDSSJ232423.47-000625.6	23	24	23.47	-00	06	25.6	UGC12578	HIPEQ2324-00	SB(s)m	9
SDSSJ233539.86+011150.6	23	35	39.86	+01	11	50.6	UGC12690	HIPEQ2335+01	SB(s)m	9
SDSSJ233631.49+001749.9	23	36	31.49	+00	17	49.9	NGC7716	HIPEQ2336+00	SAB(r)b	3
SDSSJ233723.83+002331.2	23	37	23.83	+00	23	31.2	UGC12709	HIPEQ2337+00	SAB(s)m	9
SDSSJ234020.78+011443.8	23	40	20.78	+01	14	43.8	UGC127	HIPEQ2340+01	S0/a	0

Appendix D

The ES Sample - Optical Images and HI Spectra

The Equatorial Strip - Optical Images and HI Spectra

I present optical images and HI spectra for the 201 galaxies were detected in the Equatorial Strip region discussed in Chapter 2, 3 & 4 of this thesis. The optical images are 3 band (u,g,r) colour images from the SDSS sample. The HI spectra has been obtained from the HI data cubes for the ES sample.

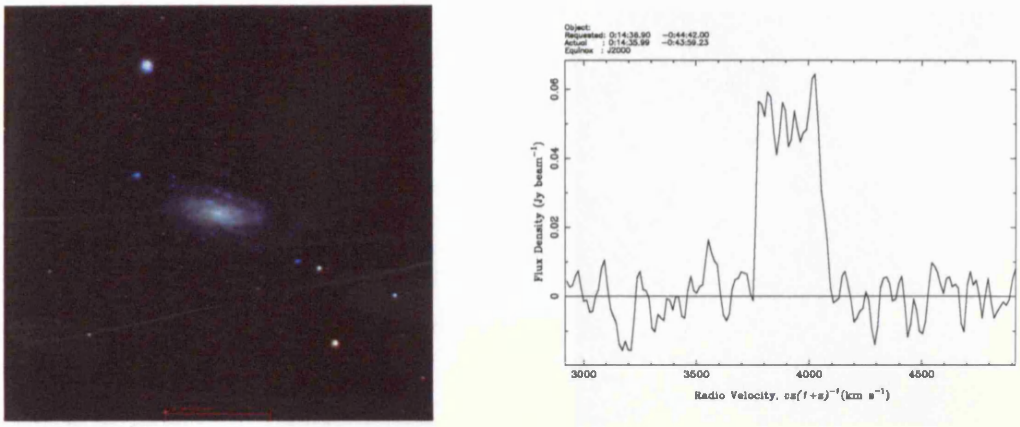

HIPEQ0014-00

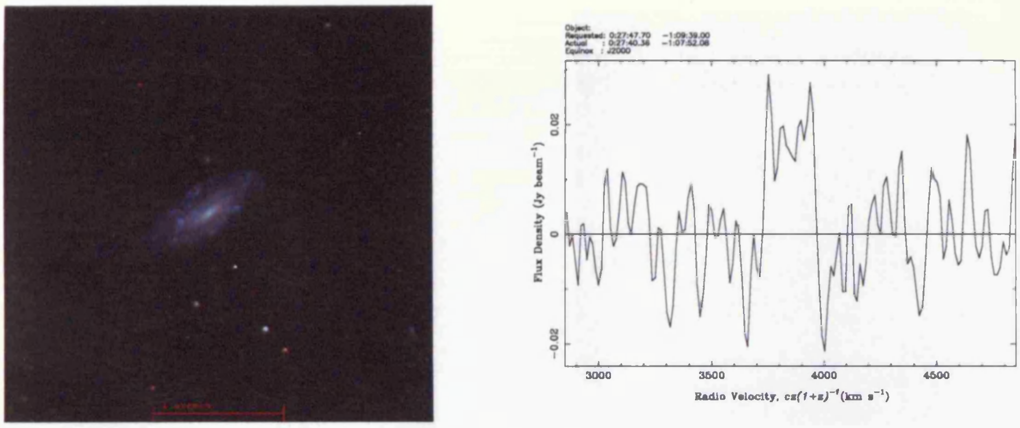

HIPEQ0027-01

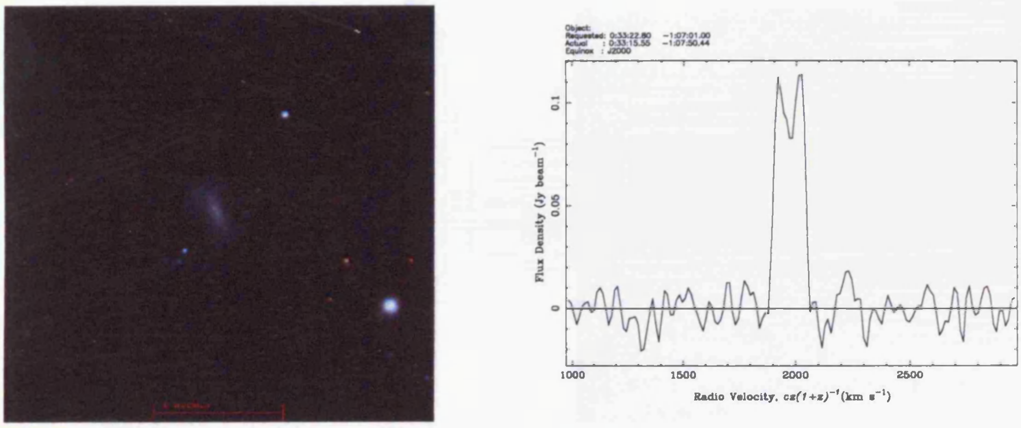

HIPEQ0033-01

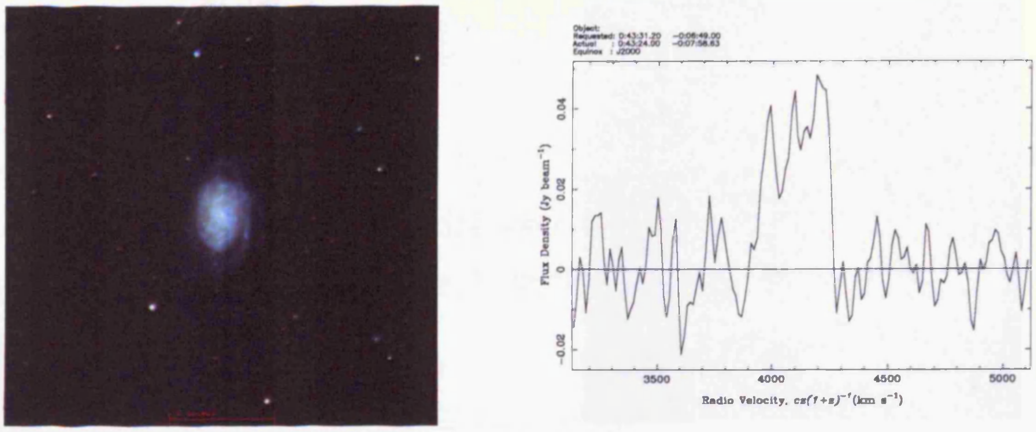

HIPEQ0043-00

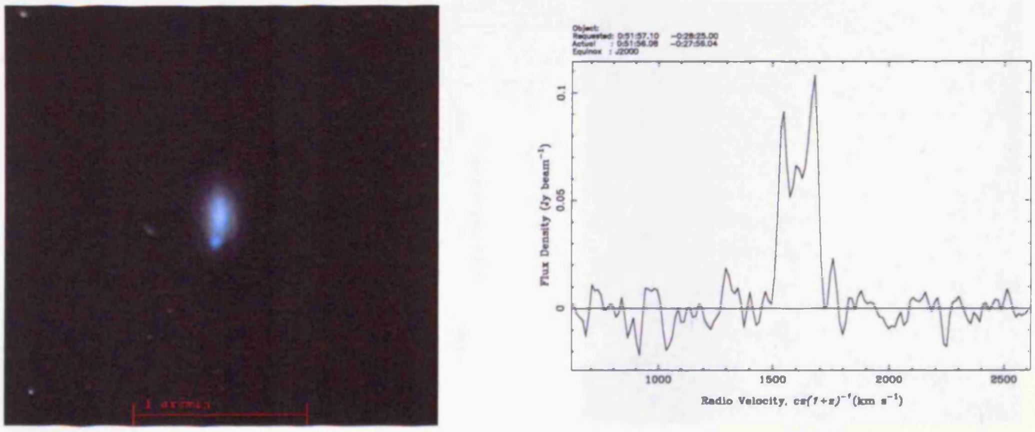

HIPEQ0051-00

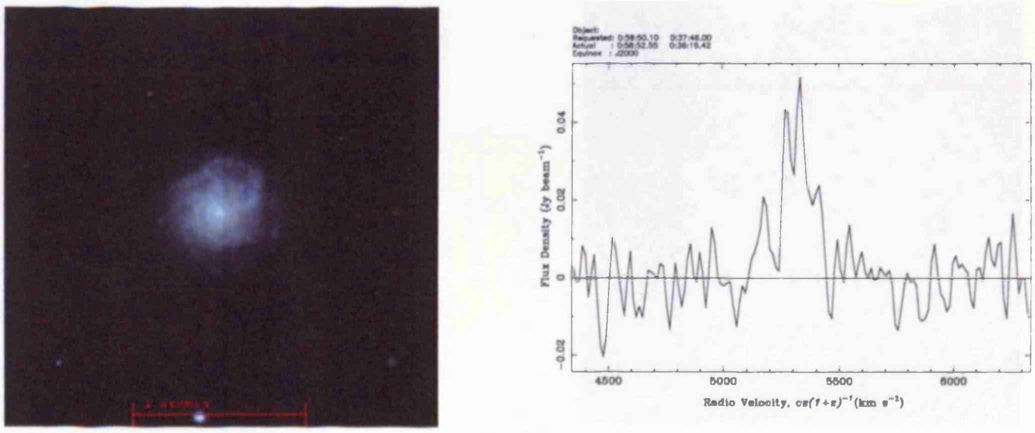

HIPEQ0058+00

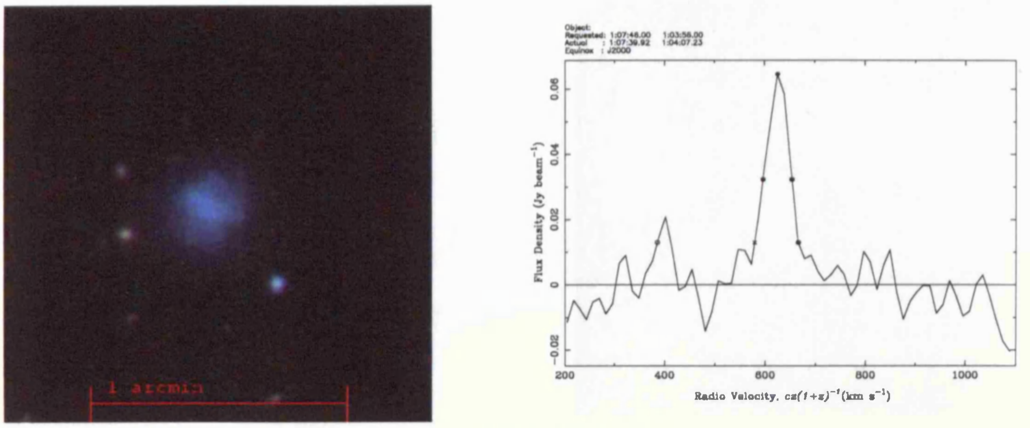

HIPEQ0107+01

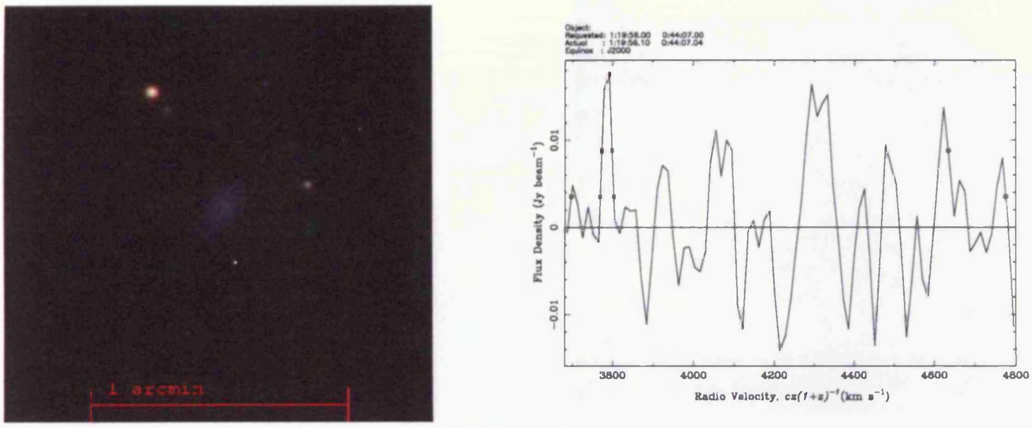

HIPEQ0119+00

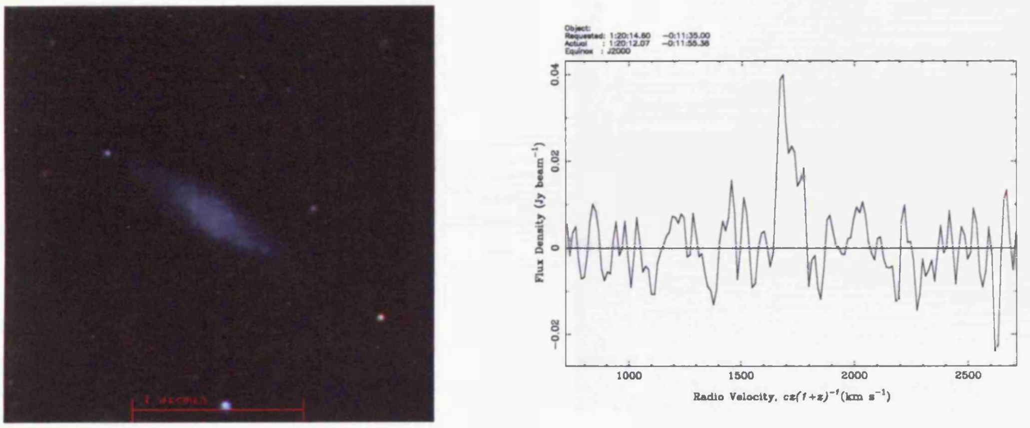

HIPEQ0120-00

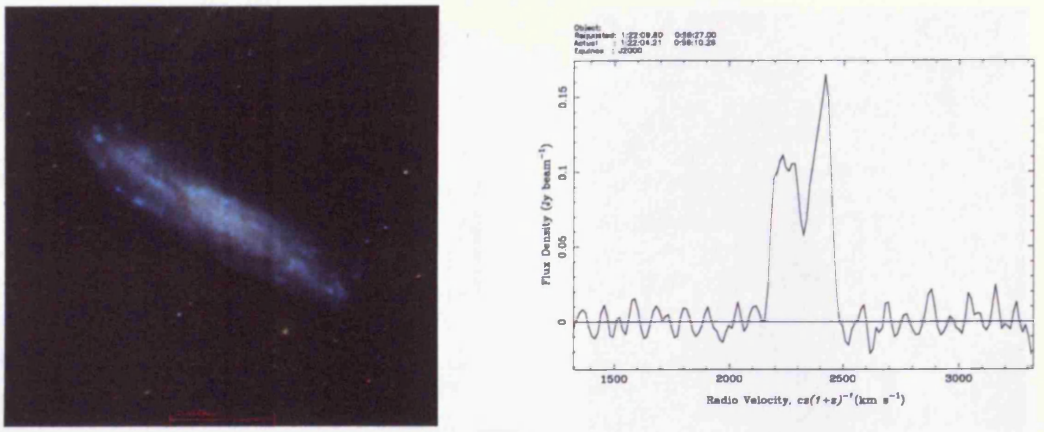

HIPEQ0122+00

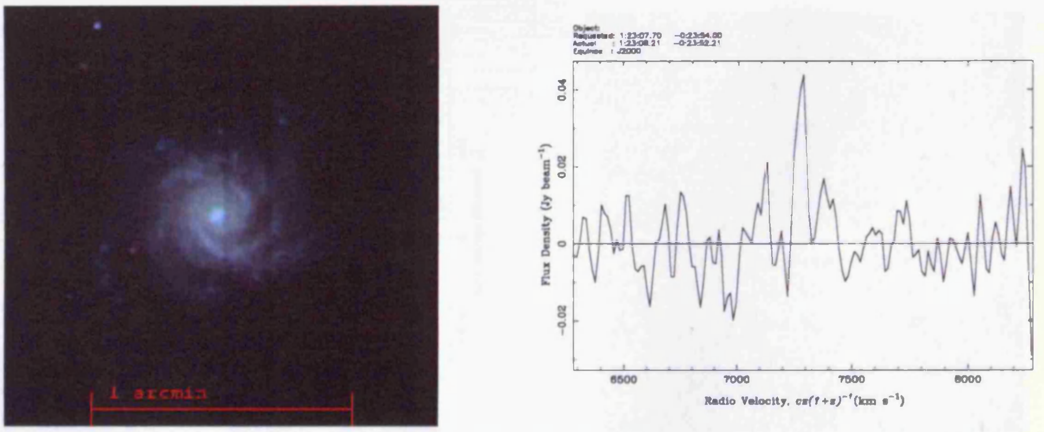

HIPEQ0123-00

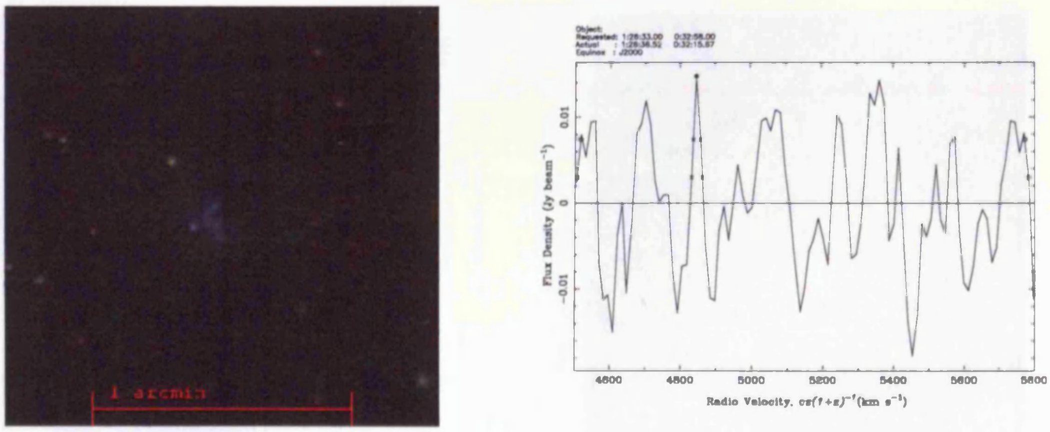

HIPEQ0126+00

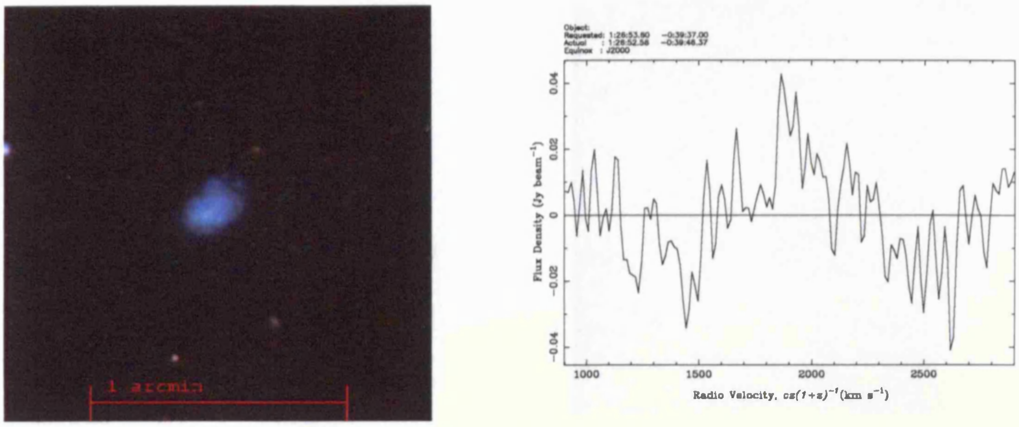

HIPEQ0126-00

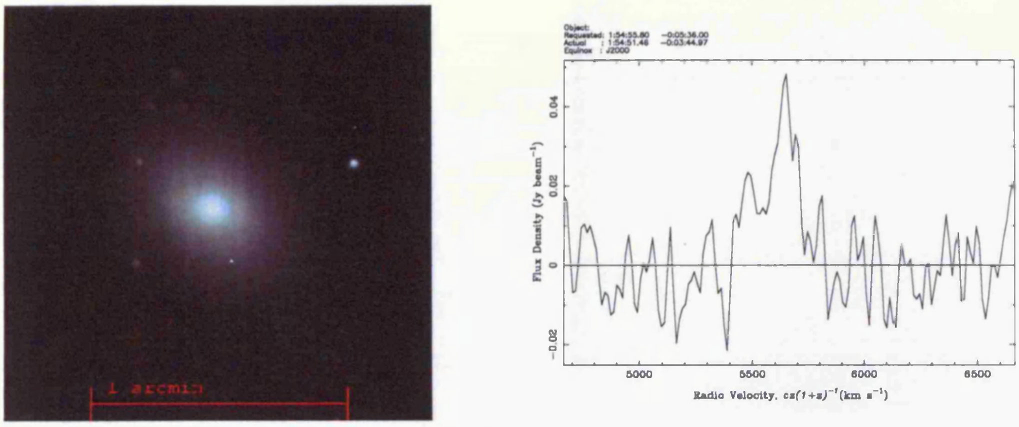

HIPEQ0154-00

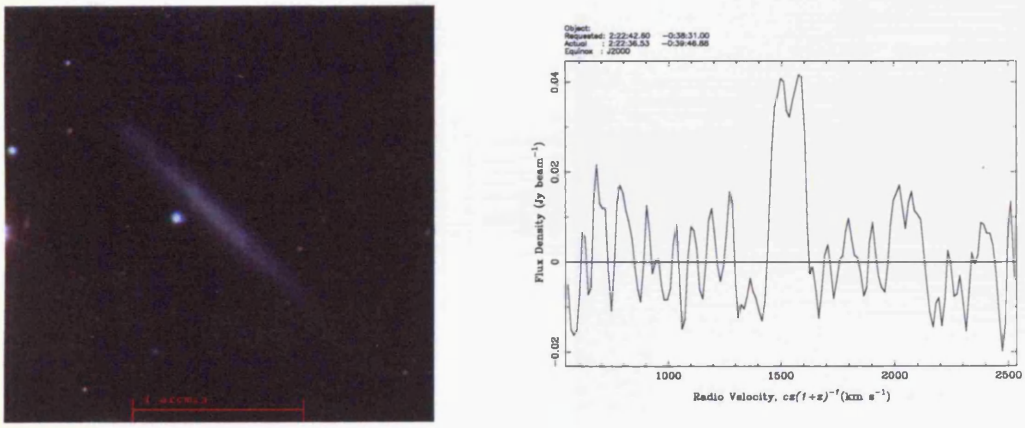

HIPEQ0222-00

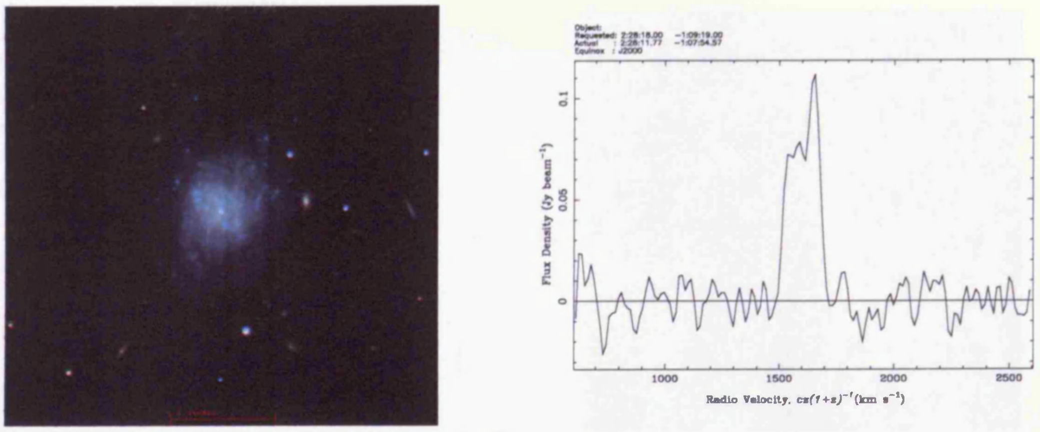

HIPEQ0228-01

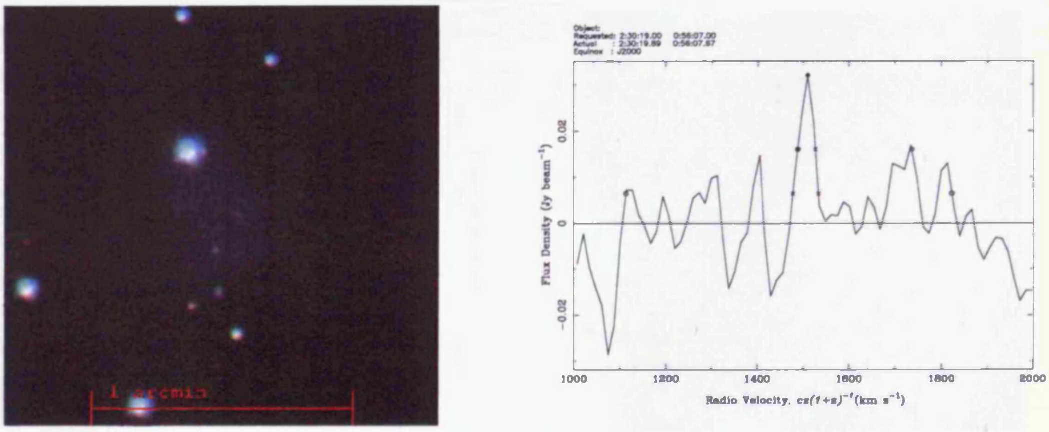

HIPEQ0230+00

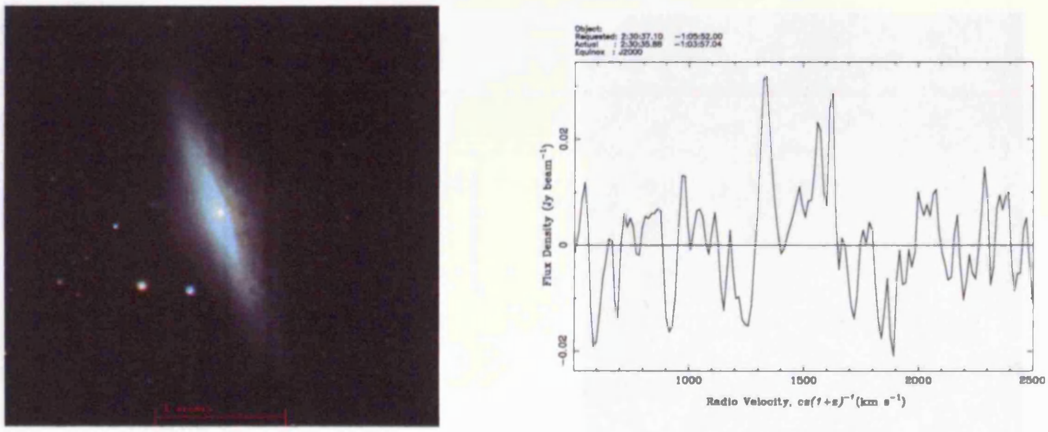

HIPEQ0230-01

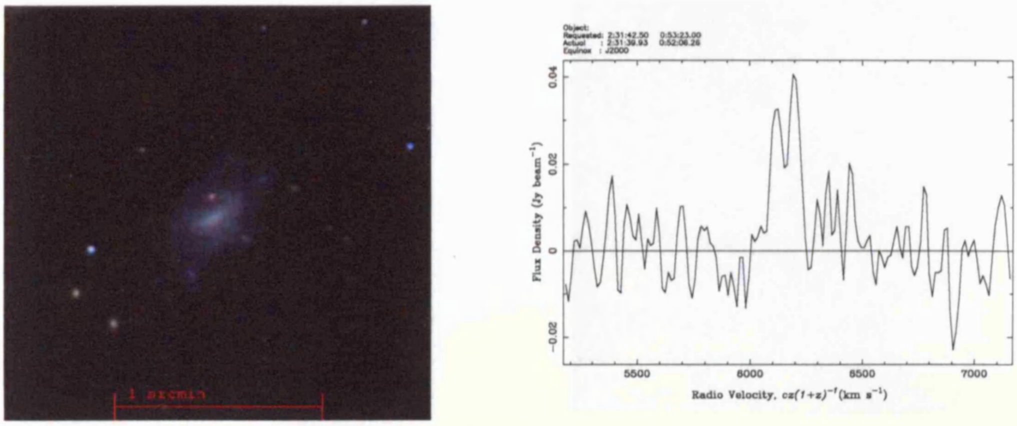

HIPEQ0231+00

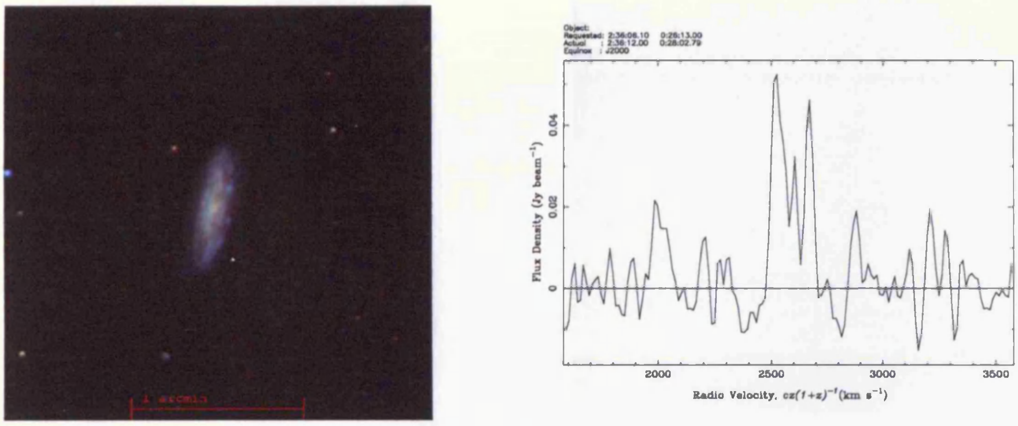

HIPEQ0236+00

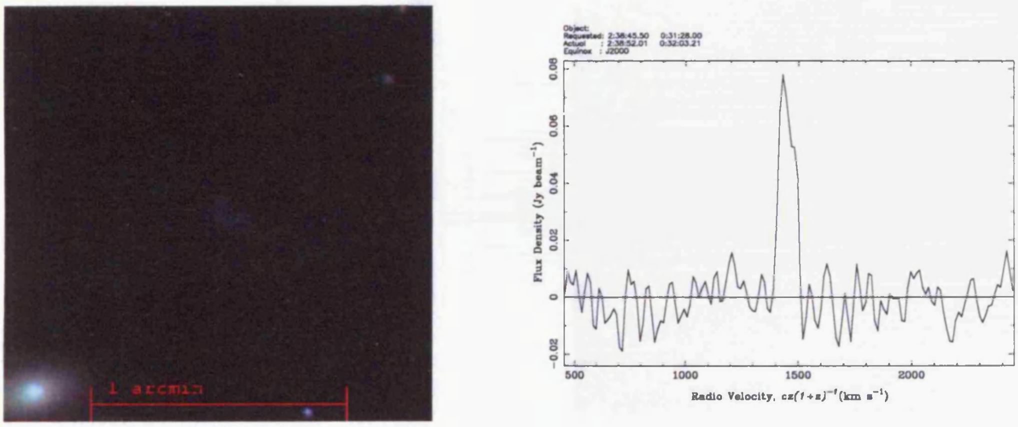

HIPEQ0238+00

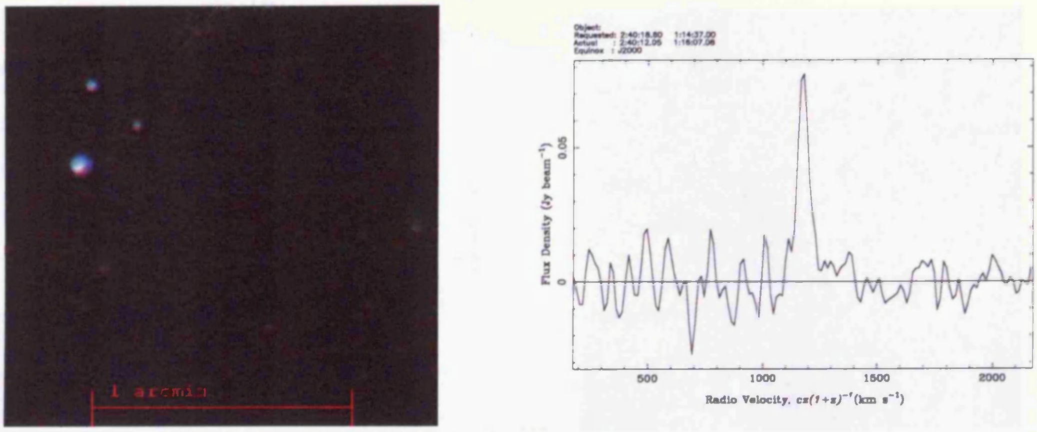

HIPEQ0240+01

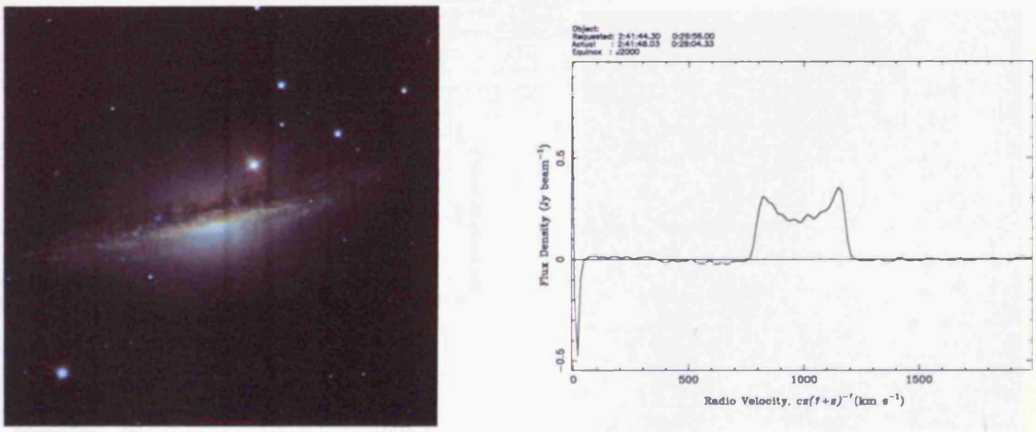

HIPEQ0241+00

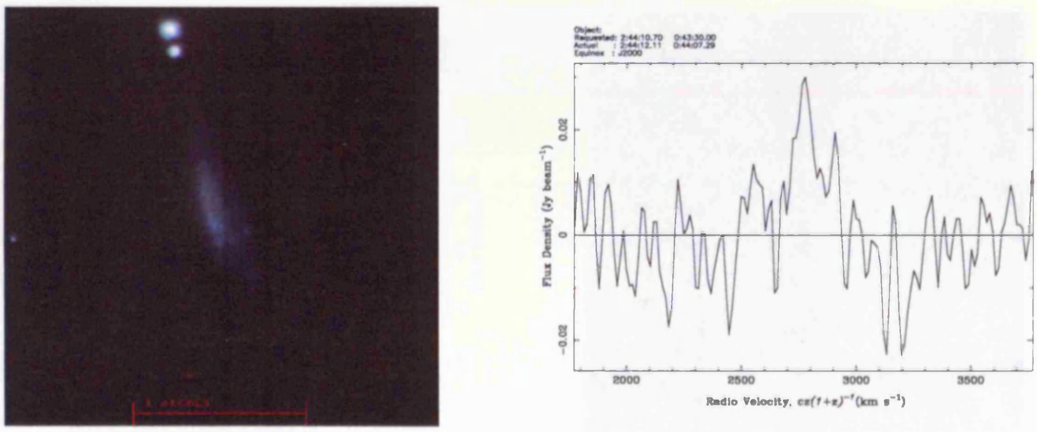

HIPEQ0244+00

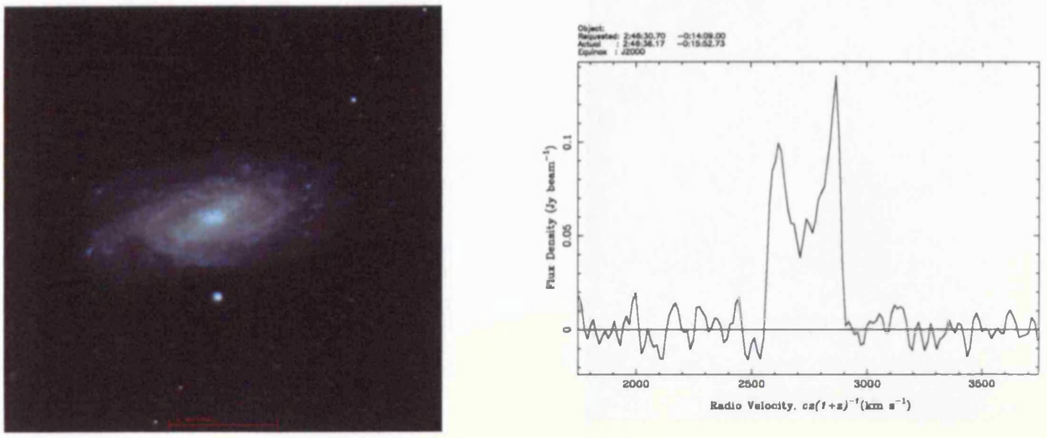

HIPEQ0246-00

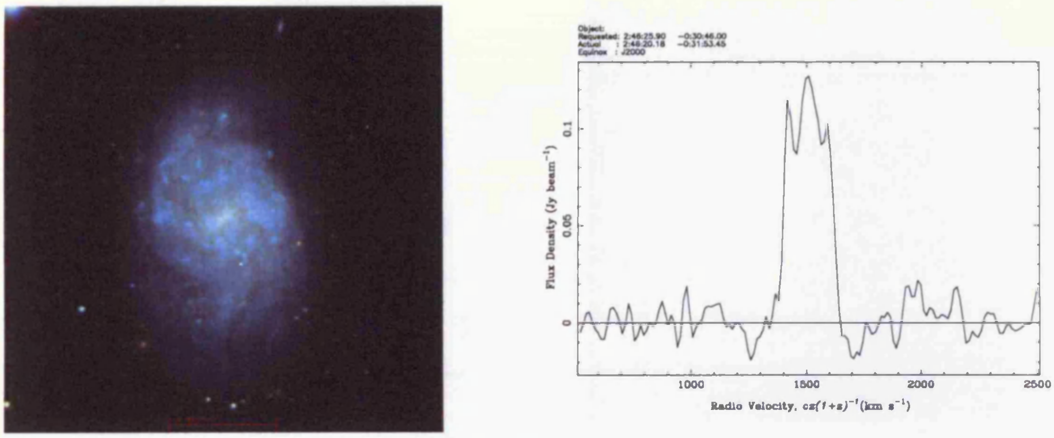

HIPEQ0246-00

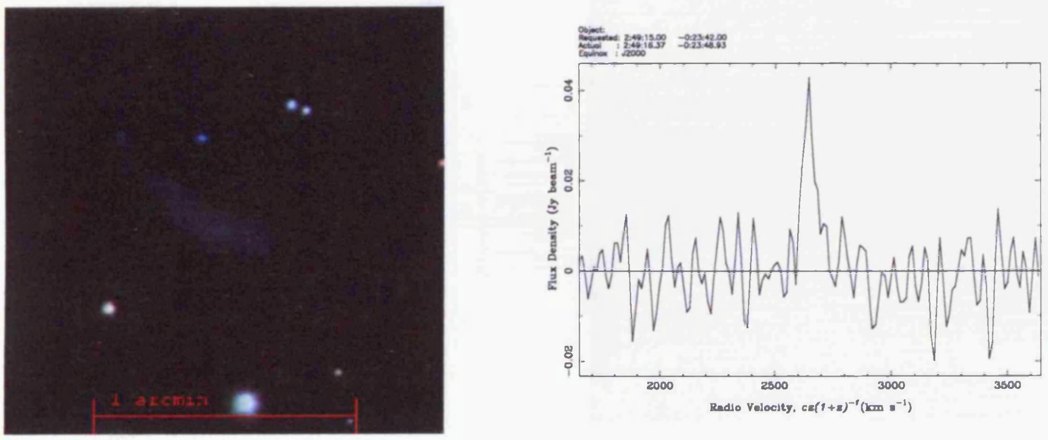

HIPEQ0249-00

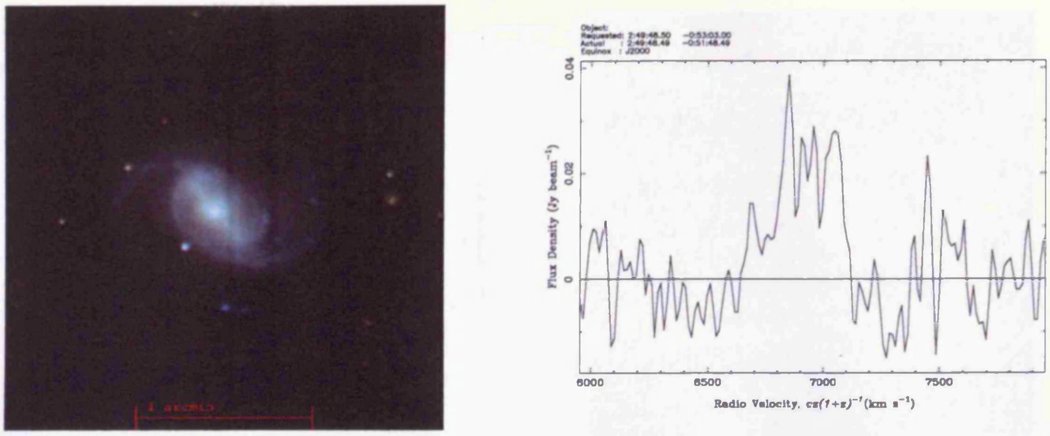

HIPEQ0249-00

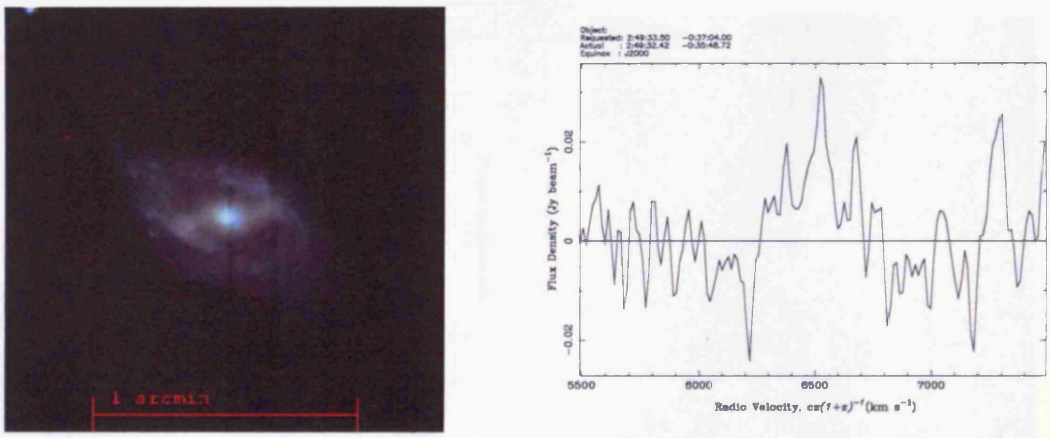

HIPEQ0249-00

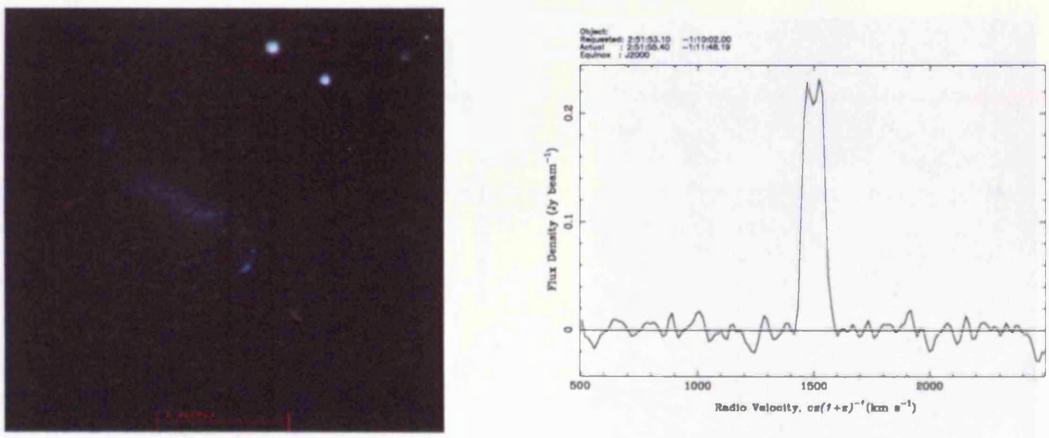

HIPEQ0251-01

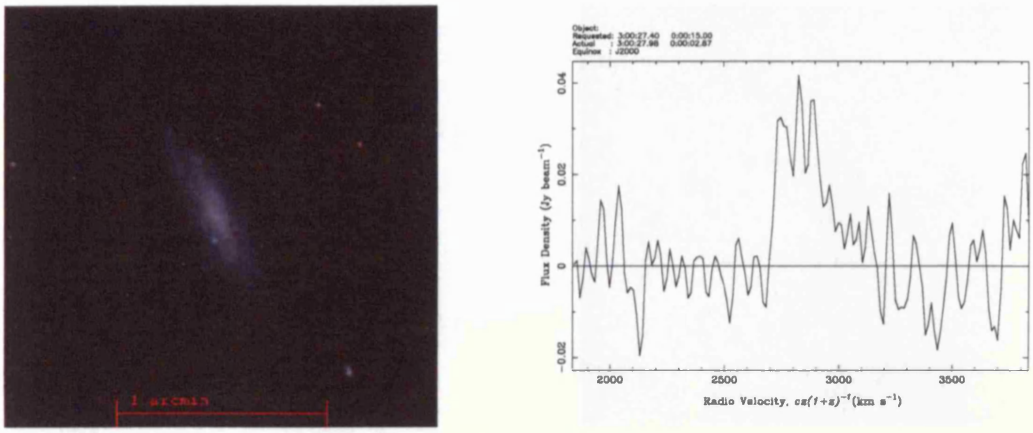

HIPEQ0300+00

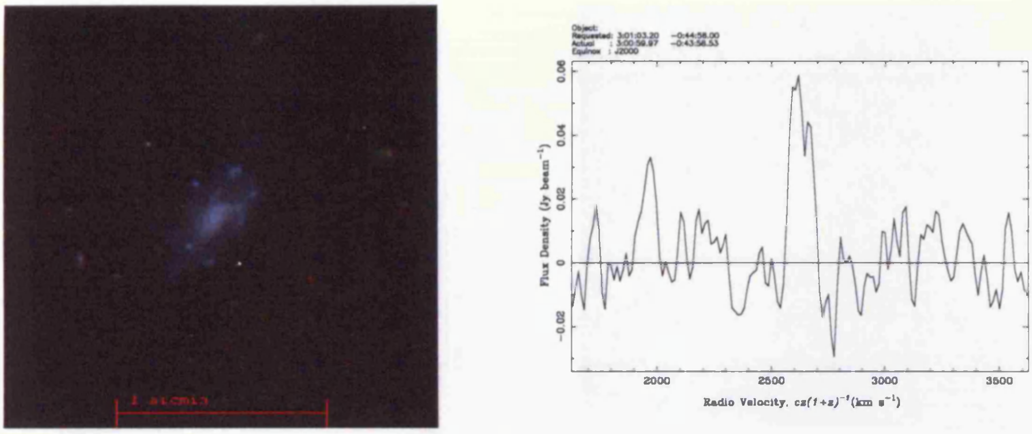

HIPEQ0301-00

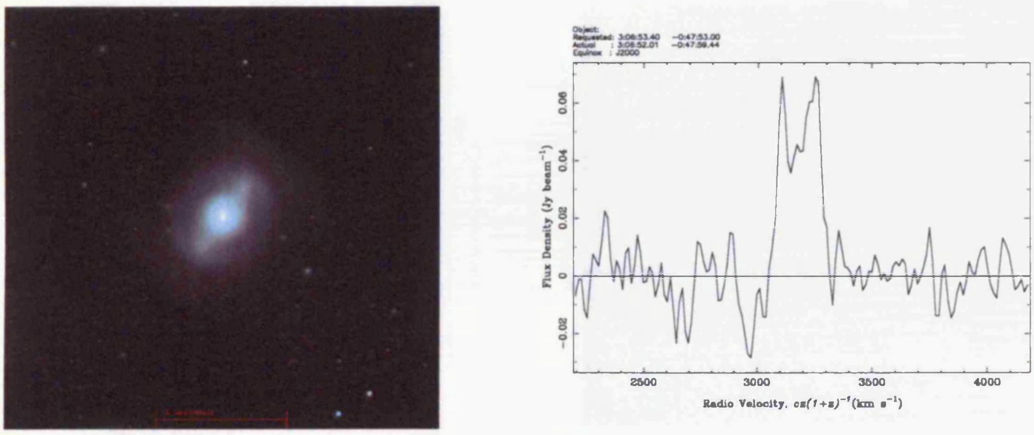

HIPEQ0306-00

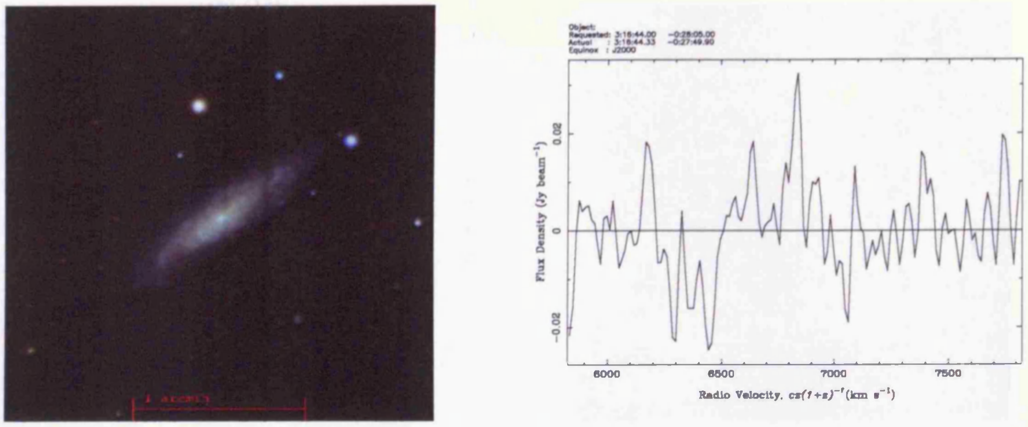

HIPEQ0316-00

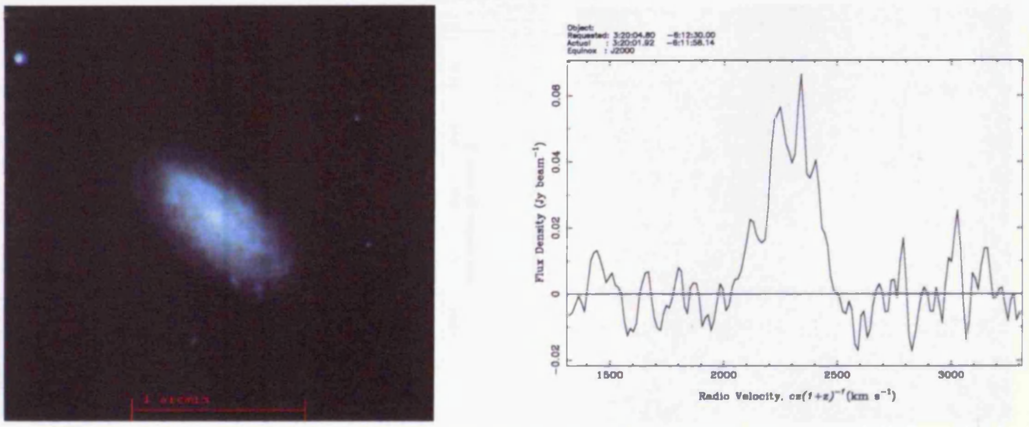

HIPEQ0320-06

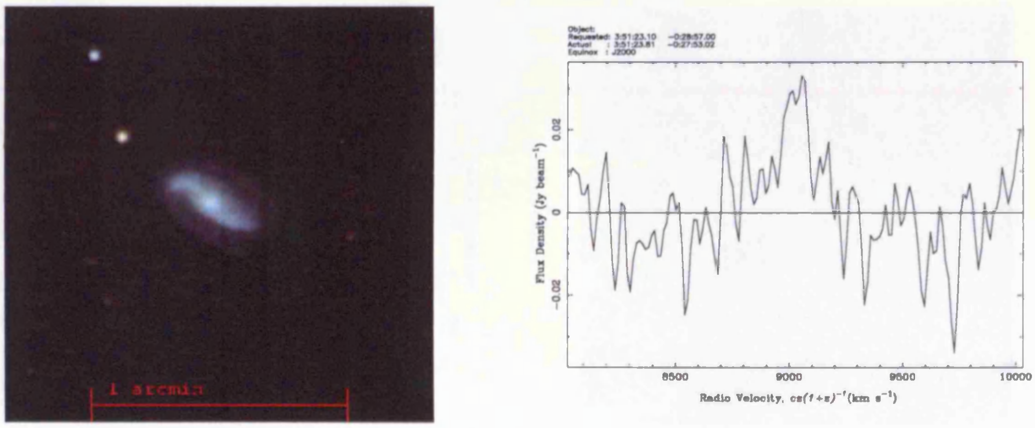

HIPEQ0351-00

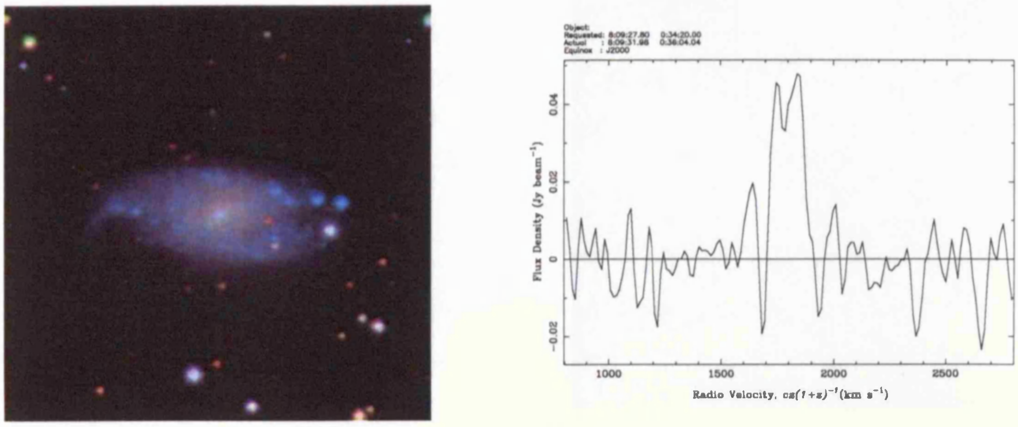

HIPEQ0809+00

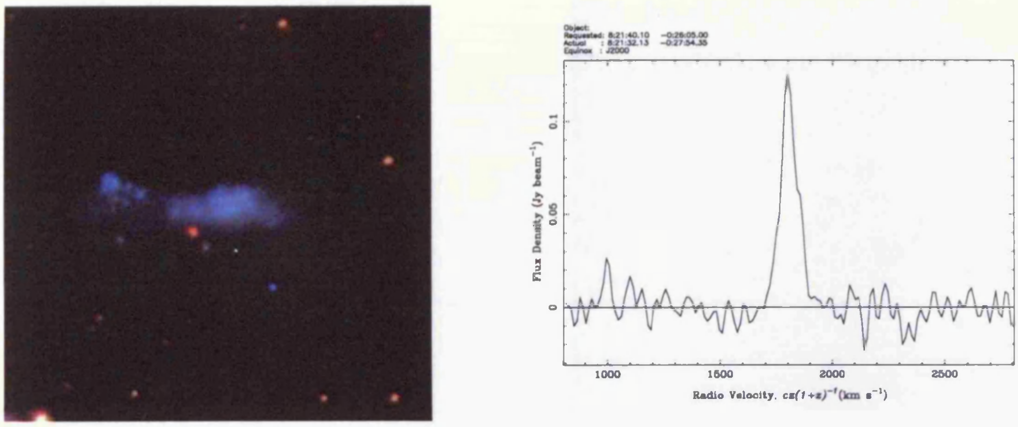

HIPEQ0821-00

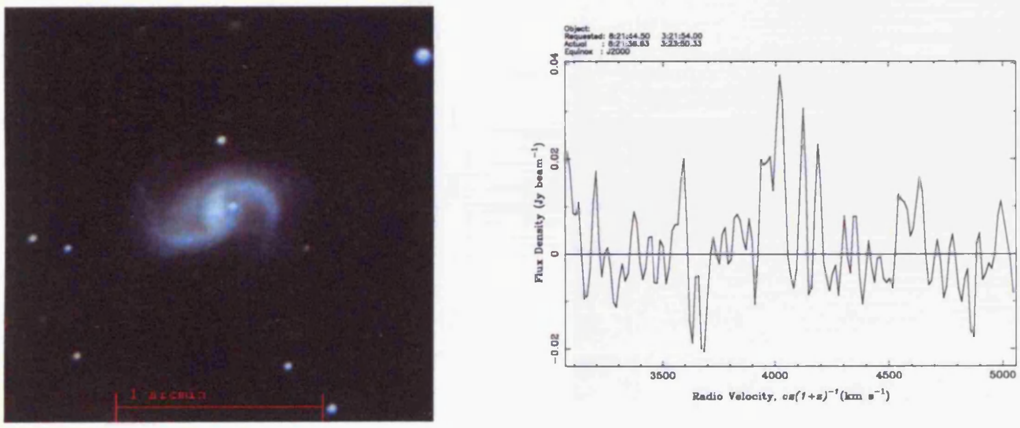

HIPEQ0821+03

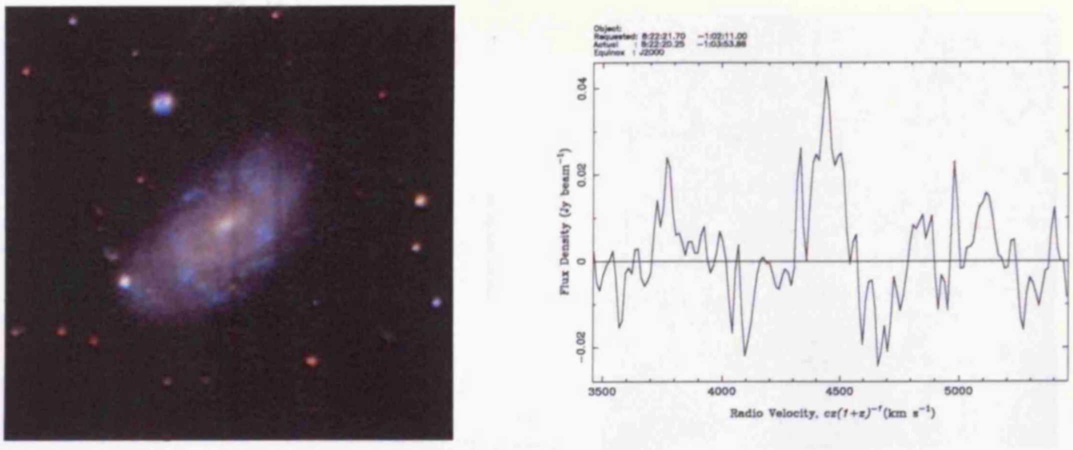

HIPEQ0822-00

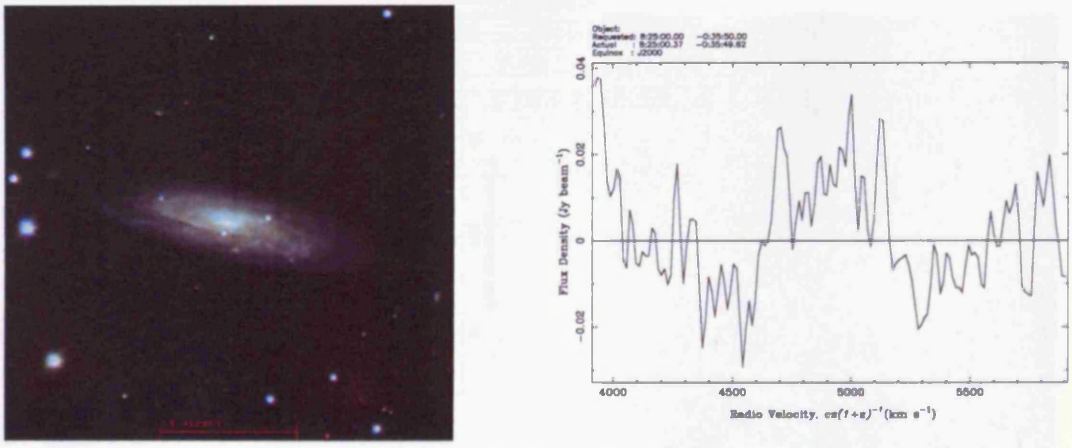

HIPEQ0825-00

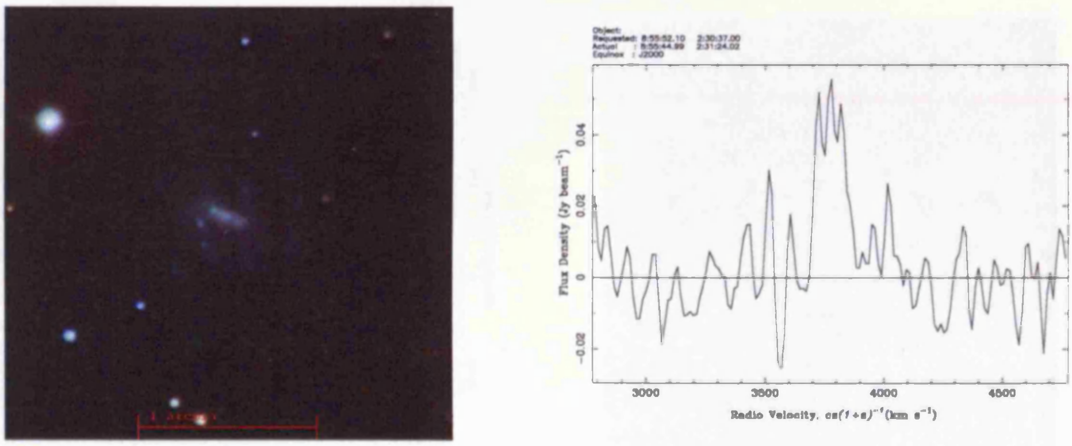

HIPEQ0855+02

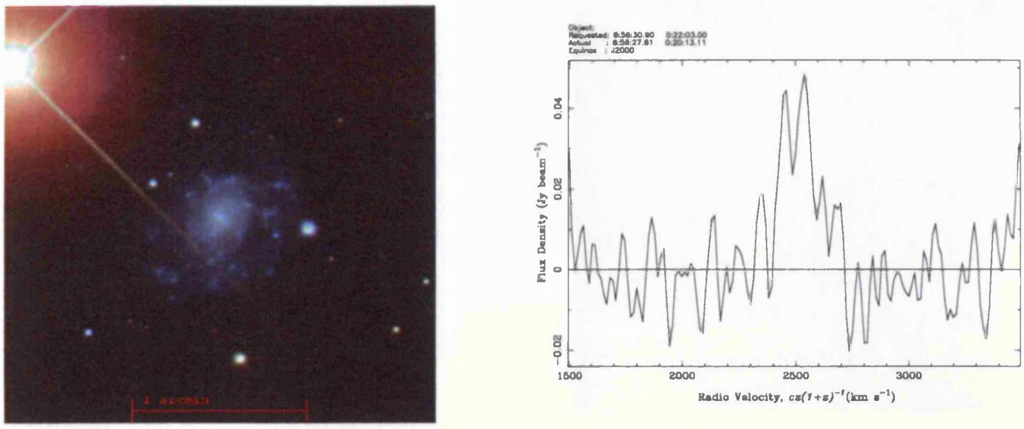

HIPEQ0856+00

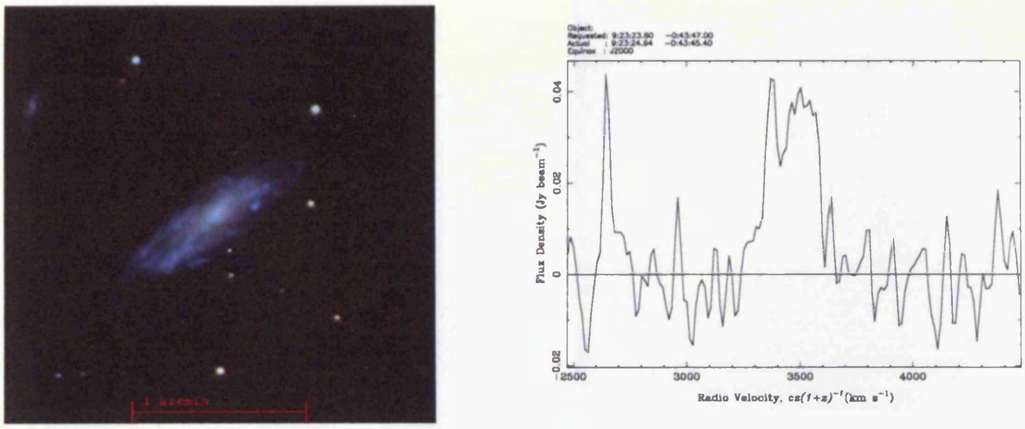

HIPEQ0923-00

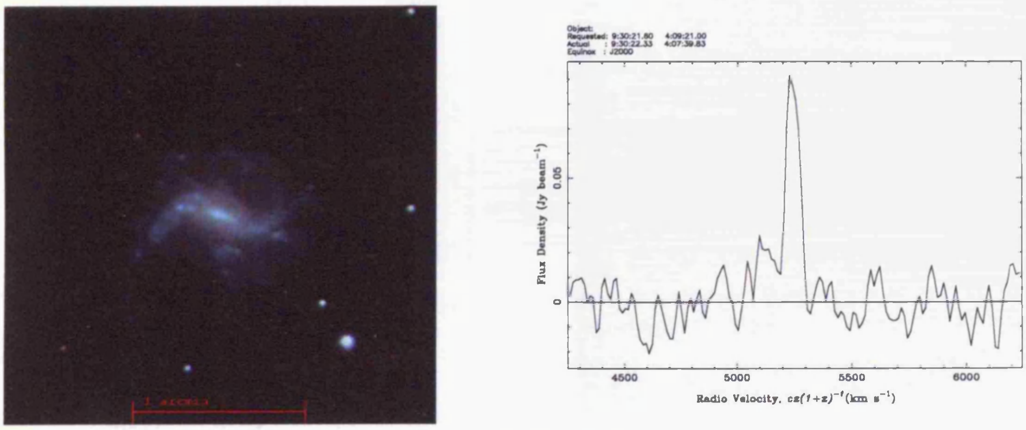

HIPEQ0930+04

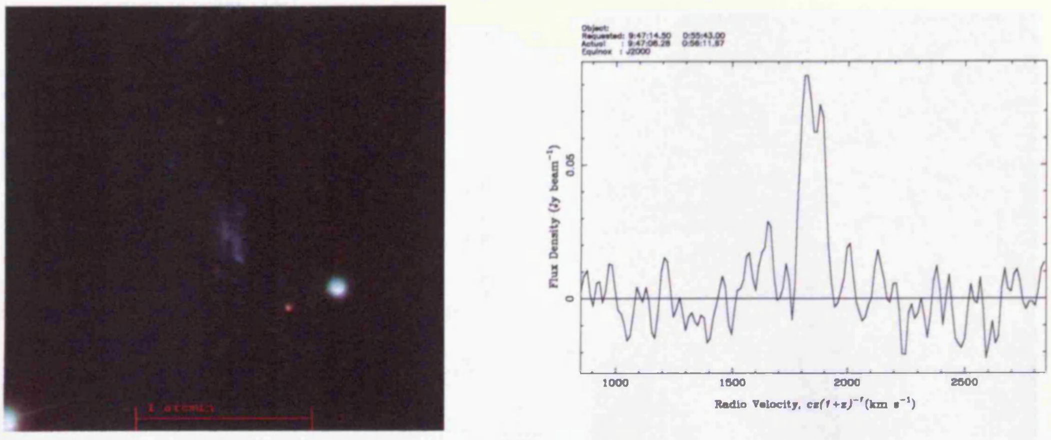

HIPEQ0947+00

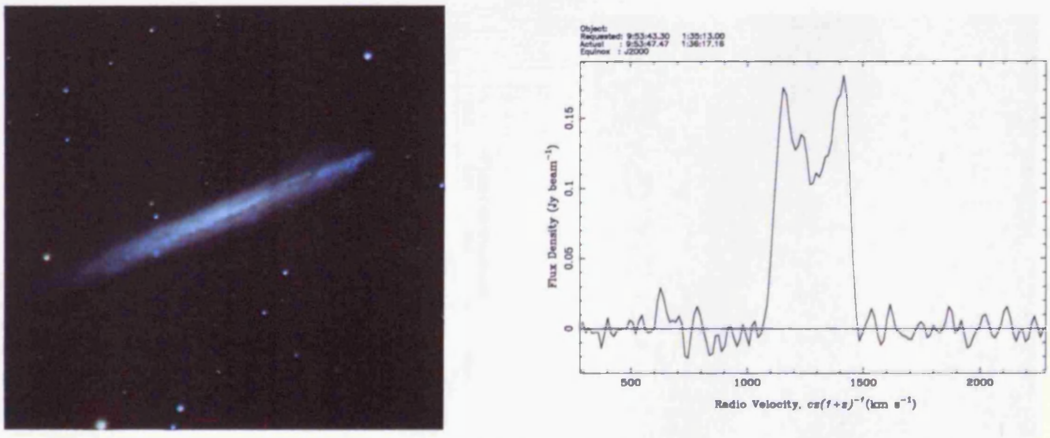

HIPEQ0953+01

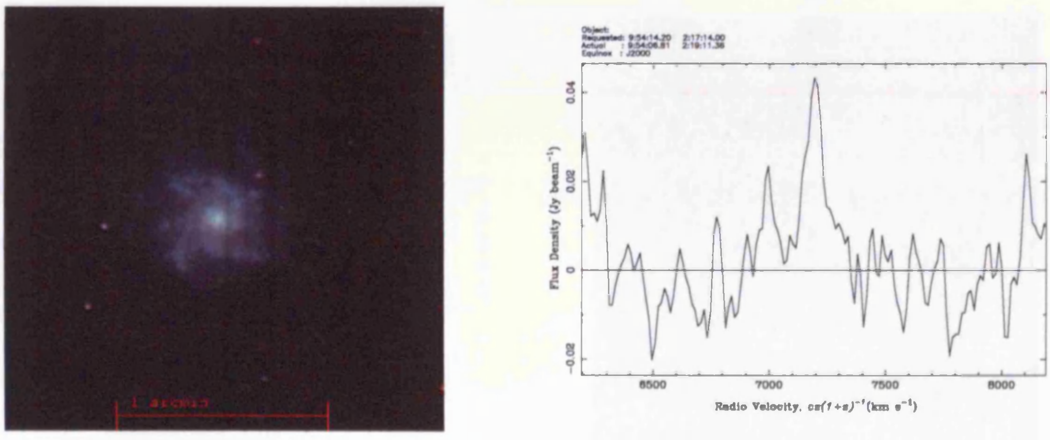

HIPEQ0954+02

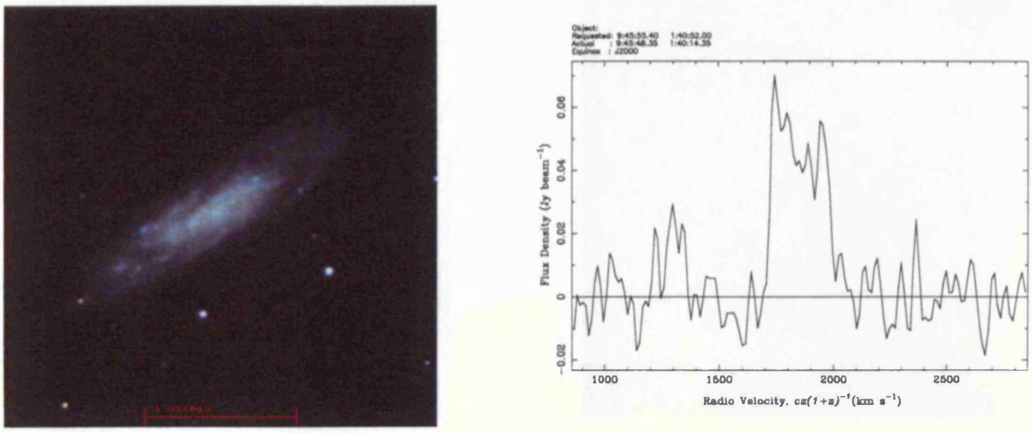

HIPEQ0945+01

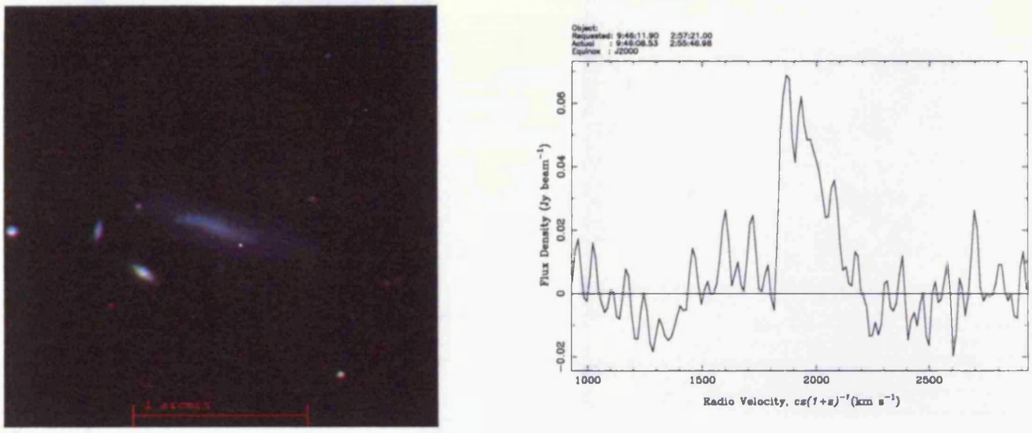

HIPEQ0946+02

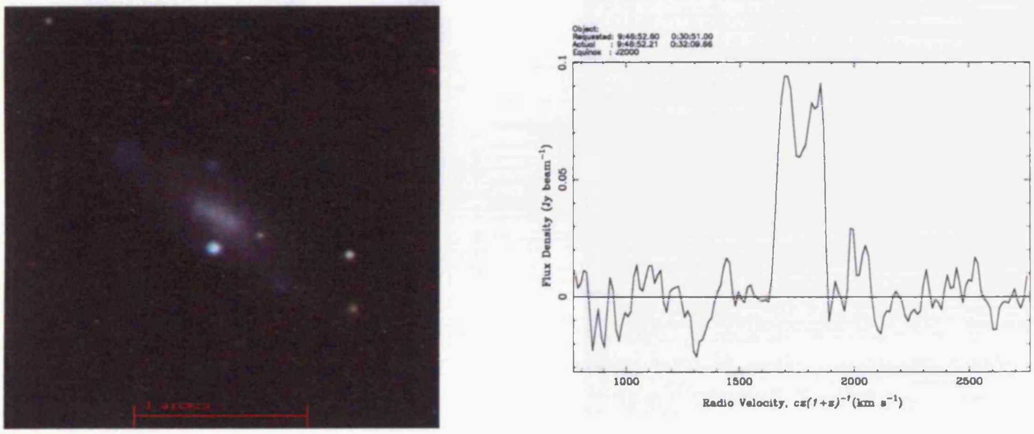

HIPEQ0947+00

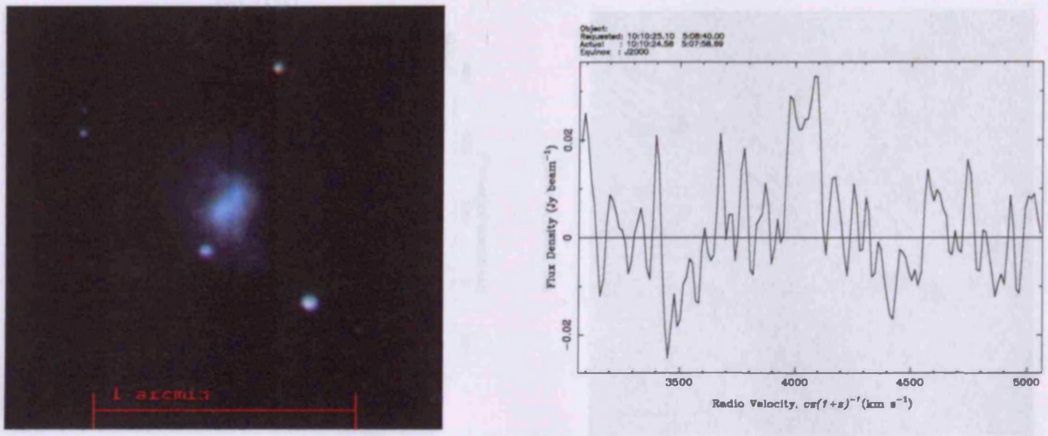

HIPEQ1010+05

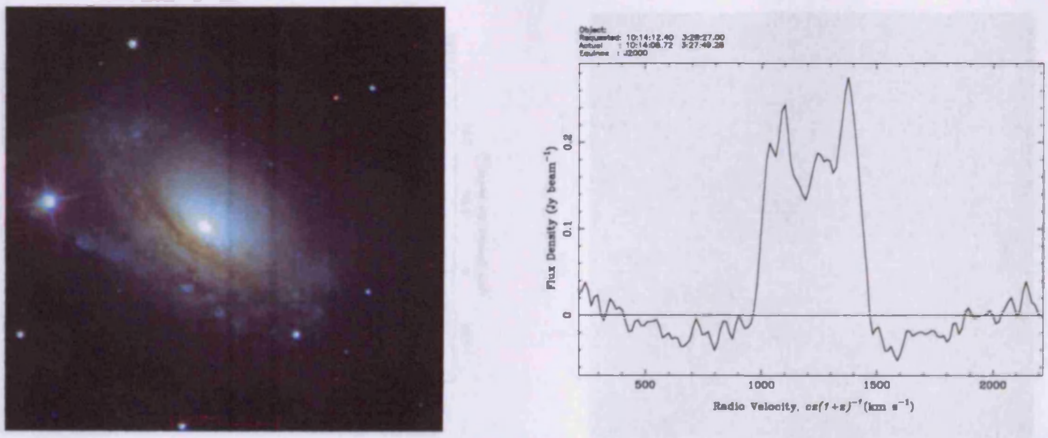

HIPEQ1014+03

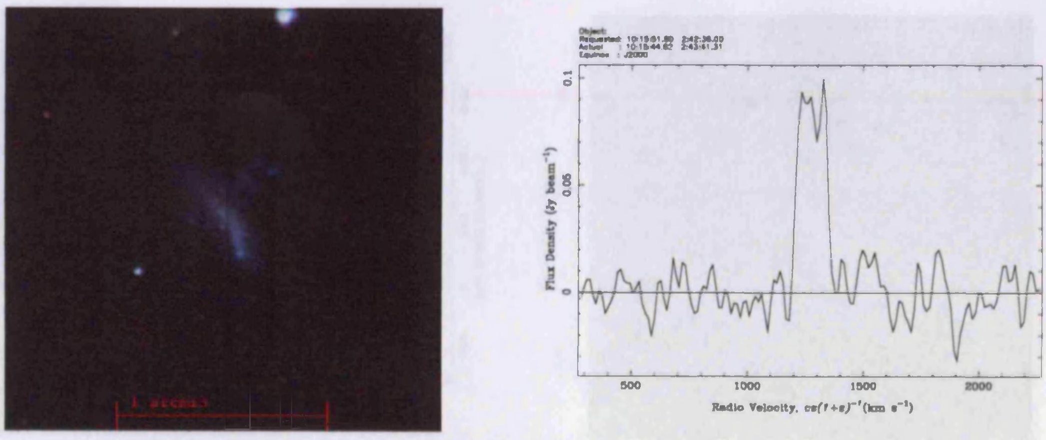

HIPEQ1015+02

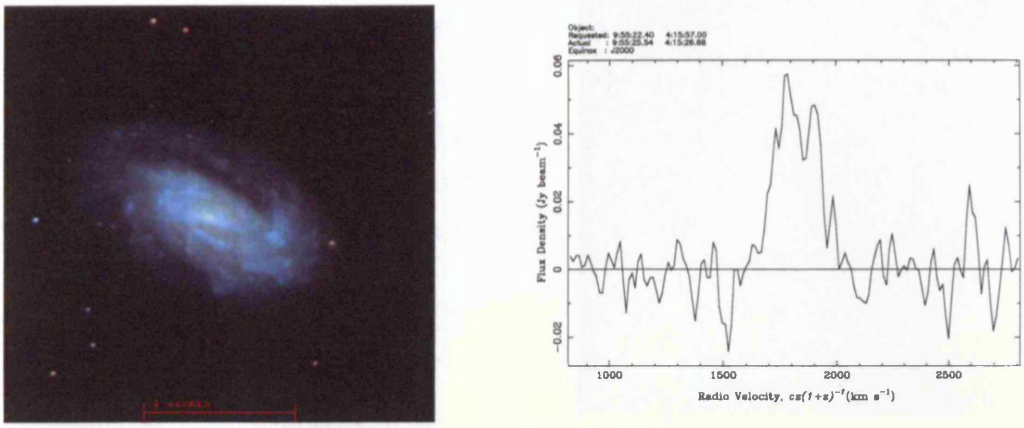

HIPEQ0955+04

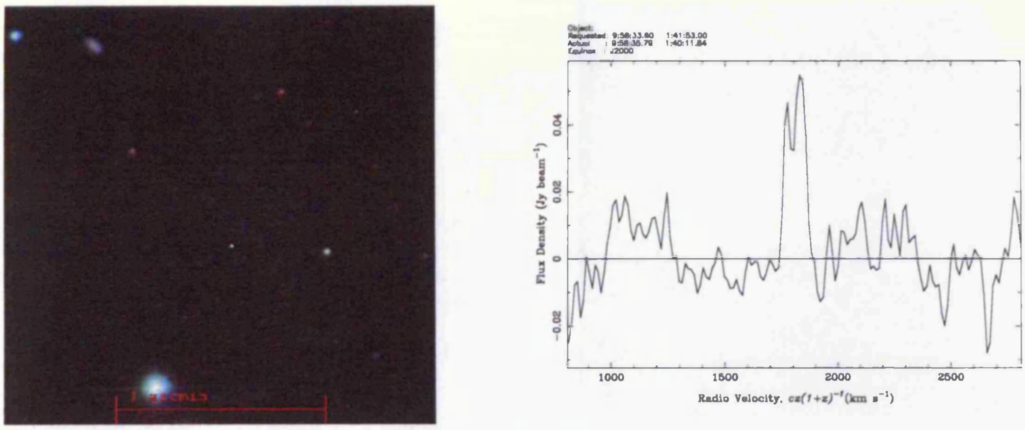

HIPEQ0958+01

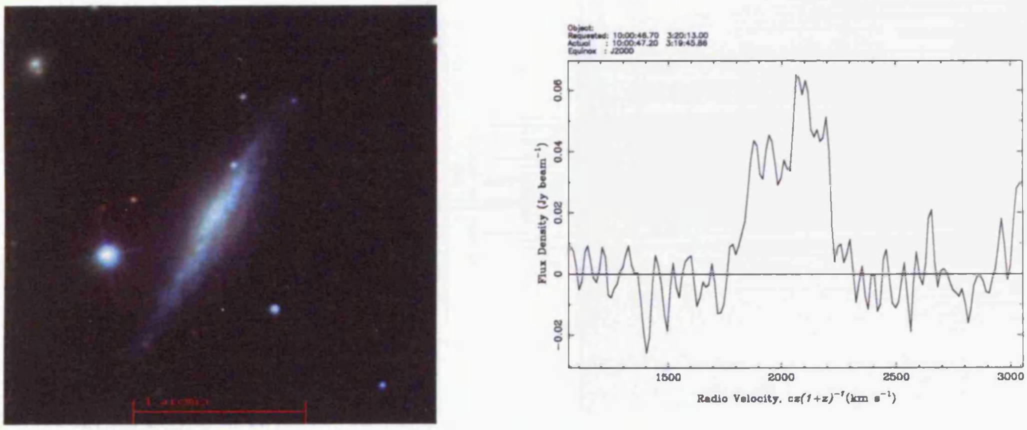

HIPEQ1000+03

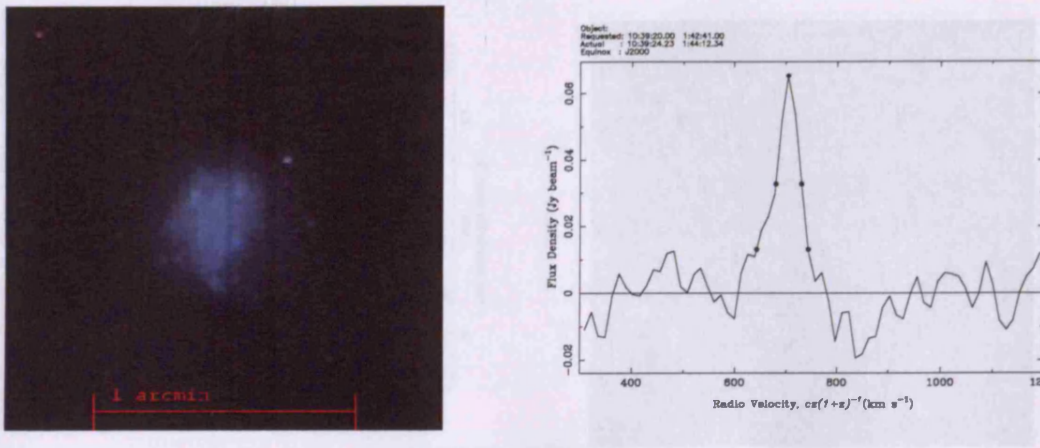

HIPEQ1039+01

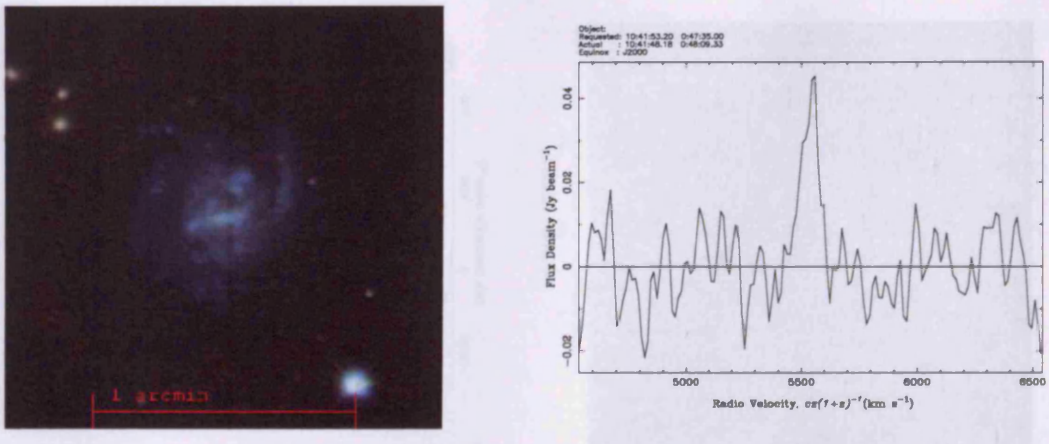

HIPEQ1041+00

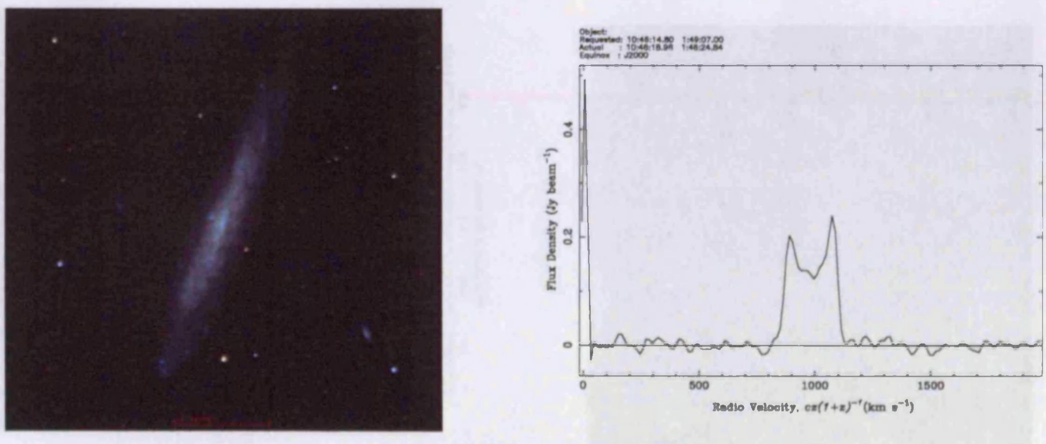

HIPEQ1046+01

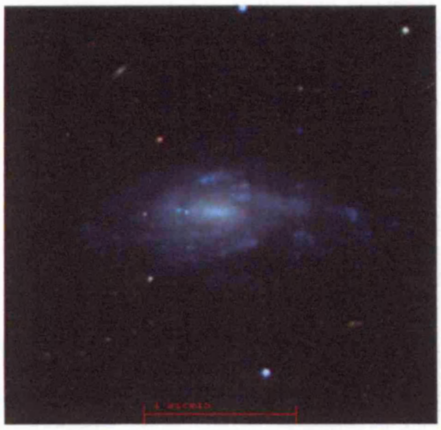

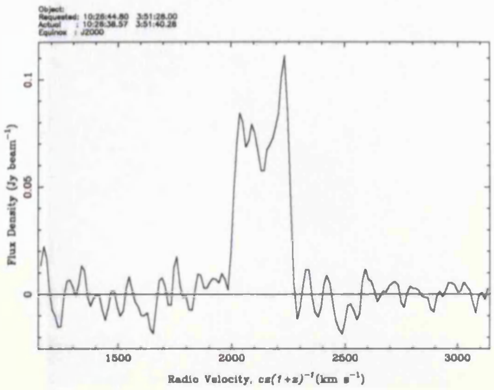

HIPEQ1026+03

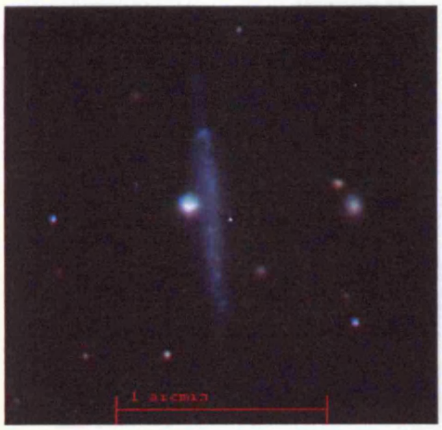

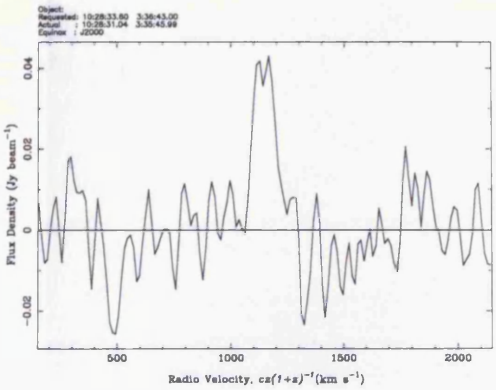

HIPEQ1028+03

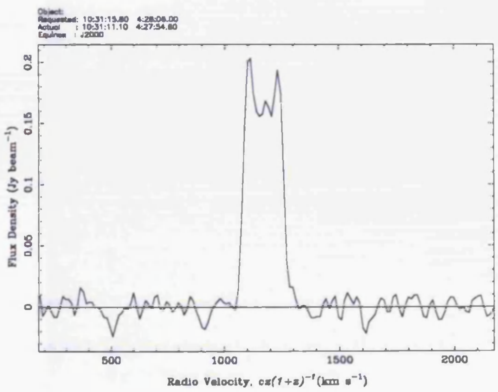

HIPEQ1031+04

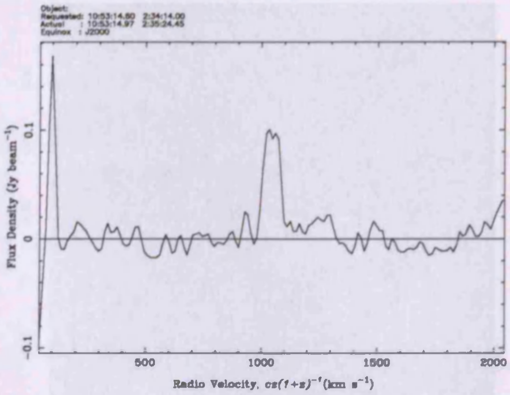

HIPEQ1053+02

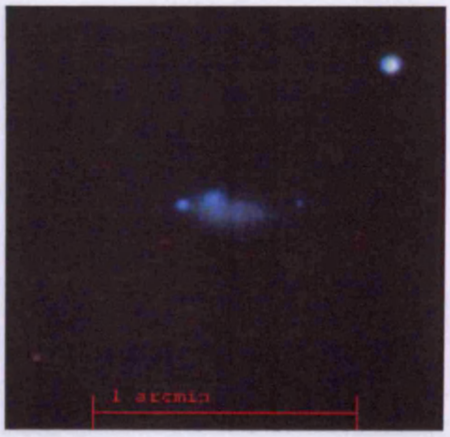

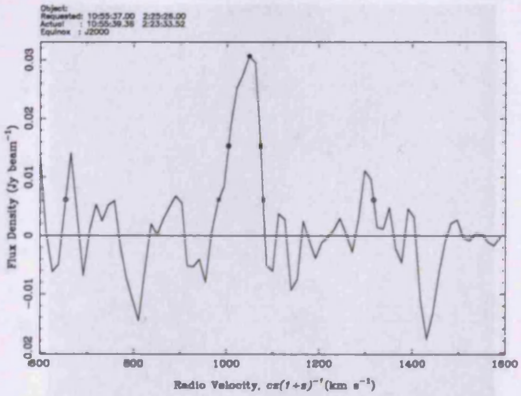

HIPEQ1055+02

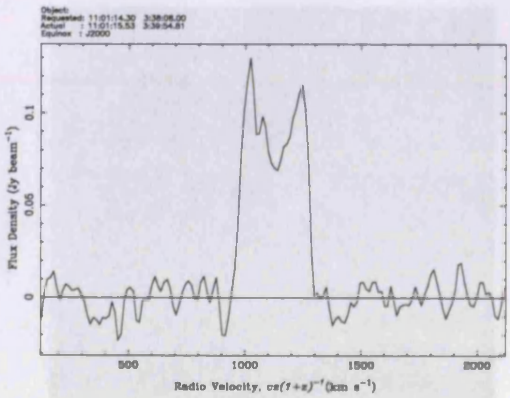

HIPEQ1101+03

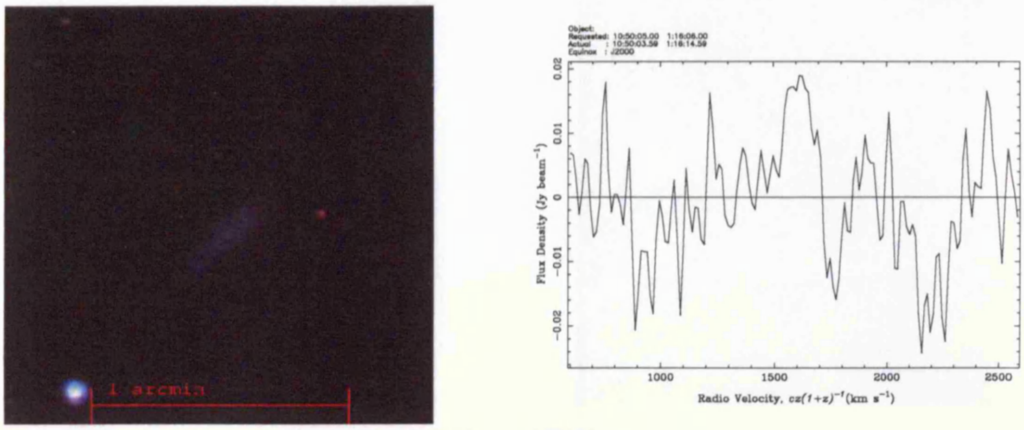

HIPEQ1050+01

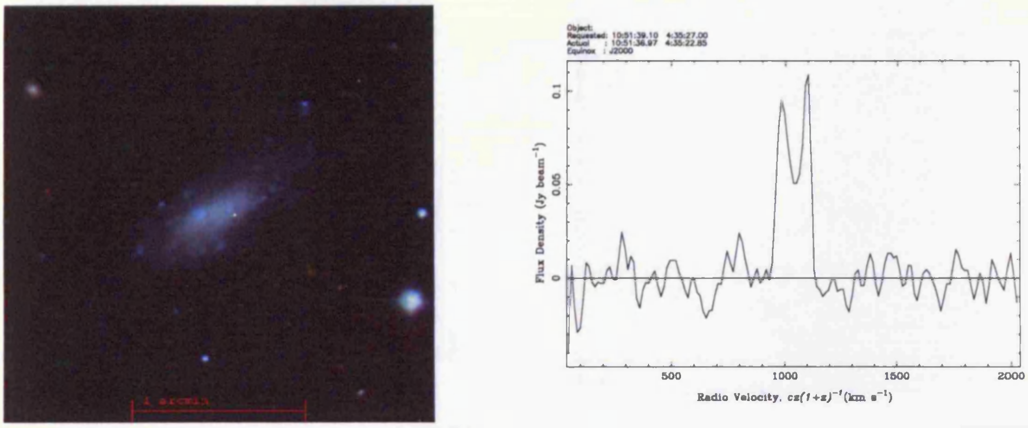

HIPEQ1051+04

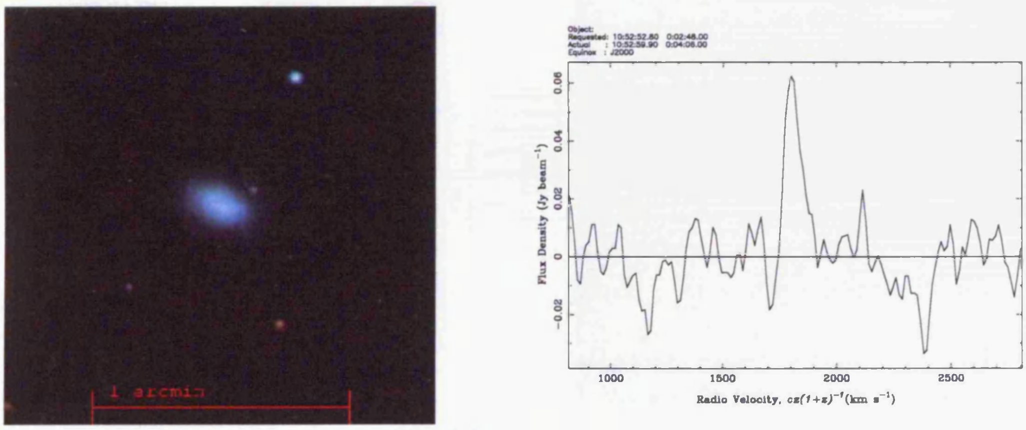

HIPEQ1052+00

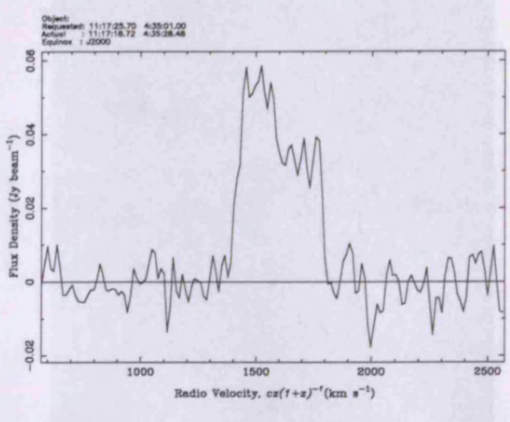

HIPEQ1117+04

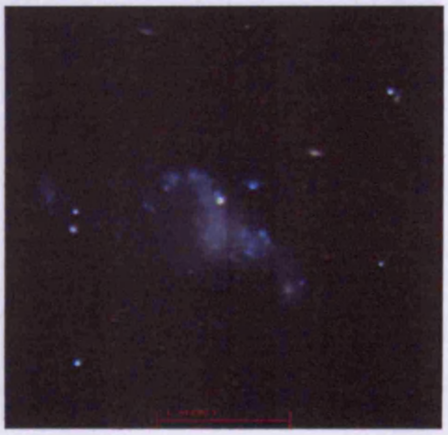

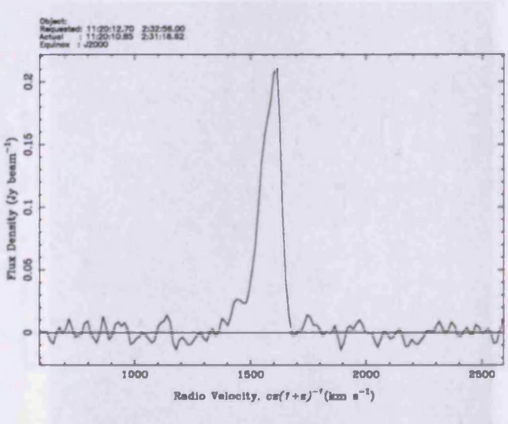

HIPEQ1119+02

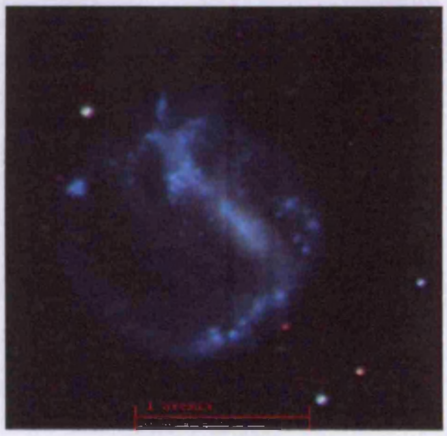

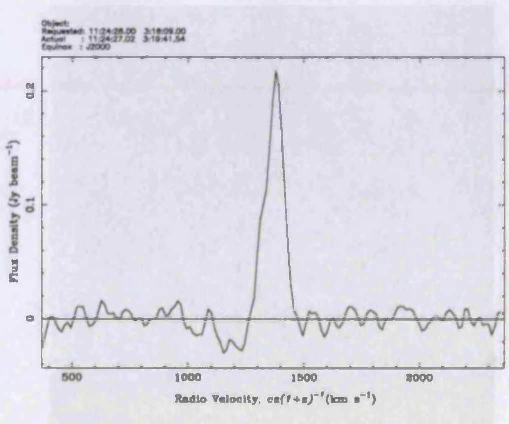

HIPEQ1124+03

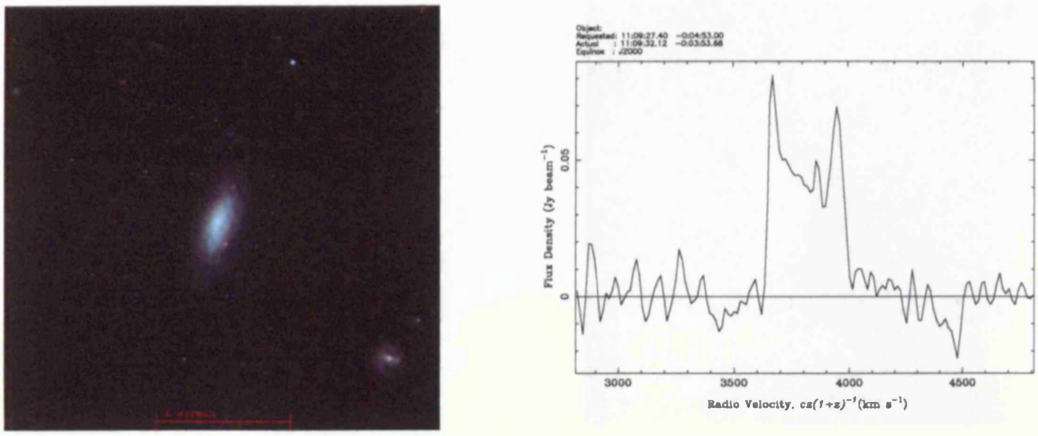

HIPEQ1109-00

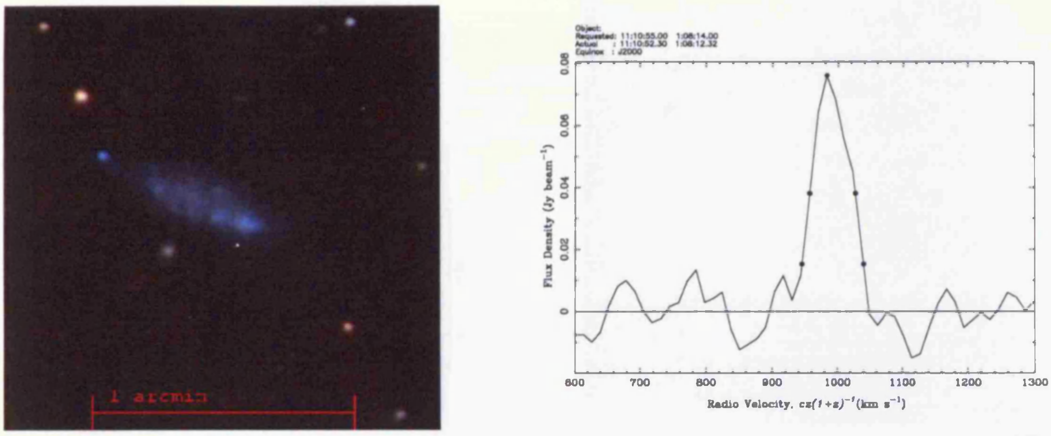

HIPEQ1110+01

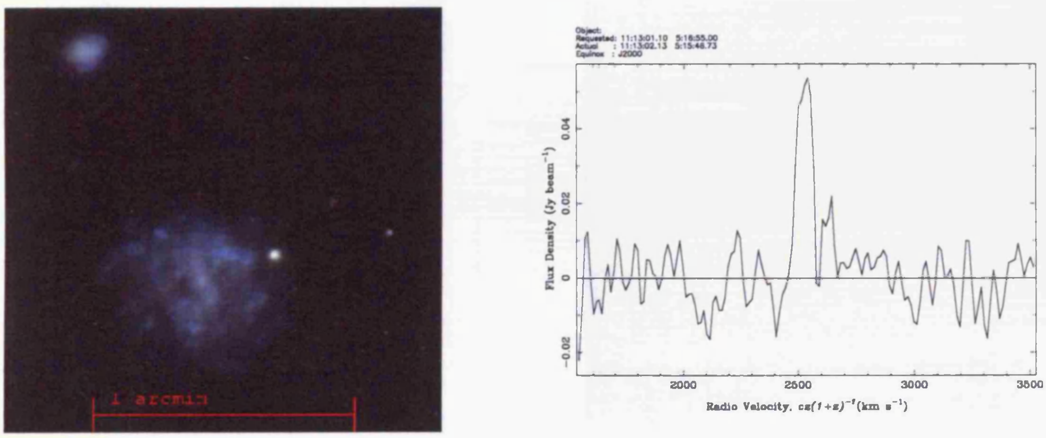

HIPEQ1113+05

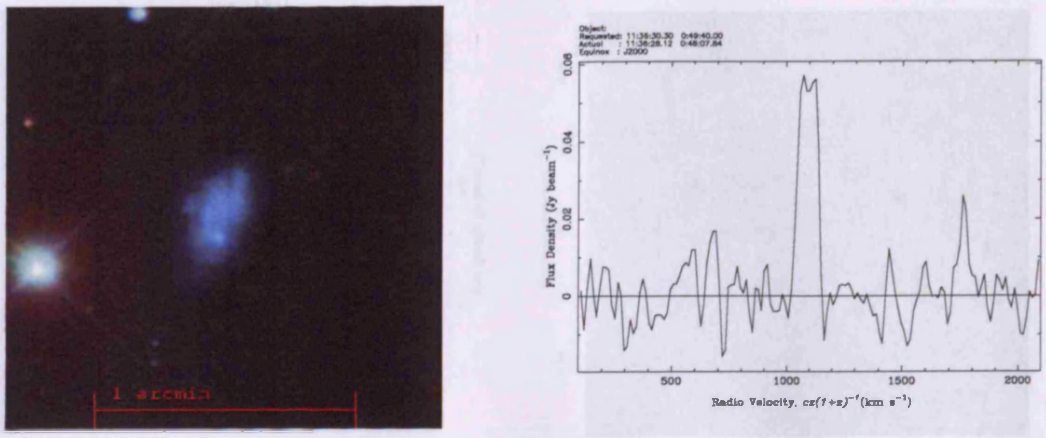

HIPEQ1136+00

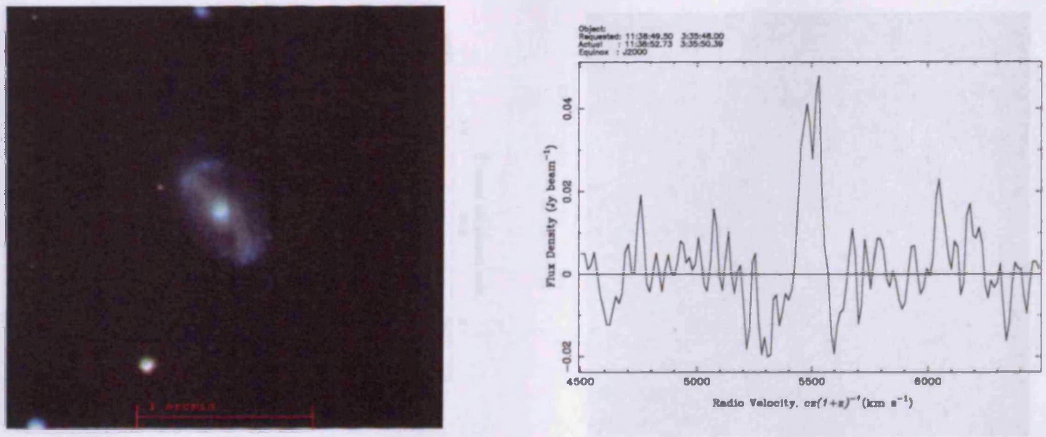

HIPEQ1138+03

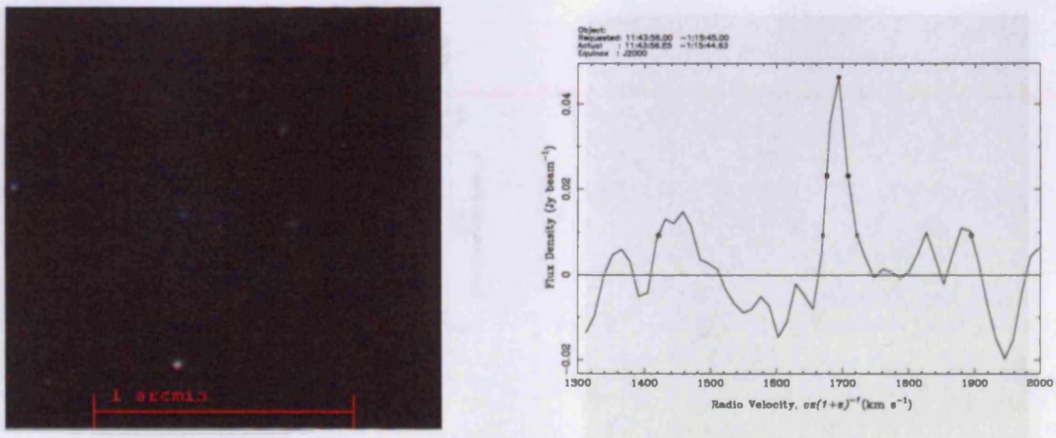

HIPEQ1143-01

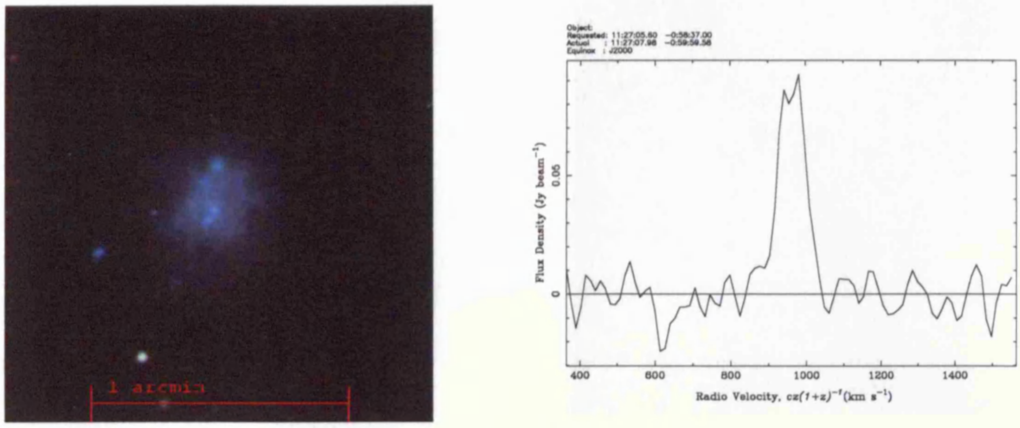

HIPEQ1127-01

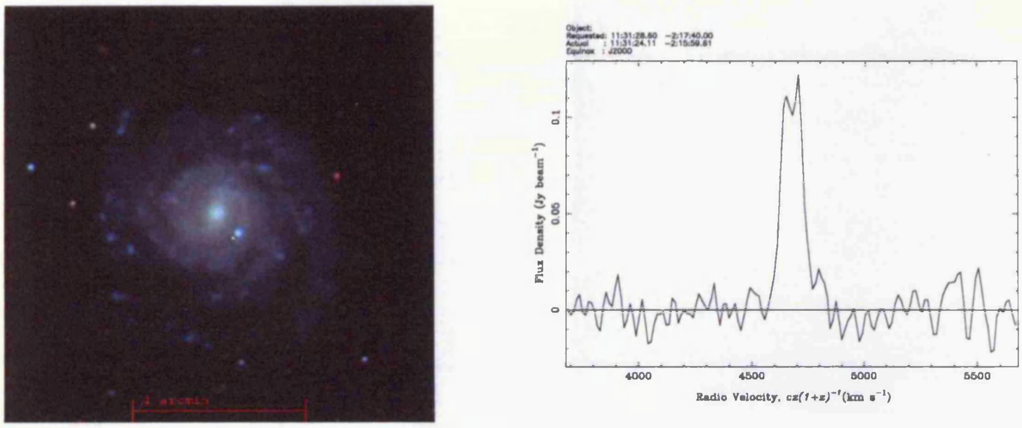

HIPEQ1131-02

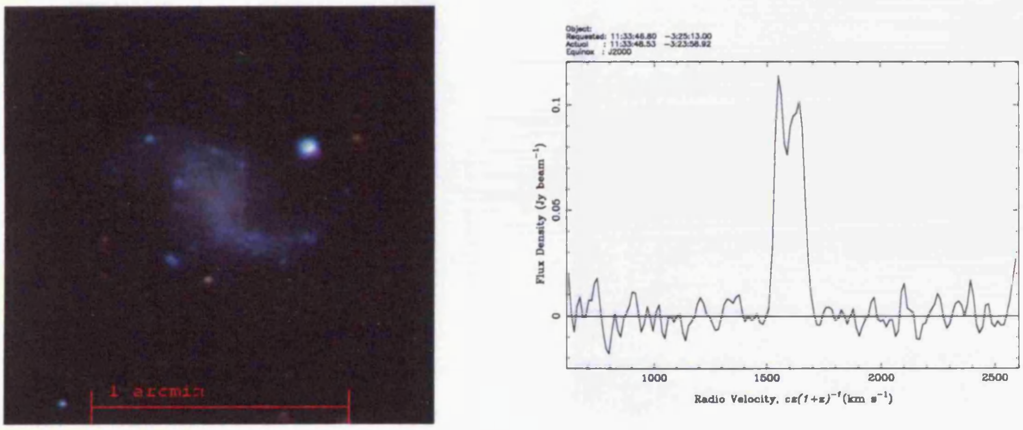

HIPEQ1133-03

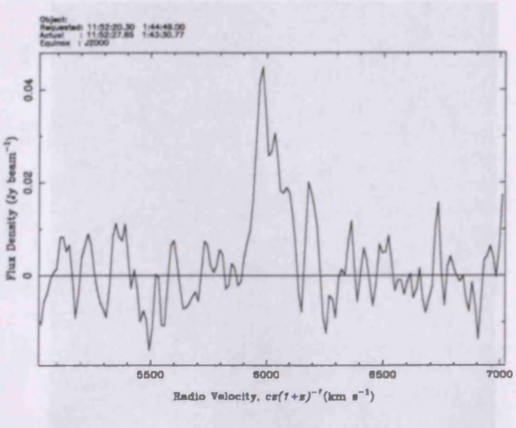

HIPEQ1152+01

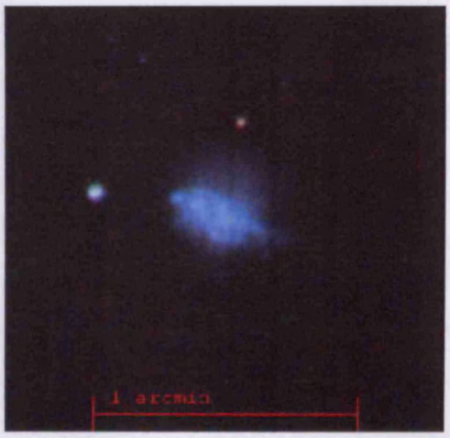

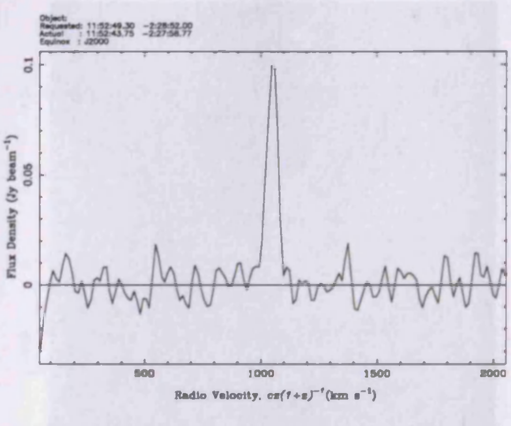

HIPEQ1152-02

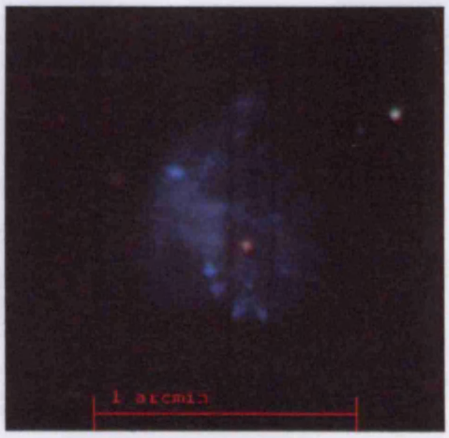

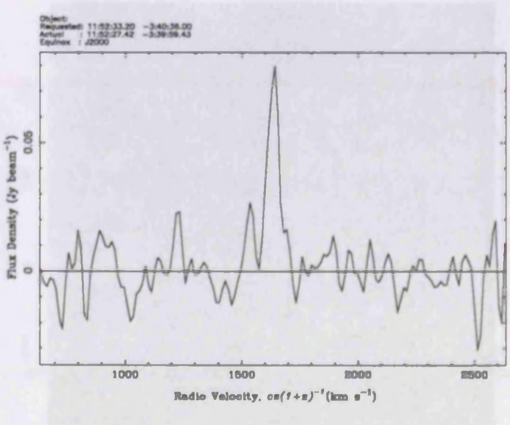

HIPEQ1152-03

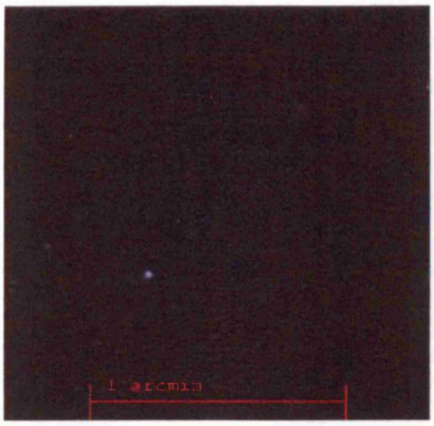

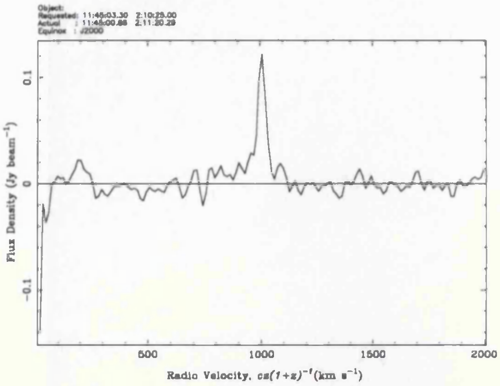

HIPEQ1145+02

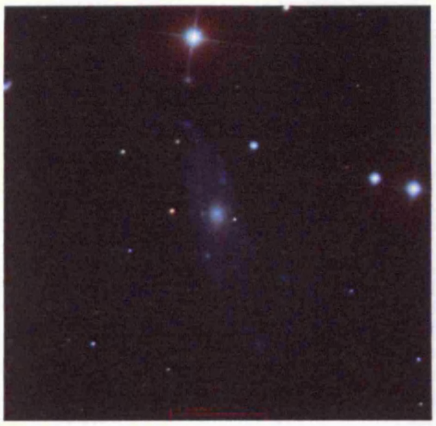

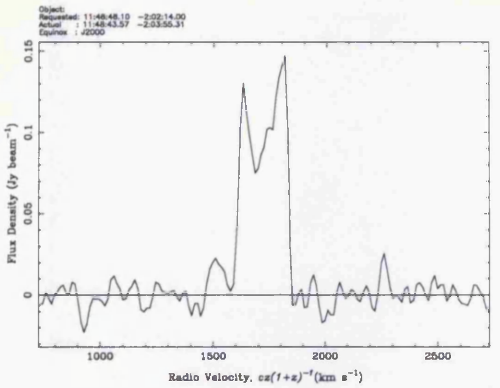

HIPEQ1148-02

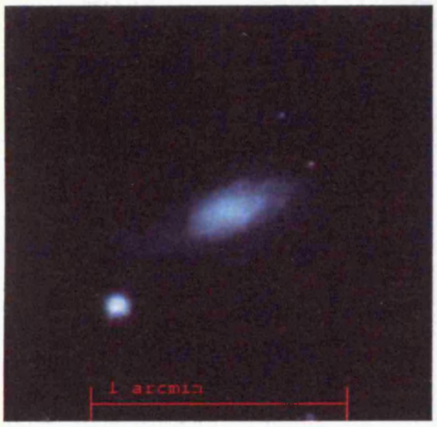

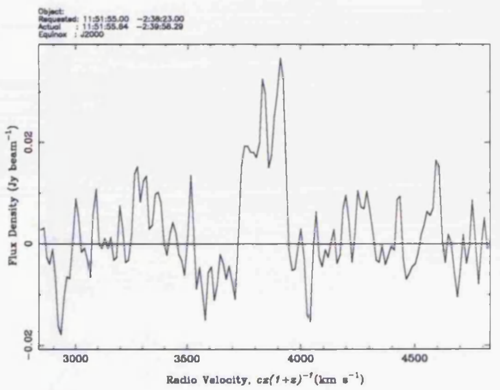

HIPEQ1151-02

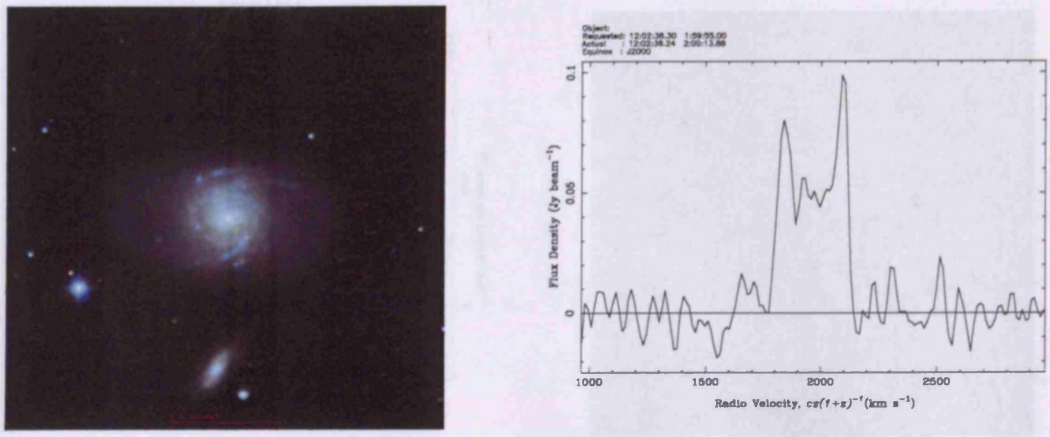

HIPEQ1202+01

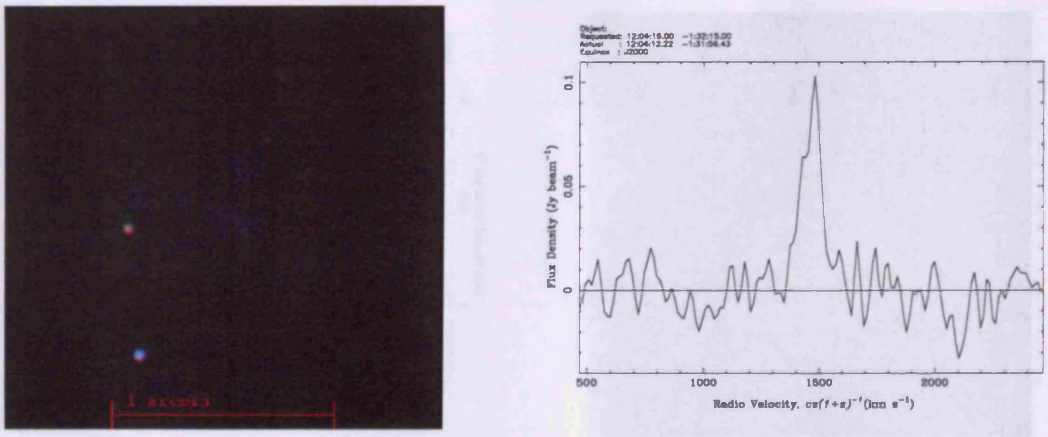

HIPEQ1204-01

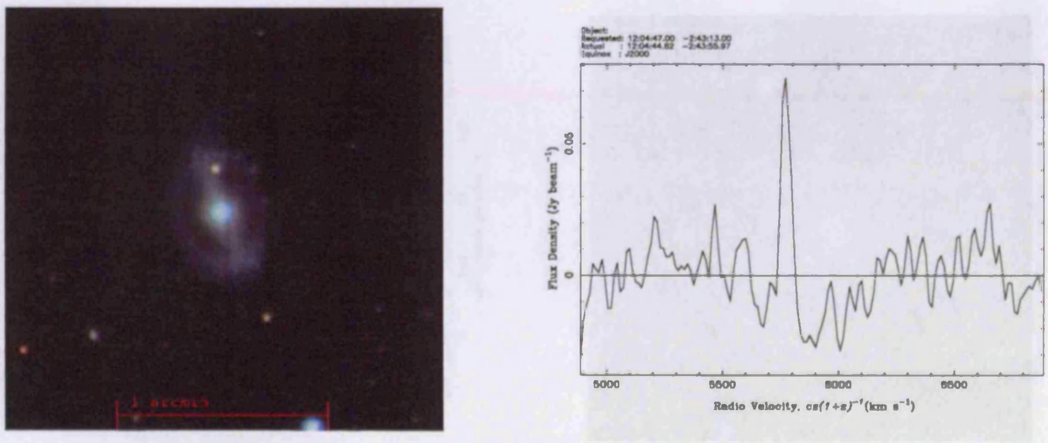

HIPEQ1204-02

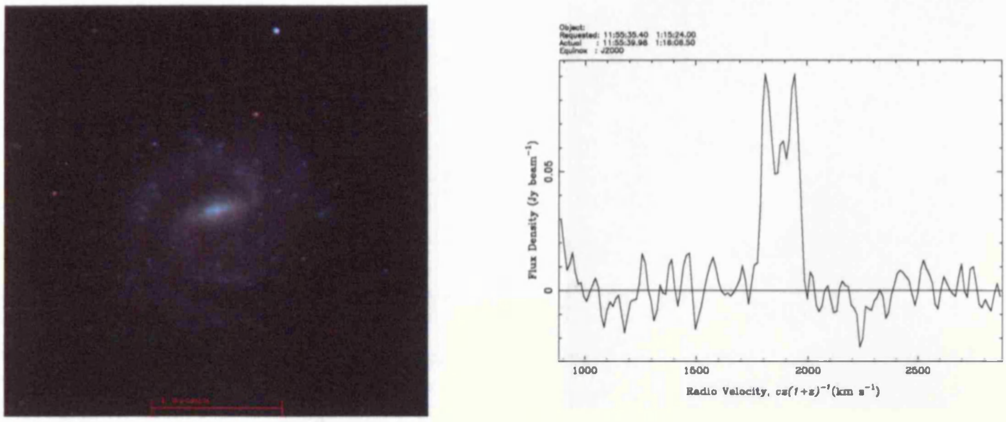

HIPEQ1155+01

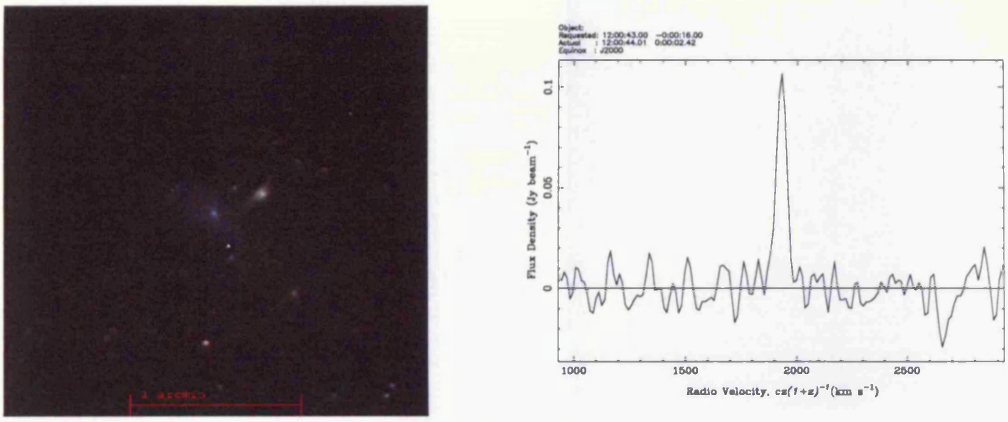

HIPEQ1200-00

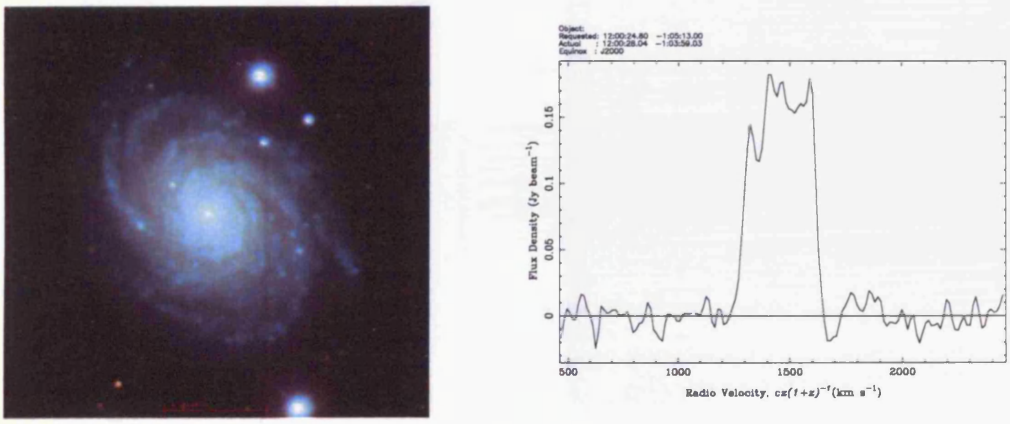

HIPEQ1200-01

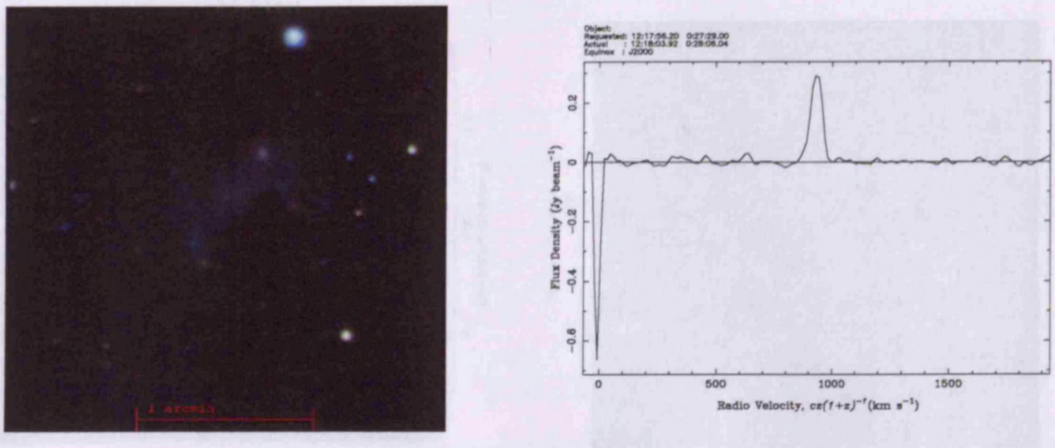

HIPEQ1218+00

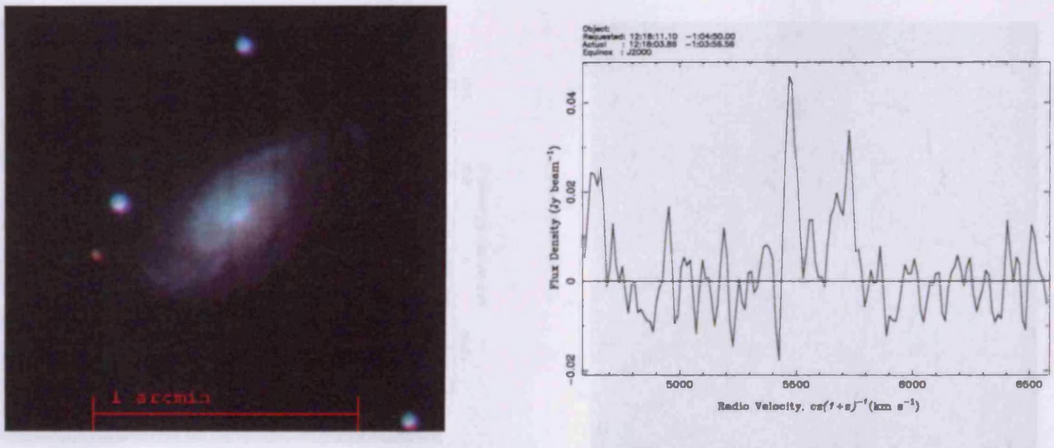

HIPEQ1218-01

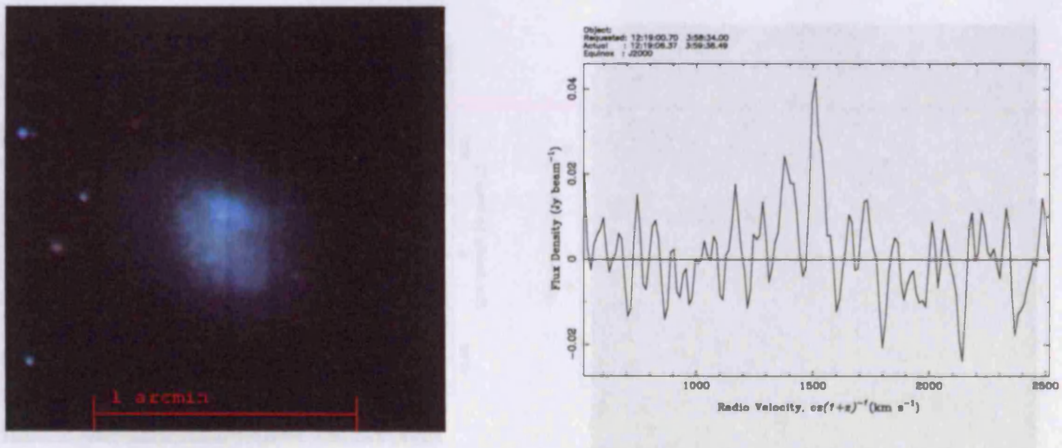

HIPEQ1219+03

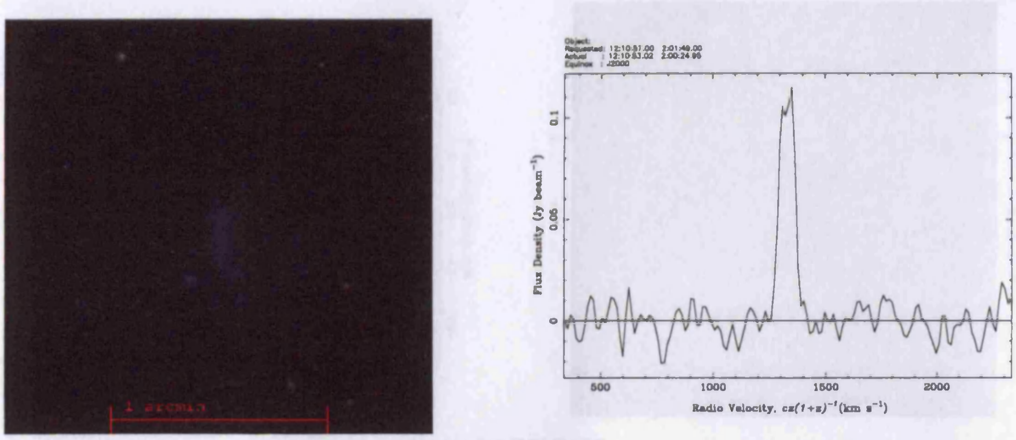

HIPEQ1210+02

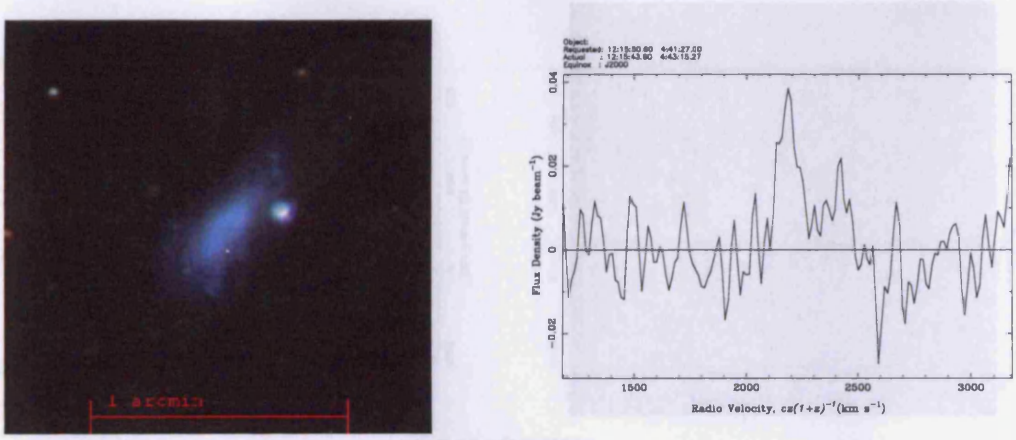

HIPEQ1215+04

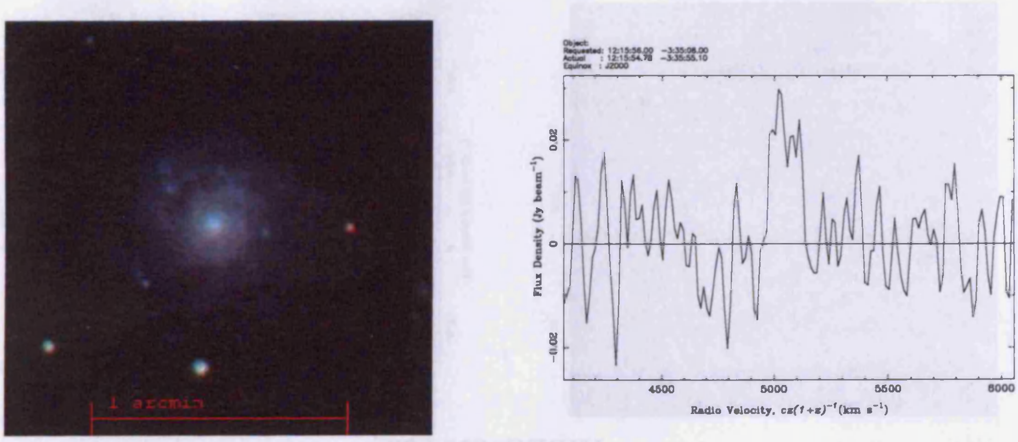

HIPEQ1216-03

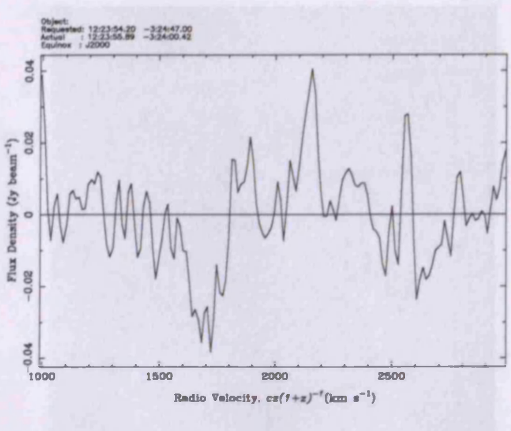

HIPEQ1223-03

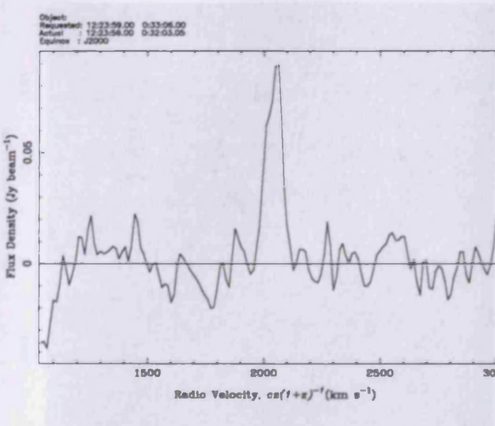

HIPEQ1224+00

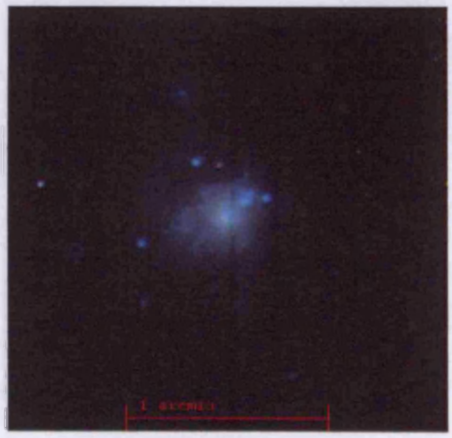

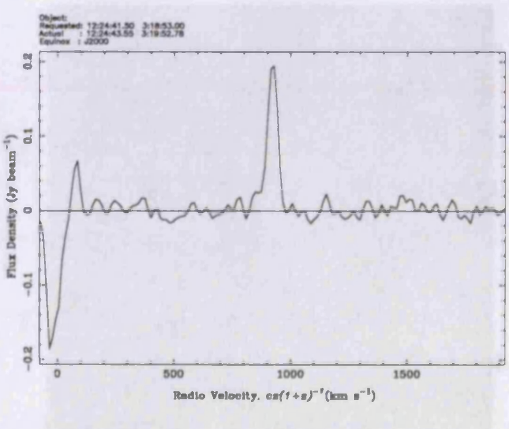

HIPEQ1224+03

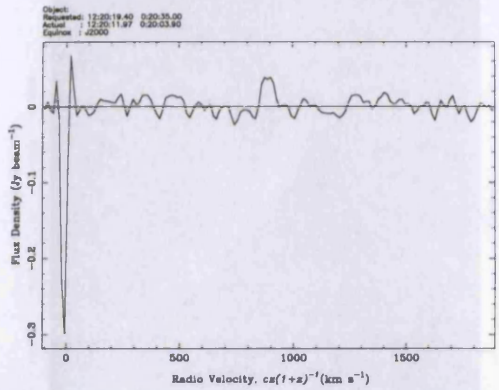

HIPEQ1220+00

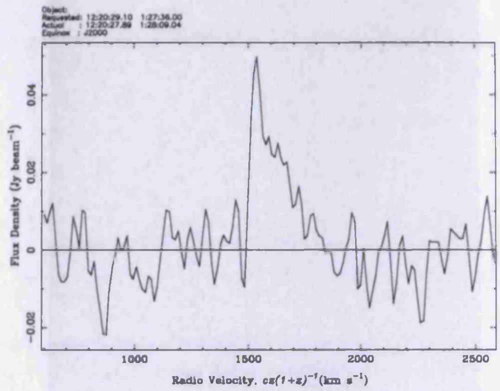

HIPEQ1220+01

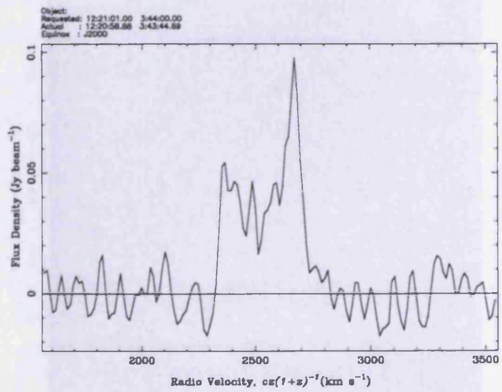

HIPEQ1221+03

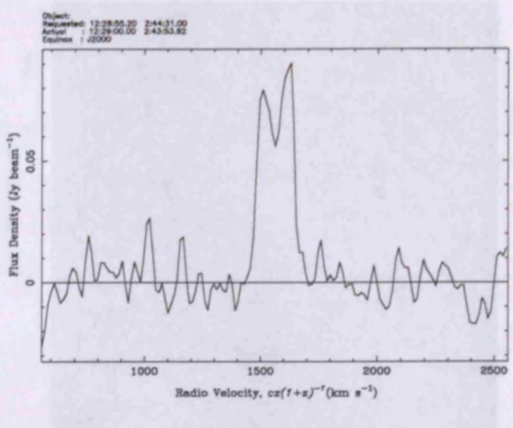

HIPEQ1228+02

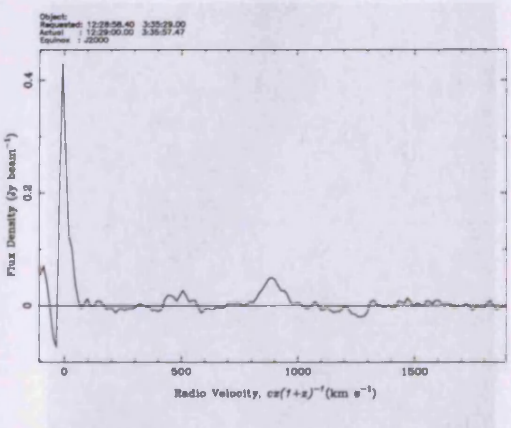

HIPEQ1228+03

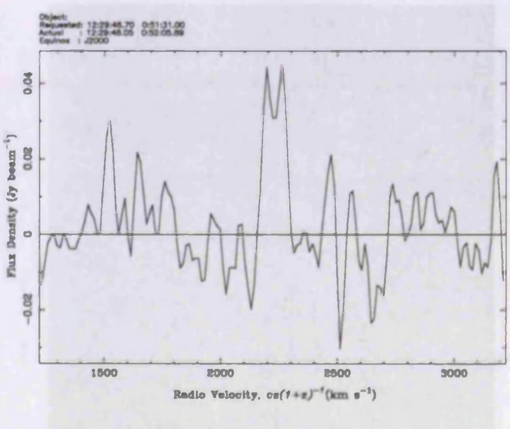

HIPEQ1229+00

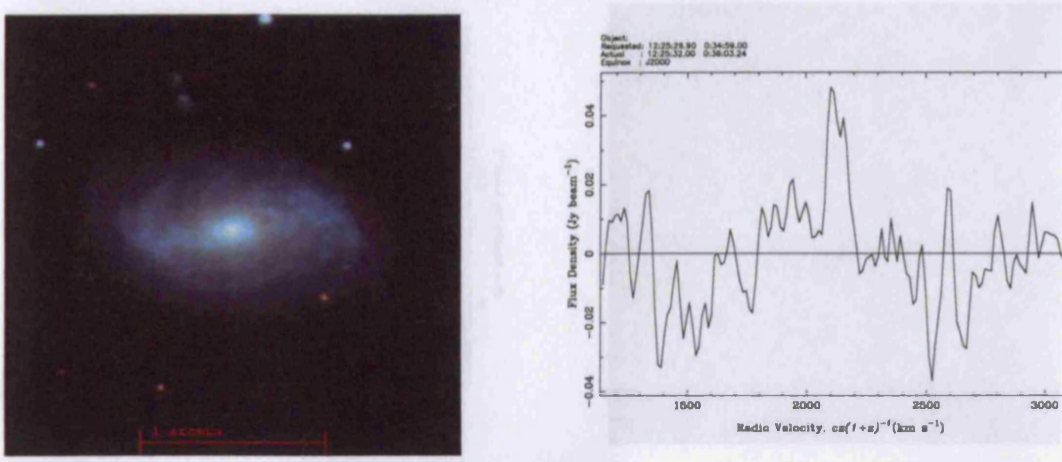

HIPEQ1225+00

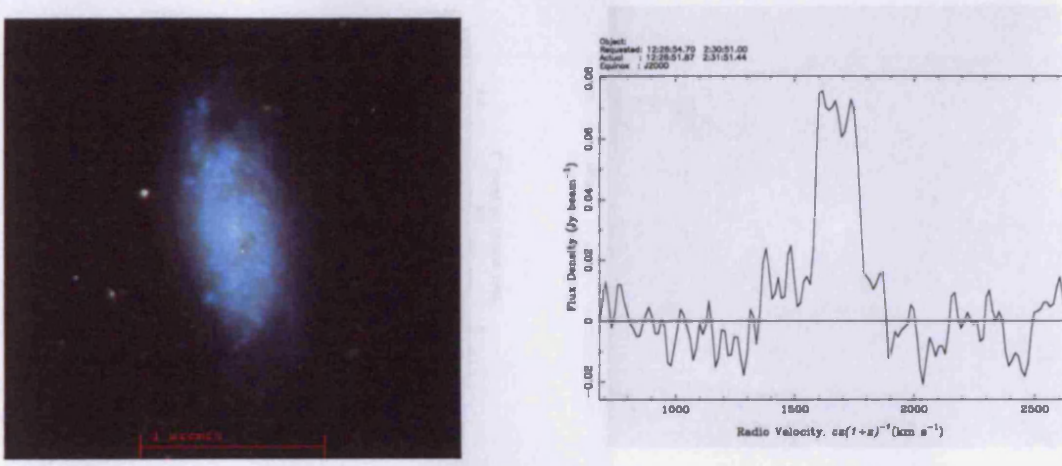

HIPEQ1226+02

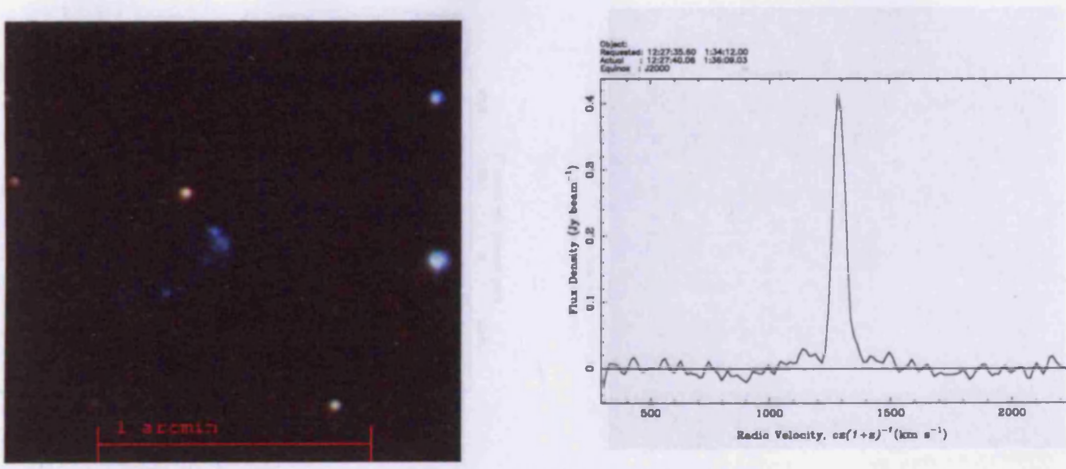

HIPEQ1227+01

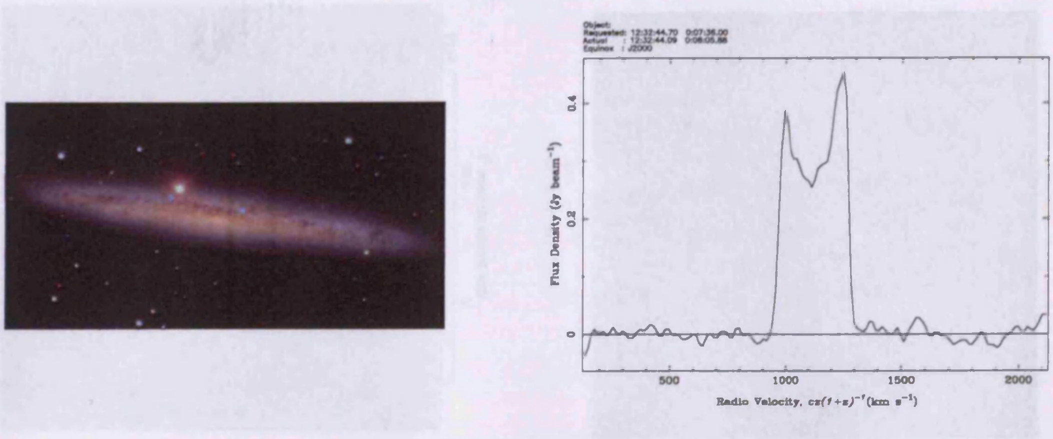

HIPEQ1232+00

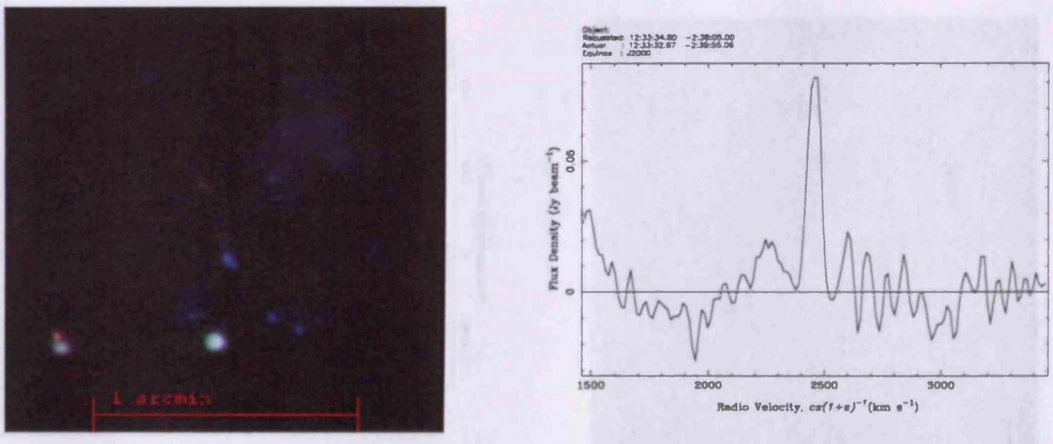

HIPEQ1233-02

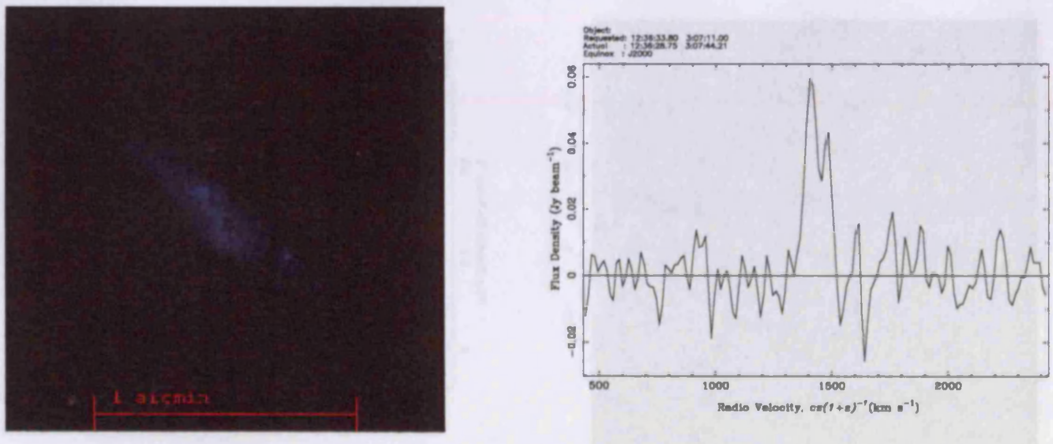

HIPEQ1236+03

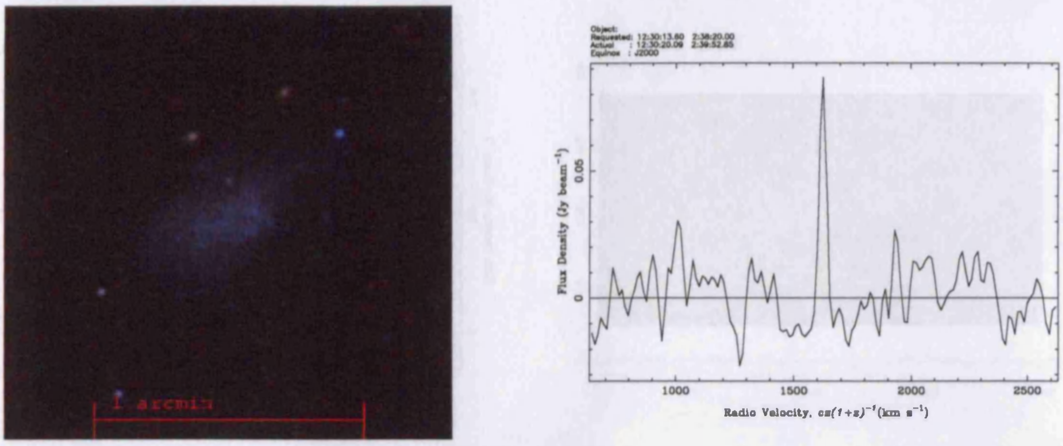

HIPEQ1230+02

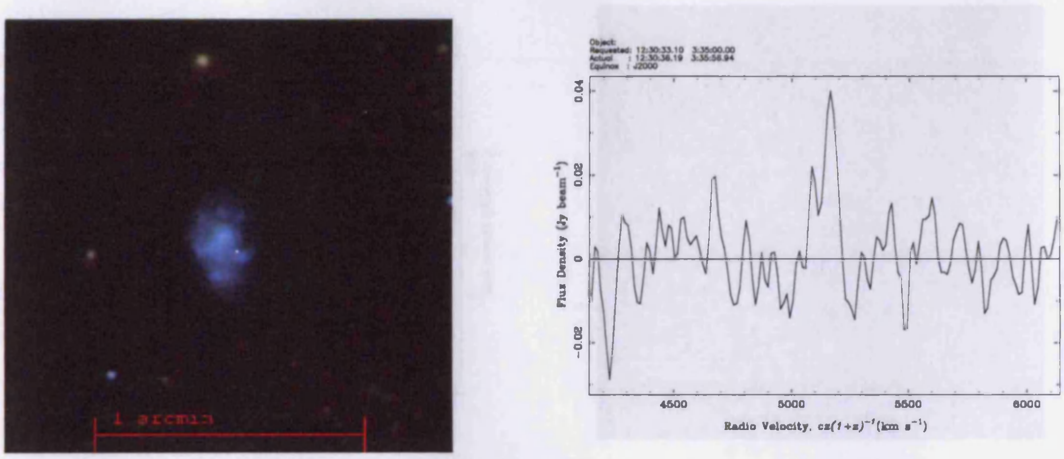

HIPEQ1230+03

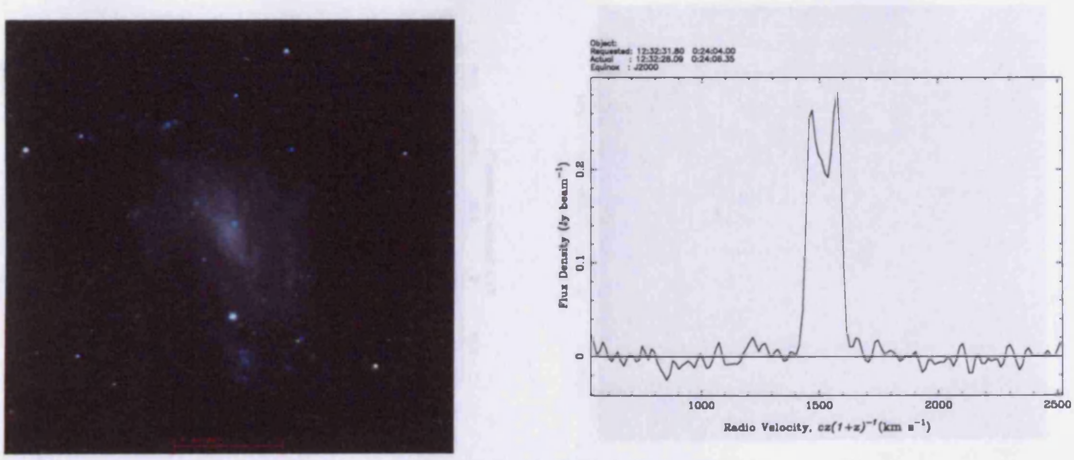

HIPEQ1232+00

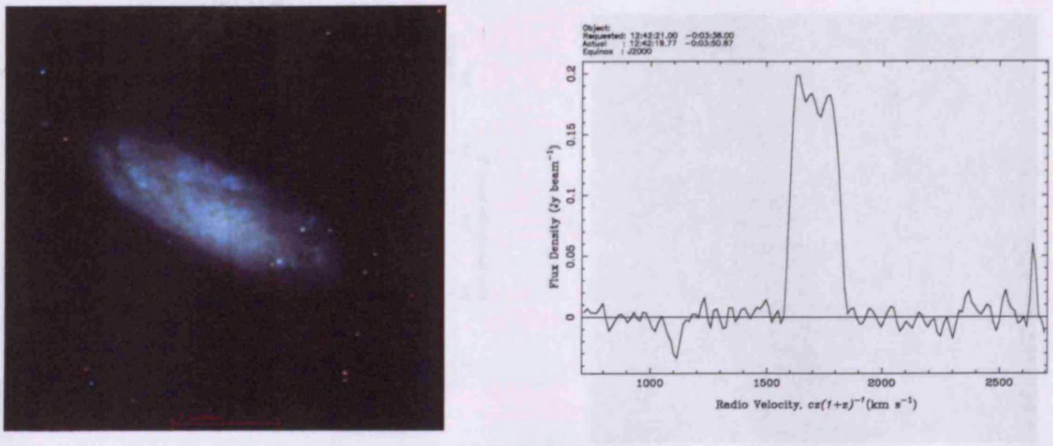

HIPEQ1242-00

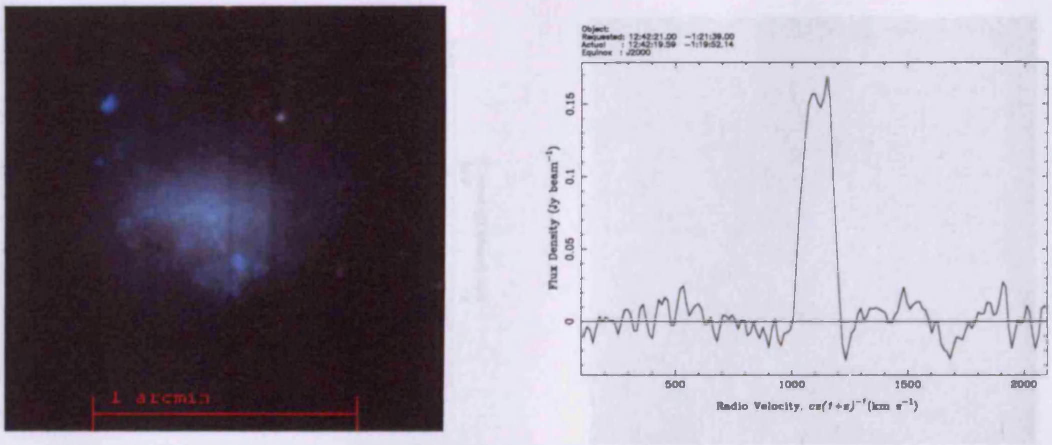

HIPEQ1242-01

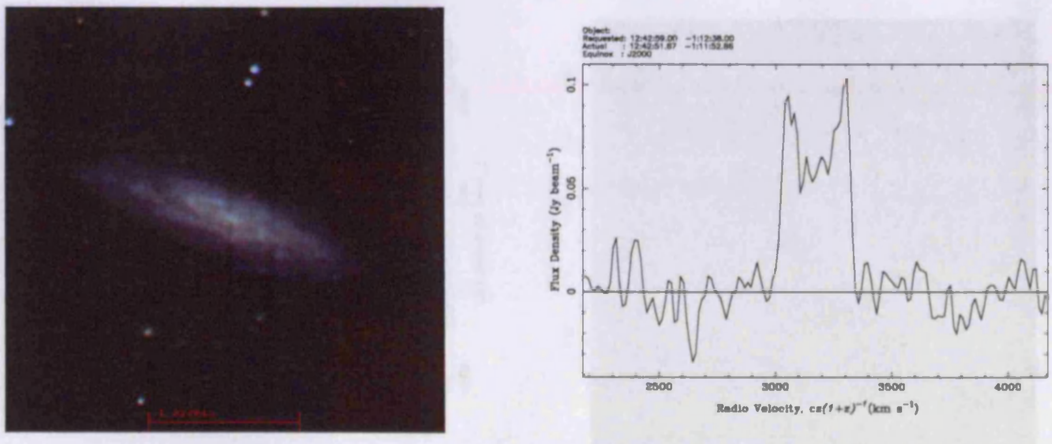

HIPEQ1242-01

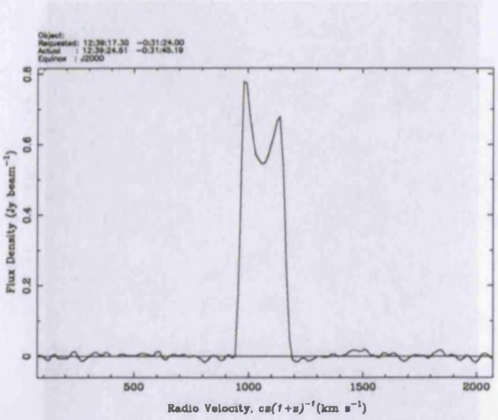

HIPEQ1239-00

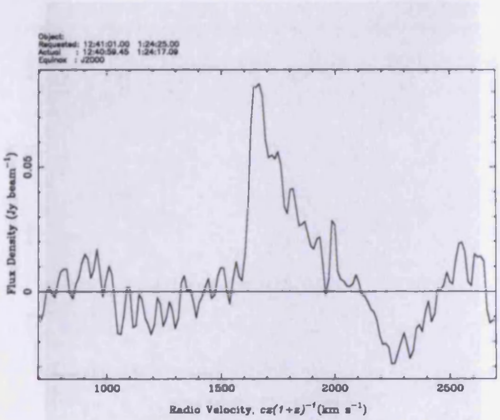

HIPEQ1241+01

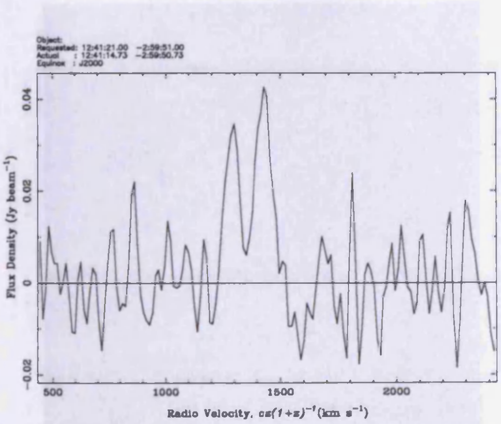

HIPEQ1241-02

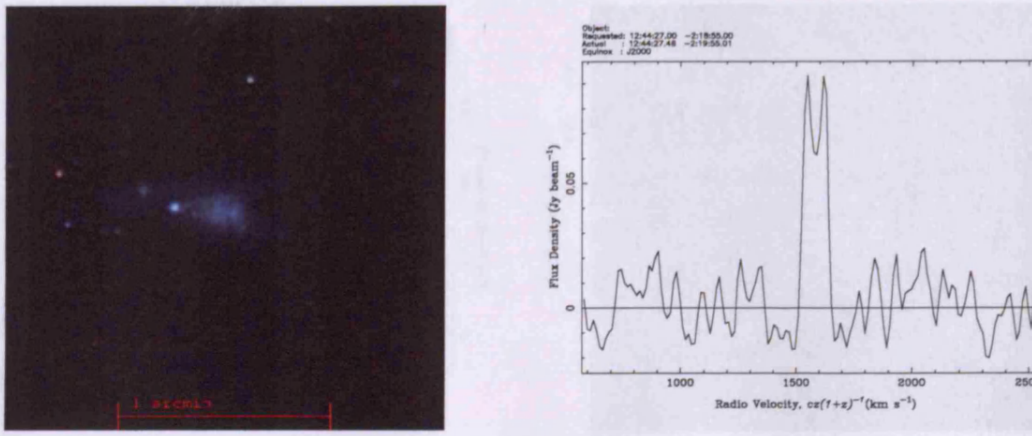

HIPEQ1244-02

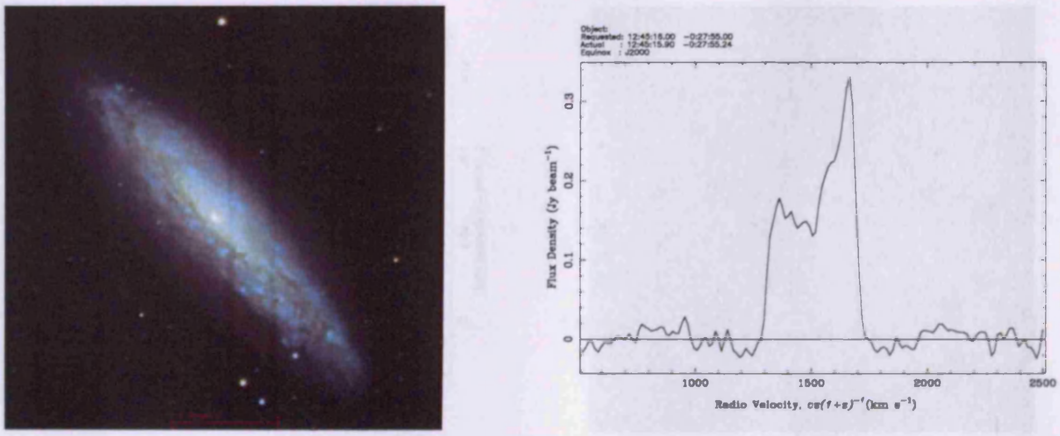

HIPEQ1245-00

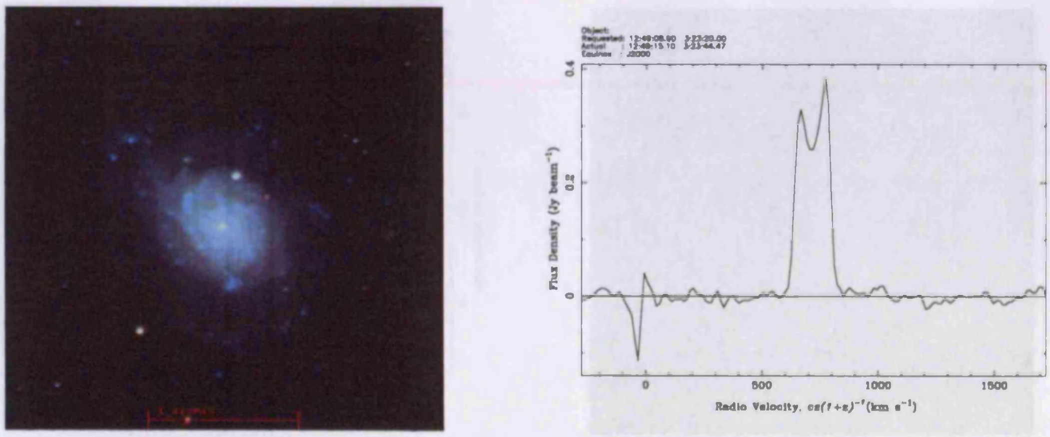

HIPEQ1249+03

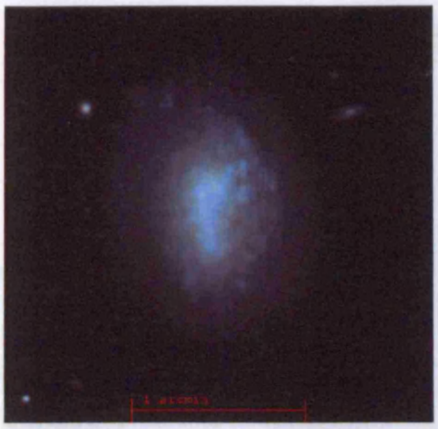

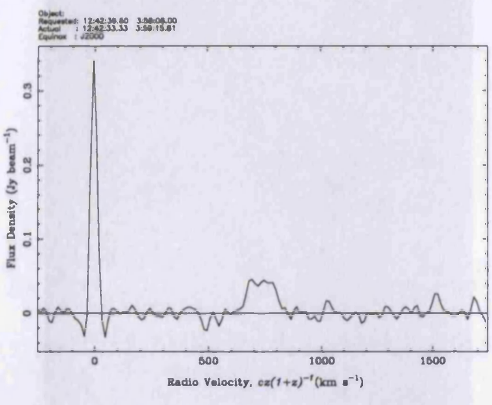

HIPEQ1242+03

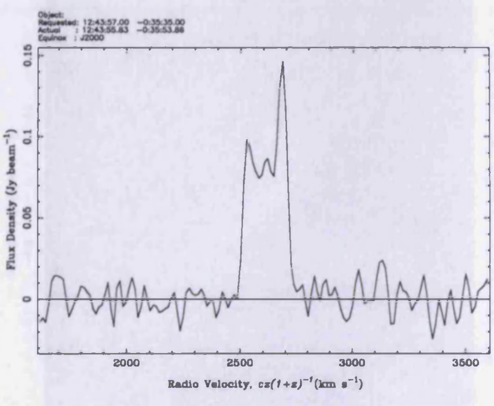

HIPEQ1243-00

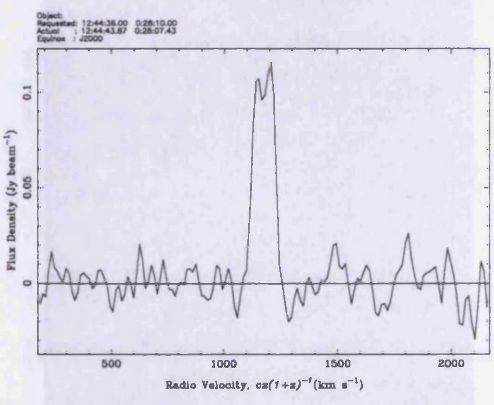

HIPEQ1244+00

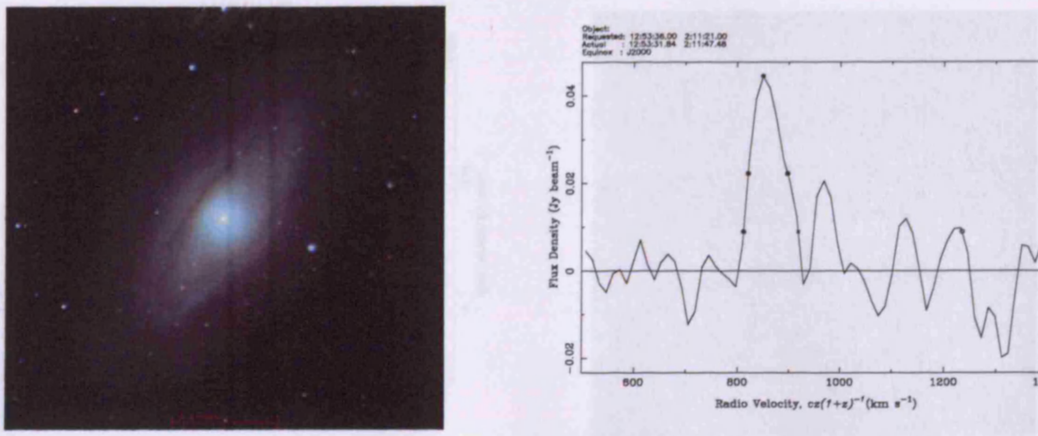

HIPEQ1253+02

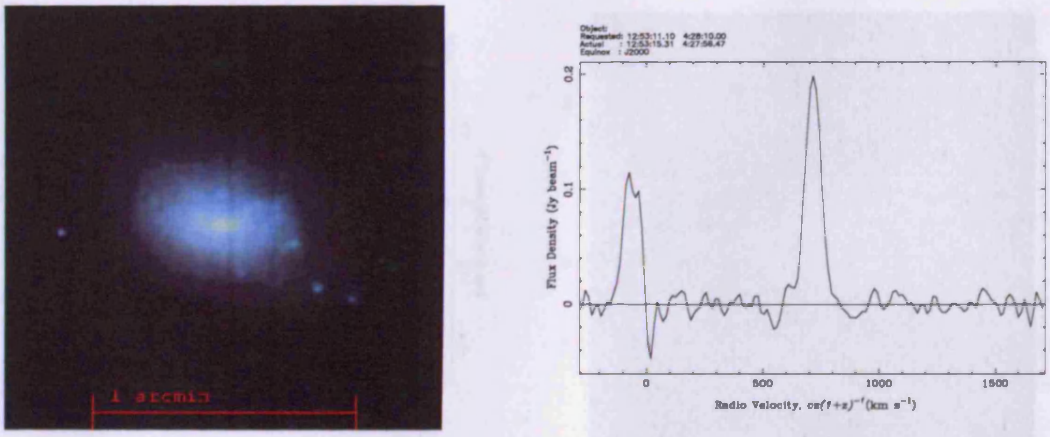

HIPEQ1253+04

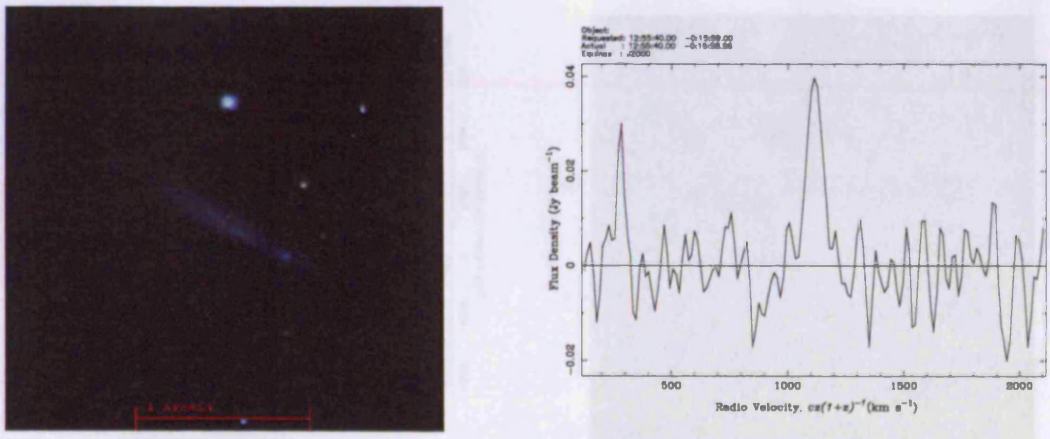

HIPEQ1255-00

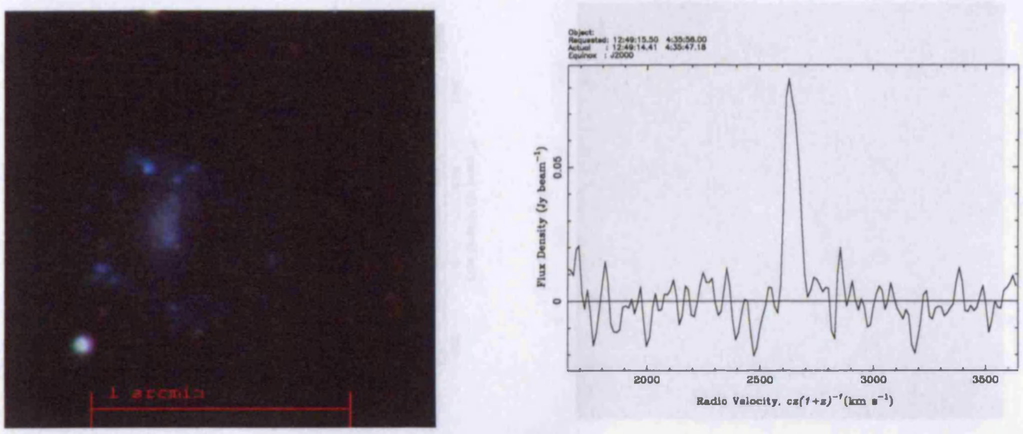

HIPEQ1249+04

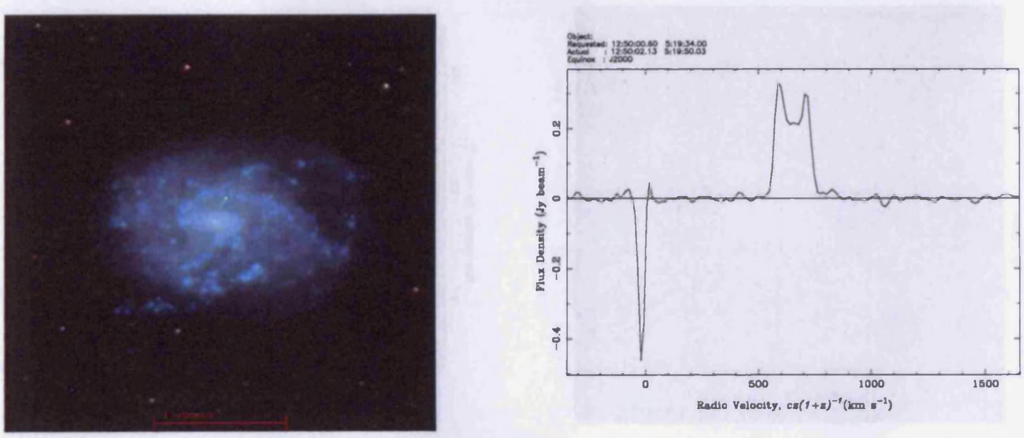

HIPEQ1250+05

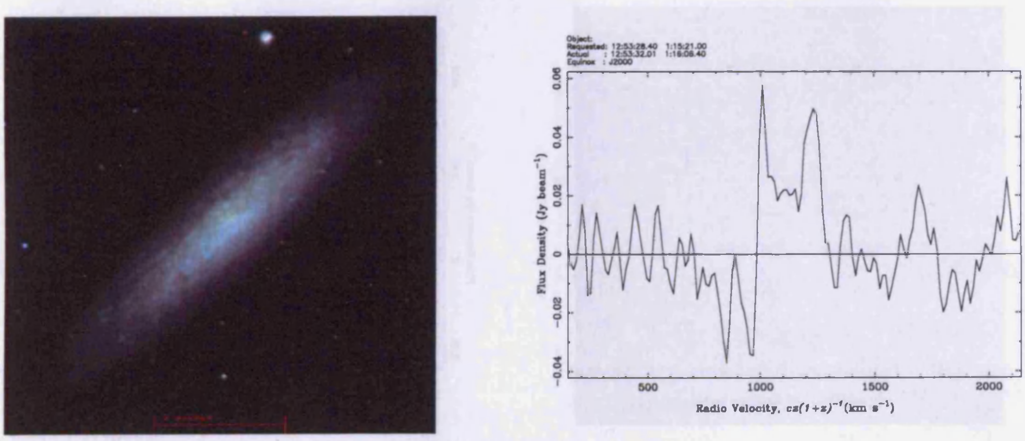

HIPEQ1253+01

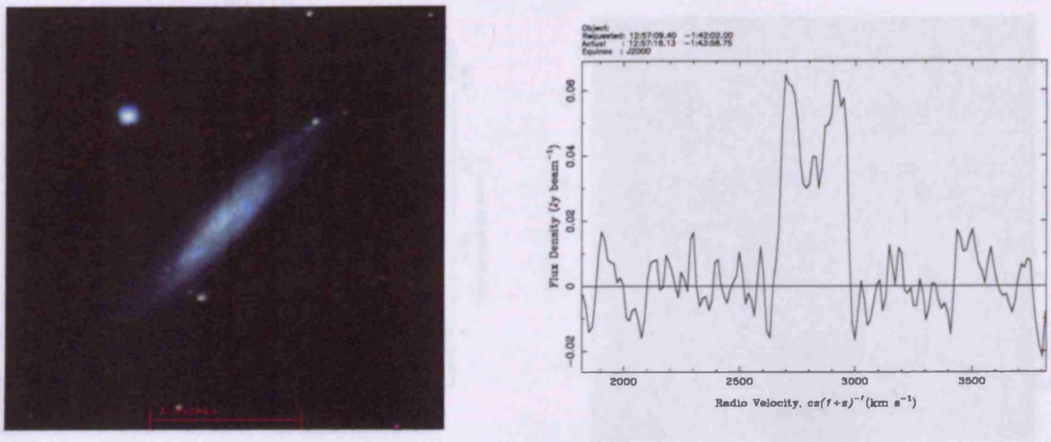

HIPEQ1257-01

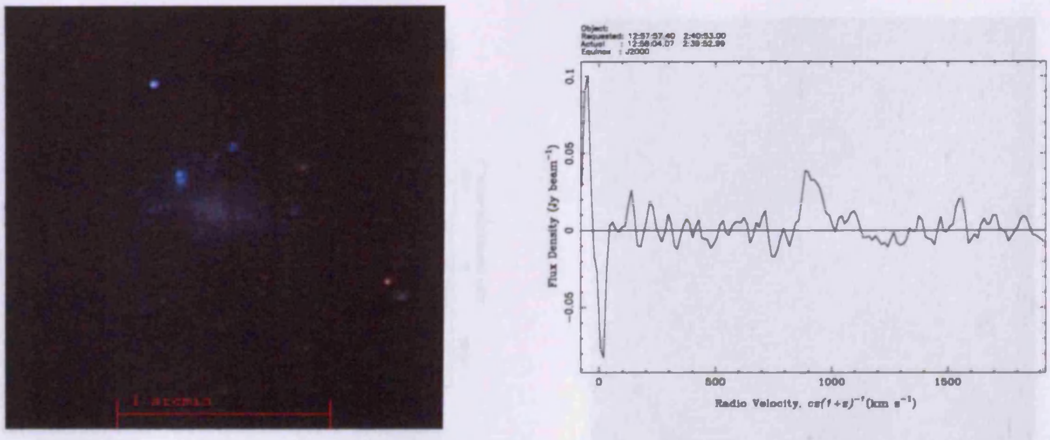

HIPEQ1257+02

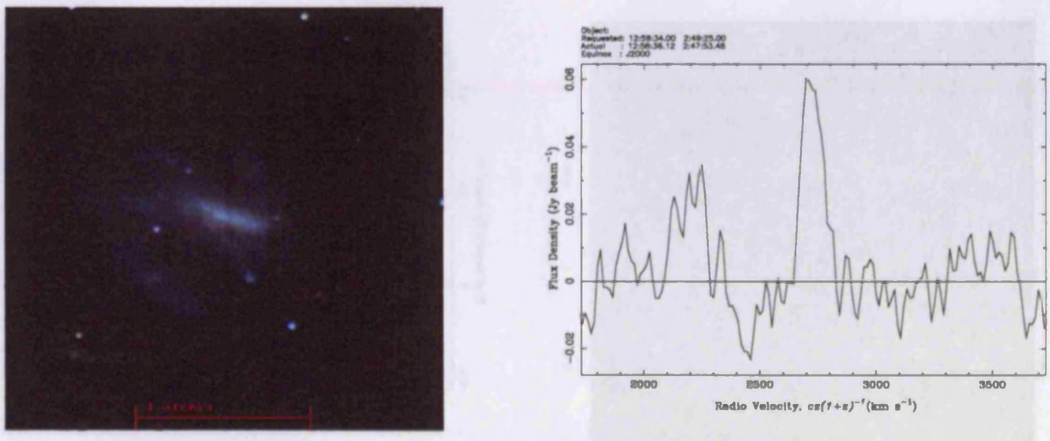

HIPEQ1258+02

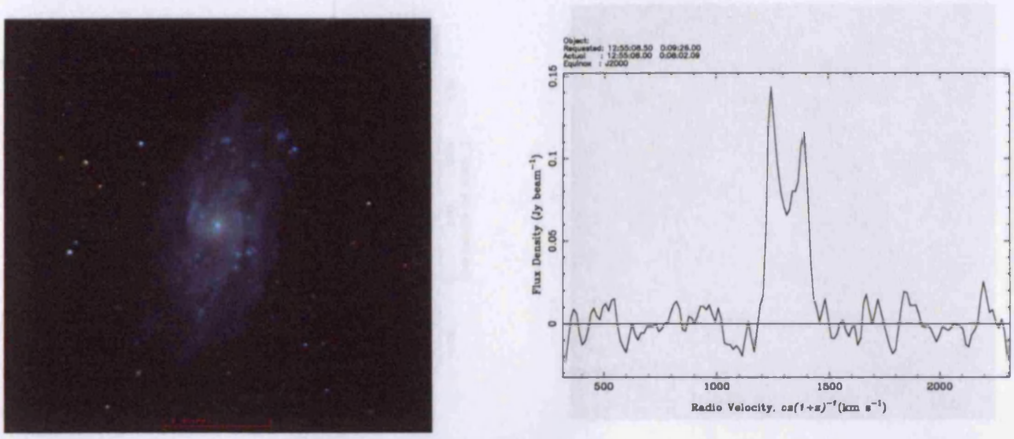

HIPEQ1255+00

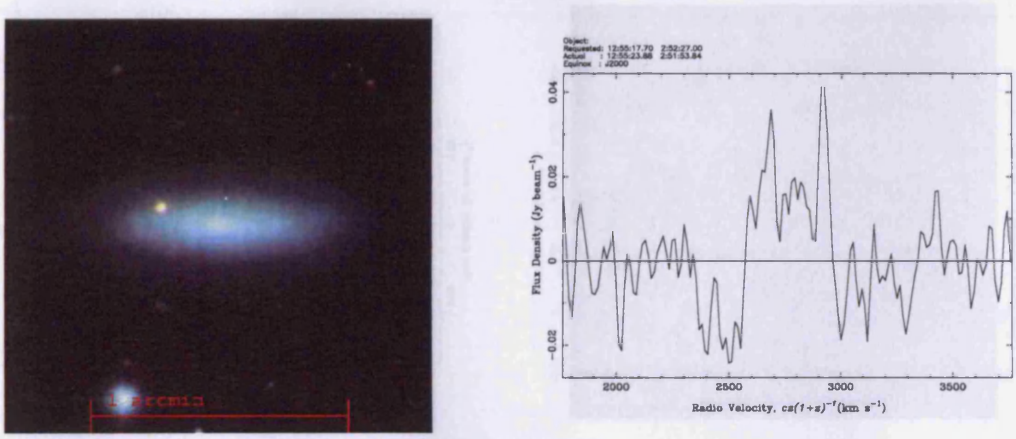

HIPEQ1255+02

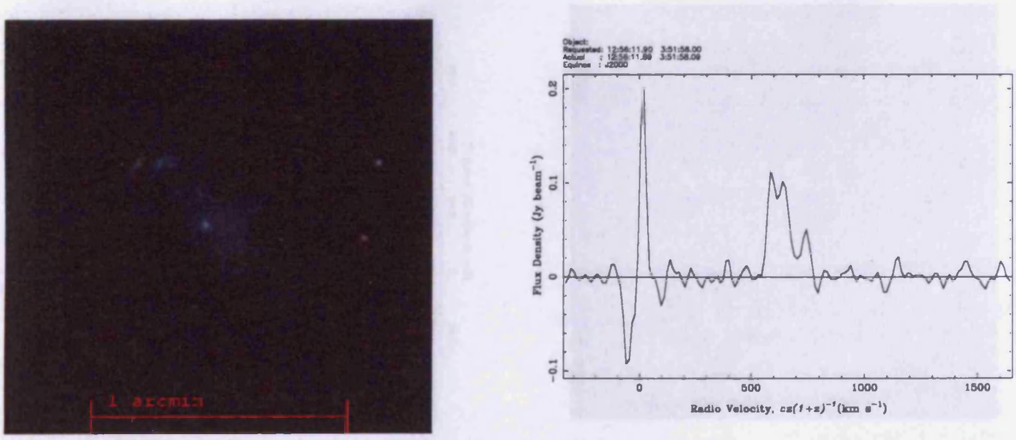

HIPEQ1256+03

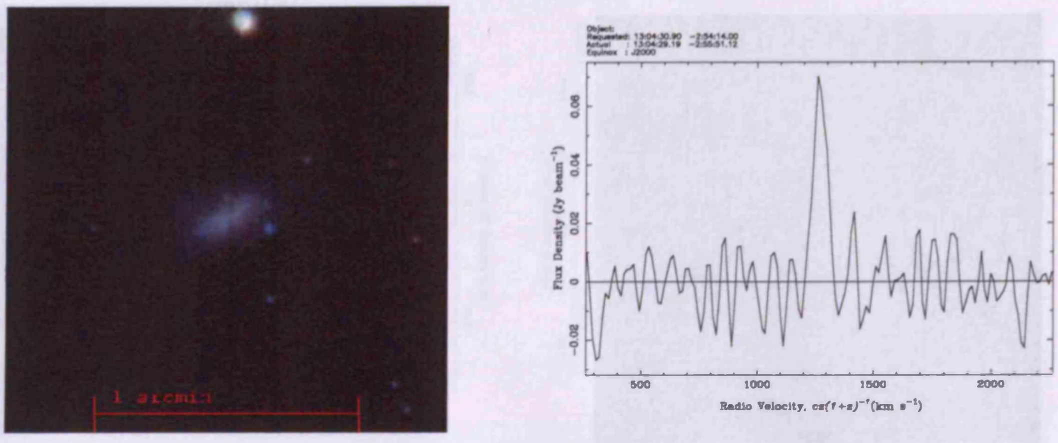

HIPEQ1304-02

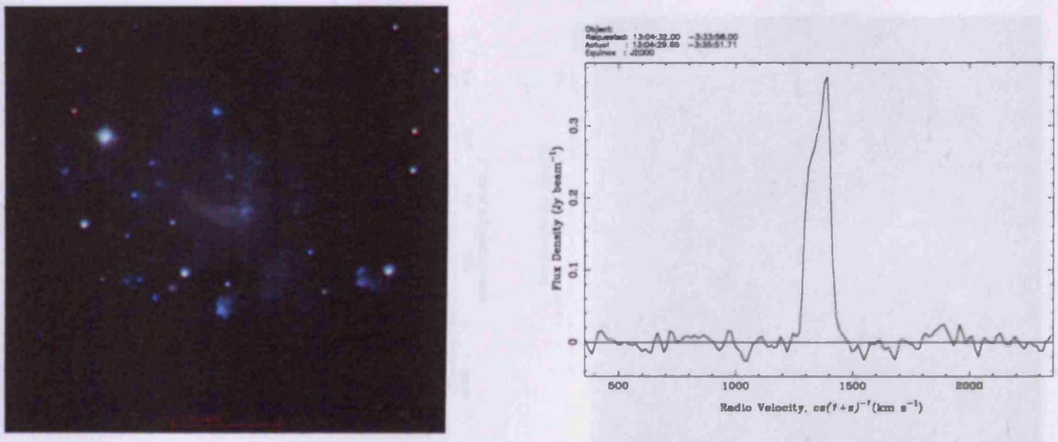

HIPEQ1304-03

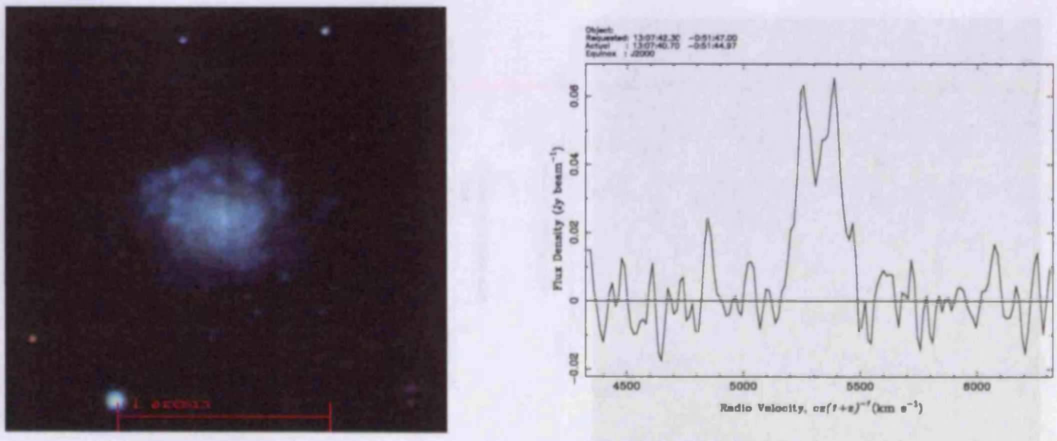

HIPEQ1307-00

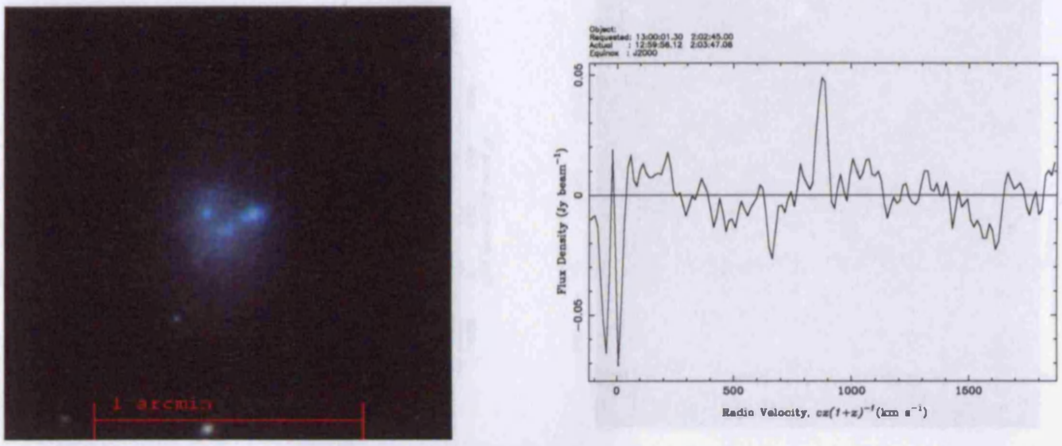

HIPEQ1300+02

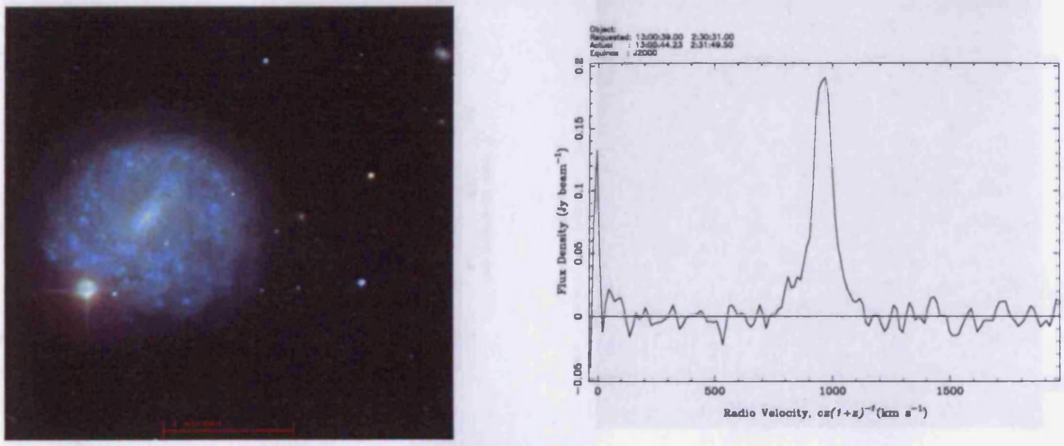

HIPEQ1300+02

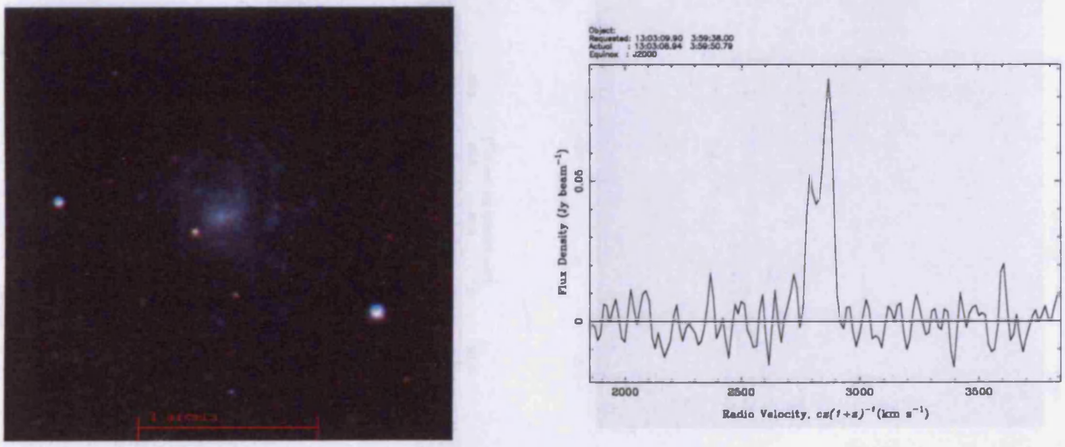

HIPEQ1303+03

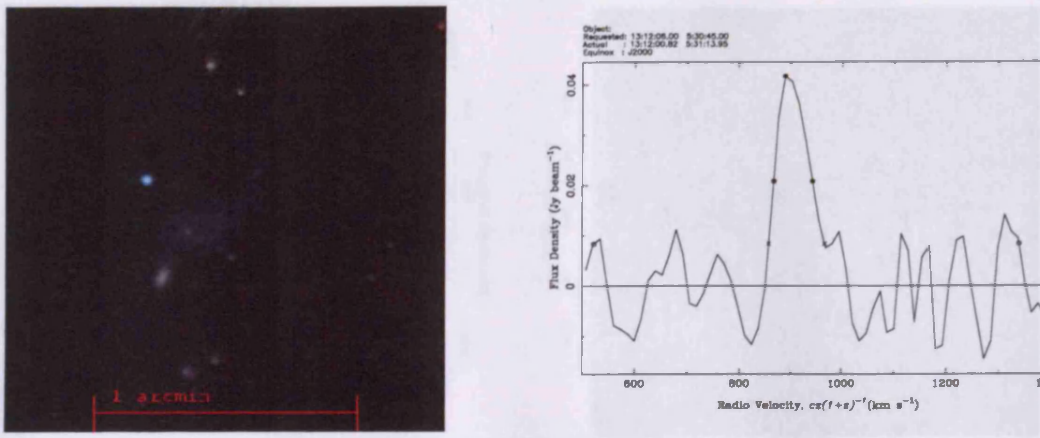

HIPEQ1312+05

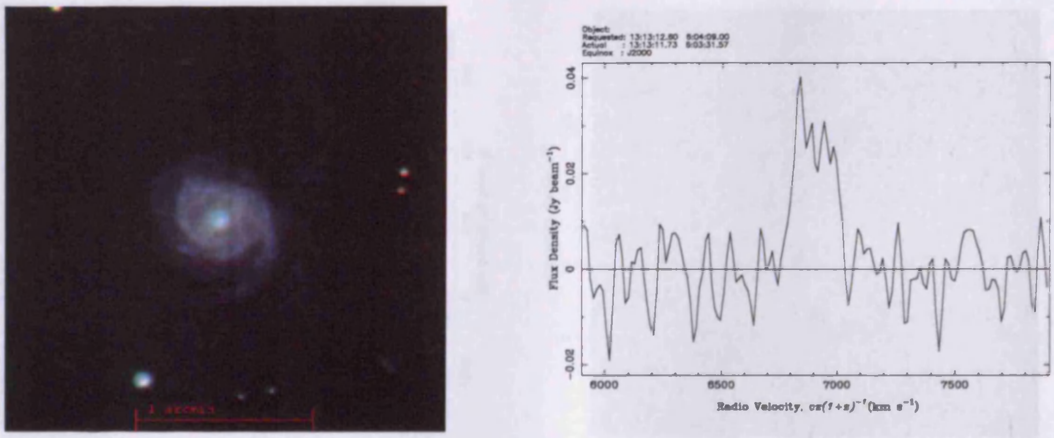

HIPEQ1313+06

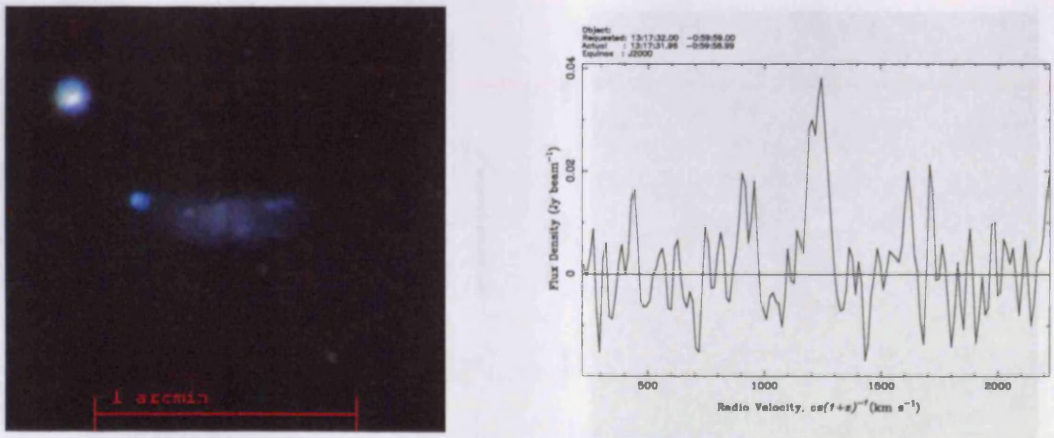

HIPEQ1317-00

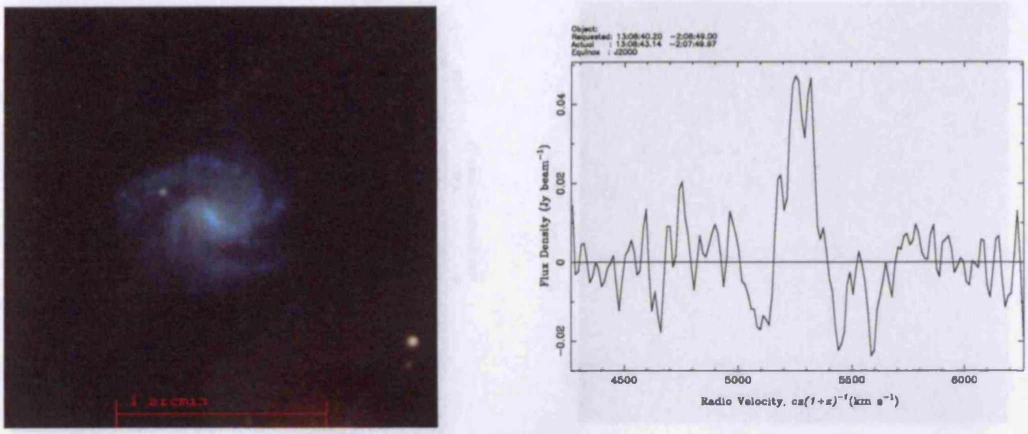

HIPEQ1308-02

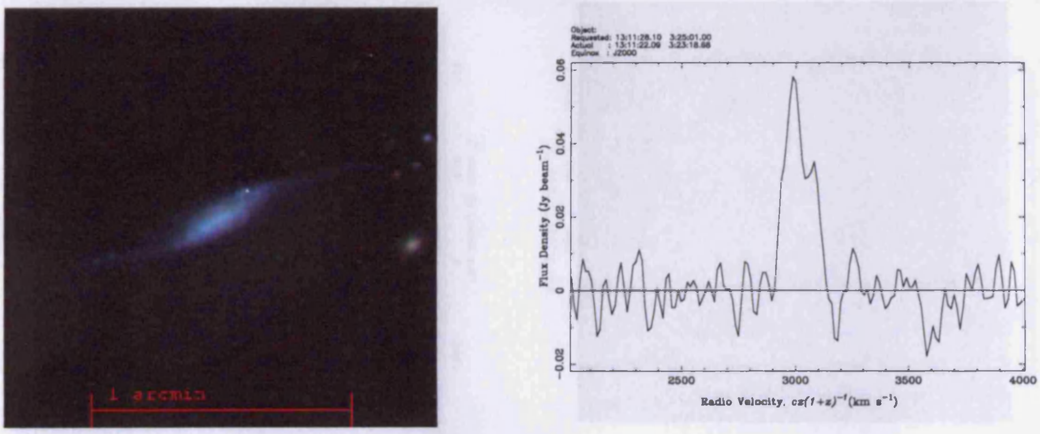

HIPEQ1311+03

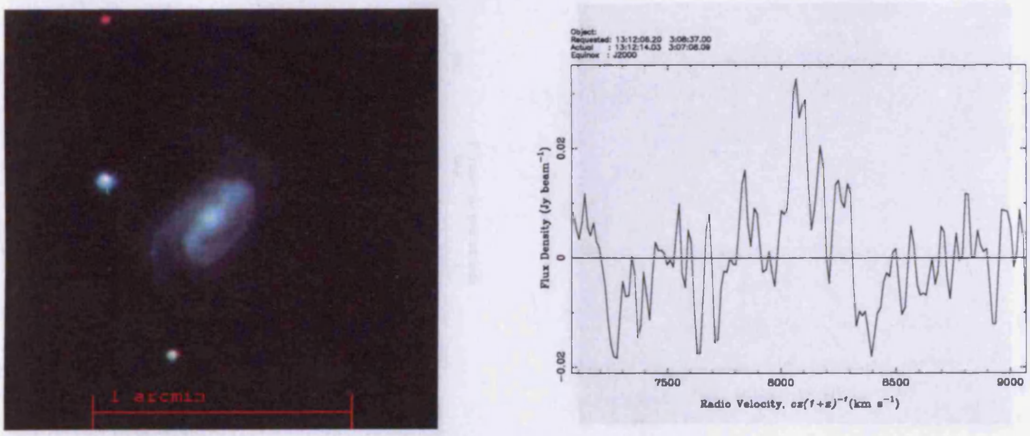

HIPEQ1312+03

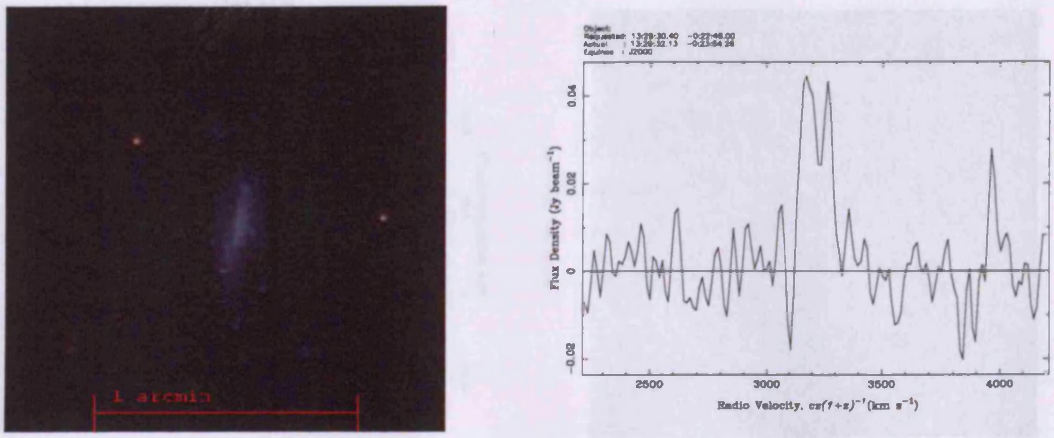

HIPEQ1329-00

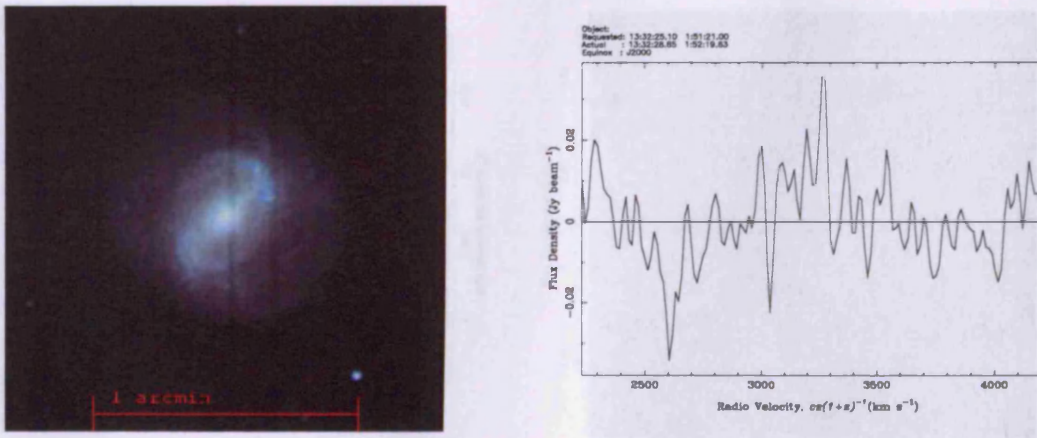

HIPEQ1332+01

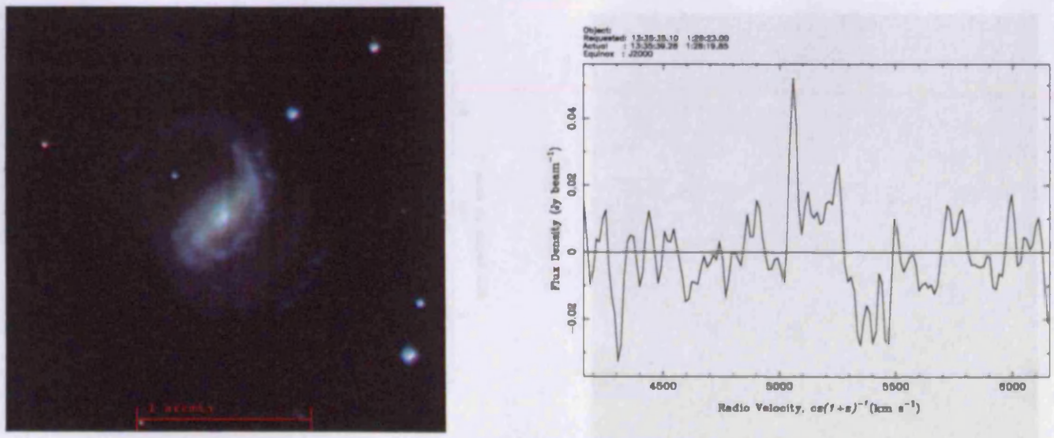

HIPEQ1335+01

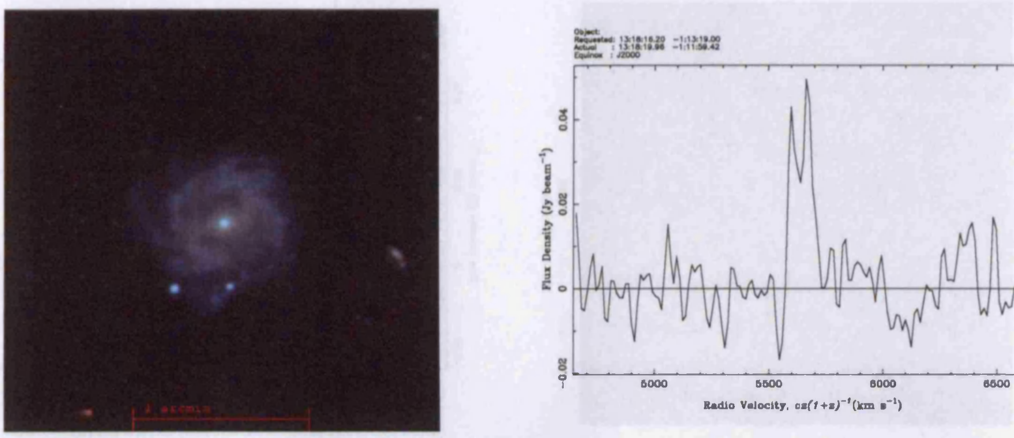

HIPEQ1318-01

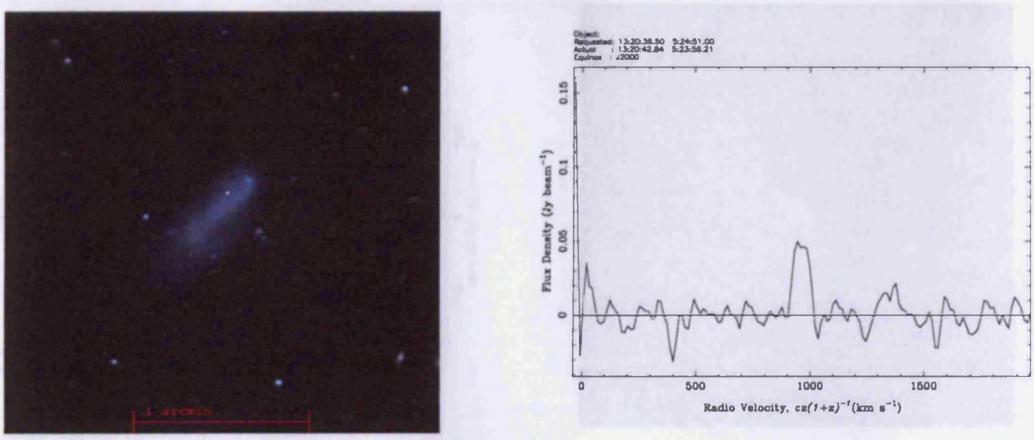

HIPEQ1320+05

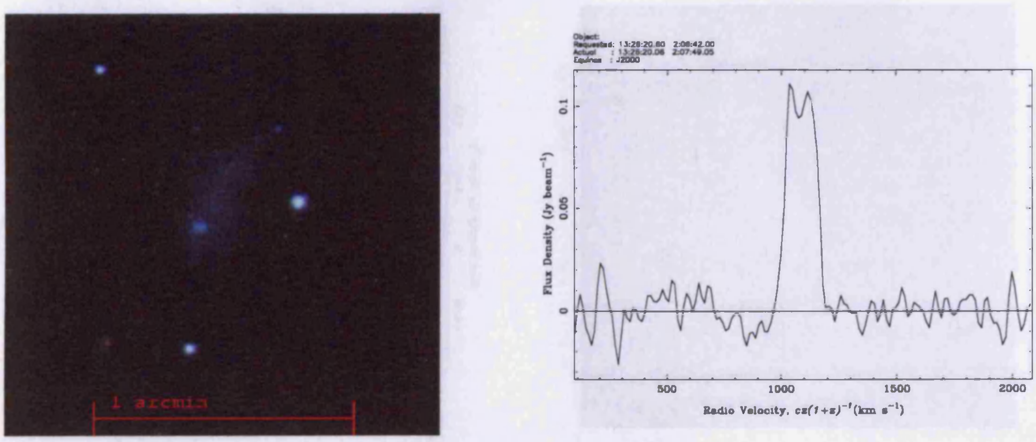

HIPEQ1327+02

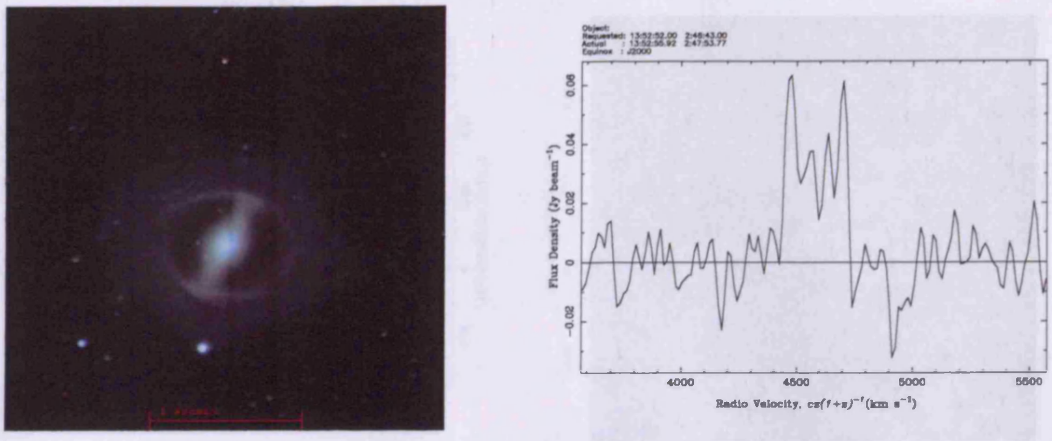

HIPEQ1352+02

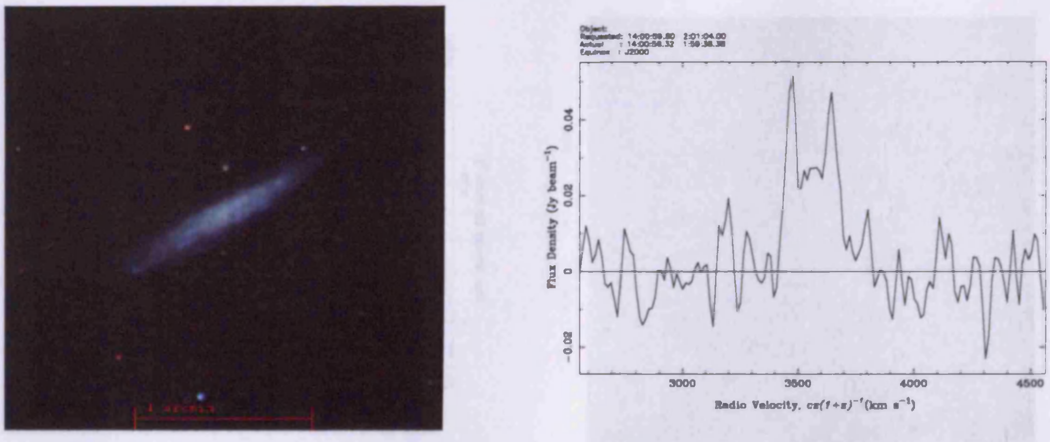

HIPEQ1400+02

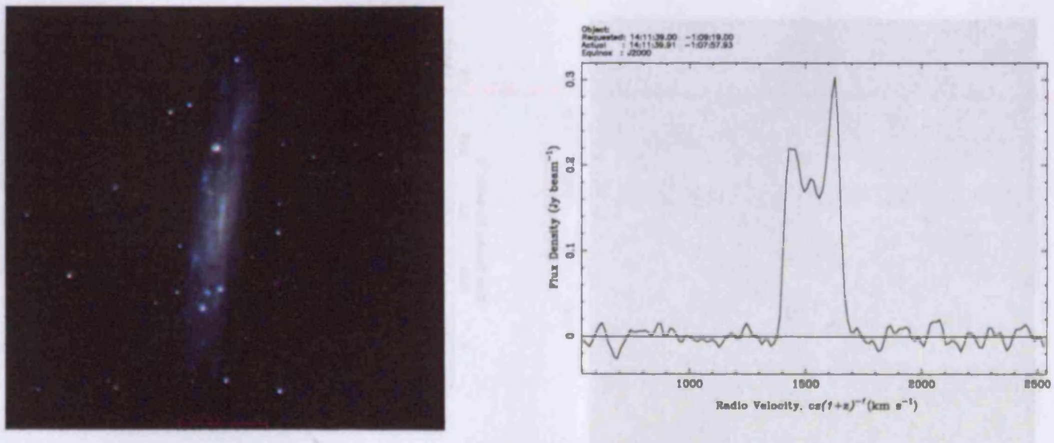

HIPEQ1411-01

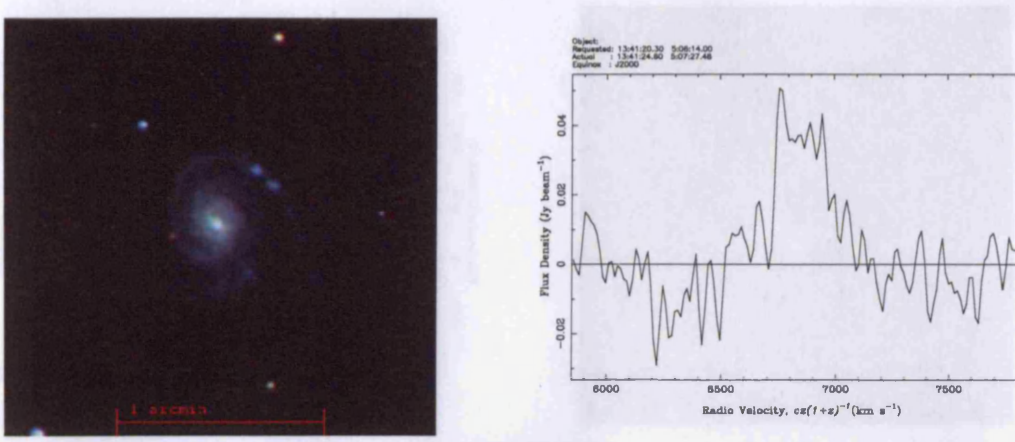

HIPEQ1341+05

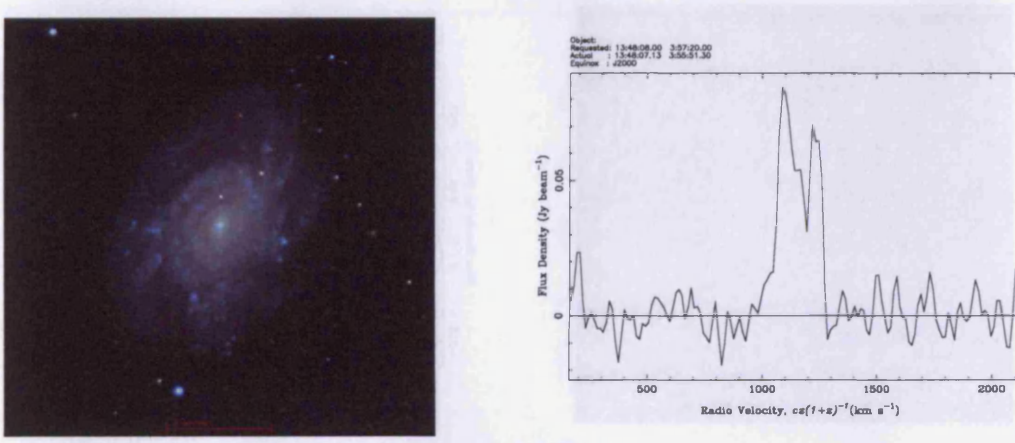

HIPEQ1348+03

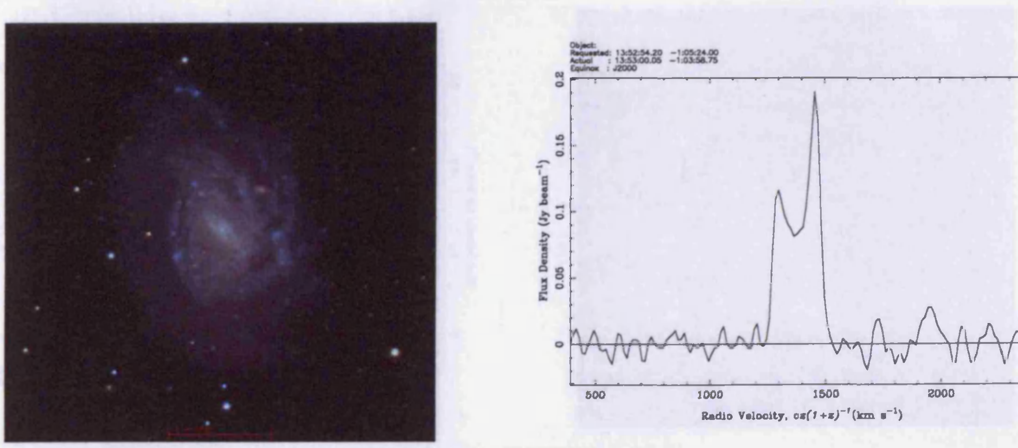

HIPEQ1352-01

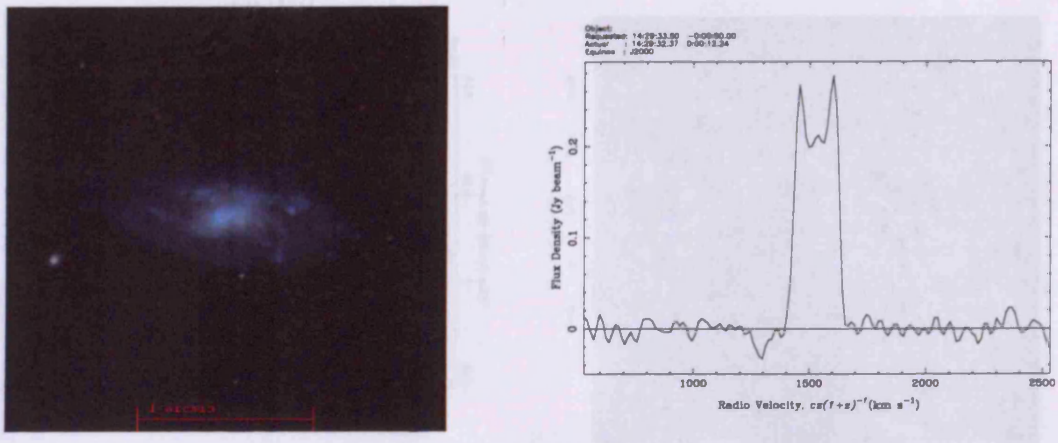

HIPEQ1429-00

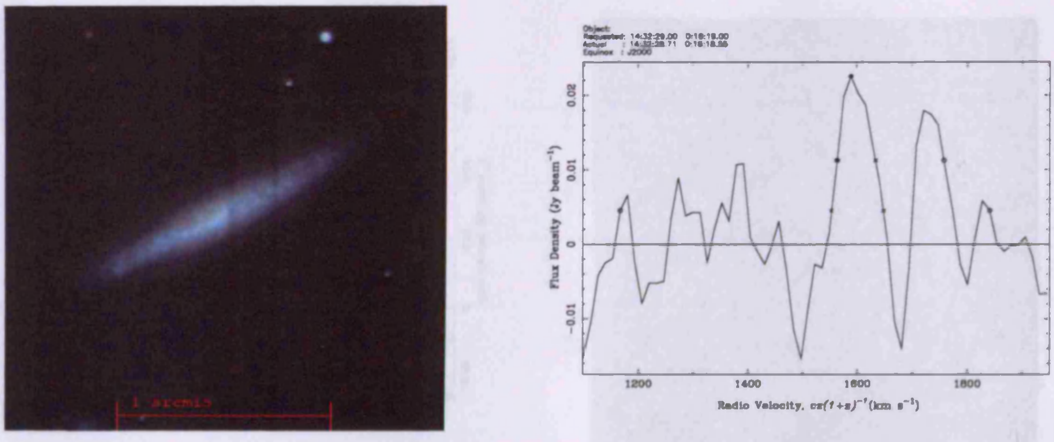

HIPEQ1432+00

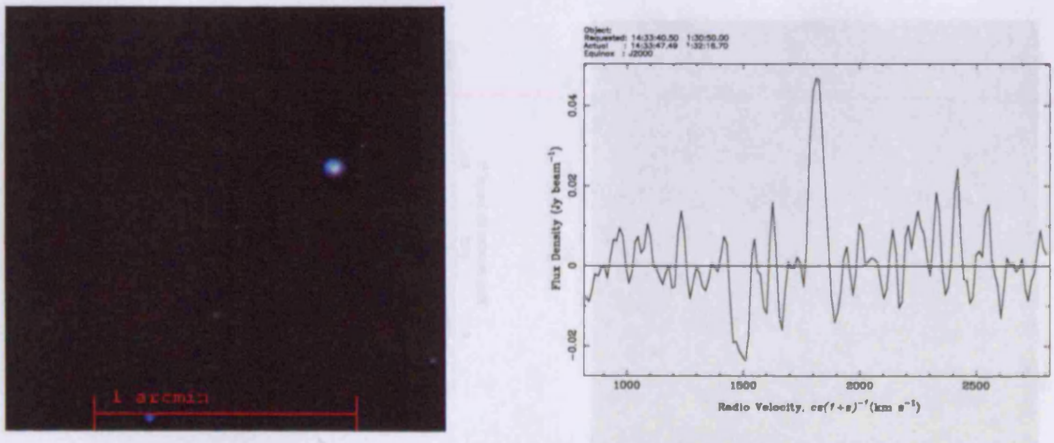

HIPEQ1433+01

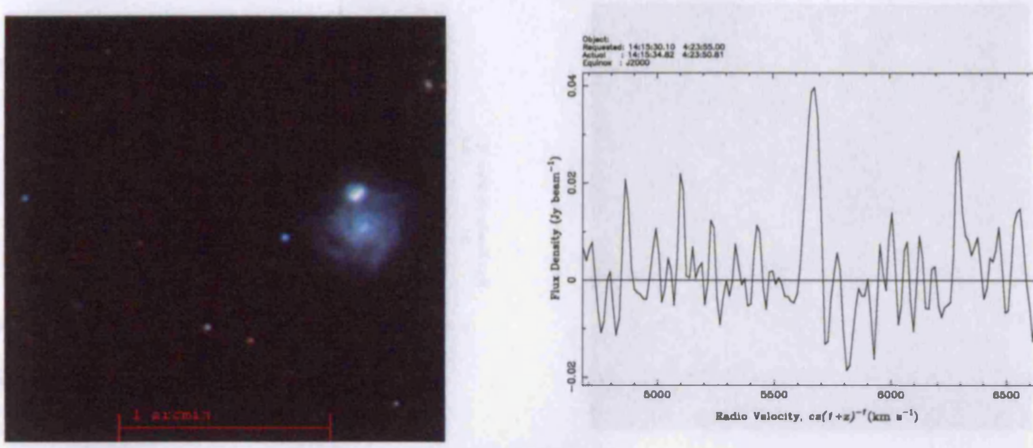

HIPEQ1415+04

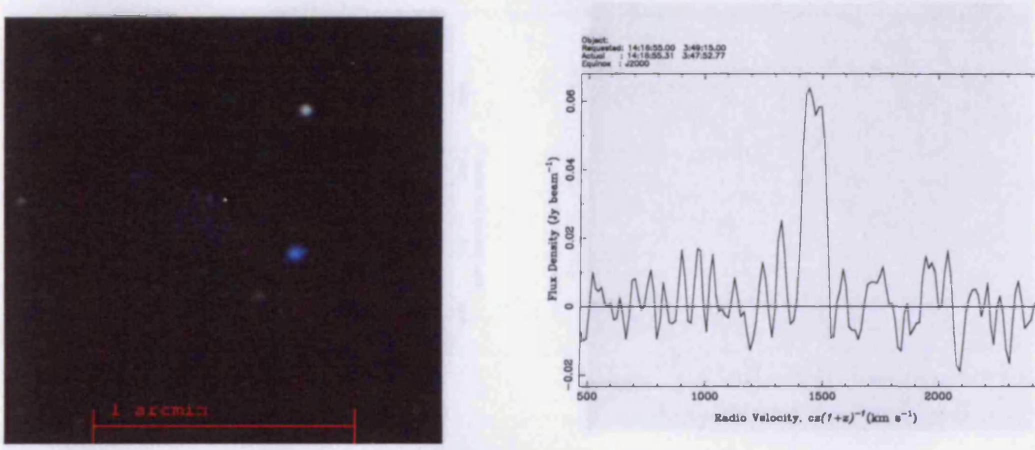

HIPEQ1416+03

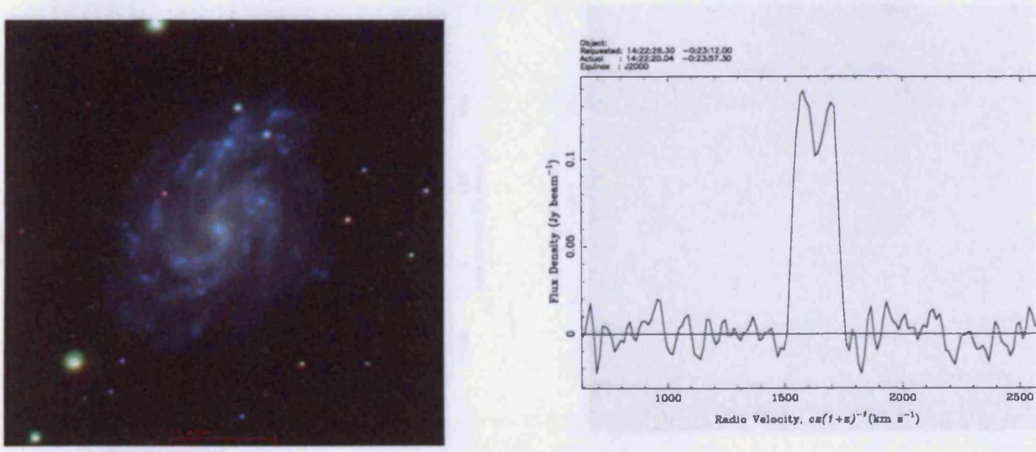

HIPEQ1422-00

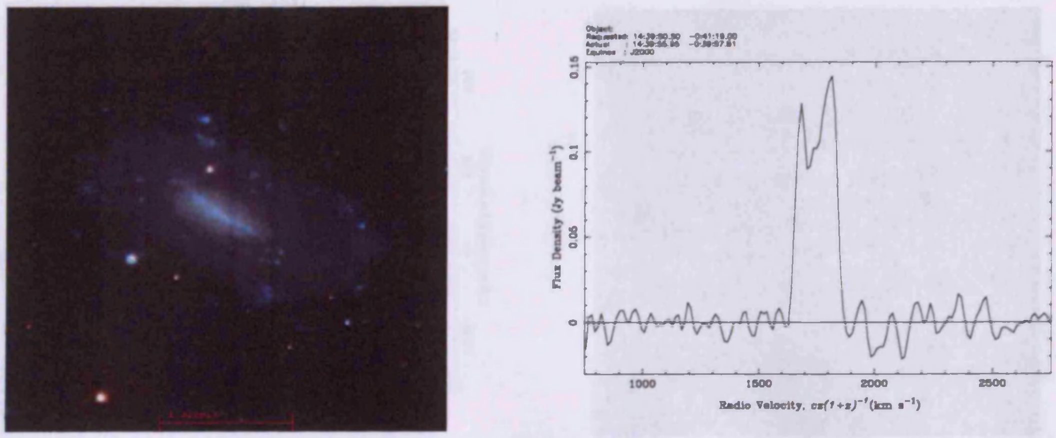

HIPEQ1439-00

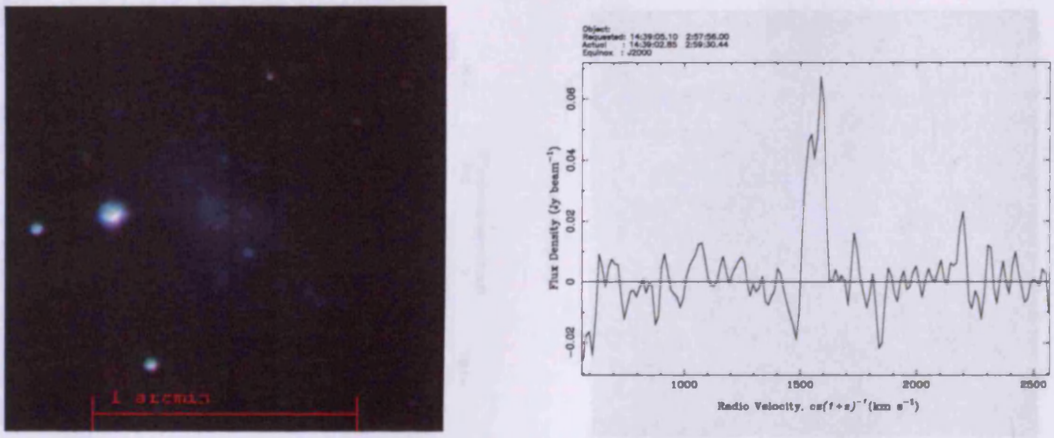

HIPEQ1439+02

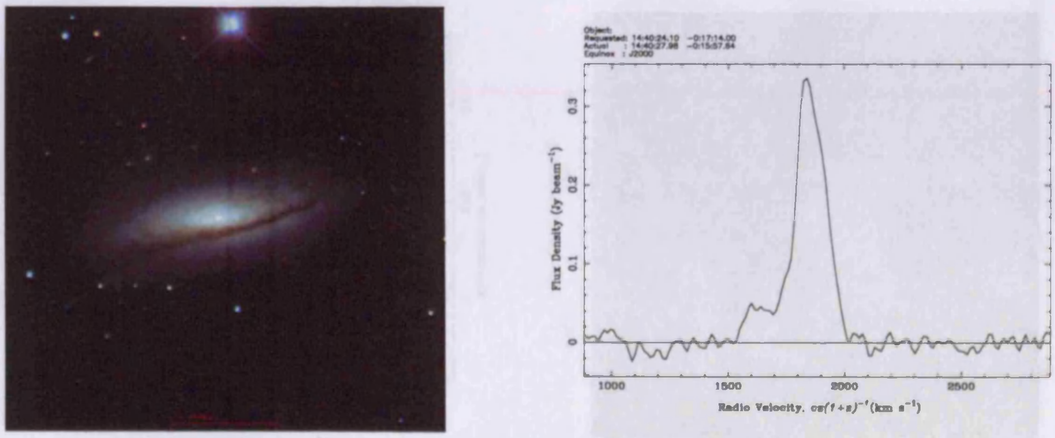

HIPEQ1440-00

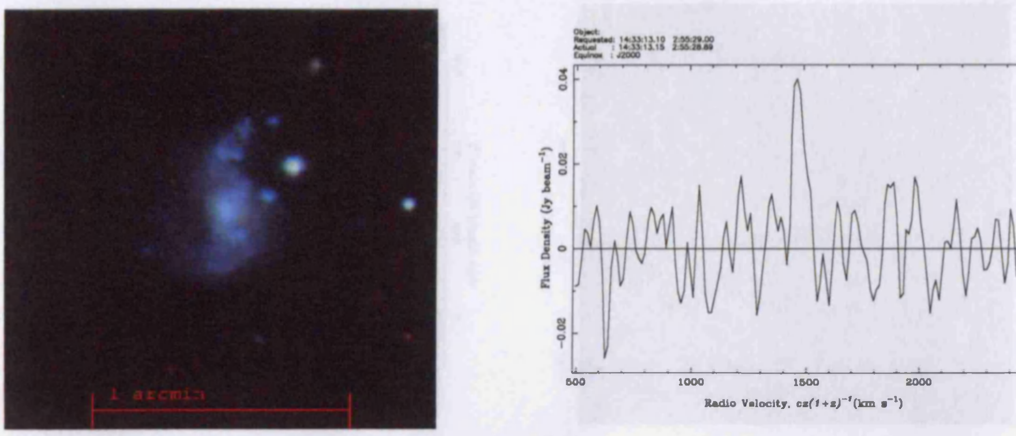

HIPEQ1433+02

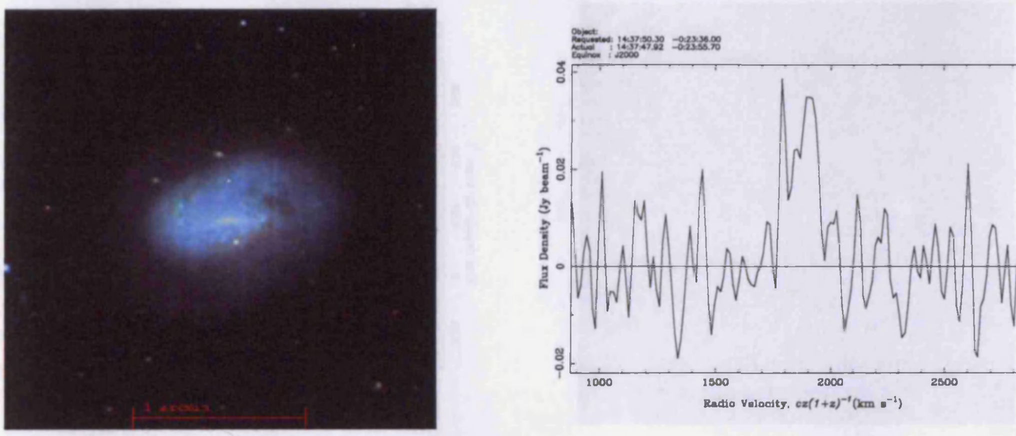

HIPEQ1437-00

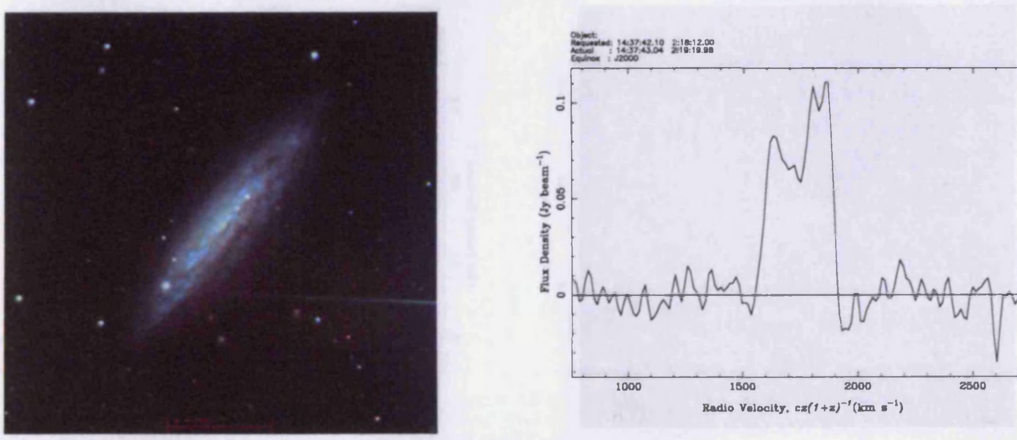

HIPEQ1437+02

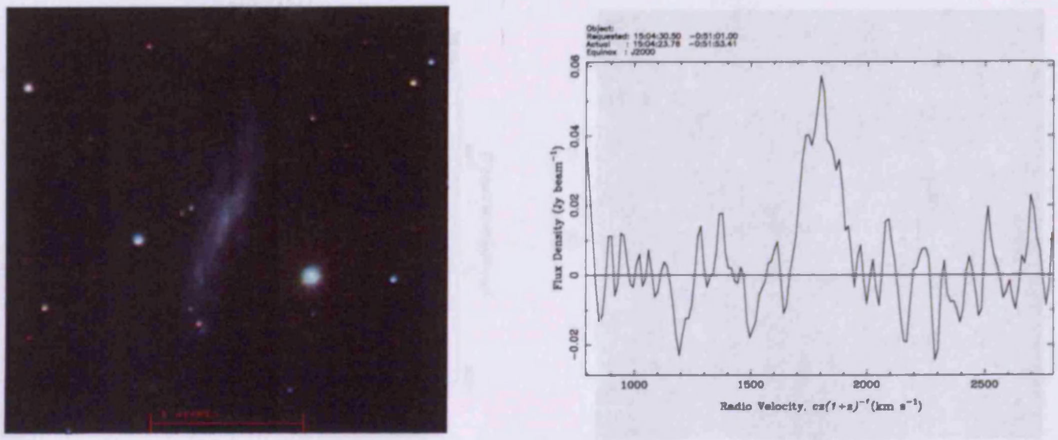

HIPEQ1504-00

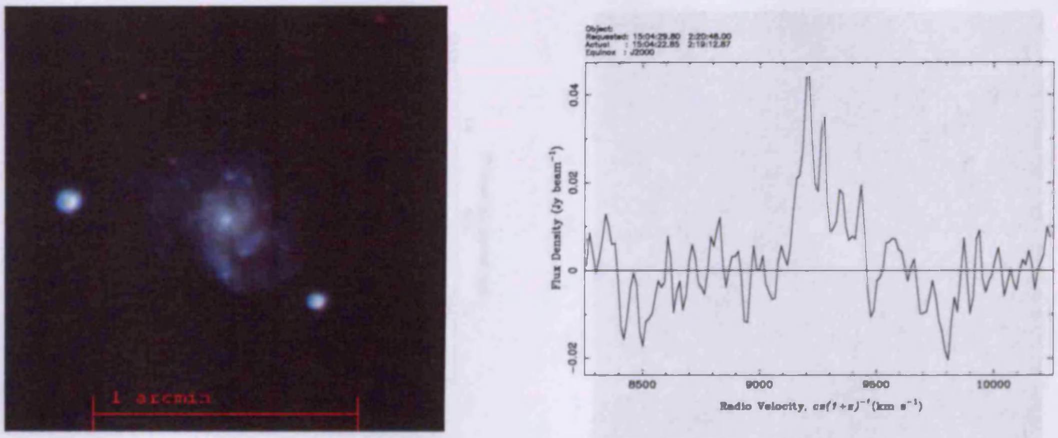

HIPEQ1504+02

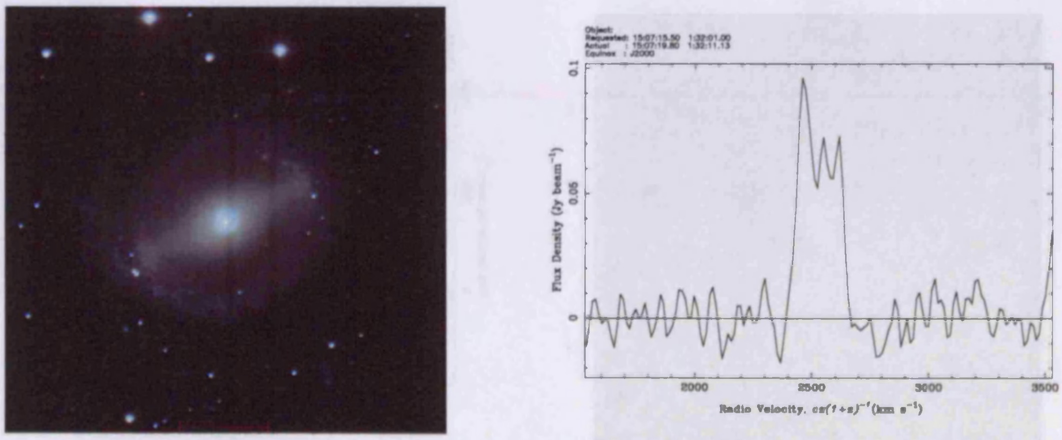

HIPEQ1507+01

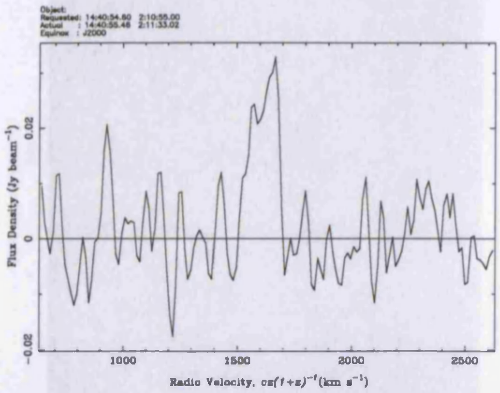

HIPEQ1440+02

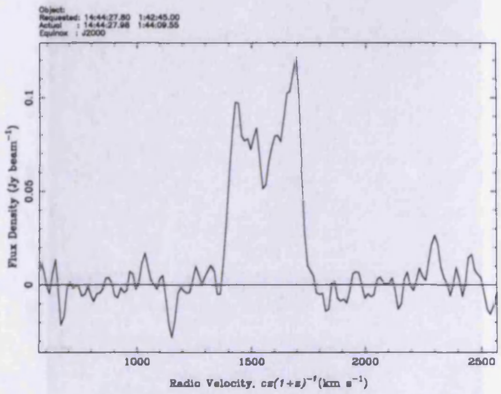

HIPEQ1444+01

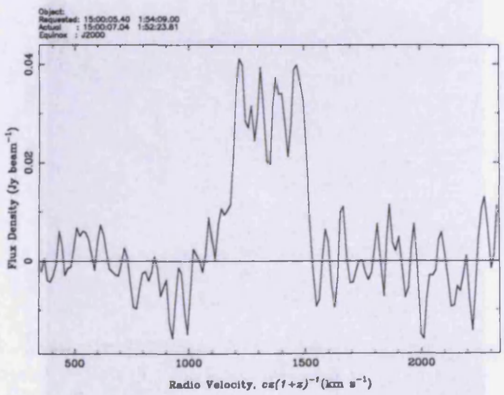

HIPEQ1500+01

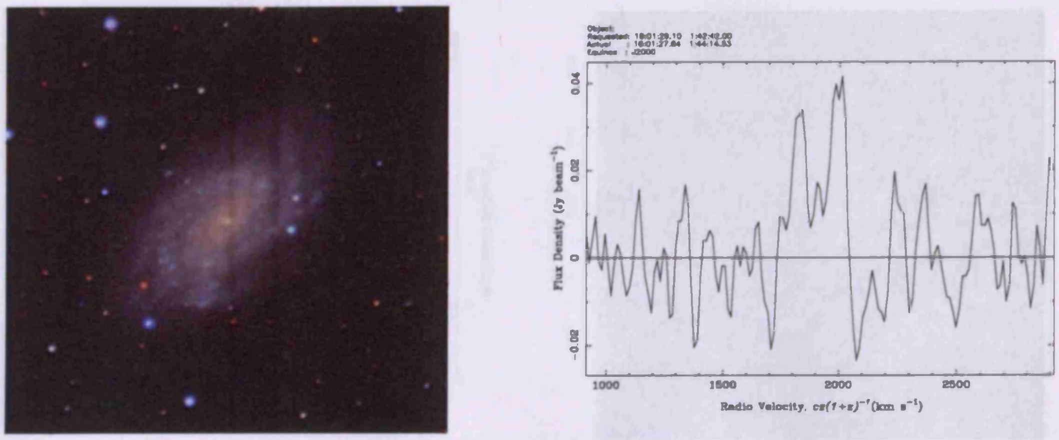

HIPEQ1601+01

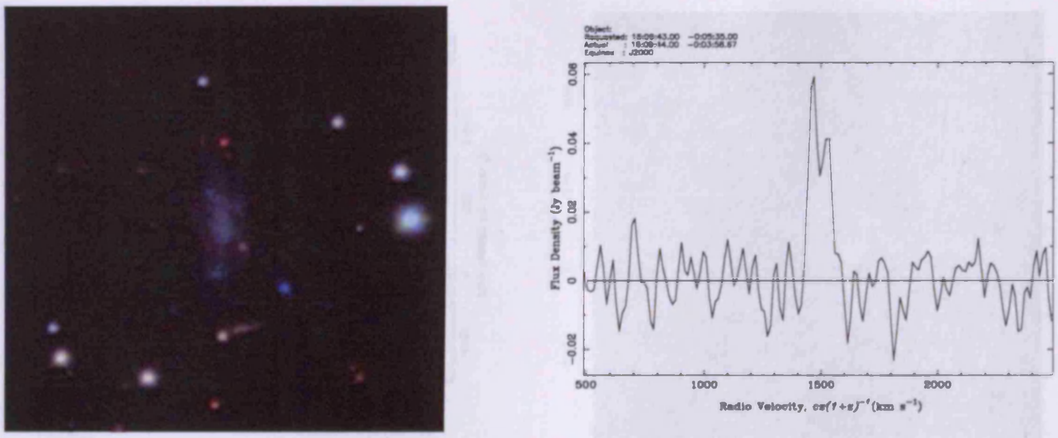

HIPEQ1609-00

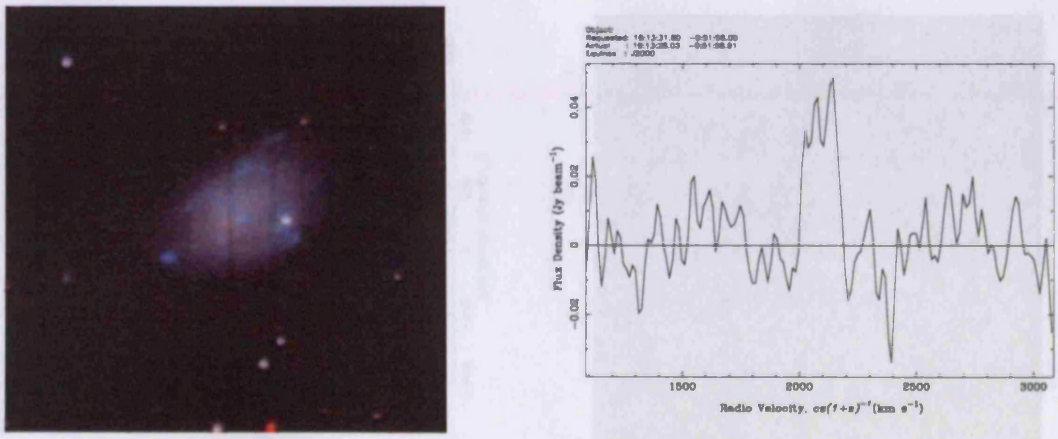

HIPEQ1613-00

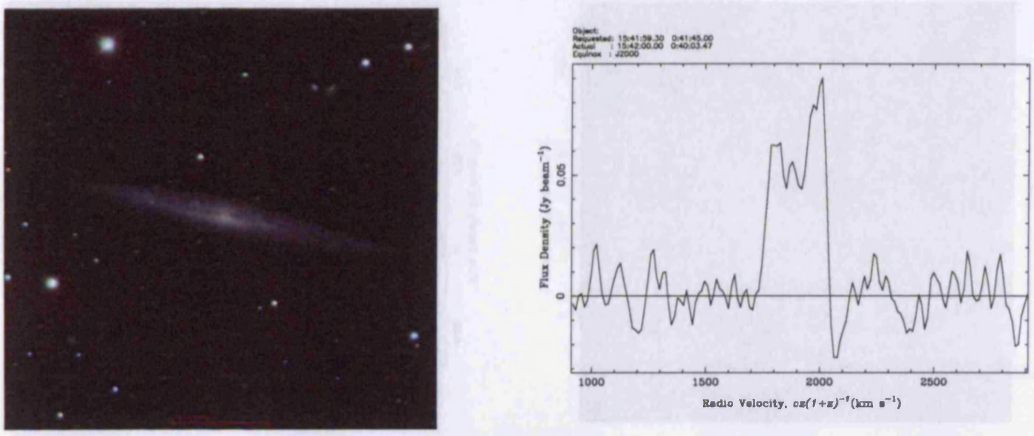

HIPEQ1542+00

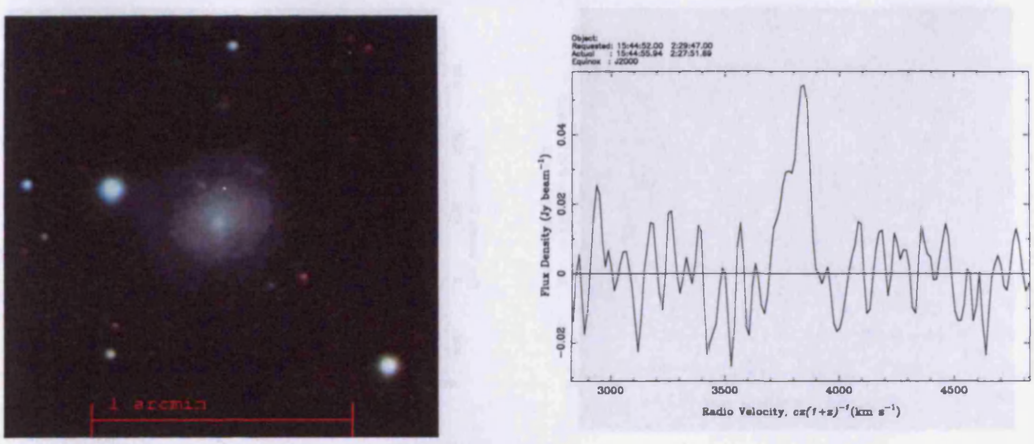

HIPEQ1544+02

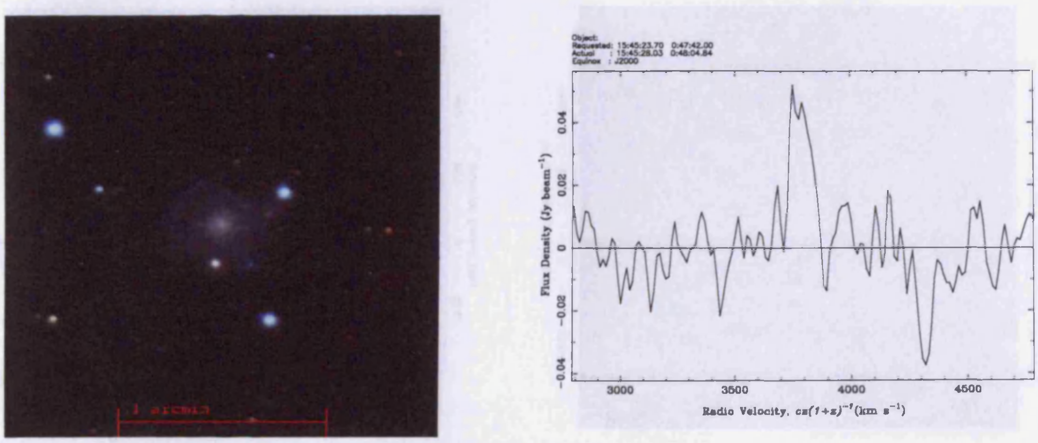

HIPEQ1545+00

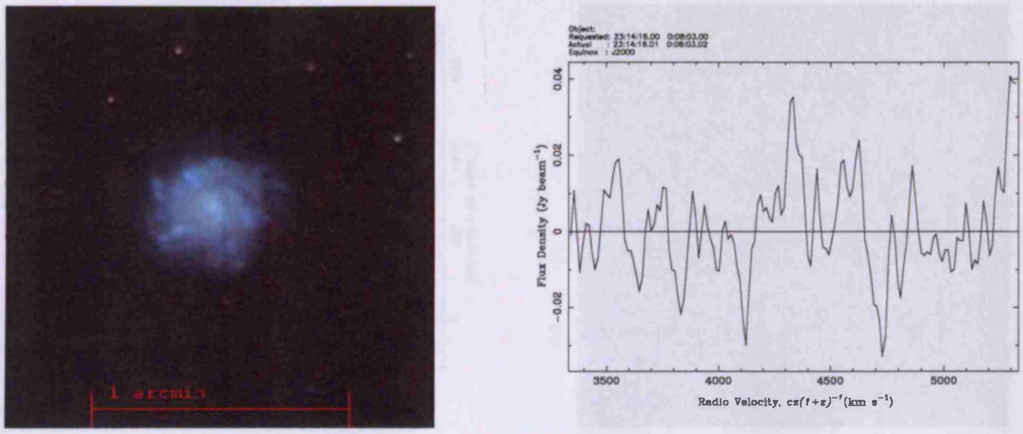

HIPEQ2314+00

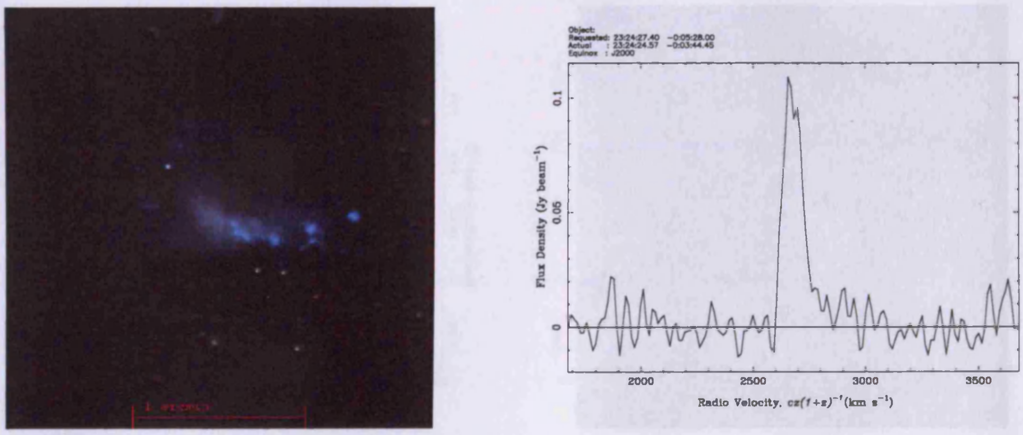

HIPEQ2324-00

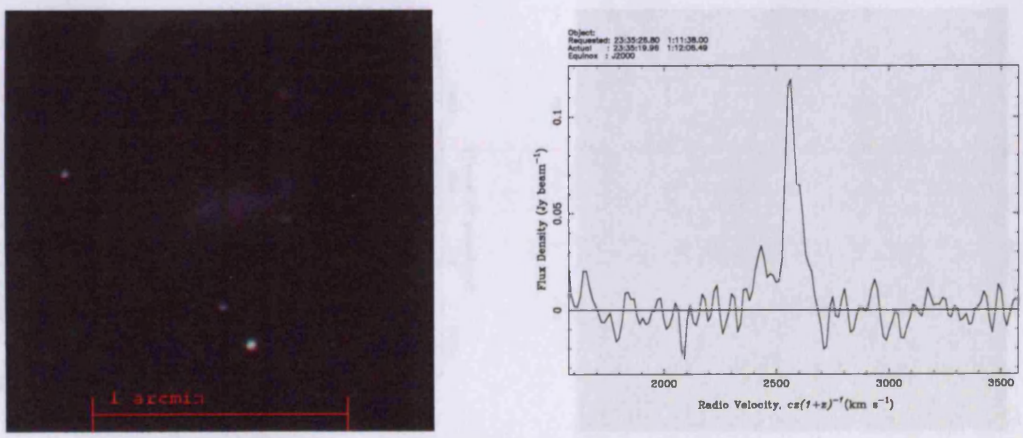

HIPEQ2335+01

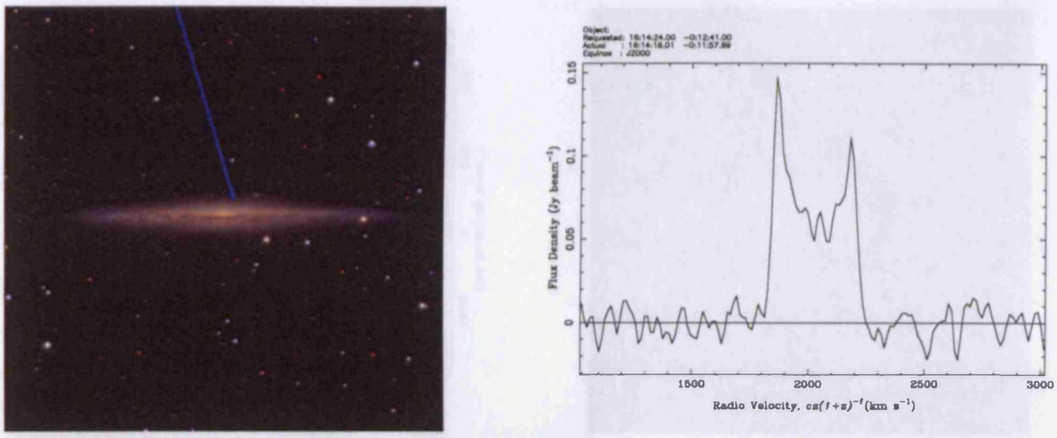

HIPEQ1614-00

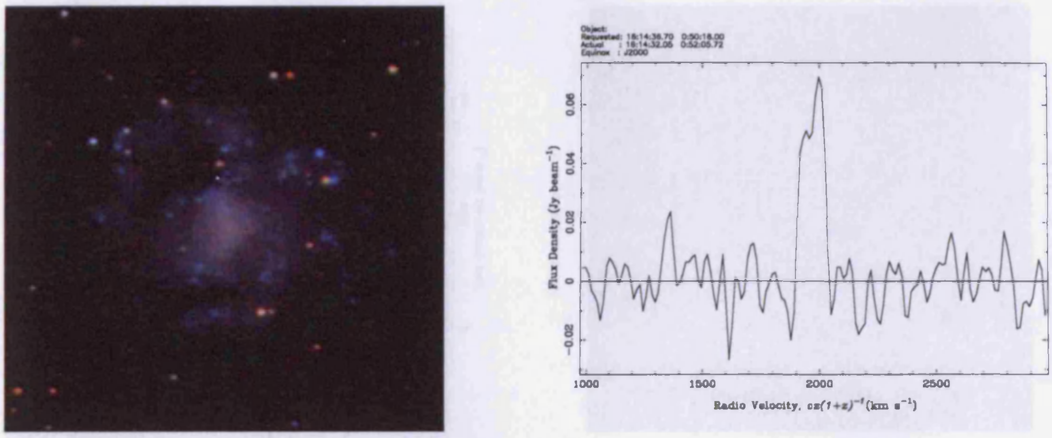

HIPEQ1614+00

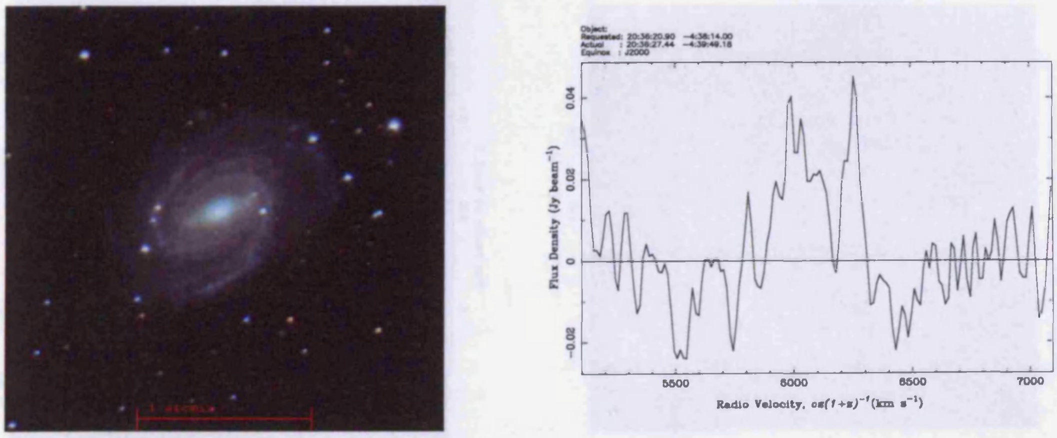

HIPEQ2036-04

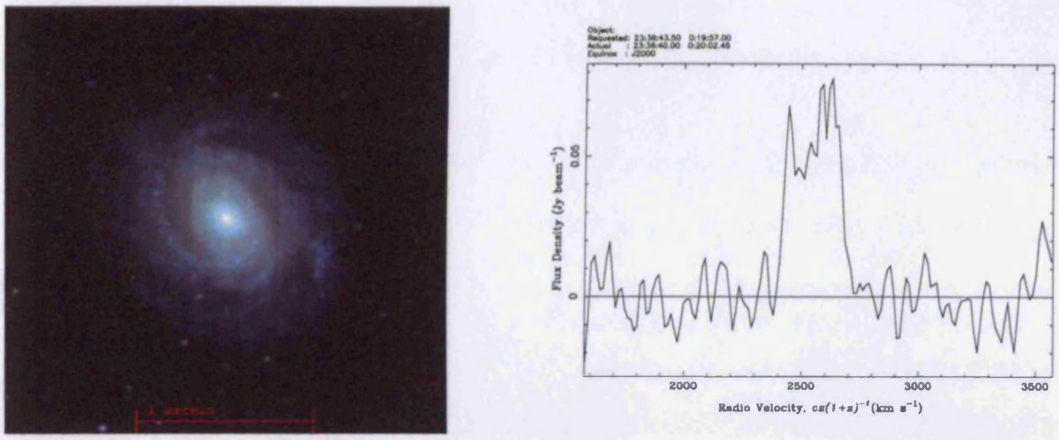

HIPEQ2336+00

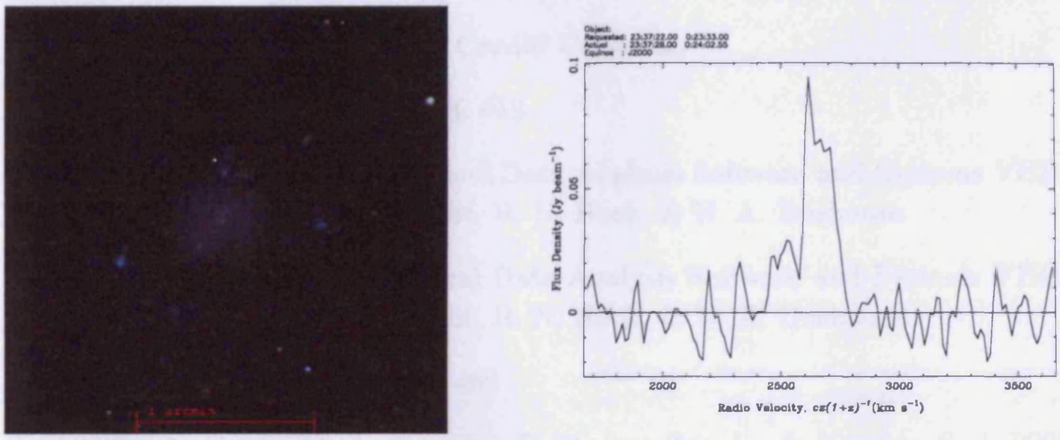

HIPEQ2337+00

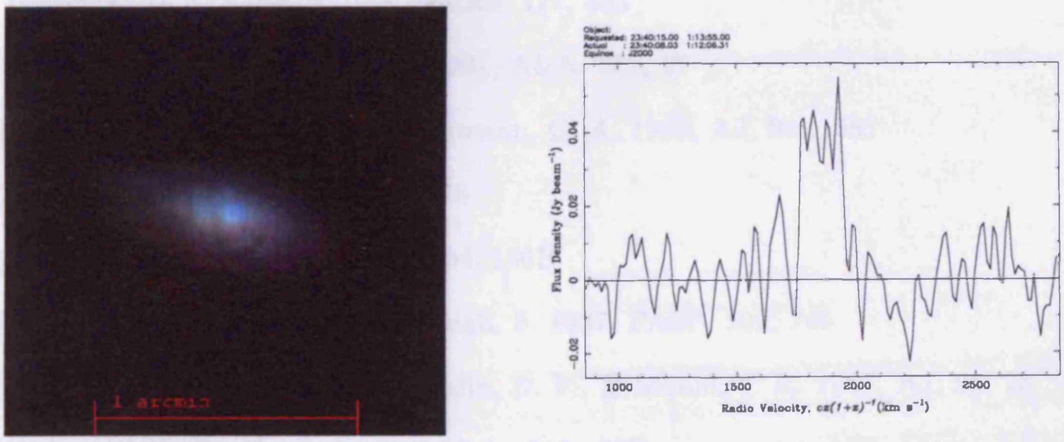

HIPEQ2340+01

Bibliography

[1] Allen, R. J. & Shu, F. H. 1979, ApJ, 227, 67

[2] Arp, H. 1965, ApJ, 142, 402

[3] Banks, G. D. 1998, Ph.D. Thesis, Cardiff University

[4] Banks, G. D. et al. 1999, ApJ, 524, 612

[5] Barnes, D. G. 1998, in 'Astronomical Data Analysis Software and Systems VIII', ASP Conf. Ser. 145, p32, eds. R. Albrecht, R. N. Hook, & H. A. Bushouse

[6] Barnes et al. 1998, in 'Astronomical Data Analysis Software and Systems VIII', ASP Conf. Ser. 145, p89, eds. R. Albrecht, R. N. Hook, & H. A. Bushouse.

[7] Barnes et al. 2001, MNRAS, 322, 486

[8] Barton, E. J., Geller, M. J., Bromley, B. C., van Zee, L., & Kenyon, S. J. 2001, AJ, 121, 625

[9] Bertin, E. & Arnouts, S. 1996, A&AS, 117, 393

[10] Bingelli, B. & Cameron, L. M. 1991, A&A, 252, 27

[11] Bingelli, B., Sandage, A., & Tammann, G. A. 1985, AJ, 90, 1681

[12] Blanton et al. 2001, AJ, 121, 2358

[13] Blanton et al. 2003, 2003ApJ...594..186B

[14] Bothun, G., Impey, C., & McGaugh, S. 1997, PASP, 109, 745

[15] Bothun, G. D.. Impey, C. D., Malin, D. F., & Mould, J. R. 1987, AJ, 94, 23

[16] Boyce, P. J., Phillipps, S., 1995A&A...296...26B

[17] Briggs, F. H. & Rao, S. 1993, ApJ, 417, 494

[18] Cawson, M. G. M., Kibblewhite, E. J., Disney, M.J., Phillipps, S. 1987, MNRAS 224, 557

[19] Cayatte, V., Kotanyl, C., Balkowski, C., van Gorkom, J.H. 1994, AJ, 107, 1003

[20] Colgan, S. W. J., Salpeter, E. E., & Terzian, Y. 1990, ApJ, 351, 503

[21] Corbelli, E. & Salpeter, E. E. 1993, ApJ, 419, 104

[22] Corbelli, E., Schneider, S. E., & Salpeter, E. E. 1989, AJ 97, 390

[23] Côté, S., Freeman, K. C., Carignan, C., & Quinn, P.J. 1997, AJ, 114, 1313

[24] Courteau, S. 1997, AJ, 114, 2402

[25] Cross, N. J. G., Driver, S. P., Lemon, D. J., Liske, J., Couch, W. J. 2002AAS...200.4006C

[26] Dalcanton, J. J., Spergel, D. N., Gunn, J. E., Schmidt, M., Schneider, D. Pl 1997, AJ, 114, 1447

[27] Davies, J. I. 1990, MNRAS, 244, 8

[28] Davies, J. I., Phillipps, S., & Disney, M. J. 1989a, MNRAS, 239, 703

[29] Davies, J. I., Phillipps, S., & Disney, M. J. 1989b, Ap&SS, 157, 299

[30] Davies, J. I., Disney, M. J., Phillipps, S., Boylce, B. J., & Couch, W. J. 1994, MNRAS, 269, 349

[31] da Costa, L. N., Numes, M. A., Pellegrini, P. S., Willmer, C., Chincarini, G., & Cowan, J. J. 1986, AJ, 91, 6

[32] da Costa, L. N., Willmer, C., Pellegrini, P. S., & Chincarini, G. 1987, AJ, 93, 1338

[33] Dekel, A. & Silk, J. 1986, ApJ, 303, 39

[34] de Blok, W. J. G., McGaugh, S. S., & van der Hulst, J. M.. 1996, MNRAS, 283, 18

[35] de Blok, W. J. G. & van der Hulst, J. M. 1998a, A&A, 335, 421

[36] de Blok, W. J. G. & van der Hulst, J. M. 1998b, A&A, 336, 49

[37] de Blok, W. J. G., van der Hulst, J. M., & Bothun, G. D. 1995, MNRAS, 274, 235

[38] de Jong, R. S. 1996a, A&AS, 118, 557

[39] de Jong, R. S. 1996b, A&A, 313, 45

[40] de Jong, R. S. 1996c, A&A, 313 377

[41] de Jong, R. S. & Lavey, C. 1999, Ap&SS, 269, 569

[42] de Jong, R. S. & van der Kruit, P. C. 1994, A&AS, 106, 451

[43] de Souza. R. E., de Mello, D. F., & Dos Anjos, S. 1997, A&AS, 135, 329

[44] de Vaucouleurs, G. 1974, in "The Formation and Dynamics of Galaxies", IAU Symp. 58, pl, ed. J. R. Shakeshaft.

[45] de Vaucouleurs, G., de Vaucouleurs, A., & Corwin, H. G. 1976 (RC2), "Second Bibitem Catalogue of Bright Galaxies", publ. University of Texas Press, Austin, US.

[46] de Vaucouleurs, G., de Vaucouleurs, A., Corwin, H. G., Jr., Buta, R. J., Paturel, G., & Fouqué, P. 1991 (RC3) "Third Bibitem Catalogue of Bright Galaxies", vols 1-3, publ. Springer-Verlag, New York, US.

[47] Disney, M. J., 1976, Nature, 263, 573

[48] Disney, M. J. & Banks, G. D. 1997, PASA, 14, 69

[49] Disney, M. J. & Phillipps, S. 1983 (DP 83), MNRAS, 205, 1253

[50] Disney, M. J., Phillipps, S., Davies, J. I., Cawson, M. G. M., & Kibblewhite, E. J. 1990, MNRAS, 245, 175

[51] Doyle, M. T., Drinkwater, M. J., Rohde, D. J., Pimbblet, K. A., Read, M., Meyer, M. J., Zwaan, M. A., Ryan-Weber, E., Stevens, J., **Garcia-Appadoo, D.A.**, and 31 coauthors, MmRAS, 361, 34D

[52] Dressler, A. 1991, ApJS, 75, 241

[53] Dreyer, J. L. E. 1888 (NGC), MmRAS, 49, 1

[54] Dreyer, J. L. E. 1895 (IC, Part 1), MmRAS, 51, 185

[55] Dreyer, J. L. E. 1908 (IC, Part 2), MmRAS, 59, 105

[56] Drinkwater, M. J., Phillipps, S., Gregg, M. D., Parker, Q. A., Smith, R. M., Davies, J. I., Jones, J. B., Sadler, & E. M. 1999, ApJ, 511, 97

[57] Drinkwater, M. J., Phillipps, S., Jones, J. B., Gregg, M. D., Dady, J. H., Davies, J. I., Parker, Q. A., Sadler, E. M., & Smith, R. M. 2000, A&A, 355, 900

[58] Driver, S. P. 1994, Ph.D. Thesis, Cardiff University

[59] Driver, S. P. & Phillipps, S., 1996, ApJ, 469, 529

[60] Eder. J. A., Oemler, A., Jr., Schombert, J. M., & Delel, A. 1989, ApJ, 340, 29

[61] Evans, Rh., Davies J. I., & Phillipps, S. 1990, MNRAS, 245, 164

[62] Fairall, A. P., Vettolani, G., & Chincarini, G. 1989, A&AS, 78, 269

[63] Ferguson, H. C. & McGaugh, S. S. 1995, ApJ, 440, 470

[64] Fish, R. A. 1964, ApJ, 139, 284

[65] Fouqué, P., Durand, N., Bottinelli, L., Gouguenheim, L., & Paturel, G. 1990, A&AS, 86, 473

[66] Freeman, K. C. 1970, ApJ, 160, 811

[67] Freeman, K. C. 1978, in "Structure and properties of nearby galaxies", IAU Symp. 77, p3, eds. E. M. Berkhuijsen & R. Wielebinski.

[68] Fukugita, M., Hogan, C. J., & Peebles, P. J. E. 1998, ApJ, 503, 518

[69] Giovanelli, R. & Haynes, M. P. 1988, in 'Galactic and extragalactic radio astronomy (2nd edition)', eds. Verschuur, G. L., & Kellermann, K. L., publ. Springer-Verlag, Berlin & New York.

[70] Giovanelli, R. & Haynes, M. P. 1989, 1989ApJ...346L...5G

[71] Henning, P. A. 1992, ApJS, 78, 365

[72] Henning, P. A. 1995, ApJ, 450, 578

[73] Henning, P. A. & Kerr, F. J. 1989, ApJ, 347L, 1

[74] Holmberg, E. B. 1958, Lund Medd. Astron. Obs. Ser. II, 136, 1

[75] Holmberg, E. 1966, in 'Galaxies and the Universe', Stars and Stellar Systems vol IX, p123, eds A. Sandage, M. Sandage, & J. Kristian, publ. University of Chicago Press, US, 1975.

[76] Hubble, E. 1929, 1929PNAS...15..168H

[77] Huchtmeier, W. K, Karachentesev, I. D., Karachentseva, V. E., & Ehle, M. 2000, A&AS, 141, 469

[78] Impey, C., & Bothun, G. 1997, ARA&A, 35, 267

[79] Impey. C., Bothun, G., & Malin, D. 1988, ApJ, 330, 634

[80] Impey, C. D., Sprayberry, D., Irwin, M. J., & Bothun, G. D. 1996, ApJS, 105, 209

[81] Irwin, M. J., Davies, J. I., Disney, M. J., & Phillipps, S. 1990, MNRAS, 245, 289

[82] Karachentsev, I. D., Karachentseva, V. E., & Parnovskij, S. L. 1993 (FGC), Astronomische Nachrichten, vol. 314, no. 3, p97.

[83] Kerr, F. J. & Henning, P. A. 1987, ApJ, 320, 99

[84] Kennicutt, R. C., Jr. 1989, ApJ, 344, 685

[85] Kibblewhite, E. J., Bridgeland, M. T., Bunclark, P. S., & Irwin, M. J. 1984, in "Astronomical Microdensitometry Conference", eds. D. A. Klinglesmith, publ. National Aeronautic and Space Administration, US.

[86] Kibblewhite, E. J., Cawson, M. G. M., Phillipps, S., Davies, J. I., & Disney, M. J. 1989, MNRAS¡ 236, 187

[87] Kilborn, V. A. 2001, Ph.D. Thesis, University of Melbourne

[88] Kilborn, V. A., Webster, R. L., & Staveley-Smith, L. 1999, PASA, 16, 8

[89] Kilborn, V. A. *et al.* 2000, AJ, 120, 1342

[90] Kilborn, Virginia A.; Boyce, Peter J.; Disney, Mike J.; **Garcia-Appadoo, Diego A.**; Grossi, Marco; Jordan, Christine A.; Lang, Robert H.; Minchin, Robert F., 2003, IAUS, 216, 209

[91] Kilborn, Virginia A.; Boyce, Peter J.; Disney, Mike J.; **Garcia-Appadoo, Diego A.**; Grossi, Marco; Jordan, Christine A.; Lang, Robert H.; Minchin, Robert F., 2003, IAUS, 216, 74

[92] Koribalski, B. S. 2001, in "Gas & Galaxy Evolution", ASP conf. ser., eds. J. E. Hibbard, M. P. Rupen, & J. H. van Gorkom, in press.

[93] Koribalski, B. S., Staveley-Smith, L., Kilborn, V. A., Ryder, S. D., Kraan-Korteweg, R. C., Ryan-Weber, E. V., Ekers, R. D., Jerjen, H., Henning, P. A.,**Garcia-Appadoo, D. A.**, and 30 coauthors, AJ, 128, 16

[94] Kormendy, J. 1977, ApJ, 217, 406

[95] Lahav, O., 2002, 2002MNRAS.333..961L

[96] Lang, Robert H., Boyce, P. J., Kilborn, V. A., Minchin, R. F., Disney, M. J., Jordan, C. A., Grossi, M., **Garcia-Appadoo, D. A.**; Freeman, K. C., Phillipps, S., Wright, A. E., 2003, MNRAS, 342, 738

[97] Lilly, S.J., Le Fevre, O., Hammer, F., 1996, ApJ, 460, 1

[98] Longmore, A. J., Hawarden, T. G., Cannon, R. D., Allen, D. A., Mebold, U., Goss, W. M., & Reif, K. 1979, MNRAS, 188, 285

[99] Longmore, A. J., Hawarden, T. G., Goss, W. M., Mebold, U., & Webster, B. L. 1982, MNRAS, 200, 325

[100] Loveday, J., Peterson, B. A., Efstathiou, G., 1992, ApJ, 390, 338

[101] Marzke, R. O., Geller, M. J., Huchra, J. P., 1994, AJ, 108, 437

[102] McGaugh, S. S. 1996, MNRAS¡ 280, 337

[103] McGaugh, S. 1999, int "The Low Surface Brightness Universe", ASP Conf. Ser. 170, eds. J. I. Davies, C. Impey, & S. Phillipps.

[104] McGaugh, S. S. & Bothun, G. D. 1994, AJ, 107, 530

[105] McGaugh, Bothun, & Schombert 1995 (MBS 95)

[106] McGaugh, S. S., Schombert, J. M., Bothun, G. D., & de Blok, W. J. G. 2000, ApJ, 533, 99

[107] Maloney, P. 1993, ApJ, 414, 41

[108] Mathewson. D. S., Cleary, M. N., & Murray, J. D. 1974, ApJ, 190, 291

[109] Mathewson, D. S. & Ford, V. L. 1996, ApJS, 107, 97

[110] Mathewson, D. S., Ford, V. L., & Buchhorn, M. 1992, ApJS, 81, 413

[111] Matthews, van Driel, & Gallagher 1998, AJ, 116, 1169

[112] Menzies, J. W., Coulson, I. M., & Sargent, W. L. W. 1989, AJ, 97, 1576

[113] Meyer, M. J., Zwaan, M., Webster, R. L., Staveley-Smith, L., Drinkwater, M. J., Barnes, D. G., Bhathal, R., de Blok, W. J. G., Disney, M. J., **Garcia-Appadoo, D. A.**, and 27 coauthors, 2004, MNRAS, 350, 1195

[114] Minchin, R. F. 1999, PASA, 16, 12

[115] Minchin, R. F., Davies, J. I., Disney, M. J., Boyce, P.,**Garcia-Appadoo, D. A.**, Jordan, C., Kilborn, V. A., Lang, R. H., Roberts, S., Sabatini, S.; van Driel, W., 2005, ApJ, 622, 21

[116] Minchin, R. F., Disney, M. J., Boyce, P.,**Garcia-Appadoo, D. A.**, de Blok, W.J.G., Banks, G. D., Ekers, R. D., Freeman, K. C., 2004, MNRAS, 355, 1303

[117] Minchin, R. F., Disney, M. J., Boyce, P.,**Garcia-Appadoo, D. A.**, de Blok, W.J.G., Banks, G. D., Ekers, R. D., Freeman, K. C., 2003, MNRAS, 346, 787

[118] Moore *et al.* 1998

[119] Morshidi, Z. 1998, Ph.D. Thesis, Cardiff University

[120] Morshidi-Esslinger, Z., Davies, J. I., & Smith, R. M. 1999a, MNRAS, 304, 297

[121] Morshidi-Esslinger, Z., Davies, J. I., & Smith, R. M. 1999b, MNRAS, 304, 311

[122] Nilson, P. 1973 (UGC), "Uppsala General Catalogue of Galaxies", publ. Royal Society of Science of Uppsala, Sweden.

[123] O'Neil, K. & Bothun, G. 2000, ApJ, 529, 811

[124] O'Neil, K., Bothun, G. D., & Cornell, M. E. 1997, AJ, 113, 1212

[125] O'Neil, K., Bothun, G. D., & Schombert, J. 2000, AJ, 119, 136

[126] O'Neil, K., Bothun, G. D., Schombert, J., Cornell, M. E., & Impey, C. D. 1997, AJ, 114, 2448

[127] Penston, M. V., Fosbury, R. A. E., Ward, M. J., & Wilson, A. S. 1977, MNRAS, 180, 19

[128] Phillipps, S. & Disney, M. J. 1983, MNRAS, 203, 55

[129] Phillipps, S., Disney, M. J., Kibblewhite, E. J., & Cawson, M. G. M. 1987, MNRAS, 229, 505

[130] Pickering, T. E., Impey, C. D., van Gorkom, J. H., & Bothun, G. D. 1997, AJ, 114, 1858

[131] Quintana, H., Ramirez, A., Melnick, J., Raychaudhury, S., & Slezak, E. 1995, AJ, 110, 463

[132] Richter, O.-G. 1984, A&AS, 58, 131

[133] Richter, O.-G. 1987, A&AS, 67, 261

[134] Roberts, M. S. 1975 in "Galaxies and the Universe", Stars and Stellar Systems vol IX, p309, eds A. Sandage, M. Sandage, & J. Kristian, publ. University of Chicago Press, US

[135] Roberts, M .S. & Haynes, M. 1994, ARA&A, 32, 115

[136] Romanishin, W., Krumm, N., Salpeter, E., Knapp, G., Strom, K. M., & Strom, S. E. 1982, ApJ, 263, 94

[137] Rosenberg, J. L. & Schneider, S. E. 2000, ApJS, 130, 177

[138] Sandage, A. 1978, AJ, 83, 904

[139] Salpeter, E. E. 1955, ApJ, 121, 161

[140] Salpeter, E. E. & Hoffman, G. L. 1996, ApJ, 465, 595

[141] Schecter, P. 1976, ApJ, 203, 297

[142] Schneider, S. E., Spitzak, J. G., & Rosenberg, J. L. 1998, ApJ, 507L, 9

[143] Schombert, J. M. & Bothun, G. D. 1988, AJ, 95, 1389

[144] Schombert.J. M., Bothun, G. D., Schneider, S. E., & McGaugh, S. S. 1992, AJ, 103, 1107

[145] Schwartzenberg, J. M., Phillipps, S., Smith, R. M., Couch, W. J., & Boyle, B. J. 1995, MNRAS, 275, 121

[146] Shostak, G. S. 1977, A&A, 54, 919

[147] Solanes, J. M., Giovanelli, R., & Haynes, M. P. 1996, ApJ, 461, 609

[148] Sorar, E. 1994, Ph.D. Thesis, Pittsburgh University

[149] Spitzak, J. G. 1996, Ph.D. Thesis, University of Massachusetts

[150] Spitzak, J. G. & Schneider, S. E. 1998, ApJS, 199, 159

[151] Sprayberry, D. 1994, Ph.D. Thesis, University of Arizona

[152] Sprayberry, D., Impey, C. D., Irwin, M. J., & Bothun , G. D. 1997, ApJ, 482, 104

[153] Staveley-Smith, L., Wilson, W. E., Bird, T. S., Disney, M. J., Ekers, R. D., Freeman, K. C., Haynes, R. F., Sinclair, M. W., Vaile, R. A., Webster, R. L., & Wright, A. E. 1996, PASA, 13, 243

[154] Theureau, G., Bottinelli, L., Coudreau-Durand, N., Gouguenheim, L., Hallet, N., Loulergue, M., Paturel, G., & Teerikorpi, P. 1998, A&AS, 130, 333

[155] Tully, R. B. & Fisher, J. R. 1977, A&A, 54, 661

[156] Turner, J. A., Phillipps, S., Davies, J. I., & Disney, M. J. 1993, MNRAS, 261, 39

[157] Van den Bergh, S. 1959, in "Publications of the David Dunlap Observatory", vol. 2, No. 5, p147, publ. University of Toronto Press, Canada.

[158] van der Hulst, J. M., Skillman, E. D., Smith, T. R., Bothun, G. D., McGaugh, S. S., & de Blok, W. J. G. 1993, AJ, 106, 548

[159] van der Kruit, P. C. 1987, A&A, 173, 59

[160] van Zee, Liese, Haynes, Martha P., Giovanelli, Riccardo, 1995, 109, 990

[161] van Zee, Liese, 1995, AAS, 187, 6305

[162] van Zee, Liese, Haynes, Martha P., alzer, John J., 1997, IAU, 2, 14

[163] van Zee, Liese, Haynes, Martha P., alzer, John J., Broeils, Adrick H, 1997, AJ, 113, 1618

[164] van Zee, Liese, 1999, ASPC, 170, 274

[165] Vorontsov-Vel'Yaminov, B. A. & Arkhipova, V. P. 1974 (MCG, part 5), Trudy Gosud. Astron. Inst. Shtemberga, 46, 1

[166] Vorontsov-Vel'Yaminov, B. A. & Arkhipova, V. P. 1968 (MCG, part 4), Trudy Gosud. Astron. Inst. Shtemberga, 38, 1

[167] Vorontsov-Vel'Yaminov, B. A. & Arkhipova, V. P. 1964 (MCG, part 2), Trudy Gosud. Astron. Inst. Shtemberga, 34, 1

[168] Vorontsov-Vel'Yaminov, B. A. & Arkhipova, V. P. 1963 (MCG, part 3), Trudy Gosud. Astron. Inst. Shtemberga, 33, 1

[169] Vorontsov-Vel'Yaminov, B. A. & Krasnogorskaya, A. A.. 1962 (MCG, part 1), Trudy Gosud. Astron. Inst. Shtemberga, 32, 1

[170] West, A. A., Dalcanton, J. J., Disney, M. J., **Garcia-Appadoo, D. A.**, 2002, AAS, 201, 5203

[171] Willmer, C. N. A., Maia, M. A. G., Mendes, S. O., Alonso, M. V., Rios, L. A., Chaves, O. L., & de Mello, D. F. 1999, AJ, 118, 1131

[172] Willmer, C. N. A., Focardi, P., Chan, R., Pilligrini, P. S., & da Cost, L. N. 1991, AJ, 101, 57

[173] Wright, A. E. & Otrupcek, R. 1990 (PKSCAT 90), "Parkes Catalogue, 1990", publ. Australia Telescope National Facility, Australia.

[174] Zwaan, M. A., van der Hulst, J. M., de Blok, W. J. G., & McGaugh, S. S. 1995, MNRAS, 273L, 35

[175] Zwaan, M. A., Briggs, F. H., Sprayberry, D., & Sorar, E. 1997, ApJ, 490, 173

[176] Zwaan, M. 2000, Ph.D. Thesis, Rijksuniversiteit Groningen, Netherlands

[177] Zwaan, M., Staveley-Smith, L., Drinkwater, M. J., de Blok, W. J. G., **Garcia-Appadoo, D. A.**, and 30 coauthors, 2003, AJ, 125, 2482

[178] Zwaan, M., Meyer, M. J., Webster, R. L., Staveley-Smith, L., Drinkwater, M. J., Barnes, D. G., Bhathal, R., de Blok, W. J. G., Disney, M. J., **Garcia-Appadoo, D. A.**, and 27 coauthors, 2004, MNRAS, 350, 1210

[179] Zwicky , F.1957, "Morphological Astronomy', publ. Springer, Germany

[180] Zwicky, F., Herzog, E., Wild, P., Karpowicz, M., & Kowal, C. T. 1968b (CGCG, vol. 6), "Catalogue of Galaxies and of Clusters of Galaxies", publ. California Institute of Technology, US.

[181] Zwicky, F., Herzog, E., Wild, P., Karpowicz, M., & Kowal, C. T. 1968a (CGCG, vol. 4), "Catalogue of Galaxies and of Clusters of Galaxies", publ. California Institute of Technology, US.

[182] Zwicky, F., Herzog, E., Wild, P., Karpowicz, M., & Kowal, C. T. 1966 (CGCG, vol. 3), "Catalogue of Galaxies and of Clusters of Galaxies", publ. California Institute of Technology, US.

[183] Zwicky, F., Herzog, E., Wild, P., Karpowicz, M., & Kowal, C. T. 1965 (CGCG, vol. 5), "Catalogue of Galaxies and of Clusters of Galaxies", publ. California Institute of Technology, US.

[184] Zwicky, F., Herzog, E., Wild, P., Karpowicz, M., & Kowal, C. T. 1963 (CGCG, vol. 2), "Catalogue of Galaxies and of Clusters of Galaxies", publ. California Institute of Technology, US.

[185] Zwicky, F., Herzog, E., Wild, P., Karpowicz, M., & Kowal, C. T. 1961 (CGCG, vol. 1), "Catalogue of Galaxies and of Clusters of Galaxies", publ. California Institute of Technology, US.